

Conceptual Considerations of the Death Valley  
Groundwater System with Special Emphasis on  
the Adequacy of This System to Accomodate  
the High-Level Nuclear Waste Repository.

Jerry S. Szymanski  
Physical Scientist  
U.S. Department of Energy  
Nevada Operations Office  
Waste Management Project Office

Las Vegas, Nevada  
November, 1987

8803310113 880315  
PDR WASTE  
WM-11 DCD

## TABLE OF CONTENTS

		<u>Page</u>
<b>SECTION 1.0</b>	<b>INTRODUCTION.</b>	1-1
<b>SECTION 2.0</b>	<b>MATHEMATICAL AND CONCEPTUAL MODELS OF GROUND-WATER FLOW SYSTEMS - STATEMENT OF THE PROBLEM.</b>	2-1
Section 2.1	General.	2-1
Section 2.2	Mathematical Models of Natural Groundwater Flow Systems.	2-3
Section 2.3	Conceptual Models of Natural Groundwater Flow Systems.	2-7
<b>SECTION 3.0</b>	<b>CONCEPTUAL FRAMEWORK FOR THE DEATH VALLEY FLOW SYSTEM.</b>	3-1
Section 3.1	General Description of Extension Dominated Tectonic Environments and Their Relationship to Groundwater Flow Systems.	3-1
Section 3.2	Conceptual Considerations of Groundwater Systems Developed in Deforming Fractured Medium.	3-9
3.2.1.	Contemporary Tectonic Environment of the Death Death Valley Flow System.	3-9
3.2.2	The Dynamic Stress Field.	3-14
3.2.3.	Hydrologic Importance of the Dynamic Stress Field	3-21
3.2.4.	Conceptual Model of Flow System in Deforming, Strongly Fractured Medium.	3-26
3.2.5.	Why is it Important to Know that the Flow System Developed in the Deforming Fractured Medium is or May be Involved?.	3-32
3.2.6.	How Can Recognition of the Involvement of the Deforming Fractured Medium in the Groundwater Flow Process be Achieved?.	3-35
Section 3.3.	Conceptual Considerations of Groundwater Systems Containing a Strong Thermal Inhomogeneity.	3-39
3.3.1.	Geothermal Setting of the Death Valley Groundwater Flow System.	3-39
3.3.2.	Simultaneous Flow of Fluid and Heat - T/H Coupled Flow.	3-43
3.3.3.	Conceptual Model of Flow System Containing Strong Thermal Inhomogeneity.	3-47
3.3.4.	Mixed vs. Forced Convection Flow Systems: Why is it important to Tell Them Apart?	3-50
3.3.5.	Forced vs. Mixed Convection Flow Systems - How to Tell the Two Apart?	3-54
Section 3.4.	Conceptual Considerations of the Two Phase, Heat-Fluid Coupled, Flow Field Developed in the Deforming Fractured Medium.	3-57
3.4.1.	General.	3-57
3.4.2.	Heat Flow Field Developed in the Deforming Fractured Medium.	3-58
3.4.3.	Coupled Fluid and Heat Flow Field Developed in the Deforming	

	<b>Fractured Medium.</b>	<b>3-64</b>
<b>SECTION 4.0</b>	<b>CHARACTERISTICS OF THE DEATH VALLEY FLOW SYSTEM IN LIGHT OF THE EXISTING DATA.</b>	<b>4-1</b>
Section 4.1.	General Description of the Death Valley Groundwater System.	4-1
Section 4.2.	The Vadose Zone of the Death Valley Groundwater System.	4-7
Section 4.3.	Configuration of the Water Table.	4-16
Section 4.4	Vertical Gradients of Hydraulic Potentials.	4-20
Section 4.5.	The In-Situ Stress State.	4-29
Section 4.6.	In-Situ Measurements of Temperature.	4-33
4.6.1.	General.	4-33
4.6.2.	Gradients of the In-Situ Temperature.	4-35
4.6.3.	Measurements of Heat Flow.	4-37
4.6.4.	Heat Flow in the Past.	4-39
4.6.5.	Summary.	4-40
Section 4.7.	Hydraulic Stressing of the Fractured Medium in the Death Valley Flow System.	4-42
4.7.1.	General.	4-42
4.7.2.	Response of Water Levels in Wells to Nuclear Detonations.	4-47
4.7.3.	Effects of Underground Nuclear Detonations on Aqueous Chemistry.	4-55
4.7.4.	Response of the Fractured Medium to Hydraulic Stressing During the Cooper-Bredehoeft Injection Tests.	4-57
4.7.5.	Summary.	4-64
Section 4.8.	Large Scale Fluctuations of Water Table as Possibly Expressed in Geologic Record Representing Late Pliocene and Quaternary Time.	4-66
<b>SECTION 5.0.</b>	<b>CONCLUSIONS AND RECOMMENDATIONS.</b>	<b>5-1</b>
Section 5.1.	Summary and Conclusions.	5-1
Section 5.2.	Recommendations.	5-15
References		(1)
Plates		-1-

## SECTION 1.0.

### 1.0. INTRODUCTION.

Options seriously considered for the isolation of high-level nuclear wastes that involve geologic media differ primarily in emplacement technique and location. Of these options, emplacement in a deep, excavated cavity, or geologic repository, is the currently favored method.

The most likely means of returning radionuclides from a sealed geologic repository to the biosphere is by dissolution and transport of the radionuclides by groundwater. The potential hazard from buried radionuclides, therefore, depends primarily upon three important aspects: a) the amount and rate of supply of radionuclides to the groundwater; b) the pathways and rate of groundwater movement; and c) the degree of geochemical retardation imposed by the geologic media.

The assessment of sites possibly suitable for a geologic repository must involve a critical evaluation of: a) the performance of the existing geologic system; b) the probable future performance of the natural system, taking into consideration evolutionary changes and potentially disruptive events; and c) the disturbance to the natural system caused by excavation, waste emplacement, sealing, and the presence thereafter of the waste facility. The assessment of risk is possible only if reasonable predictions can be made regarding the repository environment. Because actual tests and demonstrations of repository system behavior cannot be conducted under various changing conditions over representative periods of time, mathematical models must be used to evaluate the long-term behavior of the system.

Traditionally, the scientific community, concerned with development of technology to be used for purposes of achieving the disposal of radioactive materials, considered the repository siting options but only in a context of "stable geologic formations", situated in "tectonically stable areas". Roots of this perception may be related to our, human, inability to fully comprehend tectonic forces and processes and how these factors relate to long-term containment and isolation capabilities of geologic systems. It is fair to state, of course, that these reservations were expressed for saturated conditions alone. The Yucca Mountain site is different; water which is considered to be the most important factor in radionuclide transport is presently available but only in very limited quantities. What is the value of this attribute in light of the volcanotectonic setting of the site?; how do both of these factors balance each other in the context of repository performance and the uncertainties associated with it?. These are the questions which must be answered.

The most important part of understanding the role of tectonic processes, in the context of radionuclide releases, is a phenomenologic linkage between behavior of the fluid flow field which contains dissolved radionuclides and tectonically generated energy and/or substance in various forms and quantities. The subject is poorly known and the means of addressing it require rather difficult mathematical formulations which relate more to thermodynamic concepts of coupled flow than to the traditional hydrogeology.

It is likely that, for an active tectonic environment which involves extension and includes alkalic volcanism, the majority of assumptions utilized to develop mathematical models to describe "simple" groundwater flow systems are of questionable validity. Some of these assumptions are:

- Flow field involves only single phase flow;
- Three dimensional distribution of hydraulic potentials is simple and is fully describable through the configuration of the water table;
- Boundary conditions, with respect to an assumed horizontal base of the flow field, as they exist in time and space are of no importance;
- Boundary problem, as solved for a flow system consisting of surface recharge and discharge areas and composed of a non-deforming porous medium, is adequate to describe all aspects of behavior of the groundwater flow field; and
- Relationship between the flow field in the saturated zone and the flow field in the unsaturated zone is such that, in the unsaturated zone, only downward movement of water is possible.

Notwithstanding these obvious limitations, a position on tectonics and seismicity and how these subjects relate to performance of the high-level nuclear waste repository at the Yucca Mountain site has not been clearly articulated. This is true, in particular, for the relationship between tectonics and the groundwater flow system which, of course, is a key player in the performance of the high-level nuclear waste repository.

The regulatory framework, as it currently exists, tends to emphasize the issue of tectonics. However, both 10 CFR 60 and 10 CFR 960 deal with this issue in terms of vague generalities providing little help in developing siting decisions and site characterization plans. Tectonics and related hydrologic implications may have an important bearing on the compliance of a given disposal system with requirements set forth in 10 CFR 60. Conceivably, all specified performance objectives, either directly or indirectly, are involved, including:

- Pre-closure
  - Retrievability; and
  - Operational releases of radioactive materials.
- Post-closure
  - Groundwater travel time;
  - Life of waste package;
  - Release rates from engineered barriers;

- Release rates to the accessible environment.

Tectonic processes, with equal importance, come into play if one is concerned with compliance of a given disposal system with requirements set forth in 10 CFR 960. Both, pre-closure and post-closure system guidelines may be involved. Tectonics is also important with respect to many technical guidelines, both pre- and post-closure. Directly, tectonic processes govern compliance of a site with tectonic guidelines. Indirectly, other guidelines are also involved. These are: a) rock characteristics; b) geohydrology; and c) erosion.

The main purpose of the analysis presented herein is to offer a proposal regarding the relationship between the tectonics of the Yucca Mountain site region and the groundwater flow system operating at this site and in the region surrounding it. What is intended is to provoke the initiation of an understanding, on a qualitative or conceptual basis, of this groundwater flow field. This understanding could then be used: a) to develop a focused exploration program; b) to perform, if necessary, a re-evaluation of the existing data and positions based on these data; c) to develop a description of the natural system; and d) to develop a rational approach to the performance assessment and the performance allocation process.

The discussions have been divided into four parts. These parts are:

Section 2.0 - Mathematical and Conceptual Models of Groundwater Flow Systems - Statement of the Problem;

Section 3.0 - Conceptual Framework for the Death Valley Flow System;

Section 4.0 - Characteristics of the Death Valley Groundwater System in Light of the Existing Data; and

Section 5.0 - Conclusions and Recommendations.

## SECTION 2.0.

### MATHEMATICAL AND CONCEPTUAL MODELS OF GROUNDWATER FLOW SYSTEMS - STATEMENT OF THE PROBLEM.

#### 2.1. General.

Hydrologists, in their studies of natural groundwater flow systems, use mathematical models to represent these systems as a dynamic continuum in two or three dimensions. These representations can be used to estimate two very important characteristics of a given flow system, from a point of view of nuclear waste disposal. These characteristics are: a) the geometry of a flow path between any two arbitrary points or surfaces; and b) the corresponding groundwater travel time. Mathematical models can also be useful in studies of responses of the flow field to various provocations. For example, the mathematical model can be used to quantify hydrologic consequence of a climatic change or a tectonic disruption.

The mathematical representations of a flow field constitute a foundation for the analysis of transport by groundwater of buried radionuclides to the biosphere, including analysis of all significant transport attenuation processes. Through utilization of the sensitivity analyses, realistic descriptions of flow field, and reasonable assumptions about possible future disruptive processes, the mathematical models will provide the base for judgments regarding the acceptability of a site for the development of a geologic repository for nuclear waste. It is important, therefore, to understand how these models are constructed, what their limitations are, and what uncertainties are involved in their utilization.

## 2.2. Mathematical Models of Natural Groundwater Flow Systems.

Plate 2.2.-1 presents the basic structure of a mathematical model for any "simple" groundwater flow system. This structure involves three separate parts: a) the governing equation; b) the boundary conditions; and c) the initial conditions.

The governing equation is constructed by combining a law relating the groundwater velocity vector to the gradient of hydraulic potential with a continuity law which requires conservation of fluid mass. The law relating the groundwater velocity to the hydraulic gradient is commonly expressed in the form of Darcy's equation.

Boundary conditions constrain a given flow field and make solutions to the governing equation unique. The different types of boundary conditions are: a) head is known for surfaces bounding the flow region (Dirichlet conditions); b) flow is known across surfaces bounding the region (Neumann conditions); and c) some combination of (a) and (b) is known for surfaces bounding the flow region. If inconsistent or incomplete boundary conditions are specified, the flow field itself is ill defined.

The mathematical model of a flow system, in which the hydraulic potentials change with time, is a model for nonequilibrium or transient flow process. This model, in addition to the governing equation and the boundary conditions, must also include the initial conditions. These conditions are given through a set of head values at a time when the transient flow process was initiated.

There are three governing equations which are used in studies of "simple" groundwater flow systems. These equations are presented on Plate 2.2.-2, Plate 2.2.-3, and Plate 2.2.-4. Explanation of the mathematical notations used is presented on Plate 2.2.-5.

The first, most commonly used, equation is the Laplace equation. It states that the sum of the second partial derivatives of hydraulic potential with respect to  $x$ ,  $y$ , and  $z$  is equal to zero, i.e.,  $\nabla^2 h = 0$ . The flow system described by this equation is at steady-state conditions of flow. The aquifer, or a discrete portion of it, is assumed to be homogeneous and isotropic. The solution to the Laplace equation, which satisfies specific boundary conditions and specific distribution of properties of the water conducting medium (hydraulic conductivity), gives a distribution of hydraulic potentials as a function of  $x$ ,  $y$ , and  $z$ .

The second equation, which also describes the steady-state conditions of flow, is the Poisson's equation. It states that the sum of the second partial derivatives of hydraulic potential with respect to  $x$ ,  $y$ , and  $z$  is equal to a time-independent, but space variable, value, i.e.,  $\nabla^2 h = \pm R(x; y; z) \cdot T^{-1}$  (where  $T$  is transmissivity). The Poisson's equation allows for consideration of distributed or point sources and sinks of groundwater. The term  $R(x; y; z)$  expresses volume of water added per unit of time, per unit aquifer area. If  $R(x; y; z)$  is equal to zero, then the Poisson's equation reduces to the Laplace equation. Solution to the Poisson's equation, which satisfies specific boundary conditions and specific distribution of hydraulic conductivity, gives a distribution of hydraulic potentials as a function of  $x$ ,  $y$ , and  $z$ .

The third equation describes a flow field for which values of hydraulic potentials change with time. It states that the sum of the second partial derivatives of hydraulic potential with respect to  $x$ ,  $y$ , and  $z$  is equal to a time dependent value, i.e.,  $\nabla^2 h = S \cdot T^{-1} \delta h / \delta t$  (where  $S$  is storativity, it represents volume of water released from storage per unit area of aquifer, per unit decline in head). Allowing for the presence of groundwater sources and sinks, the transient flow equation becomes:  $\nabla^2 h = S \cdot T^{-1} \delta h / \delta t \pm R(x; y; z; t) \cdot T^{-1}$ . If term  $\delta h / \delta t$  is equal zero, the transient flow equation reduces to the Poisson's equation. However, if both terms  $\delta h / \delta t$  and  $R(x; y; z; t)$  are equal to zero, then the transient flow equation reduces to the Laplace's equation. Solution to the transient flow equation, which satisfies specific boundary conditions, initial conditions, and specific distribution of hydraulic conductivity and storativity, gives a distribution of hydraulic potentials as a function of  $x$ ,  $y$ , and  $z$  and as a function of time.

The above three governing equations constitute an essence of mathematical representations of groundwater flow systems as dynamic continua. They have two common characteristics. The first characteristic is that these equations, in terms of the thermodynamic concept of coupled flow, describe a single phase flow. For this flow, the groundwater velocity vector is a result of the gradient of hydraulic potential whose origin is solely related to hydraulic pressures acting at boundaries of the flow system and hydraulic losses sustained during the flow process. A role of other energy gradients, such as the temperature gradient for example, must be negligible, otherwise this flow process is misrepresented.

The second characteristic of the governing equations for the "simple" flow is that a medium in which this flow occurs, as expressed in terms of its hydraulic parameters (hydraulic conductivity and storativity), does not involve time dependency. The hydraulic parameters are considered as material properties which are independent of time or independent of other time related factors, for example the in-situ stress.

It can be expected, however, that a groundwater flow field developed in a medium which is subjected to various tectonic stimulations, operating on either continuous or episodic basis, involves other than the "simple" flow process. In this situation, none of the presented governing equations would constitute an adequate mathematical representation of the thermodynamic continuum involved.

The remainder of the discussions presented herein is devoted to an assessment of whether or not the tectonic factors play an important role in the Yucca Mountain flow field. A possibility will be explored that these factors may have a dominant, but not presently recognized, importance, in particular, with respect to the temporal aspects of behavior of this flow field.

### **2.3. Conceptual Models of Natural Groundwater Flow Systems.**

In order for a mathematical model to be an adequate, and therefore acceptable, representation of a given flow field it is necessary that this model has a rational base. This base is provided by a conceptual model which may be viewed as an interface between reality and the description of this reality provided by the mathematical model, Plate 2.3.-1. The conceptual model pertains to mental conceptions or concepts explaining a physical meaning of known characteristics of the flow field. It represents a totality of comprehension of the flow field. In order to be useful, this comprehension must be arranged within a specific framework as dictated by the requirements of the mathematical models. The characteristics of the flow field must be defined based on results of various in-situ measurements, observations, and related judgments. Only verified mathematical models, which are based on validated conceptual models, should be used for the purposes of establishing a firm base for judgments regarding the acceptability of a site for the development of a geologic repository for high-level nuclear waste.

Within the specific framework as demanded by the mathematical models, the conceptual model of the groundwater flow field may be viewed as a set of answers to the following questions:

- Does the flow field contain single or multiple phase flow?;
- Does the flow field operate in a medium with time dependent hydraulic parameters such as storetivity and hydraulic conductivity?;
- Does the flow field involve transient or steady-state flow process?;
- Does the flow field contain hydraulic sources and sinks?;
- What are the boundary and the initial conditions constraining the flow field?; and
- What is the spatial distribution of storetivity and hydraulic conductivity?.

As shown on Plate 2.3.-2, development of the conceptual model is an iterative process. The most important step in this process is the definition of characteristics of the flow field based on measurements and observations made in-situ. These characteristics, as demanded by the mathematical models, are quite specific. They include:

- Position and configuration of the water table;
- Spatial distribution of hydraulic potentials;
- Temporal changes in hydraulic potentials;
- Response of the flow field to stressing (pumping, injection, earthquakes and detonations, barometric pressure changes, earth tides, etc.);

- In-situ measurements of changes in storativity and hydraulic conductivity as a function of pore pressure (hydrofracture measurements and slug tests);
- Spatial and temporal variability of groundwater temperature;
- Spatial and temporal variability of groundwater chemistry;
- Spatial and temporal variability of the in-situ stress;
- Spatial and temporal variability of heat flow;
- Recharge-discharge balance;
- Flow mechanisms; etc.

In ordinary situations, hydrologists dealing with the problem of selecting a proper conceptual model seldom, if ever, have at their disposal the data base adequately addressing a range of conceivable conceptual alternatives which may be involved. However, these hydrologists seldom, if ever, have a need of addressing certain dynamic aspects of the flow field behavior. The situation is different, however, if one is concerned with developing the conceptual model of a flow field for purposes of evaluating the effectiveness of the nuclear waste disposal system. In this situation, the process of defining the flow characteristics must involve purposeful experimentations which are designed to obtain specific data required in order to select a proper conceptual alternative. The conceptual model of the flow field must be a result of conscious sorting out of the conceptual alternatives using the actual field data. In this process there is little room for hydrologic beliefs, customs and traditions. There is also little room for mathematical and numerical conveniences which are not supported by facts and common sense assessments of a given circumstance. There is a lot of room, however, for a fresh look at the existing data base, in particular, if this data base happens to be of extraordinary proportions.

In summary, the conceptual model of a groundwater flow field occupies a very special position in the process of searching for a geologic environment where reasonably safe and socially responsible disposal of the high-level nuclear waste can be achieved. On the following pages, therefore, this conceptual model will receive a lot of greatly deserved attention.

## SECTION 3.0.

### CONCEPTUAL FRAMEWORK FOR THE DEATH VALLEY GROUNDWATER SYSTEM.

#### 3.1. General Description of Extension Dominated Tectonic Environments and Their Relationship to Groundwater Flow Systems.

Deformational systems which are dominated by extension are commonly associated with basaltic volcanism whose composition ranges from alkalic to tholeiitic. These systems are regarded as surface manifestations of a much more fundamental tectonic process, Lipman, 1969; Chapin, 1971; Best and Brimhall, 1974; Green et al., 1974; De Paolo, 1978; Menzies et al., 1980; and, Leeman, 1982. This process involves a convective mass and heat transfer between the asthenosphere and the continental lithosphere. This dynamic transfer amounts to a diapiric upwelling of a high-temperature, less-dense, and low-viscosity asthenospheric material into the overlying lithosphere.

Plate 3.1.-1 presents the results of numerical analysis of the upwelling of asthenospheric material considered to be occurring at the Rio Grande rift, Bridwell and Potrick, 1981. The process was modeled symmetrically as a coupled, thermomechanical continuum in two-dimensions. The convective upwelling is shown as the velocity field and as the deformed mesh. The corresponding temperature field and viscosity field, as shown, are reflections of the process operating for  $6 \times 10^6$  years and causing an increase in the surface heat flow of approximately 1.0 HFU.

The process of asthenospheric upwelling introduces very significant changes into the structure of the upper mantle and the crust. These changes include:

- a) tectonic thinning of the lithosphere and the crust;
- b) development of magma bodies in the mantle and magma chambers in the crust; and
- c) locally increased temperature, and decreased density and viscosity of materials forming the upper mantle and the crust.

Plate 3.1.-2 shows effects of a mantle diapir in two dimensions. The  $1200^{\circ}\text{C}$  isotherm can be regarded as corresponding to the lithosphere-asthenosphere boundary. This isotherm is bent upward illustrating presence, in the upper mantle and the lower crust, of a significant inhomogeneity in the planar distribution of temperature. Planar distributions of density and viscosity display similar inhomogeneities.

The velocity field describing the convective flow of heat and mass in the upper mantle may be assumed to be at or near the steady-state conditions of flow (the amounts of heat and mass flowing into it equal the amounts flowing out of it). In this situation, there are two important tectonic processes which must be recognized. These processes are:

- a) The steady-state flow of heat through the crust. In terms of its planar distribution, the heat flow is nonhomogeneous -  $\delta t/\delta z \neq 0$  and therefore -  $\delta t/\delta z \neq \text{const.}$ ; and
- b) The steady state flow stresses, acting at the base of the crust. In two dimensions, these flow stresses express themselves as a shear stress gradient acting along the crustal base -  $\delta \tau_{xz}/\delta z \neq 0$ .

Plate 3.1.-3 shows two of these processes operating in association with the steady-state flow field of the perviously considered mantle upwelling. Surface heat flow is strongly nonhomogeneous. This strong inhomogeneity is caused by the planar distribution of temperature in the lower crust and by magma chambers present there. The distribution of shear stress, shown to be acting in a horizontal plane, is the result of outward flow in the upper mantle. This shear stress causes the entire crust to be subjected to a continuous extension.

Material forming the upper mantle and which contains the convective flow field, is gravitationally unstable. The hot, low-density, and low-viscosity mass tends to move buoyantly upward, thus reducing this instability. This movement causes a local uplift of the Earth surface.

The state of stress, in the crust, varies with time and space. Strain energy is being supplied into the system on a continuous basis. This energy is utilized by advancing deformation of the crust through uplift, faulting, tilting and viscous flow at deeper crustal levels.

Plate 3.1.-4 shows the distribution of shear and normal stresses developed in the crust as a function of distance from the central portion of the upper mantle convective flow field. The example shown corresponds to a convective flow system operating for about  $7 \times 10^6$  years and causing the surface heat flow of about 2.5 HFU. The stresses were computed assuming that no deformation occurs in the crust. Therefore, the stresses are not reduced to account for faulting, uplift or any other deformation. Consequently, the tensile stresses significantly exceed those which can be sustained by crustal rocks. Also, the vertical normal stress acting at the crust base exceeds the lithostatic pressure.

Both of these processes, i.e., the heat flow and the continuous introduction of strain energy, operating simultaneously lead to the establishment of two energy fields. For time scales of geologic proportions, these fields are interactive as well as dynamic or transient.

One field pertains to temperature of the crustal medium. For a given time, this field is described by a nonhomogeneous heat flux through the Earth surface. For given boundary conditions, given initial conditions, and for a given three-dimensional distribution of material properties, this flux corresponds to a set of isothermal surfaces which show a three dimensional distribution of points of equal temperature.

The other field involves the strain energy contained by the crustal medium. At a given time, this field is described by a three-dimensional deformation of the Earth surface. For given boundary conditions, given initial conditions, and for a given distribution of material properties, this deformation corresponds to

a set of equipotential surfaces which show a three dimensional distribution of points for which magnitudes of the principal stresses are the same but, for a given point, not necessarily equal to each other.

If it is assumed that: a) thickness of the system is constant; b) boundary conditions of the system remain unchanged; and, c) material properties are temperature and time scale independent, the dynamic aspects or time dependence for both fields is caused by the steady-state flow stresses operating at the base of the system.

For the strain energy field, the time dependence expresses itself as a change in position of the equipotential surfaces relative to a fixed reference surface and as a change in shape of these surfaces relative to the reference surface and relative to each other. At most times, the rate of these changes is exceedingly small. During short intervals of time, however, this rate may be dramatically increased. This occurs in association with faulting which may entail a substantial reduction of the strain energy in a substantial volume of the crustal medium.

It can be shown that, at certain stress levels, the bulk thermal conductivity of a fractured rock medium is stress dependent. It can, therefore, be expected that, if a local development of the strain energy field reaches a certain level, continued introduction of the strain energy into this field will cause time and space dependent alterations in the three dimensional distribution of thermal conductivity. Hence, although the planar distribution of heat flow remains unchanged, the time dependence in the strain energy field will cause, at least locally, a delayed time dependence in the temperature field. This time dependence will express itself as a local time dependence of the geothermal gradients.

The strain energy induced changes in the temperature field are expected to be occurring at exceedingly small rates. Also, magnitudes of changes in the local geothermal gradients are judged to be small, say somewhere within a range from 5°C/km to 15°C/km. A relatively rapid change in a local temperature field, however, may be associated with faulting which may cause a permanent change in the bulk thermal conductivity.

For the purposes of the hydrologic considerations presented below, it has been assumed that the strain energy field and the temperature field are the only factors which relate a tectonic environment and a near-surface groundwater flow system. This assumption is reasonable, in particular, if one is concerned with the tectonic environment whose main characteristics are extension and small scale basaltic volcanism.

A groundwater flow system is an energy field in itself. This field is defined by a flux of groundwater through the system boundaries. For given boundary conditions, given initial conditions, and for a given three-dimensional distribution of material properties, this flux corresponds to a set of equipotential surfaces which show a three-dimensional distribution of points of equal hydraulic potentials.

The main purpose of the hydrologic considerations presented below is an assessment of how, and to what degree, a groundwater flow field may be influenced by tectonic factors. In this case these factors are

the strain energy field and the temperature field. A real question which is being evaluated is: what are the potential hydrologic implications of the volcano-tectonic setting of the Yucca Mountain flow system? What is desired is an understanding, on a qualitative or conceptual basis, of the temporal aspects of behavior of this flow system under the influence of tectonic factors.

The discussions presented have been divided into three parts. The first part considers the relationship between the dynamic strain energy field and the groundwater flow system. The strain energy field operates in a fractured rock medium which also contains the groundwater flow field. The temperature field is considered as having no influence on either the strain energy field or the groundwater flow process.

The second part deals with the relationship between the temperature field and the groundwater flow field. It has been assumed that there is no interactive relationship between the temperature field and the strain energy field and that the strain energy field plays no role in the groundwater flow process.

The third part is concerned with a partial three way coupling between the temperature field, the strain energy field, and the groundwater flow field. It has been assumed that neither the temperature field nor the groundwater flow field influence the strain energy field. The strain energy field, however, influences both the temperature field and the groundwater flow field.

### 3.2. Conceptual Considerations of Groundwater Systems Developed in Deforming Fractured Medium.

#### 3.2.1. Contemporary Tectonic Environment of the Death Valley Flow System.

Tectonic deformation of an area corresponding to the Death Valley groundwater system during Pliocene and Quaternary periods is known based on various structural geology studies performed at or near the Nevada Test Site. Information concerning contemporary deformation of the area is also available. These data were obtained based on studies of regional and local seismicity and based on local geodetic measurements.

Long term extension rates across the Southern Great Basin, at latitude 37°N, are of the order of 1cm/year or  $+ 0.07 \times 10^{-6}$  m/m per year, Wernicke et al., 1982. These rates are average values calculated for the entire province, between the Southern Sierra Nevada and the Central Colorado Plateau, for the last  $15 \times 10^6$  years. At any given time, however, the extension seems to be confined to relatively narrow belts, as appears to be the case today in the Death Valley region, rather than being uniformly distributed across the province. Local extension rates, therefore, may be different than the average and may differ with time.

From a tectonic point of view, the groundwater system is situated within a southeastern portion of the Walker Lane, a northwest trending belt of right-lateral shearing and of continental proportions, Stewart, 1967; 1968. As shown on Plate 3.2.1.-1, the Walker Lane belt occurs in the southwestern portion of the Great Basin along the California-Nevada border. Displacements along this belt occur, in part, as dextral slip and, in part, as dextral bending. Total displacement may be as large as 130 to 190 km, Stewart et al., 1968. Some faults, located within the Walker Lane, are covered by undeformed Upper Miocene or Pliocene volcanic rocks, while others displace Pliocene and Quaternary deposits.

Plate 3.2.1.-2, Plate 3.2.1.-3, and Plate 3.2.1.-4 show the location of more prominent Late Pliocene-Quaternary faults developed in the area of the groundwater system and in the area of the proposed repository. Surface displacements of Quaternary age are known to be associated with many of the faults in this area. Movements of Late Pleistocene and Holocene age have been documented on several of these faults, Knauss, 1981; Carr, 1984; Whitney et al., 1986; and Reheis, 1986. Typically, the length of individual faults ranges from several km to tens of km. Displacements of Quaternary materials are measured in meters and were developed during repeated ruptures.

In some areas within the Walker Lane belt the structural grain is notably deflected from the regional trend. These areas appear to have been rotated about a vertical axis in response to a dextral shear couple. Recent paleomagnetic studies of a Miocene ash flow indicated that an area situated near the proposed repository has been rotated 30° clockwise since the Middle Miocene, Scott and Rosenbaum, 1986. This area is some 25 km long and is situated within the central portion of the groundwater system.

Rotations along a horizontal axis are also known in the region. Southward or southwestward tilting of, at least, the western portions of the groundwater system has been suggested by Carr, 1984. Volcanic

units emplaced 8 to  $15 \times 10^6$  years ago pinch out abruptly southward, which suggests that they were emplaced on a surface that sloped northward or north-westward. By contrast, the present topographic surface slopes generally southward from a regional topographic high in central Nevada. Southward or south-eastward tilting of 3.0 to 7.0 m/km, during the past  $3 \times 10^6$  years, is indicated by a southward decrease in the altitude of occurrence of playa deposits, Carr, 1984. Contemporary tilting is suggested by the apparent tendency of the centers of deposition, in such playas, to shift southward with time.

Seismicity of the southern Great Basin is shown on Plate 3.2.1.-5. The area shown roughly corresponds to the groundwater system. The events were recorded during a period from August 1, 1978 through December 31, 1983 by a 53 station seismic network. The pattern of local seismicity is of a widespread but diffuse background, corresponding principally to the east-west seismic belt of Greensfelder et al., 1980, punctuated by clusters of intense activity and by larger, nearly aseismic areas. The events are of low magnitude  $1 \leq M_L < 3$ . The focal depth of hypocenters ranges from 1 km to 17 km, Rogers et al., 1987. The depth distribution has two broad peaks at 0 - 2 km and 5 - 8 km and a distinct minimum at 3.5 km. Depth profiles in active areas frequently show earthquake patterns extending from the surface down to a depth of 10 km or more. Focal mechanism solutions, determined based on radiation patterns of some 29 events, indicate that strike-slip faulting is a dominant mode of elastic stress release. For most of the solutions the B-axis, which is a pole to a plane containing the slip vector, plunges steeply. Only 6 or 7 solutions yielded the B-axis whose plunge is less than  $45^\circ$ .

In 1970 trilateration networks were established, at the Nevada Test Site in the area of Yucca Flat and Pahute Mesa. The geodolite measurements were conducted by USGS personnel in 1972, 1973, and 1983, SAIC, 1984. The data obtained, for a block some 40 km long and 20 km wide and located in Yucca Flat, can be fitted to a uniform strain field. The horizontal principal strains are almost exactly N-S and E-W. The strain rate in a north-south direction is  $-0.10 \times 10^{-6}$  per year (shortening) and in an east-west direction the strain rate is  $+0.08 \times 10^{-6}$  per year (extension).

There are two tectonic models which are being considered to account for the deformation observed at and near the Nevada Test Site. The first model requires the presence of one or more subhorizontal detachment faults located at deeper crustal levels, Scott, 1985. These detachment faults would constitute a crustal expression of the steady-state flow stresses which were discussed in Section 3.1. and are shown on Plate 3.1.-3 and Plate 3.1.-4. In this model, faults observed at the surface are listric normal faults extending upward from a detachment surface. A main feature of this tectonic model is the horizontal extension developed in response to the shear displacements occurring along the detachment surface.

The second tectonic model has been proposed by Carr, 1984. According to this model the surface deformation is related to the dextral shearing within the Walker Lane shear belt. The Nevada Test Site appears to be located where a right stepping in the Walker Lane occurs. This right stepping is associated with a zone of northeast trending faults showing a left-lateral sense of slip. Based on principals of basic

wrench tectonics (Wilcox et al., 1972; Moody and Hill, 1956; deBoer, 1967), these faults may be regarded as antithetic strike-slip faults. Commonly, during an advance stage of the wrench deformation, these antithetic fractures inherit some extension aspects of the deformation and become nearly vertical, normal faults with negligible lateral displacement. Another important characteristic of the wrench deformation is the development of tension fractures and normal faults. The development of these structures occurs parallel to the acute bisectrix of the synthetic and the antithetic strike-slip faults, Wilcox et al., 1973. It is possible that north-south trending faults, which are very common at and near the Nevada Test Site, represent this type of structure, Plate 3.2.1.-4.

A main feature of the tectonic arrangements, described by the second tectonic model, is the dextral shear couple acting along margins of the Walker Lane. Extension is related to this shear couple and is localized in areas where the right stepping occurs.

For the purposes of these hydrologic considerations, it is not of great importance to know which tectonic model provides the best explanation for the observed structural arrangements and kinematic movement plans. What is important is the fact that the regional deformation occurs on a continuous basis and that it involves extension. Presence of additional factors such as compression and rotation about either a vertical axis or a horizontal axis, are important from a point of view of structural geology. These factors may only indicate presence of local inhomogeneities in the stress field. They may, nevertheless, have some regional tectonic significance. However, for purposes of these conceptual hydrologic considerations, these factors are not of great importance.

This brief summary of deformation of the Death Valley groundwater system during the Plio-Quaternary period indicates, quite clearly, that from a tectonic point of view the area is active. A substantial body of evidence points toward a complicated displacement field with surface displacement velocities far exceeding those expected to be associated with a steady-state viscous or visco-elastic flow. Consequently, an important question emerges: what are hydrologic implications of this circumstance?. Subsequent discussions are intended to provide some answers to this question. The discussions were developed keeping in mind that: a) the assessment is performed for the purposes of evaluating performance aspects of the high-level nuclear waste repository; and b) the time scales of geologic proportions are of interest.

### 3.2.2. The Dynamic Stress Field.

Plate 3.2.2.-1 presents the summary of the contemporary strain rates and of the accumulated shear strains for the surface deformation of the Death Valley groundwater system. These strain rates are far too large to be accounted for by the viscous or visco-elastic flow. Occurrences of earthquakes and of surface ruptures along numerous faults support this conclusion. It is, therefore, more than reasonable to expect that a dynamic strain energy field is involved. For such a field, the potential energy or strain energy ( $w$ ) changes with time, i.e.,  $\delta W/\delta t \neq 0$ . The rate of these changes, although exceedingly small is, at least locally, time dependent, i.e.,  $\delta W/\delta t \neq \text{const}$ . During short intervals of time, however, the rate may become

quite large, as is the case for a seismogenic fault rupture or for a fault displacement induced by vibratory ground motion.

The strain energy stored in a body by elastic straining is:

$$W = \frac{1}{2}(\sigma_1 \cdot \epsilon_1 + \sigma_2 \cdot \epsilon_2 + \sigma_3 \cdot \epsilon_3).$$

where:

$W$  - strain energy per unit volume;

$\sigma_1, \sigma_2, \sigma_3$ , - principal stresses; and

$\epsilon_1, \epsilon_2, \epsilon_3$ , - principal strains.

Before a general consideration of hydrologic significance of the dynamic strain energy field can be performed, first it is necessary to develop an understanding of the process of tectonic deformation. To this end and for the sake of simplicity, the area of interest may be considered to be composed of a number of arbitrary strain domains. This division is shown on Plate 3.2.2.-2. Size of an individual domain varies from tens of km<sup>2</sup> to hundreds of km<sup>2</sup>. It is assumed that the boundaries of all domains are respectively parallel to each other. Furthermore, it is assumed that the initial boundary tractions for each domain are equal to each other and are equal to the boundary tractions present at margins of the deformation area.

Each of these domains is assumed to contain a separate fault zone which, with time, will become the center of a focal inclusion, Brady, 1974; 1975; and 1976. For each of the faults, collapse of the focal inclusion (earthquake) occurs at different times and with a different frequency. This different response time is caused by a different length and orientation assumed for each of the faults.

This idealization of the deformation process is not an accurate description of a real deformation. In reality, some of the faults are interconnected and the boundary tractions of an individual domain are not only related to the boundary tractions of the deformation area, but they are also influenced by developments in the neighboring domains. For purposes of these conceptual hydrologic considerations, however, this inaccuracy does not entail a serious consequence.

It is convenient to think about tectonic deformation as occurring in repeated cycles of deformation. Duration or frequency of these cycles is, or may be, different for each individual strain domain. Plate 3.2.2.-3 and Plate 3.2.2.-4 presents an idealized history and the principal characteristics of such a tectonic cycle for a given strain domain.

The individual cycle can be subdivided into two phases. The first phase, or the pre-dilatant phase (Brady, 1975), begins with an onset of build-up of tectonic stress in response to a regional tectonic deformation. The rate of this local tectonic deformation is very low, but it will increase gradually. During this phase, both normal stresses ( $\sigma_{xx}$  and  $\sigma_{yy}$ ) and shear stresses ( $\tau_{xy}$  and  $\tau_{yx}$ ) show small time-dependence. In the case where shear couple is involved, the time-dependence pertains not only to the magnitude of principal stresses ( $\sigma_1$ , and  $\sigma_3$ ) but also to the orientation of these stresses. There is no frictional sliding, therefore, more or less homogenous strain conditions prevail and the stress gradients do not exist.

The second phase of deformation begins at a time when, somewhere within the strain domain, a local failure is initiated. This phase can be subdivided further into four distinct stages, Brady, 1974; 1975; and 1976. These stages are:

**Dilatant Stage:** Formation of new cracks (microcracks) occurs uniformly throughout the medium. The microcracks grow in a direction roughly parallel to the trajectory of the greatest principal stress ( $\sigma_1$ ).

**Inclusion Stage:** Clusters of microcracks develop within the medium. These zones can be represented physically as low modulus inclusions embedded within a host medium of higher modulus. As a result of this contrast, there is both a rotation and a change in magnitude of the principal stresses in the dilatant zone. Throughout the dilatant zone microcrack density is variable, therefore, the changes in the principal stresses are not only time dependent but they are also space dependent. A central portion of the dilatant zone, or the focal region, containing the highest density of microcracks is known as the inclusion.

**Closure Stage:** In this phase there is closure of the microcracks in the focal region and, in particular, within the focal inclusion. This closure is caused by an interaction between the focal region and the surrounding it medium. As the result of crack closure, the stress concentration in the focal region increases and becomes a maximum once all cracks are closed. At this time, in the interior of the inclusion, the transverse tensile stress also reaches a maximum. Macrocrack growth within the inclusion begins.

**Growth Stage:** Fault growth commences during this stage. Some phases of "growth" are slow and others catastrophic. The reopening of previously closed microcracks occurs. The system becomes unstable and the rapid growth of the macrocrack occurs once the length of the macrocrack exceeds a critical value.

Based on this description of an earthquake nucleation process, it becomes clear that during the second phase of the tectonic cycle, the strain domain is divided into two parts. The first part corresponds to an area which is situated outside the dilatant zone, Plate 3.2.2.-2. In this area, at a time when the dilatant zone is very small in volume, the stress field tends to be homogenous. The stress gradients are either very small or they do not exist at all. Both normal and shear stresses, nevertheless, display time dependence.

The second part of the strain domain corresponds to the dilatant zone, containing in its interior the focal inclusion. Within this zone time dependent stress gradients are developed.

It can be expected that, during the entire second phase of deformation, a volume represented by the dilatant zone changes continuously. During the dilatant and the inclusion stages it increases, until it reaches a certain value which is characteristic for the strain domain. This time dependent expansion of the dilatant zone, including the focal inclusion, causes time and space dependent straining of the outside zone. This, in turn, causes the development of nonhomogeneous strain conditions in this zone or the development of time dependent stress gradients.

During the closure stage of deformation, however, the interaction between the outside zone and the dilatant zone is reversed. Stretching of the outside zone reached a certain critical value. The outside zone begins to expand, thus causing contraction of the dilatant zone.

Finally, during the growth stage of deformation, the interaction between these two zones reverses itself again. Reopening of the previously closed cracks occurs and is caused by the rapid growth of the macrocrack outward from the inclusion, Plate 3.2.2.-5. At this time, the dilatant zone expands again causing renewed stretching of the outside zone.

Collapse of the focal inclusion is associated with a release of large quantities of strain energy stored in the deforming medium. Part of this energy is released in the form of vibratory ground motion. At this time, the stress field begins to return to more or less homogenous conditions of strain.

Association of the dilatant zones with the earthquake nucleation process is a well known geophysical phenomenon, Nur, 1972; Frank, 1965; Scholz and Kranz, 1974; Scholz et al., 1973; Whitcomb et al., 1973; Aggarwal et al., 1973; Sadovalsky et al., 1973; Semenov, 1969. Size of these zones, in terms of the dilatant volume ( $\Delta V$ ) and the dilatant strain ( $\Delta V/V$ ), may be considerable. Sibson et al., 1975, for example, has shown that the dilatant zone for the Matsushiro earthquake swarm, which was energetically equivalent to a single event of magnitude M 6.3, had the dilatant volume of about  $5 \times 10^6 m^3$  and the dilatant strain of about  $10^{-5}$ .

In the outside zone the displacement field, during the second phase of the tectonic cycle, can be described by: a) the Navier-Stokes equations of flow for a slow-moving, very viscous and slightly compressible fluid; and b) a set of specific boundary conditions pertaining to a given stage of the deformation (Ramsay, 1967). It can be recalled that the boundaries of deformation for the outside zone are: a) margins of the strain domain; and b) outer limits of the dilatant zone. The stress field is defined by a biharmonic equation:

$$\frac{\delta^4 \Omega}{\delta^4 x} + \frac{2\delta^4 \Omega}{\delta^2 x \delta^2 y} + \frac{\delta^4 \Omega}{\delta^4 y} = 0, \text{ or}$$

$$(\nabla^2 \Omega)^2 = 0$$

where:  $\Omega$  is a stream function chosen such that the velocities of the movement parallel to the x and y axis may be expressed as partial derivatives:  $\dot{u} = -\delta\Omega/\delta y$  and  $\dot{v} = -\delta\Omega/\delta x$ .

Solution to this equation, which satisfies the specific boundary conditions for a given stage of deformation, gives: a) the displacement velocity components; b) the strain rates; and c) the stress gradients; Ramsay, 1967.

### 3.2.3. Hydrologic Importance of the Dynamic Stress Field.

The main feature of the dynamic stress field is the time and space dependence of the principal stress. This feature may be of fundamental hydrologic importance. Analyses performed below are intended to explore this possibility.

As shown on Plate 3.2.3.-1, changing with time magnitudes of the principal stresses and/or changing orientation of these stresses must introduce corresponding time dependence of the normal and shear stresses acting along fractures. Stress and strain along these fractures are related by constitutive laws, so that incrementally:

$$\Delta\sigma_{neff} = K_n \cdot \Delta u_n, \text{ and}$$

$$\Delta\tau_j = K_s \cdot \Delta u_s, |\tau_j| < C + \sigma_{neff} \cdot \tan\phi = \tau_{max}$$

$$\text{otherwise } \tau_j = \tau_{max}$$

where:

$\Delta\sigma_{neff}$  - change in the magnitude of effective normal stress.  $\sigma_{neff} = \sigma_{nf} - p$ , ( $p$ ) is pore pressure;

$K_n$  - joint normal stiffness;

$\Delta u_n$  - normal displacement of joint;

$\Delta\tau_j$  - shear stress along joint;

$K_s$  - joint shear stiffness;

$\Delta u_s$  - shear displacement of joint;

$C$  - joint cohesion; and

$\phi$  - friction angle.

Measurements have shown that the hydraulic conductivity of fractures is sensitive to the confining pressure and this has been attributed to changes of conducting aperture caused by a change in the normal effective stress, Walsh, 1981. Various relationships have been proposed, for example Barton et al., 1985. For purposes of this conceptual analysis, a simplified but nevertheless realistic dependence has been adopted. This dependence is shown on Plate 3.2.3.-2. The conductive aperture depends linearly on confining stress (through compliance  $K_e$ ) until the closure pressure ( $\sigma_e$ ) is reached and then only a residual aperture remains. If shear dilation occurs, however, the basic relationship is assumed to be modified as indicated by the dashed line. If a joint loses all compressive effective stress, loss of block-to-block contact occurs and the conductive aperture is equal to the separation of the adjacent blocks.

Two very important hydrologic parameters are directly related to the fracture conducting aperture. These parameters are: a) the fracture hydraulic conductivity ( $K_f$ ); and, b) the fracture storetivity ( $S_f$ ).

Adopting the analogy of planer parallel plates to represent the walls of the joint, and assuming the Newtonian viscous flow (dynamic viscosity  $\mu$ , density  $\xi$ ), the fracture hydraulic conductivity is:

$$K_f = a_{con}^2 \cdot \frac{\xi \cdot g}{12\mu}, \text{ or}$$

$$K_f = a_{con}^2 \cdot \text{const.}$$

where:

$K_f$  - the fracture hydraulic conductivity; and

$a_{con}$  - the fracture conducting aperture.

The storetivity of a fracture per unit area is:

$$S_f \cong a_{con}.$$

Plate 3.2.3.-3 presents the relationship between the conducting fracture aperture and the effective normal stress assuming that the shear stress along the fracture is equal zero. This plate also shows the resulting time dependence of: a) the fracture hydraulic conductivity; b) the fracture storetivity; and, c) the depth above which both of these parameters exhibit time dependence. The relationships were developed assuming that: a) there is a limit for the normal fracture dilation; and b) the reduction in a value of

the initial confining stress ( $\sigma_e$ ) is continuous and is caused by changes in the principal stresses. At a time when  $\sigma_{nfeff}$  is reduced to a point where it is equal to the closure pressure ( $\sigma_e$ ), the hydraulic conductivity and the storativity begin to show the time dependence. Time vs. hydraulic conductivity relationship is exponential, and it is linear for the storativity. The time dependence of the depth, above which changes in the conductivity and the storativity occur, is caused by increasing with depth value of the initial confining stress. Assuming that the rate of decay in  $\sigma_{nfeff}$  is constant, more time is required to accumulate the sufficient reduction at a greater depth.

Plate 3.2.3.-4 shows an idealized joint response during shear displacement for selected values of constant normal effective stress. This plate also shows a relationship between the shear displacement ( $u_s$ ) and the shear dilation component of the conducting fracture aperture ( $a_d$ ) assuming that there is a limit to the magnitude of this component. If, at a given depth, the shear stress reaches the critical value of  $\tau_{max} = C + \tan\phi\sigma_n$  then the shear dilation component ( $a_d$ ) becomes greater than zero and dependent of the value of the shear displacement. Small incremental shear displacements cause increases in the magnitude of this component. With increasing time, joints located at a progressively greater depth become involved.

Keeping in mind the assumed time dependence of the shear stress, the diagram shown on Plate 3.2.3.-4 can be used to establish the time dependence for the shear dilation component of the fracture conducting aperture ( $a_d$ ). This relationship is shown on Plate 3.2.3.-5. Time dependence of the hydraulic parameters is also included. Increasing  $\tau$ , causes: a) the storativity; b) the hydraulic conductivity; and, c) the depth above which both of these parameters are time dependent, all to increase with time. The relationship between shear displacement ( $u_s$ ) and depth is important. It shows that the shear displacement, and with it the dilation component of fracture aperture, attains its greatest magnitude at the surface. With time this magnitude increases until a limit set by  $a_{d(t)}$  is reached. The depth at which the dilation component is greater than zero also increases with time.

In summary, it appears that the dynamic stress field or the dynamic strain energy field is of fundamental hydrologic importance. This field may cause time dependence of important hydrologic parameters, such as the hydraulic conductivity and the storativity.

#### 3.2.4. Conceptual Model of Flow System in Deforming, Strongly Fractured Medium.

A conceptual model of groundwater flow occurring in the deforming fractured medium is presented on Plate 3.2.4.-1. It is assumed that the water conducting medium is strongly fractured and, therefore, the volume of groundwater moving through the medium matrix is negligible. Most or all of groundwater moves through fractures.

A main feature of this model is a space and time dependent depth  $Z(x;t)$ . Above this depth, hydraulic parameters of the medium (the hydraulic conductivity and the storativity) are time and space dependent.

The fractured medium is assumed to be the deforming one and, therefore, the stress field is dynamic, in a sense that it is changing with time. The stress field is assumed to be evolved to a stage, so that the depth  $Z(x;t)$  is considerable relative to the total thickness of the medium ( $Z_1$ ). Taken together, these two assumptions cause that the field of hydraulic potentials is also time dependent or dynamic. If, for some reason, a change in hydraulic potentials, independent of the in-situ stress field, is introduced, a corresponding change in the in-situ stress field follows.

Below the depth  $Z(x;t)$ , the hydraulic parameters of the medium are independent of the stress field and are, therefore, time independent. There is, however, a transfer of groundwater, across a plane defined by the depth  $Z(x;t)$ . This transfer is expressed, in the governing equations of the flow system, through a term  $\pm R(x;z;t)$ . This term represents a volume of water added, per unit time and per unit aquifer area, to an infinitesimal volume of the fractured medium around the point  $p(x;z)$ . The transfer of fluid is caused by a difference in the hydraulic potentials above and below the depth  $Z(x;t)$ . The time dependence of the term  $\pm R(x;z;t)$  is caused by the time dependent nature of the difference in hydraulic potentials above and below a given depth.

The horizontal boundary of the flow system, located at the depth  $Z_1$ , is assumed to be "no-flow" boundary. For the vertical boundaries "no-flow" or "const. head" boundary conditions were assumed. The hydraulic pressures acting at these boundaries differ by the amount  $CX$ . Needless to say, the transient conditions of flow prevail.

Plate 3.2.4.-2, Plate 3.2.4.-3, Plate 3.2.4.-4, and Plate 3.2.4.-5, present an idealized history of developments in the flow system responding to the changing in-situ stress conditions in association with the tectonic cycle. For purposes of simplicity, it has been assumed that the homogeneous strain conditions exist throughout the entire cycle and that the initial value of the hydraulic potential is constant with depth.

It is assumed that the flow system contains a thick vadose zone. Prior to initiation of the tectonic straining, the flow system is under steady-state conditions of flow. The bedrock is assumed to be strongly fractured along various directions. In the zone of saturation, the fracture flow is the assumed mechanism of flow. Furthermore, the system is assumed to be situated in climatic conditions so that the recharge through the vadose zone is very small and initially, therefore, the matrix flow mechanism dominates in this zone.

As shown on Plate 3.2.4.-2, at time  $t_0$  at a very shallow depth and deeper, the effective normal stress  $\sigma_{nfeff(t_0)}$  is greater than the closure stress ( $\sigma_c$ ) and the shear stress  $\tau_{f(t_0)}$  is smaller than  $\tau_{max}$ . Therefore, only the residual fracture aperture is present. The water table is located at the depth  $dw(t_0)$ .

At time  $t_1$  only at the depth  $Z(x,t_1)$  and below it, the effective normal stress  $\sigma_{nfeff(t_1)}$  is greater than the closure stress ( $\sigma_c$ ) and the shear stress ( $\tau_{f(t_1)}$ ) is smaller than  $\tau_{max}$ , Plate 3.2.4.-3. Below this depth, therefore, the conducting fracture aperture is equal to the residual aperture.

However, above the depth  $Z(x;t_1)$  or within the vadose zone the conducting fracture aperture has been increased and with it values of the storativity and the hydraulic conductivity were also increased. In the vadose zone, therefore, a tendency toward fracture flow emerges. Because the depth  $Z(x;t_1)$  is shallower than the depth  $dw_{(t_0)}$ , the water table remains where it was during time  $t_0$ .

Plate 3.2.4.-4 presents an idealized distribution of the pore pressure with depth for an advanced stage of deformation. At time  $t_2$  the depth  $Z(x;t_2)$  is considerable and far below the water table at time  $t_0$ . Above this depth, the fractured medium is dilated which results in increased values of the hydraulic parameters. Between time  $t_1$  and time  $t_2$ , the thickness of the vadose zone increased from  $dw_{(t_1)}$  to  $dw_{(t_2)}$ . The mechanism of flow through this zone is, most likely, fracture flow caused by the increased values of fracture apertures.

The volume of water, resulting from the increased thickness of the vadose zone, was accommodated partially through increased flow, caused by the increased values of hydraulic conductivity, and partially through increased storage, caused by the increased values of storativity. The distribution of hydraulic potentials shows an important zonation. In Zone I the hydraulic potential is depth independent and its value is constant. The pore pressure increases with depth in accord with the increasing weight of water. For this zone  $\sigma_{\text{neff}(t_2)} = \sigma_c$  and/or  $\tau_{f(t_2)} = \tau_{\text{max}}$  for values of pore pressure  $p(z)$ .

In Zone II, however, the value of hydraulic potentials is depth dependent. The amount of "overpressure" is equal to  $\Delta p(z)$ . For this zone,  $\sigma_{\text{neff}(t_2)} = \sigma_c$  and/or  $\tau_{f(t_2)} = \tau_{\text{max}}$  but only for values of pore pressure  $p(z) + \Delta p(z)$ .

Zone III begins at the depth  $Z(x;t_2)$ . At this depth the value of "overpressure" reaches its maximum  $\Delta p(z) = \Delta p_{\text{max}}$ . The value of the hydraulic potential is constant and equal to the value of the hydraulic potential at time  $t_0$ .

Plate 3.2.4.-5 presents the distribution of pore pressure with depth for time  $t_3$  which represents the end of the tectonic cycle. At this time, the depth  $Z(x;t_3)$  has been reduced, from its former value  $Z(x;t_2)$ , to a very small value. This resulted in the return of the hydraulic parameters to their initial values [ $S_{(t_3)} = S_{(t_0)} < S_{(t_2)}$  and  $K_{f(t_3)} = K_{f(t_0)} < K_{f(t_2)}$ ]. The thickness of the vadose zone has been decreased from  $dw_{(t_2)}$  to  $dw_{(t_3)}$ . This decrease was caused by two factors, namely: a) the overpressure  $\Delta p_{\text{max}}$  in zone III, Plate 3.2.4.-4; and b) water released from storage between the depth interval from  $dw_{(t_2)}$  to  $Z(x;t_2)$ . In the vadose zone, the mechanism of flow is the matrix flow.

The water table is at the depth  $dw_{(t_3)}$ , which is greater than the depth  $dw_{(t_0)}$ . This position is not in accord with the value of hydraulic potentials at depth. The water table is, therefore, unstable and with time it will decay into the equilibrium position represented by  $dw_{(t_0)} = dw_{(t_1)}$ .

Plate 3.2.4.-6 shows an idealized history of the position of water table, throughout the entire tectonic cycle, for a single point  $p(x;y)$ . This history represents a summary of the discussions presented above and

is presented in the form of a hydrograph which would result from a groundwater level monitoring performed in a single well between time  $t_0$  and time  $t_3$ . It can be recalled, that the homogeneous conditions of strain were assumed to exist throughout the entire tectonic cycle and for the entire flow system. A main feature of the hydrograph is, therefore, a long term progressive lowering of the water table.

The assumption of homogeneous strain conditions is not a realistic expectation if a real deformational system is involved. There is more than one reason why one would expect that in actual situations, the nonhomogeneous stress field is involved. This has very important hydrologic implications. Because the matter soon becomes very complex only superficial evaluations are offered.

For the nonhomogeneous in-situ stress field the lowering of the water table is not necessarily uniform in both time and space. Occasionally excursions from the long term trend occur, Plate 3.2.4.-6. These excursions are of relatively small time duration and involve both positive (hydraulic mounds) and negative (hydraulic sinks) departures from the long term trend. The excursions are related to local developments in the in-situ stress field. Strain rates of deformation and values of the in-situ stresses are changed in response to local failures of various kinds. These failures may or may not be associated with, or accompanied by, vibratory ground motion. The resulting perturbations in the position of water table are of a relatively small areal extent and, therefore, are unstable because they cannot be justified by the overall distribution of hydraulic potentials. With time, they will decay into a more tolerable equilibrium position.

Plate 3.2.4.-7 presents the inferred relationship between configuration (shape) of the water table and the nonhomogenous stress field. The stress field inhomogenities are represented by a surface defined by the depth  $Z(x;y;t_n)$ . Three simple configurations were selected for this surface. These are: a) step-like; b) step-like with a depression; and, c) a tilted surface. There seem to be three important effects associated with the assumed stress field inhomogeneities. These are: a) progressive lowering; b) development of areas where local slopes of the water table are quite steep; and c) flattening or reduction in a local inclination of the water table. The configuration of the water table appears to be a result of very complex interactions between various parts of the flow system. These interactions are caused by the time and space dependence of the hydraulic parameters. The aim of these interactions is conservation of mass of fluid involved in the flow process.

### 3.2.5. Why is it Important to Know that the Flow System Developed in the Deforming Fractured Medium is or may be Involved?.

Based on the evaluations presented above it becomes clear that, in the deforming fractured medium, the position and configuration of the water table is a very special one indeed. In particular, the water table does not seem to be an expression of the durable characteristics of the flow system. Furthermore, the water table constitutes a very poor representation of the three-dimensional distribution of hydraulic potentials which motivate the real flow field.

In the case of hydrologic considerations performed for the purposes of developing the high-level nuclear waste repository in the vadose zone, two issues of fundamental importance are associated with the possibility that the flow system is developed in the deforming fractured medium. These are: a) the mechanism of flow in the vadose zone; and b) the temporal stability of the water table, including its short and long term aspects.

The flow mechanism in the vadose zone was considered in evaluating the history of developments in the flow system responding to the changing in-situ stress conditions, Section 3.2.4. In the deforming fractured medium, the depth  $Z(x;t_n)$  migrates downward with increasing time. This migration causes the conducting aperture of fractures to increase. The magnitude of this increase is depth dependent. The greatest increases occur near the ground surface and they gradually diminish downward. With the increasing value of the conducting aperture of fractures, the tendency toward fracture flow in the vadose zone increases. A relative measure of this tendency, therefore, is the depth  $Z(x;t_n)$ .

The second issue pertains to the temporal stability of the water table. In the case of the deforming fractured medium, this stability is not only related to climatic changes, it is also related to tectonic factors. Short term instabilities of the water table, such as the excursions discussed in Section 3.2.4. and shown on Plate 3.2.4.-6, if occurring with a meaningful frequency and magnitude would constitute a "pumping" mechanism for a gaseous transport through the vadose zone. Long term changes in the position and configuration of the water table may influence the radionuclide migration path and time. In extreme cases, however, these changes may cause flooding of the repository and surface expulsions of groundwater. At this point, an important question emerges. This question is: how large are the in-situ stress field related changes in the position of water table?

The answer to this question may be provided based on results of studies of: a) the relevant characteristics of the contemporary flow field; and b) the past behaviors of the flow field as recorded in geological materials of Plio-Quaternary age. As shown on Plate 3.2.4.-5, the magnitude of the "post-tectonic" rise in the water table is related to two characteristics of the contemporary flow field. These characteristics are: a) the amount of overpressure  $\Delta p_{max}$  or the value of hydraulic potentials in Zone III; and b) the difference in depths  $dw_{(t_0)}$  and  $dw_{(t_1)}$ ,  $\Delta h = dw_{(t_0)} - dw_{(t_1)}$ , which is related to the volume of water released from the storage. The difference  $\Delta h$  is related to: a) total volumetric strain ( $\Delta v/v$ ); and b) storativity of the bedrock in the unstrained state. As discussed in Section 4.4. and Section 4.7., measurements performed at the Nevada Test Site indicate that the water table changes to be expected in this flow system may be measured, at least, in tens of meters. These measurements pertain to: a) the distribution of the hydraulic potentials with depth; and b) the response of the water table to some nuclear detonations.

Changes in position of the water table may be introduced by climatic change. This causes gradual increases or decreases in volume of water passing through the surface and/or the vertical boundaries of the flow system.

It can be recalled, however, that in the deforming fractured medium, above the depth  $Z(x;t_2)$ , the in-situ stress field and the field of hydraulic potentials are coupled. Therefore, the in-situ stress independent change in the groundwater flow field, such as the climate induced change in volume of groundwater involved in the flow process, will cause adjustments in the strain energy field. These adjustments will involve displacements along fractures causing increases in the value of hydraulic parameters. The increased volume of the groundwater may, therefore, be accommodated by the increased flow rates and by the increased storage. The position of water table does not have to be significantly adjusted.

### 3.2.6. How Can Recognition of the Involvement of the Deforming Fractured Medium in the Groundwater Flow Process be Achieved?

The most important characteristic of the groundwater flow system, developed in the deforming fractured medium, is its transient behavior, i.e.,  $\nabla^2 h \neq 0 \neq \text{const.}$ . During most of time, this transient behavior involves small, in time and space, oscillations in the values of the hydraulic potentials. These oscillations can be expected to occur in conjunction with a slow continuous drift of the value of these potentials. Large scale rearrangements in the groundwater flow field, however, may be expected to be associated with tectonic disruptions. These disruptions are nothing less than large scale restructurings of the strain energy field and are associated with releases of large quantities of the strain energy stored in the medium.

Both of these characteristics can be used to achieve recognition that the deforming fractured medium is involved in the groundwater flow process. Conceivable, there are two approaches which could be utilized in this undertaking.

The first approach involves a thorough examination of the geologic record as expressed through geologic materials of the Plio-Quaternary age occurring at the ground surface or in the subsurface of the groundwater flow system. The purpose of this examination is to determine whether this record contains expressions of large scale fluctuations of the groundwater table during the Plio-Quaternary period. These fluctuations should reveal themselves as occurrences of deposits whose origin is related to groundwater. These deposits would occur in positions such that they cannot be justified by: a) the position and configuration of the contemporary water table; b) the changes in this position caused by post climatic alterations; and, c) tectonic deformations of the land surface such as: tilting, uplift and subsidence.

The second approach involves an evaluation of some specific characteristics of the contemporary groundwater flow field. These characteristics, however, must be defined based on results of involved hydrologic studies of the flow field.

The pattern of temporal behavior of the hydraulic potentials is, perhaps, the most important characteristic of the groundwater flow field. This characteristic may be used for the purposes of determining whether or not the deforming fractured medium is involved in the flow process. To this end, the results of measurements of depth to the water table made as a function of time and at several locations are required.

For the flow system, containing a thick vadose zone and situated such that an arid climate conditions prevail, presence of: a) meaningful oscillations in the position of water table; and/or b) long term continuous drift in this position; may signal that the deforming fractured medium is involved.

Another important characteristic of the contemporary flow system is the distribution of the hydraulic potentials as a function of depth. With reference to Plate 3.2.4.-4, this distribution may be used to evaluate whether or not the "overpressure"  $\Delta p_{(z)}$  is or may be present at a greater depth. However, care should be taken while interpreting the distribution of hydraulic potentials with depth. The increase in the value of hydraulic potentials may indicate either the presence of the confined aquifer conditions or it may indicate that the "overpressure" is present. It is quite easy to confuse the two.

The possibility that the deforming fractured medium is involved in the flow process may be further evaluated based on results of the in-situ stress determinations. These determinations must be performed as a function of depth and, for the sake of certainty, at several locations. Because the depth dependent distribution of the in-situ stress is required for considerable aquifer thicknesses, the in-situ stress determinations must be made utilizing the technique of hydraulic fracturing.

Involvement of the deforming fractured medium will display itself as the characteristic zonation of the in-situ stress conditions with depth, as shown on Plate 3.2.4.-4. The aquifer would appear as divided into three zones with the following in-situ stress characteristics:

Zone I - extends from the water table down to the depth  $Z_1$ . For this zone, at least locally,  $\sigma_{neff}$  is equal to the closing pressure ( $\sigma_c$ ) and/or  $\tau_f$  is equal to  $\tau_{max}$ . This occurs for values of pore pressure  $p = Z \cdot \xi$ . ( $\xi$  is density of water and  $Z$  is depth below the water table.)

Zone II - extends from the depth  $Z_1$  down to the depth  $Z(x;t_n)$ . For this zone, at least locally,  $\sigma_{neff}$  is equal to  $\sigma_c$ , and/or  $\tau_f$  is equal to  $\tau_{max}$ . This occurs for values of pore pressure  $p = Z \cdot \xi + \Delta p_{(z)}$ .

Zone III - extends from the depth  $Z(x;t_n)$  downward. For this zone,  $\sigma_{neff}$  is smaller than  $\sigma_c$ , and  $\tau_f$  is smaller than  $\tau_{max}$ . This occurs for values of pore pressure  $p = Z \cdot \xi + \Delta p_{max}$ .

As far as the involvement of deforming fractured medium in the groundwater flow process is concerned, perhaps, the most informative are observations of the response of the flow system to large scale changes in the strain energy field. A detonation of a sizeable nuclear device, say with a yield of about one megaton, will entail such large scale restructuring of the in-situ strain energy field. The resulting changes in the groundwater flow field can be monitored in both time and space using a system of properly instrumented wells. The involvement of deforming fractured medium should display itself as: a) large scale oscillations of the water table occurring long after passage of the detonation induced shock waves; and b) sustained, but localized, water table changes resulting in formation of hydraulic mounds or hydraulic sinks.

### 3.3. Conceptual Considerations of Groundwater Systems Containing a Strong Thermal Inhomogeneity.

#### 3.3.1. Geothermal Setting of the Death Valley Groundwater System.

The seismic velocity structure of the area occupied by the Death Valley groundwater system is known based on a teleseismic P-wave travel-time residual study, Monfort and Evans, 1982. The data for this study were obtained during 1980 by recording 98 teleseismic events at as many as 53 sites.

Plate 3.3.1.-1 is a map showing the seismic velocity structure of the upper crust for the region of southern Nevada. Contours shown are seismic velocity departures from the mean velocity in (%), negative velocity perturbations indicate areas of lower velocity. The most striking feature shown by this map is a low velocity trough extending from Death Valley, California to about 50 km north of the Nevada Test Site. The trough underlies the western portion of the entire Death Valley groundwater system. Within the trough, there are two highly localized low-velocity anomalies. One anomaly occurs in the area of Pahute Mesa, near or within recharge areas of the groundwater system. The other anomaly is situated in central portions of the system, near the southwestern corner of the Nevada Test Site, in the area of Skull Mountain - Wahmonie.

Plate 3.3.1.-2 is a generalized geologic map of the Death Valley - Pancake Range Volcanic Zone. The zone contains notable expressions of small scale basaltic volcanism of Plio-Quaternary age, Crow et al., 1986. Isotopic and geochemical composition of lavas related to this volcanism is remarkable. Detailed petrologic studies of these lavas were performed by Vaniman and Crowe, 1981; Vaniman et al., 1982; Semken, 1984; and Crowe et al., 1986. The results of these studies revealed that the lavas display the hawaiite affinity. Significant features of these rocks are: a) the "alkaline classification; b) presence of groundmass olivine and calcic clinopyroxene; c) scarcity of groundmass calcium-poor pyroxene; and, d) andesine-normative feldspar compositions," Crowe et al., 1986. Furthermore, the rocks are highly enriched in light rare-earth elements, even when compared to typical alkalic basalts, Vaniman et al., 1982. They exhibit a broad range of isotopic compositions. The chondrite-normalized strontium and neodymium isotopic ratios of these rocks range from  $\epsilon_{SR} = 42.2$  to  $\epsilon_{SR} = -9.0$  and from  $\epsilon_{ND} = -10.4$  to  $\epsilon_{ND} = 3.8$ , Semken, 1984.

The observed enrichment in light rare-earth elements and in strontium, coupled with low rubidium/strontium ratio, of the southern Nevada Test Site basalts, was attributed to the mantle origin of these basalts, Vaniman et al., 1982. Semken, 1984, concluded that the unique geochemical and isotopic characteristics of the basalts are best accounted for by assuming that a mixing of the lower crust materials with the upper mantle materials was involved in generation of these very special magmas. This mixing indicates the presence in the upper mantle of a descending limb of the convective flow system. Of course occurrences of these basalts at the ground surface must indicate the presence of the second, ascending limb, of the convective system.

There seems to be a remarkable correlation between the location of low velocity trough on Plate 3.3.1.-1 and the locations of the Plio-Quaternary volcanic centers, Plate 3.3.1.-2. This correlation suggests that:

- a) The map of P-wave residuals reflects real changes in seismic structure of the upper crust; and
- b) The seismic structure is related to thermally induced alterations in viscosity and rigidity of the upper crust. These alterations are most likely reflections of the convective flow system operating in the upper mantle.

It is possible, therefore, that the areas where the negative velocity perturbations occur correspond to areas where the intensity of heat flow is increased. Positive seismic velocities may indicate areas where the intensities of heat flow are reduced.

Some support for this interpretation is provided by the map of surface heat flow values, measured within and adjacent to the Nevada Test Site, and shown on Plate 3.3.1.-3. The low velocity anomaly, which is located near the southwestern corner of the Nevada Test Site, is clearly associated with the increased heat flow values measured in this area. These values range from 3.1 HFU in well Ue-25-a3, through 2.2 HFU in wells TW-3 and TW-4 to 2.0 HFU in well TW-5 and 1.81 HFU in well TWF, Sass and Lachenbruch, 1982.

The low-velocity anomaly, located near the area of Pahute Mesa, may also be associated with some local thermal perturbations. The value of geothermal gradient measured in well PM-1 ranges from 24.4°C/km to 28.8°C/km, Sass et al., 1976. In another well, however, this gradient is noticeably increased. Measurements performed in well PM-2 revealed that the value of geothermal gradient ranges from 56.8°C/km through 48.7°C/km to 38.2°C/km, Sass et al., 1976.

It is interesting to note that, relatively small changes in the surface heat flow, from one point to another, could correspond to very considerable differences in rock temperature at a greater depth. Plate 3.3.1.-4 shows changes in rock temperature as a function of depth and of value of the surface heat flow. Change in the surface heat flow value from 1.4 HFU to 2.5 HFU results, at a depth of about 15 km, in a difference in rock temperature of approximately 300°C.

Plate 3.3.1.-5 presents an actual profile of the surface heat flow for the Rio Grande rift and associated physiographic provinces of the North American continent. The corresponding seismic structure of the crust and the upper mantle is also shown. It can be noted that departures from the average P-wave velocity of few percents are associated with the increased surface heat flow values. This increase is from a range of 1.0 - 1.5 HFU, in the area where P-wave velocity is 6.8 km/sec, to a range of 2.0 - 3.0 HFU, in the area where P-wave velocity is 6.4 km/sec.

The degree of reduction in the P-wave velocity for the Rio Grande rift is quite similar to the one shown on Plate 3.3.1.-1 for the Nevada Test Site. It is reasonable, therefore, to expect that at mid-crustal levels, at the Nevada Test Site, the planar distribution of heat flow is heterogeneous and that differences in the heat flow values of about 1.5 HFU are a real possibility.

Variably distributed heat flow may play an important role in the flow process of the Death Valley groundwater system, including its transient behavior during tectonic disruptions. It seems worthwhile, therefore, to seek some understanding of the thermally influenced flow process, its hydrologic importance and, in the case of nuclear waste repository, its potential licensing implications.

### 3.3.2. Simultaneous Flow of Fluid and Heat - T/H Coupled Flow.

With increased temperature, the density of water decreases. In a column of water containing a temperature gradient, the density contrast between warm fluid, deeper within the column, and colder fluid, at a more shallow depth, introduces a buoyancy gradient acting in a vertical direction. The magnitude of this gradient depends on a change in water density caused by a given rise in temperature:

$$i_b = \frac{\alpha_w}{Z} \int_{z_2}^{z_1} t_{(z)} dz$$

where:

$i_b$  - buoyancy gradient;

$\alpha_w$  - coefficient of thermal expansion of water,  $\alpha_w = 3.85 \cdot 10^{-4}$  per °C; and

$\int_{z_2}^{z_1} t_{(z)} dz$  - change in temperature between depth  $z_1$ , and  $z_2$ .

A total hydraulic gradient combines the hydraulic pressure gradient and the buoyancy gradient in a manner shown on Plate 3.3.2.-1. If a uniform buoyancy gradient is introduced there is no resulting perturbation in the flow field. However, if a heterogeneously distributed buoyancy gradient is introduced a perturbation in the fluid flow field occurs. This perturbation displays itself as a change in the position and configuration of the fluid flow lines and as a change in the specific discharge of fluid across a reference unit area. The specific discharge of fluid, moving through a permeable medium in response to both the pressure gradient and the buoyancy gradient, is given by:

$$q_f = -L_1 \frac{\delta h}{\delta L} - L_2 \frac{\delta t}{\delta L}$$

where:

$q_f$  - specific discharge of fluid;

$L_1$  and  $L_2$  - constants of proportionality;

$\frac{\partial h}{\partial L}$  - pressure gradient; and,

$\frac{\partial t}{\partial L}$  - temperature gradient.

In most hydrologic situations  $L_1 \frac{\partial h}{\partial L} \geq L_2 \frac{\partial t}{\partial L}$ . Under these conditions assumptions that: a) the groundwater flow is fully described by Darcy's law; b) the hydraulic head distribution, at the vertical boundaries of the system, is a suitable representation of the total head; and, c) the hydraulic conductivity is the only important phenomenological coefficient, are justified.

In the groundwater flow field, developed in the area which from a volcanic point of view is active and which consequently contains a strongly heterogeneous temperature field, the value of  $L_2 \frac{\partial t}{\partial L}$  must be considerable relative to  $L_1 \frac{\partial h}{\partial L}$ . In this situation, one is facing two, more or less, interactive energy fields, i.e., the temperature field and the groundwater flow field. Interaction between these two fields is expressed as a simultaneous flow of heat and fluid under the influence of two interdependent energy gradients. This simultaneous flow of fluid and heat is a reflection of the thermodynamic concept of coupled flow. For such a flow:

$$q_f = -L_{11}i_1 - L_{12}i_2, \text{ and}$$

$$q_h = -L_{21}i_1 - L_{22}i_2.$$

where:

$q_{f,h}$  - specific discharge of fluid and heat;

$i_1$  - hydraulic pressure gradient;

$i_2$  - temperature gradient; and,

$L_{11}, L_{12}, L_{21}, L_{22}$  - phenomenological coefficients.

A mathematical model of the simultaneous flow of fluid and heat has been described by Thunvik and Braester, 1980. The model consists of a system of coupled non-linear partial differential equations. As shown on Plate 3.3.2.-2, the governing equations for the coupled flow of heat and fluid are:

- a) The equation for the conservation of fluid mass, derived from the basic conservation laws and Darcy's law; and
- b) The equation for the conservation of thermal energy.

There are also two equations of state, Plate 3.3.2.-2. These equations express a pressure and temperature dependence of water density and viscosity.

The equations can be solved utilizing the Galerkin finite element method. This method requires introduction of trial functions:

$$p = \Omega_j p_j, T = \Omega_j T_j$$

where:  $\Omega_j = \Omega_{j(x,t)}$  are basis functions, chosen to satisfy the essential boundary conditions.

Taking advantage of the orthogonality conditions in the Galerkin method one can rewrite the equation for conservation of fluid mass and the equation for conservation of thermal energy into a form shown on Plate 3.3.2.-3. Finally, applying Green's theorem to all second order terms and using the finite difference approach to the time derivatives, one can obtain a system of non-linear algebraic equations, which can be solved by an iterative procedure.

### 3.3.3. Conceptual Model of Flow System Containing Strong Thermal Inhomogeneity.

A conceptual model of a groundwater flow system, which contains a strong thermal inhomogeneity at its base, is presented on Plate 3.3.3.-1. The flow system consists of three parts. The lower part is separated from the overlying middle part by a layer which is assumed to be impermeable with respect to fluid flow but conductive with respect to heat flow. An arbitrary plane separates the middle part and the upper parts of the flow system. This plane is assumed to be conductive with respect to both fluid and heat flow.

A base of the lower part of the flow system is considered as "no fluid flow" boundary. This boundary, however, is strongly nonisothermal. The vertical boundaries are adiabatic and "no fluid flow" or "constant head" boundaries. Apart from thermal effects, differences in hydraulic pressures acting along these boundaries are small. Under these conditions, the mechanism of flow is "free" convection where most of heat is transferred by circulating fluids. The volume of fluid engaged in this steady-state hydrothermal convection flow process is constant.

A base of the middle part of the flow system is formed by the impermeable layer, which separates it from the lower part. This layer, therefore, is the "no fluid flow" boundary, but it is nonisothermal and the heat conducting boundary. These nonisothermal conditions are caused by the convective heat transfer operating in the lower part of the flow system. The vertical boundaries are adiabatic and "no fluid flow" or "constant head" boundaries. Hydraulic heads at both of these boundaries differ, however, and give a rise to the regional hydraulic gradient. Under these conditions, the mechanism of flow is "mixed" convection. Simultaneous flow of heat and fluid is caused by the hydraulic pressures acting along the vertical boundaries and by the temperature gradients present along the horizontal boundary. An arbitrary plane placed anywhere within this system, is a plane through which both fluid and heat flow occur.

A base of the near-surface flow system is formed by such an arbitrary plane. This plane is, therefore, the "fluid flow" and "heat flow" boundary. Boundary conditions at the vertical boundaries are identical to those in the middle part of the system. The mechanism of flow is also "mixed" convection.

In this situation, the main feature of the near-surface flow system is the horizontal boundary. This boundary contains "sources" through which water and heat are added into the near-surface flow system and "sinks" through which water and heat are removed from it. Consequently, the horizontal boundary, together with the regional hydraulic gradient and the distribution of material properties, controls the distribution of temperature and the distribution of hydraulic potentials in the near-surface flow system. Position and configuration of the water table will also be controlled by the underlying inhomogeneities in the coupled fluid-heat flow field. In areas underlain by the hydraulic and heat sources, the water table will tend to bend upward to form a hydraulic mound. However, in areas occurring over the potentiometric sinks, the water table will bend downward. These departures will introduce further complications into the shallow flow field. The resulting shape of the water table may be very complicated, and may include local mounds, sinks, and linear areas where slopes of the water table are considerable. This shape is the result of very complex interactions between deep and shallow areas of the flow field and involving spatially variable vertical and horizontal gradients of the hydraulic potentials and of the temperature. Consequently, correspondence between the water table and the potentiometric surfaces may be very poor.

It is interesting to note that for the flow system, which contains the "fluid-heat flow" boundary as its base, there is a special relationship between the zone of saturation and the vadose zone. These two zones can supply water to each other. An introduction of water from the saturated zone into the vadose zone occurs in association with a hydraulic mound. Such a mound attains a steady-state condition only if the volume of water flowing into it equals the volume of water flowing out of it. For a mound which has developed sufficient dimensions to reach the Earth surface, the removal of water will involve surface flow and evaporation (seep, spring etc.). In the case of less developed mounds, however, the removal of water must involve a subsurface flow through the vadose zone resulting in formation of perched waters.

The "mixed" convection flow system may or may not involve the steady-state conditions of flow. Although the pattern of temperature distribution at mid-crustal levels may be assumed to be, even for time scales of geologic proportions, reasonably stable there are, nevertheless, two complicating factors. These factors are:

- a) Coupled transfer of heat and fluid from depth will, undoubtedly, be associated with precipitation of minerals along fluid conducting fractures. This process will cause a gradual decrease in apertures of these fractures resulting in a time dependent reduction of the bulk storativity and the hydraulic conductivity of the medium; and
- b) Episodic faulting will most likely be accompanied with a more or less significant transfer of heat and fluid. This transfer will occur from the basal parts of the system where the "free" convection flow process operates, to the upper parts where the "mixed" convection flow process dominates. The resulting perturbation in the coupled fluid and heat flow field may be considerable in both time and space.

### 3.3.4. Mixed vs. Forced Convection Flow Systems: Why is it Important to Tell Them Apart?

The "forced" convection flow system is a system for which large spatial variability in the distribution of hydraulic conductivity is the main factor accounting for the convective aspects of the flow process. This variability is related solely to the lithologic composition of the crustal medium containing the flow system. The system is thermally "passive". Inhomogeneities in the temperature field are only expressions, but not the cause, of the convective nature of the flow field. In this case, the configuration and position of the contemporary water table is an expression of durable characteristics of the flow field. These characteristics are: a) the spatial distribution of hydraulic conductivity; b) the regional hydraulic gradients or location of the recharge areas relative to the discharge areas; and, c) the total volume of water involved in the flow process.

The "mixed" convection flow system is a system where thermal energy plays an important role in establishing the convective aspects of the coupled fluid-heat flow field. Such a flow field is thermally "active". Inhomogeneities in the temperature field are not only expressions, but also the cause, of the convective flow of heat and fluid. These thermal inhomogeneities are reflections of fundamental tectonic processes operating at deep crustal levels. For the "mixed" convection system, the configuration and position of the contemporary water table is not necessarily an expression of the durable characteristics of the flow field.

From a hydrologic point of view, the difference between these two flow systems is subtle. Nevertheless, this difference is of great importance. Confusing the two can entail serious errors in judgement pertaining to past and future behavior patterns of a given flow field. It is of particular importance that hydrologic considerations performed for purposes of developing the high level nuclear waste repository are free of these errors in judgement.

In performing numerical simulations of hydrologic systems for various purposes, a traditional approach has developed that is not particularly sound but which is firmly entrenched in usage. This approach amounts to the adoption of an arbitrary plane as the base of the flow system and assuming "no-flow" boundary conditions for this plane. This assumption is a reasonable one only if the "forced" convection flow process is involved. In the case of "mixed" convection, however, this assumption is not valid. "Flow" boundary conditions must be used for the base of such a flow system. Furthermore, the "flow" boundary conditions pertain to both fluid and heat. In this situation, the coupled flow of heat and fluid is involved. Consequently, mathematical models used in numerical simulations of the flow process must account for this circumstance. Calculations and interpretations based on wrong boundary conditions, assumed for the base of flow system, and based on an incorrect mathematical representation of the flow process can be grossly misleading and quite irrelevant.

The difference in boundary conditions results in a response of the "mixed" convection system to tectonic disruptions that is far more dramatic than the response of the "forced" convection system. In the

case of "forced" convection, the influence of tectonic disruptions (faulting) is limited to: a) alteration of lithologic relationships; b) additional local fracturing; and, c) change in elevation of the discharge areas relative to the recharge areas. A degree of change in these factors is relatively small and, therefore, the resulting alterations in the distribution of hydraulic conductivity and in the distribution of gradients of hydraulic potentials are likewise small. These alterations can readily be accommodated by minor changes in position and configuration of the water table.

Tectonic disruptions occurring within the "mixed" convection flow system, however, include an additional factor. This factor is the increased transfer of fluid and heat through the lower boundary of the flow system. If significant amounts of heat and fluid are involved, considerable and long lasting alterations in both position and configuration of the water table will follow. These transient conditions of flow will tend to be localized near disrupted portions of the flow system.

Changes in position of the water table can be introduced by changing climate whether or not the "forced" or the "mixed" convection system is involved. Climatic change will cause gradual increases or decreases in the volume of water passing through the boundaries of the flow system. The reaction of the water table to these changes is somewhat uniform. Its configuration is not altered in any appreciable degree, although its position may change considerably.

It is not uncommon for the climatically induced increases in the position of the water table to be recorded by occurrences, at or near the ground surface, of characteristic geologic materials. Compositions, textures and forms of the occurrence of these materials indicate that they were formed in association with paleo-springs or seeps. The map pattern of the occurrence of these deposits defines a surface whose configuration resembles the configuration of the contemporary water table.

Surface expulsion of groundwaters, caused by tectonic disruptions of the "mixed" convection flow system, will likewise be recorded through similar deposits. A map pattern of the occurrence of these deposits, however, does not display any fixed relationship to the contemporary water table. Furthermore, ages of such deposits will not bear any relationship to the history of the global climatic changes.

### 3.3.5. Forced vs. Mixed Convection Flow Systems: How to Tell the Two Apart?

Short of having at our disposal information pertaining to dramatic manifestations of geothermal conditions, such as geysers and superheated water or vapor dominated systems, it is rather difficult to distinguish between the "forced" and the "mixed" convection systems. At or near the steady-state conditions of flow, hydrologic characteristics of both systems are quite similar. These characteristics include:

- a) Complex three-dimensional distribution of the hydraulic potentials;
- b) Complicated configuration of the water table;

- c) More or less significant degree of the thermal inhomogeneity; and
- d) Inhomogeneity in the chemical composition of groundwater.

Apart from the degree of transient behavior during tectonic disruptions, there does not appear to be an unique and readily available hydrologic characteristic which could be used to distinguish one system from the other.

The problem can be solved, more or less conclusively, by relying on information provided by other disciplines of geoscience, namely, geology and geophysics. In particular, two questions seem to be appropriate. These questions are:

- a) Does the geologic record contain expressions of transient behavior during the Plio-Quaternary which are compatible with the "mixed" convection flow?; and
- b) Are geologic and geophysical characteristics of an area compatible with the assumption of strong thermal inhomogeneities at deep crustal levels?.

Information required in order to answer the above two questions include the following:

- a) Volcanic history of the area during the Plio-Quaternary;
- b) Contemporary crustal structure based on seismic, gravity, and magnetic measurements;
- c) Contemporary and paleo-thermal regimes;
- d) Character (textures, composition and origin) and location of Plio-Quaternary surface deposits which could be related to springs or seeps; and
- e) Character of Plio-Quaternary materials contained by the host rock in the subsurface (explosive breccias, veins, metasomatites, and alteration products).

### 3.4. Conceptual Considerations of the Two Phase, Heat-Fluid Coupled, Flow Field Developed in the Deforming Fractured Medium.

#### 3.4.1. General.

Examination of Plate 3.2.1.-2, Plate 3.3.1.-1, and Plate 3.3.1.-2, one against the other, reveals an interesting possibility. This possibility is that, at and near the Nevada Test Site, volcanism and faulting are related to a common cause. This is suggested by the temporal relationship between both of these processes alone. The possibility is further strengthened, however, by what appears to be a spatial relationship between the location of major faults, the location of volcanic centers, and the location of the low seismic velocity trough.

In light of this possibility, the main tectono-physical characteristics of the region, in which the Death Valley groundwater flow field operates (i.e., crustal stresses, dislocations, volcanism and heat flow), seem to be related to the deep thermal inhomogeneity which reveals itself as the pronounced anomaly in the seismic velocity structure of this region. Isotopic and geochemical characteristics of the basalts occurring in the Death Valley Pancake Range Volcanic Zone (Vaniman et al., 1982; Bergman, 1982) suggest that this inhomogeneity, in turn, is related to the convective flow of heat and mass in the mantle (Semken, 1984), Section 3.3.1. From a tectonic perspective, therefore, the gross structure of the area corresponds to an immature rift structure.

In order to understand what are potential hydrologic implications of this circumstance it is necessary to explore the mutual relationship between the groundwater flow field and two main tectonic factors, which are: a) the strain energy field; and b) the heat flow field. This is achieved through consideration of the two phase, heat-fluid coupled, flow field developed in the deforming fractured medium.

#### 3.4.2. Heat Flow Field Developed in the Deforming Fractured Medium.

Before a general consideration of the two phase coupled flow field, developed in the deforming fractured medium can be performed, first it is necessary to conceptualize the relationship between the heat flow field and the strain energy field. For the sake of simplicity, it is assumed that the relationship is one-sided, i.e., the heat flow field is influenced by the strain energy field, not the former by the latter. Furthermore, it is assumed that the fractured medium contains in pores and fractures only "stationary" fluids. The heat flow mechanism, therefore, involves only conduction and radiation and does not include convection.

This idealization of the heat flow field is not a realistic description of the actual situation. In reality, changing temperature will have a significant influence on the in-situ stress conditions of the fractured medium. The temperature change will cause volumetric changes of the medium and changes in the stress-strain relationship of this medium. Also, it is rather difficult to imagine how assumption of the "station-

ary" fluid can be valid for real circumstances. For the purposes of conceptual hydrologic considerations, however, both of these assumptions do not entail serious consequences.

The law of heat conduction for one dimension at steady-state can be expressed by the following equation:

$$q_h = -K_h \frac{\Delta t}{\Delta L}$$

where:

$q_h$  - heat flux;

$K_h$  - thermal conductivity of the medium; and

$\frac{\Delta t}{\Delta L}$  - thermal gradient.

The heat flow through the fractured medium, independently of the fluid flow, consists of three components, namely: a) the heat flow through the solid by conduction; b) the heat flow through pore space by conduction and radiation; and, c) the heat flow through fractures by conduction and radiation. The total flow can be expressed as the sum of these three components, so that:

$$q_h = q_1 + q_2 + q_3.$$

The bulk effective thermal conductivity of the fractured medium ( $K_{\text{heff}}$ ) can be regarded as related to three components which represent the thermal conductivity of the solid ( $K_{hs}$ ), of the pore space ( $K_{hp}$ ), and of the fracture space ( $K_{hf}$ ). It can be assumed that two of these components ( $K_{hs}$  and  $K_{hp}$ ) are independent of the in-situ stress and are therefore also independent of time, even for the dynamic stress field conditions. This assumption, however, cannot be justified for the component of thermal conductivity representing the fracture space ( $K_{hf}$ ). Adopting the analogy of the fluid flow, this component may be regarded as related to the fracture conducting aperture ( $a_{\text{con}}$ ), Section 3.2.3.

By performing analyses similar to those in Section 3.2.3., it can be shown that  $K_{hf}$ , and with it the bulk effective thermal conductivity of the fractured medium ( $K_{\text{heff}}$ ), is stress dependent. In the case of involvement of the dynamic stress field, this stress dependence causes the time dependence of the thermal conductivity of the medium in which this field operates.

Plate 3.4.2.-1 presents the relationship between the conducting fracture aperture and the effective normal stress. This relationship was developed assuming that the shear stress along the fracture is equal to zero. Also shown is the resulting time dependence of the thermal conductivity and the time dependence

of the depth above which the thermal conductivity is related to time. These relationships were developed assuming that: a) there is a limit for the normal fracture dilation; and b) the reduction in the value of the initial confining stress ( $\sigma_{in}$ ) is continuous and is caused by changes in the magnitude of principal stresses. At a time when  $\sigma_{nfeff}$  is reduced to a point where it is equal to the closure pressure ( $\sigma_c$ ), the thermal conductivity begins to show the time dependence. The time dependence of the depth, above which the stress and time dependent changes in the thermal conductivity occur, is caused by the increasing value of the initial confining stress with depth. Assuming that the rate of decay in  $\sigma_{nfeff}$  is constant, more time is required to attain the sufficient reduction of the confining stress at a greater depth.

Plate 3.4.2-2 presents the relationship between the shear dilation component ( $a_d$ ) of the conducting fracture aperture and the shear stress. If, at a given depth, the shear stress reaches the critical value ( $\tau_{max}$ ) then  $a_d$  becomes the shear displacement or the shear stress dependent.

Plate 3.4.2-2 shows the relationship between the conducting fracture aperture and time, assuming that the shear stress ( $\tau_s$ ) increases incrementally with time. The resulting time-dependence of the thermal conductivity and of the depth above which this occurs are also shown.

Plate 3.4.2-3 presents a conceptual model of the heat flow field developed in the deforming fractured medium. In this model, both vertical boundaries are assumed to be adiabatic. However, both horizontal boundaries are considered as heat conducting. The upper horizontal boundary ( $Z_0$ ) is isothermal, whereas the lower horizontal boundary ( $Z_1$ ) contains a distributed heat source. Intensity of this source is given by the term  $Rhz_{1(z)}$ , and is considered to be independent of time. The deforming fractured medium contains only "stationary" fluids, therefore, the heat flow mechanism is conduction and radiation.

An important feature of the model is the time and space dependent depth  $Z(x;t)$ . The time dependence of the depth  $Z(x;t)$  is a consequence of the involvement of the deforming fractured medium in the heat flow process. Below this depth, thermal properties of the fractured medium, i.e., the thermal conductivity ( $K_{heff}$ ) and the diffusivity ( $D$ ), are independent of the temperature and of the stress conditions. Hence, the heat flow is at steady-state and can be described by the Poisson's equation.

Above the depth  $Z(x;t)$ , however, the thermal properties of the fractured medium are dependent on the in-situ stress conditions. Hence, because of the involvement of the deforming fractured medium, the thermal properties must also be time dependent. The flow process, therefore, must be represented through the equation for transient or non-equilibrium flow.

If it is assumed that the intensity of the distributed heat source remains constant through time, i.e.,  $Rhz_{1(z,t)} = \text{const.}$ , the law of conservation of energy requires that the sum of the thermal energy contained in the system and the thermal energy lost from this system is constant through time. The thermal energy lost from the system is represented by the heat flux through the upper horizontal boundary.

The above observation, together with the conceptual model, can be used to deduce the main characteristics of the heat flow field developed in the deforming fractured medium. These characteristics are shown on Plate 3.4.2.-4.

The first characteristic is that the heat flow field contains the gradients of temperature developed in two or three dimensions. Inhomogeneities in the in-situ stress field cause the development of corresponding inhomogeneities in the distribution of the thermal properties of the deforming medium. These inhomogeneities display themselves as the temperature gradients.

The second characteristic is the time dependence of the thermal gradients. Near the ground surface, as the deformation process progresses, the bulk thermal conductivity of the fractured medium increases gradually. This causes the total heat flux through the upper boundary of the system to increase. The thermal energy balance, however, is maintained by reducing the amount of thermal energy stored in the fractured medium. As shown on Plate 3.4.2.-4, this reduction displays itself as: a) the time-dependent decrease in the geothermal gradient; and b) the time and space dependent downward migration of the isothermal lines.

It is interesting to note that it is rather difficult to obtain an accurate measurement of the intensity of heat flow based on measurements of the vertical temperature gradients in boreholes which are too shallow to penetrate the entire thickness of the deforming fractured medium. Putting aside hydrologic problems and problems caused by the horizontal temperature gradients, translation of the measured geothermal gradients into the intensities of heat flow requires a knowledge of the thermal conductivity.

Measurements of the thermal conductivity are, routinely, made on core samples or drill cuttings using either the Birch-type divided-bar apparatus or the needle probe technique, Sass et al., 1971. Because of the small size of the samples involved in these measurements, it is unlikely that, if the deforming fractured medium is involved, a true in-situ value of the thermal conductivity is obtained. In this case, the actual in-situ value of the thermal conductivity may be greater than the laboratory derived value and, consequently, the actual in-situ heat flow may be underestimated.

### 3.4.3. Coupled Fluid and Heat Flow Field Developed in the Deforming Fractured Medium.

Plate 3.4.3.-1 presents a conceptual model of the two phase flow field developed in the deforming fractured medium. In this model, both vertical boundaries are assumed to be adiabatic with respect to heat transfer, and "no flow" or "constant head" boundaries with respect to the transfer of fluid. The hydraulic pressures acting at these boundaries differ by a constant amount, which is represented by the term  $CX$ .

Both horizontal boundaries are considered to be the fluid and the heat conducting boundaries. The upper boundary ( $Z_0$ ) is isothermal and isobaric. The lower horizontal boundary ( $Z_1$ ) contains a distributed heat source, which is represented by the term  $Rhz_{1(z)}$ , and a distributed fluid source which is represented by the term  $Rfz_{1(z)}$ . The intensities of both sources are space dependent, but they are constant

with time. The mechanism of flow is coupled heat and fluid flow. The heat flow involves, both, convection and conduction while the fluid flow occurs through fractures.

The flow field is developed in the deforming and "strongly" fractured medium. The deformation of this medium occurs as repeated cycles of the tectonic deformation as discussed in Section 3.2.3. The deformational system contains the time and space dependent depth  $Z(x;t)$ . As was explained in Section 3.2.4., it represents a depth above which either the shear stress ( $\tau_f$ ) is equal to the critical value ( $\tau_{max}$ ) or the effective normal stress ( $\sigma_{neff}$ ) is equal to the closing pressure ( $\sigma_c$ ). Below this depth, both  $\sigma_{neff}$  and  $\tau_f$  are, respectively, either greater or smaller than  $\sigma_c$  and  $\tau_{max}$ . As the result of these stress conditions, above the depth  $Z(x;t)$ , the thermal and hydraulic conductivities ( $K_A$  and  $K_f$ ), and with them the fluid storetivity (S) and the heat diffusivity (D), are stress dependent and, therefore, time dependent. Below the depth  $Z(x;t)$ , however, all of these properties are independent of stress and time.

Plate 3.4.3.-2 presents a conceptual model of flow in the vadose zone of the two phase flow field, operating in the deforming fractured medium. In this model, both vertical boundaries are assumed to be adiabatic and "no-flow" boundaries. This assumption is not a true representation of the actual situation. However, if the distance  $X_2$  is very large relative to the depth  $Z_{wT}$ , this simplifying assumption does not entail a serious conceptual consequence. This is not so, however, if the conceptual model is intended to represent a narrow portion of the vadose zone. In this case, both vertical boundaries should be considered as the "flow" boundaries with respect to heat, fluid, and gas. Furthermore, the fluxes of heat, fluid, and gas through the vertical boundaries vary in time and space.

The flow system contains the time and space dependent depth  $Z(x;t)$ . Between points  $x_0$  and  $x_1$  this depth is assumed to be greater than the depth to the water table ( $Z_{wT}$ ). Between points  $x_1$  and  $x_2$ , however, the depth  $Z(x;t)$  is assumed to be situated above the water table.

Both horizontal boundaries are considered as the fluid and heat conducting boundaries. The upper boundary ( $Z_0$ ) is isothermal and isobaric. It contains a distributed fluid source,  $Rsf(x)$ , which represents the flux of rain water through the vadose zone. The lower boundary corresponds to the contemporary water table and is assumed to be located at the depth  $Z_{wT}(x)$ . This boundary contains a distributed heat source,  $Rhx_{wT}(x,t)$ , and a distributed fluid source-sink, which is represented by the term  $Rfx_{wT}(x,t)$ . Between points  $x_1$  and  $x_2$ , the thermal and hydraulic parameters are constant and, therefore, the intensities of the fluid sink and of the heat source vary from one point to another, but are independent of time. Between points  $x_0$  and  $x_1$ , however, the thermal and hydraulic properties are the in-situ stress dependent and, through it, they are also time dependent. Consequently, the intensities of both the heat source and the fluid sink-source are variable in time and space. These time and space dependencies represent the short term "excursions" as well as the long term restructuring of the flow field resulting from the restructuring of in-situ stress field, Section 3.2.5.

In the vadose zone, the flow of heat occurs through convection and conduction, and the flow of fluid

and gas involves the mechanism of fracture flow. The movement of fluid and gas is very complex, and is the result of interaction between three flow motivating factors, namely: a) gravity; b) heat flow; and, c) transient gradients of the gas or fluid pore pressure. These transient gradients are caused by the random flux of fluids through the lower horizontal boundary. The fluids residing in the vadose zone are the result of mixing of the infiltrating rain water with water from below the water table.

During the first phase of the tectonic cycle, when the strain energy contained by the fractured medium is at its minimum level and the pseudo-homogeneous strain conditions prevail, the depth  $Z(x;t)$  is shallow and its two-dimensional configuration is relatively plain. Progress of the deformation process is marked by a downward migration of the depth  $Z(x;t)$ . With time, during the second phase of the tectonic cycle, its value and its two-dimensional configuration become greater and more complicated, reflecting the increasingly pronounced heterogeneous nature of the strain energy field. At the end of the tectonic cycle, when large quantities of the strain energy are converted into work associated with: a) vibratory ground motion; b) permanent dislocation; and c) dislocation related heating of the medium, the depth  $Z(x;t)$  begins to return to its former position at the start of the deformation cycle. This process repeats itself, over and over again, as long as the regional tectonic activity motivating the developments remains unchanged.

The two phase coupled flow field developed in the deforming fractured medium is a remarkable thermodynamic continuum. The most striking feature of this continuum is, perhaps, its evolving nature. It should be noted that the evolving nature of geologic systems, and its potential importance with regard to the utilization of these systems for the purposes of large scale disposal of nuclear waste was emphasized by some investigators, Harper and Szymanski, 1980; Szymanski and Harper, 1980; Harper and Szymanski, 1982; Donath, 1982.

The evolution of the geologic system consisting of the heat-fluid coupled flow field developed in the deforming fractured medium can be viewed as occurring via series of similar evolutionary loops, as shown on Plate 3.4.3.-3. During the progress of evolution, the form of the continuum becomes more and more advanced. The term "form of the continuum" as used here refers to the fractured medium as expressed at any given time by: a) the intensity of fracturing; b) the deformed state; c) the balance of energy; and d) alterations in the initial litho-stratigraphic framework (dikes and sills, veins, explosive breccias, hydrothermal and metasomatic mineralization and alteration, surface deposits, such as tuffa mounds etc). Throughout this evolution, the potential energy contained in the system includes three time and space dependent components. These components are: a) the strain energy represented through the gradients of normal and shear stresses; b) the thermal energy represented through the gradients of temperature; and c) the hydraulic energy represented through the gradients of the hydraulic potentials. For the remainder of these discussions, these components will be referred to as, respectively, component A, B, and C. The sum of these components will be called the "disposable energy of the system".

A single evolutionary loop, in terms of its duration and periodicity, corresponds to the tectonic cycle of deformation, as discussed in Section 3.2.2. and shown on Plate 3.2.2.-3. During this cycle, the dispos-

able energy of the system undergoes a remarkable transformation. At the onset of deformation, during the first phase, the contribution of the A component is relatively minor. The energy balance is dominated by the components B and C. During this time, the gradients of the hydraulic potential are "strong" as are the temperature gradients. The flow field displays a strong affiliation with the "free"- "mixed" convection flow system. As the deformation process progresses, the contribution of the A component increases. At some stage of the deformation, this is associated with a progressive dilation of the fractured medium. This dilation causes an overall time and space dependent decrease in the values of the hydraulic and thermal properties of the medium. Gradually, as the stress gradients become "stronger", the gradients of hydraulic potential and temperature become "weaker". The flow system begins to lose its geothermal identity. At this time, it displays affiliation with the "mixed"- "forced" type of convection system, characteristics of which were described in Section 3.3.5. If the loss of geothermal identity is substantial the flow system will display itself, near the ground surface, as the single phase flow field developed in the deforming fractured medium. The main characteristics of this flow field were discussed in Section 3.2.4.

It is interesting to note that, while the dilation takes place, the bulk storativity of the fractured medium increases. Hence, the volume of water associated with the "weakening" of hydraulic potentials is accommodated, not only through the increased flow, but also through the increased storage. As the dilation progresses downward, the volume of this "extra" water in storage increases. This increase must be associated with the progressive transfer of a given volume of water from shallower and cooler levels to deeper and warmer levels. The transferred water must come into thermal equilibrium with the fractured medium. It can be expected, therefore, that some of the heat flowing through this medium will be used for this purpose. The deforming fractured medium, while it is being dilated, stores not only the fluid but also the thermal energy.

It is important to understand the sequence of events which takes place at the end of the tectonic cycle. To this end, it is assumed that the deforming fractured medium consists of a stack of parallel layers, with small thickness ( $\Delta z$ ), as shown on Plate 3.4.3-4. Each of these layers consists of a number of blocks of unit length (1). The blocks are separated from each other by a fracture. The mechanical properties of the medium are such that the stress vs. strain relationship involves the constant ( $E_1$ ) for blocks, and another constant ( $E_2$ ) for fractures. The initial confining stress for the entire stack consists of: a) the horizontal component of the lithostatic pressure (Poisson's effect); and b) a small compressive stress, representing the remnant tectonic stress from a previous cycle of deformation. At the onset of the current deformation, the stack was subjected to a uniform extension with a rate  $\dot{\epsilon}_{zz}$ . With time, as the deformation process progresses, the stack is transformed from the initial, undeformed, state to the deformed or dilated state, as shown on Plate 3.4.3-4. Above the depth  $Z(x;t)$ , the dilation is advanced and, therefore, the conducting fracture aperture includes more than the residual component. Below this depth, change in length of individual layers is smaller and represents the elastic response of these layers to reductions in the confining stress.

It is reasonable to expect that the end of tectonic cycle, or the collapse of the focal inclusion, will be accompanied by a large scale transfer of fluids from deeper to shallower crustal levels. This transfer involves either the mechanism of seismic pumping (Sibson et al., 1975) or is related to fault disruptions of deep portions of the flow system where either "free" or "mixed" convection flow processes operate, Section 3.3.3. It is possible that both of these mechanisms may be involved.

Plate 3.4.3.-5 presents an idealization of the response of the dilated fractured medium to a sudden build-up of the pore pressure. Two cases are considered. The first case is a uniform rise in the pore pressure. The response of the fractured medium is a more or less uniform increase in the aperture of the fractures. This occurs because the increased value of the pore pressure causes "contraction" of individual blocks of the fractured medium. The deformational system, however, remains in the dilated state.

The second case involves a local build-up of the pore pressure occurring along a few widely spaced fractures. It is assumed that the amount of fluid involved is very large, and that the transfer of fluids occurs very fast. The dilated fractured medium responds to this build-up by developing a large scale separation between blocks. This separation involves fractures along which the build-up of pore pressure took place and occurs at the expense of other areas which are not involved in the pore pressure build-up. In these areas, the blocks are pushed together and the degree of dilation is reduced.

There are two factors which control the size of the block separation. The first factor is the total amount of "recoverable" extension contained between any two given fractures involved in the pore pressure build-up. For example, if these fractures are spaced  $10^4$  feet apart, and the "recoverable" extension was accumulating at a rate of  $10^{-7}$  per year for  $10^4$  years, then the potential separation is 10 feet for each of these fractures.

The second factor is the volume of fluid involved in the pore pressure build-up for each individual fracture. As the separation between blocks increases, the volume representing the space between these blocks increases exponentially. In order for the pore pressure build-up to be sustained, this exponentially increasing space must always be filled with fluid. It can be expected that, soon after the separation begins, the volume representing space between the separating blocks will match the volume of fluid involved in the transfer. At this time, further build-up of pore pressure is arrested.

It can also be expected that: a) the transfer of fluid from depth will involve fluids which are mineralized; and b) the transfer will be sustained through the convective heat-fluid flow process, after the block separation was arrested. Precipitation of minerals along the separated fractures will, undoubtedly, be associated with this circumstance. This process will cause a gradual decrease in aperture of the separations. It will also be responsible for their complete closure and for fusing back together the fractured medium. At this time, the strain energy of the system is discharged. The system is also fused together and ready to enter another evolutionary loop.

The accretionary aspects of the evolution of the geologic system, which contains the heat-fluid coupled flow field developed in the cyclically deforming fractured medium, are very important. These aspects can be used to reveal a true identity of this system, at a time when this identity is masked by the ongoing deformation.

## SECTION 4.0.

### CHARACTERISTICS OF THE DEATH VALLEY FLOW SYSTEM IN LIGHT OF THE EXISTING DATA.

#### 4.1. General Description of the Death Valley Groundwater System.

The Death Valley groundwater system is situated in southern Nevada adjacent to parts of southeastern California, as shown on Plate 4.1.-1. The system was distinguished somewhat arbitrarily from a much larger hydrologic entity which is the Alluvial Basins Groundwater Region as described by Heath, 1984. It is centered around the Nevada Test Site, areal extent of which takes up a significant portion of the groundwater system.

It became customary to consider the Death Valley groundwater system as composed of three sub-basins, Waddell, et.al., 1984. As shown on Plate 4.1.-2., these subbasins are: a) the Oasis Valley subbasin; b) the Alkali Flat - Furnace Creek Ranch subbasin; and, c) the Ash Meadows subbasin.

The climate of the region ranges from arid on the valley floors to subhumid on the crest of the highest mountains. Altitudes range from greater than 3600 m in the Spring Mountains to below sea level in Death Valley. Precipitation ranges from less than 50 mm/year in Death Valley to greater than 700 mm/year in the Spring Mountain area. The mean daily maximum temperature, at altitude of approximately 700 m, ranges from 13°C in January to 40.5°C in July; the mean daily minimum temperature for the same months ranges from 0.5°C to 24.5°C; temperatures at greater altitudes are as much as 3°C to 10°C lower. In Death Valley temperatures greater than 49°C are common during the summer months.

Plate 4.1.-3 shows the distribution of the average annual precipitation and the location of recharge and discharge areas. The recharge areas were identified assuming that the empirical relationship between precipitation and recharge as developed by Eakin, et.al., 1963 and Eakin, 1963, is valid for this region. This relationship suggests that no recharge occurs where mean annual precipitation is less than 200 mm. The groundwater discharge occurs as spring flow, seeps, evapotranspiration, groundwater withdrawal, and outflow to other groundwater basins.

In the Death Valley groundwater system, the water conducting medium is composed of two units which involve sharply different hydraulic properties and water flow mechanisms. The first unit is the so-called "valley fill aquifer" which is composed of various detrital sediments of Late Tertiary and Quaternary age. These alluvial-fan, fluvial, fanglomerate, lakebed, and mud-flow sediments are only locally cemented and, consequently, exhibit large interstitial porosity. The groundwater flow mechanism, therefore, involves predominantly porous flow through the material matrix. The thickness and stratigraphic interrelationships of these deposits are highly variable. Thicknesses of more than 500 m occur in some areas, nevertheless, areas where the alluvium is saturated are limited and, consequently, this hydrogeologic unit is of minor

importance in controlling the groundwater flow process. The exception is beneath most of the discharge areas, where the valley fill is present in saturated thicknesses sufficient to constitute an important aquifer.

The second unit comprises the bulk of the water conducting medium of the Death Valley groundwater system. This unit consists of a great variety of sedimentary rocks; which are well indurated, slightly metamorphosed, and include limestones or marbles, quartzites, and various argillites; and of volcanic rocks, which include various pyroclastic deposits, intrusives and extrusives. The age of these rocks ranges from Precambrian-Early Cambrian, through Devonian, Carboniferous and Permian, to Tertiary. The lithologic character of these rocks is such that, by and large, the interstitial porosity is quite small and, therefore, the groundwater movement involves the mechanism of fracture flow. Locally, however, the interstitial porosity may be considerable as, for example, in the case of non-welded tuffs, fluviually reworked tuffs and tuffaceous sandstones. Hence, locally the flow mechanism may involve porous flow through the medium matrix.

The thickness of this unit is variable but involves many thousands of meters. Small portions of the total thickness, say 10 % or 20 %, are made up of rocks whose interstitial porosity is sufficient to support significant matrix flow.

It can be expected that, from a rheologic point of view and for time scales of geologic proportions, a majority of rocks comprising the water conducting medium can be represented as the Bingham substance or the B-K hybrid substance (the Bingham element in series with the Kelvin element), Price, 1966; and Ramsay, 1967. The unwelded tuffs and unaltered shales, however, may exhibit stress-strain characteristics related more to the general linear substance, rheologic representation of which involves the Maxwell element in parallel with the Hook element.

In the Death Valley groundwater basin, the spatial relationship between the various lithic types composing the water conducting medium is very complex. These relationships are the result of a very complex evolution of this medium which, during its various stages, included: sedimentary, metamorphic, volcanic, structural, and hydrothermal alteration processes. The resulting degree of litho-stratigraphic complexity is such that a three-dimensional distribution of hydraulic properties can only be known on a general and conceptual basis, regardless of the degree of subsurface exploration effort. In light of this complexity it appears that a further division of this hydrogeologic unit, as performed by some authors, is of limited practical value. This subdivision cannot be introduced into numerical modeling efforts and expressed as the three-dimensional distribution of material properties with any degree of specificity.

Notwithstanding the large degree of complexity involved, there is a very substantial data base pertaining to the Death Valley groundwater system. This data base has been developed as the result of a very substantial commitment of resources made by the U.S. Government in association with activities involving detonations of nuclear devices as well as involving the nuclear waste repository siting and evaluation process. The dollar value of this data base may be expressed in terms of billions of dollars. It should

not be a surprise, therefore, that this data base contains a lot of information which, on Plate 2.3.-2 are labeled as the "Characteristics of the Flow Field". In Section 2.3., these characteristics were judged to be necessary in order to establish a validated conceptual model of the ground water flow field. It can be recalled that the process of developing this conceptual model, for purposes of evaluating the effectiveness of the nuclear waste disposal system, was characterized as the "conscious sorting out the conceptual alternatives using the actual field data".

The following pages are devoted to this sorting out of the available conceptual alternatives. The process involves two dimensions. These are: a) the actual field data from the Nevada Test Site and its surroundings; and b) the conceptual framework as established in Section 3.0, keeping in mind the specific volcano-tectonic character of the area

The most important data, with respect to the conceptual considerations of the flow field, are, undoubtedly, the data which relate values of the hydraulic potentials in the field to time. It is understood that these data were collected during a nearly 10 year long process of evaluating the suitability of the Yucca Mountain site to accommodate the nuclear waste repository. Continuous and periodic monitoring was performed in a number of deep wells which were drilled in an area of approximately 25km<sup>2</sup>. The data, however, are not yet available in an accessible and reliable form. Therefore, the conceptual considerations undertaken herein cannot yet be carried out to their logical and completely reliable conclusion.

#### 4.2. The Vadose Zone of the Death Valley Groundwater System.

An extraordinary feature of the Death Valley groundwater system is its vadose zone. The thickness of this zone ranges from few meters, at and near the discharge areas of the system, to as much as 600 m in the central and north-eastern parts of the system.

Within the vadose zone, the water content, expressed as a percentage of the interstitial space, is highly variable. It ranges from 65 % to 75 % ( $\pm 15$  %). In local areas, however, the degree of saturation is high and may reach a state of "complete" saturation. In this situation "perched water" exists.

At the Nevada Test Site, the perched waters were encountered in many exploratory boreholes, Thordarson, 1965; Winograd and Thordarson, 1975. These waters were also encountered in some of the underground workings located in Rainier Mesa in northwestern Yucca Flat and in the Climax granitic stock of north-central Yucca Flat. The perched waters feed several springs which, at the Nevada Test Site, yield small quantities of water (less than 5 gpm). Examples of such springs are: Cane Spring; Topopah Spring; Tippipah Spring; and the Pavits Spring, Thordarson and Robinson, 1971; Schoff and Moore, 1968.

In the vadose zone, the spatial distribution of water content can be viewed as resulting from a random mixing of two basic patterns of distribution. The first pattern is a systematic change in moisture content as a function of time and depth, Ross, 1984. Near the ground surface, the water content (and consequently the suction potential) fluctuates with precipitation events and with season. At depth, however, these fluctuations damp out, and there is a constant downward flux of water under unit head gradient. The suction potential and the effective hydraulic conductivity are constant. Near the water table, saturation is high, suction potential has a small negative value, and relative permeability is substantial.

The second pattern is the random occurrence of perched waters. These waters indicate local addition and/or retention of water which may be related to many factors, some of which are: a) local lithologic composition of the medium; b) local precipitation; and, c) injection from below the water table.

In general, occurrences of the perched water present an interesting conceptual dilemma. There are two very important conceptual alternatives which come into play.

The first alternative is that the perched waters represent recent meteoric waters caught during their downward passage (infiltration) through the vadose zone by rocks whose hydraulic conductivity is very low. Most, if not all, of the researchers who concerned themselves with the Death Valley groundwater system, regarded this alternative as an adequate explanation of the origin of all perched waters occurring in this system. In this case, the perched waters should not exhibit hydraulic, thermal and chemical affiliation with waters occurring below the water table.

The second alternative is that, at least, some of the perched waters are the result of the "special relationship between the zone of saturation and the vadose zone", as discussed in Section 3.3.3. For the

"mixed" convection flow system, i.e., for the system whose horizontal boundary is both heat and fluid flow boundary, this relationship requires that both of these zones supply water to each other. It appears, therefore, that within the conceptual framework, as established in Section 3.0, some of the perched waters may be suspected to be expressions of the hydraulic mounds. These mounds would occur in areas where the in-situ stress conditions are such that a true value of hydraulic potentials can display itself in the near ground surface conditions. These potentials may or may not be related to the coupled fluid-heat flow process. In this case, the perched waters, although diluted by the fresh infiltrating water, should exhibit either hydraulic or thermal and chemical affiliation with waters occurring below the water table.

It is obvious that the selection of a correct conceptual alternative, with respect to the origin of perched waters, entail very profound implications as far as the conceptual model of the flow field is concerned. Consequently, this selection should be performed with due caution and should consider: a) the chemistry of water; b) the water temperature; c) yield or volume; and, d) the value of hydraulic potentials and their time and space dependence.

For the purpose of these considerations three areas, where occurrences of the perched water are known, were selected for further examination. These areas are: a) around the town of Beatty, Nevada; b) between Jackass Flat and Frenchman Flat, at the Nevada Test Site; and c) around Pahute and Rainier Mesas, also at the Nevada Test Site. These areas were selected because they occur in close proximity to locations of very pronounced and local low-seismic velocity anomalies, as shown on Plate 3.3.1.-1.

Plate 4.2-1 shows the hydrologic situation present in the vicinity of Beatty, Nevada. The direction of groundwater flow is from north toward south. Approximately 5 miles and 10 miles north from Beatty, (up the regional hydraulic gradient), the water table is situated at altitudes 3800 feet and 4000 feet above mean sea level, respectively. Around the town of Beatty there is a cluster of springs whose orifices are situated at altitudes 4000 feet and higher. The results of chemical analyses and of temperature measurements performed on waters discharging from these springs are presented on Plate 4.2.-2. Clearly, a deep rooted hydraulic mound, some 200 feet or 300 feet high, is present.

The mound aspects of this feature (hydraulic potentials are 200 feet or 300 feet higher than the hydraulic potentials upstream) indicate, in no uncertain terms, that more than just a simple "forced" convection flow process is involved. In order to account for this feature, either the "mixed" convection flow process, or a local in-situ stress inhomogeneity, or both of these possibilities must be assumed.

Plate 4.2-3 presents the hydrologic conditions around Skull Mountain, which is located at the Nevada Test Site between Frenchman Flat and Jackass Flat. These conditions are known based on extensive subsurface exploration. Two small springs are found in the area, namely: Cane Spring and Pavits Spring.

In the Skull Mountain area, altitudes of the regional water table range from 2410 feet to 2386 feet above mean sea level. A sharp increase in the altitude of the water table occurs west of the Mercury Highway. This increase was observed in two wells. The first well, well #73-68, was drilled to a depth of 1504

feet. Drillers first reported water at a depth of approximately 660 feet. Several days after completion of the drilling process, however, the water level stood 518 feet below land surface, which corresponds to the altitude of about 2982 feet above mean sea level. This altitude is more than 500 feet higher than the regional water table in the neighboring Frenchman Flat. A similar, sharp increase in the altitude of the water table was observed in well #77-68. At this site, the water table was encountered at altitude of approximately 2784 feet.

Further west of the Mercury Highway and west of wells #77-68 and #73-68, perched waters were encountered in three wells, namely: well #73-66 (altitudes 4066 feet and 3612 feet), well #75-66a (altitude 3924 feet), and well #75-66 (altitude 4042 feet). These perched waters occur as much as 1200 feet and 1600 feet above the "regional" water table in Frenchman Flat.

The increase in the values of hydraulic potentials with depth, as noted during drilling of well #73-68 (from altitude 2830 to altitude 2982) and, what seems to be a progressive increase in the altitude of the water table in wells #77-68 and #73-68, suggest an interesting possibility. This possibility is that the perched waters (wells #73-66, #73-66a and #75-66; and waters discharging from Cane Spring and Pavits Spring) are hydraulically connected with the underlying aquifer and are related to a deep rooted hydraulic mound. This possibility is further strengthened by the results of chemical analyses of water obtained from three depth intervals in the test well #73-66, which are shown on Plate 4.2-4. The high total dissolved solids (sulfate, chloride, sodium, and silica) content suggests that these may not be ordinary waters infiltrating down through the vadose zone. This possibility is further strengthened by the temperatures encountered, below the water table, in well #73-66. As shown on Plate 4.2-4 this temperature is 64.5°C. The spatial relationship of the occurrence of this inferred hydraulic mound to the location of the low-seismic velocity anomaly, shown on Plate 3.3.1.-1, suggests that the involvement of tectonic factors, in the hydrologic situation at Skull Mountain, should be seriously considered.

Plate 4.2-5 shows the location of Rainier Mesa relative to the boundaries of the Nevada Test Site. Plate 4.2-6 shows local hydrologic conditions at this location. These conditions are known based on extensive exploration with boreholes, and based on direct observations in a system of underground workings excavated in association with activities related to nuclear detonations.

The top of the zone of saturation has been determined based on numerous test holes drilled into the Rainier Mesa. The altitude of the water table varies up to 100 m. The mean altitude of the water table was approximately 1820 m above the mean sea level, Thordarson, 1965. The movement of water is downward from the recharge area at the top of the mesa, through the fractures of the Rainier Mesa Member, and then through the underlying Paintbrush Tuff. The groundwater travel time through the mesa is small, not greater than few years, Russell, 1987. However, upon reaching less permeable zeolitic tuffs, the groundwater forms a series of lenses which slowly drain through the fracture system of the formation, or into the tunnel system.

The perched waters are found primarily within the fractures. The majority of these water bearing fractures are normal faults characterized by small displacements, seldom exceeding several centimeters of net slip. A fracture analysis performed by Thordarson (1965) revealed that 50 to 60 percents of all normal faults yielded water, while only 2 percent of induration joints, cooling joints, and other types of fractures were water bearing. Some fractures drain and are dry within a few weeks after mining. Others, which may be relatively close by, have acted as continuous seeps since the initial excavation, albeit at much lower discharge rates than initially recorded, Thordarson, 1965.

Plate 4.2.-7 presents the results of chemical analyses performed on 24 samples of the perched water encountered in the underground workings beneath Rainier Mesa. Of interest is a relatively high content of total dissolved solids and sulfate. This becomes more intriguing if one recognizes three important facts. These facts are: a) the residence time of groundwater percolating through Rainier Mesa is very small; b) even small quantities of sulfate minerals and their weathering products have never been reported within the rocks of Rainier Mesa; and c) a study of the effects of nearby nuclear detonations, performed by Russell (1987) and described in Section 4.7.3, revealed that after detonations there are large increases in the sulfate content of the perched waters. There are only few possibilities which can explain the elevated sulfate concentrations. One possibility is that drilling activities, performed within the mesa, have contaminated the interstitial waters. Taking into account low interstitial conductivity of rocks involved, this possibility does not appear to be an attractive one. This low conductivity would inhibit the widespread dissemination of a contaminant through the matrix. Another possibility, which has been proposed by White, et.al., (1978), is that the elevated sulfate concentrations indicate the presence of relict waters. These high in sulfate waters would remain from the time of deposition of the rocks forming Rainier Mesa. This possibility does not seem to be a plausible one, because it is hard to imagine that movement of water through the vadose zone during the last  $10^7$  years did not involve matrix flow.

The third possibility, which is proposed here, is that the elevated sulfate concentrations of the interstitial and of the perched waters in fractures indicate the presence of a relict hydraulic mound. The formation of this mound would have to be related to a tectonic event which would involve local alteration of the in-situ stress field allowing for the full display of hydraulic potentials in the "mixed" convection flow field. This mound would be similar, but older, to the mound present in Beatty and one inferred to be present at Skull Mountain.

In summary, it appears that the body of evidence pertaining to some of the perched waters developed in the vadose zone of the Death Valley groundwater system permits, at least, a suspicion that these waters may be related to tectonic processes. This would be consistent with the conceptual framework, as established in Section 3.0, for the two phase coupled flow field operating in the deforming fractured medium. Should this suspicion become a reality, in light of further considerations and further in-situ experiments, the resulting implications are of very significant proportions. The following two conclusions would be warranted:

- a) The Death Valley ground water system is a system for which the position and configuration of the water table is not an expression of the durable characteristics of the flow field. Both of these parameters are a matter of tectonic consensus and, therefore, subject to a random change; and
- b) The magnitudes of potential rises of the water table, caused by tectonic processes, are very substantial and may be long lasting.

#### 4.3. Configuration of the Water Table.

The configuration of the water table is a very special characteristic of a flow field. This configuration expresses two important factors which control the flow process in this field. These factors are: a) the boundary conditions; and b) the three dimensional distribution of the hydraulic properties of the water conducting medium. In Section 3.0 it has been shown that, in the tectonic environment of the Death Valley flow system, both of these factors may be controlled by the tectonic processes. It becomes important, therefore, to evaluate whether or not the configuration of the water table in this system contains any expression that this indeed may be the case.

It can be recalled that, in Section 3.2.4. and Section 3.3.3., the configuration of the water table in a tectonically controlled flow field was described as being the result of very complex interactions involving various parts of this field. These interactions are caused by the time and space dependence of the hydraulic parameters of the medium and involve spatially variable vertical and horizontal gradients of hydraulic potentials and temperature. The resulting configuration of the water table was envisaged as including: a) hydraulic mounds; b) hydraulic sinks; c) areas where local slopes of the water table are steep; and d) areas where local flattening of the gradients of hydraulic potentials and of the water table occur.

Before analysis of the configuration of the water table are presented, it is important to define the meaning of the term "water table" on the flow system specific basis. To this end it is worthwhile to examine Plate 4.3.-1. This plate presents data pertaining to the degree of matrix saturation of the fractured medium encountered in two boreholes drilled at the Nevada Test Site, namely; USW H-1 and UE-25b#1. Core samples of rocks, from both the vadose zone and below the water table, were analyzed in the laboratory and were reported by Rush, et.al., 1983 and Lobmeyer, et.al., 1983. The results indicate that the degree of saturation, above and below the water table, does not differ by much. Below the water table, the degree of matrix saturation ranges from 70 % to 92 % - 95 %. Somewhat similar numbers were obtained from rock samples collected 100 m and 300 m above the water table.

Based on these results, the water table seems to be a plane below which most fractures contain water, but the rock matrix is not fully saturated. Above this plane, however, either none or only some fractures contain water. Nevertheless, the degree of matrix saturation is relatively high.

Plate 4.3.-2 presents the position and configuration of the water table for the Death Valley flow system. This position and configuration is known based on numerous deep wells and boreholes drilled for either the water supply or the subsurface exploration purposes. The altitude of the water table ranges from over 1900 m above sea level in the northern parts of the system, to below sea level in Death Valley.

In the Death Valley flow system the configuration of the water table is remarkable. The basic pattern displayed by this configuration consists of a few groundwater "plateaus" separated by sharp steps. Within an individual "plateau", the altitude of the water table varies little, the horizontal gradients of

hydraulic potentials seem to be quite small, measured in meters per mile or less. Between the plateaus, however, slopes of the water table as large as 10 % and 20 % are present. Changes in the altitude of the water table measured in tens to hundreds of meters occur within relatively short distances. These high hydraulic gradients occur in the recharge areas of the flow system (Plate 4.3.-3) as well as in the areas of discharge (Plate 4.3.-4). They are also present in the central portions of the flow system, between the discharge and the recharge areas. One such a notable feature extends from Beatty, Nevada, through northern Yucca Mountain, toward Yucca Flat and beyond. This feature is developed across various geohydrologic and physiographic units and across various structures. Plate 4.3.-5 and Plate 4.3.-6 show this feature in great detail for northern Yucca Mountain and eastern Yucca Flat.

It is interesting to take a look at the configuration of the water table in an area where water wells and exploratory borings are closely spaced. This spacing allows for a greater resolution in defining the configuration of water table. In Yucca Flat, numerous exploratory borings were drilled in association with activities related to the nuclear detonations testing program. Plate 4.3.-7 presents the approximate altitude of the water table beneath Yucca Flat. Along the trace of the Yucca Fault, two notable features are present. One is a hydraulic mound, some 125 feet high. The other feature is a hydraulic sink, some 25 - 50 feet deep.

In summary, this brief review of information concerning the configuration of the water table in the Death Valley flow system reveals that features expected to be present in a tectonically controlled flow field are also present in this system. Configuration of the water table includes: a) steep slopes, b) hydraulic "plateaus" where the horizontal gradients of hydraulic potentials are small; c) hydraulic mounds; and d) hydraulic sinks.

The configuration of water table, in and by itself, is not a characteristic of the flow system which allows for conclusive resolution of the question of the involvement of the tectonic factors in controlling the flow process. In the absence of other data, there are few conceptual alternatives which may, more or less completely, account for the observed configurations. The basic pattern of the configuration of the water table, which consists of the plateau-step-plateau sequence, may be accounted for by assuming that narrow groundwater barriers are locally present in the medium whose hydraulic conductivity is large otherwise. These barriers would constitute permanent and durable features of the flow system. Their origin would be, only, indirectly related to the tectonic processes. The presence of hydraulic mounds and sinks may be accounted for by assuming that man actions are involved in their formation. Examples of such actions are fluid withdrawal and fluid injection.

#### 4.4. Vertical Gradients of Hydraulic Potentials.

An important characteristic of a flow field, one which is far too often ignored, is the distribution of vertical gradients of hydraulic potentials acting in this field. The presence or absence of these gradients determines how well the actual equipotential surfaces are represented by the water table. If there are significant vertical components of the groundwater flow, the water table constitutes a very poor representation of the actual three-dimensional distribution of the hydraulic potentials. Calculations and interpretations performed based on this representation can be grossly misleading.

In terms of their origin, the vertical gradients of hydraulic potentials may be related to many factors, which either control or influence the flow process. For the purpose of these conceptual considerations, however, it is useful to recognize two broad conceptual alternatives. The first alternative is that the vertical components of flow constitute a characteristic of the flow field which is independent of tectonic factors and which, therefore, is independent of time. In this case, the vertical components are the result of: a) a local, lithology related, inhomogeneity in the three-dimensional distribution of hydraulic parameters; or b) the position of a given area in the flow system; for the "simple" flow field the vertical components occur in both the recharge (downward) and the discharge (upward) areas.

The second alternative is that the vertical gradients of the hydraulic potentials are related to tectonic processes and may, therefore, be time dependent. For the "mixed" convection flow system, for example, the vertical gradients are related to the "heat and fluid" flow boundary conditions present at the base of the flow system, Section 3.3.3. In areas underlain by the hydraulic and heat sources, the upward directed components of flow must be present. The downward components of flow, however, will be present in areas which are situated over the potentiometric and heat sinks.

For a flow field operating in the deforming fractured medium, the apparent vertical gradients are related to the deformation process of this medium, as discussed in Section 3.2.4. In the case of an advanced stage of deformation, the characteristic distribution of hydraulic potentials or pore pressure with depth includes the "overpressure"  $\Delta p(z)$ , as shown on Plate 3.2.4.-4. This distribution requires that there is an upward, vertical component of flow.

At the onset of a new tectonic cycle, however, the distribution of hydraulic potentials with depth is different. This distribution is shown on Plate 3.2.4.-5. It involves the "underpressure" gradually decaying with time. The value of this "underpressure" reaches its maximum at some depth and becomes smaller with the decreasing depth. This distribution causes, at a time when a new deformation cycle begins, a downward vertical component of flow.

With the above introduction, it seems appropriate to examine the data base in order to establish whether or not the vertical components of flow, occurring in the Death Valley flow system, show any signs of being associated with tectonic processes. To this end three areas, located within the Nevada Test Site,

were selected for closer examination. These areas are: a) the area around Pahute Mesa; b) the area of Yucca Flat; and c) the area corresponding to the proposed repository site at Yucca Mountain.

In the area of Pahute Mesa, the vertical gradients of hydraulic potentials are known based on measurements of pore pressure with depth. These measurements were performed in 16 deep wells. Discreet intervals were isolated with packers from the remainder of the borehole. The results of these measurements were reported by Blankenagel and Weir, 1973. They are presented on Plate 4.4.-1 and Plate 4.4.-2.

Plate 4.4.-3, shows an idealized overall distribution of the hydraulic potentials with depth in the area of Pahute Mesa. Within the first 2500 feet of the "saturated" zone, the hydraulic potential are independent of depth and their value is constant. The pore pressure increases linearly with depth, in accord with the increasing weight of water. Below a depth of approximately 2500 feet from the water table, the distribution of hydraulic potentials changes. As shown on Plate 4.4.-1 and Plate 4.4.-3, the boreholes situated in the western portion of Pahute Mesa revealed that the hydraulic potentials increase with depth. In these boreholes, therefore, there is an upward, vertical component of flow. The boreholes drilled in the eastern portion of Pahute Mesa, however, revealed that the value of the hydraulic potentials decreases with depth, indicating that there is a downward, vertical component of flow.

Examination of Plate 4.4.-2 reveals an interesting and very important characteristic of the flow field. In boreholes for which values of the hydraulic potentials decrease with depth, the water level as measured in an open hole reflects the underlying "underpressure". Evidently, the boreholes act as conduits through which water contained in the shallow intervals, drains into the deeper intervals where lower values of the hydraulic potentials exist. However, in boreholes for which the value of the hydraulic potentials increases with depth, the water level, as measured in an open hole, does not show at all the high pressures occurring at depth, Plate 4.4.-3. Evidently water enters the borehole at a depth where higher pressures exist, rises upward toward interval of lower pressure where it must enter the formation without noticeably raising the fluid level in the borehole. This seems to be a very curious circumstance indeed. There is only one logical explanation for it. The height of water column in the borehole must be controlled by the in-situ stress present in the fractured medium. Either the effective normal stress ( $\sigma_{nfeff}$ ) is equal to the closure pressure ( $\sigma_c$ ) or the shear stress ( $\tau_f$ ) is equal to the value of  $\tau_{max}$ , as discussed in Section 3.2.3. The system seems to be quite delicately balanced. A small rise in the value of pore pressure causes dilation of some fractures and, through it, causes increases in their hydraulic conductivity. These fractures can now accommodate additional volumes of water. It becomes clear that either the deformed or the deforming fractured medium is involved. This involvement occurs down to a depth of approximately 2500 feet below the water table.

The special distribution of hydraulic potentials at depths greater than 2500 feet below the water table, may be explained by assuming that, at Pahute Mesa, the "heat-fluid flow" boundary conditions are present at the base of the flow system. Either a potentiometric and heat sink is present in the eastern part of Pahute Mesa, or the entire area contains a weak hydrothermal convection cell. This cell would be expressed, at the base of the flow system, as the heat and fluid source in line with the heat and fluid sink.

Three lines of evidence support this conclusion. First, as shown on Plate 3.3.1.-1, Pahute Mesa is underlain by a pronounced and local low-seismic velocity anomaly. In this setting presence of the hydrothermal convection cell should not be surprising. Second, measurements of the in-situ temperature with depth, performed in the area of Pahute Mesa, revealed presence of substantial horizontal and vertical gradients of the in-situ temperature, Plate 4.4.-6. Between well PM-2 and well UE-20f, the horizontal temperature gradient, at depth of approximately 700 m, is equal to about 30°C/5 miles. Also, in wells UE-20f and UE-19gs, there seems to be an increase in the value of geothermal gradients, very similar to the increase postulated in Section 3.4.2. Third, chemical analysis of water samples obtained from deep wells in Pahute Mesa revealed presence of noticeable horizontal gradients involving the chemical composition of groundwater, Plate 4.4.-6 and Plate 4.4.-5. The content of sulfate and chloride is noticeably increased where the upward vertical components of flow were observed.

The vertical gradients of hydraulic potentials are also known from the area of Yucca Flat. These gradients are known based on observations of the position of water table made during drilling of a number of exploratory boreholes. It appears that systematic measurements of the hydraulic potentials as a function of depth were not performed.

Plate 4.4.-7 presents a general hydrogeologic situation in the vicinity of Yucca Flat. The characteristic feature of this area is a difference between the value of hydraulic potentials in the Tertiary volcanic rocks and the value of these potentials in older, mainly, sedimentary rocks of Paleozoic age. From one place to another, this difference ranges from considerable to small. There is, however, a consistent pattern. The values of hydraulic potentials decrease with depth indicating that there is a downward, vertical component of flow. Observations made during drilling of two holes, well #88-66 and well #83-69a penetrating the Tertiary volcanic rocks, provided an opportunity to take a closer look at the distribution of this component with depth, Winograd and Thordarson, 1975. "When well #88-66 was 2045 feet deep, the static water level was 1915 feet beneath the surface. After the well had been deepened to 2535 feet and cased (but not cemented) to 2121 feet, the water level was 1959 feet beneath the surface. No further changes were made in the well for 5 months thereafter, but the water level gradually declined another 20 feet. After penetration of carbonate rocks, at a depth of 2550 feet, the water level in the well fell to 2055 ± 2 feet. The water level within the well remained at this depth during subsequent deepening of the well to a depth of 3411 feet", Winograd and Thordarson, 1975.

A similar decline in the value of hydraulic potentials was documented in well #83-69a in west-central Yucca Flat. "At well depths of 1875 and 1970 feet the measured static water level was 1716 feet beneath the land surface. After the hole was deepened to 2430 feet, the water level dropped to 1732 feet below the land surface. Later the hole was deepened to 2620 feet, and the static water level was 1780 feet below the land surface", Winograd and Thordarson, 1975.

Plate 4.4.-8, presents an idealized pattern of changes in the value of pore pressure as a function of depth in wells #88-66 and #83-69a. The characteristic feature of this pattern is the progressive decline in

the value of hydraulic potentials with depth. In well #88-66 this decline occurs in the sequence of Tertiary volcanic rocks. In the sequence of Paleozoic carbonate rocks, encountered at depth, the value of hydraulic potentials is constant. In well #83-69a, however, the decline occurs in both the Tertiary volcanics and the Paleozoic carbonates.

The pattern of changes in the value of hydraulic potentials with depth observed in the area of Yucca Flat is strikingly similar to the pattern shown on Plate 3.2.4.-5. In Section 3.2.4., the latter pattern was postulated to be characteristic of an area which had experienced the large scale restructuring of the in-situ stress field and entered a new tectonic cycle of deformation.

Based on this similarity, it is reasonable to suspect that the distribution of hydraulic potentials with depth in Yucca Flat may be related to tectonic processes. Some support for this interpretation may be inferred from the results of chemical analysis of water samples from well #81-67, Schoff and Moore, 1964. These results indicate that "mixed" water, or sodium-potassium-calcium-magnesium type, occurs in the sequence of Tertiary volcanics. Furthermore, active faults are known to be present in the area of Yucca Flat (Knauss, 1981), therefore, significant changes in the in-situ stress conditions, in not too distant past, should not be surprising.

The vertical gradients of hydraulic potentials are also present in the area of Yucca Mountain. These gradients are known based on downhole measurements of pore pressure performed in 7 deep exploratory wells, namely: UE-25b#1, UE-25p#1, USW H-1, USW H-3, USW H-4, USW H-5, AND USW H-6. The location of these wells is shown on Plate 4.4.-9.

The measurements of downhole pore pressure were made at discreet intervals which were isolated, from the remainder of the borehole, with packers. The results of these measurements were reported by Robison, 1984. They are presented on Plate 4.4.-10.

Plate 4.4.-11 shows an idealized distribution of the pore pressure with depth in the area of Yucca Mountain. Between the water table and a depth of approximately 1200 m, the value of hydraulic potentials is more or less constant and independent of depth. Below this depth, however, higher values of the hydraulic potentials were encountered in three boreholes. These boreholes are: UE-25 p#1, USW H-1, and USW H-3. The highest difference in the value of pore pressure  $\Delta p_{(z)}$  was observed in borehole USW H-1 where it was equal to approximately 53 m. In boreholes UE-25 p#1 and USW H-3, the difference  $\Delta p_{(z)}$  was 20 m and 22 m, respectively.

Similarly as in the area of Pahute Mesa, the water levels as measured in open holes do not show the higher pressures occurring at greater depths. Again, it is clear that either the deformed or the deforming fractured medium is involved. The results of in-situ stress determinations, performed at four sites in the area using the hydrofracture technique, fully support this conclusion. These results were reported by Stock, et.al., 1985, and Stock, et.al., 1986. They are also presented and discussed in Section 4.5.

In summary, the examination of data reveals that the vertical gradients of hydraulic potentials occurring in the Death Valley flow system display all characteristics of being related to tectonic processes. In two cases, the area of Pahute Mesa and the area of Yucca Mountain, either the deformed or the deforming fractured medium is clearly present. In the case of Yucca Flat, the distribution of pore pressure with depth may be related to a recent faulting event. This event, most probably, occurred along the Yucca Fault. Furthermore, the characteristic spatial distribution of the vertical components of flow in the area of Pahute Mesa, may be related to the hydrothermal convection cell. This cell appears to be dampened by the limit equilibrium in-situ stress conditions present within the first 2500 feet of the zone of saturation.

#### 4.5. The In-Situ Stress State.

Hydrologists seldom, if ever, use in their considerations of groundwater flow systems information concerning the in-situ stress field. They prefer to consider the fractured medium as a medium whose hydraulic properties, i.e. the storativity and the hydraulic conductivity, are fixed in space. Furthermore, it is assumed that the value of these parameters is unrelated to time or other time-dependent factors. It is in petroleum industry, stimulation in particular, where the in-situ stress state receives its greatly deserved attention. It is recognized that the in-situ stress controls the relationship between the effective normal stress ( $\sigma_{\text{neff}}$ ) and the closing pressure ( $\sigma_c$ ) as well as between the shear stress ( $\tau_f$ ) and the resistance of the medium against frictional sliding, which is  $\tau_{\text{max}}$ . Hence, the in-situ stress also controls the relationship between formation pore pressure and its storativity and hydraulic conductivity.

In Section 3.2.2., a thought was advanced that, in the case of Death Valley flow system, the in-situ stress field may vary in time and space. This characteristic would result in control by the in-situ stress field of the storativity and of the hydraulic conductivity and, through them, the distribution of hydraulic potentials. Similarly, the in-situ stress field would control the thermal conductivity and, through it, the distribution of geothermal gradients.

There is no doubt that the in-situ stress field is the important factor which may either control or influence the flow process. It seems appropriate, therefore, to review what is known about the in-situ stress field in the Death Valley groundwater system.

At the Nevada Test Site numerous in-situ stress determinations were made. These determinations were performed using either the overcoring technique or the hydraulic fracturing technique. The results of these experiments were widely reported in literature, for example Ellis and Edge, 1976; Haimson, et.al., 1974; Ellis and Maguer, 1980; Smith et.al., 1980; Haimson, 1981; Stock, et.al., 1985; and Stock, et.al., 1986.

For the purposes of these considerations two areas, at the Nevada Test Site, were selected for closer examination of the in-situ stress conditions. These areas are: Rainier Mesa and Yucca Mountain.

A three-dimensional determination of the in-situ stress, beyond the influence of tunnel openings, was performed in U-12e.18 drift excavated into Rainier Mesa. The measurements were made with the USBM three-component borehole deformation gage, using the overcoring technique. Magnitudes and orientations of the principal stresses were calculated based on results of these measurements. They were reported by Miller, et.al., 1975 and are shown on Plate 4.5.-1, and Plate 4.5.-2.

Plate 4.5.-3 presents the Mohr's three-dimensional representation of the in-situ stresses measured at Rainier Mesa. The Coulomb criterion for shear failure is also shown. It was assumed that the cohesion (C) of natural fractures is equal to zero, and that the coefficient of friction for these fractures ranges from

0.47 ( $\phi = 25^\circ$ ) to 0.58 ( $\phi = 30^\circ$ ). In this situation, the ratio  $\tau_{\max}/\tau_f$ , for most favorably oriented for shear slip fractures, is equal to approximately 1.0 indicating that near the limit equilibrium in-situ stress conditions exist. Small increase in the value of pore pressure will cause the initiation of shear sliding along some fractures. The value of shear stress is controlled by the value of pore pressure. Conversely, small increase in the value of shear stress will cause the initiation of shear sliding and the resulting increase in the value of hydraulic conductivity for some fractures. In this situation, the shear stress controls the value of pore pressure. It becomes clear that the system is quite delicately balanced, in a sense, that the in-situ stress and the pore pressure are coupled via the principal of effective stress.

At Yucca Mountain, the in-situ stress determinations were made in four deep wells, namely: USW G-1; USW G-2; USW G-3; and, UE-25p #1. The location of these wells is presented on Plate 4.5-4. The measurements were made down to a depth of approximately 1700m, in both the vadose zone and the "saturated" zone. The results of these measurements were reported by Stock, et.al., 1985 and Stock, et.al., 1986. They are shown on Plate 4.5-5, Plate 4.5-6, Plate 4.5-7, and Plate 4.5-8.

A characteristic feature of the in-situ stresses, measured at the Yucca Mountain, is that in most cases the value of minimum horizontal stress is very close to a line which represents resistance of fractures against frictional sliding. This line has been drawn assuming that the cohesion (C) of pre-existing fractures is negligible, and that the coefficient of friction for these fractures is somewhere within a range of 0.6-1.0. Again, the data indicate quite clearly that the limit equilibrium is present. Consequently, the in-situ stress and the pore pressure are coupled and, obviously, either the deformed or the deforming fractured medium is involved.

In summary, even casual overview of the results of in-situ stress determinations reveals that, in the Death Valley flow system, the in-situ stress plays a very important, perhaps dominant, role. This conclusion is in full agreement with expectations deduced based on the volcano-tectonic character of the area, Section 3.1., and based on the history of tectonic deformation of the area, including the contemporary deformation, Section 3.2.1. Furthermore, the contemporary straining and seismicity together with the pattern of Plio-Quaternary deformation and faulting in the area all indicate that the evolving, i.e. changing with time, or the dynamic strain energy field must be involved. Any hydrologic consideration not accounting for this circumstance will, undoubtedly, contain serious errors in judgment amounting to a complete misunderstanding and, therefore, misrepresentation of the flow field.

#### **4.6. In-Situ Measurements of Temperature.**

##### **4.6.1. General.**

The results of measurements of the in-situ temperature can provide important insights into the flow process operating in a hydrologic system. Specifically, these measurements can yield data which can provide, either directly or indirectly, answers to a number of important hydrogeologic questions. Of particular relevance, to the Death Valley groundwater system, are the following three questions: a) does the flow field involve the single or the two phase flow process, i.e. is there an involvement of the "mixed" convection flow process?; b) is the flow field developed in the deforming fractured medium?; and, c) does the flow field involve the two phase, heat-fluid coupled, flow occurring in the deforming fractured medium?.

As discussed in Section 3.3.3., presence of the "mixed" convection should reveal itself through two thermal characteristics of the flow field. These characteristics are: a) the relatively high heat flow; and, b) the relatively high degree of thermal inhomogeneity, i.e. presence of significant gradients of the in-situ temperature. Based on the thermal characteristics alone, however, it is quite easy to confuse the "mixed" and the "forced" convection flow systems. In order to distinguish the two apart, it is necessary to introduce other characteristics of the flow field and of the medium, Section 3.3.4.

In Section 3.4.2., it has been shown that the involvement of the deforming fractured medium in the heat flow process will also reveal itself through the thermal characteristics of the flow field. These characteristics are: a) the presence of horizontal gradients of the in-situ temperature, Plate 3.4.2.-4; b) the specific sharp increase in the value of geothermal gradient with depth, Plate 3.4.2.-4; and, c) the time dependence of both the horizontal and the vertical gradients of the in-situ temperature.

It is expected that the thermal signature of the two phase, heat-fluid coupled, flow field developed in the deforming fractured medium will combine characteristics of the two above systems. In this field, the convective aspects of the flow process will be displayed with a corresponding intensity but only below some depth. Near the ground surface, however, the convective flow will be attenuated or dampened by the limit equilibrium conditions of the in-situ stress field. Such flow field is characterized by a large degree of variability of its behavior with time, Section 3.4.3.

Examination of the data base pertaining to thermal characteristics of the Death Valley groundwater system is presented below. This examination has been divided into three parts. These parts are: a) Section 4.6.2 describing gradients of the in-situ temperature; b) Section 4.6.3. describing results of the in-situ heat flow measurements; and, c) Section 4.6.4. dealing with the heat flow in the past. Summary of interpretations of the data base is presented in Section 4.6.5.

#### 4.6.2. Gradients of the In-Situ Temperature.

Within the Death Valley flow system, measurements of the in-situ temperature, as a function of depth, were carried out in more than 50 deep wells, Plate 4.6.2.-1. These impressive data were summarized and reported by Sass, et.al., 1980. Plates 4.6.2.-2 through 4.6.2.-8 present these data in a form of distribution of the in-situ temperature with depth. Six different areas located at the Nevada Test Site are represented.

Examining the depth distributions of the in-situ temperature, it becomes clear that the flow field is characterized by a large degree of thermal inhomogeneity. Sass and Lachenbruch, 1982, and Sass, et.al., 1980, attributed this inhomogeneity to "local groundwater circulations". These authors, nevertheless, recognized the convective aspects of the flow system in at least one area or possibly two areas. One of these areas is around well UE-25a3 and another is situated around well PM-2, Plate 4.6.2.-1.

Within the Death Valley flow system, at a constant depth of 500 m, the in-situ temperatures range from about 20°C (well TW7 on Plate 4.6.2.-4, and well TW1 on Plate 4.6.2.-3) to as much as 48°C and 52°C (well TWF on Plate 4.6.2.-6 and well PM-2 on Plate 4.6.2.-2) Values of the geothermal gradient range from 15°C/km - 20°C/km (well TW1 on Plate 4.6.2.-3 and well UE-4a on Plate 4.6.2.-4) to 43°C/km - 58°C/km (in well TWF on Plate 4.6.2.-6 and well PM-2 on Plate 4.6.2.-2).

The pattern outlined by the spatial distribution of thermal inhomogeneity, if viewed together with the seismic velocity structure of the area shown on Plate 3.3.1.-1, is very revealing. East of the contour line, which on Plate 3.3.1.-1 represents the zero seismic velocity perturbation, the in-situ temperatures are low, for example Plate 4.6.2.-3 and Plate 4.6.2.-5. However, west of this contour line the in-situ temperatures are noticeably higher (well UE-18t on Plate 4.6.2.-3; Plate 4.6.2.-2; Plate 4.6.2.-6; and Plate 4.6.2.-7). Furthermore, two local seismic velocity anomalies, one in the area of Pahute Mesa and another in the southwestern corner of the Nevada Test Site, are clearly reflected in the pattern of spatial distribution of thermal inhomogeneities. The highest in-situ temperatures, as measured near the ground surface, occur over both of these anomalies, for example well PM-2 on Plate 4.6.2.-2; wells TWF, TW-5, TW-3, and J-11 on Plate 4.6.2.-6, and well UE-25a3 on Plate 4.6.2.-7.

Based on the above observations, it appears that in addition to the "local groundwater circulations" there is another factor involved. This factor is the nonhomogeneous heat flow through the base of the flow system. As shown by the seismic velocity structure of the upper crust, Plate 3.3.1.-1, this nonhomogeneous heat flow is clearly related to the fundamental tectonic fabric of the area.

It is interesting to note that, the deformational aspects of the area are also reflected in the three-dimensional distribution of the in-situ temperature. Two observations are of particular relevance. First, two areas where the limit equilibrium conditions of the in-situ stress field exist (i.e. Pahute Mesa, Section

4.4.; and Yucca Mountain, Section 4.4. and Section 4.5.), contain wells in which the distribution of values of the geothermal gradient with depth shows the distinct sharp increase. This increase was described in Section 3.4.2. and is presented on Plate 3.4.2.-4. The wells which show this increase are: UE-19gs and UE-20f, Plate 4.6.2.-3; and USW H-1 and USW G-1, Plate 4.6.2.-7.

Second, in the area of Yucca Flat, the local hydrologic conditions were interpreted to be the result of a recent tectonic event, possibly on the Yucca Fault, Section 4.4. According to this interpretation the contemporary near-surface groundwaters are free of tectonic influences. Consequently, the in-situ temperature field is characterized by a considerable degree of uniformity, for example Plate 4.5.2.-4 and Plate 4.5.2.-5 (wells TWE and UE-15b are exceptions; they, most likely, represent a different tectonic configuration).

#### 4.6.3. Measurements of Heat Flow.

The results of measurements of the contemporary heat flow, performed in the Death Valley groundwater system, were published by Sass, et.al., 1976; Sass, et.al., 1980; and, Sass and Lachenbruch, 1982. These results were obtained by combining the in-situ measurements of temperature, Section 4.6.2., with measurements of the thermal conductivity. The latter measurements were performed in the laboratory using either core samples or drill cuttings, Sass, et.al., 1976.

The intensities of heat flow, within and adjacent to the Nevada Test Site, are presented on Plate 4.6.3.-1 and Plate 4.6.3.-2. The values of this intensity range from 0.7 HFU - 1.3 HFU, through 1.8 HFU - 2.2 HFU to 3.1 HFU. Obviously, a very heterogeneous temperature field is involved.

Within the Southern Great Basin, a large area was distinguished, based on the results of measurements of the intensity of heat flow. In this area anomalously low, from a regional point of view, heat flow values occur. This area includes the Nevada Test Site and was named the Eureka Low by Sass, et.al., 1977. The anomaly was attributed to a complex hydrologic disturbance of an unspecified nature.

The location of the Eureka Low is presented on Plate 4.6.3.-3. This plate also presents the 2.5 HFU heat flow intensity contour which have been established by Swanberg and Morgan, 1978. The contour is based on the silica contents of groundwater. These silica contents indicate that the intensities of heat flow, for most of the Eureka Low including the Nevada Test Site, are equal to or greater than 2.5 HFU. Recognizing this contradiction, Sass and Lachenbruch, (1982), concluded that: a) groundwater "is carrying off much of the earth's heat in the upper 3 km and delivering it elsewhere"; and, b) "the regional heat flow from beneath the zone of hydrologic disturbance in the Eureka Low may be the same as that characteristic of the Great Basin in general ( $80 \text{ mWm}^{-2}$  or 2 HFU) or it could be as high as  $100 \text{ mWm}^{-2}$  or 2.5 HFU".

A mystery posed by the Eureka Low can be readily solved by recognizing that the deforming fractured medium is involved in the heat flow process. There are two factors which together explain the dilemma. The first factor was discussed in Section 3.4.2. The values of thermal conductivity as derived

based on the laboratory measurements underestimate the actual in-situ values, because they do not account for the dilated nature of the deforming fractured medium. Consequently, the intensities of heat flow are also underestimated. The second factor was discussed in Section 3.4.3. It was shown that the deforming medium, while it is being dilated, stores not only fluid but also the thermal energy. This causes the apparent decrease in the intensity of heat flowing through the deforming fractured medium.

#### 4.6.4. Heat Flow in the Past.

The intensity of heat flow in the past, specifically during Late Quaternary, was estimated at only one location. This location is the Yucca Mountain itself. Samples of calcitic veins, emplaced along some fractures, were collected from drill cores extracted from the vadose zone in three boreholes, namely: UE-25 a#1; USW G-2; and, USW G-3. The location of these boreholes is shown on Plate 4.6.4.-1.

The samples were analysed for uranium and stable isotope contents, and were dated by the uranium-series method. The results of these analyses were reported by Szabo and Kyser, 1985. They are also shown on Plate 4.6.4.-2 and Plate 4.6.4.-3. Two calcite samples yielded an average date of  $28 \times 10^3$  years B.P., four calcite deposits yielded an average date of about  $170 \times 10^3$  years B.P., and four calcite deposits have an average date of about  $280 \times 10^3$  years B.P. In addition four calcite samples yielded minimum dates of precipitation of greater than  $400 \times 10^3$  years B.P.

Plate 4.6.4.-4 presents the stable isotope data for the calcites from Yucca Mountain. The presentation is in a form of  $\delta^{18}\text{O}$  vs.  $\delta^{13}\text{C}$  plot. Temperatures shown represent the calculated isotopic composition of calcite in equilibrium with meteoric water having the  $\delta^{18}\text{O}$  value of (-9) and the  $\delta^{13}\text{C}$  values of either (-11.5) or (-8). Fractionation factors for oxygen are those suggested by O'Neil, et.al., 1969, and for carbon are those derived by Friedman, 1970.

Plate 4.6.4.-5 presents an estimate of the in-situ paleo-temperatures based on the stable isotope content of the calcite samples. This estimate is also presented on Plate 4.6.5.-6 which, in addition, shows the contemporary in-situ temperatures within Yucca Mountain. Differences between the contemporary and the in-situ paleo-temperatures are substantial ranging from few °C near the ground surface to as much as 15°C at a depth of about 600 m. This suggests, but does not prove, that the in-situ temperatures at the Yucca Mountain vary through time in accord with the conceptual model of heat flow in the deforming fractured medium, Section 3.4.3. It is possible that at the onset of a new evolutionary loop of the system the values of geothermal gradients are 5°C - 15°C per km higher than at the end of this loop.

#### 4.6.5. Summary.

The review of thermal characteristics of the Death Valley groundwater system reveals that there are indications of heavy involvement of tectonics in the flow process. The flow field appears to be characterized by a substantial degree of thermal inhomogeneity in three dimensions. At a depth of approximately

2 km or 3 km, the intensity of heat flow is high and may be the same as that characteristic of the Great Basin in general. At the base of the flow field, distribution of the intensity of heat flow appears to be heterogeneous. This distribution seems to be related to the fundamental tectonic fabric of the area, as shown by the seismic velocity structure of the upper crust. In this situation, the possibility that the "mixed" convection or two phase, heat-fluid coupled, flow process is involved in the flow field should be seriously considered.

The characteristic increase in the value of geothermal gradients with depth, observed in some deep wells, together with the possible time-dependence of the value of these gradients, indicates that the strain energy field may be involved in the heat flow process. This strengthens the earlier conclusion that the deforming fractured medium is, locally, the dominant factor in the flow field.

As the consequence of above discussions, the question: does the flow field involve the two phase, heat-fluid coupled, flow process occurring in the deforming fractured medium?, seems to have an affirmative answer. This question, without any doubt, is of paramount importance as far as the utilization of the Death Valley flow field for the purposes of permanent disposal of high-level nuclear wastes is concerned.

#### 4.7. Hydraulic Stressing of the Fractured Medium in the Death Valley Flow System.

##### 4.7.1. General.

Hydrologic observations made during hydraulic stressing of a fractured medium can reveal important characteristics of the flow system. Specifically, the results of these observations can be used to evaluate whether or not the deforming fractured medium is involved in the flow process. Furthermore, these results can provide some help in evaluating, on qualitative basis, how significant are the in-situ stress related changes in the hydraulic conductivity and the storativity of the fractured medium. These information, in turn, can be used to estimate a magnitude of the potential hydrologic disturbances resulting from the large scale restructuring of the in-situ strain energy field. Of course, these estimates must be made with reference to a specific flow field and accounting for local hydrologic conditions.

The hydraulic stressing of the fractured medium occurs in association with many natural or man-made processes and activities. Drilling of a well or an exploratory borehole using drilling fluids, amounts to local hydraulic stressing of the fractured medium. The values of applied hydraulic pressures are small if the potentiometric surface is located near the ground surface. However, if drilling is performed in a situation involving a thick vadose zone, the applied hydraulic pressures may be very high.

The hydraulic stressing occurs in association with testing of a completed well using the Cooper-Brederhoeft "slug" injection test procedure. The hydraulic pressures applied may be very high. For example, the hydraulic pressures used in testing wells at Yucca Mountain were in a range of 10 bars to 40 bars.

Passage of a vibratory ground motion through the fractured medium also causes the hydraulic stressing of this medium. This transient stressing may result from either a natural earthquake or a man-made detonation of a nuclear device. During the passing of vibratory ground motion, the fractured medium is alternately compressed and dilated through many cycles of strain. During a single cycle, part of the fractured medium, perhaps 1/4 of the shock wave wavelength wide, may be under either compressional or extensional strain for a time equal to about 1/4 of the shock wave period.

The magnitude of dynamic strain caused by an earthquake with magnitudes  $M_s = 7.0$  and  $M_s = 7.5$  was estimated by Wood, 1985. As shown on Plate 4.7.1.-1, the dynamic strain, produced by such an earthquake, ranges from  $10^{-3}$ , near the earthquake epicenter, to  $10^{-5}$  some 200 km - 250 km away from the epicenter. The Handley nuclear detonation produced the peak dynamic strain of about  $1.5 \times 10^{-5}$ , at a distance of about 200 km (Wood, 1965). The Handley nuclear device had a reported yield of about 1 megaton, which is equivalent to an earthquake with  $M_s = 6.5$ . It is reasonable to expect that the dynamic strain resulting from the  $M_s = 7.0 - 7.5$  earthquake is of the order of  $10^{-4}$ , at a distance of 30 km. As shown on Plate 4.7.1.-1, the shock wave induced potential increases in the value of pore pressure are very high in the range of tens of bars.

The deforming fractured medium is characterized by two important features, Section 3.2.4. The first feature is that the in-situ strain energy field is spatially heterogeneous, i.e. the fractured medium contains gradients of both the normal stress and the shear stress. The second feature is that, locally, the strain energy field is at the conditions of limit equilibrium (either  $\sigma_{n\text{eff}} = \sigma_c$  or  $\tau_f = \tau_{\text{max}}$ ). In this situation, even small increases in the value of pore pressure, introduced into the medium, cause the development of local instabilities leading to the establishment of local perturbations in the in-situ strain energy field. It is important to understand these perturbations and their role in the hydraulic stressing of the medium as well as in controlling the hydraulic response of this medium during and after the stressing. To this end it is useful to examine Plate 4.7.1.-2; Plate 4.7.1.-3, and Plate 4.7.1.-4.

Plate 4.7.1.-2 presents the assumed initial distribution of the in-situ stresses along a fracture. It has been assumed that the location of this fracture, relative to the  $\sigma_1$  stress trajectory, is such that the gradients of both the normal and the shear stress are present along the fracture plane. Consequently, the value of shear stress ( $\tau_f$ ) varies along the fracture plane, it is highest near the fracture center and diminishes with distance away from it. In contrast, the magnitude of normal effective stress ( $\sigma_{n\text{eff}}$ ) is highest near the fracture ends and diminishes toward the fracture center. Along the fracture plane, the value of pore pressure ( $p$ ) is constant, and the value of  $\tau_{\text{max}(y)}$  varies in accord with the distribution of  $\sigma_{n\text{eff}(y)}$ .

Plate 4.7.1.-3 presents the in-situ stress perturbation resulting from a local build-up of the pore pressure  $p(y)$ . This build-up causes that the value of normal effective stress  $\sigma_{n\text{eff}(y)}$  is reduced by a variable amount  $\sigma_{n\text{eff}(y)}^1$ . Reduction in the value of  $\tau_{\text{max}(y)}$  by a variable amount  $\tau_{\text{max}(y)}^1$  follows. Near the fracture center, this reduction is sufficient to cause the development of a local shear dislocation. As a result, the value of  $\tau_f(y)$  is reduced by a variable amount  $\tau_f^2(y)$ . Reacting to the shear dislocation, the fracture wall-rock is compressed in the upper half of the fracture and stretched in the lower half. This straining gives rise to an additional gradient of the normal stress  $\sigma_{n(y)}$ . As the magnitude of shear dislocation diminishes with distance ( $x$ ) away from the fracture plane, the magnitude of additional normal stress ( $\sigma_n^1$ ) also diminishes. This causes that, in addition to the normal stress gradient  $\sigma_n^1(y)$ , there is also an additional gradient of the shear stress  $\tau_{xy(x)}$ , Plate 4.7.2.-4.

Emergence of the additional stress gradients [ $\sigma_n^1(y)$  and  $\tau_{xy(x)}$ ] causes locally the initial in-situ stress trajectories to change their position with respect to the fracture plane. These trajectories also change their configuration relative to their former configuration. Both of these changes constitute the essence of the in-situ stress perturbation resulting from the local pore pressure build-up. These changes are not, however, in accord with the overall configuration of the in-situ strain energy field and, therefore, cannot be tolerated for a long time. With time, both of the additional stress gradients will decay to a more tolerable position of equilibrium, as shown on Plate 4.7.1.-4.

Following discussions presented in Section 3.2.3., it can be inferred that the shear dislocation, induced by the pore pressure build-up, causes important changes in the fracture hydraulic conductivity ( $K_{\text{eff}}$ ) and

stretivity ( $S_f$ ). These changes are shown on Plate 4.7.1.-4. The shear dislocation related dilation of the fracture results in increase of the value of both the fracture hydraulic conductivity and the storetivity. When the in-situ strain energy field eradicates the stress perturbation, the value of both of these parameters diminishes, and with time returns to normal.

The above described perturbation of the in-situ strain energy field involves a transfer of the strain energy from the fracture plane to the wallrock. This perturbation does not involve significant removal of the strain energy from the field via vibratory ground motion, permanent dislocation, and associated thermal effects. However, if such removal is triggered by the pore pressure build-up the reaction of the fractured medium is different. In this case, there is a permanent reduction in the strain energy around the fracture, values of both the normal stress and the shear stress are changed. The value of normal effective stress increases and the value of shear stress diminishes. Consequently, the hydraulic conductivity and the storetivity of the medium are reduced. This reduction occurs in a volume of the fractured medium from which the strain energy was removed.

Examination of hydrologic observations made during the hydraulic stressing of the fractured medium in the Death Valley flow system is presented below. This examination has been subdivided into three parts. These parts are: a) Section 4.7.2, describing response of water levels in wells to nuclear detonations; b) Section 4.7.3., describing effect of nuclear detonations on groundwater discharge from tunnels and on groundwater chemistry; and, c) Section 4.7.4., describing response of the fractured medium to the Cooper-Brederhoest injection tests. Summary of interpretations is presented in Section 4.7.5.

#### 4.7.2. Response of Water Levels in Wells to Nuclear Detonations.

Measurements of the response of the flow system to shock waves were performed, at the Nevada Test Site, in association with detonation of few nuclear devices. Best known are the responses to two important events, namely: the Handley Event and the Bilby Event.

The Bilby Event occurred on September 13, 1963, in Yucca Flat, at the Nevada Test Site. The nuclear device had a reported yield of approximately 200 kilotons, and was buried 2339 feet below the land surface. In Yucca Flat, the Bilby Event was the first nuclear explosion detonated within the zone of "saturation". The results of hydrogeologic observations made in association with this event were published by Garber (1971) and Corchary and Dinwiddie (1975). The location of the detonation site is shown on Plate 4.7.2.-1. The response of the fluid pressure to the Bilby Event, as measured in three observation wells, is shown on Plate 4.7.2.-2. The event caused the fluid pressure to rise about 250 feet in the observation well U3-4, located 2000 feet from the detonation site. The observation wells #7 and E, situated 4000 feet and 8000 feet away, recorded the fluid pressure rise of about 65 feet and 10 feet, respectively.

After the event, borehole U3-cn PS #2 was drilled into the Bilby rubble chimney. The water level rise, in the rubble chimney, was observed during a period from November, 1963, to May, 1968. The results of these measurements were reported by Garber (1971) and are presented on Plate 4.7.2.-3.

Considering together the data on Plate 4.7.2.-2 and Plate 4.7.2.-3 the following sequence of events may be reconstructed. Prior to detonation of the Bilby device the water table, in the vicinity of the explosion site, was at an altitude about 2425 feet above mean sea level. The shock wave generated by the Bilby Event produced the dynamic fluid over-pressure value of which ranged from 250 feet, 2000 feet away from the detonation site, to 10 feet, 8000 feet away from the detonation site. Between September 13, 1963, and November 8, 1963, the fluid level declined to an altitude of about 2090 feet, i.e. 335 feet below the fluid level prior to the detonation time. The continuous rise of the water level, from an altitude of 2090 feet to an altitude about 2410 feet, was observed from November 8, 1963, to May 8, 1968.

The local hydrologic conditions in the area of Yucca Flat, and presumably around the Bilby detonation site, were discussed in Section 4.4. It can be recalled that, the characteristic feature of this area is the progressive decline of the value of hydraulic potentials with increasing depth, as shown on Plate 4.4.-8. The distribution of hydraulic potentials with depth indicates the presence of "underpressure" in deeper portions of the zone of "saturation". The value of this "underpressure" ranges from 527 feet in well #87-62, through 140 feet in well #88-66, to 64 feet in well #83-69a, Winograd and Thordarson, 1975.

In light of these local hydrologic conditions, the following interpretation of behavior of the fluid pressure through time, at the Bilby detonation site, seems to be reasonable. The detonation induced shock wave produced the dynamic fluid overpressure value of which diminished with the increasing distance away from the detonation site. Locally, around the detonation site, the dynamic overpressure and the shock wave caused the development of perturbation in the in-situ strain energy field, increase in the conducting aperture of fractures, and resulting enhancement of the vertical conductivity of the Tertiary volcanics. Evidently, the perturbation of the in-situ strain energy field involved only transfer of the strain energy which was not accompanied by reduction of the overall energy balance. This perturbation was not in accord with the overall configuration of the strain energy field. Consequently, it provoked a reaction on the part of this field. This reaction was to strain back, with time, the "rebellious" volume of the fractured medium. In the meantime, taking advantage of the increased vertical hydraulic conductivity, the groundwater drained from the higher intervals into the deeper intervals where values of the hydraulic potentials are lower. With time, as the restoration of the strain energy field took place, the conducting aperture of fractures was being gradually reduced. The values of hydraulic potentials were adjusted accordingly by a lateral radial inflow of water from outside of the detonation induced stress anomaly. These adjustments displayed themselves as a rise of the fluid level in borehole U3-cn PS#2, during a period from November, 1963, to May, 1968.

The Handley Event occurred on March 26, 1970, in the area of Pahute Mesa at the Nevada Test Site. The nuclear device had a reported yield of approximately one megaton. It was detonated in emplacement hole U-20m, location of which is shown on Plate 4.7.2.-4. Many measurements and observations pertaining to the deformational and hydrologic effects of the Handley Event were made. The results of these measurements and observations were described by Dudley, et.al., 1971 and Morris, 1971.

Measurements of ground deformation, within a few km of the Handley detonation site, were made by high-precision leveling and by Geodimeter distance measurements. Level data showed subsidence caused by cavity collapse and possible compaction out to at least 1.2 km from the detonation point. These data also showed displacements across faults. Surface fracturing resulting from the explosion were typical radial and concentric fractures associated with the surface collapse area. Displacements along faults were observed as much as 8 km away. A maximum of 60 cm of vertical displacement occurred on a fault east of the detonation site. Prior to the Handley Event, a long-term creep was observed along the Boxcar Fault.

In anticipation of the Handley Event, pressure transducers to measure water levels were installed in 13 pre-existing wells. The most distant monitoring site was 112 km northwest of the detonation site. The location of some of the monitoring sites is shown on Plate 4.7.2.-5.

The dynamic fluid overpressure produced by the Handley shock wave is presented on Plate 4.7.2.-6. Within a distance of about 5 km of the detonation site, the value of overpressure is equal to nearly 100 m. The overpressure attenuated with distance from the detonation point. In well UE-18r, located 20 km away, the value of dynamic overpressure was equal 7.0 m. Beyond a distance of 50 km, the value of overpressure was less than 2.0 m.

In association with the Handley Event of particular importance are hydrologic observations made in the proximity to the detonation site. Four wells situated in Pahute Mesa (PM-1; PM-2; UE-20; and, UE-20p) and one well situated between Buckboard Mesa and Pahute Mesa (UE-18r) were observed at the detonation time. Water levels and pressures were recorded in these wells for three months after the Handley Event, through June, 1970. The location of these wells is shown on Plate 4.7.2.-7. The results obtained were reported by Dudley, et.al., 1971 and Corchary and Dinwiddie (1975), they are also presented on Plate 4.7.2.-8; Plate 4.7.2.-9; and, Plate 4.7.2.-10.

The monitoring of the dynamic fluid overpressure, in response to the Handley shock wave, was only partially successful. Apparently, the Rustrak recorders utilized in monitoring of Pahute Mesa wells were too slow to reveal cyclic responses to the shock wave. Nevertheless, the dynamic fluid overpressure of more than 92 m was recorded in well UE-20f, located about 5 km from the detonation site.

Sustained and oscillatory pore pressure changes were monitored for more than a month after the Handley Event. As shown on Plate 4.7.2.-6, these changes were observed in two wells, namely: UE-20f and UE-20p. In well UE-20f significant changes in the water level were recorded for 214 minutes after the detonation time. These changes are summarized on Plate 4.7.2.-7. The magnitude of greatest positive excursion was 24.5 m. There were many positive excursions with magnitudes ranging from 5 m to 15 m. The magnitude of greatest negative excursion was -28.7 m, and there were numerous excursions in a range of -10 m. During the first 214 minutes after the detonation, the maximum change in fluid level was observed to be equal to 53.2 m. The activity ended abruptly, but a residual increase in the value of hydraulic potentials of about 1.1 m remained. Well UE-20f has shown significant sustained fluid pressure increases

after some previous detonation, most notably the Jorum Event, Dudley, et.al., 1971. This well, approximately 4172 m deep, penetrates into the aftershock hypocentral zone of a seismic event triggered by the Benham detonation, Hamilton and Healy, 1959.

In well UE-20p, located approximately 5 km north of the detonation site, a drop in the water level of about 3 m was recorded at the detonation time. This drop was followed by a 45 minute recovery to 0.5 m above the pre-detonation water level. This peak decayed in about 15 minutes. A sustained rise in the fluid pressure of about 23 m occurred on March 29, 1970. This rise was followed by a further erratic increase in the water level. As shown on Plate 4.7.2.-8, the value of maximum rise of fluid level was about 50 m. The recording of water level at well UE-20p, was interrupted on March 30, 1970, when the cable was pulled from the recorder shelter by an unidentified person. On May 6, 1970 another rise in the water level occurred. The recorder was off scale ( $> + 8$  m) for 10 of the 14 days of fluid pressure excursion, Plate 4.7.2.-8.

The well casing in borehole UE-20p is perforated from a depth of 348 m to a depth of 783 m. At this depth interval, high values of the hydraulic conductivity were observed. The water level was at a depth of about 280 m below the ground surface. In this situation, large fluid pressure increases in the well could dissipate through upward seepage causing a slight increase in the water table elevation. Obviously, very large volumes of water must have been involved to produce the recorded changes of the fluid pressure in this well.

The local hydrologic conditions in the area of Pahute Mesa, and around the Handley detonation site, were discussed in Section 4.4. It can be recalled that, there are two characteristic features interpreted and/or observed in this area. The first feature is the presence, in the first 2500 feet of the "saturated" zone, of the limit equilibrium in-situ stress conditions. The second feature is spatial distribution of the hydraulic potentials, as shown on Plate 4.4.-1 and Plate 4.4.-3. In the western portion of Pahute Mesa, at a depth of 2500 feet below the water table, the "overpressure"  $\Delta p_{(z)}$  is clearly developed. The value of this "overpressure" may be considerable, as in the case of well UE-20f where the measured value of  $\Delta p_{(z)}$  was equal to 142 feet, Plate 4.4.-1 and Plate 4.4.-2.

In light of these local hydrologic conditions, the following interpretations of behavior of the fluid pressures with time, around the Handley detonation site, seems to be reasonable. The detonation induced shock wave produced the dynamic fluid overpressure value which was in a range of 100 m, at a distance of approximately 5 km away from the detonation point. The dynamic overpressure together with the shock wave triggered a large scale restructuring in the in-situ strain energy field, Section 3.2.4. and Section 4.7.1. This restructuring manifested itself through seismic shocks, fault displacements and distortions of the land surface, Morris, 1971. The removal of stored strain energy resulted in the reduction of magnitude of the shear stresses along some fractures and/or in the increase of magnitude of the effective normal stresses. These changes, in turn, caused the reduction of both the hydraulic conductivity and the storetivity of the

fractured medium. These reductions displayed themselves as the fluid pressure rises observed in two monitoring wells. Water involved in these rises is either water released from the storage or it comes from the "overpressure" zone at depth, as discussed in Section 3.2.4. Evidently, the pore pressure build-ups were too high relative to the magnitude of shock wave induced changes in the in-situ stresses. Consequently, dilation of the previously closed fractures occurred resulting in increasing the values of hydraulic conductivity and storativity. The fluid pressure dropped and fractures closed again. This process repeated itself over and over again until the system found a new equilibrium configuration. This new equilibrium configuration may require the presence of local hydraulic mounds in areas from which the strain energy was removed. It is quite possible that these mounds are responsible for "surprisingly high water levels found in some exploratory and emplacement holes", Corchary and Dinwiddie, 1975.

#### 4.7.3. Effects of Underground Nuclear Detonations on Aqueous Chemistry.

The effects of underground nuclear detonations on discharge from nearby sources and the resulting changes in aqueous chemistry, including content of the stable isotopes, were investigated by Russell, 1987. The studies were conducted in underground workings beneath Rainier Mesa. Two announced nuclear detonations were performed in these workings, one on April 6, 1985 and the other on April 10, 1986.

A tunnel seep discharge was monitored before and after the detonations. The discharge record obtained in association with the April 10, 1986 explosion is presented on Plate 4.7.3.-1. A twofold increase in the groundwater discharge is present. The "bomb" pulse lasted for approximately eighteen days.

Every five days, samples of groundwater discharging from two different seeps were collected and analyzed in the laboratory. The results of these analyses revealed that, corresponding with the increased discharge, there is also an increase in the total dissolved solids of the seep water. Changes in the content of specific ions with time are presented on Plate 4.7.3.-2, Plate 4.7.3.-3, Plate 4.7.3.-4 and Plate 4.7.3.-5. The data presented on these plates represent response of two different seeps to two different detonations. The increase in concentration for most dissolved species occurring at the times of detonations is clearly indicated by the data. The April 6, 1986, explosion was associated with a particularly large increase in concentration of sodium, sulfate, and bicarbonate. The large increase in sulfate is important because the presence of even small quantities of sulfate minerals or their weathering products have never been reported within the rock formations of Rainier Mesa. The changes in water chemistry, before and after the April 6, 1985 explosion in the form of Stiff diagram, are presented on Plate 4.7.3.-6. Plate 4.7.3.-7 is the Stiff representation of changes in the groundwater chemistry associated with the April 10, 1986 detonation.

The groundwater samples were also analyzed to determine their stable isotope content. The results obtained are shown on Plate 4.7.3.-8 and Plate 4.7.3.-9. There are large changes in isotopic signatures as represented by both oxygen-18 and deuterium.

Based on the above data, it is clearly evident that a shock wave resulting from an underground nuclear detonation mobilizes water from some sources. These waters are both chemically and isotopically

different from the "normal" water contained in fractures of Rainier Mesa. The question of importance is: what is the source of the additional water?. Two interpretations seem reasonable. On one hand, it is possible that the shock wave is forcing out the interstitial fluids from the rock matrix into fractures, Russell, 1987. According to this interpretation, the source of the additional water are rocks of the vadose zone. If this interpretation is correct, it indicates that the pore water is different from the fracture water. This pore water would represent either the relict water remaining from the time of rock deposition or water from the relict hydraulic mounds, as discussed in Section 4.2.

On the other hand, it is equally possible that the additional water comes from below the water table. The shock wave, through the dynamic fluid overpressure, is causing closure of some fractures resulting in injection of water into the vadose zone. The additional water represents either water released from the storage or water from the "overpressure" zone trying to form a hydraulic mound. It is not known, however, that the "overpressure" exists at the location of Rainier Mesa.

#### 4.7.4. Response of the Fractured Medium to Hydraulic Stressing During the Cooper-Bredehoeft Injection Tests.

It is assumed here that the fractured medium fails in a brittle or semi-brittle manner according to the combined Griffith-Navier-Coulomb envelope of failure. This envelope is represented by curve ABC on Plate 4.7.4.-1. If the stress circle touches the failure envelope between B and C a shear failure results. If the stress circle touches the failure envelope between A and B a hybrid extension-shear failure develops. Only if the stress circle touches the envelope at point A will pure tensile failure result. For tensile failure the Griffith criterion requires that the stress difference ( $\sigma_1 - \sigma_3$ ) is smaller than  $4T$ ; and for shear and hybrid extension-shear failure the stress difference ( $\sigma_1 - \sigma_3$ ) must be greater than  $4T$ . The failure criterion for the weakest type of the fractured medium is given by line OX on Plate 4.7.4.-1, which represents the failure envelope of material with zero cohesion (pre-existing fractures).

The principal of effective stress states that, at failure, the stress circle represents two components. These components are: the bedrock stress ( $\sigma_1 - \sigma_3$ ) and the pore pressure ( $p$ ). The effective stress difference  $(\sigma_1 - \sigma_3)_{eff}$  is equal to  $(\sigma_1 - \sigma_3) - p$ . According to this principle, failure of the fractured medium can be induced either by increasing the bedrock stress or by increasing the pore pressure.

Keeping in mind these elementary remarks and following discussions in Section 3.2.3., it is possible to conceptualize a constitutive relationship between the hydraulic conductivity of a fracture ( $K_f$ ) and the pore pressure ( $p$ ). This relationship is presented on Plate 4.7.4.-2. It consists of three segments. The first segment pertains to all values of the effective stress difference  $(\sigma_1 - \sigma_3)_{eff}$  smaller than those required by the Navier-Coulomb criterion for shear failure. In this case, the value of hydraulic conductivity ( $K_f$ ) is a function of the residual aperture of fractures ( $a_{res}$ ). The value of hydraulic conductivity is constant, in a sense that it is not related to the value of pore pressure.

The second segment pertains to values of the effective stress difference  $(\sigma_1 - \sigma_3)_{\text{eff}}$  greater than those required by the Navier-Coulomb criterion for shear failure and greater than values required by the Griffith criterion for tensile failure. The hydraulic conductivity ( $K_f$ ) is a function of the conducting aperture of the fracture ( $a_{\text{con}} = a_{\text{res}} + a_n + a_d$ ), Section 3.2.3. Because the value of  $a$  is related to the value of pore pressure, the value of hydraulic conductivity ( $K_f$ ) must also be related to it in a manner shown on Plate 4.7.4.-2.

The third segment pertains to values of the effective stress difference  $(\sigma_1 - \sigma_3)_{\text{eff}}$  satisfying the Griffith criterion for tensile failure and the Navier-Coulomb criterion for shear failure. The value of hydraulic conductivity ( $K_f$ ) is a function of the separation between fracture walls ( $a_{\text{con}} = a_{\text{sep}}$ ). Very small increases in the value of pore pressure cause very large increases in the value of hydraulic conductivity.

Plate 4.7.4.-3 presents an idealization of the expected relationship between the velocity of slug movement, in injection tubing as measured during the Cooper-Bredehoeft injection tests, and the value of applied pore pressure -  $\Delta p$ . The relationship is shown for four different in-situ stress conditions assumed to be present in the fractured medium prior to the application of pore pressure -  $\Delta p$ .

With the above introduction it seems appropriate to examine response of the fractured medium to hydraulic stressing as observed during the Cooper-Bredehoeft injection tests. Within the Death Valley flow system, extensive testing of the fractured medium was performed at Yucca Mountain. The testing was carried out in eight deep wells, namely: USW H-1; USW H-3; USW H-6; USW H-5; USW H-6; UE-25b #1; UE-25p #1; and, USW G-4. The location of these wells is shown on Plate 4.7.4.-4. The results obtained are presented on Plate 4.7.4.-5 through 4.7.4.-12.

The injection testing was performed below the water table, to a depth of approximately 2.0 km. Inflatable packers were used to isolate test zones; tests were performed at intervals where hole size and configuration of borehole walls allowed setting of the packers. Thickness of the test intervals ranged from tens of meters to several hundreds of meters. Water was injected into the interval between two packers, or between one packer and the bottom of a test borehole. Decline of hydraulic head with time, i.e. the speed of slug movement in the injection tubing, was monitored in the isolated intervals.

The hydraulic pressures applied during the testing were very substantial. They ranged from a minimum of 196 m (well USW H-6, test #10) to a maximum of 546 m (well USW G-4). The majority of the injection tests, however, were performed applying the values of hydraulic pressure ranging from 300 m to 500 m.

In light of the in-situ stress conditions, as established at Yucca Mountain based on the hydrofracture experiments (Section 4.5.), it can be expected that the high values of the applied hydraulic pressures were more than sufficient to introduce local failures in the fractured medium. Furthermore, values of the effective stress difference  $(\sigma_1 - \sigma_3)_{\text{eff}}$ , which have been generated during the injection testing, appear to be

sufficient to meet both the Navier-Coulomb criterion for shear failure and the Griffith criterion for tensile failure. It seems, therefore, that for the fractured medium at Yucca Mountain the injection tests offered an excellent opportunity to test in-situ the validity of constitutive relationship between the hydraulic conductivity ( $K_f$ ) and the pore pressure ( $p$ ), as proposed on Plate 4.7.4.-2.

Examination of Plates 4.7.4.-5 through Plate 4.7.4.-12, in conjunction with information presented on Plate 4.7.4.-3, reveals that the results of Cooper-Bredehoeft injection tests performed at the Yucca Mountain indicate that hydraulic opening of fractures commonly occurred during the injection testing. This conclusion is consistent with the conclusion drawn earlier by Thordarson, et.al., (1985) based on the results of the injection tests in well USW H-3. This conclusion is in full accord with the results of hydrofracture experiments as reported by Stock, et.al., (1985), Stock, et.al., (1986), and described in Section 4.5. Furthermore, the results of injection tests seem to indicate that all four in-situ stress conditions assumed on Plate 4.7.4.-3 are present in the fractured medium at Yucca Mountain.

The assumed in-situ stress conditions represented on Plate 4.7.4.-3a display themselves in the injection test data least frequently. They are evident in the injection test data from: well USW H-1 (Plate 4.7.4.-5, Plate 4.7.4.-5a, and Plate 4.7.4.-5b); well USW H-6, at depths ranging from 1118 m to 1220 m (Plate 4.7.4.-9d and Plate 4.7.4.-9e); and well UE-25b #1 at depths ranging from 1006 m to 1220 m (Plate 4.7.4.-10b). For these conditions, the injection data indicate the velocity of slug movement measured in tens of cm per minute or in meters per minute.

The in-situ stress conditions assumed on Plate 4.7.4.-3b for the relationship between the velocity of slug movement and the value of pore pressure seem to be evident more frequently in the injection test data. They were encountered in the following wells: well USW H-3 at depth of 851 m - 917 m (Plate 4.7.4.-6); well USW H-4 at depth of 555 m - 604 m (Plate 4.7.4.-7c); well USW H-5 at depths of 790 m - 796 m, 949 m - 1010 m, and 1015 m - 1033 m (Plate 4.7.4.-8, and Plate 4.7.4.-8c); well USW H-6 at depth intervals of 835 m - 869 m and 871 m - 1220 m (Plate 4.7.4.-9c and Plate 4.7.4.-9d); well UE-25b #1, at a depth of 477 m - 579 m (Plate 4.7.4.-10a); and well USW G-4, at depth intervals from 792 m to 838 m (Plate 4.7.4.-12c). For these cases, if the value of pore pressure is high the velocity of slug movement is measured in tens of meters per minute. For the lower pressure, however, the velocity of slug movement is lower, within the range of a few meters per minute or less. The curve relating the velocity of slug movement to the value of pore pressure displays a characteristic single break.

The relationship between the velocity of slug movement and the magnitude of pore pressure shown on Plate 4.7.4.-3c is characterized by a very distinct pattern. There are two breaks in the curve relating the velocity of slug movement and the value of pore pressure. The first break,  $\Delta p_2$ , marks the termination of satisfying the Griffith criterion by the value of effective stress difference  $(\sigma_1 - \sigma_3)_{eff}$ . The second break,  $\Delta p_3$ , identifies the value of effective stress difference for which the Navier-Coulomb criterion for shear failure is no longer satisfied. Results of the injection tests from the following wells display this characteristic

pattern: USW H-3, depth intervals 911 m - 972 m, 972 m - 1219 m, 1063 m - 1124 m, and, 1126 m - 1219 m (Plate 4.7.4.-6a and Plate 4.7.4.-6b), and well USW G-4, depth 792 m - 838 m (Plate 4.7.4.-12c).

The results of injection tests from Yucca Mountain, most commonly, display the pattern shown on Plate 4.7.4.-3d. The curve relating the speed of slug movement and the value of pore pressure shows only one break,  $\Delta p_4$ , similarly as the curve on Plate 4.7.4.-3b. The difference, however, is that now the slug travels at a speed value which is measured in hundreds of meters per minute. Examples of this most extraordinary behavior can be seen in the results of injection tests from the following wells: USW H-3, depth interval 792 m - 850 m (Plate 4.7.4.-6); USW H-4, depth intervals 652 m - 701 m, 703 m - 735 m, 783 m - 832 m, 832 m - 850 m, 1195 m - 1219 m (Plate 4.7.4.-6, Plate 4.7.4.-7, Plate 4.7.4.-7a, Plate 4.7.4.-7b, Plate 4.7.4.-7c, Plate 4.7.4.-7g); USW H-5, at depth intervals 796 m - 815 m, 887 m - 947 m, 888 m - 949 m (Plate 4.7.4.-8, Plate 4.7.4.-8b; USW H-6, at depth 606 m - 640 m (Plate 4.7.4.-9); UE-25b #1 at depth intervals of 514 m - 579 m, 505 m - 579 m, 792 m - 1220 m, 820 m - 860 m, 779 m - 819 m, and 581 m - 621 m (Plate 4.7.4.-10, Plate 4.7.4.-10c, Plate 4.7.4.-10d, Plate 4.7.4.-10e); UE-25p #1, at depth 1044 m - 1114 m (Plate 4.7.4.-11e); and USW G-4, at depth intervals 702 m - 747 m, 850 m - 875 m, 875 m - 899 m, and 899 m - 915 m (Plate 4.7.4.-12, Plate 4.7.4.-12c, and Plate 4.7.4.-12f).

The results of Cooper-Bredehoeft injection tests, if viewed in light of the information provided on Plate 4.7.4.-3, seem to be of an extraordinary hydrologic and geologic significance. These results appear to indicate that the  $K_f$  vs.  $p$  constitutive relationship, as shown on Plate 4.7.4.-2, is valid for the fractured medium at Yucca Mountain. They also appear to indicate that a degree of heterogeneity in the in-situ strain energy field is very substantial. This degree of heterogeneity must indicate that the dynamic strain energy field is involved.

#### 4.7.5. Summary.

The review of hydrologic observations made in association with the hydraulic stressing of the fractured medium in the Death Valley flow system revealed few important characteristics of this flow field. First, the flow system appears to operate in the deforming fractured medium. The hydrologic observations made during and after two detonations of nuclear devices are consistent with this conclusion. Similarly, assumption of the deforming nature of the fractured medium is consistent with the results of Cooper-Bredehoeft injection tests performed at Yucca Mountain.

Second, local hydrologic conditions appear to control the response of the fractured medium to hydraulic stressing occurring in association with the detonation of nuclear devices. These local hydrologic conditions, in turn, seem to be controlled by the tectonic factors, as discussed in Section 4.4., Section 4.5., and Section 4.7.2. Types of the hydraulic response observed at Yucca Flat and at Pahute Mesa appear to support the assumption of heavy involvement of tectonics in controlling the Death Valley flow field.

Third, the post-detonation hydrologic responses of the fractured medium indicate that the size of hydrologic disturbances resulting from the large-scale restructuring of the in-situ strain energy field may be

considerable. These responses may be interpreted as indicating that the volumetric strain of the fractured medium in the "strained" state is large relative to the "relaxed" state. This volumetric strain causes both the hydraulic conductivity and the storativity to be significantly changed during the transformation from one state into the other.

Fourth, the in-situ strain energy field, at least locally at Yucca Mountain, appears to be characterized by a substantial degree of internal heterogeneity. The results of injection tests indicate that, locally, the fractured medium is at conditions of limit equilibrium with respect to both the Griffith criterion for tensile failure and the Navier-Coulomb criterion for shear failure. If this interpretation is correct, then the flow field at Yucca Mountain should display both systematic and erratic drifts in the value of hydraulic potentials with time, as shown on Plate 3.2.4.-6.

#### 4.8. Large Scale Fluctuations of Water Table as Possibly Expressed in Geologic Record Representing Late Pliocene and Quaternary Time.

If interpretations advanced in Section 4.1. through Section 4.7. are, at least, partially correct then the geologic record representing Late Pliocene and Quaternary times must contain some expression of the large scale fluctuations of the water table. These fluctuations should reveal themselves as occurrences of deposits whose origin is related to the deep-seated groundwaters. These deposits would occur at the ground surface in a form of tuffa mounds and/or aprons with associated feeder dikes, and in the subsurface in a form of veins, fragmentation breccias and metasomatic replacements of wallrock. Furthermore, the deposits would occur at altitudes which can not be justified by: a) the position and configuration of the contemporary water; b) the changes in this position related to past climatic alterations; and, c) tectonic deformation, such as: tilting, uplift, and subsidence.

As discussed in Section 3.4.3. and shown on Plate 3.4.3.-3, termination of an individual evolutionary loop of the two-phase, coupled heat-fluid, flow field developed in the deforming fractured medium is expected to be associated with precipitation of minerals along the separated fractures and, possibly, on the ground surface. It can be recalled that this termination involves the transformation of the flow field from the "weak" geothermal state into the "strong" geothermal state. At the time of termination, the flow process exhibits strong "mixed" convection aspects and is responsible for "fusing back together the dilated fractured medium". The resulting mineralization is very important with regard to conceptual understandings of the Death Valley flow field. This mineralization can confirm directly that the flow field, indeed, operates in the deforming fractured medium and that it includes the two-phase, coupled heat-fluid, flow process. Furthermore, the mineralization can yield data which may be used to determine a duration of a single evolutionary loop of the system and a magnitude of the associated hydrologic disturbances.

A review of geologic literature pertaining to the Death Valley flow system was performed. The purpose of this review was to establish whether or not the geologic record representing Plio-Quaternary time contains any indications of large scale fluctuations of the water table. The results of this review are presented below.

In the vicinity of Yucca Mountain, various vein deposits of calcite, opaline silica, including opal CT (opal with cristobalite- and tridymite-type structure), with lesser quartz and sepiolite are associated with Late Plio-Quaternary faults and Late Pliocene to Holocene surficial deposits, Swadley, et.al., 1984. The faults which contain the calcite-silica veins are; Windy Wash fault, Solitario Canyon fault, Bow Ridge fault, Paintbrush fault, and Fran Ridge fault. The location of these faults is shown on Plate 4.8.-1.

The calcite-silica deposits occur as veins emplaced along fault planes in both the unconsolidated alluvium of Late Quaternary age and in the Late Miocene bedrock. They also occur as aprons developed over the unconsolidated alluvial and eolian sediments. Thickness of the calcite-silica deposits ranges from tens

of centimeters to a maximum of about two meters. Typically, the deposits exhibit banded texture suggesting several generations of deposition.

The veins emplaced within the Bow Ridge fault and within the Windy Wash fault contain thin stringers of uncemented basaltic ash that displays petrographic and chemical affinity with one of two volcanic centers located nearby, Whitney, et.al., 1986. The age of these centers has been determined, based on radiometric dating of the associated lavas, to be approximately  $1.2 \times 10^6$  years B.P. and possibly less than  $0.1 \times 10^6$  years B.P., Vaniman, et.al., 1982; and Crowe and Vaniman, 1985.

Traces of the Windy Wash fault, the Solitario Canyon fault, the Bow Ridge fault, the Paintbrush fault, and the Fran Ridge fault are marked by occurrences of very distinct breccias, Plate 4.8.-2. Commonly, these breccias form the wallrock of the calcite-silica veins. They are clearly older than the emplaced within them veins. Thickness of the breccia zones is highly variable, ranging from tens of meters to several hundreds of meters. The breccia consists of angular fragments of the country rock in a matrix composed mainly of silica and calcite. Remarkable features of these breccias are: a) a very large volumetric strain which ranges from several percents to tens of percents; and b) a very homogenous nature of the volumetric strain, i.e. the amount of dilation appears to be equal in any three mutually perpendicular directions. Both of these features indicate that the breccias are "fragmentation" or "explosive" breccias, formation of which is the result of large and very fast build-ups of pore pressure.

Various origins for the calcite-silica veins have been proposed including precipitation from low temperature descending water and from elevated temperature ascending water. It was also considered that, the deposits may have formed by multiple processes involving deep-seated groundwaters, perched groundwaters, surficial runoff waters, or water flow induced by seismic activity.

Stable isotope analyses were performed on three samples representing the calcite-silica deposits. Two of these samples represent deposits from the Bow Ridge fault and one sample represents the veins from the Fran Ridge fault. The samples have the following  $\delta^{18}\text{O}$  and  $\delta^{13}\text{C}$  per mil isotopic composition referenced to Standard Mean Ocean Water (SMOW) and the Pee Dee Belemnite (PDB) respectively, O'Neil, 1984, and 1985:

	<u><math>\delta^{18}\text{O}</math> (SMOW)</u>	<u><math>\delta^{13}\text{C}</math> (PDB)</u>
<u>The Bow Ridge fault</u>		
Sample: T-14 FB (calcite)	19.6	-5.3
Sample: T-14-3a-w (calcite)	20.3	-7.5
<u>The Fran Ridge fault</u>		
Sample: FR 6 (calcite)	19.8	-7.0

Plate 4.8.-3 presents the comparison of the stable isotope composition of the three samples with the stable isotope composition of samples of the calcite veins described in Section 4.6.4. The comparison sug-

gests that the temperatures of formation of the minerals, represented by samples T-14 FB, T-14-3a-w, and FR-6, range from approximately 24°C to about 27°C.

Plate 4.8.-4 presents a comparison of these temperatures with the in-situ contemporary temperatures as measured in wells USW G-2, USW G-1, and USW H-1. The temperature of formation of minerals composing the calcite-silica veins appears to be 5°C and 8°C higher than the contemporary temperature of rock near the ground surface. This may suggest, but does not prove, that warmer subsurface fluids are responsible for deposition of the calcite-silica veins.

In close proximity to Yucca Mountain lake beds, or most likely pond or seep deposits, were described by Hoover, et.al., 1981. These sediments occur near the southern end of Crater Flat (Plate 4.8.-5) at altitudes 120 m and 150 m higher than the altitude of the contemporary water table. They consist of white to buff, laminated to thick-bedded, poorly indurated, sandy and tuffaceous marls, siltstones, and diatomites. Bedding characteristics and presence of the diatomaceous beds quite clearly indicate the environment of aqueous deposition. The diatoms identified in three samples indicate "...alkaline, at times slightly saline, shallow water. Many of the species identified are found in alkaline, somewhat saline spring systems, but they are not restricted to this environment", Hoover, et.al., 1981.

Near the southern end of Crater Flat, the occurrence of spring deposits were also described by Hoover, et.al., 1981. These spring deposits consist of pale brown, vuggy tuffa to white relatively dense siliceous calcium carbonates containing scattered large pores. They form mounds, diameter of which ranges from 5 m to 20 m.

It appears that some of the above deposits were dated by Szabo, et.al., (1981), using the uranium-thorium method. Samples #199 and #106 are of particular relevance. The locations of these samples are shown on Plate 4.8.-5. Sample #199 represents a "nodular tuffa spring deposit". It gave the uranium-thorium age of about  $3 \times 10^4$  years B.P., indicating that "suggested spring activity was at altitude of about 838 m as late as 30,000 years ago. Present water table is about 120 m lower, Winograd and Thor-darson (1975)". Sample #106 represents "seep deposited tuffa or calcrete intercalated in Q2 alluvium - shows some evidence of spring- water deposition". The sample yielded the uranium-thorium age of  $78 \times 10^3 \pm 5 \times 10^3$  years B.P. It was collected at an altitude of about 940 m above mean sea level. This altitude is about 200 m higher than the altitude of the contemporary water table.

At Yucca Mountain, the veins composed of calcite and silica are known to occur in the subsurface. Szabo and Kyser, (1985) reported the results of radiometric and stable isotope analysis performed on samples of the calcite-silica veins emplaced along some fractures in the vadose zone. These results were discussed in Section 4.6.4.

As shown on Plate 4.6.4.-4, the elevated temperatures of formation of minerals composing the calcite veins suggest that their origin may be related to deep seated groundwaters, rather than to the infiltrating

meteoric water as assumed by Szabo and Kyser, 1985. Radiometric ages of these veins, range from more than  $4 \times 10^5$  years B.P. to  $3 \times 10^3$  and  $2.6 \times 10^3$  years B.P.

Veins which are most likely related to the deep seated fluids occur in other cores extracted from the vadose zone at Yucca Mountain. Examples of these veins are: borehole RF-3, at depth ranging from 238 feet to 248 feet; borehole UE-25A #4, at depth from 318 feet to 336 feet; and borehole UE-25A #5, at depth from 281 feet to 290 feet. The veins, however, were not investigated in any detail and therefore neither their age nor composition are known.

Carr, et.al., (1986) reported the occurrence of metasomatic alteration of possibly hanging wall of a large fault at the contact between the Paleozoic carbonates and the Tertiary tuffs. Borehole UE-25p #1 intersected 33 m of calcified ash-flow tuff at a depth ranging from 1172 m to 1205 m and immediately above the fault. Locally, secondary calcite comprises more than 50 percent of the total rock volume. Clearly, a long history of migration of the carbonate-rich fluids from the nearby fault into the country rock is evident. In order to account for the 33 m thick zone of metasomatic alteration, the assumption of significant horizontal gradients of hydraulic potentials is required.

At the Nevada Test Site, surficial deposits composed of carbonate, opaline silica, and gypsum are known from other locations. According to Szabo, et.al. (1981), carbonates occur in a variety of forms in surficial and subsurficial deposits. These carbonates accumulate in soil horizons in different forms. "They commonly fill fractures along faults, form dense, strongly cemented deposits in alluvium and are precipitated by spring water. The carbonates were broadly classified into five groups. The hard, dense and finely crystallized carbonates precipitating from groundwater are referred to as travertines. The softer and more porous forms of the precipitated carbonates are defined as tuffaceous travertines. The surficial conglomerates or rock fragments and minerals, strongly cemented by authigenic carbonates are called calcretes. The secondary accumulations of cementing carbonate in the host material of a soil environment are identified as soil caliches. Finally, the dense calcium carbonate in fractures in drill cores is referred to as calcite veins", Szabo, et.al., 1981, pg. 2.

Samples of all types of these carbonates have been collected from various locations throughout the Nevada Test Site and dated using the uranium-series method by Szabo, et.al., 1981. The locations of sample sites are shown on Plate 4.8.-5. The analytical data and the uranium-series ages of various carbonates are presented on Plate 4.8.-6. The uranium-series ages of travertines and tuffaceous travertines range from more than  $7 \times 10^5$  years B.P. to  $3 \times 10^3$  years B.P. The samples of these materials were collected at altitudes ranging from 100 m to several hundreds of meters above the contemporary water table.

Samples of carbonates (travertine, calcrete, and caliche) were dated from the Carpetbag, Yucca, Boundary, and Cane Spring faults by Knauss (1981) using the uranium-series method. Locations of sample sites are shown on Plate 4.8.-7. Travertine and tuffaceous travertine deposits were identified along the Cane Spring fault (samples: CSF #1 and CSF #2) and along the Boundary fault (samples: BF LLL1-1

and BF USGS5-5a). The author defined the terms "travertine" and "tuffaceous travertine" as "...hard, dense, finely crystalline carbonate that precipitates from groundwater, the modifier tuffaceous denotes a softer, more porous variety of travertine". Plate 4.8.-8 presents the uranium-series ages of the four samples of travertine and tuffaceous travertine. Both, the carbonate ages calculated using the graphic-isochron plot method of Szabo, et.al., (1978; 1981) and, for comparison, the uncorrected ages based simply on the leach raw data are shown. The ages of travertines from the Cane Spring fault are:  $4.1 \times 10^4$  years B.P. for sample CSF #1, and  $2 \times 10^3$  years B.P. for sample CSF #2. The travertines occurring along the Boundary fault yielded ages greater than  $4 \times 10^5$  years B.P.

The location of Cane Spring fault is shown on Plate 4.3.-3. The fault is located in close proximity to a possible hydraulic mound, presence of which was inferred in Section 4.3. Near the Cane Spring fault, altitude of the ground surface, is nearly 1600 feet higher than the contemporary water table in Frenchman Flat.

The following quotation is from Winograd and Doty (1980), pg. 61: "Two calcitic fracture fillings found in Paleozoic carbonate rocks at sampling Site 4 are examples of veins apparently having little relation to modern or pluvial groundwater levels despite uranium-thorium dates, of 72,000 and 100,000 years. These samples were collected by W.J. Carr (U.S. Geological Survey, Denver, Colo.) at an altitude of approximately 1140 m, or about 200 m above the level of the playa in Frenchman Flat. While we tentatively accept the ages, the assumption that this calcitic material was precipitated within a regional zone of saturation during pluvial times is premature". The location of sampling Site 4 is shown on Plate 4.8.-9.

At the Nevada Test Site, a few meters thick deposit of gypsum was found near Wahmonie. The deposit occurs at the ground surface, in a topographic setting that precludes playa deposition, and in the area where the vadose zone is approximately 2000 feet thick. Following quotation is from the Draft Environmental Assessment (DOE, 1984), pg. 2-14: "In addition to the altered granite, local surface deposits from recent warm springs indicate upward seepage of ground water, possibly from great depth".

A spectacular swarm of calcitic veins occurs along the western edge of the Funeral-Greenwater Mountain Range, forming the eastern margin of the Death Valley tectonic depression. The swarm occurs along the trace of the Furnace Creek Fault. This swarm was described by Winograd and Doty, 1980; and Winograd, et.al., 1985.

The veins occur in near-vertical fractures in well cemented fanglomerates of the Funeral Formation of Pliocene age. The veins vary from a millimeter to a meter in thickness, locally occur in swarms, and are commonly finely laminated. They can be traced vertically for tens of meters and horizontally for over hundreds of meters.

In places, visible transitions of vein to tuffa mound can be observed. It is very clear, therefore, that the veins mark the sites of fossil discharges of groundwater at the ground surface. The veins originated

as low-temperature, less than 50°C, precipitates from calcite saturated waters rising along the extension fractures. Three samples of the veins have been dated using the uranium-series method. The radiometric ages obtained range from  $1.7 \times 10^6$  years B.P. to  $10^5$  years B.P., Winograd et.al., 1985.

Plate 4.8.-10 is a diagrammatic NE/SW section illustrating topography of the Funeral-Greenwater Mountain Range, from Death Valley, California to Ash Meadows and Amargosa Deserts, Nevada. The direction of regional groundwater flow is from the northeast toward the southwest, as shown on Plate 4.1.-2. In the Amargosa Desert, the altitude of ground surface is approximately 2400 feet above mean sea level, in Death Valley the ground surface drops to below the sea level.

The swarm of calcitic veins occurs at altitudes ranging from approximately 2900 feet to 3100 feet above mean sea level. These altitudes are more than 500 feet above the altitudes of land surface downstream and upstream along the regional flow path. There are two possibilities that may account for this apparent paleo-hydrologic anomaly. Either the Funeral-Greenwater Mountain Range has been uplifted some 500 feet relative to the Amargosa Desert during the last  $10^5$  years B.P. or the calcitic veins reflect occurrences of the tectonic hydraulic mounds during the time span from  $1.7 \times 10^6$  years B.P. to  $10^5$  years B.P. The published data base does not allow for a conclusive resolution of this question. Nevertheless, the results of recent hydrologic studies performed in the area of Furnace Creek Ranch - Franklin Lake playa by Czarnecki (1987) revealed that configuration of the contemporary water table, below the Greenwater Range, contains a similar hydrologic anomaly, as shown on Plate 4.8.-10. Potentiometric data, reported by Czarnecki (1987), indicate that a groundwater "divide" may exist in the Greenwater Range, between the Amargosa Desert and Death Valley. Hydraulic head under the Greenwater Range is as great as 875 m, whereas in the Amargosa Desert the hydraulic head is about 615 m, and in Death Valley it is about sea level. Clearly, a contemporary hydraulic mound, some 260 m high, is present. The question which emerges is: is this mound the result of groundwater recharge from the ground surface, or the tectonic factors or are responsible for the formation of this mound?. As shown on Plate 4.1.-3, the average annual precipitation in the area of Funeral-Greenwater Range, ranges from 2 inches per year to a maximum of 6 inches per year. In light of this information, the assumption that local surface recharge is responsible for the Greenwater Range mound does not appear to be a reasonable one.

Plate 4.11.-10 presents the comparison between history of the global climatic changes during the Pleistocene Epoch and the radiometric ages of travertines from the Nevada Test Site. This history is expressed as a plot of the average water temperature in the Atlantic Ocean with time and a plot of the "average steppe index" from the Black Sea with time, Hsu, 1978. Clearly, the ages of travertines from the Nevada Test Site do not bear any relationship to the history of global climatic changes. This seems to imply that the global climatic changes should not be held responsible for deposition of these travertines.

In summary, the geologic record representing Late Pliocene and Quaternary times appears to contain possible expressions of the large scale fluctuations of the water table. This conclusion, if correct, together

with the interpretations presented in Section 4.1. through Section 4.7. seem to form a harmonious picture of the Death Valley flow system. Although it is rather difficult to judge the reliability of the information from geologic literature, the picture seems to be remarkably consistent. The two-phase, coupled heat-fluid, flow field developed in the deforming fractured medium seems to be clearly present. The magnitudes of hydrologic disturbances, possible in this flow field, seem to be very large, measured in tens and hundreds of meters. The duration of a single evolutionary loop of the system, at and near Yucca Mountain, appears to be less than  $10^5$  years.

## SECTION 5.0.

### CONCLUSIONS AND RECOMMENDATIONS

#### 5.1. Summary and Conclusions.

Having performed the analysis presented in Section 2.0, Section 3.0, and Section 4.0, the following three conclusions seem to be reasonable and warranted at this time:

i) Examination of the extensive data base pertaining to the Death Valley groundwater system, in light of the conceptual framework as established in Section 3.0., reveals that this flow field is considerably different than the flow system currently envisaged by the NNWSI Project. The conceptual model of this flow system, as used in performing site suitability assessments for purposes of developing the Final Environmental Assessment for the Yucca Mountain site and for purposes of establishing an approach to the forthcoming site characterization activities, is far too simple and much too far removed from reality. Simply stated this conceptual model ignores completely the volcano-tectonic setting of the Yucca Mountain site.

The currently adopted conceptual model considers a single phase, steady-state, flow process which is assumed to be fully describable by the Laplace equation. In this model, it is assumed that the water table constitutes a meaningful and durable expression of the characteristics of the flow system. The position of the water table is assumed to be related solely to the volume of fluid passing through the system's boundaries. This volume of fluid is a function of climatic conditions and remains constant as long as these conditions remain unchanged. Consequently, it is assumed that all moisture in the vadose zone is the result of infiltration of a small portion of rainfall. Furthermore, it is assumed that the movement of water involves the mechanism of matrix flow and that this movement occurs under the influence of gravity alone.

Within the context of the currently considered conceptual model the influence of tectonic disruptions is limited to: a) local alteration of stratigraphic relationships; b) additional local fracturing; and, c) minor changes in the altitude of discharge areas relative to the altitude of recharge areas. A tectonically induced change in these factors is relatively small and, therefore, the resulting alterations in the three-dimensional distribution of hydraulic conductivity and of the gradients of hydraulic potentials are likewise small. These alterations can readily be accommodated by minor changes in the position and configuration of the water table. It follows then that, the impact of these alterations on the migration of radionuclides from the repository is small.

A completely different picture emerges if one considers the volcano-tectonic setting of the Yucca Mountain site and of the groundwater system operating at this site. As indicated in Section 3.1., and Section 3.3, the setting of Yucca Mountain contains the continental alkalic basalts of Late Pliocene and Quaternary age. These basalts, as a matter of fact, are trace-element enriched hawaiites with isotopic compositions indicative of the mantle origin. The isotopic and geochemical characteristics of these rocks are best

accounted for by assuming that the convective mass and heat transfer occurs in the upper mantle. From a point of view of regional hydrology, this mantle upwelling appears to be responsible for two very important, tectonophysical factors.

The first factor is high and, most importantly, spatially heterogeneous heat flow. This heat flow and the gravitational hydraulic pressures acting at the flow system boundaries are the energy sources which together are responsible for the movement of groundwater. In a thermodynamic sense, therefore, the flow process is the two phase, heat-fluid coupled, flow or the "mixed" convection flow. In such a flow field, an arbitrary plane adopted as the base of the flow field must be considered as the "flow" boundary with respect to flow of both heat and fluid. Mathematical models used in numerical simulations of the flow process in this field must account for this circumstance, otherwise calculations and interpretations may be grossly misleading and, with reference to the Death Valley flow system, are quite irrelevant.

The second factor is the strain energy which, because of the mantle upwelling, is being supplied into the flow field on continuous basis. The resulting dynamic strain energy field plays an important role in controlling the resistance offered by the fractured medium against the coupled flow of heat and fluid. Near the ground surface, the strain energy field controls the conducting aperture of fractures and, therefore, it also controls the bulk thermal and hydraulic conductivities of the medium. Also controlled are the hydraulic storativity and the thermal diffusivity of this medium. As the strain energy field changes with time, the thermal and hydraulic parameters also change. Consequently, the entire flow system acts as a three way, H - F - M, coupled thermodynamic continuum. For the purposes of these conceptual considerations, this continuum has been simplified and referred to as the two phase, heat-fluid coupled, flow field developed in the deforming fractured medium.

The continuum evolves through a series of similar evolutionary loops which, for a given area within the flow field, are closely tied to the deformational cycles of this area, Section 3.4.3.. During a single evolutionary loop, the energy balance of the continuum undergoes a remarkable transformation. At the onset of the deformation cycle, the gradients of the in-situ stress are "weak", allowing for existence of "strong" gradients of the in-situ temperature and of the hydraulic potentials. At this time, the water table is high and the flow field shows strong "mixed" convection aspects. With the advance of the deformation, however, the in-situ stress gradients become "stronger" and the fractured medium enters the "dilated" state. The values of the thermal and hydraulic parameters of the fractured medium increase and become time dependent. These time dependent increases in the value of these parameters cause that the gradients of temperature and of hydraulic potentials to "weaken". The water table deepens and, near the ground surface, the flow system loses its strong "mixed" convection or geothermal aspects.

The termination of the deformational cycle is associated with a large, but local discharge of the accumulated distortional strain energy from the system. The in-situ stress gradients "weaken", allowing for the reappearance of the normal "strong" gradients of the in-situ temperature and of the hydraulic potentials.

The water table returns to its high position and the convective heat-fluid flow process returns to its normal intensity. At this time, the bedrock separations which resulted from the discharge of strain energy are being filled with minerals precipitating from the convecting fluids.

As demonstrated in Section 4.0., assumption of the two phase, heat-fluid coupled, flow field developed in the deforming fractured medium is in full accord with all known characteristics of the Death Valley groundwater system. This is in sharp contrast to the conceptual model of this system used to: a) perform assessments of suitability of Yucca Mountain for site characterization; and, b) develop strategies for demonstrating compliance of this site with all applicable Federal regulations. Not accounting for the true nature of the flow field will, undoubtedly, entail serious errors in judgement amounting to a complete misunderstanding and, therefore, misrepresentation of the flow field.

ii) Conceptualization of hydrologic processes operating in the vadose zone of the two phase flow field developed in the deforming fractured medium yields a completely different picture than the one currently envisaged by the NNWSI Project. Two issues of fundamental importance are associated with the possibility that the flow system is developed in the deforming fractured medium. These issues are: a) the mechanism of flow in the vadose zone; and, b) the temporal stability of the water table, including its short and long term aspects, and involving both climatic and tectonic factors. Two other issues of fundamental importance are associated with the possibility that the flow field involves the two phase, heat-fluid coupled, flow process. These issues are: a) the chemistry of the interstitial pore water in the vadose zone; and, b) the spatial and temporal distribution of heat flow through the vadose zone.

There are two relative measures of a tendency toward fracture flow in the vadose zone. These measures are: a) the depth to which the limit equilibrium in-situ stress conditions are developed; and, b) the difference in the degree of rock matrix saturation in the vadose zone and in the "saturated" zone. Results of the in-situ stress determinations performed at Yucca Mountain, Section 4.5., and of the Cooper-Brederhoeft injection tests, Section 4.7.4., indicate that the depth of the limit equilibrium in-situ stress conditions is considerable, more than 1200 m, and is substantially below the water table. Results of laboratory measurements of the degree of rock matrix saturation, Section 4.3., revealed that the difference in the degree of saturation of the rock matrix in the vadose zone, below a depth of approximately 220 m, relative to the degree of the matrix saturation below the water table, is not substantial by any standards. Consequently, in light of these data, an expectation that the movement of water through the vadose zone of Yucca Mountain involves the mechanism of interstitial porous flow does not appear to have a proper foundation. This is true, in particular, if one is concerned with the movement of water through rocks with small interstitial porosity as in the case of the densely welded Topopah Spring Member of the Paintbrush Tuff.

In the case of the deforming fractured medium, the temporal stability of the water table is not only related to global or regional climatic fluctuations, but it is also related to tectonic factors, in particular,

the in-situ stress conditions. As discussed in Section 3.2.3., both short term and long term instabilities of the water table can be expected at the Yucca Mountain site.

The short term instabilities involve several meters, perhaps tens of meters, of displacement of the water table. They are short lived, say days or weeks at most, and occur with a frequency related to the degree of heterogeneity in the local strain energy field. These short lived instabilities are caused by the minor restructuring of the strain energy field which may or may not require an external triggering mechanism. Fault creep, local and temporary uplift or subsidence, vibratory ground motion induced slip, etc. are examples of the manifestation of these restructurings. As discussed in Section 4.1., results of the continuous and periodic measurements of the position of the water table, performed at Yucca Mountain in a number of deep wells during the last 10 years, are not yet available in an accessible and reliable form. Consequently, it is not known whether or not the short lived instabilities of the water table were observed at the Yucca Mountain site. These instabilities, however, are very important because they can directly confirm that the deforming fractured medium is, indeed, involved in the flow process. Furthermore, these instabilities, if occurring with a meaningful frequency and magnitude, would constitute a "pumping" mechanism for gaseous transport through the vadose zone.

The long term displacements of the water table involve tens and perhaps hundreds of meters. They are caused by the large scale restructuring of the strain energy field occurring at the end of a deformation cycle and with a frequency measured in terms of tens of thousands of years. These displacements would directly impact the radionuclide migration path and the radionuclide migration time. In extreme cases, however, these displacements can result in the flooding of the repository and in expulsion of groundwater at the ground surface.

The critical point of the overall conceptual considerations of the flow field at Yucca Mountain is whether or not the geologic record representing Late Pliocene and Quaternary time contains expressions of the large scale displacements of the water table in the past. As discussed in Section 4.8., there are indications that this indeed may be the case. Detailed studies of the calcite-silica-sepiolite vein deposits, however, were not performed. Consequently, the current data base does not allow a conclusive resolution of this question. Nevertheless the possibility that these veins are a record of large scale displacements of the water table in the past is real, and by all means not remote.

The assumption that the Yucca Mountain flow field is developed in the deforming fractured medium and that it involves the two phase flow process, leads to the following question: what is the origin and chemistry of the interstitial water in the vadose zone?. If this assumption is correct then it follows that the interstitial water represents past hydraulic mounds developed in association with the high water levels present at the end of cycles of deformation. The chemistry of this water would be considerably different than the chemistry of water currently passing through fractures of the medium. In the vadose zone, downward movement of the infiltrating rain water may involve the mechanism of interstitial porous flow, but

only during the early stages of deformation when the in-situ stress gradients are "weak" and the fractured medium is in a "relaxed" stage. It is highly unlikely that a significant replacement of the relict interstitial water by the infiltrating rain water could occur at this time. This replacement could be significant, but only during a more advanced state of deformation, when the water table is deeper. At this time, however, the in-situ stress gradients are "strong" and it is unlikely that the infiltration of the water involves the mechanism of interstitial porous flow.

As far as it can be determined, there are no published data pertaining to the chemistry of interstitial waters from the vadose zone of Yucca Mountain. Consequently, there is no basis to either confirm or reject the above hypothesis. Nevertheless, there are some unpublished data which seem to indicate that the chemistry of interstitial water is considerably different than the chemistry of water contained in fractures. These data were obtained by Dr. A. Yang (U.S. Geological Survey, Denver, CO) through chemical analysis of samples of the interstitial water which have been mechanically squeezed out of cores extracted from Yucca Mountain.

It can be expected that the flux of heat through the vadose zone, in the two phase flow field developed in the deforming fractured medium, is very heterogeneous in both the temporal sense and the spatial sense. This heterogeneity is related to the in-situ stress control of the thermal conductivity of the fractured medium. It is likely, therefore, that the intensities of heat flowing through some fractures are very substantial and are variable in time. In this situation, the flow of heat may be an important factor in the local upward movement of vapors and gases through the vadose zone. This heterogeneous heat flow would also complicate the movement of infiltrating rain water.

Very little information concerning the spatial and temporal distribution of heat flux through the vadose zone of Yucca Mountain is available at the present time. The results of measurements of the in-situ temperature, as published, were obtained shortly after the completion of drilling. Consequently, it is very unlikely that the results of these measurements represent a true picture of the spatial distribution of the intensity of heat flow. Also, it appears that the results of repetitive measurements of the in-situ temperature are not yet available and, therefore, little is known with regard to the temporal variability of heat flow.

iii) The conceptual model of the flow field, indicated by the currently available data from the Yucca Mountain site, points toward serious limitations of this site to effectively isolate radionuclides from the biosphere. These limitations are greater by far than those currently recognized by the NNWSI Project. Without recognizing these limitations, the issue resolution strategies, as expressed in the current version of the Site Characterization Plan, are interesting propositions, but are of very limited practical value. The resulting misunderstanding of the hydrologic processes operating in the vadose zone results in overly optimistic assessments of the licensability of the Yucca Mountain site.

In light of the conceptual model of the flow field, as proposed in Section 3.0. and Section 4.0., the

most important licensing concern is the potential rise of the water table. If this tectonically induced rise is possible at all at the Yucca Mountain site, then the geochronologic data presented in Section 4.8., indicate that the annual probability of an occurrence of this rise is more than  $10^{-5}$ , perhaps within a range from  $3 \times 10^{-4}$  to  $5 \times 10^{-4}$ . In this situation, and in the context of performance requirements set forth in 10 CFR 60 and 40 CFR 191, the rise of the water table constitutes the "anticipated process and event". As such, the rise of the water table must be accounted for in demonstrating compliance of the Yucca Mountain disposal system with three long term performance objectives set forth in 10 CFR 60. These performance objectives are: a) the life of waste package; b) the release rates of radionuclides from the engineered barrier system; and, c) the release of radionuclides into the accessible environment.

The rise of the water table would significantly alter the radionuclide migration path and the radionuclide migration time. Furthermore, the water table rise, by providing substantial volumes of water, would also alter the radionuclide migration rate. Occurrence of the water rise during early stages of the life of the repository, when temperature of the waste packages and of the fractured medium surrounding them is above the boiling point of water, would result in a particularly strong impact on the overall repository performance. Vaporization of water entering the repository would cause substantial increases in the vapor pore pressure and, therefore, would accelerate the gaseous transport from the repository to the ground surface. Subsequent cooling of the repository, to below the boiling point of water, may be accompanied by a long term convective flow of fluids from the repository to the ground surface.

It can be expected that the chemistry of fluids entering the repository, in association with the tectonic rise of water table, is different than the chemistry of fluids currently residing in fractures of the flow system. The impact of the tectonic rise of water table on the life of waste package, therefore, is two-fold. Corrosion of waste packages will be accelerated not only because of the increased amounts of water contacting these packages, but also because of the more adverse chemistry of this water.

The tectonically induced rise of the water table, with a magnitude sufficient to flood the repository, is not the only licensing concern resulting from the proposed conceptual model of flow system. The model indicates significant consequences with respect to the ground water travel time requirement set forth in 10 CFR 60. Compliance of the Yucca Mountain site with this requirement can be demonstrated, but only by assuming that the rain water infiltrates through the vadose zone via the mechanism of interstitial porous flow. In the case of fracture flow, if infiltration occurs at all, the travel time of rain water is, most certainly, substantially less than  $10^3$  years.

The gaseous transport from the repository to the ground surface is another licensing concern resulting from the proposed conceptual model of the flow system. This transport is caused by the short lived instabilities of the water table and by the heterogeneous heat flow through the vadose zone. The gaseous transport may have some impact on the compliance of the Yucca Mountain site with two performance objectives set forth in 10 CFR 60. These performance objectives are: a) the release rate of radionuclides from the engineered barrier system; and, b) the overall release of radionuclides into the accessible environment.

Finally, the proposed conceptual model requires the chemistry of interstitial pore water in the vadose zone to be different from the chemistry of water currently residing in fractures. The chemistry of interstitial water is important with respect to considerations of regulatory compliance of the Yucca Mountain site. Three long term performance objective, set forth in 10 CFR 60, may be impacted. These performance objectives are: a) the life of waste package; b) the release rates of radionuclides from the engineered barrier system; and, c) the overall radionuclide release from the repository into the accessible environment.

It should be recognized that all of the above licensing concerns regarding the Yucca Mountain site are not new concerns. They were raised previously, in one form or another by various parties, most notably by the U.S. Nuclear Regulatory Commission and the State of Nevada. The proposed conceptual model of the flow system reinforces these concerns and provides an uniform theoretical background for these concerns.

## 5.2. Recommendations.

The proposed conceptual model of the flow system poses a number of questions regarding suitability of the Yucca Mountain site to accommodate safely the high-level nuclear waste repository. Recognizing the serious nature of these questions, and keeping in mind the long established policy of the U.S. Department of Energy to address the critical suitability issues first, the following four recommendations are offered:

i) A thorough examination should be performed of the data collected during the last 10 years of monitoring the position of the water table at Yucca Mountain. The main purpose of this examination is to establish whether or not short lived instabilities of the water table are occurring at the Yucca Mountain site. Furthermore, it is important to determine the frequency of occurrence of these instabilities as well as their magnitude;

ii) Complete and conclusive investigation of the calcite-silica-sepiolite deposits occurring at the Yucca Mountain site should be performed. This investigation should be carried out in both surface and subsurface and should include extensive radiometric age determinations. The purpose of this investigation is to establish whether or not the geologic record representing the Late Pliocene and Quaternary times contains expression of large scale fluctuations of the water table. Specifically, a firm position must be established whether or not flooding of the repository is the "anticipated process and event" within the context of regulatory requirements set forth in 10 CFR 60 and in 40 CFR 191.

iii) Investigation of the chemistry of water contained in the vadose zone of Yucca Mountain should be performed. It is recommended that a few borings be drilled for this purpose. The boreholes should be drilled with air and the drilling process should be designed to detect the presence of perched waters. If these waters are encountered, the drilling process should be halted and samples obtained for subsequent chemical analysis in the laboratory. The investigation should include chemical analyses of samples of the interstitial pore water mechanically squeezed out from cores following the procedure developed by Dr. A. Yang of the U.S. Geological Survey. The main purpose of these investigations is to establish whether or not: a) the vadose zone contains the perched water; and, b) the perched water and the interstitial pore water are chemically different from the fracture water.

iv) Investigation of the known perched waters occurring in the vadose zone of the Death Valley flow system should be performed. There are two outstanding candidates for this investigation. They are: a) the perched water in the vicinity of Skull Mountain, as described in Section 4.2.; and, b) the apparent hydraulic mound under the Greenwater Range, as discussed in Section 4.8. The main purpose of this investigation is to determine the origin of the water forming both of these hydrologic features. There are only two possibilities. Either they are ordinary meteoric waters infiltrating through the vadose zone, or they are related to the tectonically induced hydraulic mounds. The temperature and chemical composition of these waters should be sufficient to distinguish one from the other.

The investigations recommended above were designed to obtain data which are judged to be required to carry the conceptual considerations undertaken herein to their logical and reliable conclusion. Presence of: a) short lived instabilities of the water table; b) expressions of large scale instabilities of the water table during the last  $10^5$  years; c) perched waters with chemical compositions indicative of below the water table origin; and, d) meaningful difference in the chemistry of interstitial pore water relative to the fracture water, would confirm that the proposed conceptual model of the flow field is correct. In this situation, serious consideration should be given to abandoning the Yucca Mountain site and declaring it as unsuitable for the purposes of permanent disposal of the high-level nuclear wastes. In all sincerity, the U.S. Government would be well advised to perform the recommended investigations prior to the commitment of substantial resources, such as those associated with the Site Characterization Process and the in-situ testing in the Exploratory Shaft.

## LIST OF PLATES

- Plate 2.2.-1      **Mathematic model of "simple" groundwater system**
- Plate 2.2.-2      **Laplace's equation**
- Plate 2.2.-3      **Poisson's equation**
- Plate 2.2.-4      **Transient flow equation**
- Plate 2.2.-5      **Explanation of mathematical notations**
- Plate 2.3.-1      **Role of mathematical and conceptual models**
- Plate 2.3.-2      **Conceptual model of groundwater flow system**
- Plate 3.1.-1      **Numerical analysis of a process of upwelling of asthenospheric materials into lithosphere for the Rio Grande Rift**
- Plate 3.1.-2      **Effect of a mantle upwelling on lithospheric structure**
- Plate 3.1.-3      **Surface heat flow and shear stresses in upper mantle and lower crust resulting from convective flow of heat and mass in the upper mantle**
- Plate 3.1.-4      **Continuum crustal stresses and surface uplift resulting from convective flow of heat and mass in the upper mantle**
- Plate 3.2.1.-1     **The Walker Lane shear belt and major associated faults**
- Plate 3.2.1.-2     **Major Late Pliocene and Quaternary faults in the Nevada Test Site region, their relation to the Death Valley - Pancake Volcanic Zone**
- Plate 3.2.1.-3     **Quaternary faults near proposed repository area**
- Plate 3.2.1.-4     **Quaternary faults near proposed repository site**
- Plate 3.2.1.-5     **Seismicity of the Southern Great Basin. Period August 1, 1978 through December 31, 1983**
- Plate 3.2.2.-1     **Summary of strain rates and of accumulated shear strain for the region of Death Valley groundwater basin**
- Plate 3.2.2.-2     **Division of deformation area into individual strain domains**
- Plate 3.2.2.-3     **Idealization of tectonic cycle for an individual strain domain**
- Plate 3.2.2.-4     **Idealization of changes in stress field during tectonic cycle**

- Plate 3.2.2.-5 Spatial and temporal variation of crack closure during the growth stage
- Plate 3.2.3.-1 Stress on a fracture as a function of magnitude and orientation of principal stresses
- Plate 3.2.3.-2 Joint conducting aperture model
- Plate 3.2.3.-3 Relationship between time and hydraulic parameters caused by reduction in  $\sigma_{\text{eff}}$
- Plate 3.2.3.-4 Idealized joint response during shear displacement
- Plate 3.2.3.-5 Relationship between time and hydraulic parameters caused by increases in  $\tau_j$
- Plate 3.2.4.-1 Conceptual model of flow system in deforming fractured medium
- Plate 3.2.4.-2 Deforming fractured medium - idealized history of changes in hydraulic potential
- Plate 3.2.4.-3 Deforming fractured medium - idealized history of changes in hydraulic potential
- Plate 3.2.4.-4 Deforming fractured medium - idealized history of changes in hydraulic potential
- Plate 3.2.4.-5 Deforming fractured medium - idealized history of changes in hydraulic potential
- Plate 3.2.4.-6 Idealized history of the position of the water table for a single point P(x;y)
- Plate 3.2.4.-7 Nonhomogeneous strain - its relationship to configuration of the water table
- Plate 3.3.1.-1 Seismic velocity structure of the upper crust from teleseismic P-wave residuals for the region of southern Nevada
- Plate 3.3.1.-2 Generalized geologic map of the death Valley Pancake Range Volcanic Zone
- Plate 3.3.1.-3 Regional heat flow values within and adjacent to the Nevada Test Site
- Plate 3.3.1.-4 Crustal temperature as a function of depth and surface heat flow
- Plate 3.3.1.-5 Surface heat flow and seismic crustal structure for the Rio Grande rift and associated physiographic provinces of the north American Continent
- Plate 3.3.2.-1 Total hydraulic gradients combines buoyancy and pressure gradient
- Plate 3.3.2.-2 Mathematical model for simultaneous flow of heat and fluid
- Plate 3.3.2.-3 Governing equations in the Galerkin finite element method
- Plate 3.3.2.-4 Explanation of symbols used on Plate 3.3.1.-2 and Plate 3.3.1.-3
- Plate 3.3.3.-1 Conceptual model of flow system which contains a strong thermal inhomogeneity at its base

- Plate 3.4.2.-1 Relationship between time and thermal conductivity caused by incremental reduction in  $\sigma_{nter}$
- Plate 3.4.2.-2 Relationship between time and thermal conductivity caused by incremental increase in  $\tau_f$
- Plate 3.4.2.-3 Conceptual model of "simple" heat flow through deforming fractured medium
- Plate 3.4.2.-4 Main characteristics of the heat flow field developed in the deforming fractured medium
- Plate 3.4.3.-1 Conceptual model of two phase heat-fluid coupled flow field developed in the deforming fractured medium
- Plate 3.4.3.-2 Conceptual model of flow in vadose zone of the two phase heat-fluid coupled flow field developed in the deforming fractured medium
- Plate 3.4.3.-3 Evolutionary path of the coupled fluid and heat flow field developed in the deforming fractured medium
- Plate 3.4.3.-4 Idealized response of the fractured medium during uniform extension
- Plate 3.4.3.-5 Idealized response of the fractured medium to sudden changes in pore pressure
- Plate 4.1.-1 Location of the Death Valley groundwater system
- Plate 4.1.-2 Subdivision of the Death Valley groundwater system
- Plate 4.1.-3 Precipitation, recharge and discharge areas for the Death Valley groundwater system
- Plate 4.2.-1 Local hydrologic conditions at Beatty, Nevada
- Plate 4.2.-2 Results of chemical analyses of water samples from springs and wells, Beatty, Nevada
- Plate 4.2.-3 Local hydrologic conditions near Skull Mountain at the Nevada Test Site
- Plate 4.2.-3a Explanation of symbols used on Plate 4.2.-3
- Plate 4.2.-4 Results of chemical analyses of water from three depth intervals in test well 73-66
- Plate 4.2.-5 Location of Rainier Mesa at the Nevada Test Site
- Plate 4.2.-6 Schematic diagram illustrating local hydrology of the Rainier Mesa
- Plate 4.2.-7 Results of chemical analyses of 24 samples of perched waters from Rainier Mesa
- Plate 4.3.-1 Degree of saturation above and below water table

- Plate 4.3.-2 Configuration of water table in Death Valley flow system
- Plate 4.3.-3 Configuration of water table in Pahute Mesa (recharge area of the Death Valley flow system)
- Plate 4.3.-4 Configuration of water table in Amargosa Desert (discharge area of the Death Valley flow system)
- Plate 4.3.-4a Explanation of symbols used on Plate 4.3.-4
- Plate 4.3.-5 Configuration of water table at Yucca Mountain
- Plate 4.3.-6 Configuration of water table in Yucca Flat and Emigrant Valley
- Plate 4.3.-6a Explanation of symbols used on Plate 4.3.-6
- Plate 4.3.-7 Configuration of water table in Yucca Flat
- Plate 4.4.-1 Vertical components of flow in the area of Pahute Mesa
- Plate 4.4.-2 Results of downhole measurements of distribution of hydraulic potentials, Pahute Mesa.
- Plate 4.4.-3 Idealized changes in hydraulic potentials in the Pahute Mesa
- Plate 4.4.-4 Water chemistry map for Pahute Mesa
- Plate 4.4.-5 Results of chemical analyses of water samples from Pahute Mesa
- Plate 4.4.-5a Results of chemical analyses of water samples from Pahute Mesa (cont.)
- Plate 4.4.-6 Downhole temperature for three boreholes in Pahute Mesa
- Plate 4.4.-7 General hydrogeology of Yucca Flat
- Plate 4.4.-8 Idealized changes in pore pressure with depth in wells 88-66 and 83-69a located in Yucca Flat
- Plate 4.4.-9 Location map for deep wells at Yucca Mountain
- Plate 4.4.-10 Water levels - Yucca Mountain
- Plate 4.4.-10a Water levels - Yucca Mountain (cont.)
- Plate 4.4.-11 Idealized changes of pore pressure with depth at Yucca Mountain
- Plate 4.5.-1 The results of in-situ stress determinations in Rainier Mesa

- Plate 4.5.-2 Three-dimensional representation of the in-situ stresses measured in Rainier Mesa
- Plate 4.5.-3 Mohr's representation of the in-situ stresses at Rainier Mesa
- Plate 4.5.-4 Location map showing wells where hydrofracture experiments were made at Yucca Mountain
- Plate 4.5.-5 Results of in-situ stress determinations in well USW G-1, Yucca Mountain
- Plate 4.5.-6 Results of in-situ stress determinations in well USW G-2, Yucca Mountain
- Plate 4.5.-7 Results of in-situ stress determinations in well USW G-3, Yucca Mountain
- Plate 4.5.-8 Results of in-situ stress determinations in well UE-25p #1, Yucca Mountain
- Plate 4.6.2.-1 Location of wells where in-situ temperature measurements were performed
- Plate 4.6.2.-2 Composite temperature profile, Pahute Mesa
- Plate 4.6.2.-3 Composite temperature profile, Rainier Mesa and environments
- Plate 4.6.2.-4 Composite temperature profile, Yucca Flat area
- Plate 4.6.2.-5 Composite plot of temperatures below 100 m, Syncline Ridge area
- Plate 4.6.2.-6 Composite temperature profile, for the Southern Nevada Test Site
- Plate 4.6.2.-7 Temperatures in wells deeper than 600 m, Yucca Mountain
- Plate 4.6.2.-8 Temperatures from UE-25a1 and the "conductor holes," Yucca Mountain Pahute Mesa
- Plate 4.6.3.-1 Intensities of heat flow in near ground surface rocks at the Nevada Test Site
- Plate 4.6.3.-2 Intensities of heat-flow at the Nevada Test Site
- Plate 4.6.3.-3 Map of Western United States showing intensities of heat flow
- Plate 4.6.4.-1 Location of boreholes where calcite samples from Yucca Mountain were collected
- Plate 4.6.4.-2 Analytical data from fracture filling calcites from Yucca Mountain
- Plate 4.6.4.-2a Analytical data from fracture filling calcites from Yucca Mountain (cont.)
- Plate 4.6.4.-3 Calculated uranium series ages of fracture filling calcite from Yucca Mountain
- Plate 4.6.4.-4 Plot of  $\delta^{18}\text{O}$  vs.  $\delta^{13}\text{C}$  values of calcites from Yucca Mountain

- Plate 4.6.4.-5 Estimate of paleo-temperatures based on stable isotope content of calcites from Yucca Mountain
- Plate 4.6.4.-6 Comparison of contemporary and Late Quaternary in-situ temperatures at Yucca Mountain
- Plate 4.7.1.-1 Potential increase in pore pressure caused by vibratory ground motion
- Plate 4.7.1.-2 Assumed initial in-situ stress configuration along a fracture
- Plate 4.7.1.-3 Perturbation of the in-situ stress caused by local build-up of pore pressure
- Plate 4.7.1.-4 Perturbation of the in-situ stress caused by local build-up of pore pressure and resulting change in hydraulic parameters
- Plate 4.7.2.-1 Location of detonation site of the Bilby nuclear device
- Plate 4.7.2.-2 Dynamic fluid overpressure caused by the Bilby shock wave
- Plate 4.7.2.-3 Fluid level rise in U-3cn PS #2
- Plate 4.7.2.-4 Location of detonation site of the Handley nuclear device
- Plate 4.7.2.-5 Location of off-site wells monitored during the Handley Event
- Plate 4.7.2.-6 Dynamic fluid overpressure produced by the shock wave of the Handley detonation
- Plate 4.7.2.-7 Location of monitoring wells in the Pahute Mesa, Handley detonation
- Plate 4.7.2.-8 Hydrologic response in Pahute Mesa to the Handley detonation
- Plate 4.7.2.-9 Hydrologic response to the Handley Event in well UE-20f
- Plate 4.7.2.-10 Hydrologic response to the Handley Event in well UE-20p
- Plate 4.7.3.-1 Increased discharge from a seep caused by the April 10, 1986, nuclear detonation
- Plate 4.7.3.-2 Change in aqueous chemistry caused by the April 6, 1985, detonation
- Plate 4.7.3.-3 Change in aqueous chemistry caused by the April 6, 1985, detonation
- Plate 4.7.3.-4 Change in aqueous chemistry caused by the April 10, 1986 nuclear detonation
- Plate 4.7.3.-5 Change in aqueous chemistry caused by the April 10, 1987, nuclear detonation
- Plate 4.7.3.-6 Stiff diagrams of aqueous chemistry before and after the April 6, 1985, nuclear detonation

- Plate 4.7.3.-7** Stiff diagrams of aqueous chemistry before and after the April 10, 1986, nuclear detonation
- Plate 4.7.3.-8** Change in deuterium content caused by two nuclear detonations
- Plate 4.7.3.-9** Change in oxygen-18 content caused by two nuclear detonations
- Plate 4.7.4.-1** Mohr's representation of stresses in two dimensions and combined Griffith/Navier-Coulomb failure envelope
- Plate 4.7.4.-2** Constitutive relationship between hydraulic conductivity of fracture and pore pressure
- Plate 4.7.4.-3** Idealization of relationship between velocity of slug movement and value of pore pressure for different assumed in-situ stress conditions
- Plate 4.7.4.-4** Location of wells where the Cooper-Brederhoeft injection tests were performed
- Plate 4.7.4.-5** Results of the Cooper-Brederhoeft injection tests in well USW H-1
- Plate 4.7.4.-5a** Results of the Cooper-Brederhoeft injection tests in well USW H-1
- Plate 4.7.4.-5b** Results of the Cooper-Brederhoeft injection tests in well USW H-1
- Plate 4.7.4.-6** Results of the Cooper-Brederhoeft injection tests in well USW H-3
- Plate 4.7.4.-6a** Results of the Cooper-Brederhoeft injection tests in well USW H-3
- Plate 4.7.4.-7** Results of the Cooper-Brederhoeft injection tests in well USW H-4
- Plate 4.7.4.-7a** Results of the Cooper-Brederhoeft injection tests in well USW H-4
- Plate 4.7.4.-7b** Results of the Cooper-Brederhoeft injection tests in well USW H-4
- Plate 4.7.4.-7c** Results of the Cooper-Brederhoeft injection tests in well USW H-4
- Plate 4.7.4.-7d** Results of the Cooper-Brederhoeft injection tests in well USW H-4
- Plate 4.7.4.-7e** Results of the Cooper-Brederhoeft injection tests in well USW H-4
- Plate 4.7.4.-7f** Results of the Cooper-Brederhoeft injection tests in well USW H-4
- Plate 4.7.4.-7g** Results of the Cooper-Brederhoeft injection tests in well USW H-4
- Plate 4.7.4.-8** Results of the Cooper-Brederhoeft injection tests in well USW H-5
- Plate 4.7.4.-8a** Results of the Cooper-Brederhoeft injection tests in well USW H-5

Plate 4.7.4.-8b Results of the Cooper-Bredehoeft injection tests in well USW H-5

Plate 4.7.4.-8c Results of the Cooper-Bredehoeft injection tests in well USW H-5

Plate 4.7.4.-8d Results of the Cooper-Bredehoeft injection tests in well USW H-5

Plate 4.7.4.-8e Results of the Cooper-Bredehoeft injection tests in well USW H-5

Plate 4.7.4.-9 Results of the Cooper-Bredehoeft injection tests in well USW H-6

Plate 4.7.4.-9a Results of the Cooper-Bredehoeft injection tests in well USW H-6

Plate 4.7.4.-9b Results of the Cooper-Bredehoeft injection tests in well USW H-6

Plate 4.7.4.-9c Results of the Cooper-Bredehoeft injection tests in well USW H-6

Plate 4.7.4.-9d Results of the Cooper-Bredehoeft injection tests in well USW H-6

Plate 4.7.4.-9e Results of the Cooper-Bredehoeft injection tests in well USW H-6

Plate 4.7.4.-10 Results of the Cooper-Bredehoeft injection tests in well UE-25b #1

Plate 4.7.4.-10a Results of the Cooper-Bredehoeft injection tests in well UE-25b #1

Plate 4.7.4.-10b Results of the Cooper-Bredehoeft injection tests in well UE-25b #1

Plate 4.7.4.-10c Results of the Cooper-Bredehoeft injection tests in well UE-25b #1

Plate 4.7.4.-10d Results of the Cooper-Bredehoeft injection tests in well UE-25b #1

Plate 4.7.4.-10e Results of the Cooper-Bredehoeft injection tests in well UE-25b #1

Plate 4.7.4.-10f Results of the Cooper-Bredehoeft injection tests in well UE-25b #1

Plate 4.7.4.-11 Results of the Cooper-Bredehoeft injection tests in well UE-25p #1

Plate 4.7.4.-11a Results of the Cooper-Bredehoeft injection tests in well UE-25p #1

Plate 4.7.4.-11b Results of the Cooper-Bredehoeft injection tests in well UE-25p #1

Plate 4.7.4.-11c Results of the Cooper-Bredehoeft injection tests in well UE-25p #1

Plate 4.7.4.-11d Results of the Cooper-Bredehoeft injection tests in well UE-25p #1

Plate 4.7.4.-11e Results of the Cooper-Bredehoeft injection tests in well UE-25p #1

Plate 4.7.4.-11f Results of the Cooper-Bredehoeft injection tests in well UE-25p #1

Plate 4.7.4.-11g Results of the Cooper-Bredehoeft injection tests in well UE-25p #1

- Plate 4.7.4.-11h Results of the Cooper-Bredehoeft injection tests in well UE-25p #1
- Plate 4.7.4.-11i Results of the Cooper-Bredehoeft injection tests in well UE-25p #1
- Plate 4.7.4.-11j Results of the Cooper-Bredehoeft injection tests in well UE-25p #1
- Plate 4.7.4.-11k Results of the Cooper-Bredehoeft injection tests in well UE-25p #1
- Plate 4.7.4.-11l Results of the Cooper-Bredehoeft injection tests in well UE-25p #1
- Plate 4.7.4.-11m Results of the Cooper-Bredehoeft injection tests in well UE-25p #1
- Plate 4.7.4.-12 Results of the Cooper-Bredehoeft injection tests in well USW G-4
- Plate 4.7.4.-12a Results of the Cooper-Bredehoeft injection tests in well USW G-4
- Plate 4.7.4.-12b Results of the Cooper-Bredehoeft injection tests in well USW G-4
- Plate 4.7.4.-12c Results of the Cooper-Bredehoeft injection tests in well USW G-4
- Plate 4.7.4.-12d Results of the Cooper-Bredehoeft injection tests in well USW G-4
- Plate 4.7.4.-12e Results of the Cooper-Bredehoeft injection tests in well USW G-4
- Plate 4.7.4.-12f Results of the Cooper-Bredehoeft injection tests in well USW G-4
- Plate 4.8.-1 Location of faults containing calcite-silica veins of Quaternary age - Yucca Mountain
- Plate 4.8.-2 Geologic section across Yucca Mountain showing location and thickness of breccias
- Plate 4.8.-3 Comparison of stable isotope composition of three surface samples of calcite-silica veins to isotopic composition of calcite veins from subsurface
- Plate 4.8.-4 Comparison of temperature of formation of calcite-silica deposits, based on isotopic composition of three samples, with contemporary temperature at Yucca Mountain
- Plate 4.8.-5 Location of samples analyzed and dated by Szabo, et.al., 1981
- Plate 4.8.-6 Analytical data and uranium series ages of carbonates at the Nevada Test Site
- Plate 4.8.-6a Analytical data and uranium series ages of carbonates at the Nevada Test Site (cont.)
- Plate 4.8.-6b Analytical data and uranium series ages of carbonates at the Nevada Test Site (cont.)
- Plate 4.8.-6c Analytical data and uranium series ages of carbonates at the Nevada Test Site (cont.)

- Plate 4.8.-7**      **Location map of samples analysed and dated by Knauss (1981)**
- Plate 4.8.-8**      **Radiometric ages of samples of travertine and tuffaceous travertine analyzed by Knauss (1981)**
- Plate 4.8.-9**      **Location map - sampling Site 4**
- Plate 4.8.-10**     **Idealization of contemporary and paleo-hydrologic situation between Death Valley and Amargosa Desert**
- Plate 4.8.-11**    **Comparison of ages of travertines from Nevada Test Site with global temperature fluctuations during Pleistocene**

## REFERENCES

- Aggarwal, Y.P., Sykes, L.R., Armbruster, J., and Sbar, M.L., 1973. Premonitory Changes in Seismic Velocities and Prediction of Earthquakes, Nature 241.
- Barton, N., Bandis, S., and Bakhter, K., 1985. Strength, Deformation and Conductivity Coupling of Rock Joints. Int. J., Rock Mech. Min. Sci. and Geomech. Abstr., 22, 3.
- Bentley, C.B., 1984. Geohydrologic Data for Test Well USW G-4, Yucca Mountain Area, Nye County, Nevada. USGS-OFR-84-063, Open-File Report, U.S. Geological Survey, Denver, Colo.
- Bentley, C.B., Robison, J.H., and Spengler, R.W., 1983. Geohydrologic Data for Test Well USW H-5, Yucca Mountain Area, Nye County, Nevada. USGS-OFR-83-853, Open-File Report, U.S. Geological Survey, Denver, Colo.
- Bergman, S.C., 1982. Petrogenetic Aspects of the Alkali Basaltic Lavas and Included Mega Crystals and Nodules from the Lunar Crater Volcanic Field, Nevada, U.S.A. Ph.D. Dissertation, Princeton University.
- Best, M.G., and Brimhall, W.H., 1974. Late Cenozoic Basaltic Magmas in the Western Colorado Plateaus and the Basin and Range Transition Zone, U.S.A., and Their Bearing on Mantle Dynamics. Geol. Soc. Am. Bull. 85.
- Birdwell, R.J., 1978. The Rio Grande Rift and a Diapiric Mechanism for Continental Rifting. Tectonics and Geophysics of Continental Rifts. Ramberg, I.B., and Neumann, E.R., (eds).
- Birdwell, R.J., and Potzick, C., 1981. Thermal Regimes, Mantle Diapirs and Crustal Stresses of Continental Rifts. Tectonophysics, 73.
- Blankennagel, R.K., and Weir, J.E., Jr., 1973. Geohydrology of the Eastern Part of Pahute Mesa, Nevada Test Site, Nye County, Nevada, U.S. Geological Survey Professional Paper 712-B, Washington, D.C.
- Brady, B.T., 1974. Theory of Earthquakes, I. A Scale Independent Theory of Rock Failure. Birkhauser Verlag, Basel. Pageoph, Vol. 112.
- Brady, B.T., 1975. Theory of Earthquakes, II. Inclusion Theory of Crustal Earthquakes. Birkhauser Verlag, Basel. Pageoph, Vol. 113.
- Brady, B.T., 1976. Theory of Earthquakes, Part III. Inclusion Collapse Theory of Deep Earthquakes. Birkhauser Verlag, Basel. Pageoph, Vol. 114.
- Carr, W.J., 1984. Regional Structural Setting of Yucca Mountain, Southwestern Nevada, and Late Cenozoic Rates of Tectonic Activity in Part of the Southwestern Basin, Nevada and California, USGS-OFR-84-854, Open-File Report, U.S. Geological Survey, Denver, Colo.
- Carr, M.D., Waddell, S.J., Vick, G.S., Stock, J.M., Monsen, S.A., Harris, A.G., Cork, B.W., and Byers, F.M., Jr., 1986. Geology of Drill Hole UE25p 1: A Test Hole into Pre-Tertiary Rocks near Yucca Mountain, Southern Nevada, USGS-OFR-86-175, Open-File Report, U.S. Geological Survey, Menlo Park, Calif.
- Chapin, C.E., 1971. The Rio Grande Rift, Part 1, Modifications and Additions. New Mex. Geol. Soc. Guideb. - San Luis Basin, 22nd Field Conf.

- Corchary, G.S., Dinwiddie, G.A., 1975. Field Trip to Nevada Test Site. U.S. Geological Survey.
- Craig, R.W., Reed, R.L., and Spengler, R.W., 1983. Geohydrologic Data for Test Well USW H-6 Yucca Mountain Area, Nye County, Nevada. USGS-OFR-83-856, Open-File Report, U.S. Geological Survey, Denver, Colo.
- Craig, R.W., and Robinson, J.H., 1984. Geohydrology of Rocks Penetrated by Test Well UE-25p #1, Yucca Mountain Area, Nye County, Nevada. USGS-WRI-84-4248, Water-Resources Investigations Report, U.S. Geological Survey, Denver, Colo.
- Crowe, B.M., and Vaniman, D.T., (comps.), 1985. Research and Development Related to the Nevada Nuclear Waste Storage Investigations, January 1 - March 31, 1984. LA-10154-PR, Los Alamos National Laboratory, Los Alamos, N. Mex.
- Crowe, B.M., Wohletz, K.H., Vaniman, D.T., Gladney, E., and Bower, N., 1986. Status of Volcanic Hazard Studies for the Nevada Nuclear Waste Storage Investigations. LA-9325-MS, Vol. II, Los Alamos National Laboratory, Los Alamos, N. Mex.
- Czarnecki, J.B., 1987. Should the Furnace Creek Ranch - Franklin Lake Playa Ground-Water Subbasin Simply Be the Franklin Lake Playa Ground-Water Subbasin? Amer. Geophys. Union, (abs.).
- Czarnecki, J.B., and Waddell, R.K., 1984. Finite-Element Simulation of Ground-Water Flow in the Vicinity of Yucca Mountain, Nevada-California. USGS-WRI-84-4349, Water-Resources Investigations Report, U.S. Geological Survey, Denver, Colo.
- DeBoer, J., 1967. Paleomagnetic Tectonic Study of Mesozoic Dike Swarm in the Appalachians. Jour. Geophys. Res., V.72, No. 8.
- DePaolo, D.J., 1978. Study of Magma Sources, Mantle Structure, and the Differentiation of the Earth Using Variations of  $^{143}\text{Nd}/^{144}\text{Nd}$  in Igneous Rocks. Ph.D. Thesis, Cal. Tech.
- DOE. (U.S. Department of Energy), 1984. Draft Environmental Assessment, Yucca Mountain Site, Nevada Research and Development Area, Nevada. DOE/RW-0012, Washington, D.C.
- Donath, F., 1982. The isolation of High-Level Nuclear Wastes in a Geologic Repository. Radiation Research, 91.
- Dudley, W.W., Wollitz, L.E., Jr, Baldwin, D.A., Claassen, H.C., 1971. Geologic and Hydrologic Effects of the Handley Event, Pahute Mesa, Nevada Test Site (Effects on Wells and Aquifers). USGS-474-95.
- Eakin, T.E., Schoff, S.L., Cohen, P., 1963. Regional Hydrology of a Part of Southern Nevada: A Reconnaissance. USGS-TEI-833, Trace Elements Investigations Report, U.S. Geological Survey, Denver, Colo.
- Ellis, W.L., and Magner, J.E., 1980. Compilation of Results of Three-Dimensional Stress Determinations Made in Rainier and Aqueduct Mesas, Nevada Test Site, Nevada, USGS-OFR-80-1098, Open-File Report, U.S. Geological Survey, Reston, Va.
- Ellis, W.L., and Ege, J.R., 1976. Determination of In-Situ Stress in U12g Tunnel, Rainier Mesa, Nevada Test Site, Nevada. USGS-474-219.
- Frank, F.C., 1965. On Dilatancy in Relation to Seismic Sources. Rev. Geophys. 3,484-503.

- Friedman, I., 1970. Some Investigations of the Deposition of Travertine from Hot Springs - I. The Isotopic Composition of a Travertine-Depositing Spring. *Geochemical et. Cosmochimica Acta*, V.34.
- Garber, M.S., 1971. Hydraulic Test and Quality of Water Data from Hole U-3cr PS #2, Bilby Site, Nevada Test Site. USGS-474-105.
- Green, D.H., Edgar, A.D., Beasley, P., Kiss, E., Ware, N.G., 1974. Upper Mantle Source for Some Hawaiites, Mugearites, and Benmoreites. *Contrib. Min. Petrol.*, V.48.
- Greensfelder, R.W., Kintzer, F.C., Somerville, M.R., 1980. Seismotectonic Regionalization of the Great Basin and Comparison of Moment Rates Computed from Holocene Strain and Historic Seismicity. *Geological Society of America Bulletin Part II*, Vol. 91, pp. 2039-2111.
- Haimson, B.C., 1981. A Comparative Study of Deep Hydrofracturing and Overcoring Stress Measurements at Six Locations with Particular Interest to the Nevada Test Site. U.S. National Committee for Rock Mechanics. National Academy of Sciences.
- Haimson, B.C., Lacoumb, J., Jones, A.H., and Green, S.J., 1974. Deep Stress Measurements in Tuff at the Nevada Test Site. *Advances in Rock Mechanics*, Vol IIa, National Academy of Sciences.
- Harper, T.R., and Last, N.C., 1987. Numerical Modelling of Fracture System Hydraulic Conductivity Changes During Fluid Injection. Workshop on forced fluid flow through "strong" fractured rock masses, Gerchy, France. For submission to *Annales Geophysicae*. Now: Koninklijke/Shell Exploratie en Productie Laboratorium.
- Harper, T.R., and Szymanski, J.S., 1982. Complex Geologic Characterization of the Repository Environment. *Underground Space*, Vol. 6. Pergamon Press, Ltd.
- Harper, T.R., and Szymanski, J.S., 1980. A Perspective of Geological Characterizations Required for Subsurface Nuclear Waste Disposal. *Subsurface Space*, Proceedings of the International Symposium (Rockstore '80), Stockholm, Sweden, Bergman, M. (ed.).
- Heath, R.C., 1984. Ground-water Regions of the United States, Geological Survey Water Supply Paper 2242, U.S. Geological Survey, Washington, D.C.
- Hsu, K.J., 1978. When the Black Sea Was Drained. *Scientific American*, 238, 5:52-63.
- Hoover, D.L., 1968. Genesis of Zeolites, Nevada Test Site, Nevada Test Site, E.B. Eckel (ed.), Geological Society of America Memoir 110.
- Hoover, D.L., Swadley, W.C., and Gordon, A.J., 1981. Correlation Characteristics of Surficial Deposits with a Description of Surficial Stratigraphy in the Nevada Test Site Region. USGS-OFR-81-512, Open-File Report, U.S. Geological Survey, Denver, Colo.
- Lahoud, R.G., Lobmeyer, D.H., and Whitfield, M.S., Jr., 1984. Geohydrology of Volcanic Tuff Penetrated by Test Well UE-25b-1, Yucca Mountain, Nye County, Nevada. USGS-WRI-84-4253, Water-Resources Investigations Report, U.S. Geological Survey, Denver, Colo.
- Leeman, W.P., 1982. Tectonic and Magmatic Significance of Strontium Isotopic Variations in Cenozoic Volcanic Rocks from the Western United States. *Geol. Soc. Amer. Bull.*, V. 93.
- Lipman, P.W., 1969. Alkalic and Tholeiitic Basaltic Volcanism Related to the Rio Grande Depression, Southern Colorado and Northern New Mexico. *Geol. Soc. Am. Bull.* 80.

- Lobmeyer, D.H., Whitfield, M.S., Lahoud, R.R., and Bruckheimer, L., 1983. Geohydrologic Data for Test Well UE-25b #1, Nevada Test Site, Nye County, Nevada. USGS-OFR-83-855, Open-File Report, U.S. Geological Survey, Denver, Colo.
- Lomnitz, C., 1974. Global Tectonics and Earthquake Risk, Developments in Geotectonics 5, Elsevier Scientific Publishing Company.
- Maldonado, F., 1958. Geologic Map of the Jackass Flatts Area, Nye County, Nevada. Miscellaneous Investigations Series Map I-1519, U.S. Geological Survey, Denver, Colo.
- Menzies, M.A., and Murthy, V.R., 1980. Nd and Sr Isotope Geochemistry of Hydrous Mantle Nodules and Their Host Alkali Basalts: Implications for Local Heterogeneities in Metasomatically-Veined Mantle. Earth Plan. Sci. Lett., V. 46.
- Miller, C.H., Miller, D.R., Ellis, W.L., and Ege, J.R., 1975. Determination of In Situ Stress at U12e-18 Working Point, Rainier Mesa, Nevada Test Site. USGS-474-217.
- Monfort, M.E., and Evans, J.R., 1982. Three-Dimensional Modeling of the Nevada Test Site and Vicinity From Teleseismic P-Wave Residuals. USGS-OFR-82-409.
- Moody, J.D., and Hill, M.J., 1956. Wrench-Fault Tectonics. Geol. Soc. Am. Bull., V.67, No.9.
- Morris, R.H., 1971. Geologic and Hydrologic Effects of the Handley Event, Pahute Mesa, Nevada Test Site. (Geologic Effects) USGS-474-95.
- Nur, A., 1972. Dilatancy, Pore Fluids and Premonitory Variations of ts/tp travel times. Bull. Seismal. Soc. Am. 62.
- O'Neil, J.R., 1984. Letter Report from J.R. O'Neil (USGS) to D. Vaniman (LANL), December 19, 1984; regarding stable isotope analyses of three samples from Yucca Mountain.
- O'Neil, J.R., 1985. Letter Report from J.R. O'Neil (USGS) to S. Levy (LANL), April 29, 1985; regarding stable isotope analysis and oxygen isotope temperatures of samples.
- O'Neil, J.R., Clayton, R.N., and Mayeda, T.K., 1969. Oxygen Isotope Fractionation in Divalent Metal Carbonates. Jour. Chem. Physics, V. 51.
- Price, N.J., 1966. Fault and Joint Development. Pergamon Press, New York.
- Ramsay, J.G., 1967. Folding and Fracturing of Rocks. McGraw-Hill Book Company.
- Reheis, M., 1986. Preliminary Study of Quaternary Faulting on the East Side of Bare Mountain, Nye County, Nevada. USGS-OFR-86-576, Open-File Report, U.S. Geological Survey, Denver Colo. p. 14.
- Robison, J.H., 1984. Ground-Water Level Data and Preliminary Potentiometric-Surface Maps, Yucca Mountain and Vicinity, Nye County, Nevada. USGS-WRI-84-4197, Water-Resources Investigations Report, U.S. Geological Survey, Lakewood, Colo.
- Rogers, A.M., Harmsen, S.C., Carr, W.J., and Spence, W., 1983. Southern Great Basin Seismological Data Report for 1981 and Preliminary Data Analysis. USGS-OFR-83-669, Open-File Report, U.S. Geological Survey, Denver, Colo.

- Rogers, A.M., Harmsen, S.C., and Meremonte, M., 1987. Evaluation of the Seismicity of the Southern Great Basin and Its Relationship to the Tectonic Framework of the Region. USGS-OFR-87, Open-File Report, U.S. Geological Survey, Denver, Colo.
- Ross, B., 1984. A Conceptual Model of Deep Unsaturated Zones with Negligible Recharge. Water Resources Research, Vol. 20, No. 11.
- Rush, F.E., Thordarson, W., and Bruckheimer, L., 1983. Geohydrologic and Drill-Hole Data for Test Well USW H-1, Adjacent to Nevada Test Site, Nye County, Nevada. USGS-OFR-83-141, Open-File Report, U.S. Geological Survey, Denver, Colo.
- Rush, F.E., Thordarson, W., and Pyles, D.G., 1984. Geohydrology of Test Well USW H-1, Yucca Mountain, Nye County, Nevada. Investigations Report USGS-WRI-84-4032, U.S. Geological Survey, Denver, Colo.
- Russell, C.E., 1987. Hydrogeologic Investigations of Flow in Fractured Tuffs, Rainier Mesa, Nevada Test Site. M.S. Thesis, University of Nevada.
- Sadovsky, M.A., Nersesow, I.L., Nigmatullaev, S.K., Latynina, L.A., Lukk, A.A., Semenov, A.N., Simbireva, I.G., and Vlomov, R.I., 1972. The Process Preceding Strong Earthquakes in Some Regions of Middle Asia. Tectonophysics, 14.
- SAIC (Science Application International Corporation), 1985. Tectonic Stability and Expected Ground Motion at Yucca Mountain, Report of a Workshop at SAIC - La Jolla August 7-8, 1984 and January 25-26, 1985. DOE/NV/10270-2 (Rev. 1).
- Sass, J.H., and Lachenbruch, H., 1982. Preliminary Interpretation of Thermal Data from the Nevada Test Site. USGS-OFR-82-973, Open-File Report, U.S. Geological Survey, Denver, Colo.
- Sass, J.H., Lachenbruch, A.H., Munroe, R.J., Greene, G.W., and Moses, T.H., Jr., 1971. Heat Flow in the Western United States. Journal of Geophysical Research, Vol. 76, No. 26, pp. 6376-6413.
- Sass, J.H., Diment, W.H., Lachenbruch, A.H., Marshall, B.V., Munroe, R.J., Moses, T.H., Jr., and Urban, T.C., 1976. A New Heat-Flow Contour Map of the Conterminous United States. USGS-OFR-76-756, Open-File Report, U.S. Geological Survey.
- Sass, J.H., Lachenbruch, A.H., and Mase, C.W., 1980. Analysis Of Thermal Data From Drill Holes UE-24a3 and UE-25a-1, Calico Hills and Yucca Mountain, Nevada Test Site. USGS-OFR-80-826, Open-File Report, U.S. Geological Survey.
- Scholz, C.H. and Kranz, R., 1974. Notes on Dilatancy Recovery. Jour. Geophys. Res. 79. No. 14.
- Scholz, C.H., Sykes, L.R., and Aggarwal, Y.P., 1973. The Physical Basis for Earthquake Prediction. Science 181, No. 4102.
- Schoff, S.L., and Moore, J.E., (Comps.) 1964. Chemistry and Movement of Ground Water, Nevada Test Site. USGS-TEI-838, U.S. Geological Survey, Denver, Colo.
- Scott, R.B., 1984. Internal Deformation of Blocks Bounded by Basin-and Range Style Faults. Geological Society of America, Abstracts with Programs, Vol. 16, no. 6, p. 649.
- Scott, R.B., 1986. Extensional Tectonics at Yucca Mountain, Southern Nevada. Geological Society of America, Abstracts with Programs, 1986, Rocky Mountain Section, Flagstaff, Ariz., April 30-May 2, 1986, Vol. 18, No. 5, p.411.

- Scott, R.B., and Bonk, J., 1984. Preliminary Geologic Map of Yucca Mountain, Nye County, Nevada, with Geologic Sections. USGS-OFR-84-494, Open-File Report, U.S. Geological Survey, Denver, Colo.
- Scott, R.B., and Rosenbaum, J.G., 1986. Evidence of Rotation about a Vertical Axis during Extension at Yucca Mountain, Southern Nevada. Transactions, American Geophysical Union, EOS, Vol. 67, No. 16, p. 358.
- Semenov, A.M., 1969. Variations in Travel Time of Transverse and Longitudinal Waves Before Violent Earthquakes. *Isv. Earth Physics*, 4.
- Sibson, R.H., Moore, J. M<sup>c</sup>M., and Rankin, A.H., 1975. Seismic Pumping - a Hydrothermal Fluid Transport Mechanism. *Jl. Geol. Soc. Lond.*, Vol. 131.
- Smith, W.C., Vollendorf, W.C., and Warren, W.E., 1980. In-Situ Stress from Hydraulic Fracture Measurements in G Tunnel, Nevada Test Site. Sandia National Laboratories Report, SAND 80-1138.
- Stewart, J.H., Albers, J.P., and Poole, F.G., 1986. Summary of Regional Evidence for Right-Lateral Displacement in the Western Great Basin. *Geological Society of America Bulletin*, Vol. 79, No. 10, pp. 1407-1414.
- Stewart, J.H., 1985. East-Trending Dextral Faults in the Western Great Basin: An Explanation for Anomalous Trends of Pre-Cenozoic Strata and Cenozoic Faults. *Tectonics*, Vol. 4, No. 6, pp. 546-564.
- Stock, J.M., Healy, J.H., Hickman, S.H., and Zoback, M.D., 1985. Hydraulic Fracturing Stress Measurements at Yucca Mountain, Nevada, and Relationship to the Regional Stress Field. *Journal of Geophysical Research*, Vol. 90, No. B10, pp. 8691-8706.
- Stock, J.M., Healy, J.H., Svitek, J., and Mastin, L., 1986. Report on Televiwer Log and Stress Measurements in Holes USW G-3 and UE-25p #1, Yucca Mountain, Nye County, Nevada. USGS-OFR-86-369, Open-File Report, U.S. Geological Survey, Menlo Park, Calif.
- Swadley, W.C., Hoover, D.L., and Rosholt, J.N., 1984. Preliminary Report on Late Cenozoic Faulting and Stratigraphy in the Vicinity of Yucca Mountain, Nye County, Nevada. USGS-OFR-84-788, Open-File Report, U.S. Geological Survey, Denver, Colo.
- Szabo, B.J., 1984. Uranium-Series Dating of Fault-Related Fracture and Cavity-Filling Calcite and Opal in Drill Cores from Yucca Mountain, Southern Nevada. *Geological Society of America, Abstracts with Programs, Annual Meeting, Reno, Nev., November 5-8, 1984*, Vol. k16, No. 6, pp. 672-673.
- Szabo, B.J., and Kyser, T.K., 1985. Uranium, Thorium Isotopic Analyses and Uranium-Series Ages of Calcite and Opal, and Stable Isotopic Compositions of Calcite from Drill Cores UE-25a 1, USW G-2, and USW G-3/GU3, Yucca Mountain Nevada. USGS-OFR-85-224, Open-File Report, U.S. Geological Survey, Denver, Colo.
- Szabo, B.J., and O'Malley, P.A., 1985. Uranium-Series Dating of Secondary Carbonate and Silica Precipitates Relating to Fault Movements in the Nevada Test Site Region and of Caliche and Travertine Samples from the Amargosa Desert. USGS-OFR-85-47, Open-File Report, U.S. Geological Survey, Denver, Colo.

- Szabo, B.J.; Carr, W.J.; and Gottschall, W.C., 1981. Uranium-Thorium Dating of Quarternary Carbonate Accumulations in the Nevada Test Site Region, Southern Nevada. USGS-OFR-81-119, Open-File Report, U.S. Geological Survey, Denver, Colo.
- Szymanski, J.S., and Harper, T.R., 1980. Assessment of the Future Evolution of Geologic Systems Intended for the Development of a Nuclear Waste Repository. Proceedings of the International Symposium (Rockstore '80), Stockholm, Sweden. Bergman, M. (ed.)
- Thordarson, W., Rush, F.E., and Waddell, S.J., 1985. Geohydrology of Test Well USW H-3, Yucca Mountain, Nve County, Nevada. USGS-WRI-84-4272, Water-Resources Investigations Report, U.S. Geological Survey, Lakewood, Colo.
- Thordarson, W., and Robison, B.P., 1971. Wells and Springs in California and Nevada Within 100 Miles of the Point 37 deg. 15 min. N., 116 deg., 25 min. W., on Nevada Test Site. USGS-474-85, U.S. Geological Survey, Denver, Colo.
- Thordarson, W., 1965. Perched Ground Water in Zeolitized-Bedded Tuff, Rainier Mesa and Vicinity, Nevada Test Site. U.S. Geol. Survey TEI 862.
- Thunvik, R., and Braester, C., 1982. Hydrothermal Conditions Around a Radioactive Waste Repository. Scientific Basis for Nuclear Waste Management V. Materials Research Society Symposia Proceedings, Vol. II, Lutze, W. (ed).
- Vaniman, D.T., Crowe, B.M., and Cladney, E.S., 1982. Petrology and Geochemistry of Hawaiite Lavas from Carter Flat, Nevada. Contributions to Mineralogy and Petrology, Vol 80, Springer-Verlag.
- Waddell, R.K., 1982. Two-Dimensional, Steady-State Model of Ground-Water Flow, Nevada Test Site and Vicinity, Nevada-California. USGS-WRI-82-4085, Water-Resources Investigations Report, U.S. Geological Survey, Denver, Colo.
- Waddell, R.K., 1984. Solute-Transport Characteristics of Fractured Tuffs at Yucca Mountain, Nevada Test Site - A Preliminary Assessment. Geological Society of America Abstracts with Programs, Vol. 16, No. 6, p. 684.
- Walsh, J.B., 1981. Effect of Pore Pressure and Confining Pressure on Fracture Permeability. Int. J. Rock Mech. Min. Sci. Geomech. Abstr., 18.
- Wernicke, B., Spencer, J.E., Burchfiel, B.C., and Guth, P.L., 1982. Magnitude of Crustal Extension in the Southern Great Basin. Geology, Vol. 10.
- Whitcomb, J.A., Garmany, J.D., and Anderson, D.L., 1973. Earthquake Prediction: Variation of Seismic Velocities Before the San Fernando Earthquake. Science, 180.
- White, A.F., 1979. Geochemistry of Ground Water Associated with Tuffaceous Rocks, Oasis Valley, Nevada. US Geological Survey Professional Paper 712-E, Washington, D.C.
- White, A.F., Claassen, H.C., and Benson, L.V., 1980. The Effect of Dissolution of Volcanic Glass on the Water Chemistry in a Tuffaceous Aquifer, Rainier Mesa, Nevada. USGS-WSP1536-Q, Water-Supply Paper, U.S. Geological Survey, Washington, D.C.
- Whitfield, M.S., Jr., Eshom, E.P., Thordarson, W., and Schaefer, D.H., 1985. Geohydrology of Rocks Penetrated by Test Well USW H-4, Yucca Mountain, Nve County, Nevada. USGS-WRI-85-4030, Water-Resources Investigations Report, U.S. Geological Survey, Denver, Colo.

- Whitney, J.W., Shroba, R.R., Simonds, F.W., and Harding, S.T., 1986. Recurrent Quaternary Movement on the Windy Wash Fault, Nye County, Nevada [abs.]. Geological Society of America, Abstracts with Programs, p. 787.
- Wilcox, R.E., Harding, T.P., and Seeley, D.R., 1973. Basic Wrench Tectonics. A.A.P.G. Bul., V. 57, No. 1.
- Winograd, I.J., Szabo, B.J., Riggs, A.C., and Kolesar, P.T., 1985. Two-Million-Year Record of Deuterium Depletion in Great Basin Ground Waters. Science, V.227.
- Winograd, I.J., and Doty, G.C., 1980. Paleohydrology of the Southern Great Basin, with Special Reference to Water Table Fluctuations Beneath the Nevada Test Site During the Late (?) Pleistocene. USGS-OFR-80-569, Open-File Report, U.S. Geological Survey, Reston, Va.
- Winograd, I.J., and Thordarson, W., 1975. Hydrogeologic and Hydrochemical Framework, South-Central Great Basin, Nevada-California, with Special Reference to the Nevada Test Site. U.S. Geological Survey Professional Paper 712-C, Washington, D.C., pp. C1-C126.
- Wood, S.H., 1985. Regional Increase in Groundwater Discharge After the 1983 Idaho Earthquake; Coseismic Strain Release, Tectonic and Natural Hydraulic Fracturing. USGS-OFR-85-290.

TRANSIENT OR NON-EQUILIBRIUM FLOW	STEADY STATE CONDITIONS OF FLOW	<p><u>GOVERNING EQUATION</u></p> <p>CONTINUITY EQUATION. LAW RELATING VELOCITY VECTOR TO THE GRADIENT OF HYDRAULIC POTENTIAL.</p>
		<p><u>BOUNDARY CONDITIONS</u></p> <p>DIRICHLET CONDITIONS; NEUMANN CONDITIONS;AND "MIXED" CONDITIONS.</p>
	<p><u>INITIAL CONDITIONS</u></p> <p>SET OF HYDRAULIC POTENTIAL VALUES AT THE ONSET OF NONEQUILIBRIUM FLOW.</p>	

Mathematical model of "simple" groundwater flow system.

CONTINUITY EQUATION

$$\frac{\delta q_x}{\delta x} + \frac{\delta q_y}{\delta y} + \frac{\delta q_z}{\delta z} = 0$$

DARCY'S LAW

$$q_x = -K \frac{\delta h}{\delta x}; \quad q_y = -K \frac{\delta h}{\delta y}; \quad q_z = -K \frac{\delta h}{\delta z}$$

LAPLACE'S EQUATION

$$\frac{\delta^2 h}{\delta x^2} + \frac{\delta^2 h}{\delta y^2} + \frac{\delta^2 h}{\delta z^2} = 0; \quad \text{OR}$$

$$\nabla^2 h = 0$$

Laplace's equation.

CONTINUITY EQUATION

$$\frac{\delta q_x}{\delta x} + \frac{\delta q_y}{\delta y} + \frac{\delta q_z}{\delta z} = R_{(x,y,z)} \cdot \Delta z^{-1}.$$

DARCY'S LAW

$$q_x = -K \frac{\delta h}{\delta x}; \quad q_y = -K \frac{\delta h}{\delta y}; \quad q_z = -K \frac{\delta h}{\delta z}.$$

POISSON'S EQUATION

$$\frac{\delta^2 h}{\delta x^2} + \frac{\delta^2 h}{\delta y^2} + \frac{\delta^2 h}{\delta z^2} = -R_{(x,y,z)} \cdot T^{-1}; \quad \text{OR}$$

$$\nabla^2 h = -R_{(x,y,z)} \cdot T^{-1}.$$

Poisson's equation.

CONTINUITY EQUATION

$$\frac{\delta q_x}{\delta x} + \frac{\delta q_y}{\delta y} + \frac{\delta q_z}{\delta z} = R_{(x,y,z,t)} \cdot \Delta z^{-1} - S \cdot \Delta z^{-1} \frac{\delta h}{\delta t}$$

DARCY'S LAW

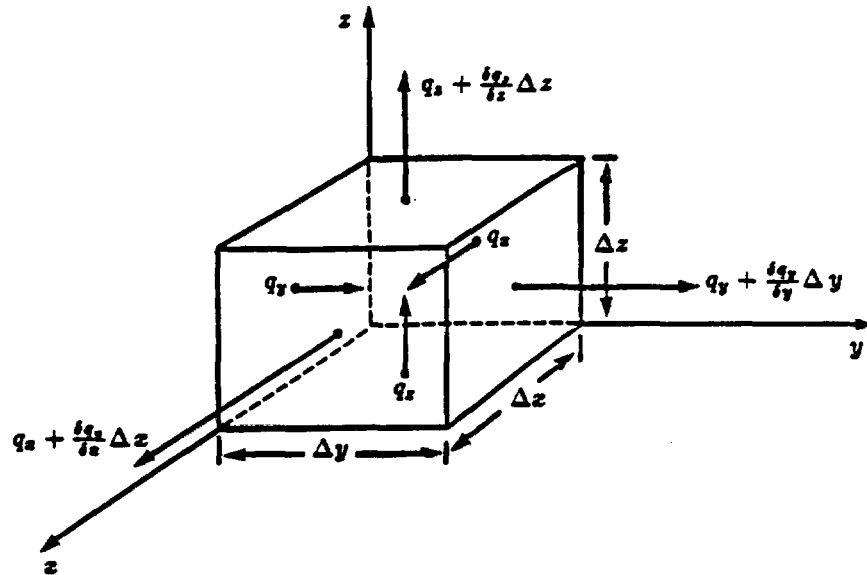
$$q_x = -K \frac{\delta h}{\delta x}; \quad q_y = -K \frac{\delta h}{\delta y}; \quad q_z = -K \frac{\delta h}{\delta z}$$

TRANSIENT FLOW EQUATION

$$\frac{\delta^2 h}{\delta x^2} + \frac{\delta^2 h}{\delta y^2} + \frac{\delta^2 h}{\delta z^2} = S \cdot T^{-1} \frac{\delta h}{\delta t} - R_{(x,y,z,t)} \cdot T^{-1} \quad \text{OR}$$

$$\nabla^2 h = S \cdot T^{-1} \frac{\delta h}{\delta t} - R_{(x,y,z,t)} \cdot T^{-1}$$

Transient flow equation.



$\Delta V = \Delta x \Delta y \Delta z$  - VOLUME;

$\frac{\delta q_x}{\delta x} \Delta x$  - NET CHANGE IN THE DISCHARGE RATE IN x DIRECTION;

$\frac{\delta q_y}{\delta y} \Delta y$  - NET CHANGE IN THE DISCHARGE RATE IN y DIRECTION;

$\frac{\delta q_z}{\delta z} \Delta z$  - NET CHANGE IN THE DISCHARGE RATE IN z DIRECTION;

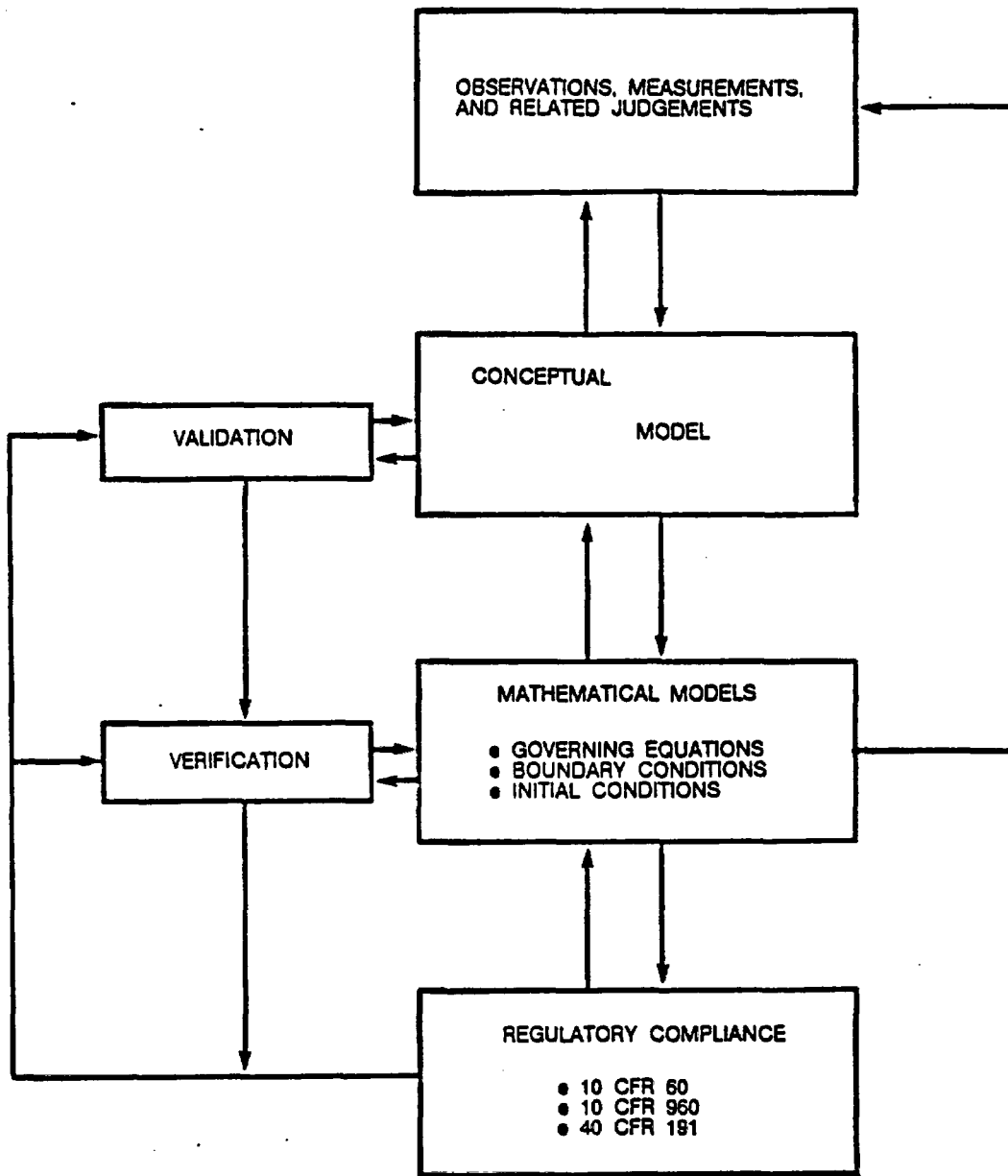
$R_{(x;y;z)}$  - VOLUME OF WATER ADDED PER UNIT TIME PER UNIT AQUIFER VOLUME TO THE INFIMITESIMAL VOLUME AROUND A POINT (x;y;z);

$S = \frac{-\Delta V_w}{\Delta z \Delta y \Delta h}$  - STORETIVITY, REPRESENTS THE VOLUME OF WATER RELEASED FROM STORAGE PER UNIT AREA OF AQUIFER PER UNIT DECLINE IN HEAD;

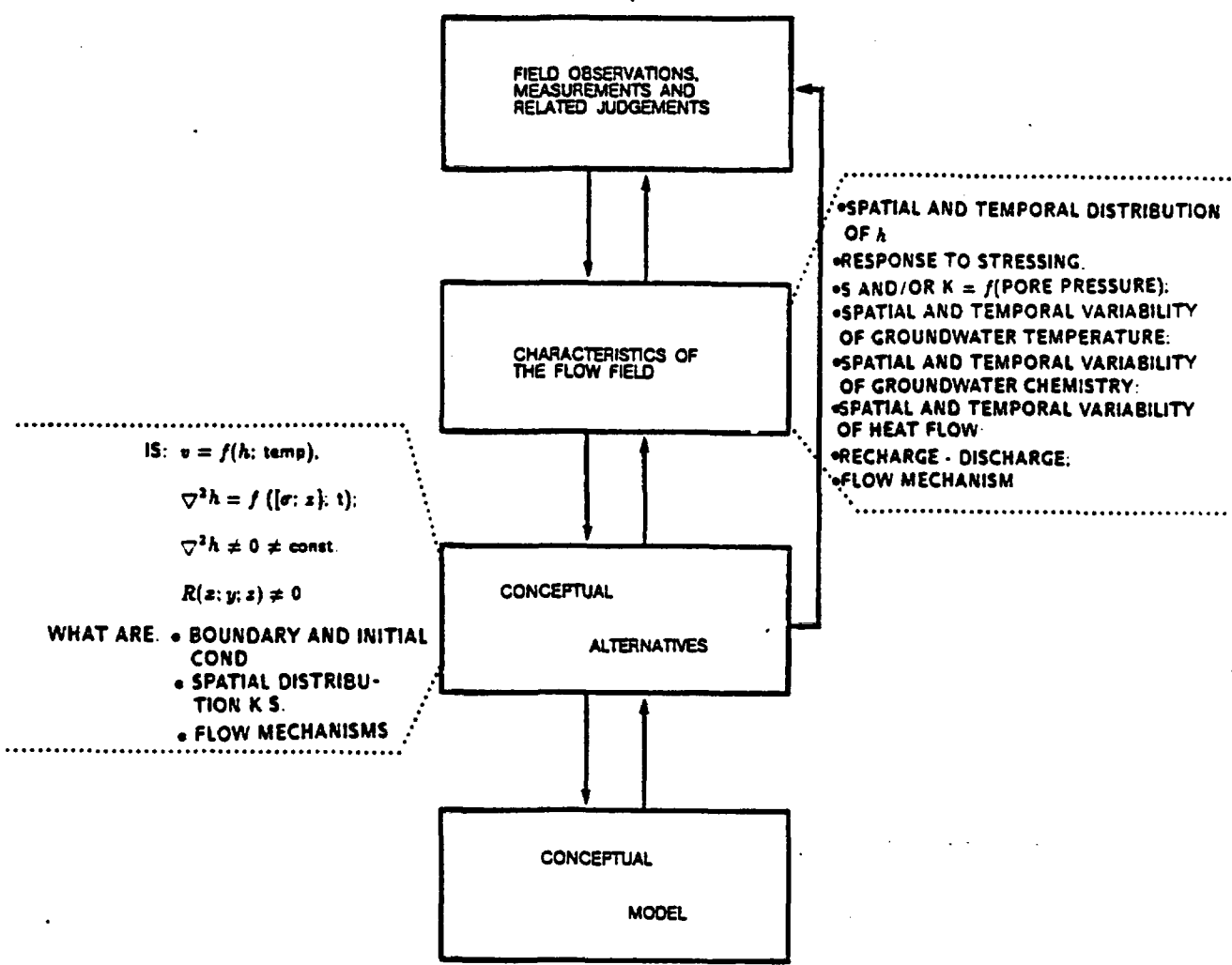
$\frac{\Delta V_w}{\Delta t} = -S \frac{\delta h}{\delta t} \Delta x \Delta y$  - RATE OF RELEASE FROM STORAGE;

$T$  - TRANSMISSIVITY

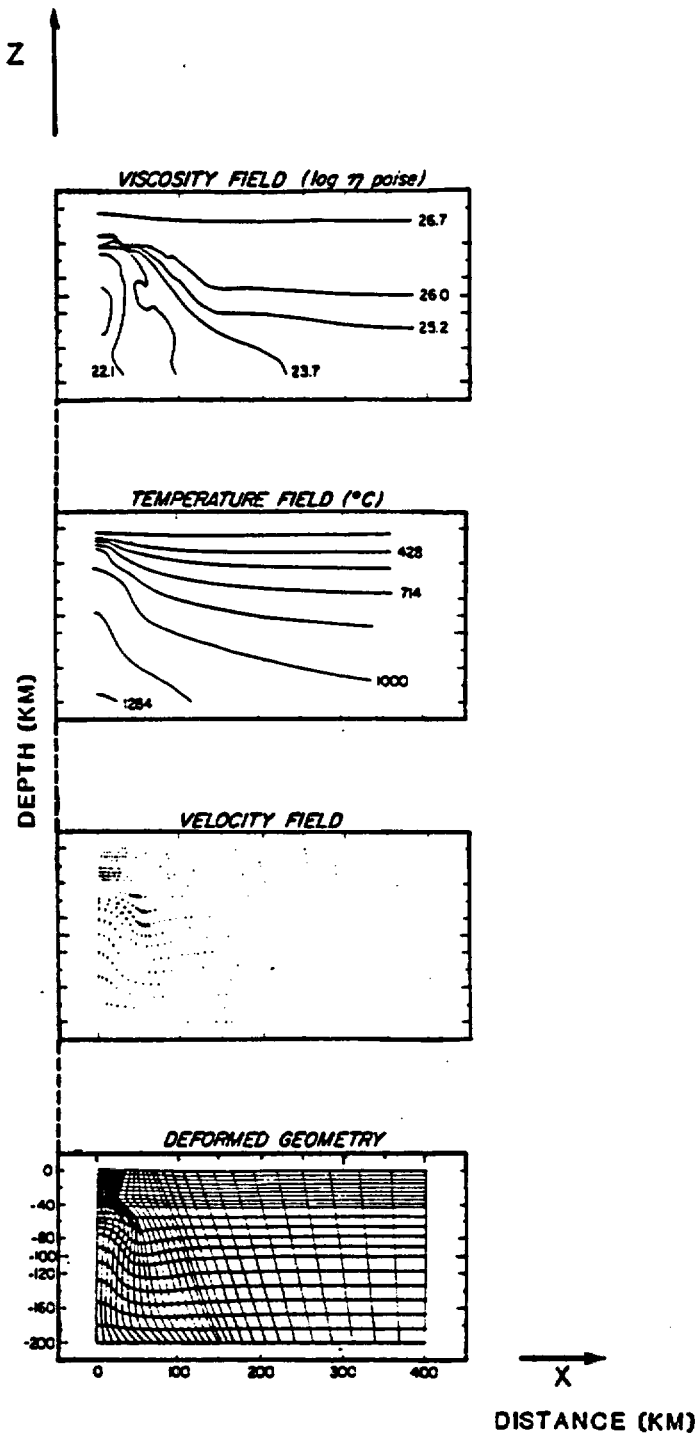
Explanation of mathematical notations.



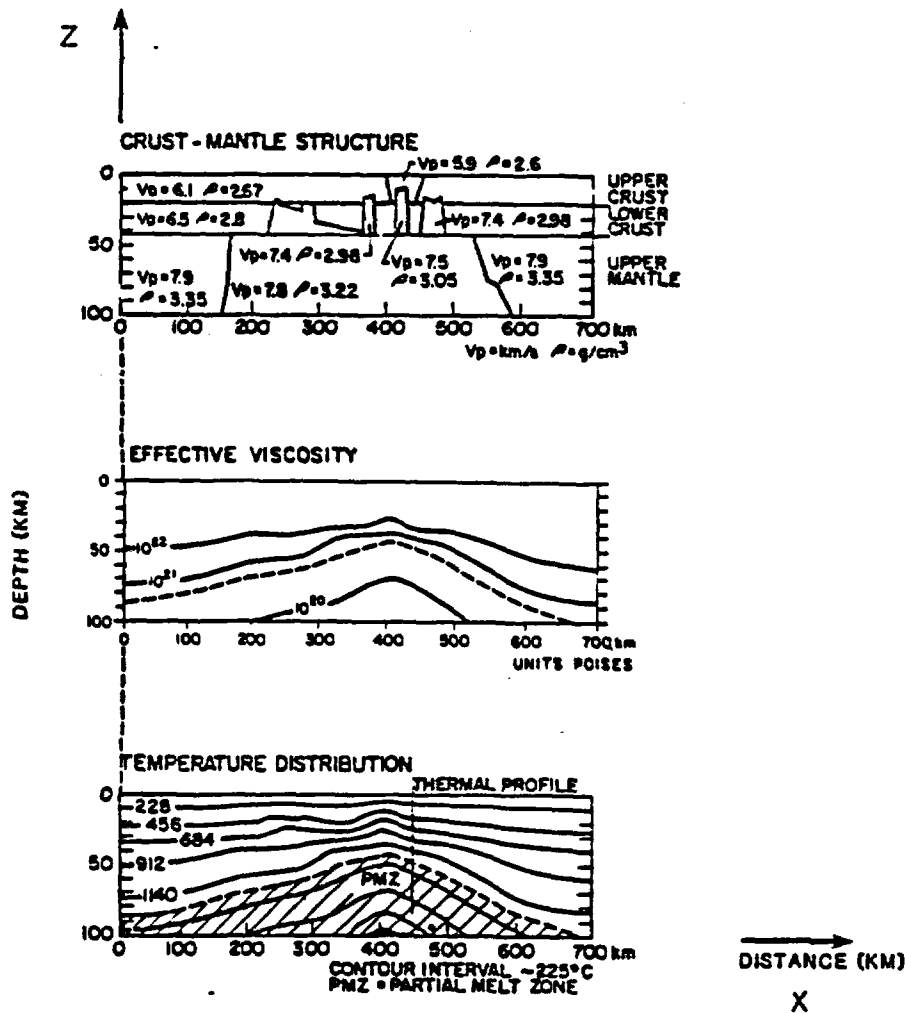
Role of mathematical and conceptual models.



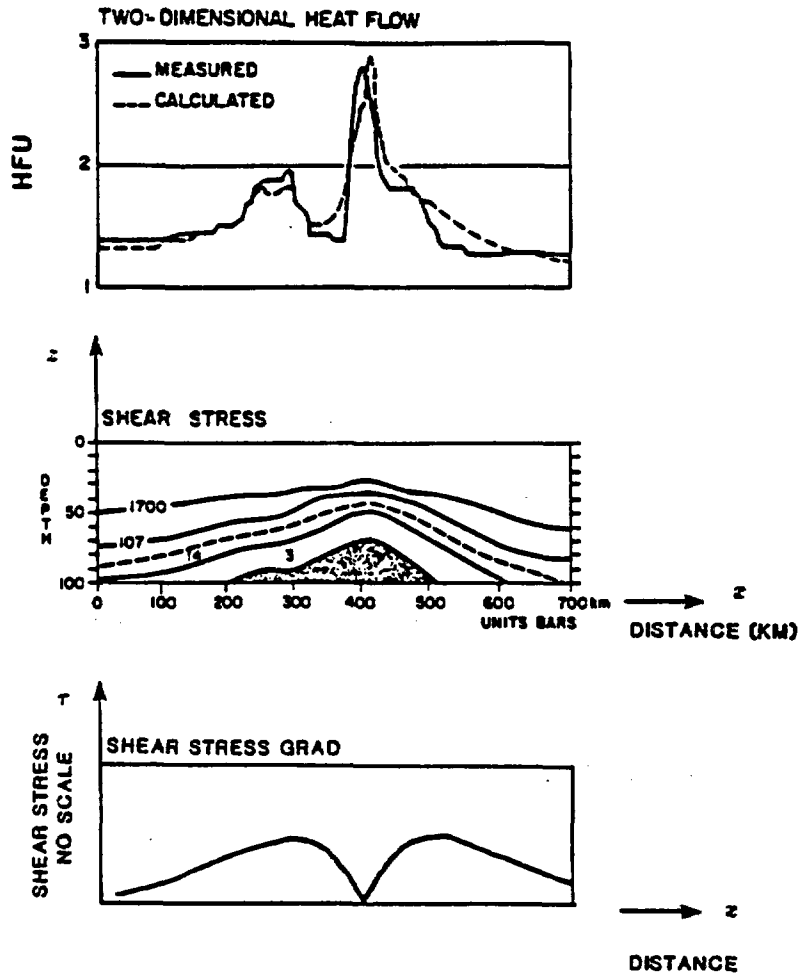
Conceptual model of groundwater flow system.



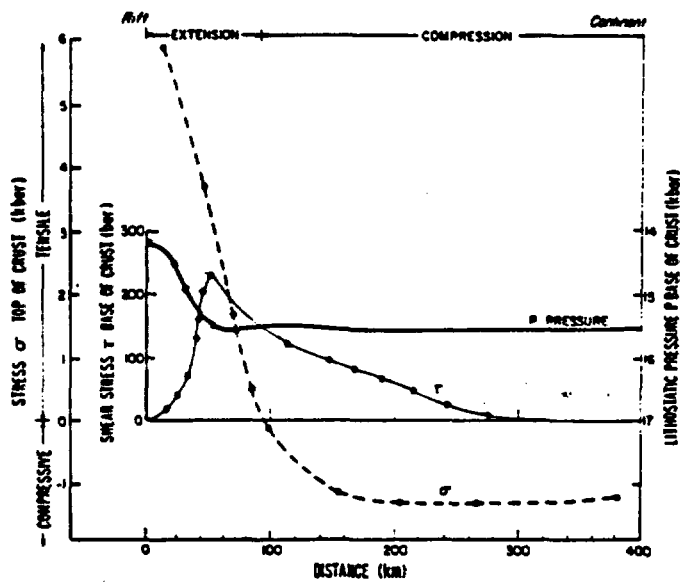
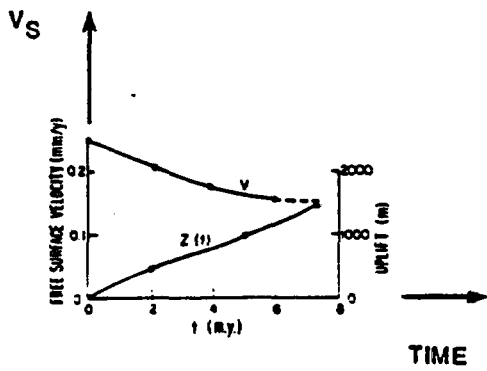
Numerical analysis of a process of upwelling of asthenospheric materials into lithosphere for the Rio Grande Rift  
 Bridwell R J Potzick 1981



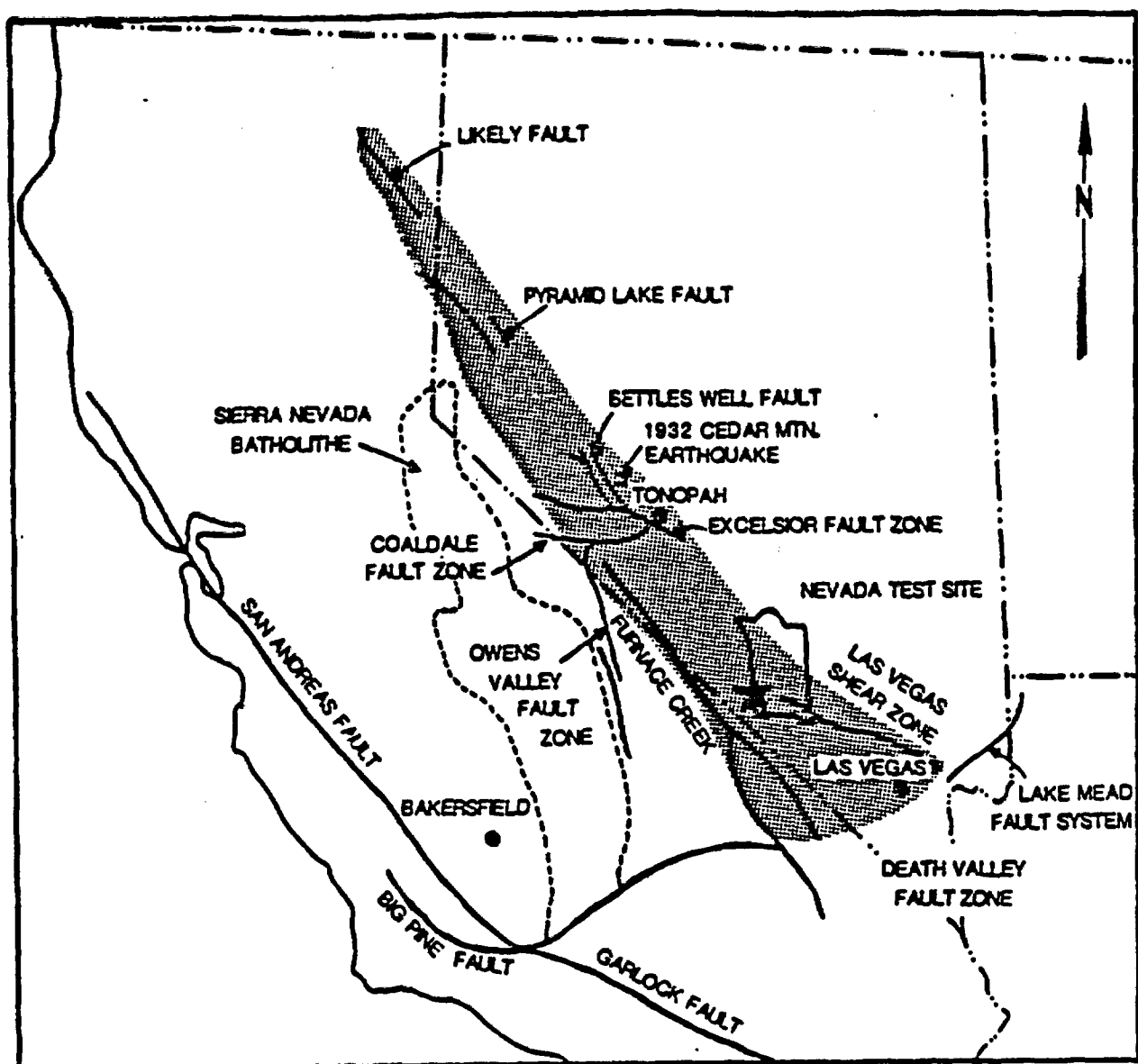
Effect of a mantle upwelling on lithospheric structure. Bridwell R.J. 1978



Surface heat flow and shear stresses in upper mantle and lower crust resulting from convective flow of heat and mass in the upper mantle. Bridwell R.J., 1978.



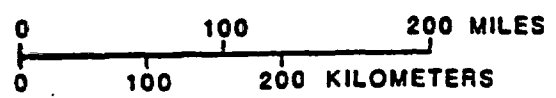
Continuum crustal stresses and surface uplift resulting from convective flow of heat and mass in the upper mantle.  
 Bridwell R.J. Potzick, 1981.



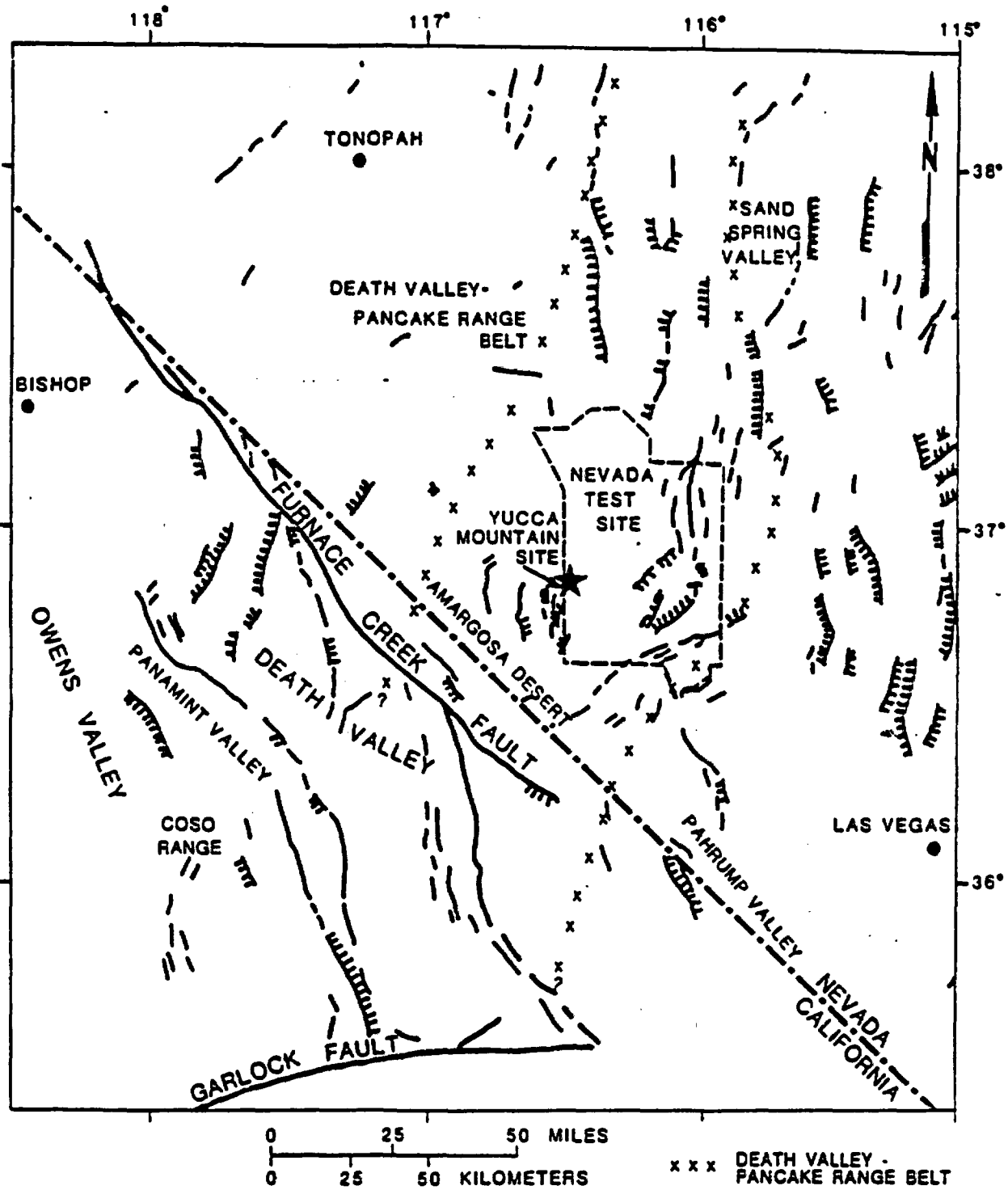
WALKER LANE



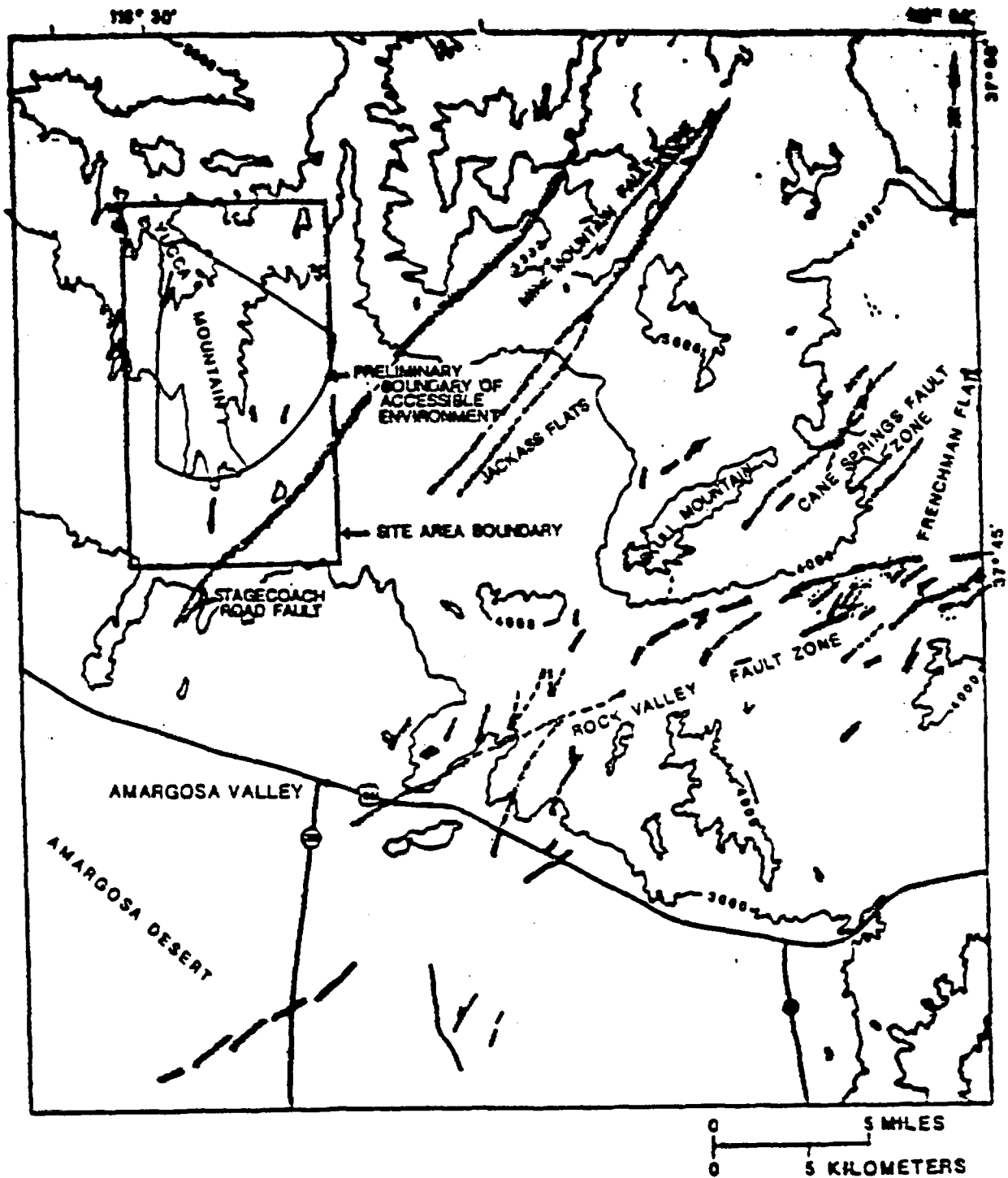
YUCCA MOUNTAIN AREA



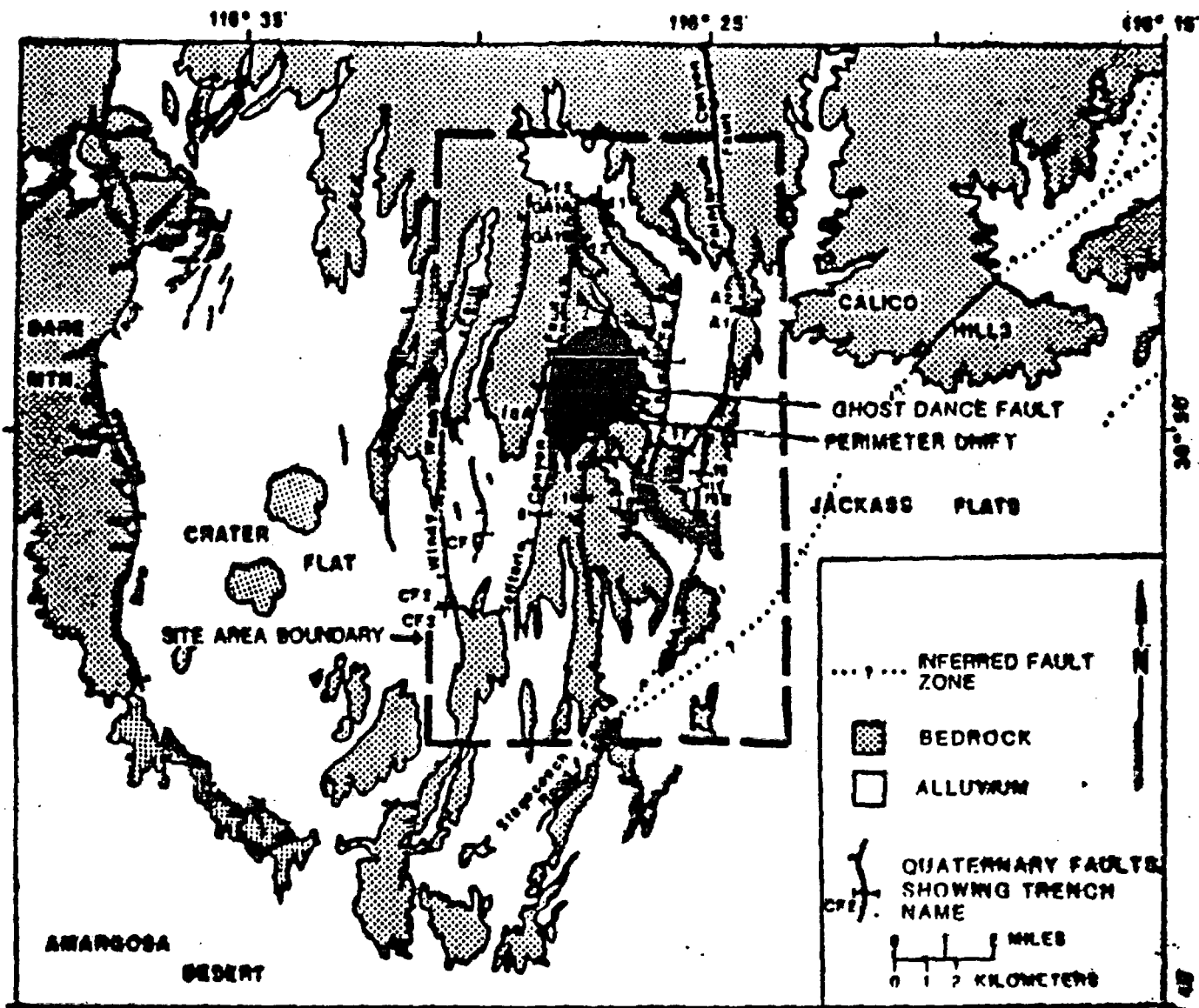
The Walker Lane shear belt and major associated faults. Modified from Stewart (1985)



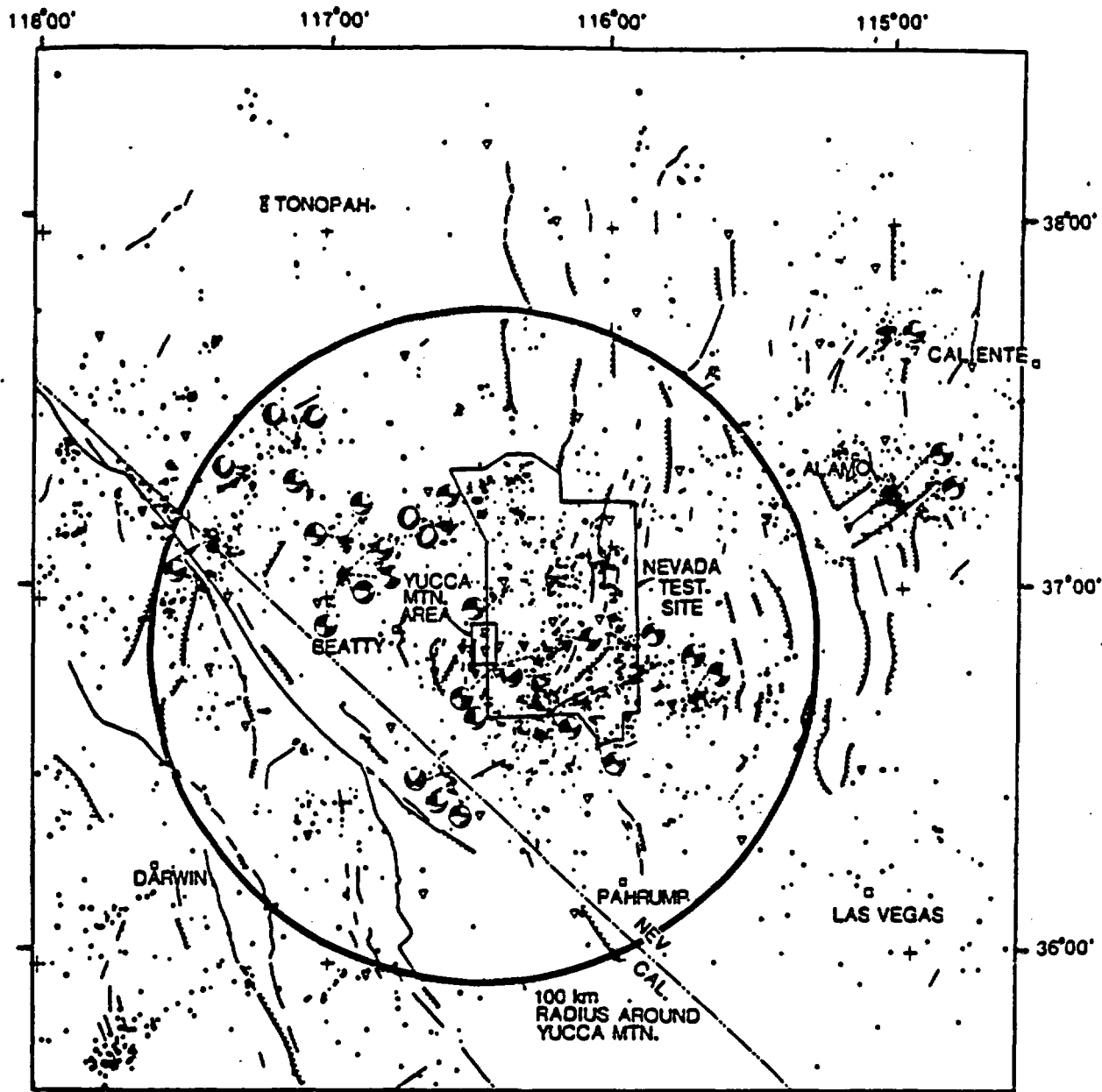
Major late Pliocene and Quaternary faults in the Nevada Test Site region, their relation to the Death Valley-Pancake volcanic zone. Modified from Carr (1984).



Quaternary faults near proposed repository area. Modified from Maldonado, 1985.



Quaternary faults near proposed repository site. Modified from Maldonado, 1985.



ALL IMPORTANT QUATERNARY FAULTS ARE SHOWN OUT TO A 100 km RADIUS OF YUCCA MOUNTAIN. MAP IS INCOMPLETE IN SOME AREAS BEYOND THAT CIRCLE.

— UNUSUALLY LINEAR MTN. FRONT WHERE PERSISTENT FAULT ACTIVITY HAS MAINTAINED A PROMINENT SCARP IN BEDROCK. A STEEP LINEAR MTN. SEGMENT WHERE YOUNG DEPOSITS ARE NOT OBVIOUSLY OFFSET.

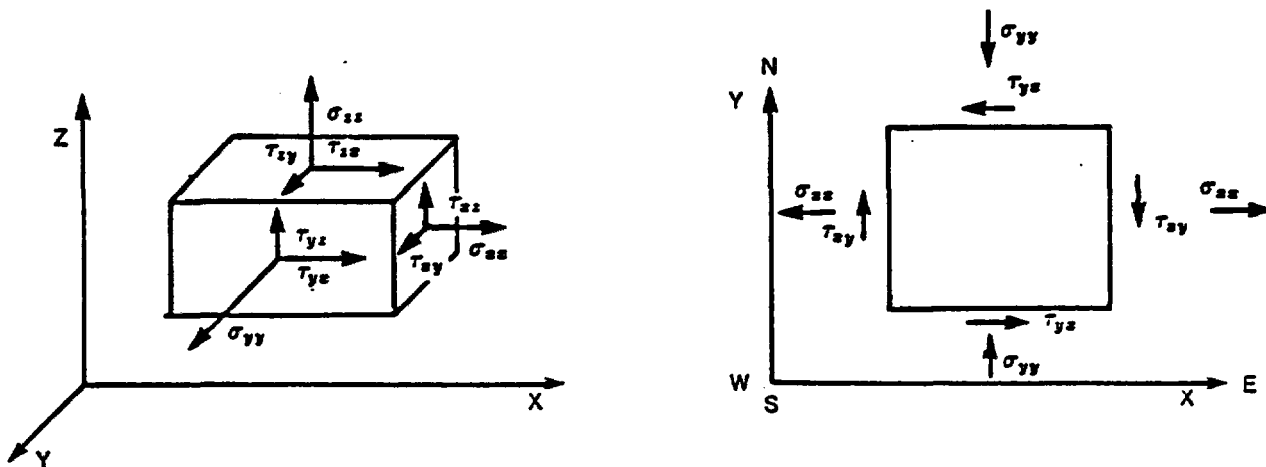
— FAULT KNOWN OR SUSPECTED TO HAVE HAD A SURFACE MOVEMENT IN LAST 2-3 MILLION YEARS

— LINE OF VOLCANIC VENTS OF QUATERNARY AGE

● SINGLE AND COMPOSITE FOCAL MECHANISMS LOWER HEMISPHERE PROJECTION OF THE FOCAL SPHERE WHERE SHADED AND UNSHADED QUADRANTS REPRESENT COMPRESSIONAL AND DILATIONAL FIRST MOTIONS RESPECTIVELY.

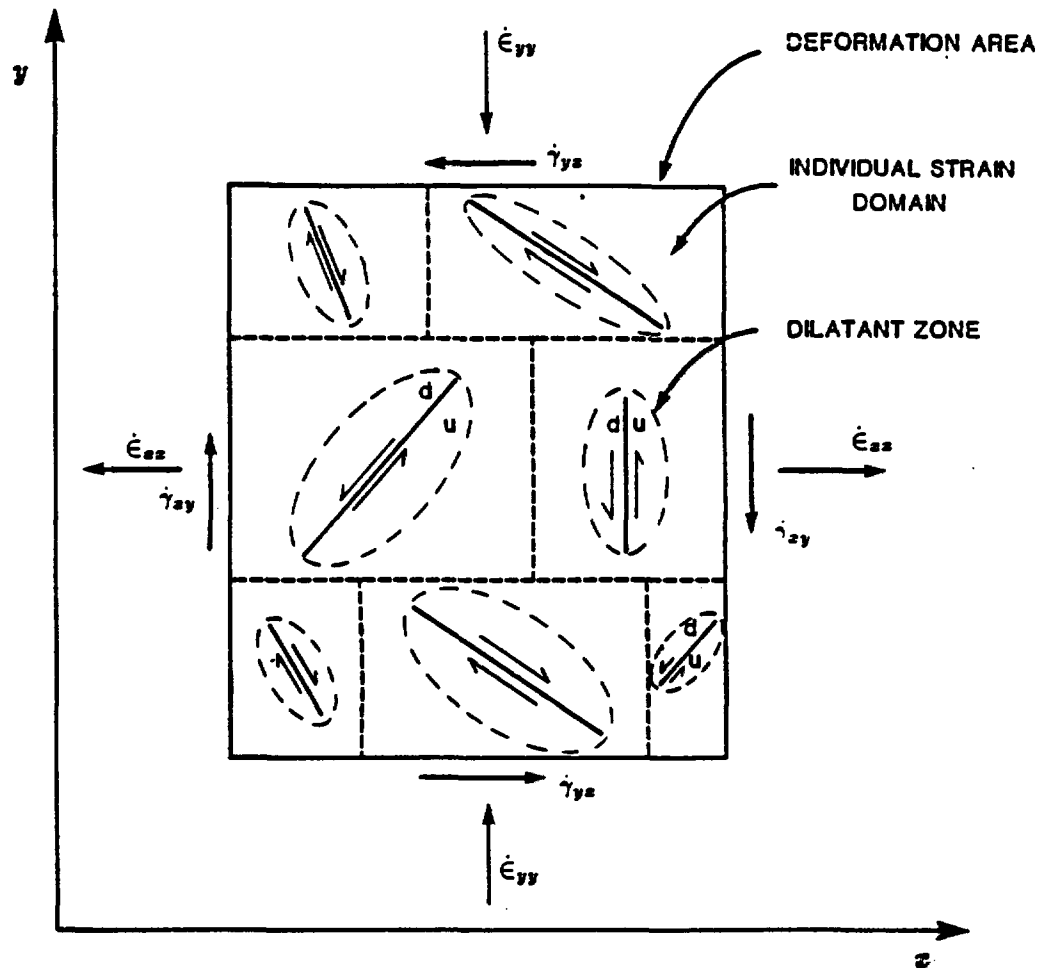
SEISMOGRAPH STATION  
 $0 < M_L < 1$       $2 \leq M_L < 3$   
 $1 \leq M_L < 2$       $3 \leq M_L$

Seismicity of the Southern Great Basin. Period August 1, 1978 through December 31, 1983. From Rogers et al., 1983 and 1987.

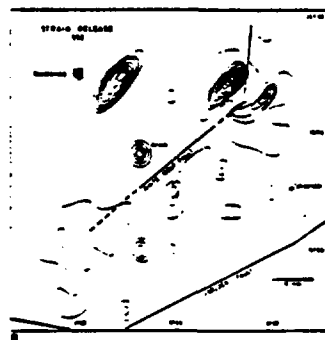


STRAIN COMPONENT	STRAIN RATE OR STRAIN ACCUMULATION	SOURCE
$\epsilon_{xx}$	$\dot{\epsilon}_{xx} = 0.07 \times 10^{-6}/\text{per year}$	WERNICKE et. al. 1982.
	$\dot{\epsilon}_{xx} = 0.08 \times 10^{-6}/\text{per year}$	SAIC, 1984.
	$\dot{\epsilon}_{xx} = 2 \times 10^{-6}/\text{per year}$	GREENSFELDER et. al. 1980.
$\epsilon_{yy}$	$\dot{\epsilon}_{yy} = -0.10 \times 10^{-6}/\text{per year}$	SAIC, 1984
$\gamma_{xy}$	$\gamma_{xy} = \int_0^{12 \times 10^6} \int_0^{25} \gamma_{xy}(y) dy \cdot dt$ $= \tan 30^\circ \text{ in } 25 \text{ km in}$ $\approx 12 \times 10^6 \text{ years}$	SCOTT AND ROSENBAUM, 1986.
$\gamma_{zy}$	$\gamma_{zy} = 3 - 7 \times 10^{-3} \text{ in}$ $3 \times 10^6 \text{ years}$	CARR, 1984.

Summary of strains rates and of accumulated shear strain for the region of Death Valley groundwater basin.



OBSERVED PHOTOELASTIC FRINGES  
IN A FAULT MODEL IN GELATIN.  
FROM LOMNITZ, 1974



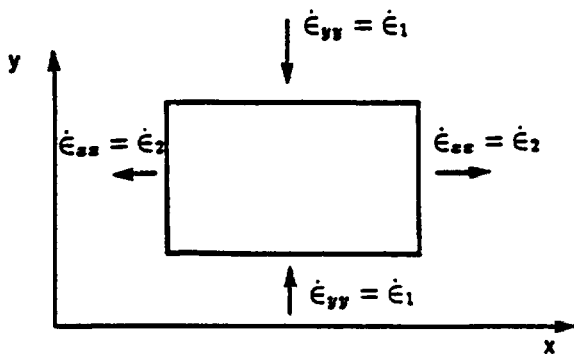
STRAINS CALCULATED FROM THE ENERGY  
RELEASE OF THE KERN COUNTY AFTERSHOCK  
SEQUENCE FROM LOMNITZ, 1974

Division of deformation area into individual strain domains

LOG TIME  
→

COMPLETE TECTONIC CYCLE				
PHASE I	PHASE II			
	DILATANT STAGE	INCLUSION STAGE	CLOSURE STAGE	GROWTH STAGE
<p>SLOW BUILD-UP OF TECTONIC STRESS.</p> <p>NORMAL AND SHEAR STRESSES EXHIBIT TIME-DEPENDENCY.</p>	<p>RATE OF LOCAL TECTONIC STRAINING INCREASES. INHOMOGENEITIES IN THE STRESS FIELD (NORMAL AND SHEAR STRESS GRADIENTS) BECOME MORE PRONOUNCED WITH TIME. AT THE END, LARGE AND FAST CHANGES IN THE CUMULATIVE STRAIN ENERGY OCCUR IN ASSOCIATION WITH A SEQUENCE OF SEISMIC EVENTS.</p>			
MORE OR LESS HOMOGENOUS STRAIN	NON-HOMOGENOUS STRAIN			
$\frac{\delta(\sigma_{xx}, \tau_{xy})}{\delta t} \neq 0$ $\frac{\delta(\sigma_{yy}, \tau_{yz})}{\delta t} \neq 0$	$\frac{\delta(\sigma_{xx}, \tau_{xy})}{\delta t} \neq 0 \neq \text{const. } \underline{\text{time-dependence of stress}}$ $\frac{\delta(\sigma_{yy}, \tau_{yz})}{\delta t} \neq 0 \neq \text{const.}$ $\frac{\delta(\sigma_{xx}, \tau_{xy})}{\delta x} \neq \text{const. } \underline{\text{stress gradients}}$ $\frac{\delta(\sigma_{yy}, \tau_{yz})}{\delta y} \neq \text{const.}$ $\frac{\delta^2(\sigma_{xx}, \tau_{xy})}{\delta t \cdot \delta x} \neq 0 \underline{\text{time dependence of stress gradients}}$ $\frac{\delta^2(\sigma_{yy}, \tau_{yz})}{\delta t \cdot \delta y} \neq 0$			

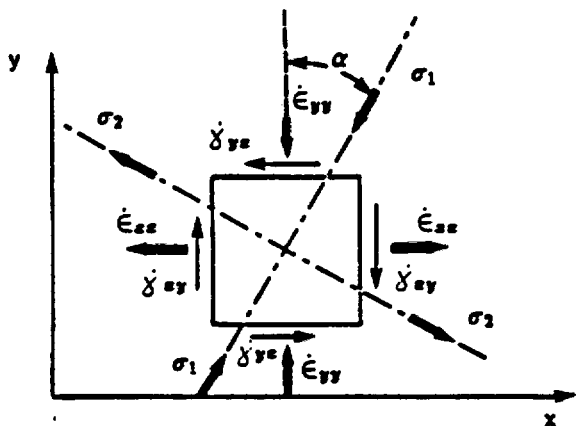
Idealization of tectonic cycle for an individual strain domain.



HOMOGENOUS STRAIN

$$\frac{\delta\sigma_1}{\delta t} \neq 0; \text{ and}$$

$$\frac{\delta\sigma_2}{\delta t} \neq 0.$$

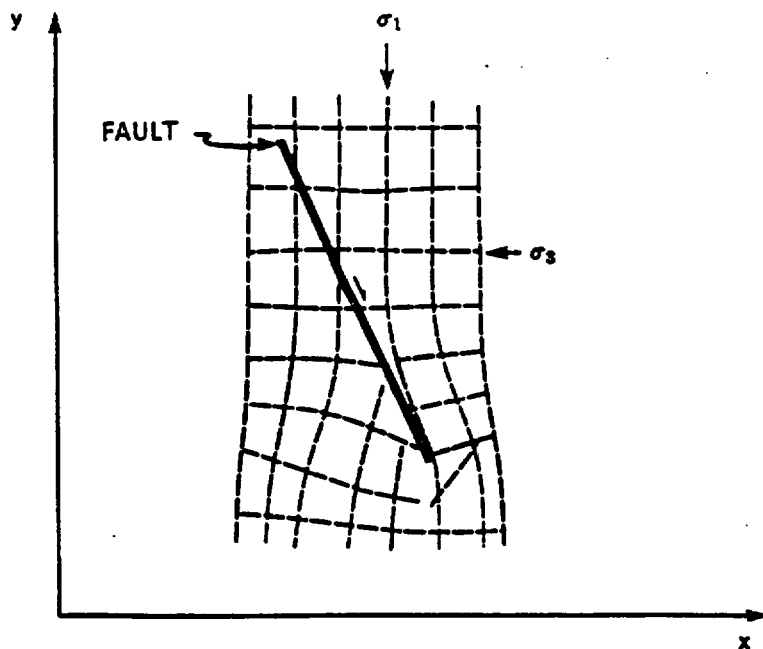


HOMOGENOUS STRAIN  
INCLUDES SHEAR COUPLE

$$\frac{\delta\sigma_1}{\delta t} \neq 0;$$

$$\frac{\delta\sigma_2}{\delta t} \neq 0; \text{ and}$$

$$\frac{\delta\alpha}{\delta t} \neq 0.$$

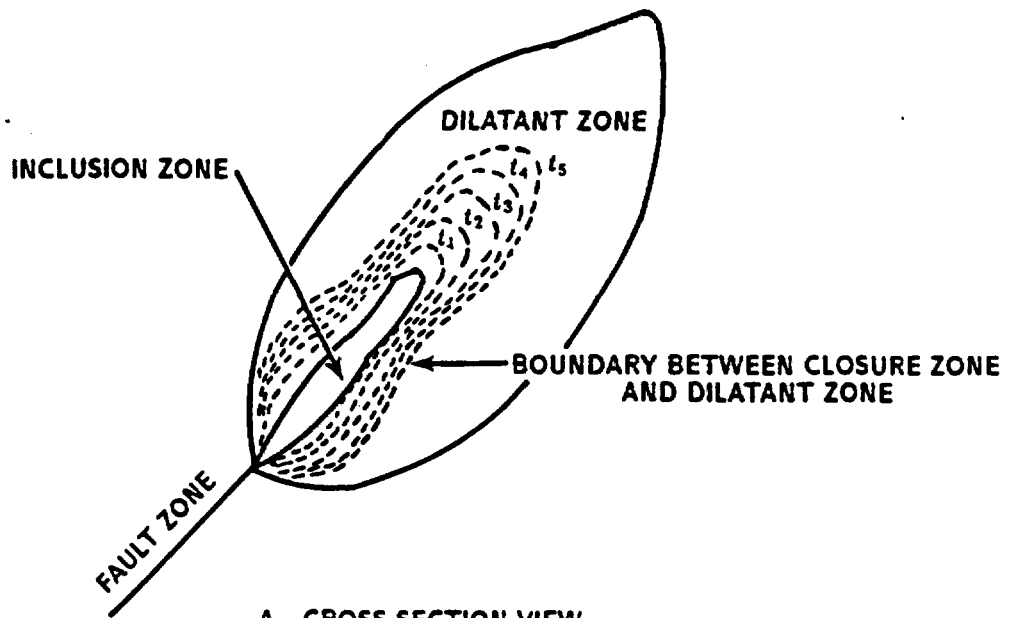


NON-HOMOGENOUS STRAIN

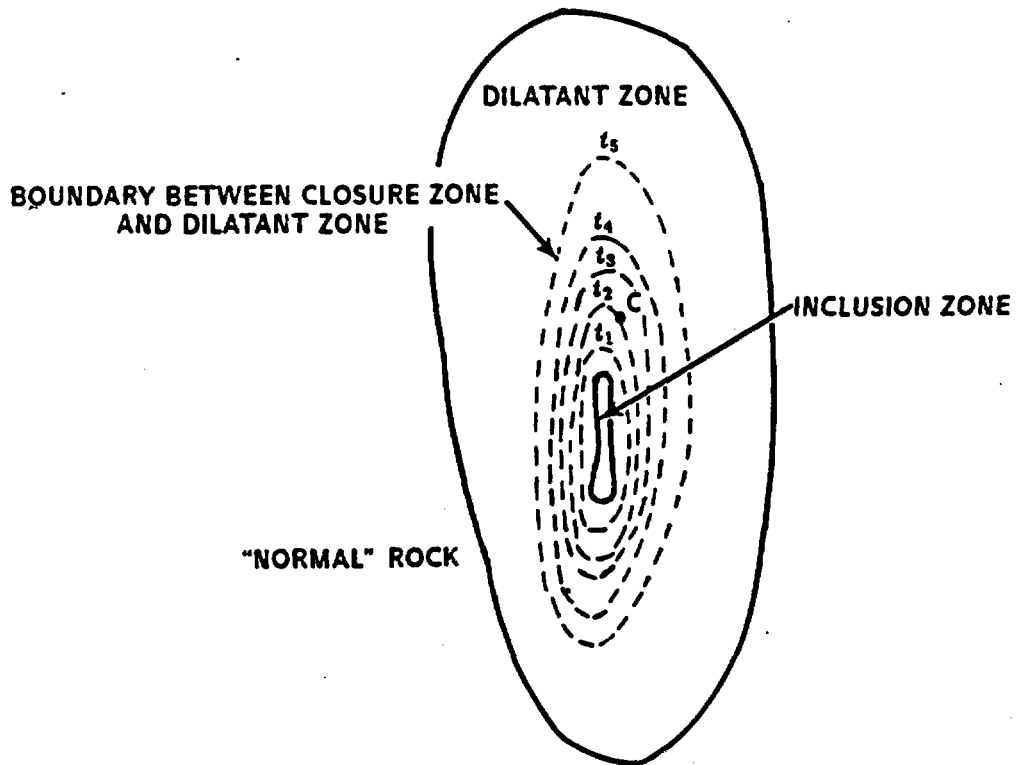
$$\frac{\epsilon^2(\sigma_{xx}, \tau_{xy})}{\sigma_z \sigma_t} = 0; \text{ and}$$

$$\frac{\epsilon^2(\sigma_{yy}, \tau_{yz})}{\sigma_z \sigma_t} \neq 0.$$

Idealization of changes in stress field during tectonic cycle.

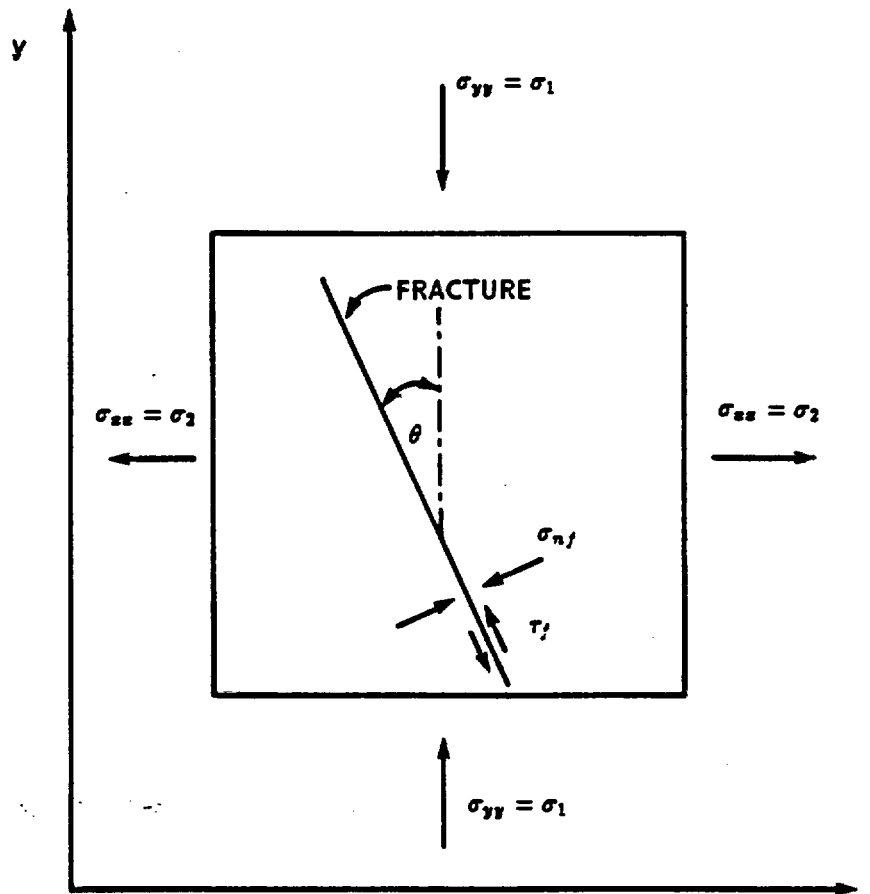


A - CROSS SECTION VIEW



B - PLAN VIEW

Spatial and temporal variation of crack closure during the growth stage. Brady, 1975.

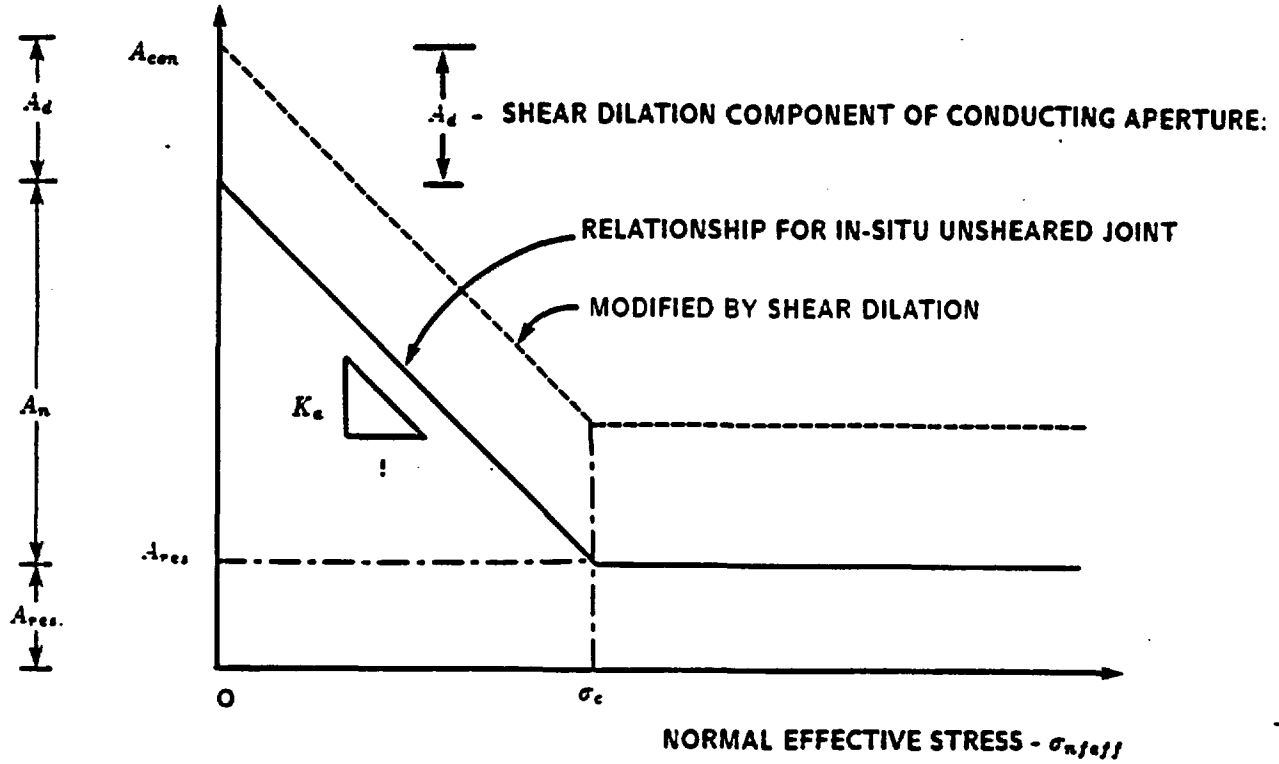


$$\sigma_{n_f} = \frac{1}{2}(\sigma_1 + \sigma_2) + \frac{1}{2}(\sigma_1 - \sigma_2) \cos 2\theta; \text{ and}$$

$$\tau_f = \frac{1}{2}(\sigma_1 - \sigma_2) \cdot \sin 2\theta.$$

Stress on a fracture as a function of magnitude and orientation of principal stresses.

**CONDUCTING APERTURE**



$$A_{con} = A_{res.} + r\sigma_{nfeff} \cdot K_e - A_d$$

$$r = 1 \text{ if } 0 < \sigma_{nfeff} < \sigma_c$$

$$\text{OTHERWISE}$$

$$r = 0$$

**WHERE:**

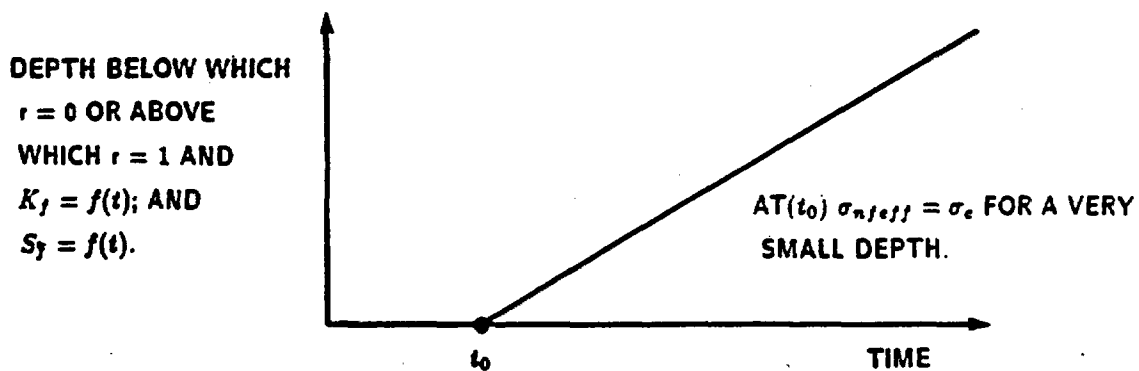
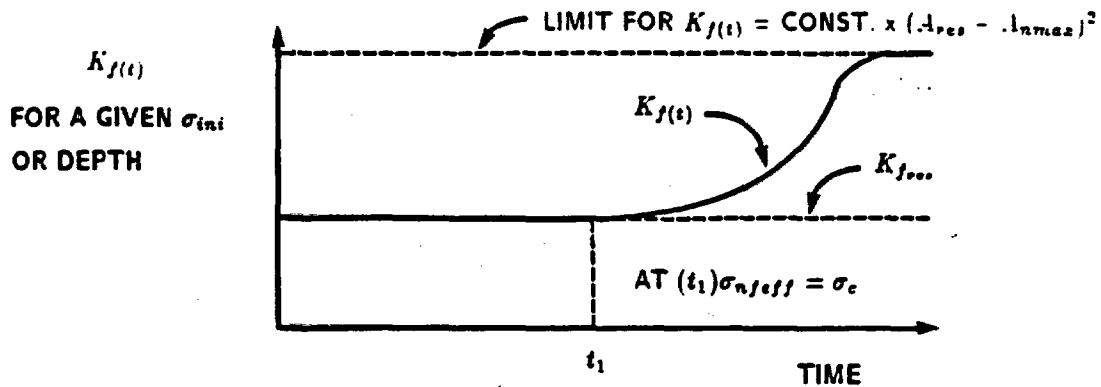
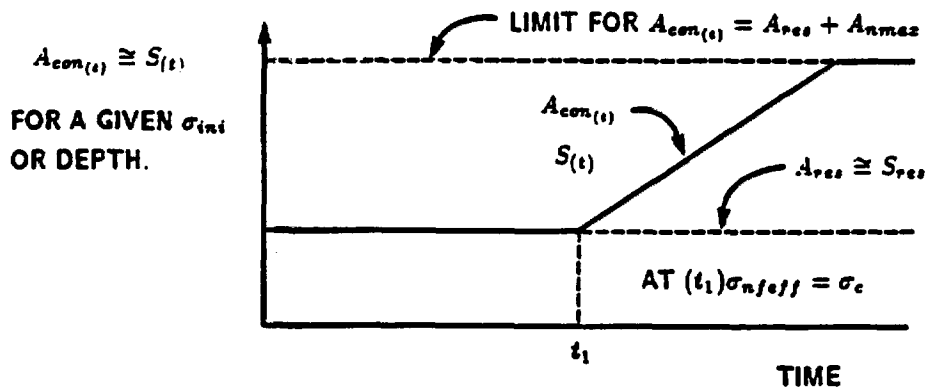
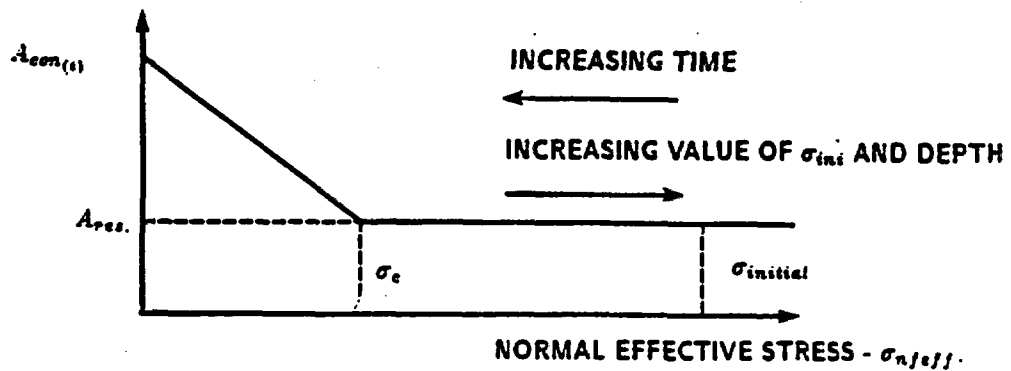
$A_{con}$  - FRACTURE CONDUCTING APERTURE:

$A_{res.}$  - FRACTURE RESIDUAL APERTURE:

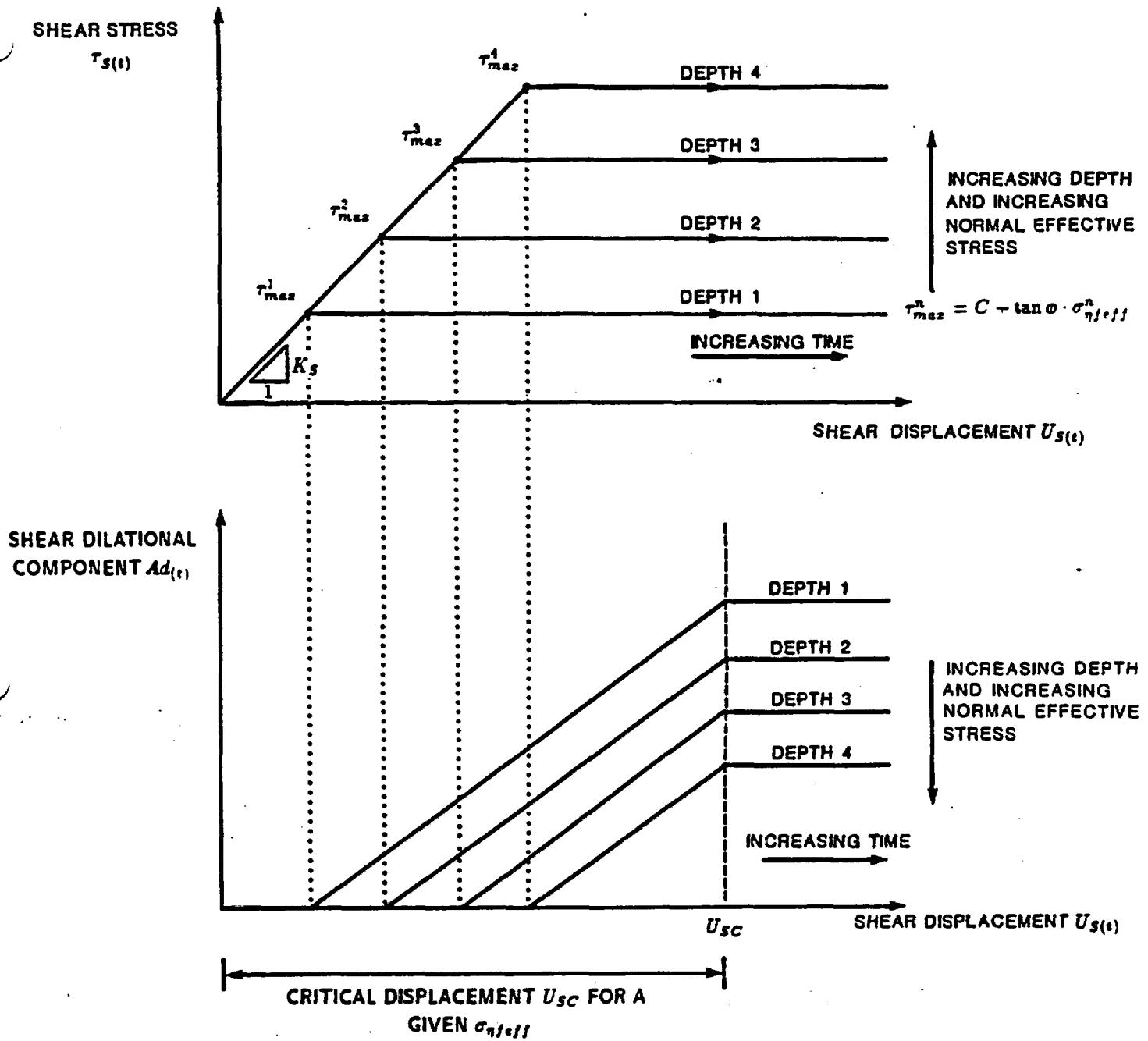
$A_d$  - SHEAR DILATION COMPONENT OF CONDUCTING APERTURE

$r\sigma_{nfeff}K_e = A_n$  - NORMAL DILATION COMPONENT OF CONDUCTING APERTURE: AND

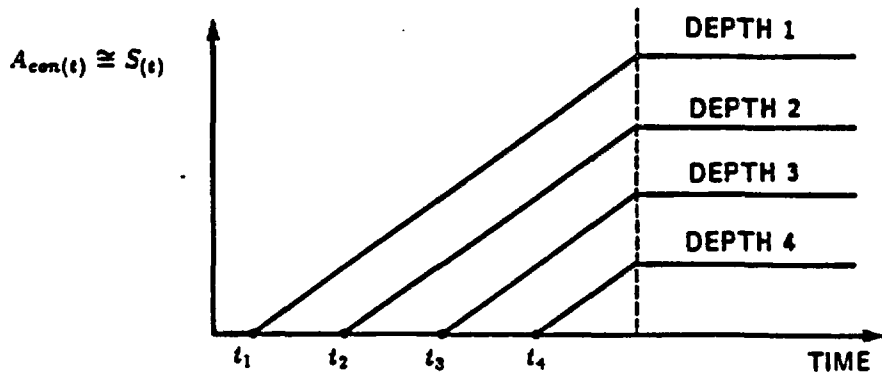
$K_e$  - COMPLIANCE



Relationships between time and hydraulic parameters caused by reduction in  $\sigma_{n,eff}$ .

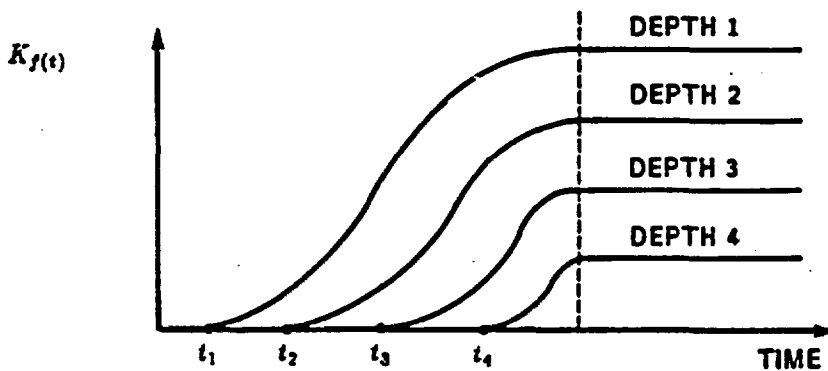


Idealized joint response during shear displacement. Modified from Harper T.R. and Last N.C., 1987.

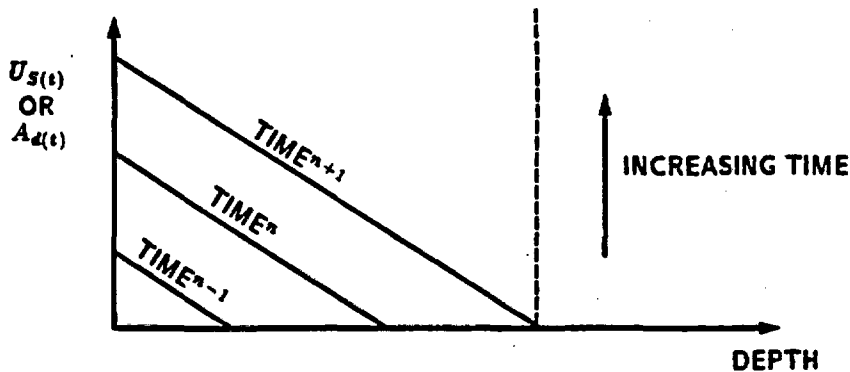
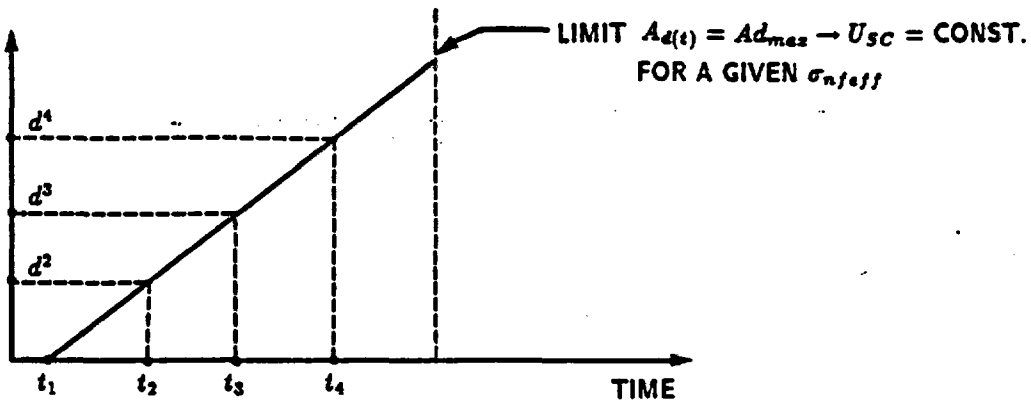


$A_{con}(t) = A_{res} - A_{d(t)}$   
 $A_{d(t)} > 0$  IF  $\tau_{S(t)} \cong \tau_{max}$   
 OTHERWISE  
 $A_{d(t)} = 0$

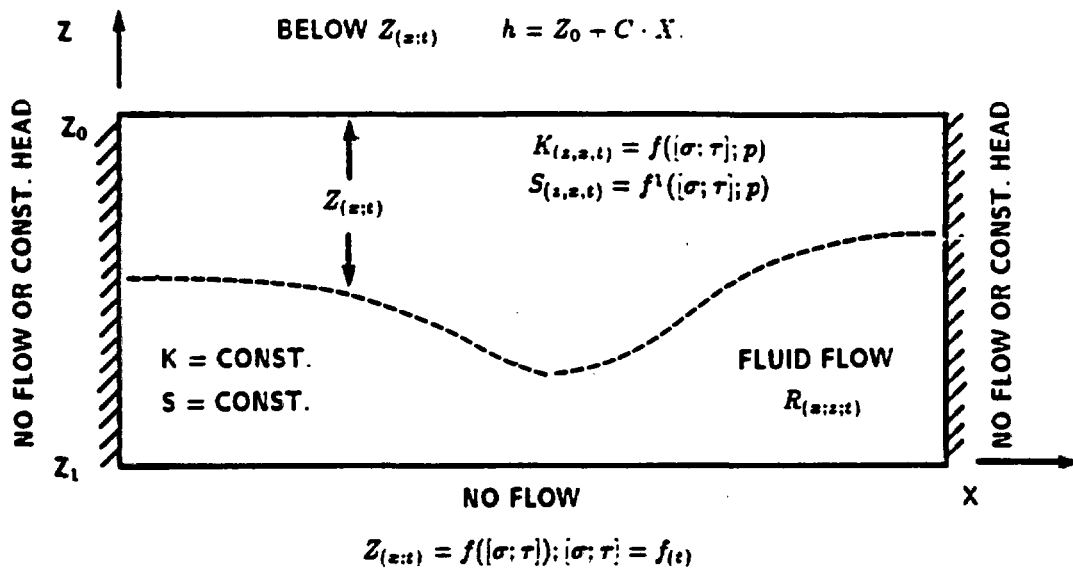
$t_n$  - TIME REQUIRED FOR  $\tau_{S(t)}^n$  TO REACH  $\tau_{max}^n$



DEPTH BELOW WHICH  $\tau_{S(t)}^n < \tau_{max}^n$  AND THEREFORE  $A_d = 0$



Relationships between time and hydraulic parameters caused by increase in  $\tau_f$ .



**GOVERNING EQUATION**

ABOVE  $Z(x;t)$

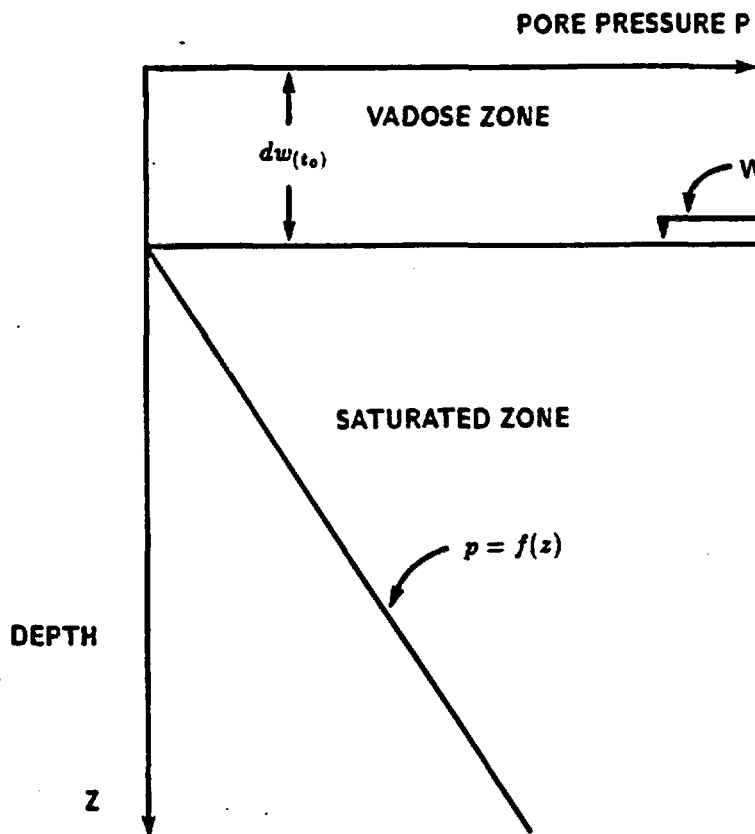
$$\frac{\delta^2 h}{\delta x^2} + \frac{\delta^2 h}{\delta z^2} = S_{(x,z;t)} \cdot [K_{(x,z;t)} \cdot Z_{(x;t)}]^{-1} \cdot \frac{\delta h}{\delta t} \pm R_{(x,z;t)} \cdot [K_{(x,z;t)} \cdot (Z_1 - Z_{(x;t)})]^{-1}$$

BELOW  $Z(x;t)$

$$\frac{\delta^2 h}{\delta x^2} + \frac{\delta^2 h}{\delta z^2} = S \cdot [K(Z_1 - Z_{(x;t)})]^{-1} \cdot \frac{\delta h}{\delta t} \pm R_{(x,z;t)} [K_{(x,z;t)} (Z_1 - Z_{(x;t)})]^{-1}$$

Conceptual model of flow system in deforming fractured medium.

$t_{(0)}$  - START OF TECTONIC DEFORMATION



AT TIME  $t_{(0)}$ , AT DEPTH  $\rightarrow 0$  AND BELOW:

$$\sigma_{\eta f e f f(t_0)} > \sigma_c \rightarrow r = 0 \text{ and } A n_{(t_0)} = 0$$

AND/OR

$$\tau_{f(t_0)} < \tau_{max} \rightarrow \Delta U_{s(t_0)} = 0 \text{ AND}$$

$$A d_{(t_0)} = 0$$

$$A_{con(t_0)} = A_{res.} = \text{CONST.}$$

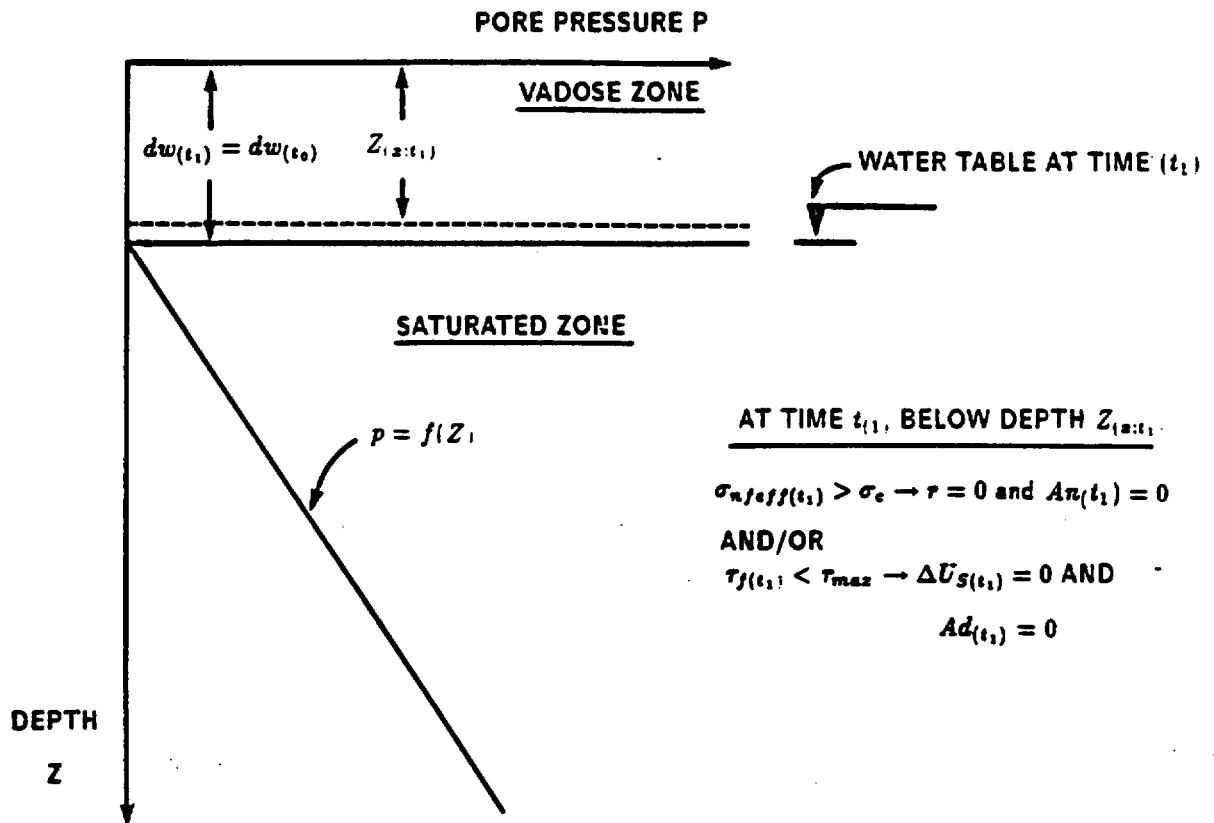
$$S_{(t_0)}^{Uz} = S_{(t_0)}^{Sz}$$

$$K_{(t_0)}^{Uz} = K_{(t_0)}^{Sz}$$

$$K_{z(t_0)} = K_{y(t_0)}$$

Deforming fractured medium - idealized history of changes in hydraulic potential.

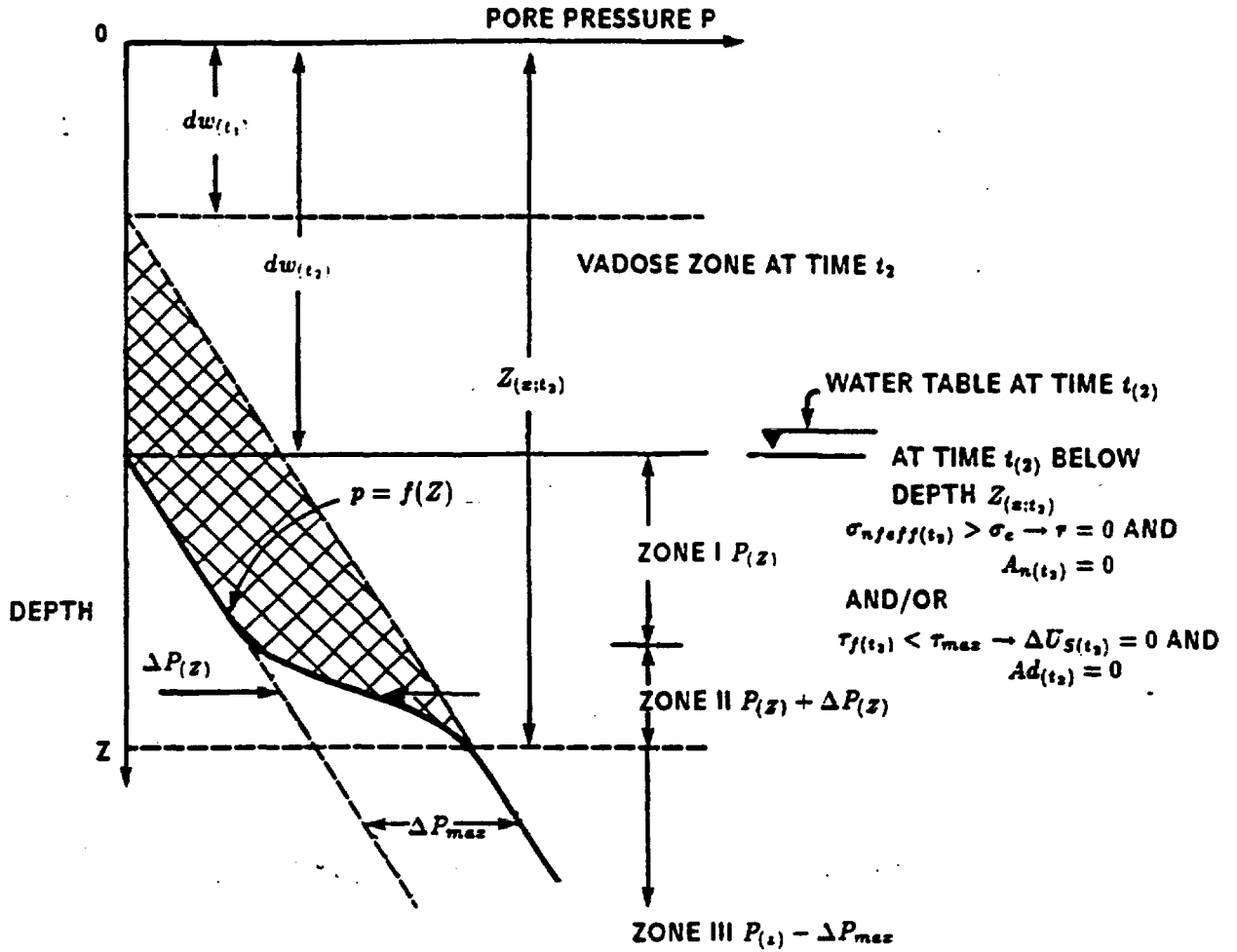
$t_1$  - EARLY STAGES OF TECTONIC DEFORMATION



ABOVE DEPTH $Z_{(z:t_1)}$	BELOW DEPTH $Z_{(z:t_1)}$
$A_{con}(t_1) = A_{res} + A_n(t_1) - Ad(t_1)$	$A_{con} = A_{res} = \text{CONST.}$
$S_{(t_1)}^{Uz} = S_{(t_0)}^{Uz} + \Delta S_{(t_1)}^{Uz}$	$S_{(t_1)}^{Sz} = S_{(t_0)}^{Sz}$
$K_{(t_1)}^{Uz} = K_{(t_0)}^{Uz} + \Delta K_{(t_1)}^{Uz}$	$K_{(t_1)}^{Sz} = K_{(t_0)}^{Sz}$
$K_x \neq K_y$	$K_x = K_y$

Deforming fractured medium - idealized history of changes in hydraulic potential.

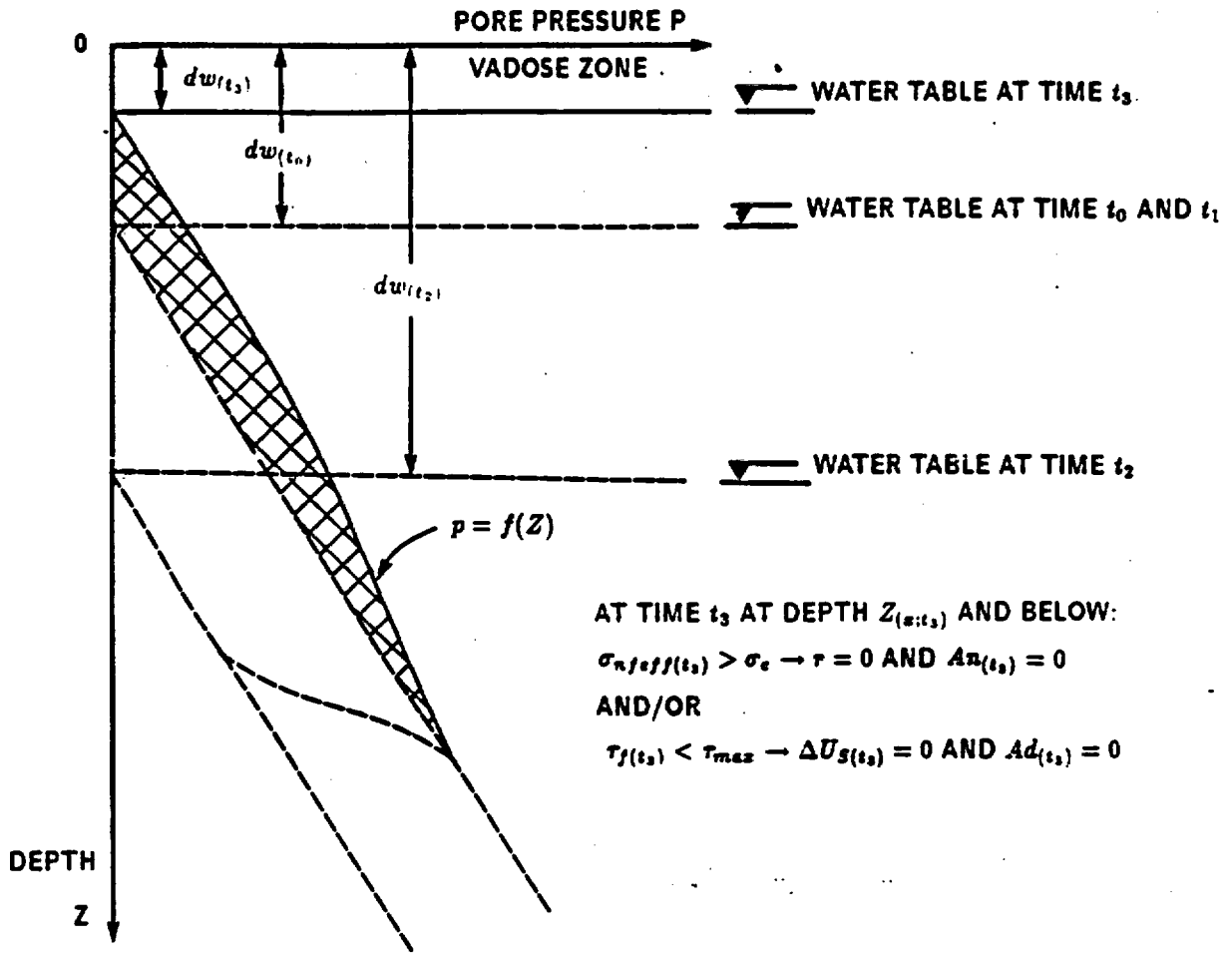
$t_2$  - ADVANCED STAGES OF TECTONIC DEFORMATION



ABOVE DEPTH $Z(z;t_2)$	BELOW DEPTH $Z(z;t_2)$
$\lambda_{con}(t_2) = \lambda_{res} + \lambda_n(t_2) + \lambda_d(t_2)$	$\lambda_{con}(t_2) = \lambda_{res} = \text{CONST.}$
$S_{(t_2)}^{Uz} = S_{(t_0)}^{Uz} + \Delta S_{(t_1)}^{Uz} + \Delta S_{(t_2)}^{Uz}$	$S_{(t_2)}^{Sz} = S_{(t_0)}^{Sz}$
$S_{(t_2)}^{Sz} = S_{(t_0)}^{Sz} + \Delta S_{(t_1)}^{Sz} + \Delta S_{(t_2)}^{Sz}$	$K_{(t_2)}^{Sz} = K_{(t_0)}^{Sz}$
$K_{f(t_2)}^{Uz} = K_{f(t_0)}^{Uz} + \Delta K_{f(t_1)}^{Uz} + \Delta K_{f(t_2)}^{Uz}$	$K_x = K_y$
$K_{f(t_2)}^{Sz} = K_{f(t_0)}^{Sz} + \Delta K_{f(t_1)}^{Sz} + \Delta K_{f(t_2)}^{Sz}$	
$K_x \neq K_y$	
<b>FRACTURE FLOW</b>	

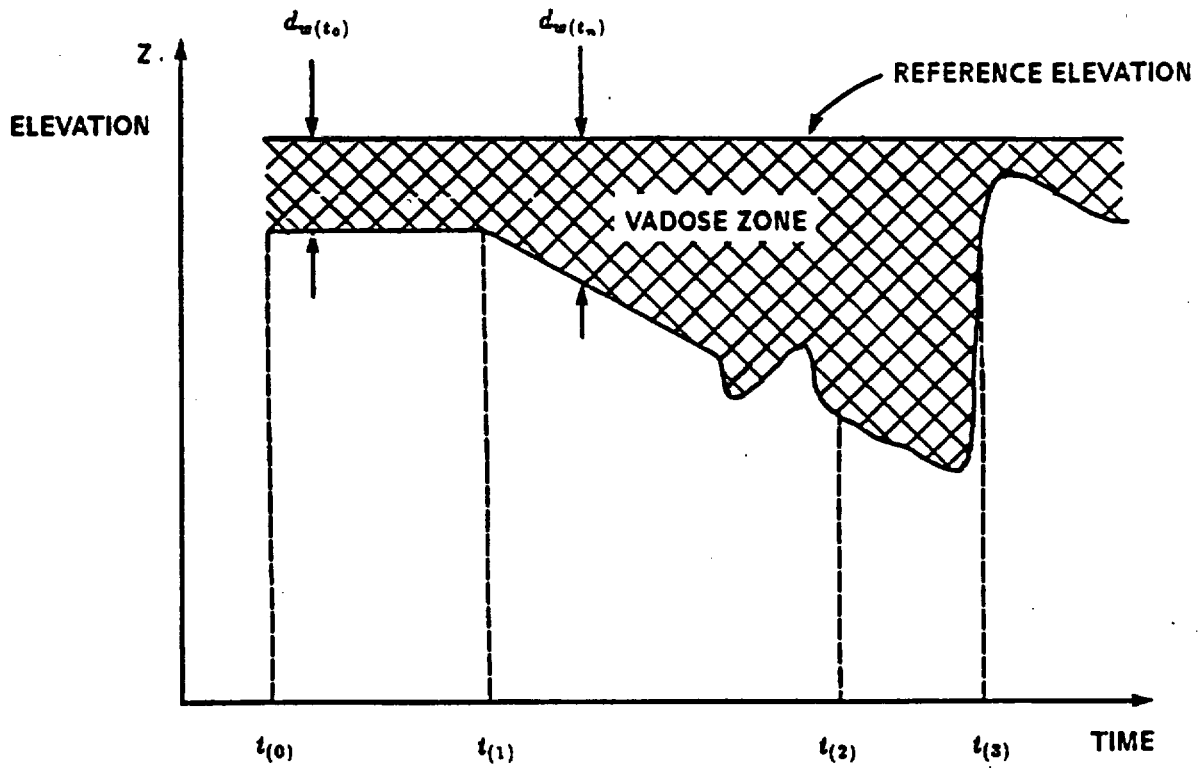
Deforming fractured medium - idealized history of changes in hydraulic potential.

$t_3$  - END OF THE TECTONIC CYCLE



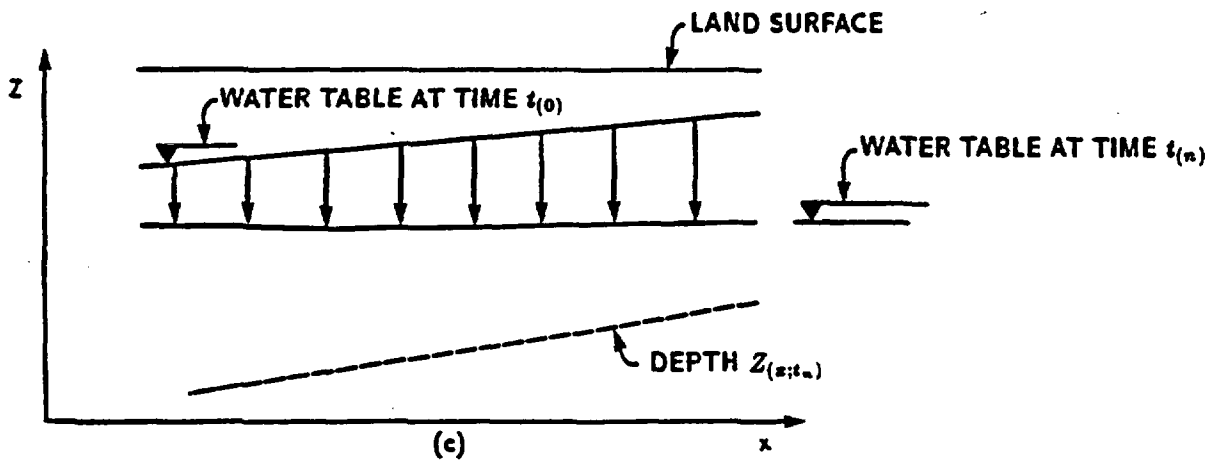
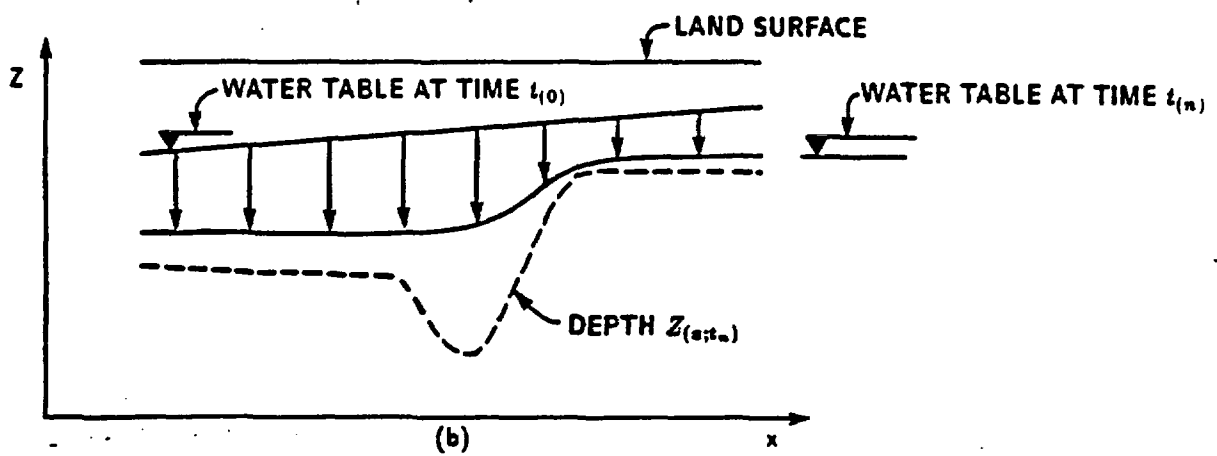
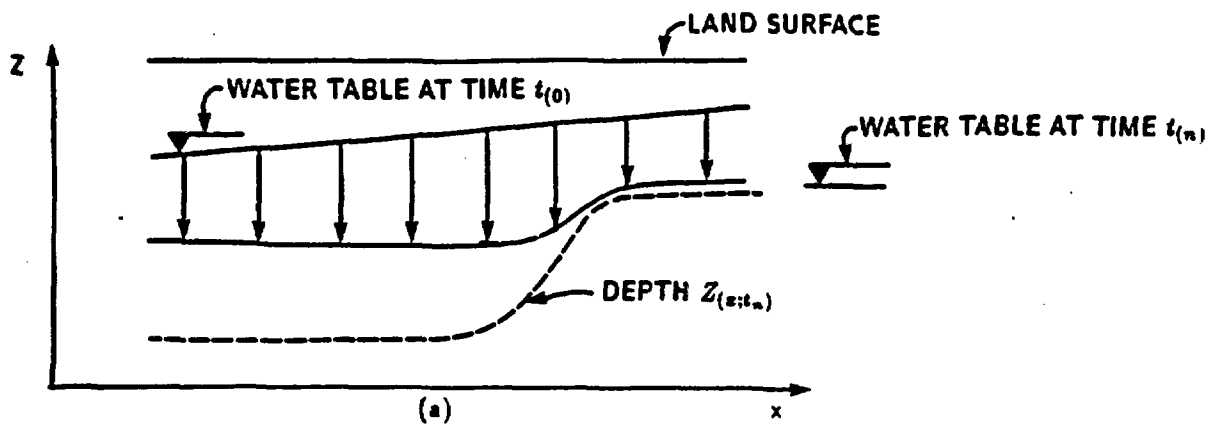
AT DEPTH $Z_{(z;t_3)}$ AND BELOW
$A_{con(t_3)} = A_{res}$
$S_{(t_3)}^{Uz} = S_{(t_0)}^{Uz} < S_{(t_2)}^{Uz}$
$S_{(t_3)}^{Sz} = S_{(t_0)}^{Sz} < S_{(t_2)}^{Sz}$
$K f_{(t_3)}^{Uz} = K f_{(t_0)}^{Uz} < K f_{(t_2)}^{Uz}$
$K f_{(t_3)}^{Sz} = K f_{(t_0)}^{Sz} < K f_{(t_2)}^{Sz}$
<b>POROUS OR EQUIVALENT FLOW</b>

Deforming fractured medium - idealized history of changes in hydraulic potential.

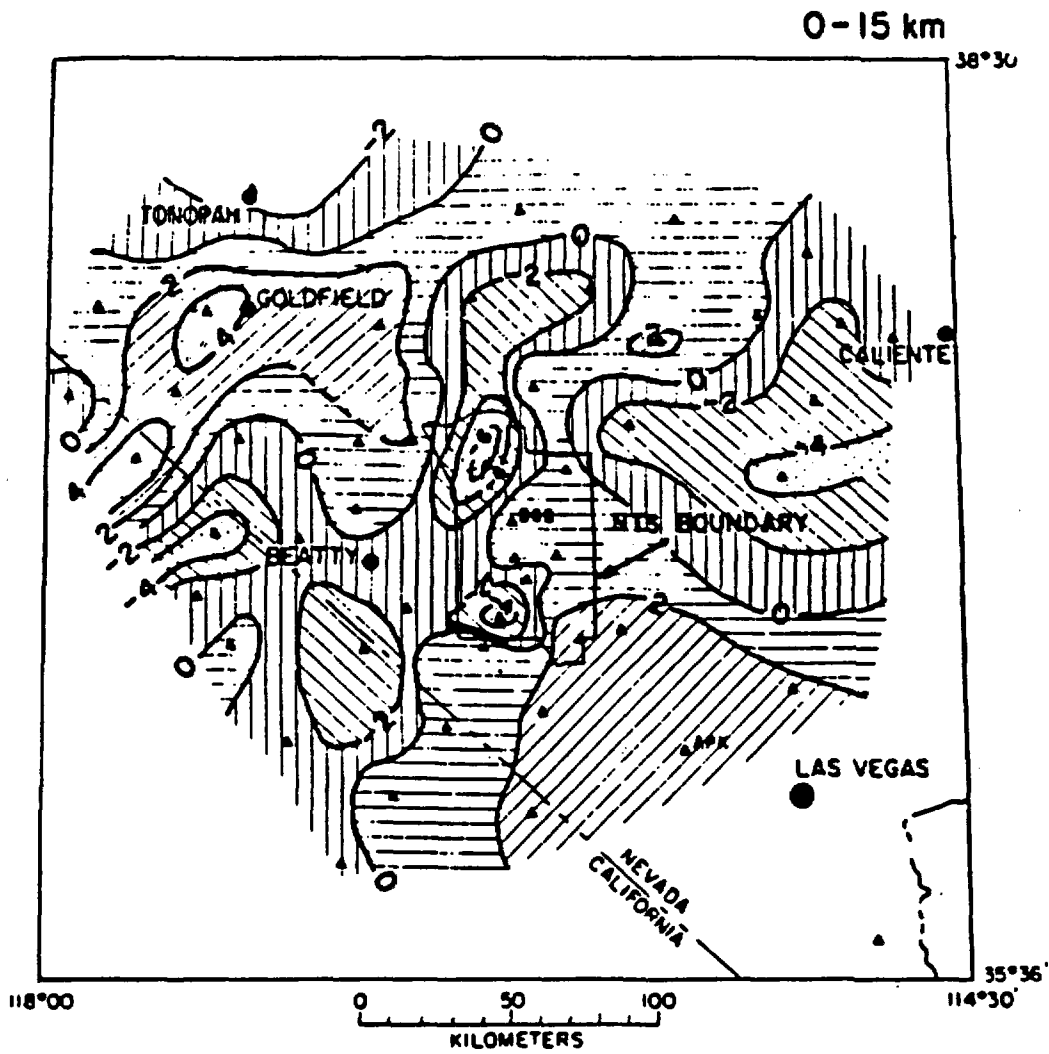


Note: The drawing is diagramatic - no relationship between initial thickness of the vadose zone and magnitude of tectonic lowering of the water table is implied.

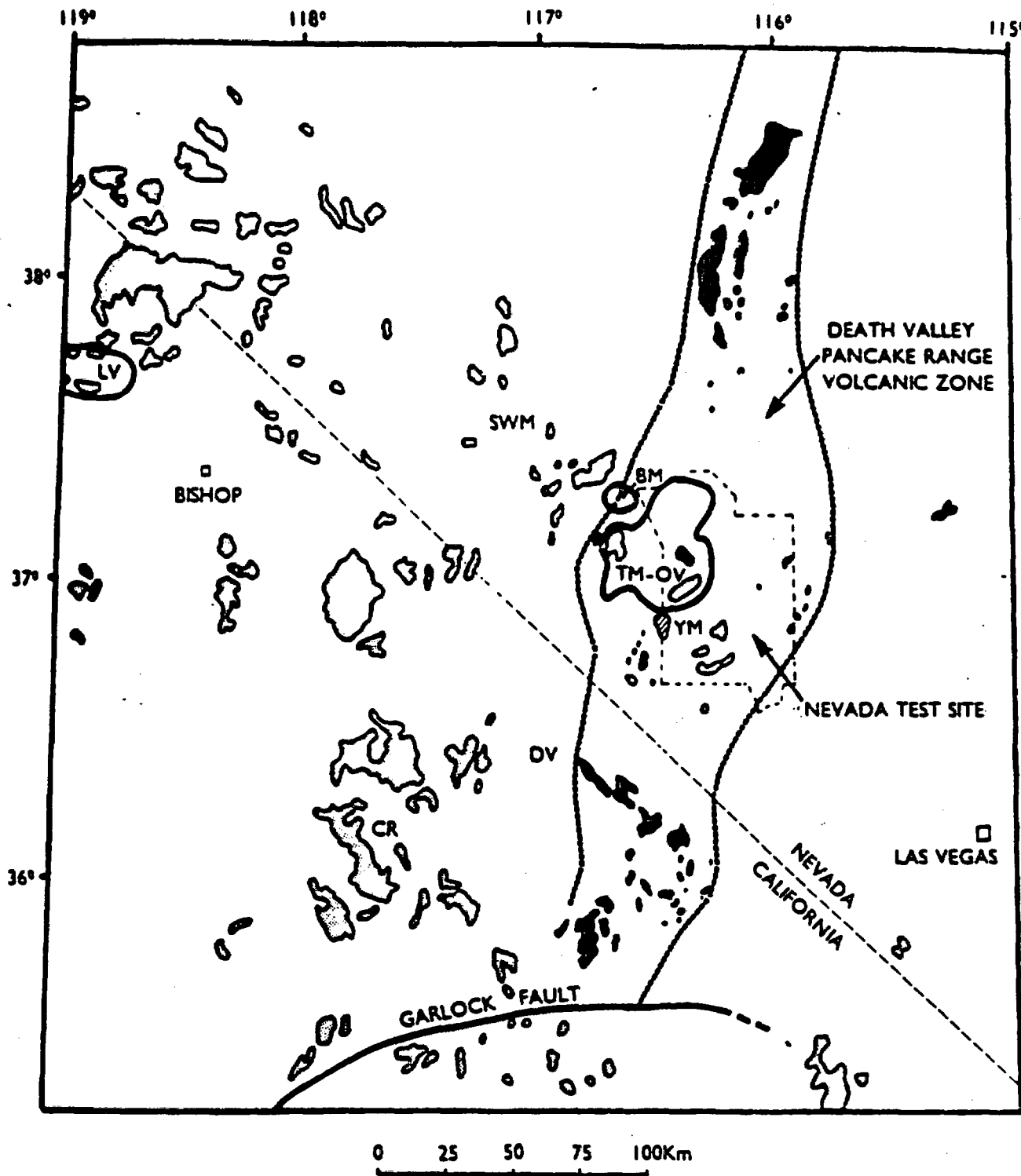
Idealized history of the position of the water table for a single point P(x,y).



Non-homogeneous strain - it's relationship to configuration of the water table.

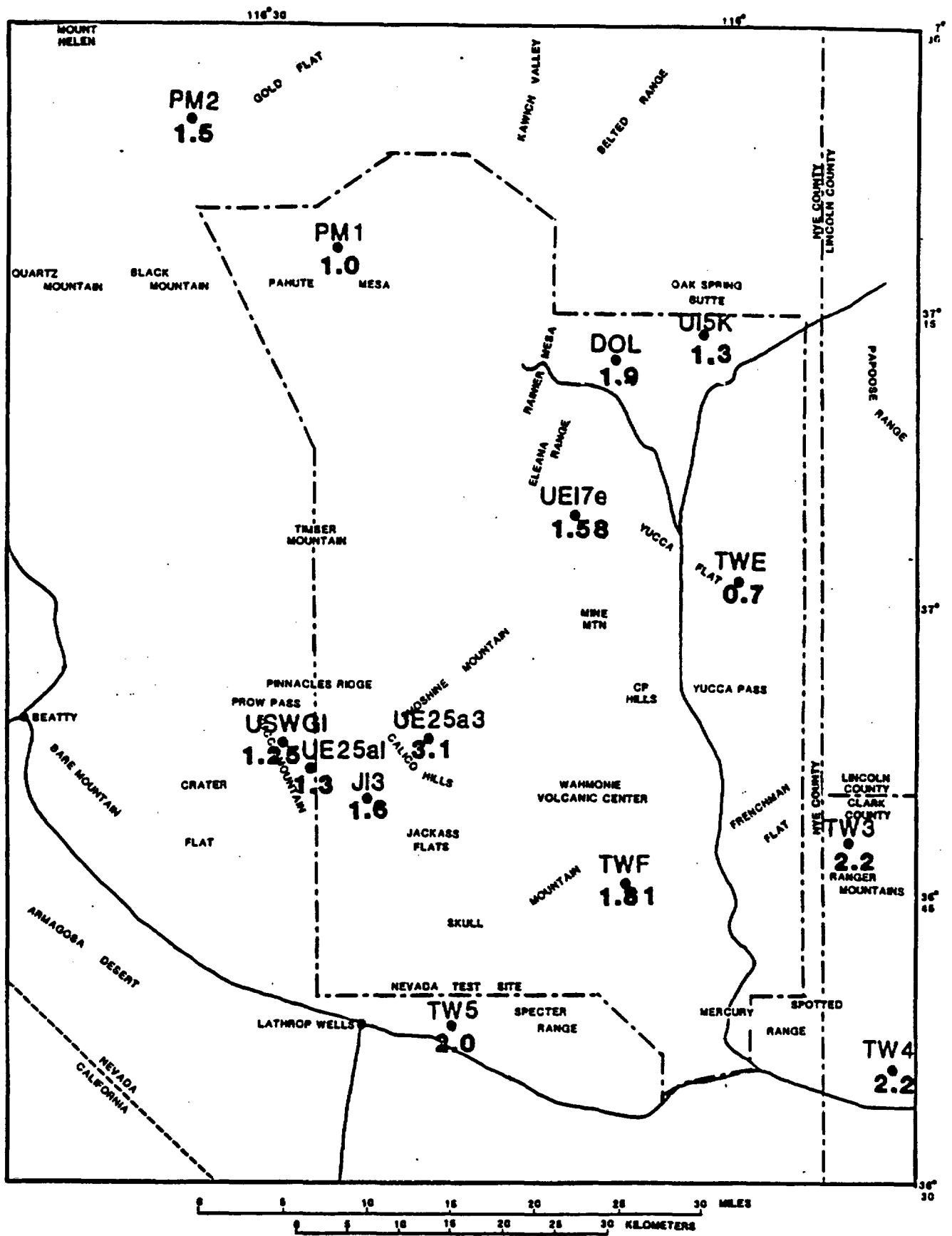


Seismic velocity structure of the upper crust from teleseismic P-wave residuals for the region of southern Nevada.  
 Monfort and Evans. 1982.

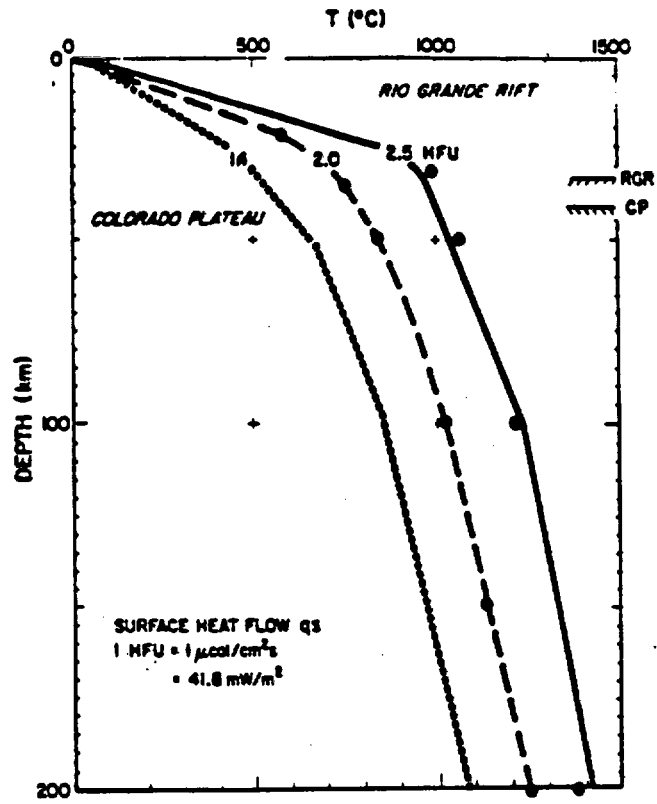


Explanation: SWM Stonewall. BM: Black Mountain; TM-OV: Timber Mountain-Oasis Valley caldera complex; YM: Yucca Mountain exploration block; LV: Long Valley; DV: Death Valley; and CR: Coso Range. Black-shaded areas are volcanic rocks of the DV-PR volcanic zone; light-shaded areas are part of the western Cordillera rift zone.

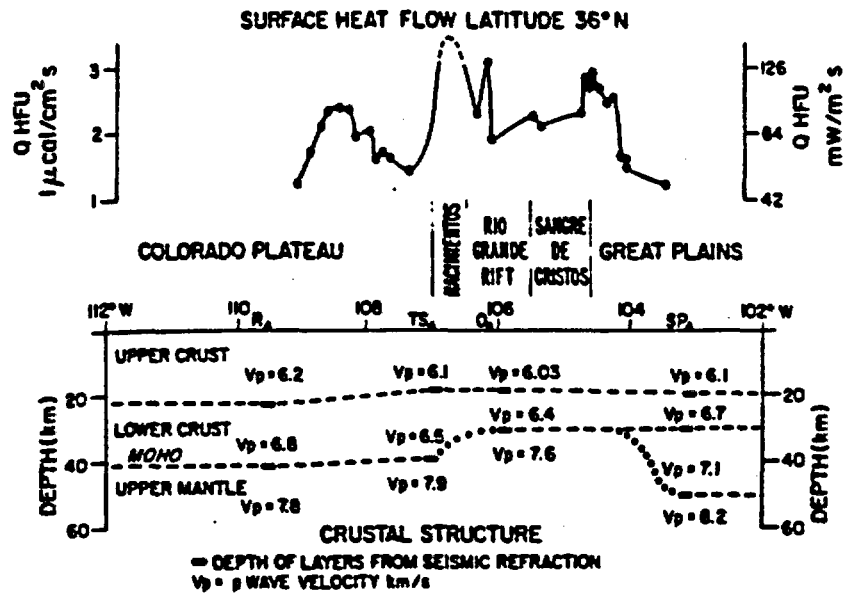
Generalized geologic map of the Death Valley Pancake Range Volcanic Zone. Crowe et. al. 1986



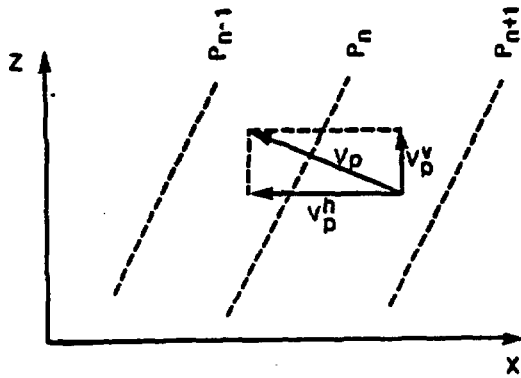
Regional heat-flow values within and adjacent to the Nevada Test Site. Sass J H and Lachenbruch, 1982.



Crustal temperature as a function of depth and surface heat flow. Bridwell R.J. and Potzick. 1981

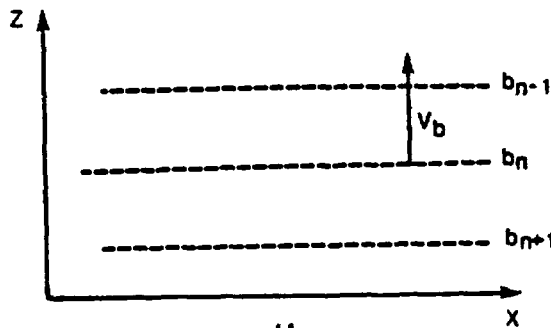


Surface heat flow and seismic crustal structure for the Rio Grande rift and associated physiographic provinces of the North American Continent. Bridwell R.J. and Potzick, 1981.



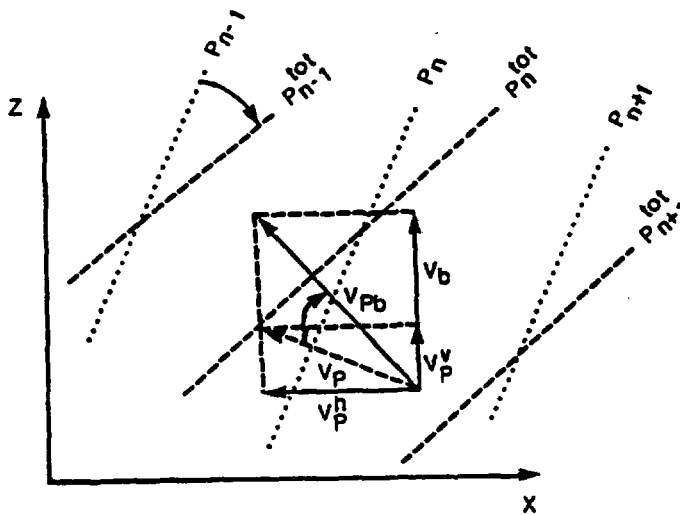
PRESSURE GRADIENT.  
 $V_p$ -VELOCITY

+



BUOYANCY GRADIENT.  
 $V_b$ -VELOCITY

||



TOTAL HYDRAULIC GRADIENT.  
 $V_{Pb}$ -VELOCITY

Total hydraulic gradient combines buoyancy and pressure gradient.

## GOVERNING EQUATIONS

### CONSERVATION OF FLUID MASS:

$$\rho^f (c^f - c^s) p_{,t} - \phi \rho^f \beta T_{,t} - (\rho^f \frac{k}{\mu} ij (p_{,j} - \rho^f g_j))_{,i} = 0 \quad \text{AND}$$

### CONSERVATION OF THERMAL ENERGY:

$$((\rho C)^* T)_{,t} - (\lambda^* T_{,i})_{,i} + (\rho^f C^f (\frac{k}{\mu} ij (p_{,j} - \rho^f g_j)) T)_{,i} = 0.$$

## EQUATIONS OF STATE

$$\rho^f = \rho^f(p, T), \quad \mu^f = \mu^f(p, T).$$

Note: For explanation of symbols used see plate 3.3.2-4.

CONSERVATION OF FLUID MASS:

$$\langle \phi \rho^f (c^f + c^s) p_{,t} \rangle_{\Psi_I} - \langle \phi \rho^f \beta T_{,t} \rangle_{\Psi_I} - \langle \rho^f \frac{k}{\mu} i_j (p_{,j} - \rho^f g_j) \rangle_{\Psi_I} = 0 \quad \text{AND}$$

CONSERVATION OF THERMAL ENERGY:

$$\langle ((\rho C)^s T)_{,t} \rangle_{\Psi_I} - \langle (\lambda T_{,ii}) \rangle_{\Psi_I} + \langle \rho^f C^f \left( \frac{k}{\mu} i_j (p_{,j} - \rho^f g_j) \right) T \rangle_{\Psi_I} = 0$$

Note: For explanation of symbols used see plate 3.3.2-4.

Governing equations in the Galerkin finite element method. Thuvik R. and Braester C., 1982.

Symbol	Description
c	compressibility
C	specific heat capacity
g	acceleration of gravity
k	permeability
p	pressure
Q	heat flow rate
t	time
T	temperature
$x_i$	Cartesian coordinate
$\beta$	coefficient of thermal volume expansion of the fluid
$\lambda$	thermal conductivity
$\mu$	dynamic viscosity
$\phi$	porosity
$\Psi$	basis function

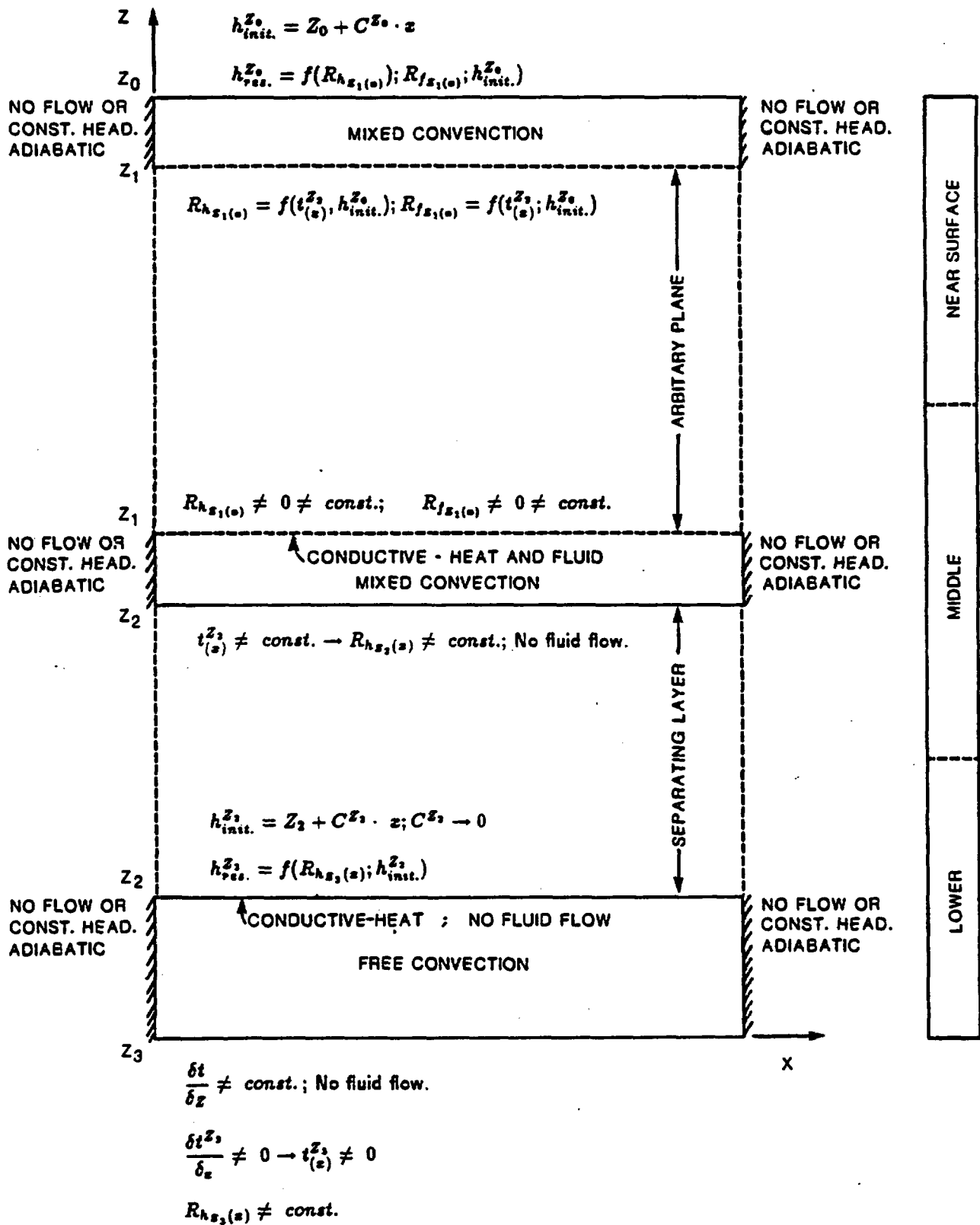
$$\langle f(x), g(x) \rangle = \int_V f(x)g(x) dv, \text{ inner product}$$

#### superscripts

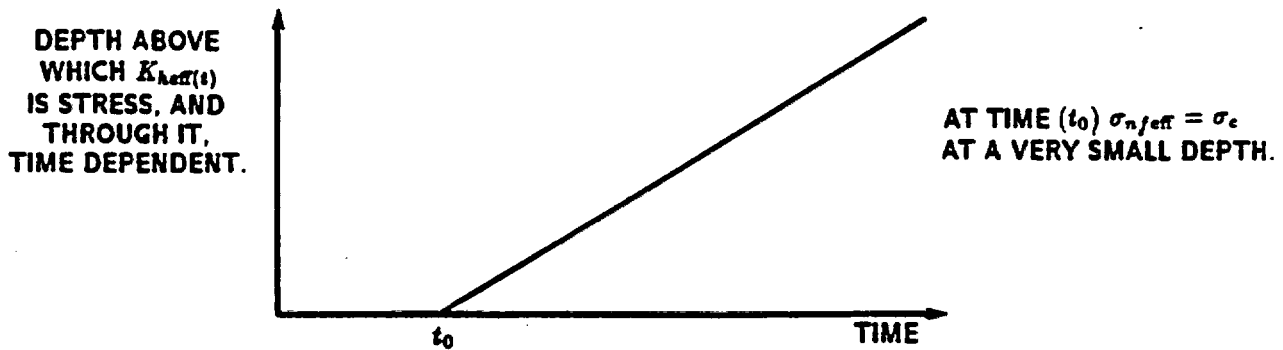
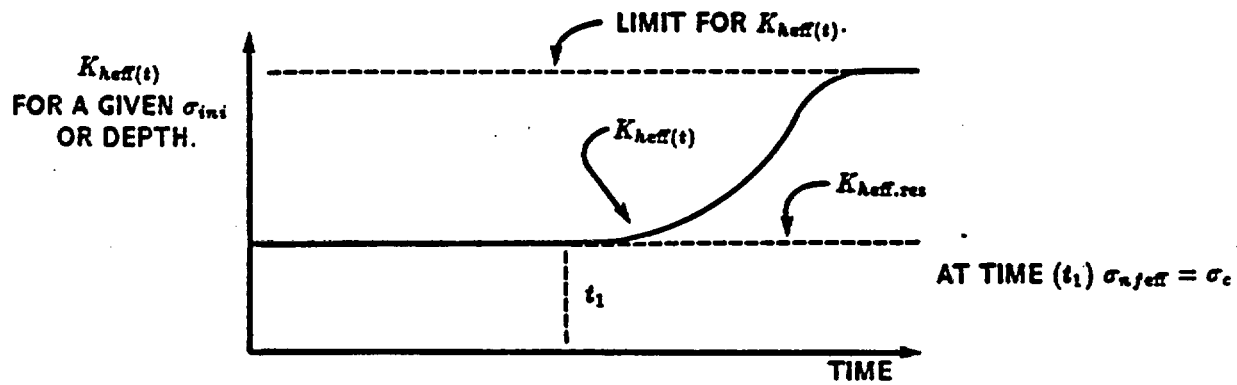
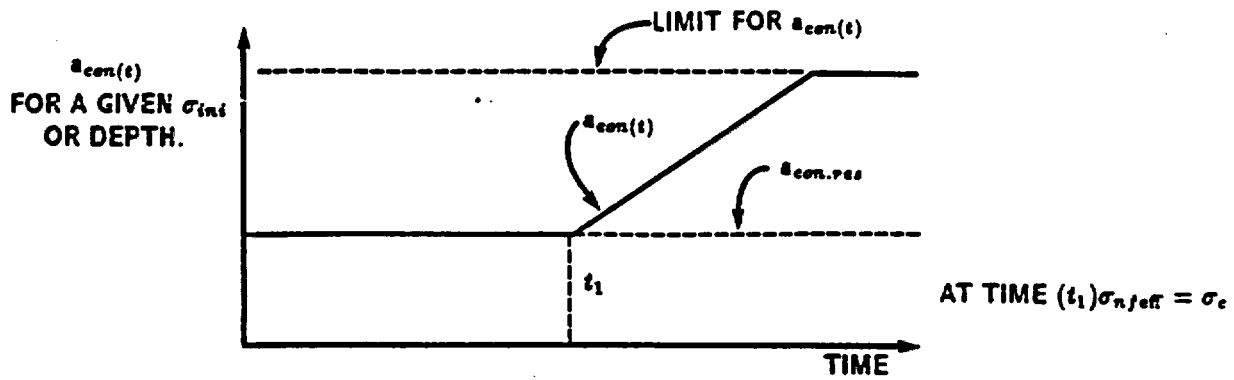
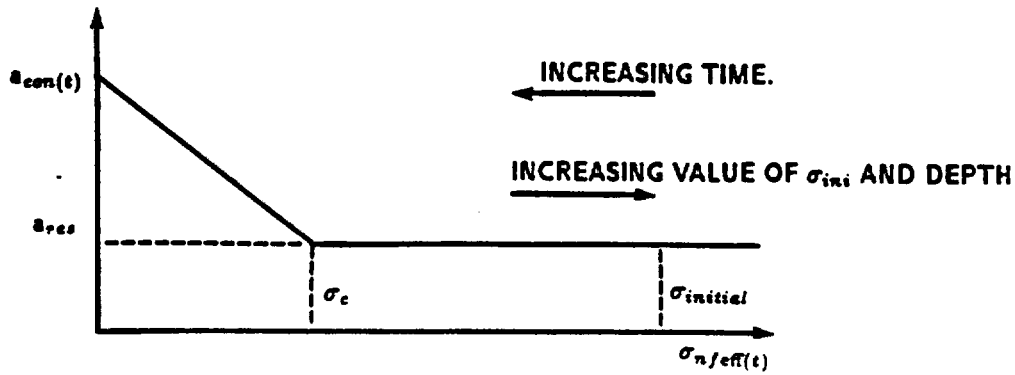
f	fluid
r	rock
*	equivalent medium

#### subscripts

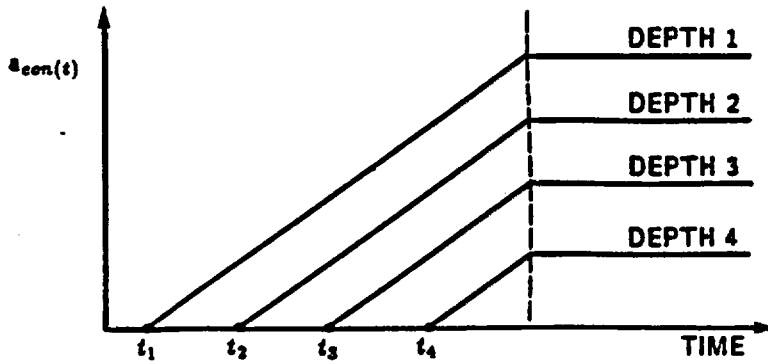
$i, j$	indices used for Cartesian tensor notation, repeated indices indicate summation over these indices ( $i=j=1,2,3$ )
$p_{,t}$	partial time derivative of p
$p_{,j}$	gradient of p
I	node index



Conceptual model of flow system which contains a strong thermal inhomogeneity at its base.



Relationship between time and thermal conductivity caused by incremental reduction in  $\sigma_{n/eff}$ .

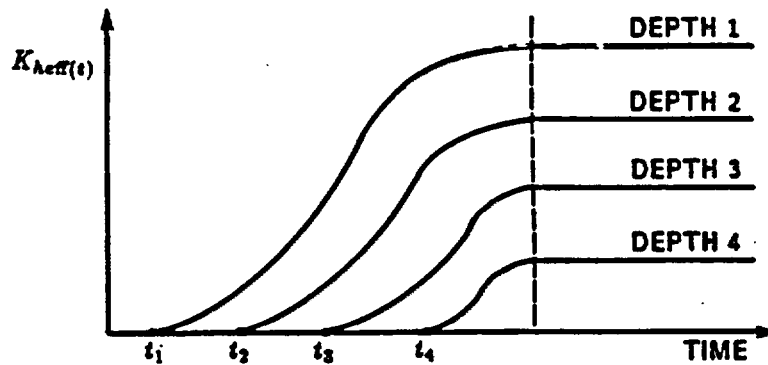


$$\sigma_{\text{con}}(t) = \sigma_{\text{res}} + \sigma_d(t)$$

$$\sigma_d(t) > 0 \text{ if } \tau_s(t) = \tau_{\text{max}}$$

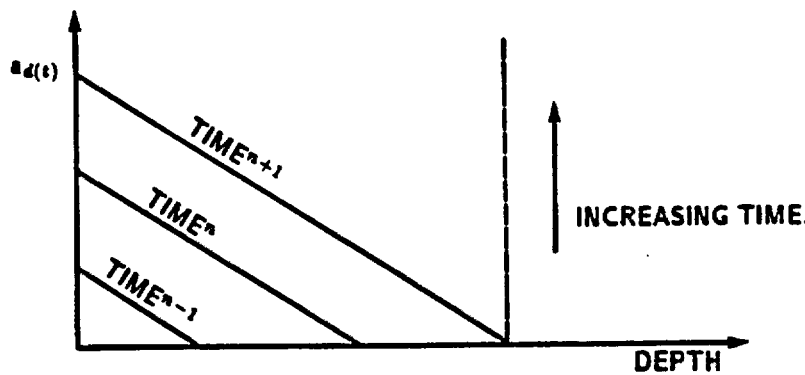
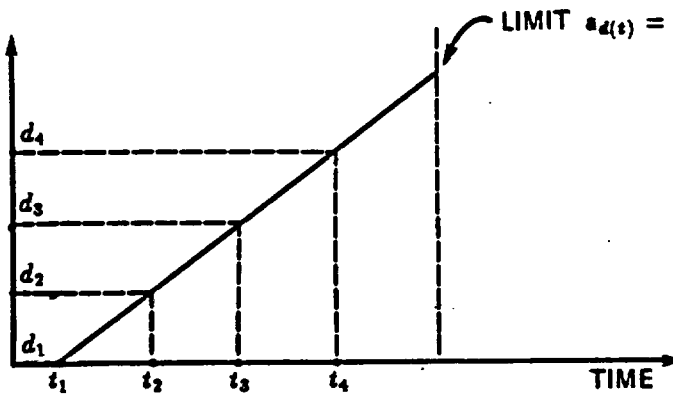
$$\text{OTHERWISE } \sigma_d(t) = 0$$

$t_n$  - TIME REQUIRED FOR  $\tau_s(t)$  to reach  $\tau_{\text{max}}$

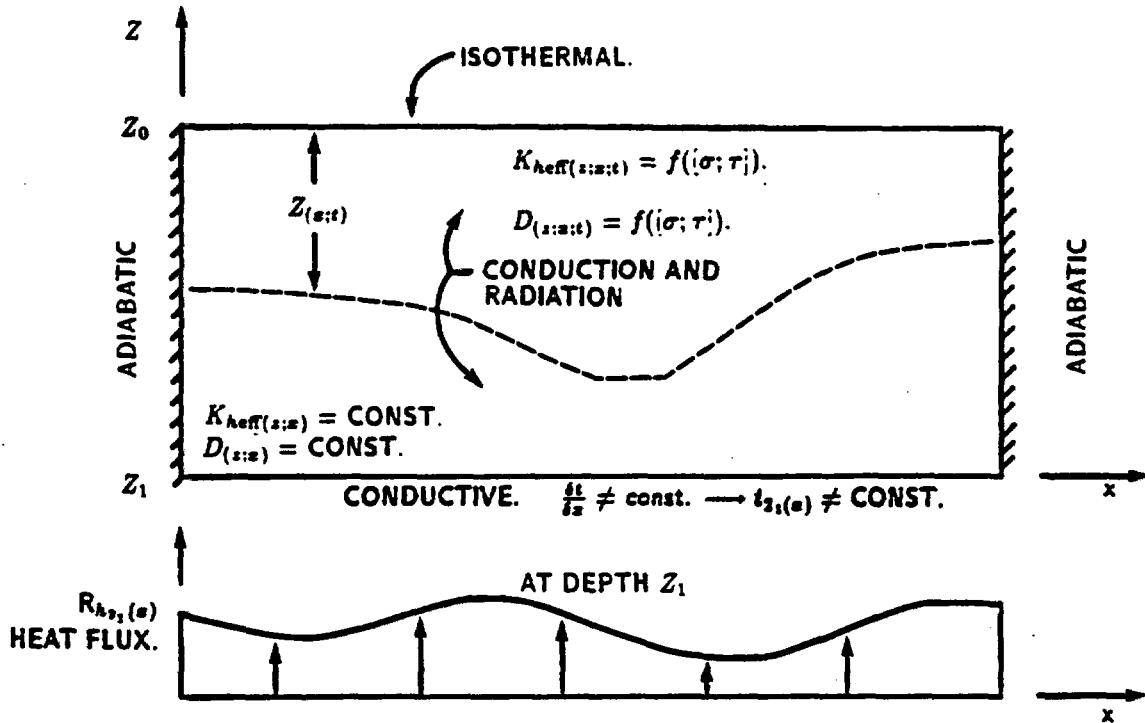


AT TIME  $t_1$ , AT DEPTH 1  
 $\tau_s(t_1) = \tau_{\text{max}}$

DEPTH BELOW WHICH  
 $\tau_s < \tau_{\text{max}}$   
AND THEREFORE  
 $\sigma_d = 0$



Relationship between time and thermal conductivity caused by incremental increases in  $\tau_s$ .



$$Z(z;t) = f((\sigma; \tau)): \quad (\sigma; \tau) = f(t)$$

$$R_{h_{s_1}}(z;t) = \text{CONST.} - \text{NO CHANGE IN HEAT FLUX THROUGH TIME.}$$

$$K_{\text{heff}}(z;x;t;\text{temp}) = \text{CONST.} - \text{THERMAL CONDUCTIVITY IS TEMPERATURE INDEPENDENT.}$$

#### GOVERNING EQUATIONS:

- BELOW DEPTH  $Z(z;t)$  - STEADY STATE. - POISSON'S EQUATION.

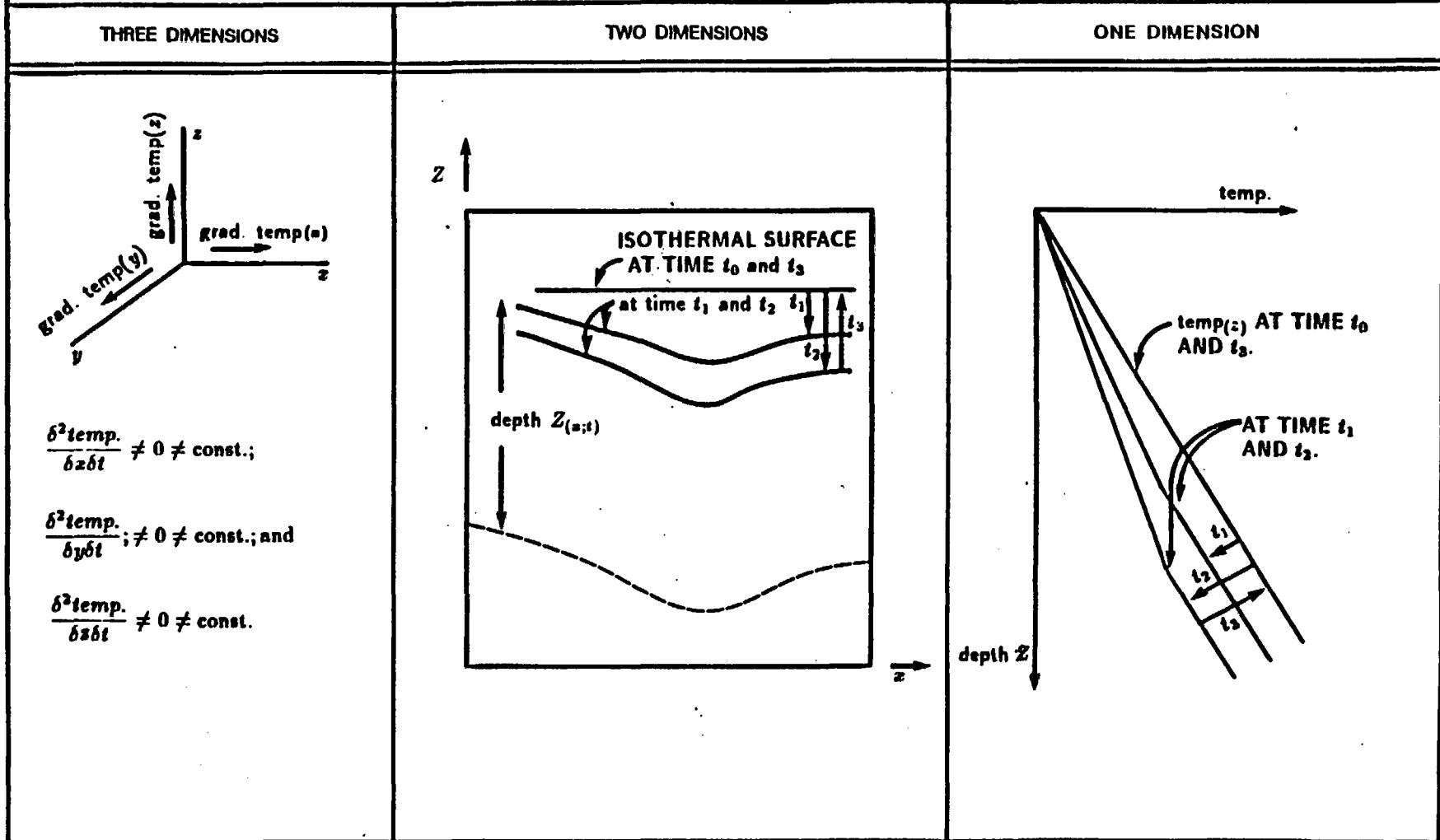
$$\frac{\delta^2 \text{temp.}}{\delta x^2} + \frac{\delta^2 \text{temp.}}{\delta z^2} = -R_{h_{s_1}}(z) \cdot K_{\text{heff}}^{-1}$$

- ABOVE DEPTH  $Z(z;t)$  - TRANSIENT FLOW.

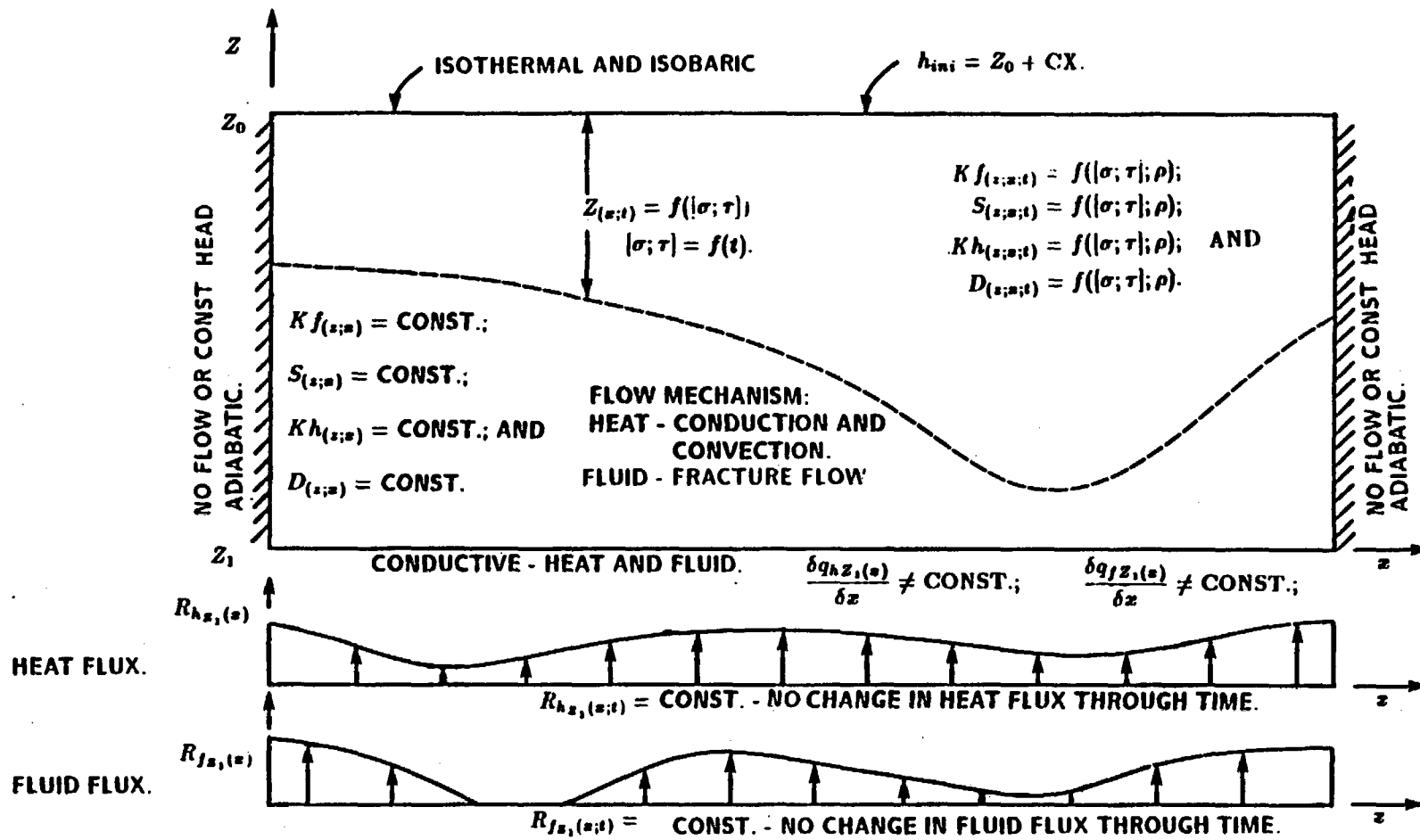
$$\frac{\delta^2 \text{temp.}}{\delta x^2} + \frac{\delta^2 \text{temp.}}{\delta y^2} = D_{(z;x;t)}^{-1} \cdot \frac{\delta \text{temp.}}{\delta t} - R_{h_{s_1}}(z) \cdot K_{\text{heff}}^{-1}(z;x;t)$$

Conceptual model of "simple" heat flow trough deforming fractured medium

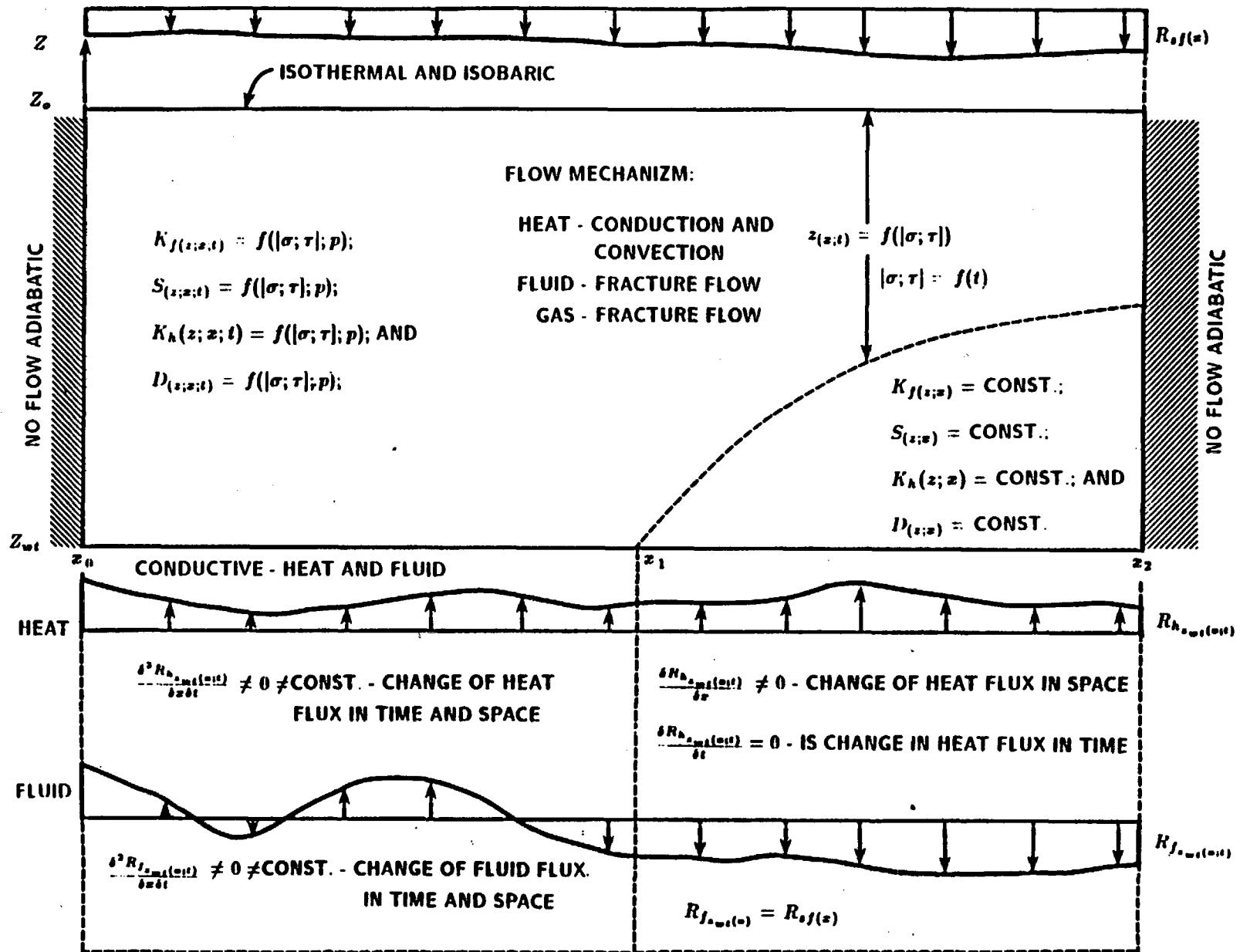
HEAT FLOW FIELD DEVELOPED IN THE DEFORMING FRACTURED MEDIUM WITH  $R_{h_{s_1}(z;t)} = \text{CONST.}$   
 HAS THE FOLLOWING CHARACTERISTICS.



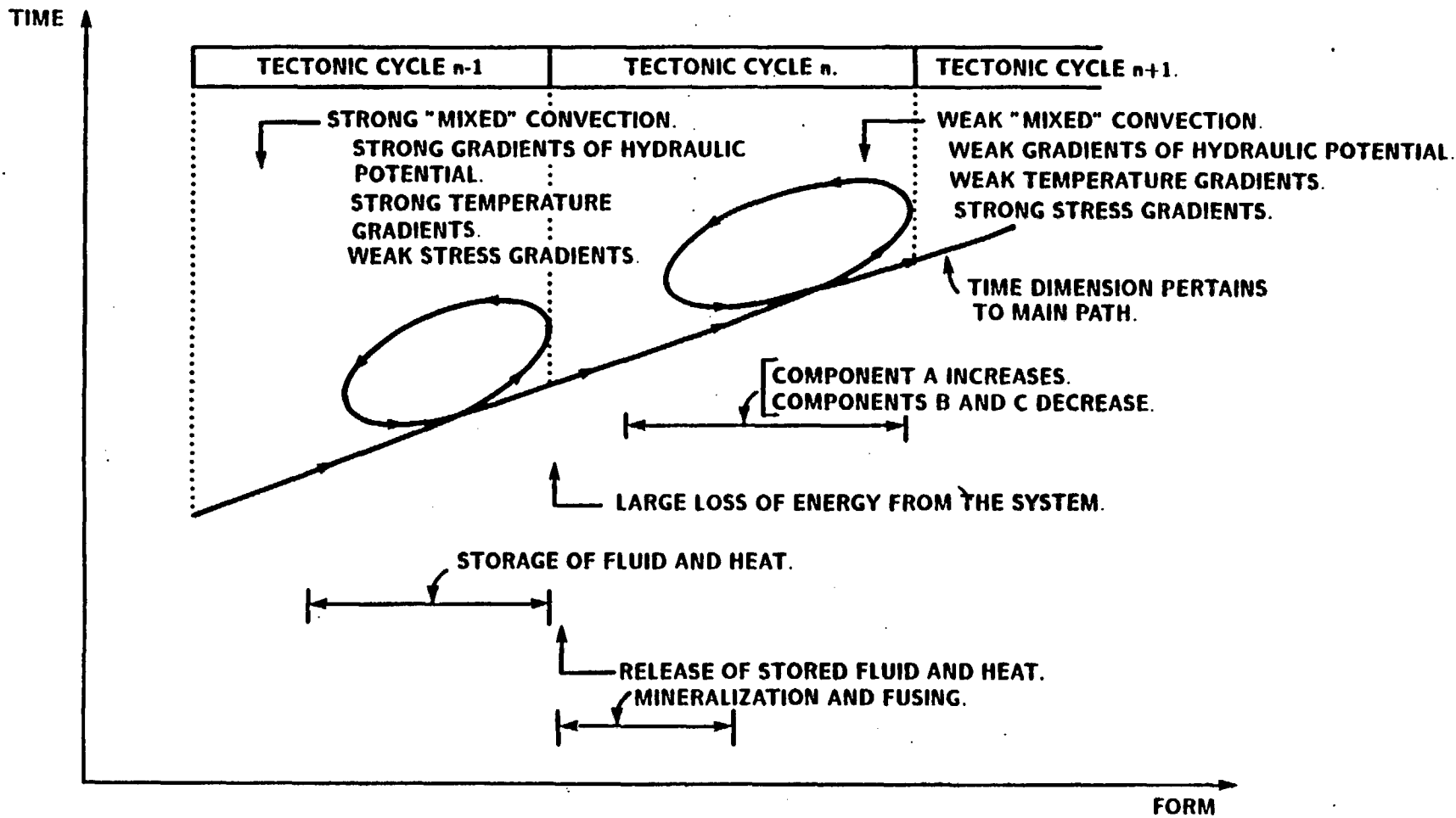
Main characteristics of the heat flow field developed in the deforming fractured medium.



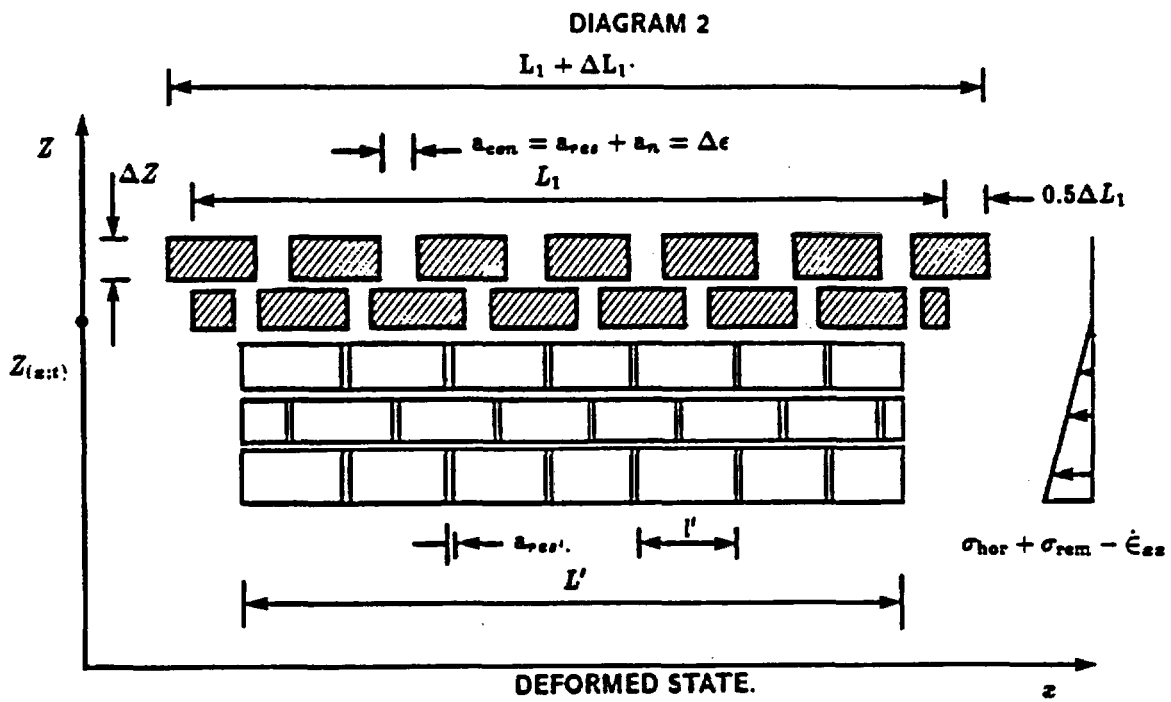
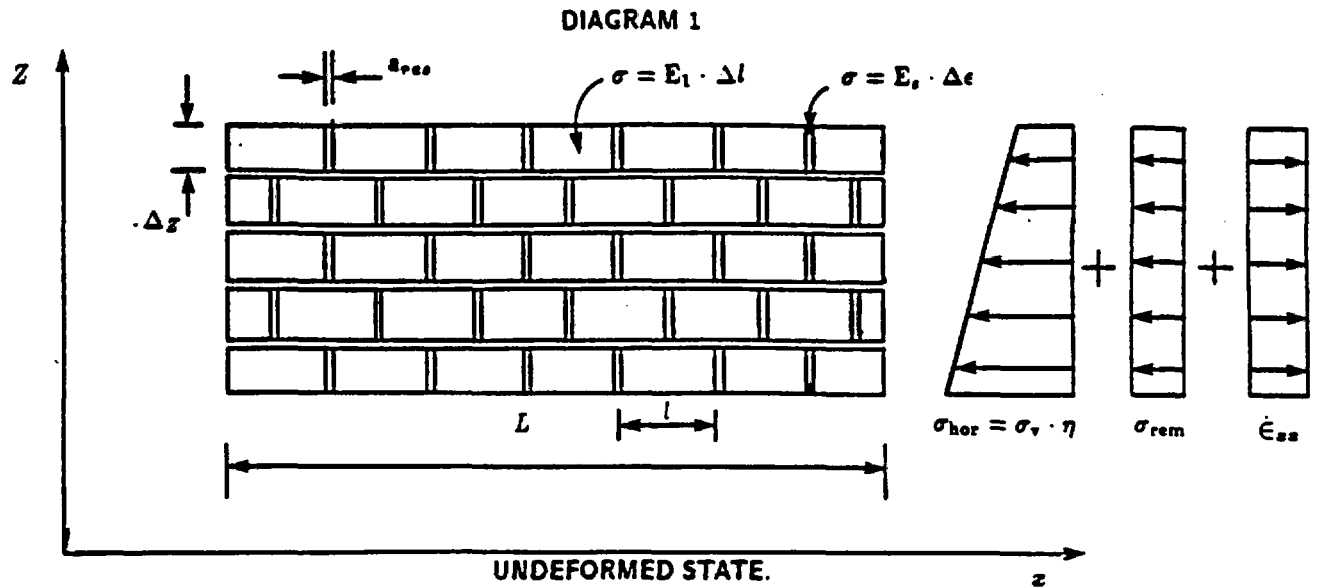
Conceptual model of two phase, heat-fluid coupled, flow field developed in the deforming fractured medium.



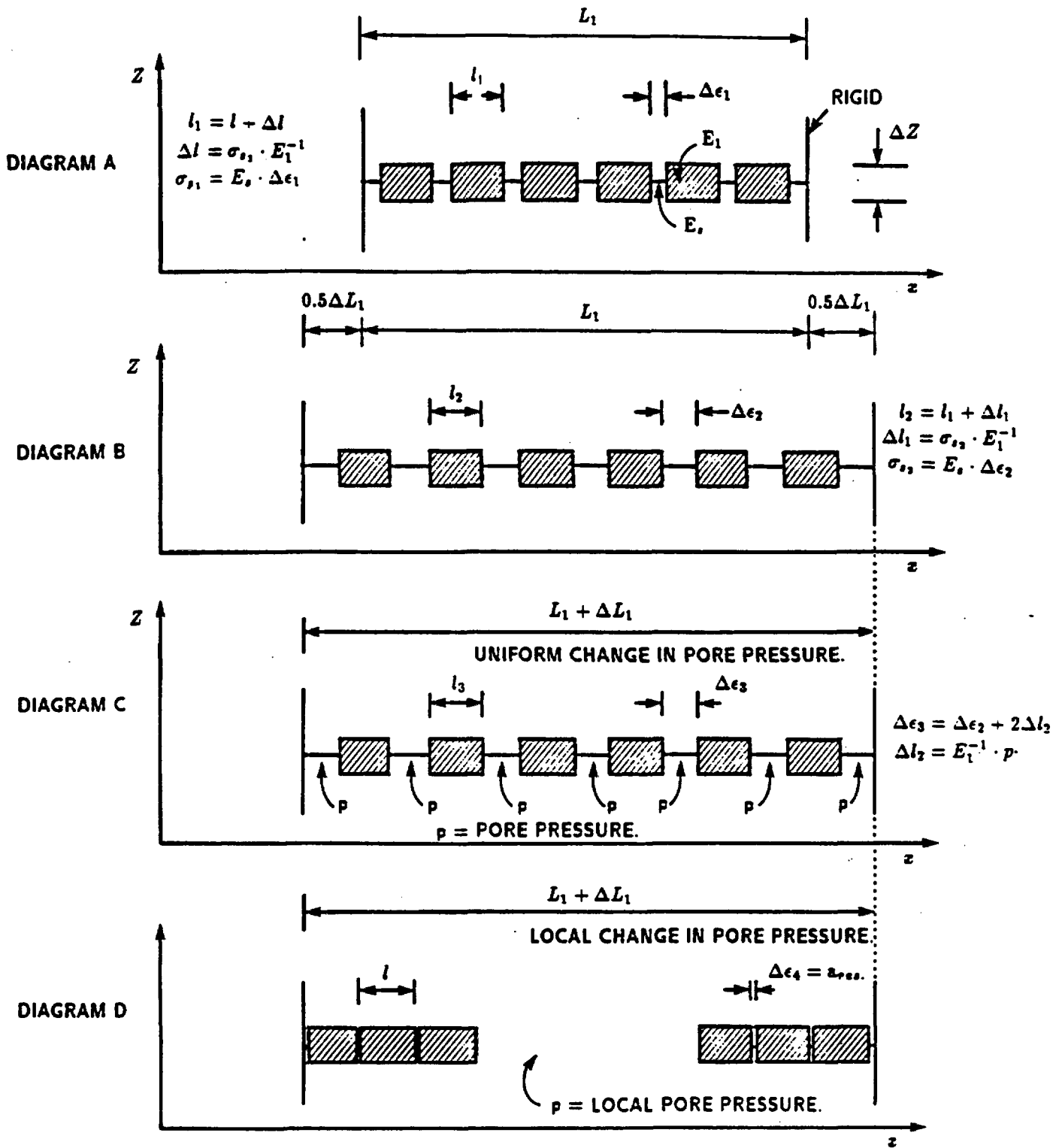
Conceptual model of flow in vadose zone of the two phase, heat-fluid coupled, flow field developed in the deforming fractured medium.



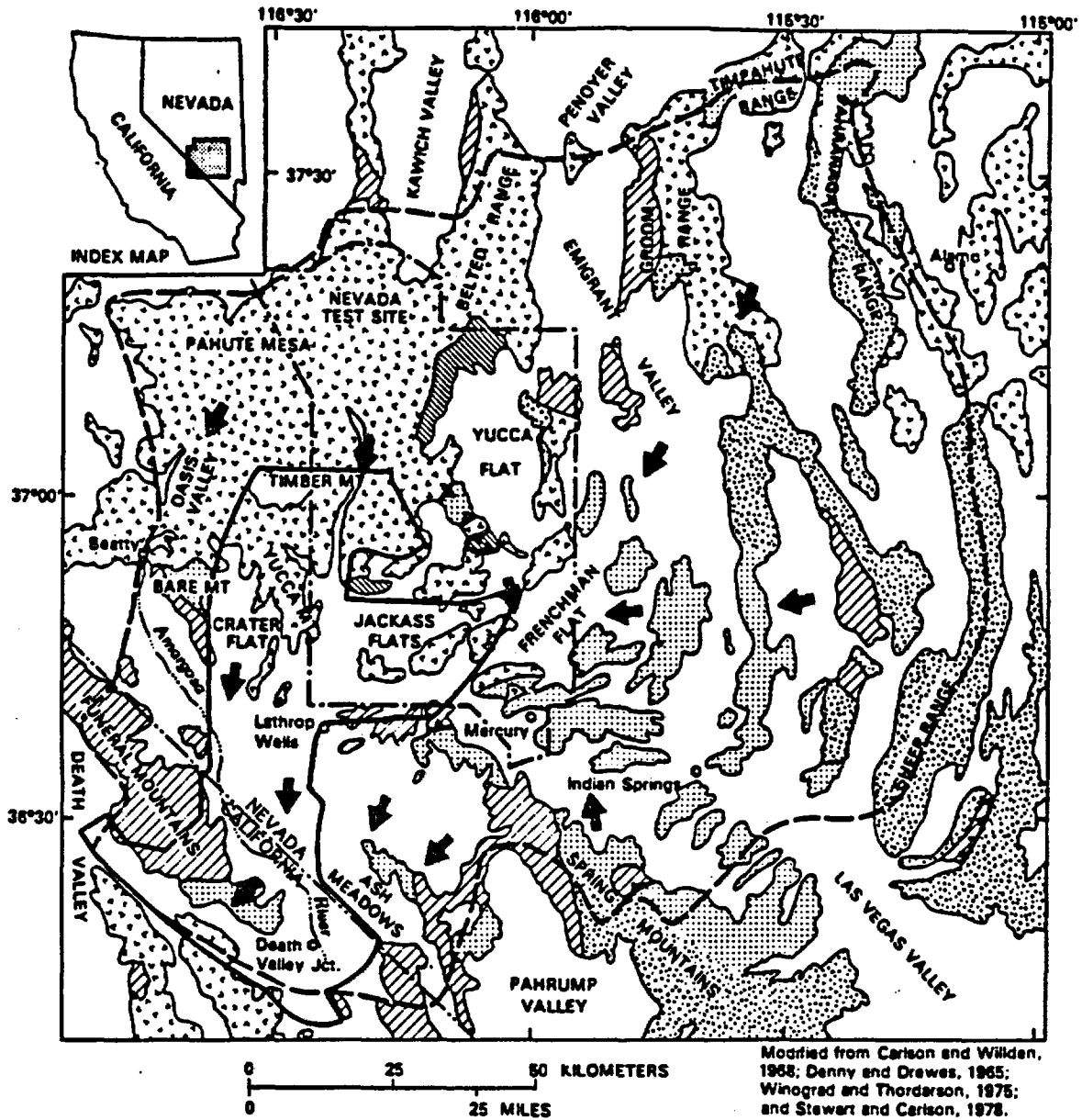
Evolutionary path of the coupled fluid and heat flow field developed in the deforming fractured medium.



Idealized response of the fractured medium during uniform extension.



Idealized response of the dilated fractured medium to sudden changes in pore pressure.

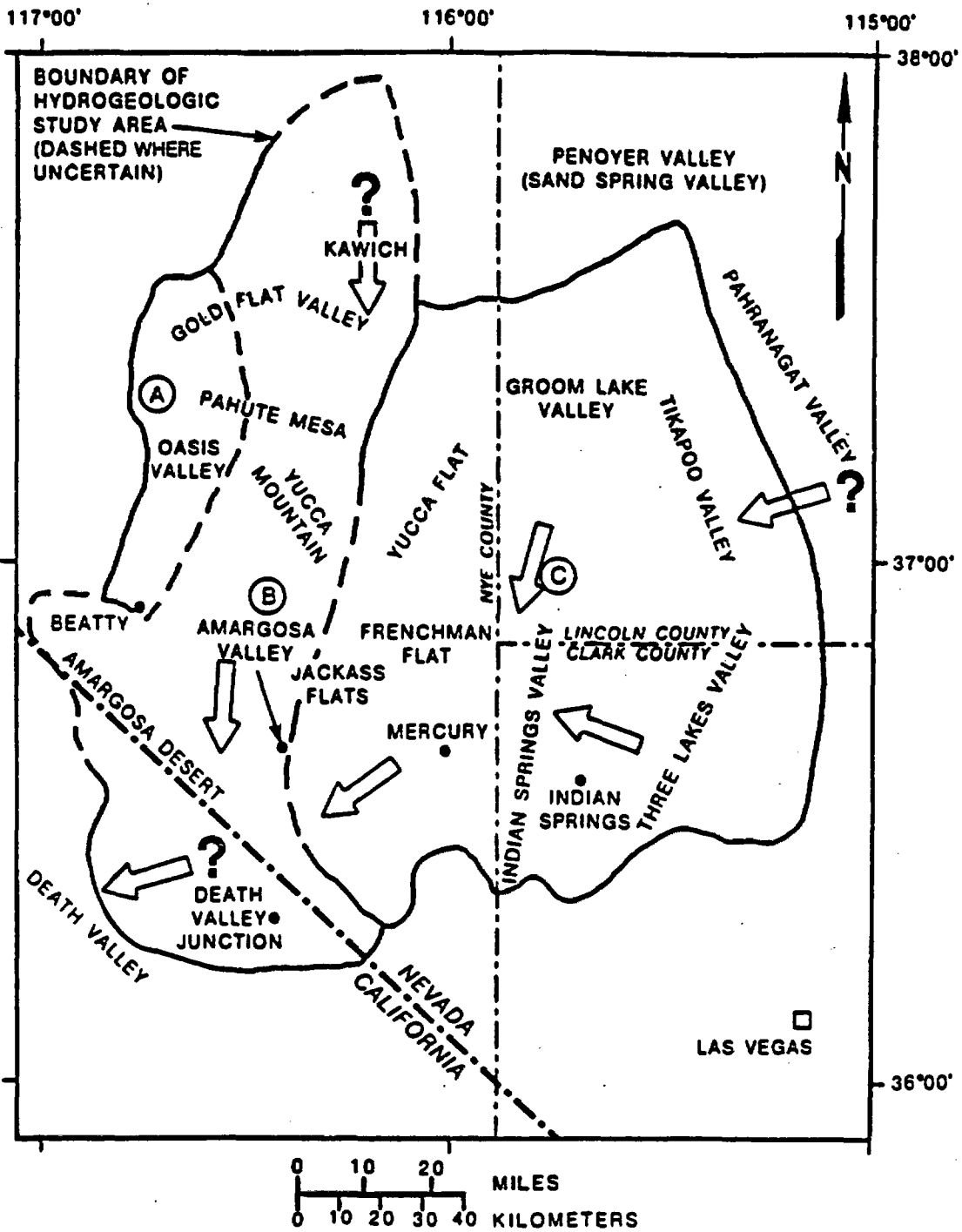


Modified from Carlson and Willden, 1968; Denny and Drewes, 1965; Winograd and Thordarson, 1975; and Stewart and Carlson, 1978.

**EXPLANATION**

- |                                     |   |   |
|-------------------------------------|---|---|
| <b>QUATERNARY</b>                   | Alluvium, lake beds, and minor volcanic rocks                                   | Lower carbonate aquifer   |
| <b>TERTIARY</b>                     | Tuff, rhyolite, and associated volcanic rocks                                   | <b>PALEOZOIC (CAMBRIAN) AND PRECAMBRIAN</b>   |
| <b>MESOZOIC (Minor - not shown)</b> |   | Lower classic aquitard  |
| <b>PALEOZOIC</b>                    | Undifferentiated upper classic aquitard, and lower and upper carbonate aquifers | <b>SYMBOLS</b>  |
| Upper classic aquitard              |   | Contact   |
|                                     |   | Trust fault with sawteeth on upper plate  |
|                                     |   | Regional model boundary (Waddell, 1982) (approximate boundary of ground-water system) |
|                                     |   | Subregional model boundary (this report)  |
|                                     |   | Approximate direction of ground water flow  |

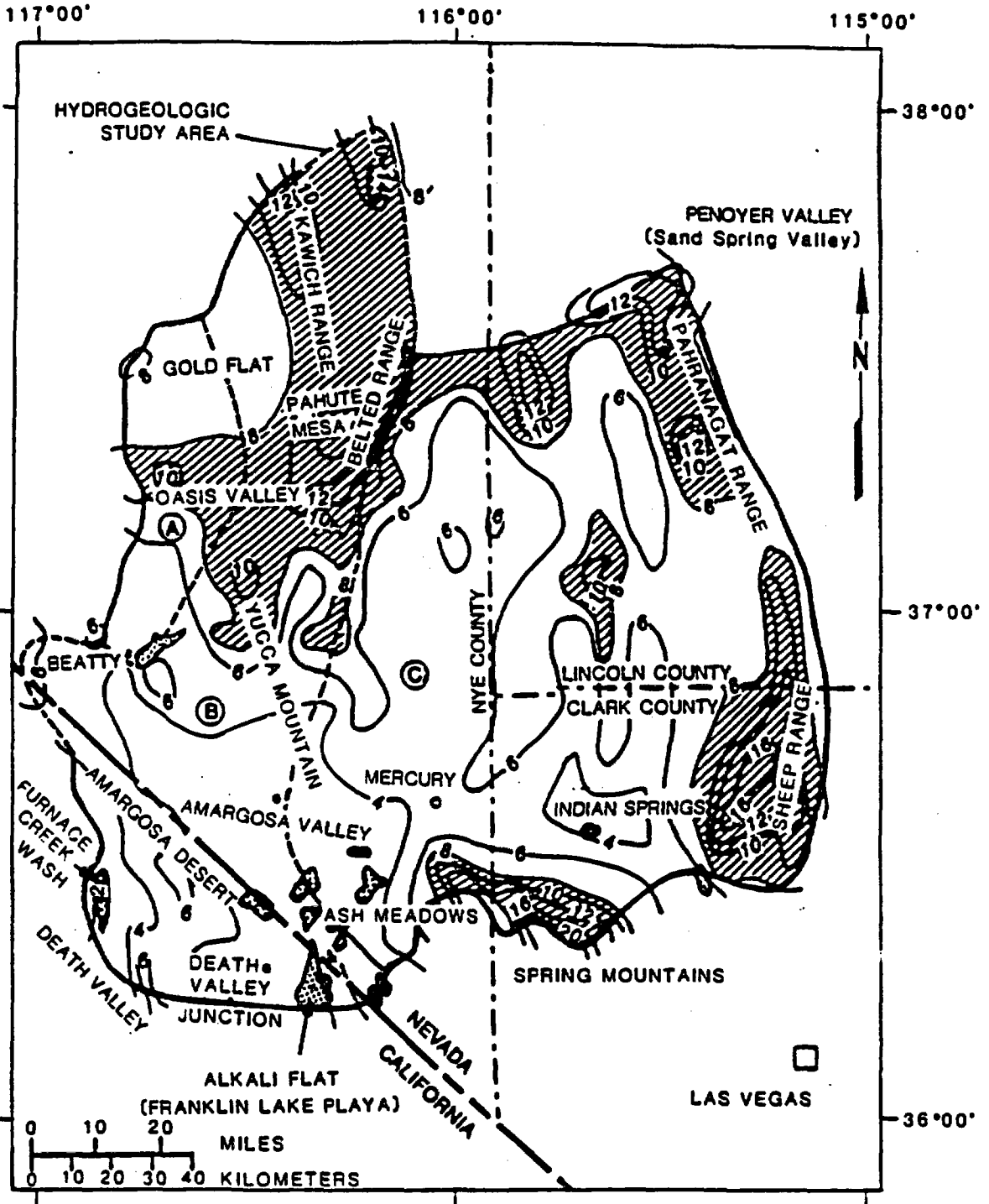
Location of the Death Valley groundwater system. From Czarnecki and Waddell (1984).



➔ GENERAL DIRECTION OF REGIONAL GROUND-WATER FLOW (QUESTION MARK INDICATES UNCERTAINTY)

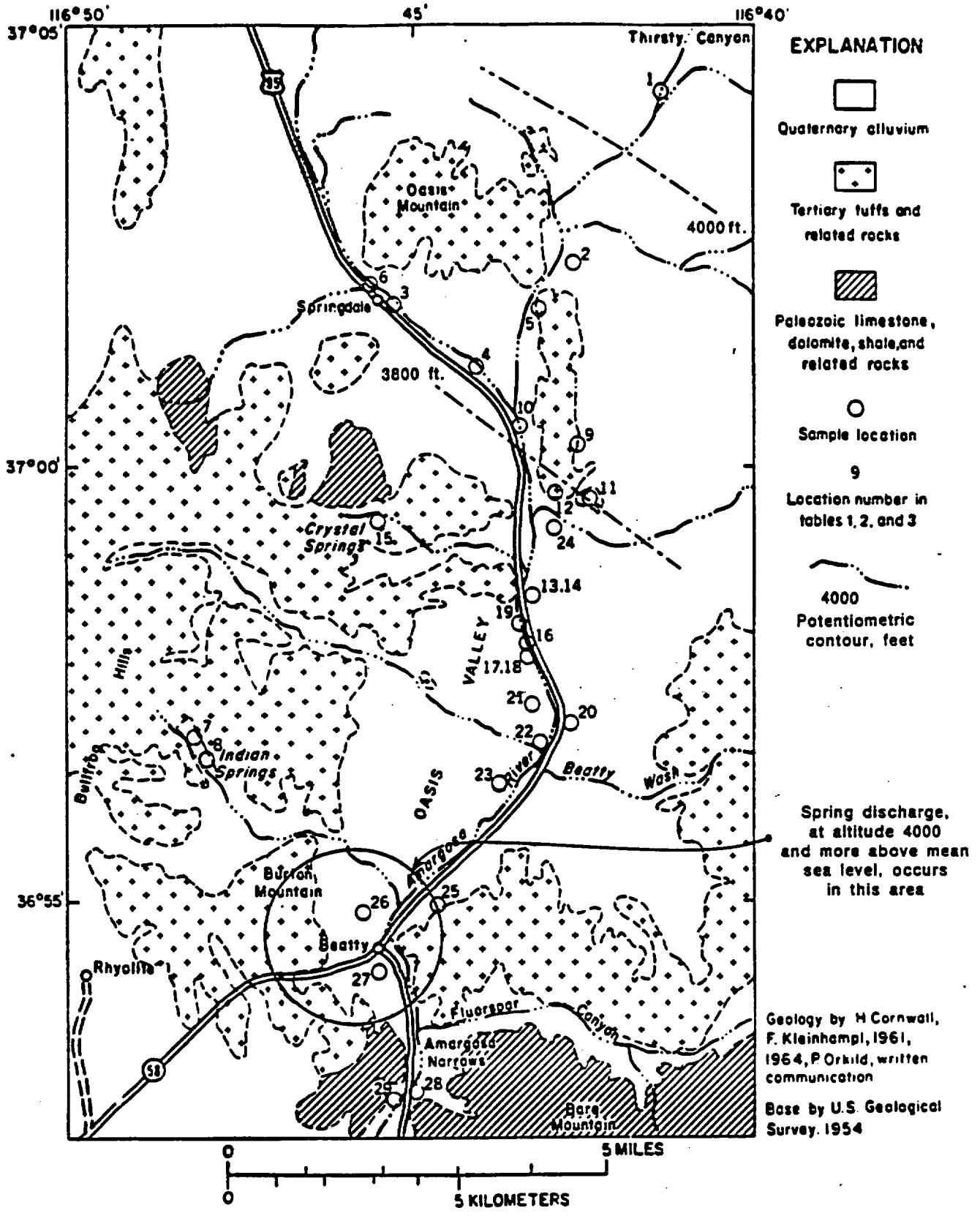
- A. OASIS VALLEY SUBBASIN
- B. ALKALI FLAT-FURNACE CREEK RANCH SUBBASIN
- C. ASH MEADOWS SUBBASIN

Subdivision of the Death Valley groundwater system. Modified from Winograd and Thordarson (1975), Waddell (1982) and Waddell et al., 1984.



-  RECHARGE AREAS
-  DISCHARGE AREAS
-  BOUNDARY OF HYDROGEOLOGIC STUDY AREA; DASHED WHERE UNCERTAIN
-  SUBBASIN BOUNDARY
-  (A) OASIS VALLEY SUBBASIN
-  (B) ALKALI FLAT-FURNACE CREEK RANCH SUBBASIN
-  (C) ASH MEADOWS SUBBASIN
-  -o- LINE OF EQUAL AVERAGE ANNUAL PRECIPITATION, IN INCHES

Precipitation, recharge and discharge areas for the Death Valley groundwater system. From Winograd and Thordarson (1975), Waddell (1982) and Waddell et al., (1984).



Local hydrologic conditions at Beatty, Nevada. Modified from White (1979) and Winograd and Thordarson (1975).

TABLE 2.—Analysis of selected major chemical constituents

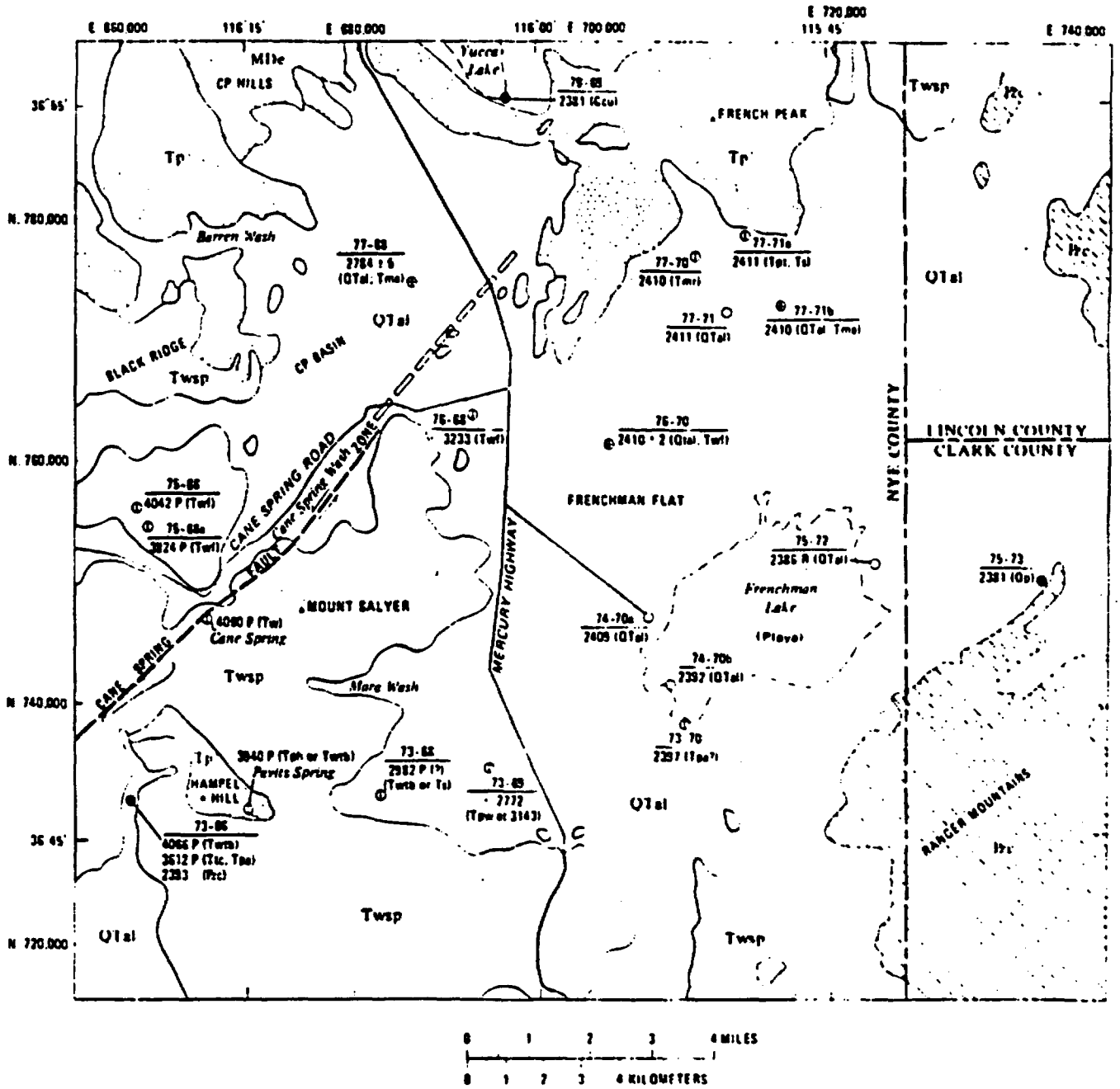
(Sampling-site numbers keyed to figures, samples collected July 3-6, 1967 Qal=Alluvium of Quaternary age. T= Volcanics of Tertiary age (Concentrations in millimoles per liter, except as indicated)

Sampling-site number	Probable aquifer source	Temperature (°C)	pH	Dissolved constituents									Total dissolved solids (mg/L)
				calcium (Ca)	magnesium (Mg)	sodium (Na)	potassium (K)	bicarbonate (HCO <sub>3</sub> )	chloride (Cl)	fluoride (F)	sulfate (SO <sub>4</sub> )	silica (SiO <sub>2</sub> )	
1	TTTTT	23.0	8.1	0.18	0.01	6.22	0.21	3.39	1.44	0.22	0.86	0.95	454
2	TTTTT	18.0	7.7	0.85	0.06	7.44	2.22	4.57	1.83	9.99	1.06	1.03	573
3	TTTTT	19.8	7.6	0.88	0.18	4.35	2.00	3.75	1.18	13	0.85	1.18	421
4	TTTTT	22.0	7.6	0.78	0.22	5.96	0.00	5.08	1.04	12	1.00	1.03	523
5	TTTTT	22.0	7.8	0.78	0.19	7.35	0.23	4.85	1.92	23	1.07	0.90	584
6	TTTTT	22.5	7.8	0.80	0.19	4.35	0.20	3.80	1.13	0.9	0.61	1.20	424
7	TTTTT	22.8	8.7	0.01	0.01	2.57	0.04	1.90	0.39	0.2	0.15	0.73	192
8	TTTTT	21.0	7.9	0.15	0.04	2.44	0.04	2.07	0.42	0.2	0.18	0.8	213
9	TTTTT	21.0	8.2	0.40	0.04	5.31	0.12	3.01	1.27	0.15	0.9	0.7	421
10	TTTTT	21.0	7.7	0.65	0.18	9.70	0.22	6.23	2.26	0.27	1.35	1.03	726
11	TTTTT	24.0	8.1	0.35	0.03	8.53	0.06	5.41	1.82	0.32	1.13	0.63	583
12	TTTTT	18.8	7.6	0.35	0.02	6.79	0.18	4.79	1.18	0.24	0.95	0.85	511
13	TTTTT	26.8	7.8	0.45	0.02	7.53	0.20	4.39	1.33	0.32	1.32	1.07	572
14	TTTTT	24.8	7.8	0.42	0.02	7.13	0.19	4.15	1.21	0.36	1.25	1.07	546
15	TTTTT	24.8	7.7	0.55	0.15	2.18	0.08	2.33	0.86	0.03	0.23	0.75	251
16	TTTTT	31.8	7.7	0.88	0.12	10.09	0.22	6.10	1.95	0.32	1.65	1.00	750
17	TTTTT	23.8	7.7	0.82	0.13	10.57	0.21	6.44	2.03	0.32	1.74	0.93	783
18	TTTTT	26.8	7.9	0.85	0.13	10.70	0.21	6.46	2.03	0.32	1.74	0.90	777
19	TTTTT	21.0	7.8	0.82	0.12	6.83	0.20	3.65	0.99	0.32	1.21	0.90	509
20	TTTTT	21.8	8.0	0.80	0.21	5.00	0.20	3.03	2.82	0.37	2.27	0.98	396
21	TTTTT	18.0	9.1	0.25	0.19	13.70	0.23	8.39	1.92	0.34	1.76	0.75	997
22	TTTTT	21.0	8.2	0.21	0.00	10.83	0.06	5.08	0.76	0.20	0.73	0.77	737
23	TTTTT	34.0	8.3	0.30	0.03	4.87	0.12	2.84	1.27	0.14	0.85	0.83	355
24	TTTTT	21.0	8.2	0.32	0.11	5.39	0.15	3.03	0.73	0.20	0.73	1.00	414
25	TTTTT	24.8	7.9	0.80	0.18	4.61	0.19	3.21	1.07	0.02	0.97	0.90	384
26	TTTTT	21.8	7.9	0.88	0.13	4.57	0.28	3.47	2.06	0.32	1.86	0.80	440
27	TTTTT	20.0	7.7	0.15	0.15	11.14	0.28	6.49	2.06	0.32	1.36	1.10	814
28	TTTTT	18.8	7.8	0.15	0.15	11.05	0.28	6.39	2.17	0.31	1.91	1.12	820
29	TTTTT	20.0	7.7	0.88	0.23	12.82	0.28	7.20	2.82	0.33	2.80	1.12	1,040

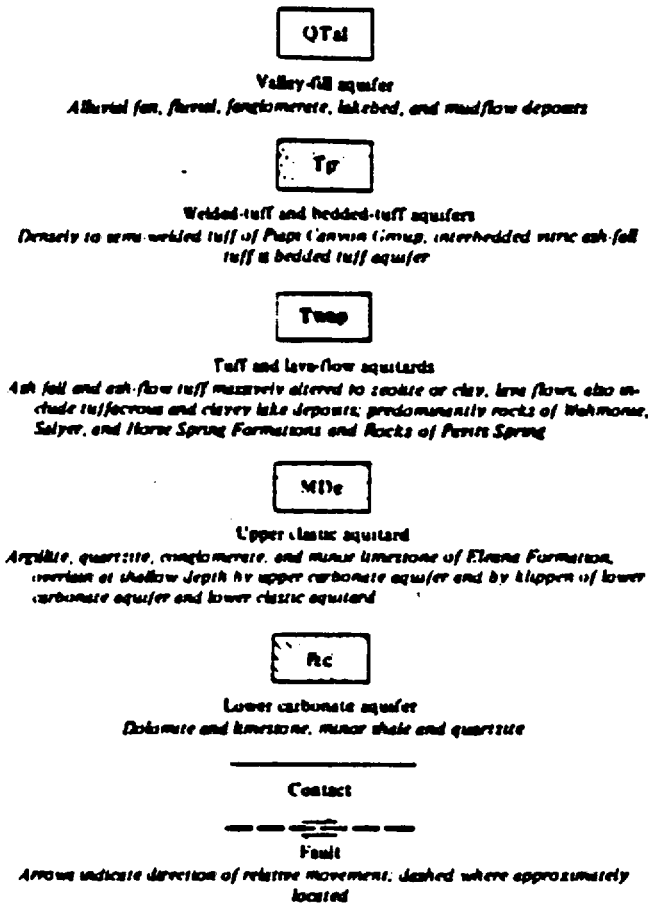
Sampling-site number	Dissolved constituents					
	Iron (Fe)	Copper (Cu)	Iron (Fe)	Aluminum (Al)	Manganese (Mn)	Potassium (K)
1		0.03	0.36	0.22	0.17	0.03
2	21.3	.01	.18	.26	1.71	.09
3	45.3	.13	.20	.15	2.05	.09
4	53.6	.03	.18	.074	4.45	.17
5	31.4	.05	.32	.45	2.17	.18
6	47.1	.02	.32	.37	2.17	.09
7	15.7	.02	.07	.41	.10	.01
8	16.6	.02	.16	.55	.34	.02
9	17.6	.02	.36	.45	1.08	.06
10	41.6	.02	.14	.26	3.19	.14
11	19.4	.05	.27	.11	1.48	.04
12		.03	.81	1.48	.46	.04
13	18.5	.09	.43	.26	1.37	.17
14	17.6	.05	1.52	.03	1.37	.19
15	10.2	.03	.25	.15	.51	.02
16	36.0	.03	.89	3.34	2.51	.03
17	35.1	.08	1.07	.19	2.86	.03
18	30.5	.03	.53	.26	2.97	.03
19	15.7	.05	.18	.04	1.37	.20
20	14.8	.05	1.07	1.11	.23	.02
21	38.8	.03	1.25	.26	4.56	.11
22	34.2	.05	8.41	.93	1.03	.02
23		.06	.20	.30	.23	.01
24	16.6	.02	.16	.52	.68	.04
25	20.3	.05	.18	.26	.86	.02
26	43.4	.03	1.07	.11	1.37	.04
27	46.2	.03	.89	1.12	1.37	.06
28	53.6	.06	.16	1.67	.11	.07
29						

(No analyses for sample site 29)

Results of chemical analyses of water samples from springs and wells, Beatty, Nevada. From White (1979).



Local hydrologic conditions near Skull Mountain at the Nevada Test Site. From Winograd and Thordarson (1975).



TERTIARY AND QUATERNARY

TERTIARY

DEVONIAN AND MISSISSIPPIAN

CAMBRIAN TO DEVONIAN

**HYDRAULIC SYMBOLS**

NOTE: All altitudes in feet; datum is mean sea level; potentiometric contours not drawn for reasons outlined in text

75-72  
● 2301 (QTal)

Test well  
Well tapping lower carbonate aquifer; upper number is well number; lower number is altitude of static water level; symbol in parentheses is formation tapped

73-66  
○ 4085 P (Tma)  
● 3512 P (Tt, Tml)  
● 2383 (Tt)

Test well  
Well tapping tuff aquitard and lower carbonate aquifer; upper number is well number; lower numbers are altitude of static water level; P, perched water; symbols in parentheses are formations tapped

73-68  
< 2772  
○ (Tpt at 3143)

Test well  
Well tapping Tertiary hydrogeologic units; upper number is well number; lower number is altitude of static water level; symbol and number in parentheses are formation tapped and its altitude; symbol < denotes well was dry

75-72  
○ 2384 R (QTal)

Test well or water well  
Well tapping valley-fill aquifer; upper number is well number; lower number is altitude of static water level; R, reported water level; symbol in parentheses is formation tapped

77-77b  
● 2418 (QTal; Tma)

Test well  
Well tapping both valley-fill aquifer and Tertiary hydrogeologic units; upper number is well number; lower number is altitude of static water level; symbols in parentheses are formations tapped

○ 4088 P (Tml)  
Spring

Number is altitude; P, perched or semiperched; symbol in parentheses is formation supplying spring

-----  
Dry lakebed

=====

Inferred ground-water barrier  
Width of symbol not intended to represent width of barrier, which may range from several tens to a few thousand feet

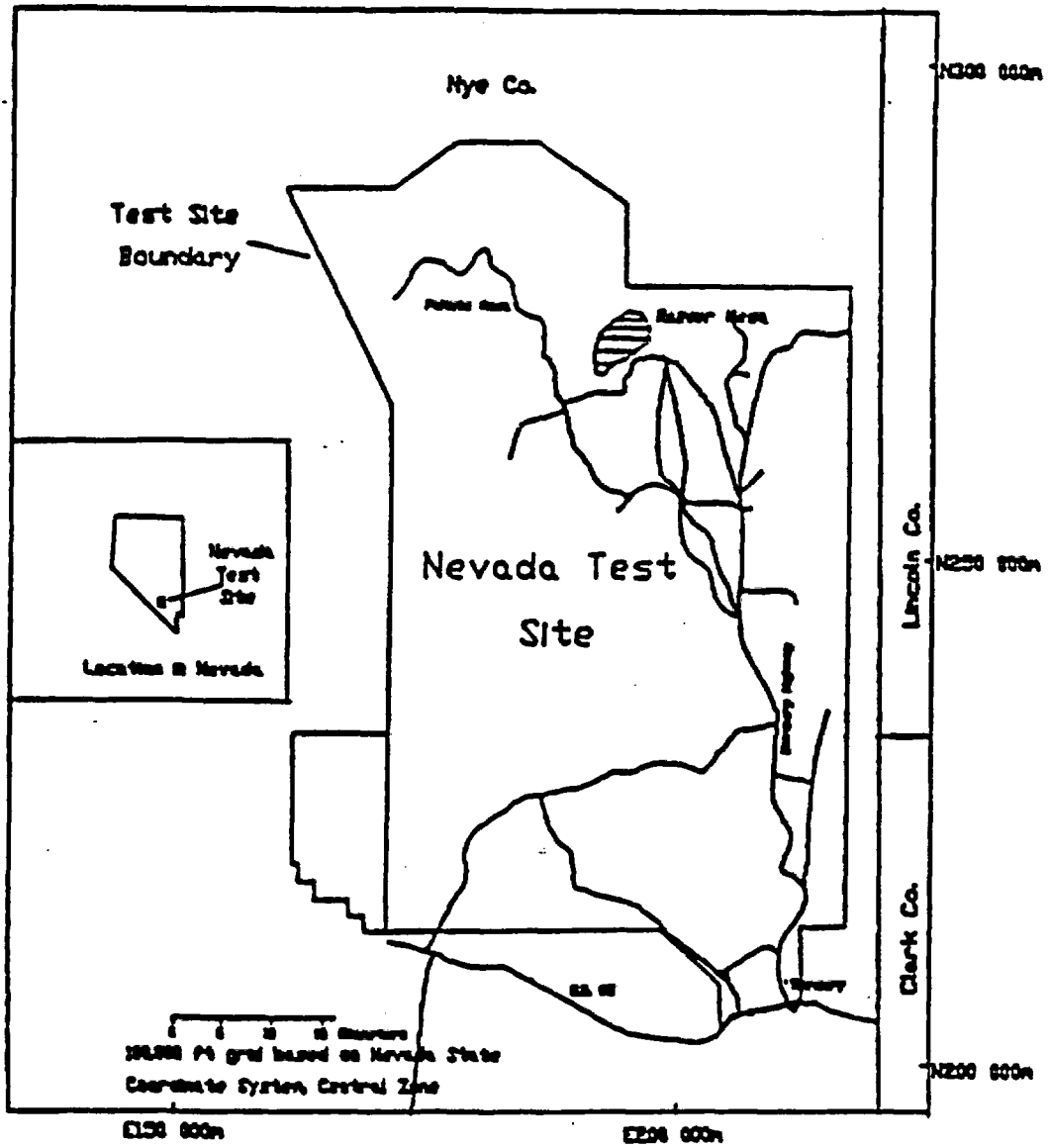
SYMBOL	GEOLOGIC UNIT	HYDROGEOLOGIC UNIT
QTal	Valley fill	Valley-fill aquifer
Tma	Ammonite Tanks Member of Timber Mountain Tuff	Tuff aquifers and aquitard and lava-flow aquitard
Tmr	Rainier Mesa Member of Timber Mountain Tuff	
Tpt	Topopeah Spring Member of Paintbrush Tuff	
Tph	Sandstone and tuff of Hoppel Hill (lower part of Papp Canyon Group)	
Tpw	Tuff and sandstone of Papp Canyon Group, and tuff, sandstone, and lithic tuff of Wahmonie Formation undifferentiated	
Tv	Wahmonie Formation undifferentiated	
Twf	Dacite and rhyodacite lava flows of Wahmonie Formation	
Twtb	Tuff, sandstone, and lithic tuff breccia of Wahmonie Formation	
Ts	Salyer Formation undifferentiated	
Tlc	Tuff of Crater Flat	
Tpa	Rocks of Pavits Spring	Lower carbonate aquifer
Rc	Paleozoic carbonate rock	
Op	Pigouap Group	
Cca	Cassara Formation, upper half	

Explanation of symbols used on Plate 4.2-3. From Winograd and Thordarson (1975).

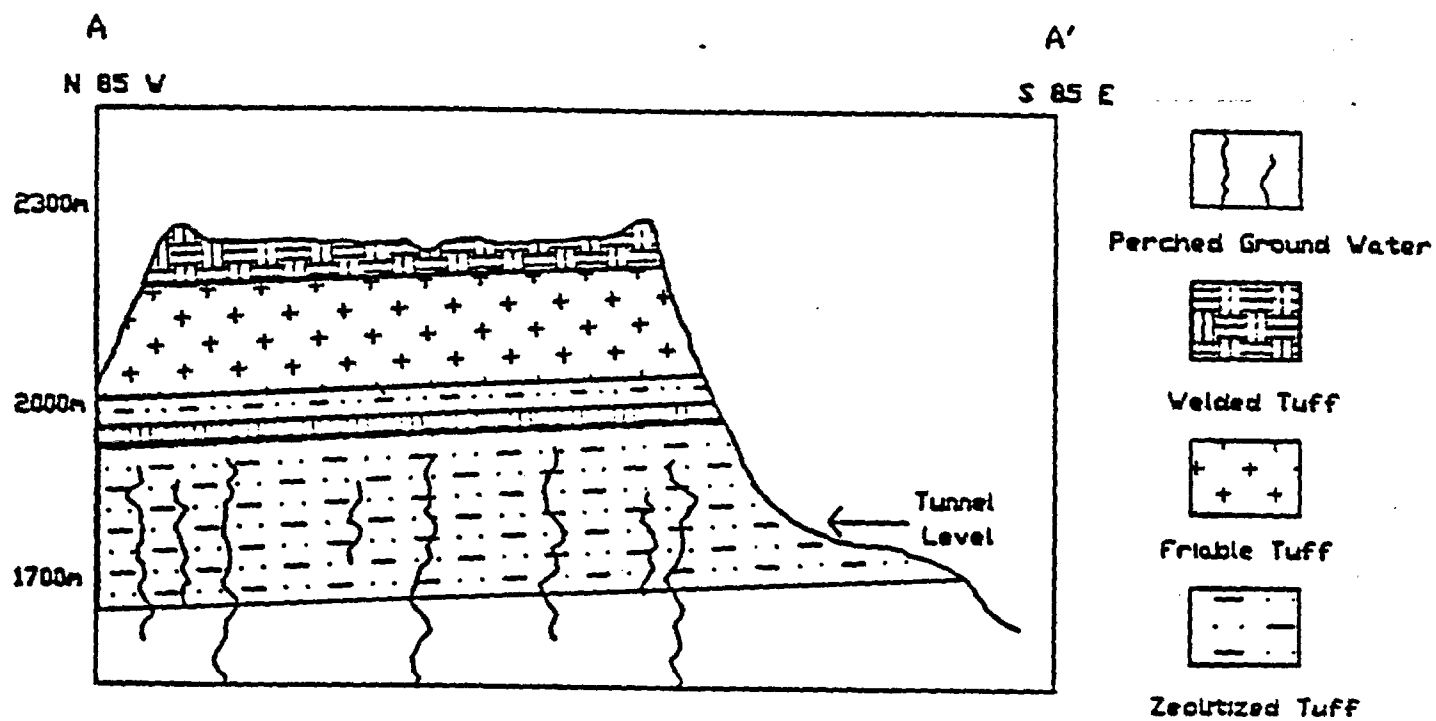
[Analysis by U. S. Geol. Survey, Denver, Colo.]

Depth interval (ft) .....	77-883	1,865-1,886	3,140-3,400
<b>Major constituents, in milligrams per liter</b>			
Silica (SiO <sub>2</sub> ) .....	32	14	31
Calcium (Ca) .....	13	4.0	81
Magnesium (Mg) .....	10	0	30
Sodium (Na) .....	99	424	63
Potassium (K) .....	6.4	4.4	8.6
Bicarbonate (HCO <sub>3</sub> ) .....	199	718	273
Carbonate (CO <sub>3</sub> ) .....	0	88	0
Sulfate (SO <sub>4</sub> ) .....	34	110	181
Chloride (Cl) .....	32	35	11
<b>Physical characteristics and computed values</b>			
Dissolved solids, in milligrams per liter calculated .....	327	981	634
Hardness in milligrams per liter CaCO <sub>3</sub> .....			
Total .....	37	10	233
Noncarbonate .....	0	0	65
Specific conductance .....			
micromhos per cm at 25°C .....	692	1,640	751
pH .....	7.3	8.8	7.3
Temperature (°C) .....	22.0	31.8	64.6

Results of chemical analyses of water from three depth intervals in Test Well 73-66. From Winograd and Thor-darson (1975).



Location of Rainier Mesa at the Nevada Test Site. From Russell (1987)



Schematic diagram illustrating local hydrology of the Rainier Mesa. From Russell (1987).

Map number and area (pl. 3)	Hydrogeologic setting	Number of samples <sup>1</sup>	Ca+Mg		Na+K		HCO <sub>3</sub> +CO <sub>3</sub>	
			Range	Median	Mean	Range	Median	Mean

DA-1 Rainier Mesa ----- Minor recharge area: ground water perched in tuff aquard sampled.

24 0.01-1 .1 .3 0.72-4.3 1.4 1.7 0.79-2.3 1.2(2) 1.3

SO <sub>4</sub> +Cl	Ca+Mg Ca+Mg+Na+K x 100 (percent)	HCO <sub>3</sub> +CO <sub>3</sub> HCO <sub>3</sub> +CO <sub>3</sub> +SO <sub>4</sub> +Cl x 100 (percent)	SiO <sub>2</sub> (mg/l)		Dissolved solids (mg/l) (Residue on evaporation at 180°C)		Data source
			Range	Median	Mean	Range	

0.23-1.1 0.48(23) 0.80

7

71

34-126

82

94

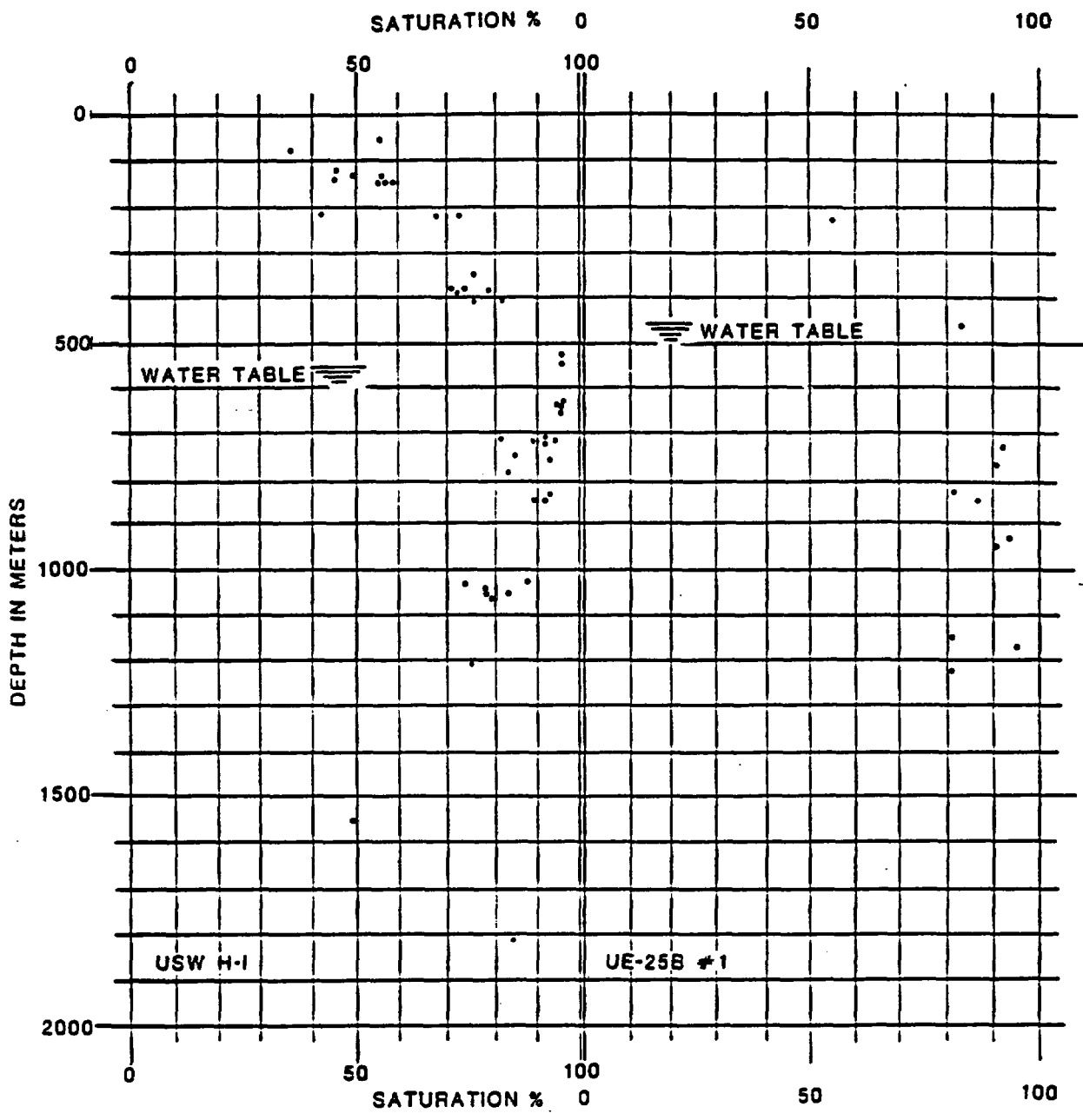
91-424

192

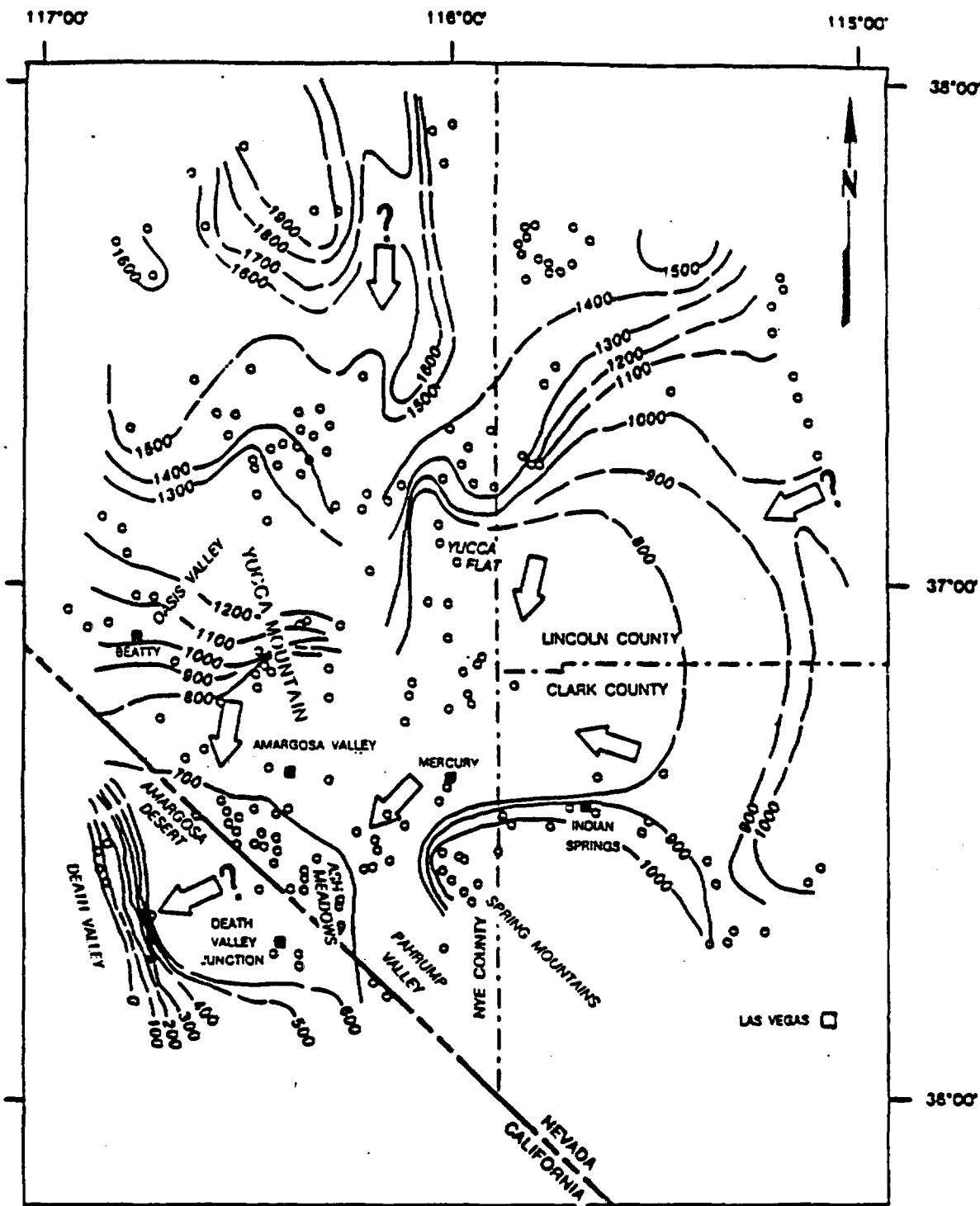
220

Clebach and Barber (1960).

Results of chemical analyses of 24 samples of perched waters from Rainier Mesa. From Winograd and Thordarson (1975).



Degree of saturation above and below water table. From Lahoud et al.. (1984), and Rush et al.. (1983).

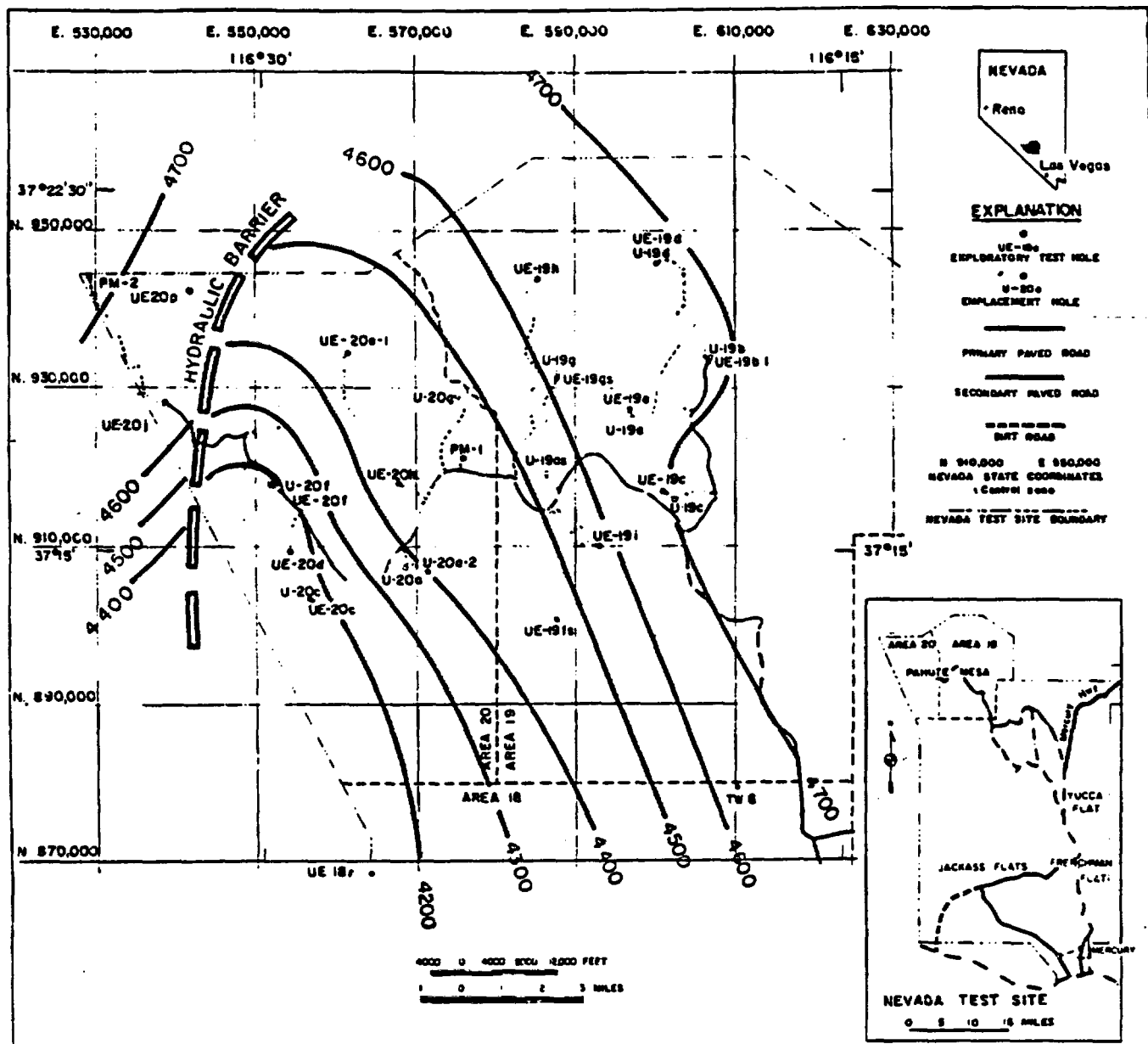


**KEY TO SYMBOLS**

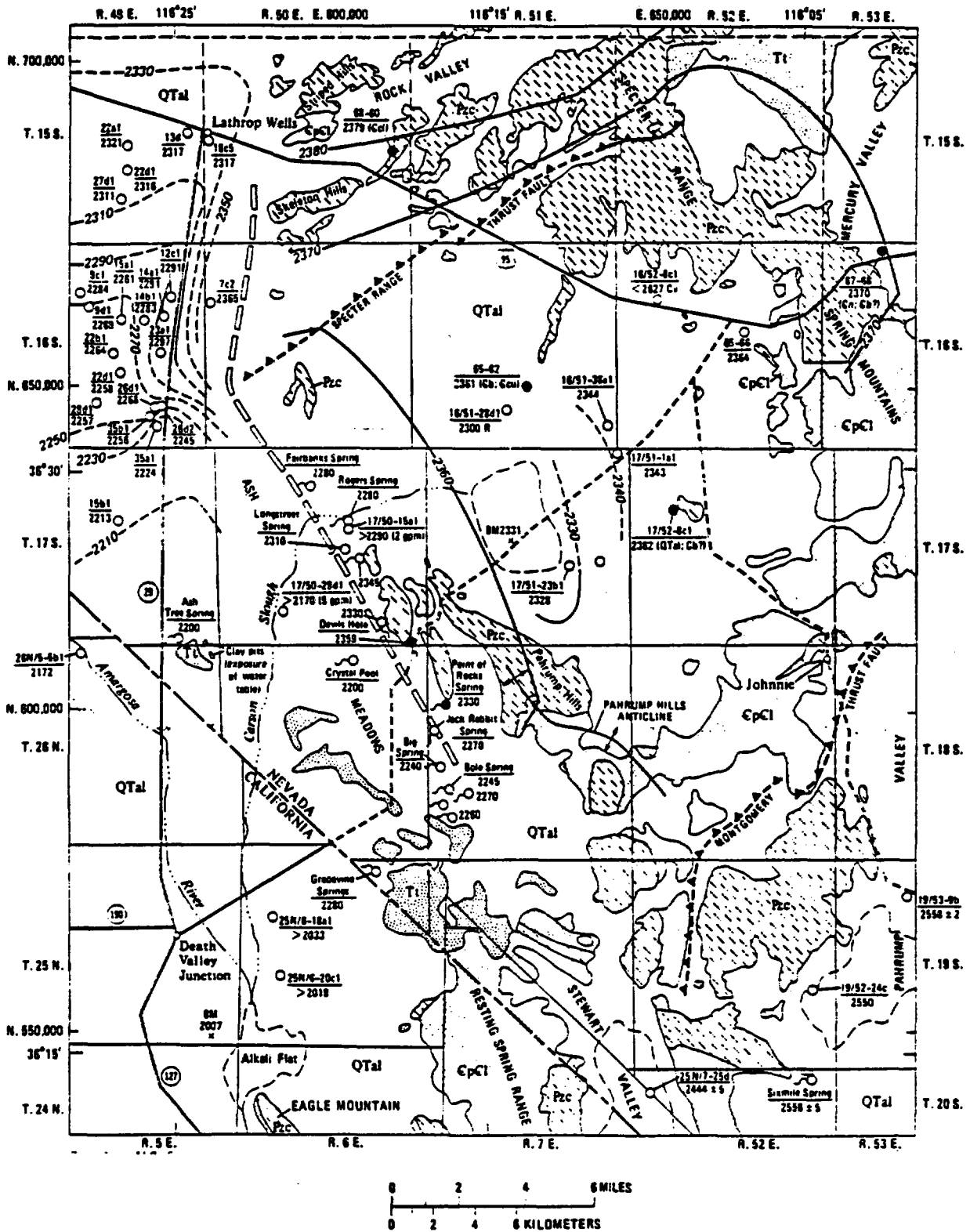
- 1200 — LINE OF EQUAL POTENTIOMETRIC LEVEL, IN METERS ABOVE SEA LEVEL. DASHED WHERE APPROXIMATE. CONTOUR INTERVAL 100 M
- ➔ DIRECTION OF GENERAL GROUND-WATER FLOW (QUESTION MARK INDICATES UNCERTAINTY)
- DATA POINT

0 10 20 MILES  
0 10 20 30 40 KILOMETERS

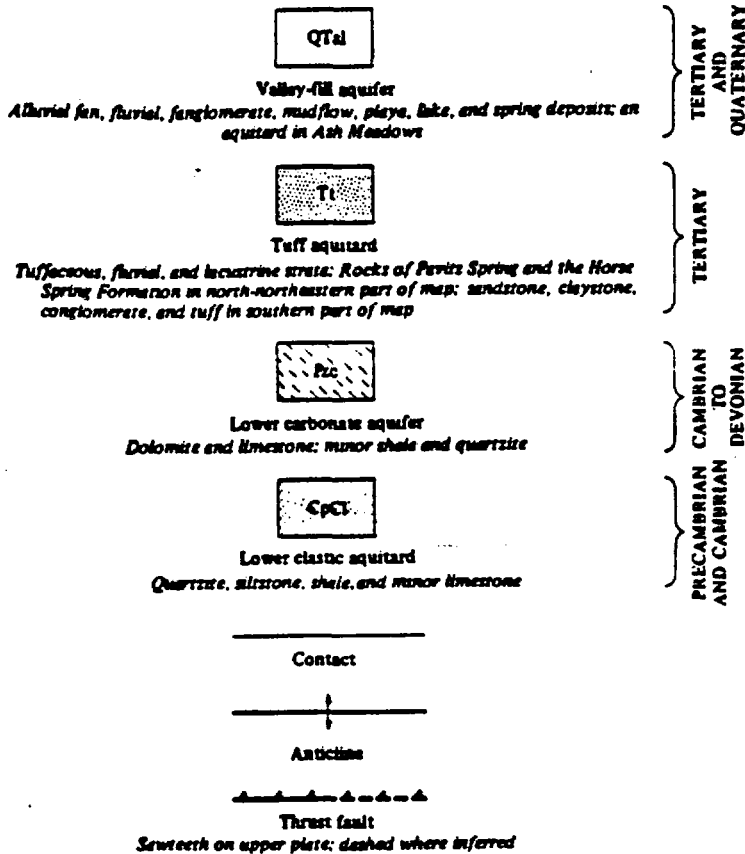
Configuration of water table in Death Valley flow system. Modified from Waddell et al., (1984).



Configuration of water table in Pahute Mesa (recharge area of the Death Valley flow system). From Corchary and Dinwiddie (1975).



Configuration of water table in Amargosa Desert (discharge area of the Death Valley flow system). From Winograd and Thordarson (1975).

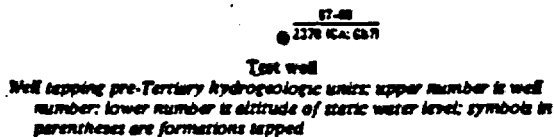


**HYDROGEOLOGIC AND GEOLOGIC UNITS**

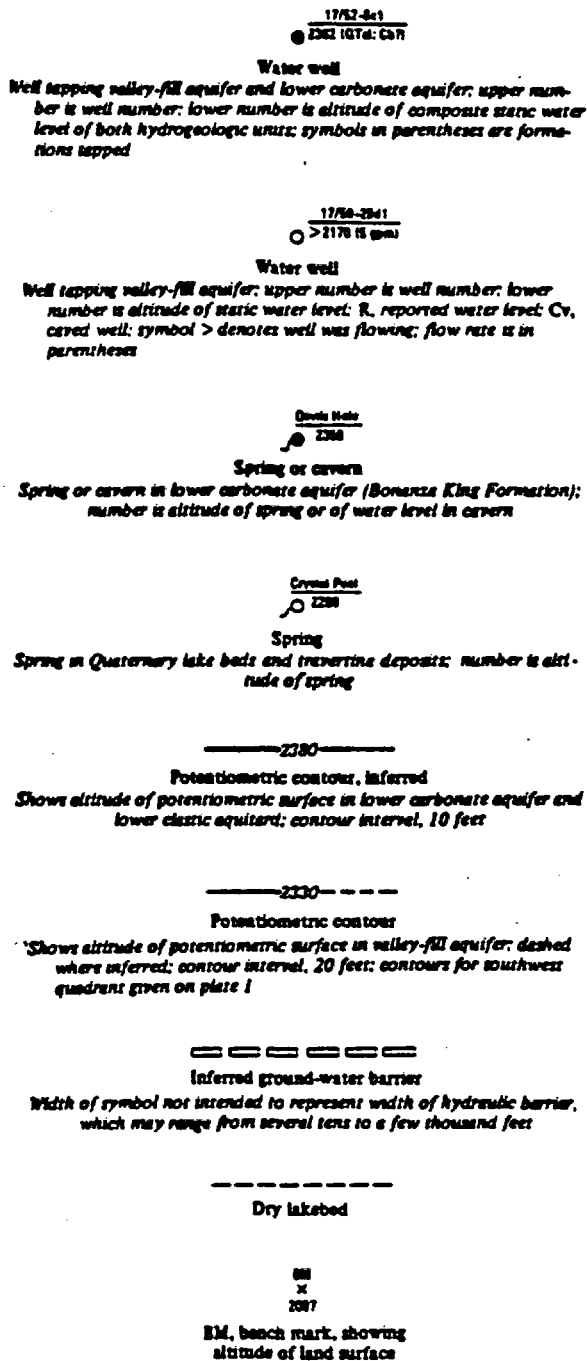
SYMBOL	GEOLOGIC UNIT	HYDROGEOLOGIC UNIT
Ca	Nopah Formation	Lower carbonate aquifer
Cb	Bonanza King Formation	
Cca	Carrara Formation, upper part	
Ccl	Carrara Formation, lower part	Lower clastic aquitard

**HYDRAULIC SYMBOLS**

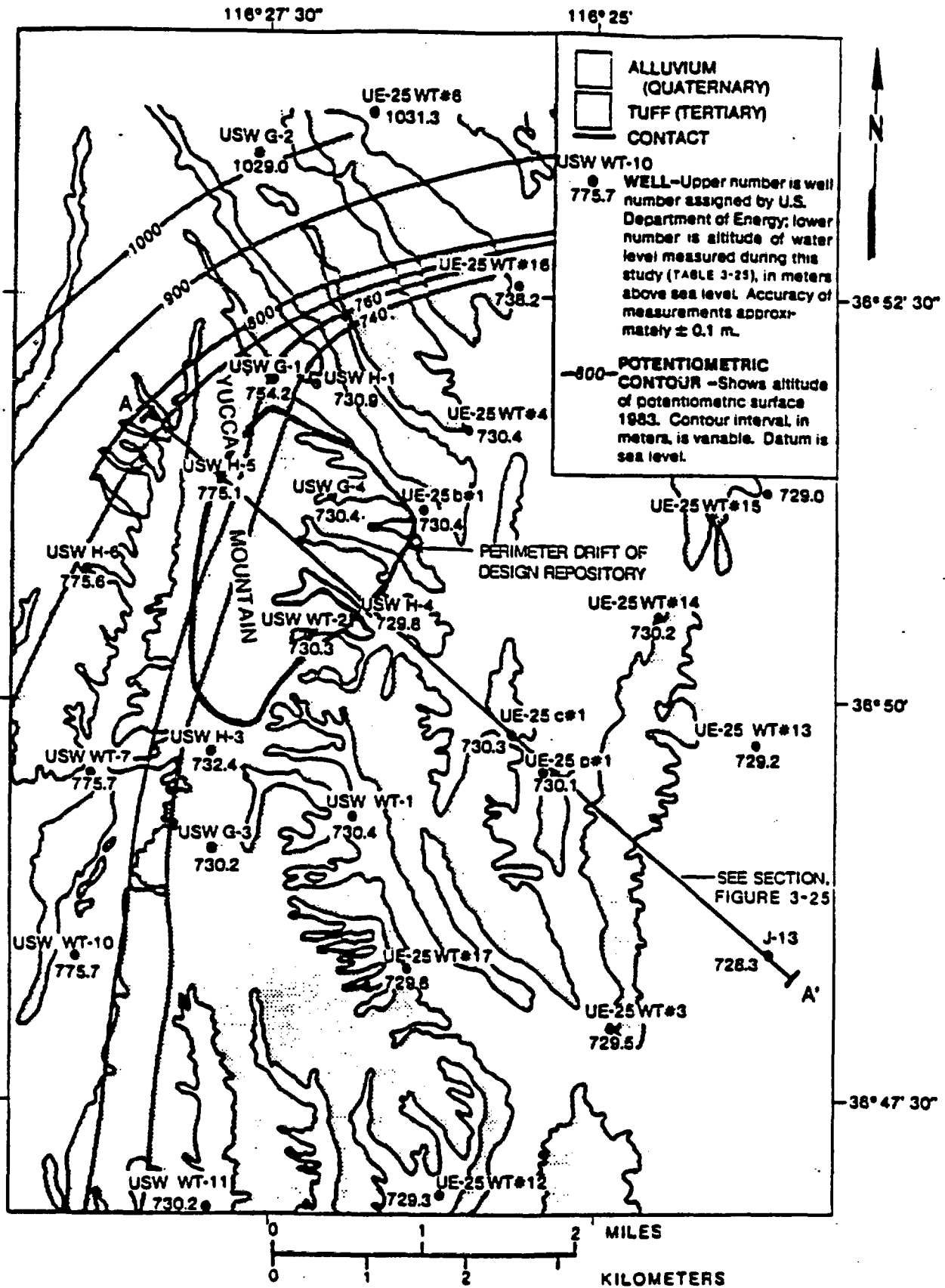
**NOTE:** All altitudes and contours in feet; datum is mean sea level. Areas of significant evapotranspiration are at Ash Meadows and at Alkali Flat and vicinity



TERTIARY AND QUATERNARY  
TERTIARY  
PRECAMBRIAN, CAMBRIAN TO DEVONIAN  
AND CAMBRIAN

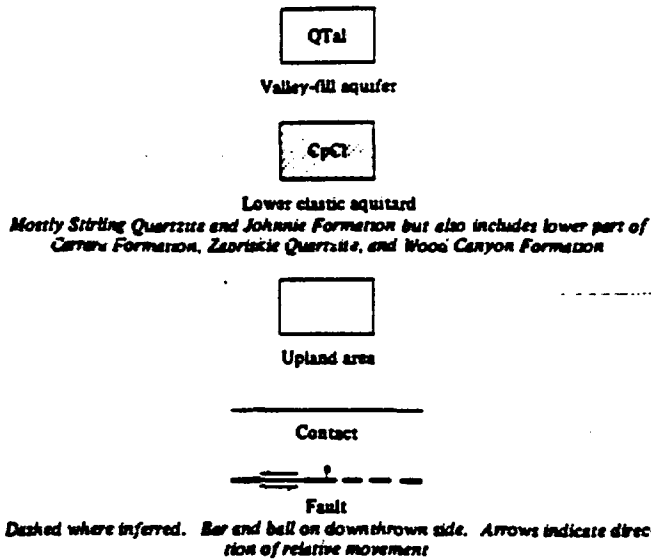


Explanation of symbols used on Plate 4.3-4. From Winograd and Thordarson (1975).



Configuration of water table at Yucca Mountain. Modified from Robison (1986).





PRECAMBRIAN, TERTIARY AND QUATERNARY

**HYDRAULIC SYMBOLS**

Note: All altitudes and contours in feet; datum is mean sea level



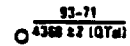
Test well

Well tapping pre-Tertiary hydrogeologic units; upper number is well number; lower number is altitude of static water level; symbol in parentheses is formation tapped



Test well

Well tapping Tertiary tuff aquifer; upper number is well number; lower number is altitude of static water level; symbol in parentheses is formation tapped



Test well

Well tapping Quaternary and Tertiary valley-fill aquifer; upper number is well number; lower number is altitude of static water level; symbol in parentheses is formation tapped



Potentiometric contour

Shows altitude of potentiometric surface in Cenozoic hydrogeologic units; dashed where inferred; contour interval variable



Potentiometric contour

Shows altitude of potentiometric surface in pre-Tertiary hydrogeologic units; dashed where inferred; contour interval variable

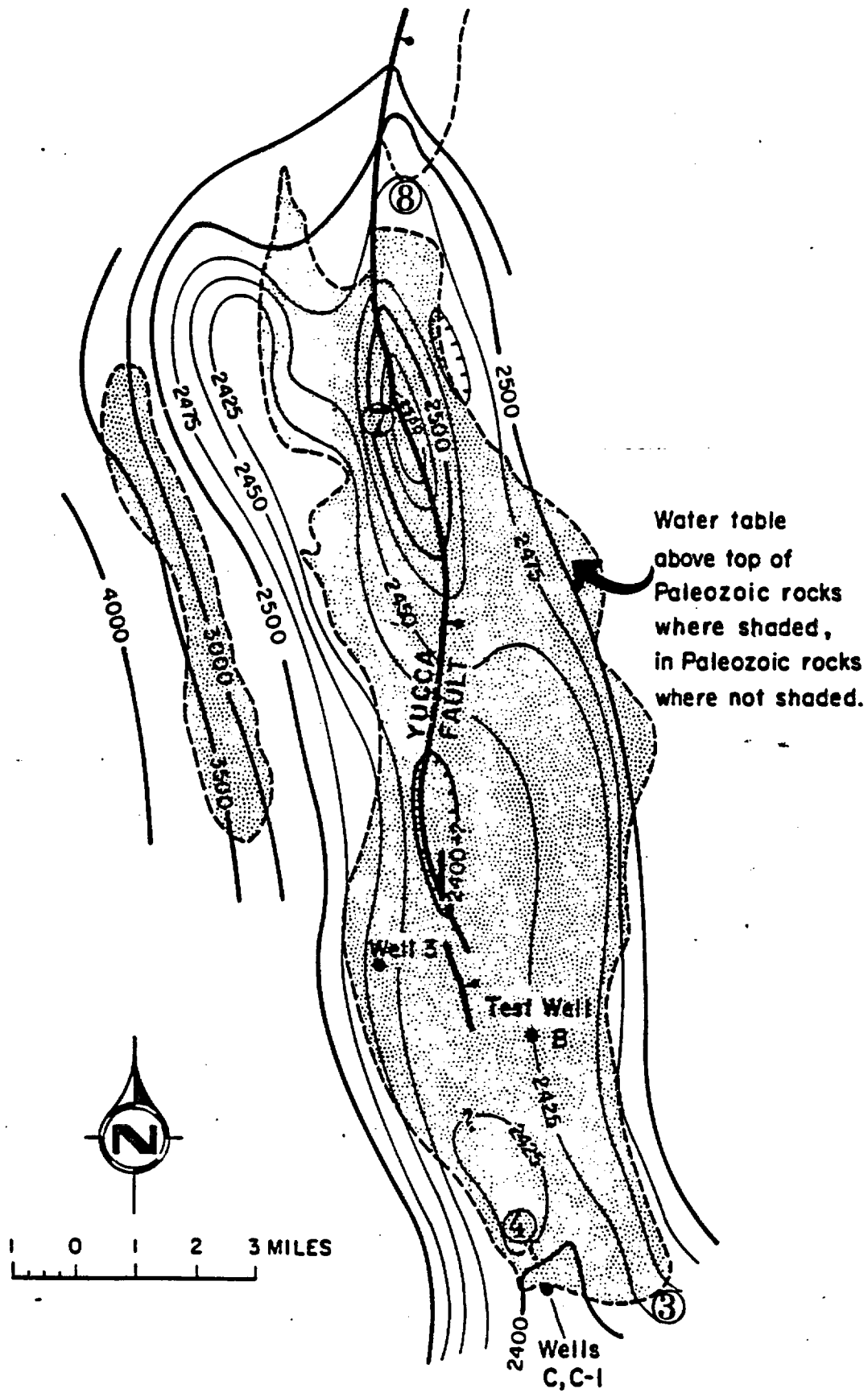


Test well, dashed where projected

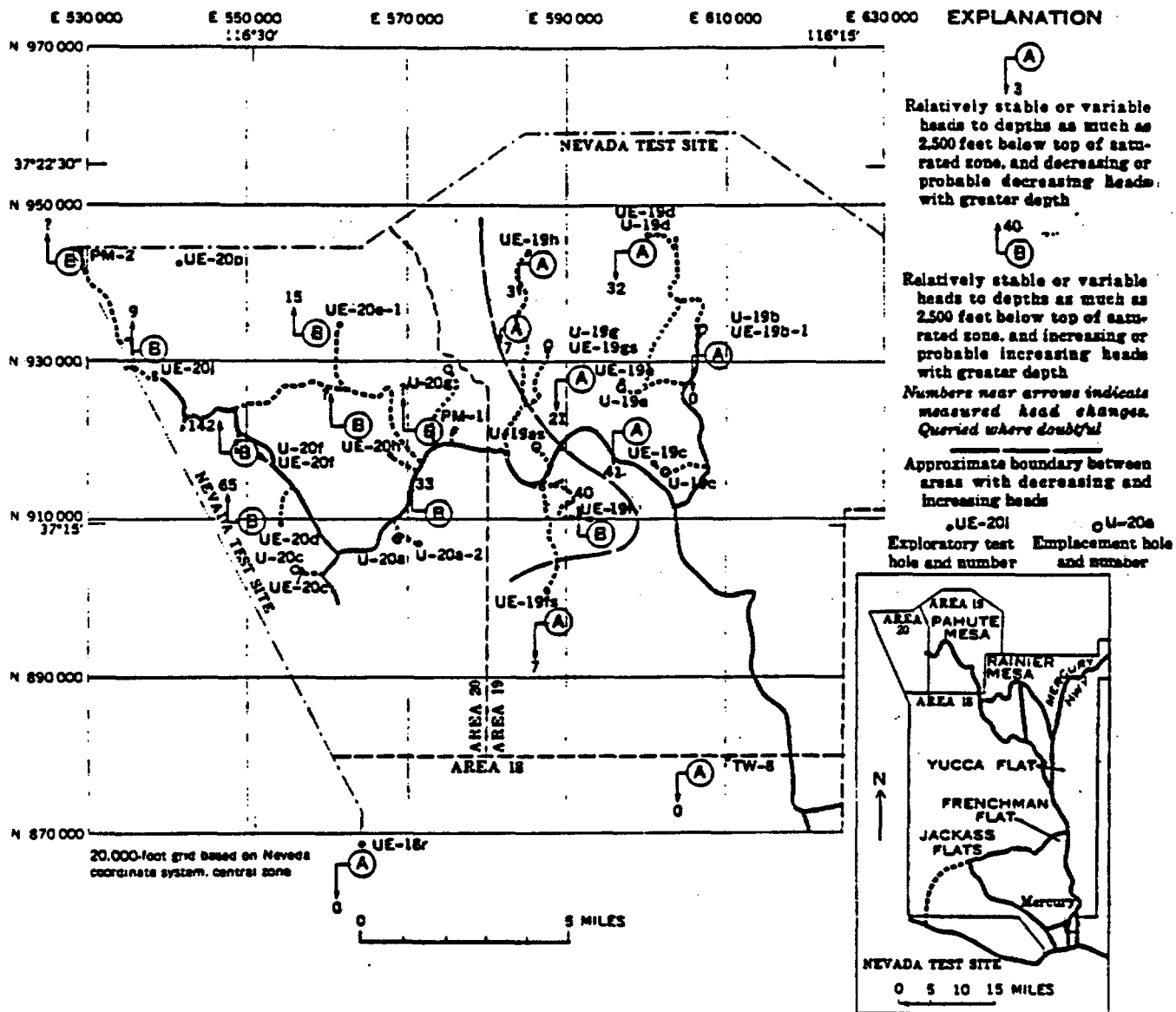
**HYDROGEOLOGIC AND GEOLOGIC UNITS**

SYMBOL	GEOLOGIC UNIT	HYDROGEOLOGIC UNIT
QTal	Quaternary and Tertiary valley fill	Valley-fill aquifer
Tpi	Piapi Canyon Group and Indian Trail Formation undifferentiated	Tuff aquifer and aquitard
Tp	Ash-fall(?) tuff of Piapi Canyon(?) Group	
Trk	Rhyolite of Kawich Valley	Lower carbonate aquifer
Pcc	Paleozoic carbonate rocks	
Cb	Bonanza King Formation	Lower clastic aquitard
CpCl	Lower Cambrian and Precambrian clastic rocks	
pCa	Stirling Quartzite and Precambrian clastic and carbonate rocks	
pCa	Noonday(?) Dolerite	

Explanation of symbols used on Plate 4.3-6. From Winograd and Thordarson (1975).



Configuration of water table in Yucca Flat. From Corchary and Dinwiddie (1975)



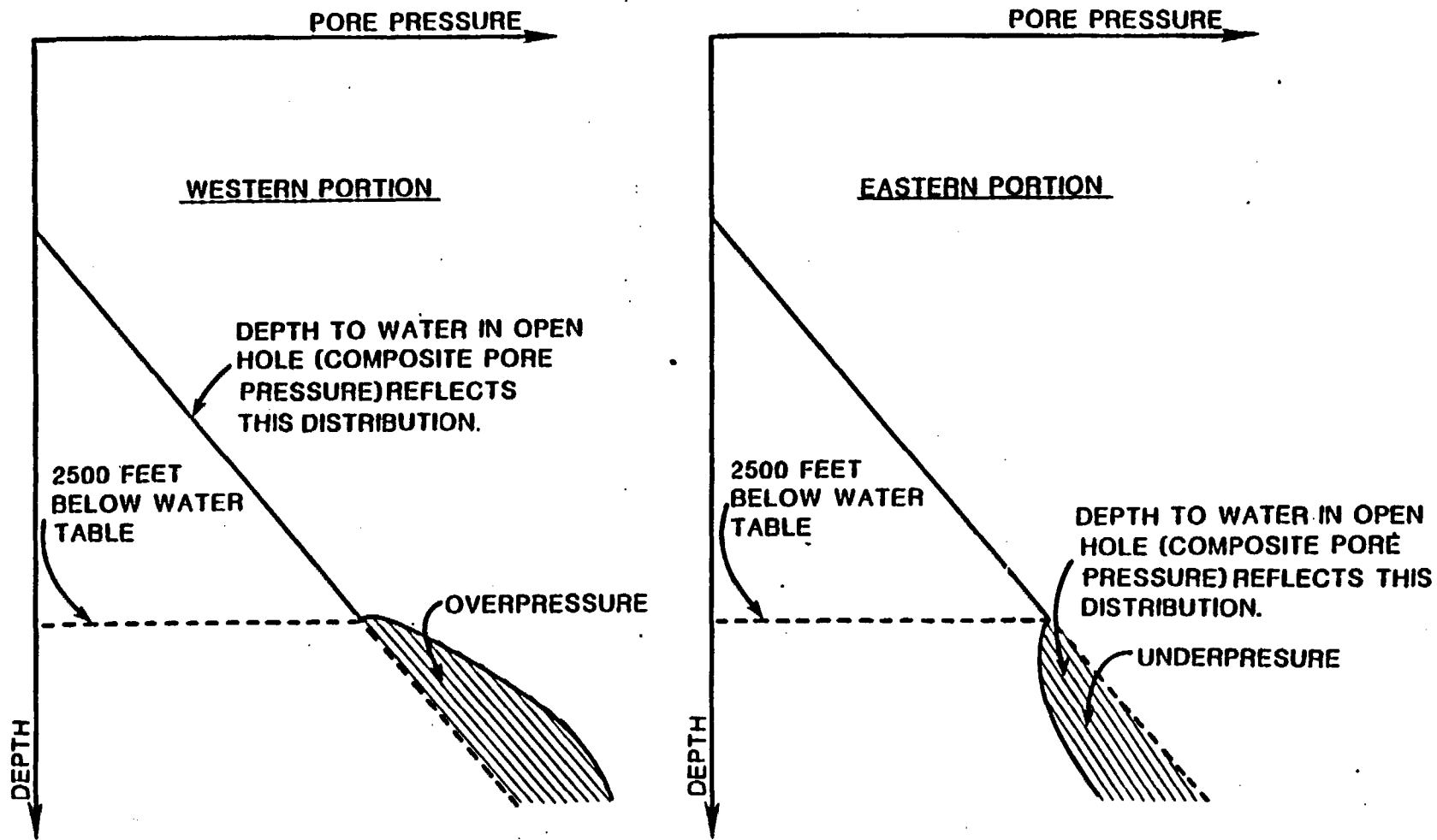
Vertical components of flow in the area of Pahute Mesa. From Blankennagel and Weir (1973).

(All depths in feet below land surface. Intervals isolated with packers in PM-1 and PM-2 were too impermeable to yield data on head changes)

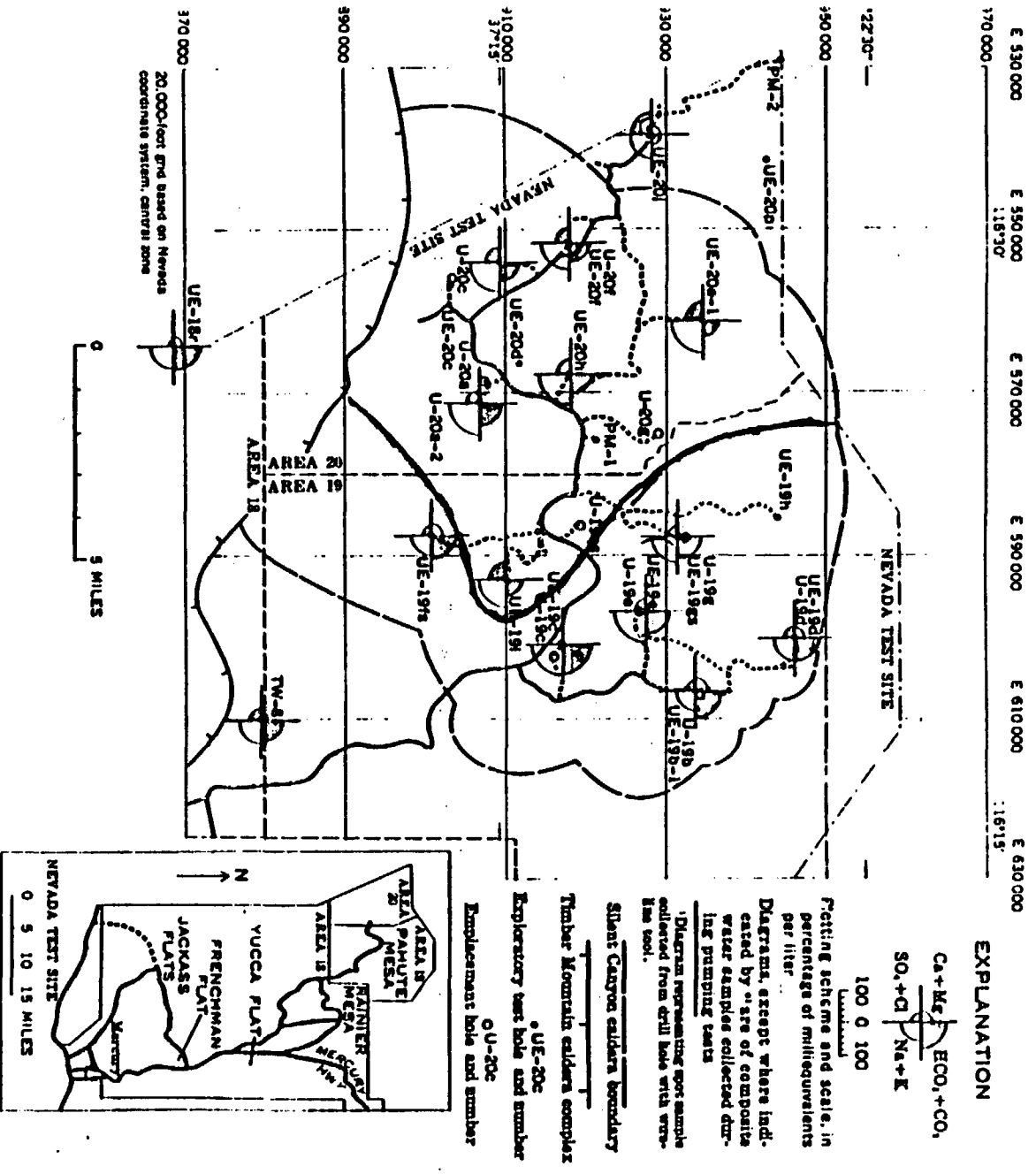
Exploratory hole	Depth to water in open hole	Interval(s) isolated with packers	Depth to water for isolated interval(s)	Principal rock types in isolated interval(s)	Depth of interval(s) with highest permeability
UE-19b-1	2,117	2,176-4,060	2,117	Rhyolite	2,610-2,640, 2,720-2,760
UE-19c	2,345	2,319-2,874	2,319 (?)	Rhyolite and rhyolite breccia	3,050-3,075
		2,884-3,224	2,343	do	
		4,033-4,231	2,360	Rhyolite	
UE-19d	2,177	2,500-3,483	2,177	Rhyolite	3,300-3,350
		3,472-3,852	2,186	do	
		3,844-4,042	2,178	do	
		4,626-4,784	2,180	do	
		4,810-4,968	2,206	do	
		5,823-6,583	2,210	do	
UE-19e	2,240	2,619-2,779	2,232	Welded tuff and zeolitized tuff	2,650-2,690, 4,970-4,990
		4,802-6,004	2,253	do	
UE-19fs	2,305	2,753-3,218	2,302	Rhyolite	2,880-2,950, 3,150-3,160
		3,520-3,838	2,304	do	
		4,146-4,480	2,309	Rhyolite and tuff	
UE-19gs	2,045	2,802-2,970	2,043	Rhyolite	2,940-2,970, 4,785-4,790
		4,636-4,834	2,050	Welded tuff	
		6,920-7,118	2,049	Tuffaceous sandstone	
UE-19h	2,112	2,200-2,396 2,408-3,705	2,109 2,112	Rhyolite and welded tuff do	2,378-2,388 (est.)
UE-19i	2,258	2,910-3,068	2,220	do	3,400-3,470, 3,750-3,765
		3,460-3,618	2,258	do	
		4,100-4,258	2,218	do	
U-20a-2	2,066	2,067-2,608	2,064	Rhyolite	2,400-2,682, 2,895-3,085, 3,648-3,838
		2,492-2,682	2,066	do	
		2,895-3,085	2,065	do	
		3,090-3,280	2,064	do	
		3,648-3,838	2,042	do	
		4,048-4,238	2,051	do	
		4,355-4,500	2,033	do	
UE-20d	2,075	2,578-2,776	2,078	Rhyolite	2,578-2,730
		4,118-4,316	2,018	do	
UE-20e-1	1,822	2,774-2,972	1,828	Rhyolite	3,550-3,660
		3,480-3,678	1,835	Rhyolite and vitrophyre	
		4,020-4,218	1,828	Zeolitized bedded tuff and welded tuff	
UE-20f	1,954	4,540-6,395	1,820	do	3,150-3,345, 4,568-4,765
		2,598-2,796	1,946	Rhyolite and vitrophyre	
		3,150-3,345	1,988	do	
		3,338-3,536	1,954	do	
		4,350-5,249	1,857	do	
UE-20h	2,116	8,972-9,170	1,846	do	3,042-3,170, 4,040-4,060
		2,575-2,743	2,111	Rhyolite	
		2,741-3,210	2,116	do	
		3,350-3,518	2,111	Zeolitized bedded tuff	
		3,705-3,873	2,114	do	
		3,892-4,060	2,116	Rhyolite breccia	
UE-20j	1,270	4,070-4,238	2,117	do	2,060-2,150, 2,957-3,557
		1,858-2,056	1,245	Welded tuff	
		2,051-2,249	1,247	do	
		2,253-2,461	1,249	do	
		2,670-2,868	1,261	do	
		2,957-3,155	1,270	do	
		3,359-3,832	1,273	do	
		4,023-5,690	1,264	Rhyolite and tuff	
UE-18r <sup>2</sup>	1,372	1,440-5,004	1,372	Welded tuff	1,660-1,675 2,350-2,360 3,550-3,560
				do	
				Rhyolite	
TW-8 <sup>2</sup>	1,068	1,320-5,490	1,068	Rhyolite and welded tuff	1,290-2,010

<sup>1</sup>Depth to water when hole was drilled to 4,548 ft. After hole was cased to 4,690 ft and drilled to 13,684 ft, depth to water was 1,772 ft.  
<sup>2</sup>South of Pahute Mesa.

Results of downhole measurements of distribution of hydraulic potentials, Pahute Mesa. From Blankennagei and Weir (1973).



Idealized changes in hydraulic potentials in the Pahute Mesa.



Water chemistry map for Pahute Mesa. From Blankenagel and Weir (1973).

TABLE 10. — Selected chemical analyses of water

(Chemical analyses in milligrams)

Hole	Date of sample collection	Interval sampled (ft)	Major producing zone(s) (ft)	Temperature (°C)	Silica (SiO <sub>2</sub> )	Aluminum <sup>a</sup> (Al)	Iron <sup>a</sup> (Fe)	Manganese <sup>a</sup> (Mn)	Calcium (Ca)	Magnesium (Mg)	Strontium (Sr)	Sodium (Na)
UE-18r <sup>d</sup>	1-29-44	1,629-4,004	—	32.2	48	<.01	0.02	<.01	26	1.0	<.01	31
U-18as	6-7-45	3,195	—	—	68	.04	.02	<.01	2.6	1.1	<.01	200
	6-7-45	3,195	—	—	68	.09	.14	<.01	1.4	1.1	<.01	189
	6-7-45	3,195	—	—	64	.05	.02	<.01	2.6	1.1	<.01	263
UE-18b-1	6-21-44	2,190-4,600	2,740	31.6	47	.03	.25	.06	20	1.7	<.01	43
	10-12-44	2,190-4,600	2,740	30.0	41	.04	.41	1.4	24	2.4	<.01	42
UE-18c	6-7-44	2,421-4,820	3,040-3,075	33.3	41	<.01	.04	.01	13	1.0	<.01	29
	3-9-44	3,059	3,040-3,075	31.1	30	<.01	.04	.00	13	1.1	<.01	141
UE-19d	3-24-44	724-4,500	3,300-3,450	32.2	28	.03	.59	<.01	23	2.1	<.01	173
	6-27-44	2,540-7,639	3,300-3,450	46.0	58	.02	.06	<.01	44	6.0	<.01	150
	6-27-44	2,540-7,639	3,300-3,450	45.0	49	.06	.06	<.01	23	1.4	<.01	143
	3-9-44	3,320	3,300-3,450	34.4	65	<.01	<.01	.43	65	2.4	<.01	163
	3-9-44	4,200	3,300-3,450	34.4	55	<.01	.02	.46	67	2.4	<.01	153
UE-19e	4-22-45	2,475-4,005	2,650-2,690; 4,970-4,990	—	50	.03	.99	.02	.5	1.1	<.01	50
	8-1-44	2,475-4,005	2,650-2,690; 4,970-4,990	35.0	58	<.01	.03	.03	3.7	1.1	<.01	43
UE-19fa	3-18-44	2,545-4,778	—	37.7	56	.02	<.01	.03	11	1.6	<.01	29
UE-19fs	3-27-45	2,650-4,508	2,540; 2,970; 4,270	41.6	48	.04	<.07	.01	12	1.1	<.01	43
	8-2-44	2,650-7,500	2,540; 2,970; 4,270	41.6	50	.01	<.01	.01	2.5	1.1	<.01	34
UE-19l	9-2-45	2,894-4,000	3,460-3,616	47.2	39	.08	<.01	<.05	5.6	1.1	<.01	75
U-20a-2	10-14-44	2,064-4,600	—	26.6	41	.05	.13	<.01	5.9	1.1	<.01	63
UE-20d	3-16-44	2,064-4,600	—	—	45	<.01	.09	.01	6.1	1.1	<.01	55
	3-9-44	2,920	2,570-2,720; 4,250-4,460	—	37	<.01	.05	.01	1.4	1.1	<.01	31
	3-9-44	3,200	2,570-2,720; 4,250-4,460	41.6	46	.04	.07	.01	1.4	1.1	<.01	33
	7-27-44	2,444-4,500	2,570-2,720; 4,250-4,460	40.0	47	<.01	<.01	<.01	4.3	1.1	<.01	35
	7-27-44	2,444-4,500	2,570-2,720; 4,250-4,460	40.0	62	<.01	<.01	.02	21	1.1	<.01	63
	8-12-44	2,444-4,500	2,570-2,720; 4,250-4,460	—	45	.09	<.01	.39	3.5	1.1	<.01	107
UE-20e-1	6-5-44	1,825-4,295	3,530-3,660	47.2	44	.02	.12	<.01	.4	1.1	<.01	112
	3-9-44	2,900	3,530-3,660	32.5	36	.01	.02	<.01	.2	1.1	<.01	33
UE-20f	8-11-44	4,454-13,626	4,670-4,698	45.8	47	.07	.56	.14	4.3	1.1	<.01	118
U-20f	3-23-44	4,028	4,630	41.1	38	.04	<.01	.01	.9	1.1	<.01	66
	5-27-44	4,025	4,025	41.6	39	.05	<.01	.02	.4	1.1	<.01	66
UE-20h	8-28-45	2,504-7,207	4,900-4,970	32.2	49	.02	<.01	.03	.3	1.1	<.01	34
UE-20j	10-21-44	1,740-5,690	2,050-2,250; 2,960-3,830	33.9	44	.01	4.3	<.01	46	1.1	<.01	123
TW-5 <sup>a</sup>	10-15-44	1,043-1,360	1,200-1,750	25.1	45	<.01	<.01	<.01	8.8	.8	<.01	30

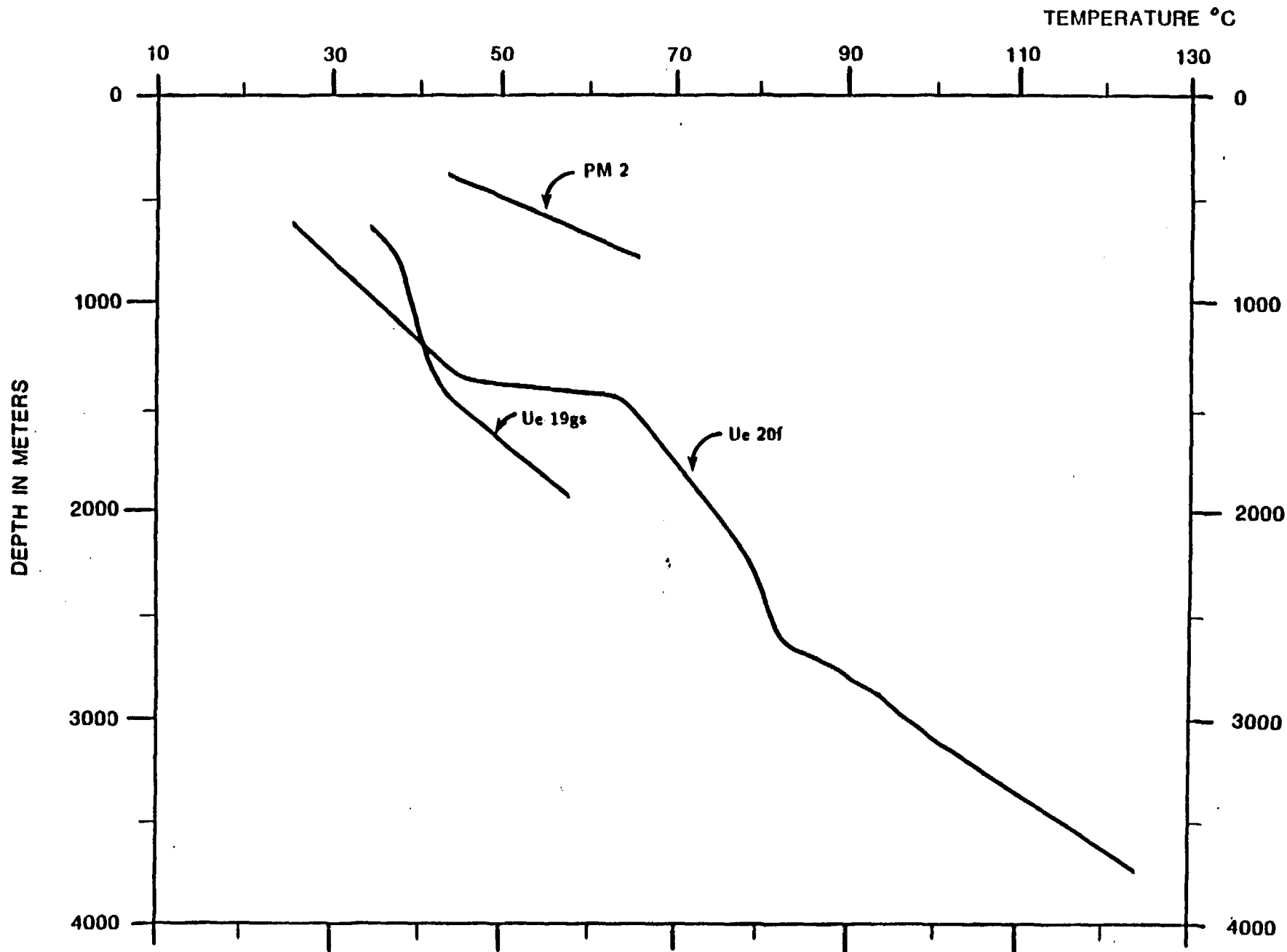
<sup>a</sup>In solution at time of analysis or collection.  
<sup>b</sup>South of Pahute Mesa.

Results of chemical analyses of water samples from Pahute Mesa. From Blankennagel and Weir (1973).

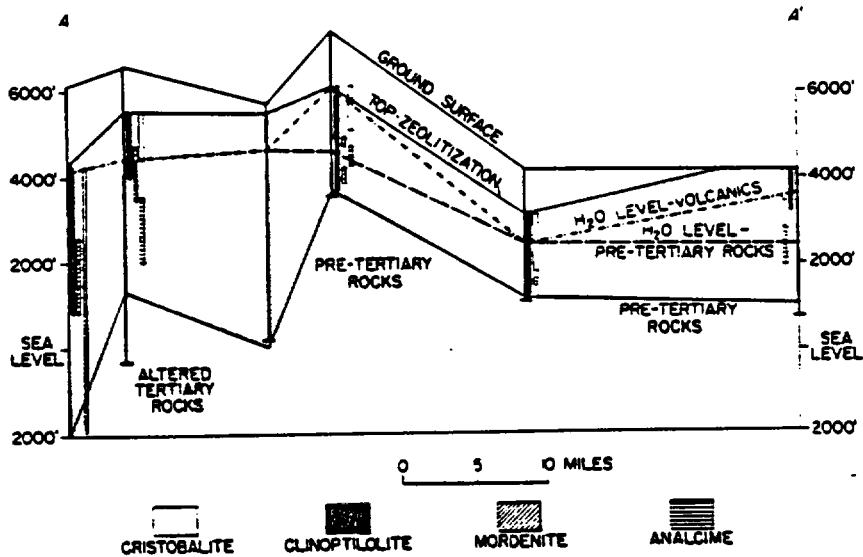
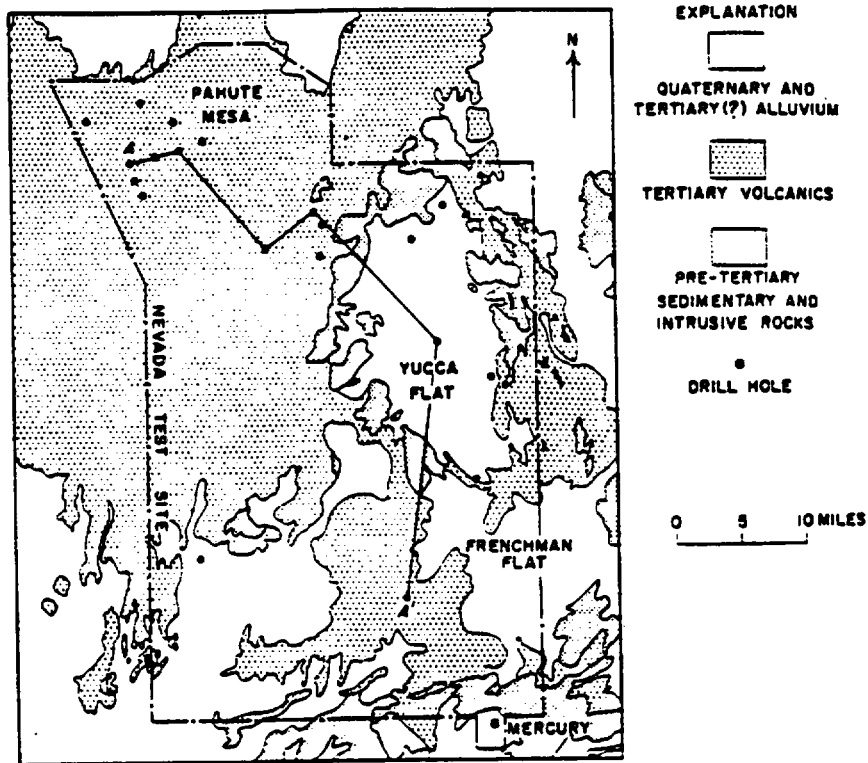
Well	Date of sample collection	Interval sampled (ft)	Major producing zone(s) (ft)	Hardness as CaCO <sub>3</sub>										Specific conductance (microhm/cm at 25°C)	pH					
				Lithium (Li)	Selenium (Se)	Carbonate (CO <sub>3</sub> )	Bicarbonate (HCO <sub>3</sub> )	Sulfate (SO <sub>4</sub> )	Chloride (Cl)	Fluoride (F)	Nitrate (NO <sub>3</sub> )	Phosphate (PO <sub>4</sub> )	Dissolved solids (residue on evaporation at 180°C)			Calcium, magnesium	Noncarbonate			
UE-19 <sup>a</sup>	1-29-44	3,629-5,004	.....	0.10	0.11	0	252	24	7.8											
U-19 <sup>a</sup>	6-7-45	3,195	.....	.41	.04	39	174	26	10											
	6-7-45	3,195	.....	.42	.07	0	205	27	11											
	6-7-45	3,195	.....	.05	.04	52	201	51	12											
UE-19b-1	6-21-44	2,190-4,500	2,740	.....	.03	0	190	24	18											
UE-19c	10-10-44	2,190-4,500	2,740	.....	.03	0	190	21	6.5											
	6-7-44	2,421-4,520	3,040-3,075	.04	.05	0	62	4.4	2.5											
	2-9-45	3,050	3,040-3,075	.20	.....	0	490	7.7	4.3											
UE-19d	2-24-44	2,660-4,500	3,200-3,430	.20	.04	0	424	.....	4.4											
	6-27-44	2,660-7,859	3,200-3,430	.....	.....	0	320	.....	0.0											
	6-27-44	2,560-7,859	3,200-3,430	.....	.....	0	320	.....	7.5											
UE-19e	2-9-45	3,200	3,200-3,430	.20	.....	0	421	.....	0.0											
	2-9-45	4,200	3,200-3,430	.20	.....	0	450	.....	4.0											
	4-22-45	2,475-5,005	2,650-2,920	.16	.....	0	36	.....	1.2											
UE-19f	2-1-44	2,475-5,005	2,650-2,920; 4,970-4,990	.06	.01	0	30	.....	2.7											
	2-1-44	2,475-5,005	2,650-2,920; 4,970-4,990	.06	.01	0	30	.....	2.7											
	2-1-44	2,475-5,005	2,650-2,920; 4,970-4,990	.06	.01	0	30	.....	2.7											
UE-19fa	2-15-45	2,605-4,770	.....	.02	.....	0	26	.....	0.0											
UE-19fb	2-27-45	2,650-4,500	2,940; 2,970; 4,270	.....	.....	0	145	.....	0.0											
	2-2-45	2,650-7,500	2,940; 2,970; 4,270	.04	.01	0	123	.....	2.0											
	2-2-45	2,650-7,500	2,940; 2,970; 4,270	.04	.01	0	123	.....	2.0											
UE-19f	2-2-45	2,650-8,000	3,460-3,510	.05	.01	0	98	.....	7.0											
U-20a-2	10-14-44	2,000-4,500	.....	.....	.....	0	102	.....	1.1											
UE-20d	2-10-45	2,000-4,500	.....	.06	.....	0	106	.....	1.1											
	2-8-45	2,920	2,570-2,720; 4,250-4,460	.00	.....	0	122	.....	2.0											
	2-8-45	3,200	2,570-2,720; 4,250-4,460	.00	.....	0	120	.....	2.1											
UE-20e	7-27-45	2,440-4,500	2,570-2,720; 4,250-4,460	.00	.01	0	107	.....	2.3											
	7-25-45	2,440-4,500	2,570-2,720; 4,250-4,460	.00	.01	0	143	.....	2.4											
	7-25-45	2,440-4,500	2,570-2,720; 4,250-4,460	.00	.01	0	143	.....	2.4											
UE-20f-1	6-12-45	2,440-4,500	2,570-2,720; 4,250-4,460	.00	.01	4	192	.....	2.4											
	6-5-44	1,925-5,995	3,550-3,860	.....	.....	0	130	.....	4.4											
	2-8-45	2,600	3,550-3,860	.07	.....	0	110	.....	2.0											
UE-20f	2-11-44	4,450-13,685	4,570-4,800	.....	.....	0	104	.....	6.0											
U-20f	2-25-45	4,025	4,030	.09	.01	10	105	.....	6.0											
UE-20h	6-27-45	4,025	4,025	.00	<.01	14	90	.....	7.0											
	6-25-45	2,500-7,207	4,000-4,070	.02	<.01	0	107	.....	2.7											
	10-21-44	1,740-5,590	2,050-2,250	.....	.....	0	150	.....	1.0											
TW-0 <sup>b</sup>	10-15-44	1,000-1,960	1,200-1,750	.....	.....	0	78	.....	7.0											

<sup>a</sup>In solution at time of analysis or collection.  
<sup>b</sup>South of Pahute Mesa.

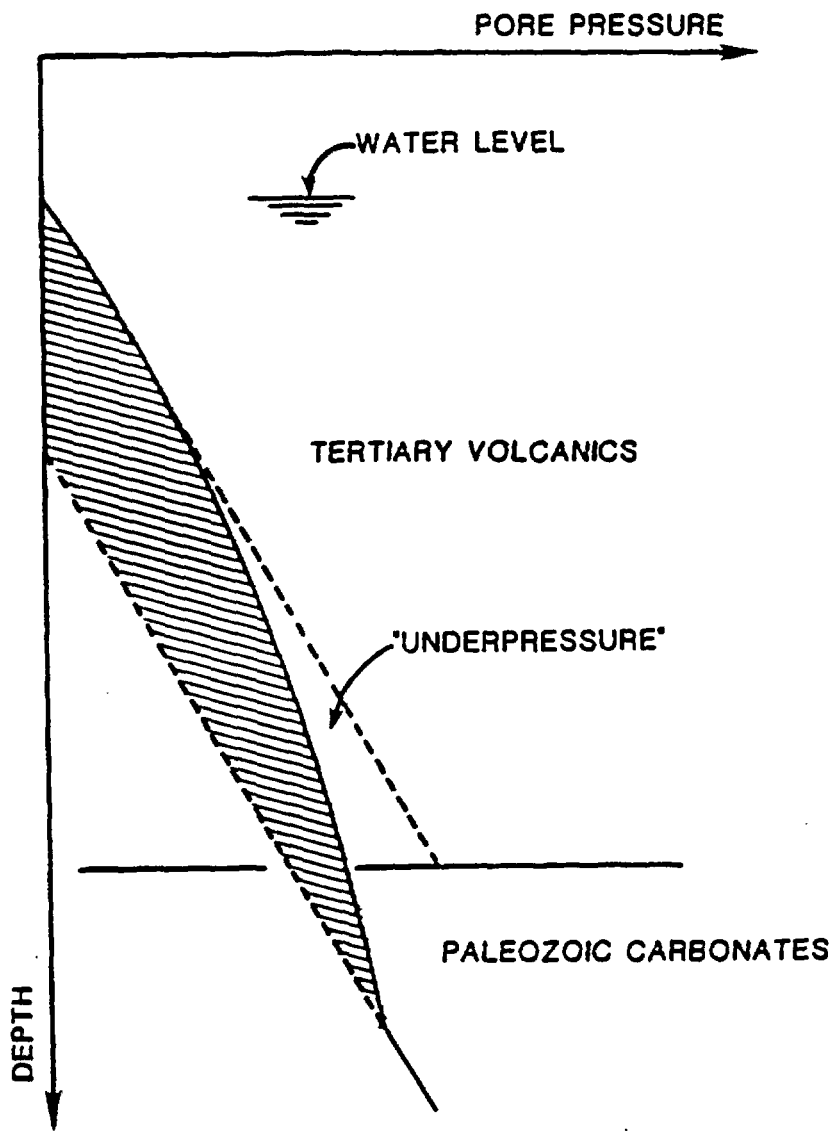
Results of chemical analyses of water samples from Pahute Mesa (continued). From Blankennagel and Weir (1973)



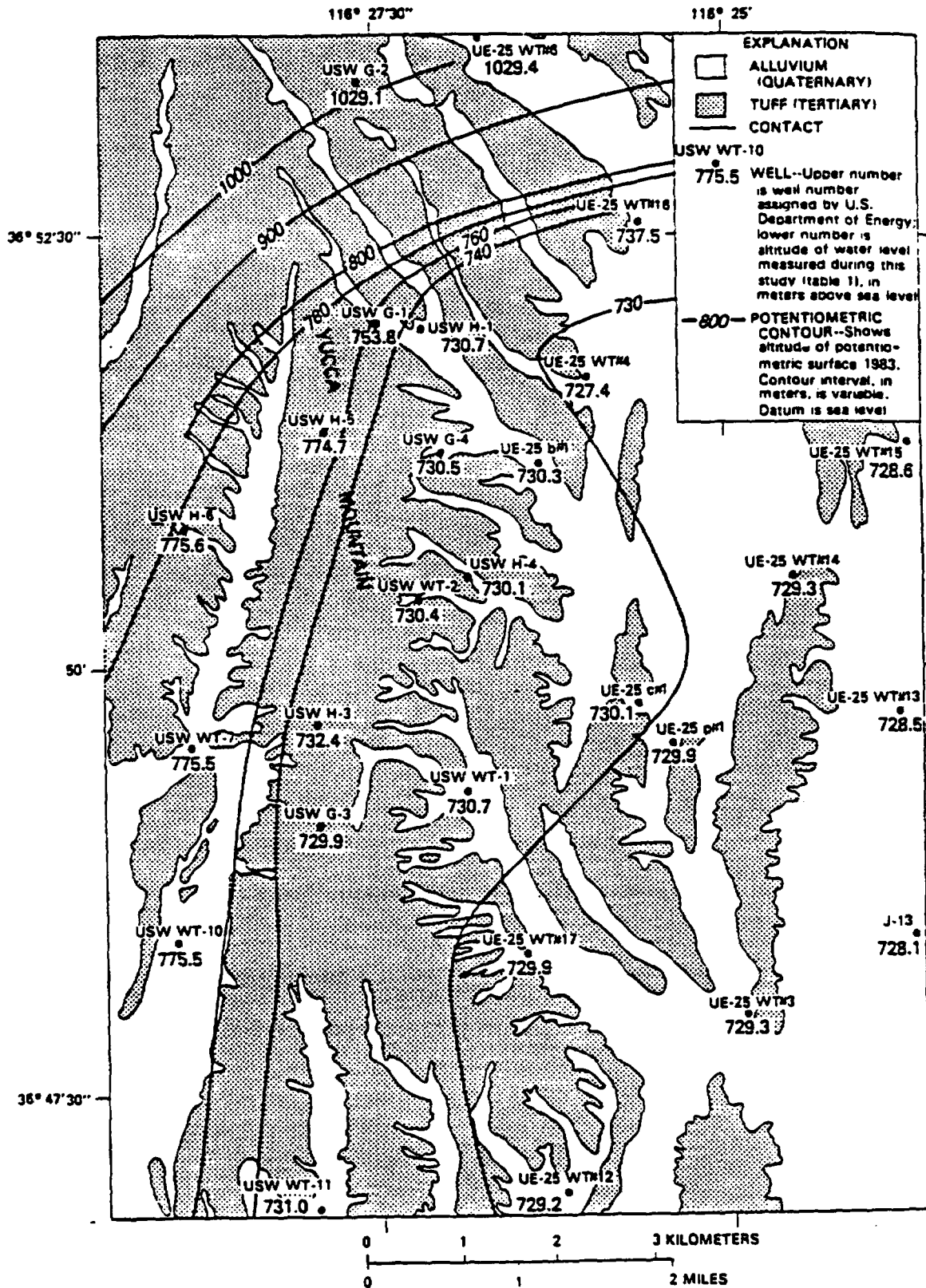
Downhole temperature for three boreholes in Pahute Mesa. From Sass and Lachenbruch (1982).



General hydrogeology of Yucca Flat. From Hoover (1968).



Idealized changes in pore pressure with depth in Wells 88-66 and 83-69a located in Yucca Flat.



Location map for deep wells at Yucca Mountain. From Robison (1984).

Hole or well number: Designation assigned by U.S. Department of Energy.

Location: Nevada State Coordinate System Central Zone (feet).

Hole Depth: Total depth drilled.

Land-surface altitude: Altitude above National Geodetic Vertical Datum of 1929 at well, reported by Holmes & Harver, Inc., contractor to U.S. Department of Energy.

Depth correction: Correction needed to adjust measured depth or altitude to true value because of hole deviation from vertical. The correction is computed for a depth approximately equal to the depth of the measured water level; this correction is obtained from a down-hole gyroscopic survey.

Date measured: Date of a water-level measurement.

Interval: Depth interval of the hole represented by the water-level measurement. Composite levels represent mixed hydraulic heads of the entire interval between the water table or lower end of the casing and the bottom of the hole. Where a specific interval is indicated, the zone was isolated, using inflatable packers for the straddled interval during permeability testing, or using a single packer installed to determine hydraulic head differences above and below the packer.

Depth to water: Depth based on direct measurements of water levels using down-hole wireline equipment, adjusted for depth correction (where available), except where noted.

Altitude: Computed altitude of water level above National Geodetic Vertical Datum of 1929, based on land-surface altitude and measured depth to water (corrected).

Hole or well number	Location (feet)		Hole depth (meters)	Land-surface altitude (meters)	Depth correction (meters)	Date measured	Water level (corrected) <sup>1</sup>			
	North	East					Interval (meters)	Depth to water (meters)	Altitude (meters)	
UE-25b#1	765,243	566,416	1220	1200.6	0.25	12/03/83	Composite	470.6	730.8	
							08/01/83	471-1199	470.3	730.3
							do.	1199-1220	472.2	728.4
UE-25c#1	757,095	569,680	914	1130.4	.06	11/07/83	Composite	400.3	730.1	
UE-25p#1	756,171	571,485	1805	1114	.02	Feb. 1983	383- 500	383.9	729.9	
						do.	500- 550	383.5	730.4	
						do.	739- 789	383.3	730.6	
						do.	764- 834	383.1	730.8	
						do.	834- 904	381.1	732.7	
						do.	904- 974	382.2	731.7	
						do.	974-1044	380.9	733.0	
						do.	1044-1114	379.4	734.5	
						do.	1110-1180	361.7	752.2	
						do.	1117-1301	360.5	753.4	
						do.	1180-1301	355.0	750.9	
						May 1983	1297-1308	362.0	751.9	
						do.	1297-1338	362.3	751.6	
						do.	1341-1381	362.3	751.6	
						do.	1381-1420	362.4	751.5	
						do.	1423-1463	362.5	751.4	
						do.	1463-1509	362.4	751.5	
						do.	1509-1585	362.5	751.4	
						do.	1597-1643	362.7	751.2	
						do.	1643-1689	360.0	750.9	
						do.	1734-1780	363.1	750.8	
						do.	1780-1805	363.0	750.9	
						11/07/83	1297-1805	364.7	749.2	

Water levels - Yucca Mountain. From Robison (1984)

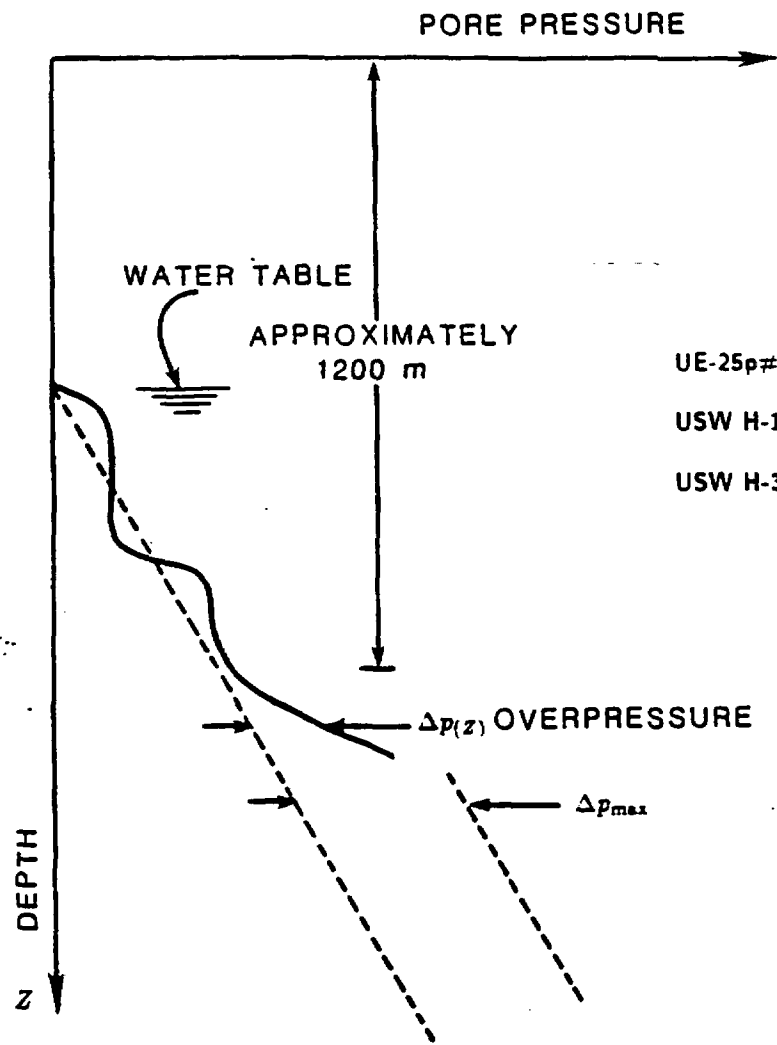
Hole or well number	Location (feet)		Hole depth (meters)	Land-surface altitude (meters)	Depth correction (meters)	Date measured	Water level (corrected) <sup>1</sup>		
	North	East					Interval (meters)	Depth to-- water (meters)	Altitude (meters)
USW G-1	770,500	561,000	1829	1325.5	0.67	03/23/82	Composite	571.7	753.8
USW G-2	778,824	560,504	1831	1554.0	.16	09/17/82	Composite	524.9	1029.1
USW G-3	752,780	558,483	1533	1480.2	.57	11/30/83	Composite	750.3	729.9
USW G-4	765,807	563,082	915	1269.6	1.53	04/27/83	Composite	539.5	730.1
USW H-1	770,254	562,388	1829	1302.8	.19	02/25/82	Composite	572.1	730.7
						11/01/83	572- 673	572.4	730.5
						do.	716- 765	572.4	730.5
						do.	1097-1123	571.7	731.2
						do.	1783-1814	518.2	784.7
USW H-3	756,542	558,452	1219	1483.3	.08	11/19/82	Composite	750.8	732.5
						11/03/83	751-1190	750.9	732.4
						do.	1190-1219	729.0	754.1
USW H-4	761,643	563,911	1219	1248.6	.45	12/30/82	Composite	518.7	730.1
						06/16/83	518-1181	518.2	730.8
						do.	1181-1219	518.1	730.9
USW H-5	766,634	558,909	1219	1478.5	0.08	12/22/83	Composite	704.2	774.3
						11/07/83	704-1091	703.8	774.7
						do.	1091-1219	703.8	774.7
USW H-6	763,299	554,075	1220	1301.7	.05	12/15/82	Composite	526.6	775.1
						10/24/83	526-1187	526.1	775.6
						do.	1187-1220	524.7	777.0
USW WT-1	753,941	563,739	515	1201.7	.33	10/31/83	Composite	471.0	730.7
USW WT-2	760,661	561,924	628	1301.4	.53	11/01/83	Composite	571.0	730.4
UE-25 WT#3	745,995	573,384	348	1029.8	.27	10/31/83	Composite	300.5	729.3
UE-25 WT#4	768,512	568,040	482	1167.1	.46	11/01/83	Composite	438.9	728.2
UE-25 WT#6	780,576	567,524	383	1312.9	.24	10/31/83	Composite	283.9	1029.4
USW WT-7	755,570	553,891	491	1197.0	.03	10/24/83	Composite	421.2	775.9
USW WT-10	748,771	553,302	430	1123.2	.03	10/24/83	Composite	347.7	775.5
USW WT-11	739,070	558,377	441	1094.4	.12	10/24/83	Composite	363.9	730.5
UE-25 WT#12	739,726	567,011	399	1074.6	.20	10/31/83	Composite	345.4	729.2
UE-25 WT#13	756,884	578,843	352	1031.8	.01	10/31/83	Composite	303.3	728.5
UE-25 WT#14	761,651	575,210	399	1076.1	.09	11/07/83	Composite	346.2	729.9
UE-25 WT#15	766,116	579,806	415	1082.8	.19	12/01/83	Composite	354.2	728.6
UE-25 WT#16	774,420	570,395	519	1210.5	.06	12/01/83	Composite	472.7	737.8
UE-25 WT#17	748,420	566,212	443	1124.5	.48	11/07/83	Composite	394.6	729.9
J-11	740,968	611,764	405	1050	--	03/22/73	Composite	317.4	732.6
J-12	733,509	581,011	347	953.5	--	12/05/83	Composite	226.2	727.3
J-13	749,209	579,651	1063	1011.3	--	10/31/83	Composite	283.2	728.1
USW VII-1	743,356	533,626	762	963.5	--	02/12/81	Composite	184.2	779.3
USW VII-2	748,320	526,264	1219	974.4	--	04/23/83	Composite	164.0	*810.4

<sup>1</sup>Where more than one water-level altitude is reported for a well, the value shown on the map is underscored in the table.

<sup>2</sup>Water level probably not stabilized.

<sup>3</sup>Composite of interval open to rocks of Paleozoic age.

<sup>4</sup>Water level estimated from geophysical logs.



- UE-25p#1  $\Delta p(z) = 20\text{m}; Z = 1300\text{m}.$
- USW H-1  $\Delta p(z) = 53\text{m}; Z = 1123 - 1733\text{m}.$
- USW H-3  $\Delta p(z) = 22\text{m}; Z = 1200\text{m}.$

Idealized changes of pore pressure with depth at Yucca Mountain

Principal compressive stress				
Stress axis	Magnitude <sup>1</sup> (psi)	Bearing (degrees)	Inclination from <sup>2</sup> horizontal (degrees)	Standard deviation of magnitude (psi)
Minimum	404	S. 75° E.	-12	62
Maximum	1,006	S. 4° W.	+40	55
Intermediate	864	S. 28° W.	-48	61

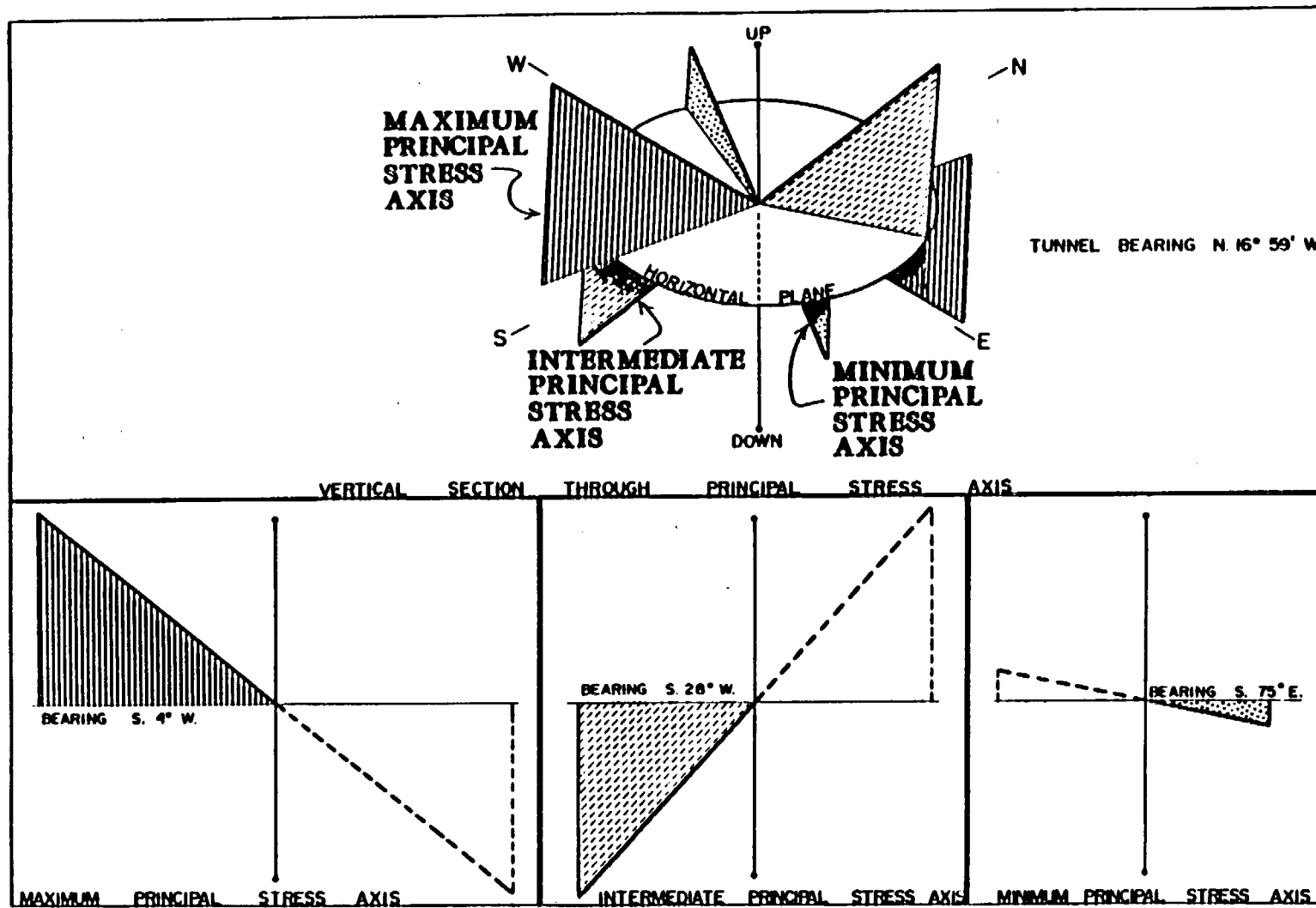
Stress components with respect to the X (east), Y (north), and Z (vertical) coordinate system					
Normal compressive stress component	Magnitude of normal component (psi)	Standard deviation of normal component magnitude (psi)	Shear stress component	Magnitude <sup>3</sup> of shear component (psi)	Standard deviation of shear component magnitude (psi)
$\sigma$ X	453	58	$\tau$ XY	113	42
$\sigma$ Y	920	55	$\tau$ YZ	-94	37
$\sigma$ Z	902	48	$\tau$ ZX	87	42

<sup>1</sup>Compressive stresses are designated by positive sign.

<sup>2</sup>Positive sign indicates inclination above the horizontal plane.

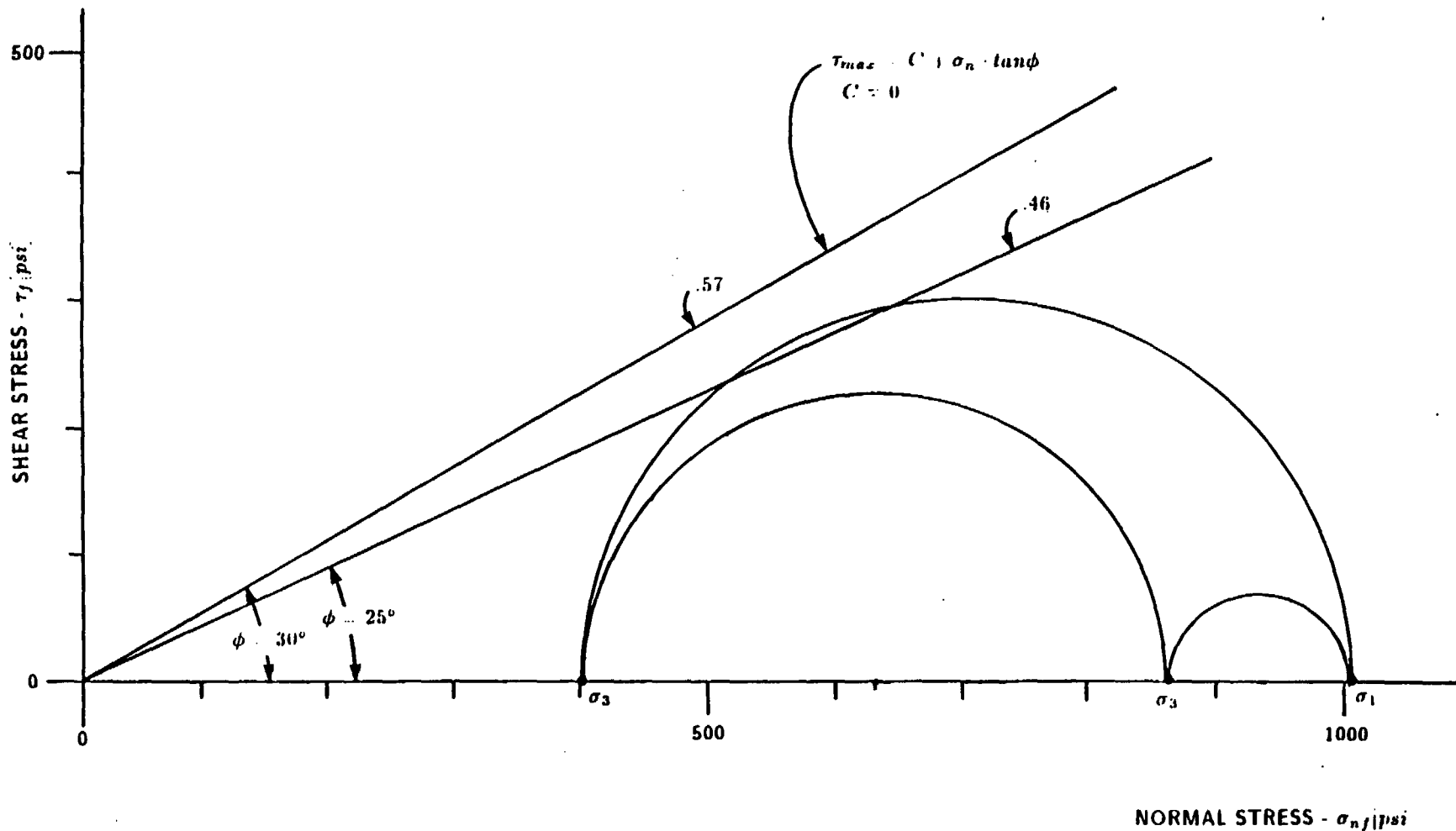
<sup>3</sup>Sign indicates the direction of shear stress. A positive sign is dextral (right-handed), a negative is sinistral (left-handed).

The results of in-situ stress determination in Rainier Mesa. From Miller et al., (1975)

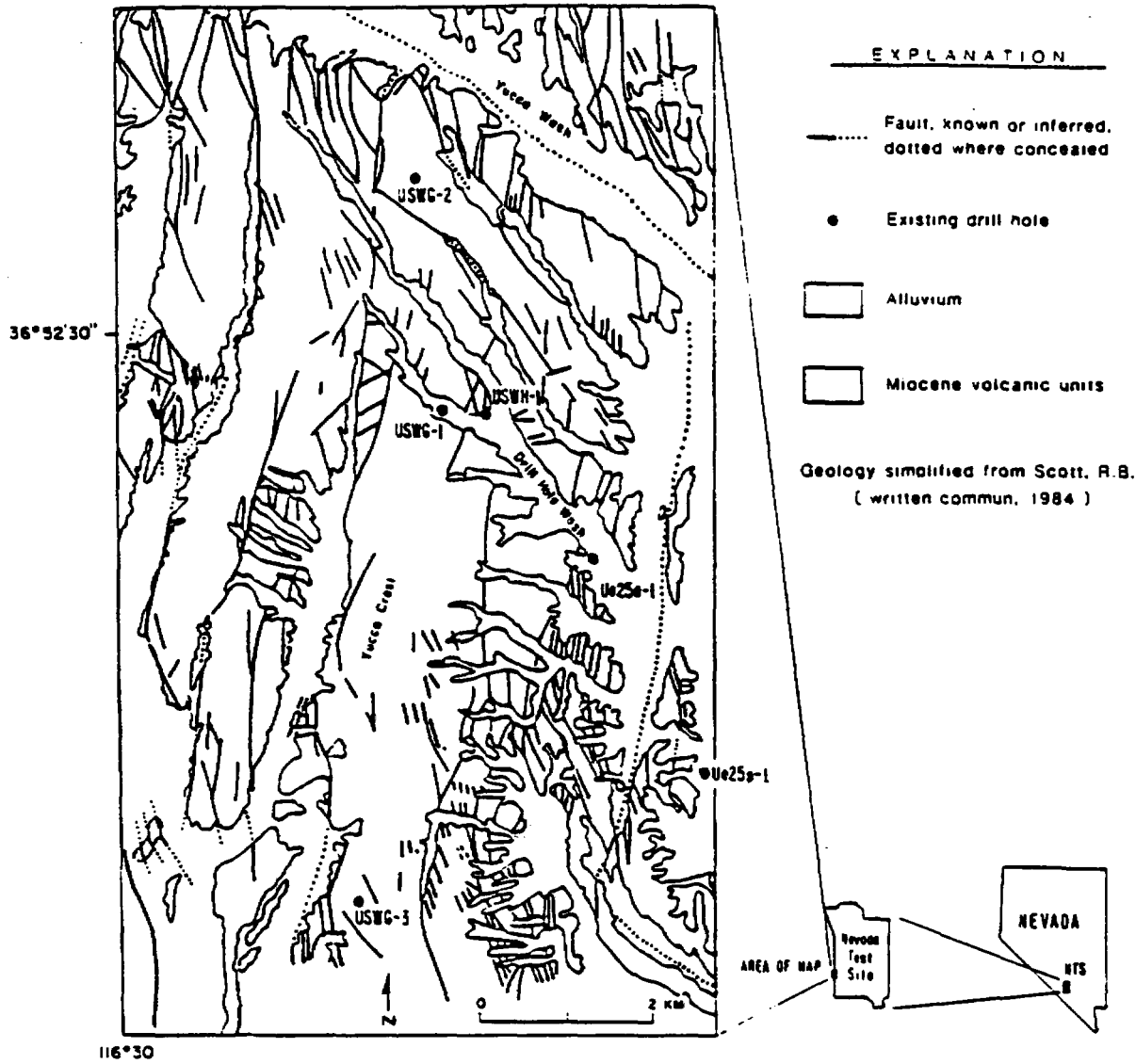


Three-dimensional representation of the in-situ stresses measured in Rainier Mesa. From Miller et al., (1975)

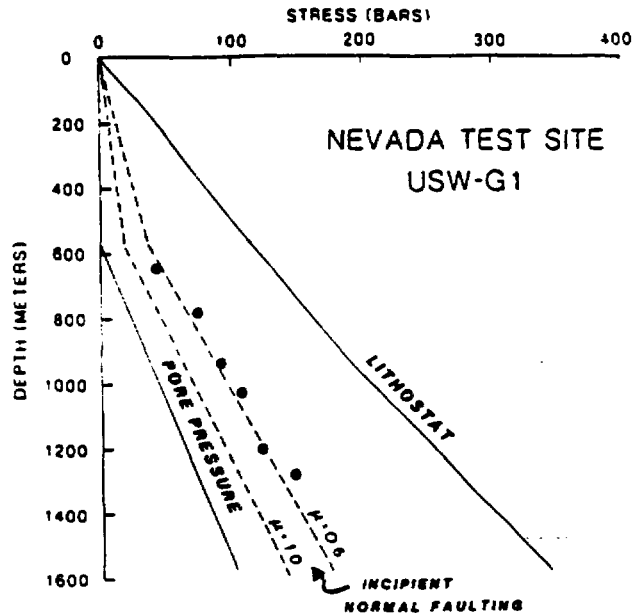
NOTE: 50 TO 60 PERCENT OF ALL NORMAL FAULTS CONTAIN WATER. THORDARSON (1965) SIGNIFICANT PORE PRESSURES MAY BE INVOLVED.  $\sigma_{n\text{eff}} = \sigma_n - p$



Mohr's representation of in-situ stress at Rainier Mesa.

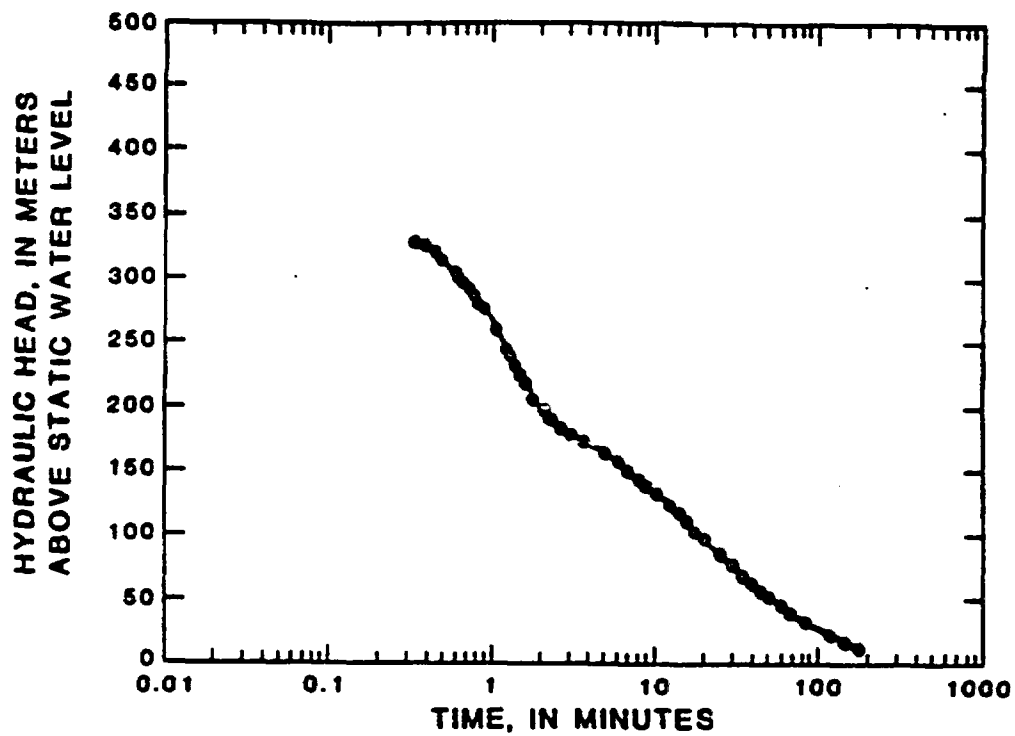


Location map showing wells where hydrofracture experiments were made at Yucca Mountain. From Stock et. al. (1986).

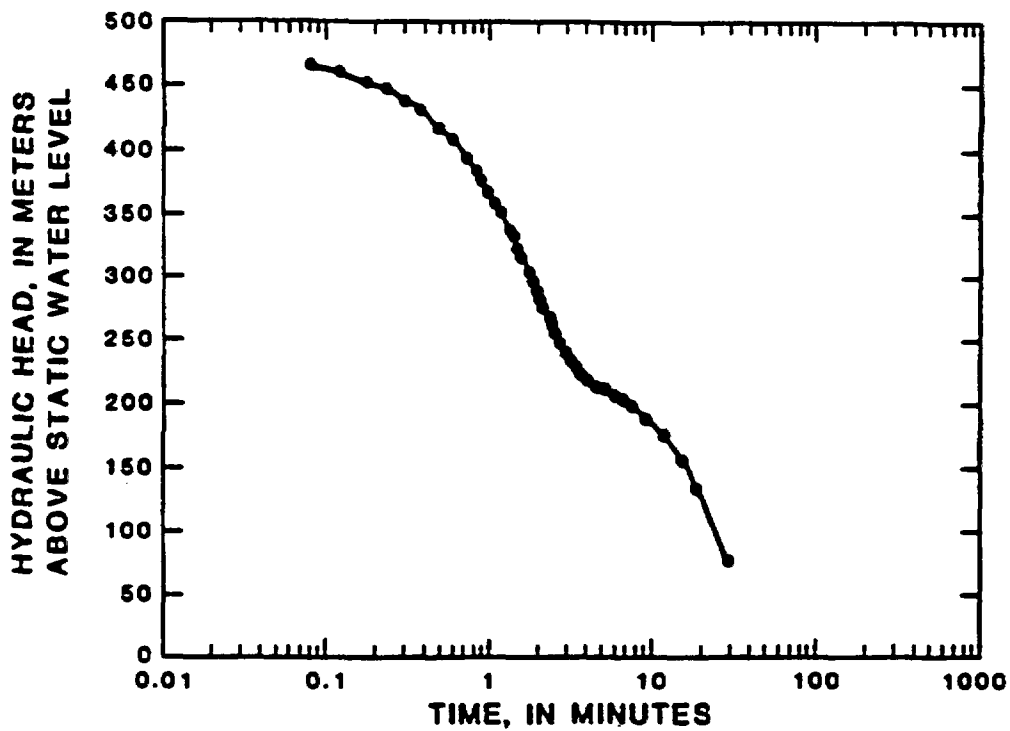


Hydraulic Fracturing Data					Principal Stresses		
Depth, m	Breakdown Pressure, MPa	Shut-In Pumping Pressure, MPa	Hydrostatic Pressure, MPa	Pore Pressure,*† MPa	Minimum Horizontal Stress, MPa	Vertical Stress MPa*	Comments
<i>USW G-1</i>							
646	8.3	4.2 ± 0.2	6.2	0.7	4.2 ± 0.2	12.9	Minimum horizontal stress from flat subhydrostatic pumping pressure attained during second cycle. $S_2$ may thus be several bars too high due to pressure gradient in fracture.
792	10.2	7.2 ± 0.2	7.9	2.2	7.2 ± 0.2	15.9	Same as above.
945	13.2	9.0 ± 0.2	9.2	3.6	9.0 ± 0.2	19.2	Same as above.
1038	13.5	10.6 ± 0.2	10.3	4.5	10.6 ± 0.2	21.4	Minimum horizontal stress from stable instantaneous shut-in pressures attained in final cycles.
1218	18.8	12.1 ± 0.2	12.0	6.3	12.1 ± 0.2	25.5	Same as above.
1288	23.8	14.8 ± 0.2	12.8	7.0	14.8 ± 0.2	27.2	Same as above.

Results of in-situ stress determinations in well USW G-1, Yucca Mountain. From Stock et. al., (1985)

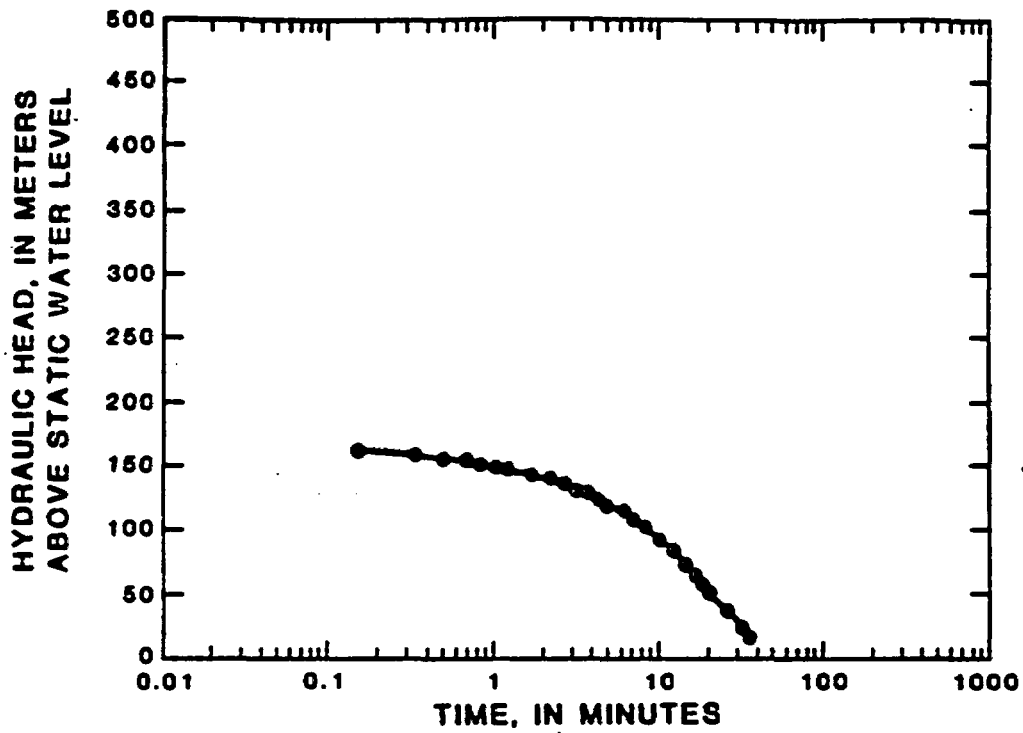


TEST INTERVAL 555m - 604m.

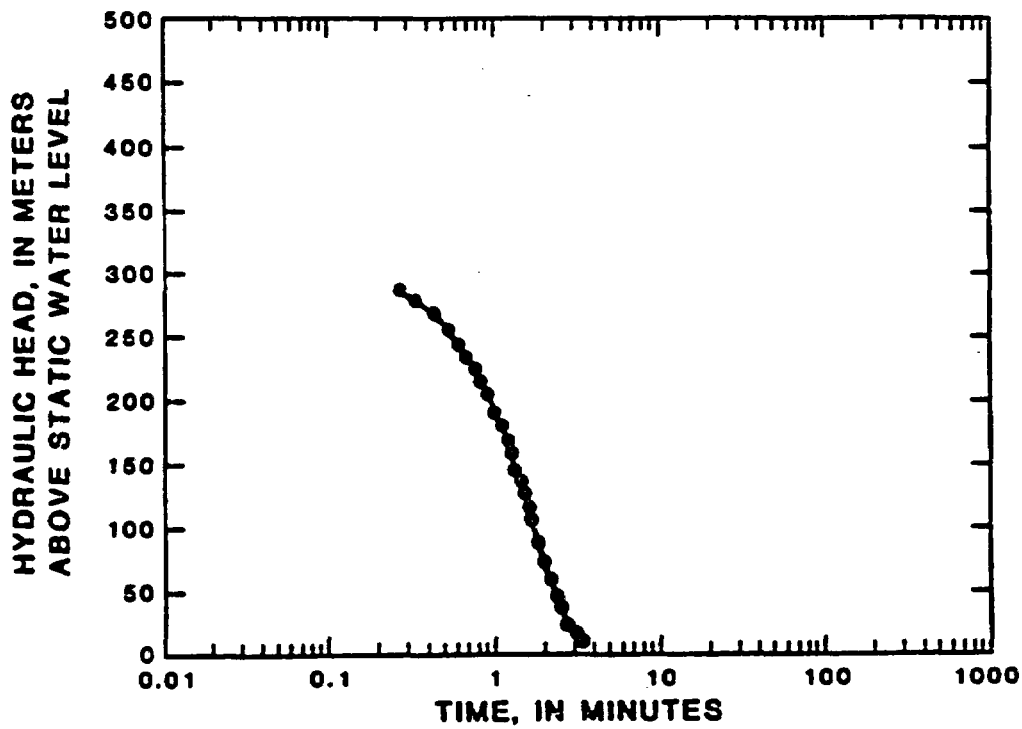


TEST INTERVAL 604m - 652m.

Results of the Cooper-Brederhoeft injection tests in well USW H-4. From Whitefield et al. (1984).

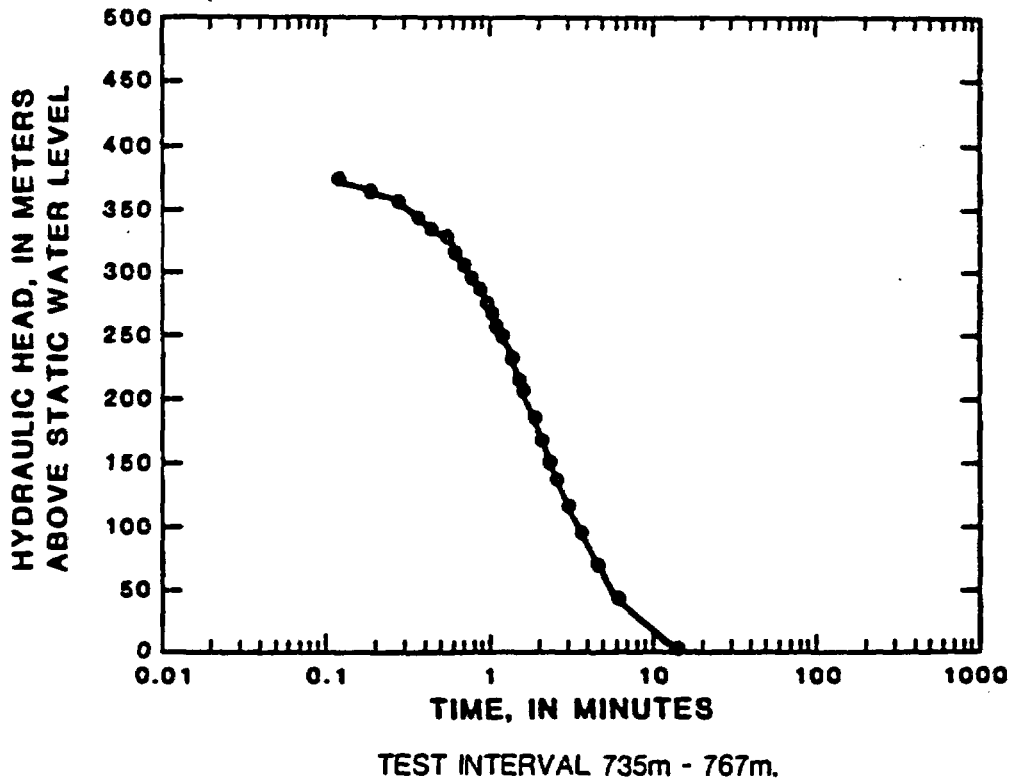
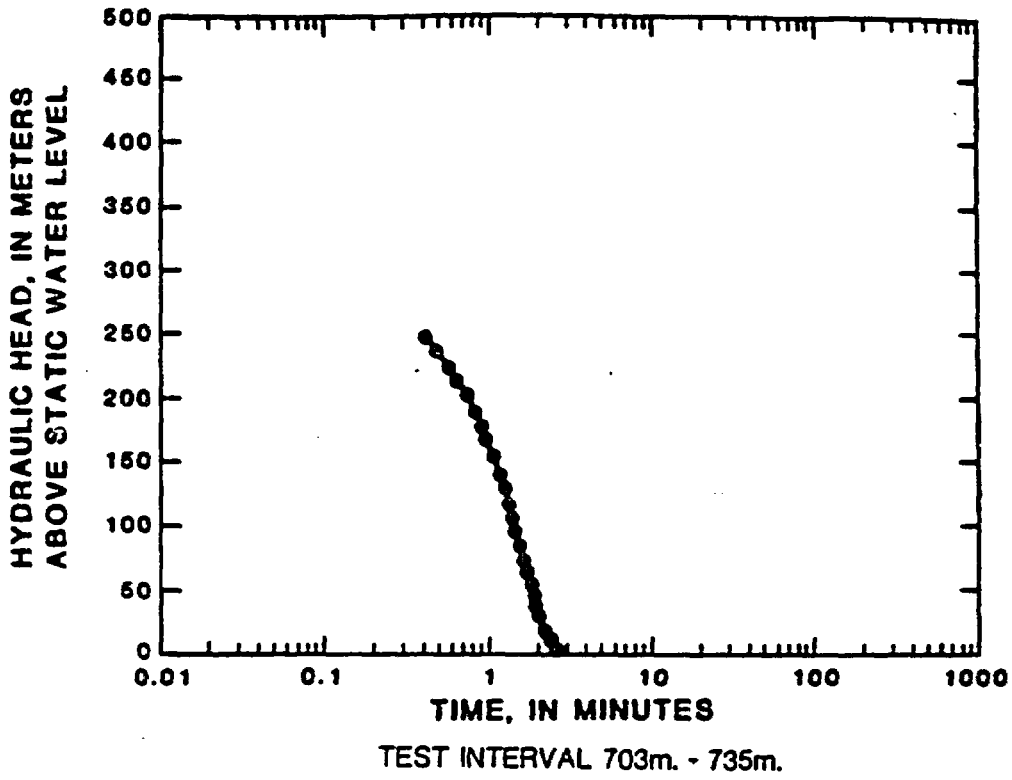


TEST INTERVAL 604m - 652m.

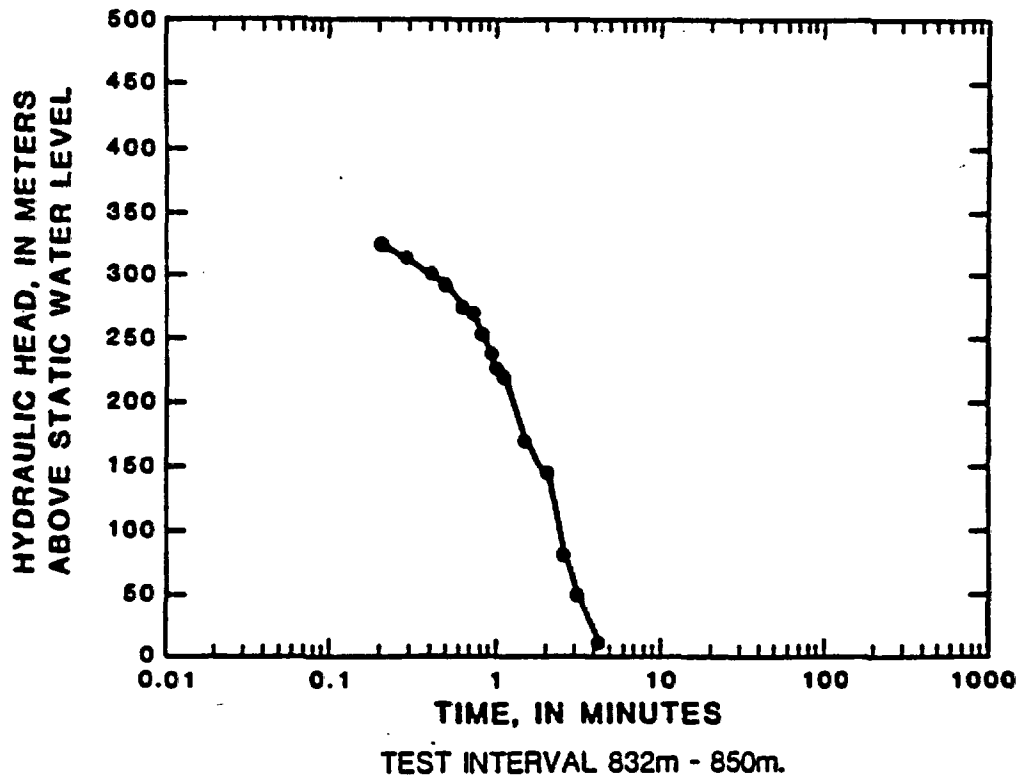
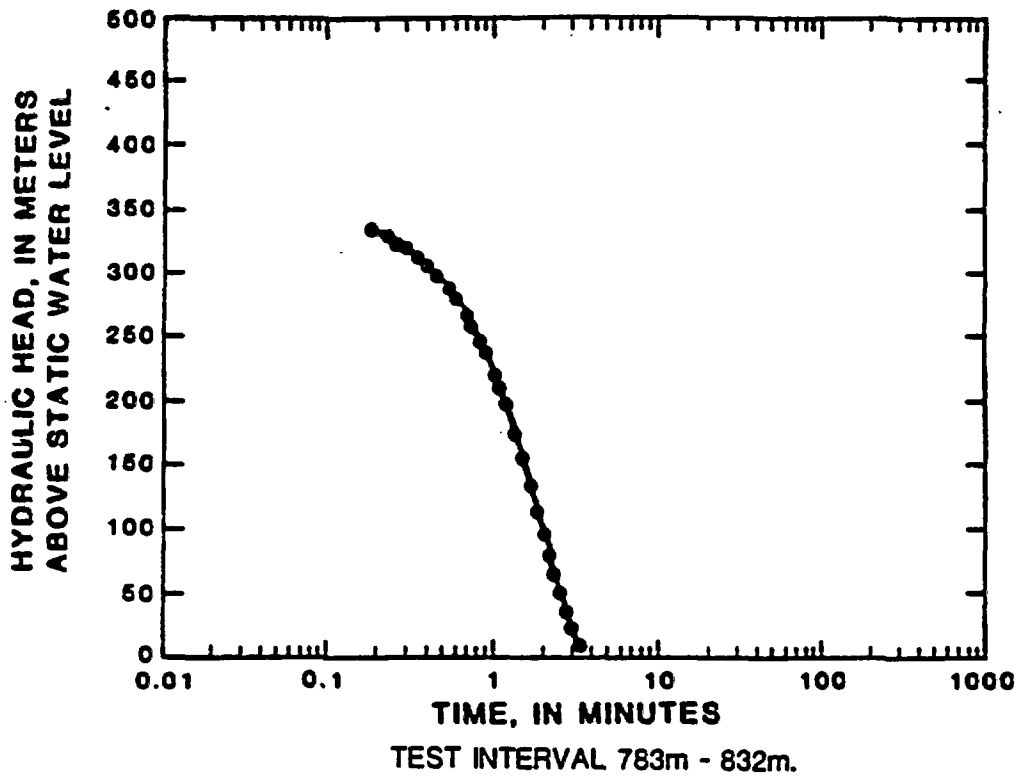


TEST INTERVAL 652m - 701m.

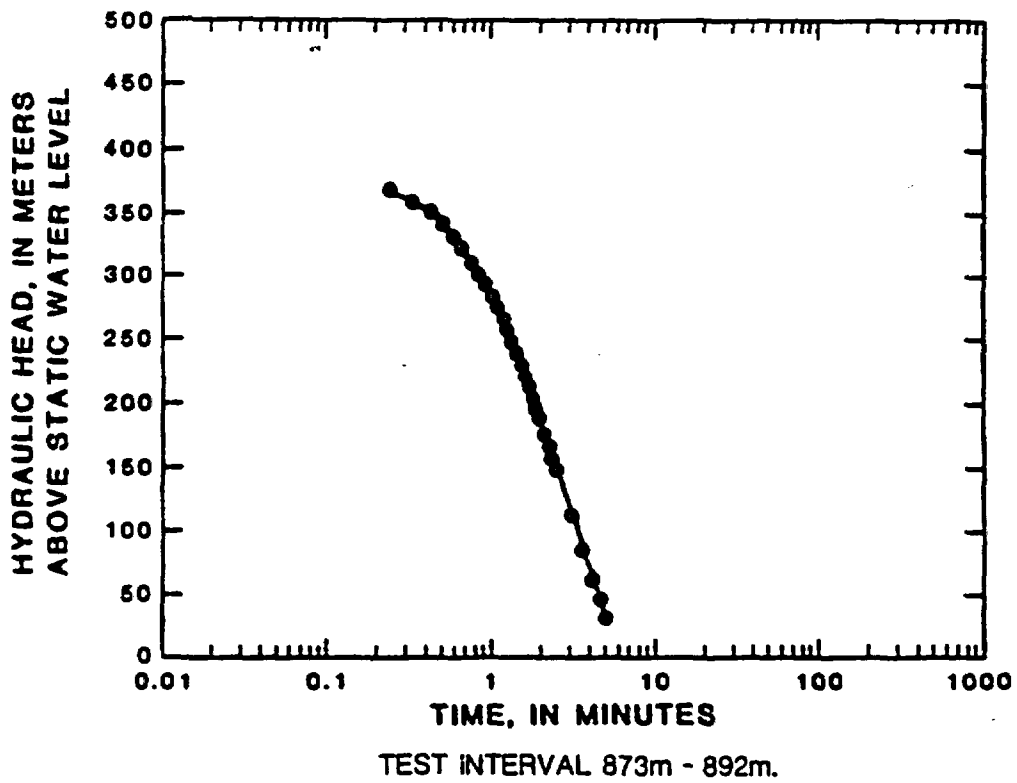
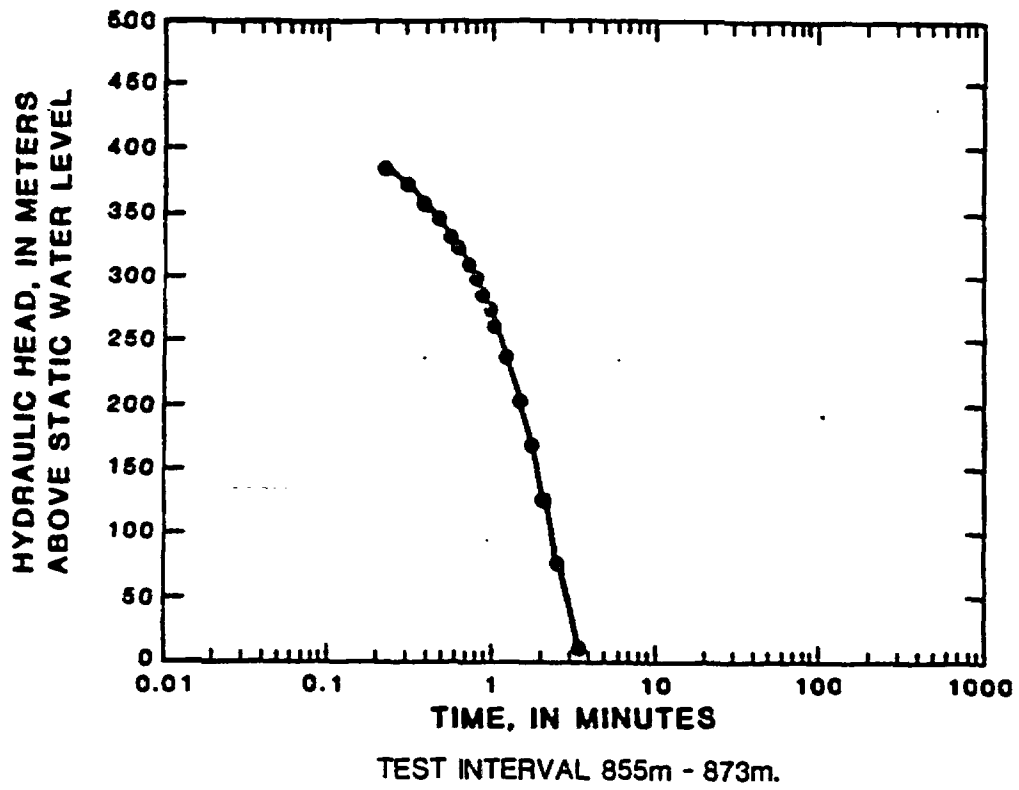
Results of the Cooper-Bredehoeft injection tests in well USW H-4. From Whitefield et al. (1984).



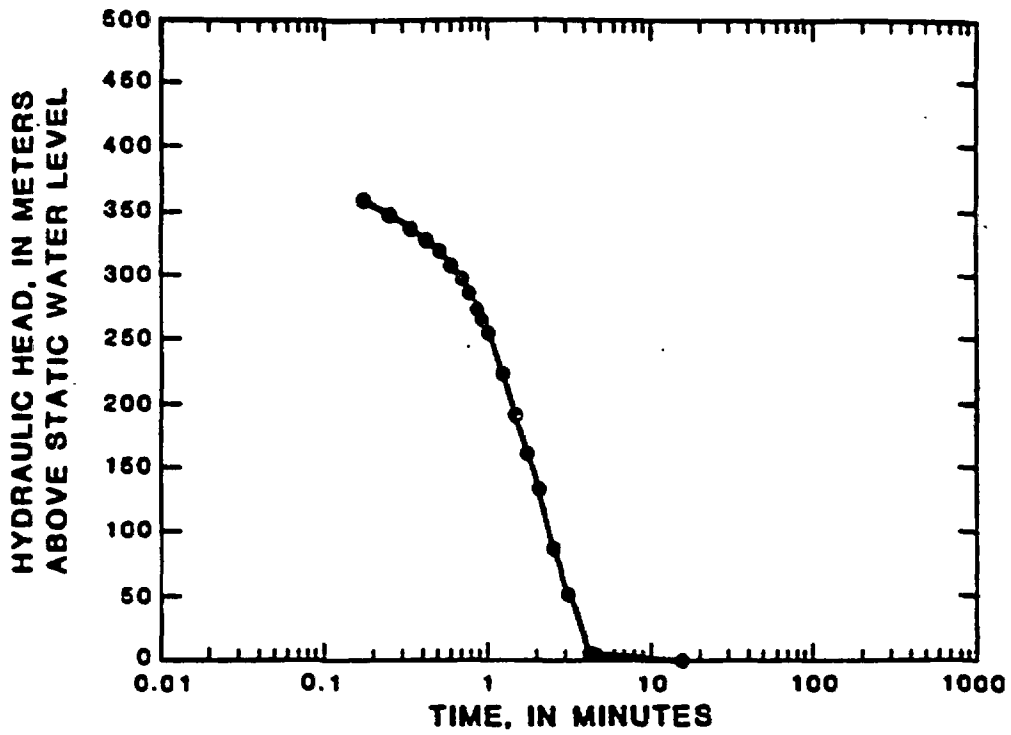
Results of the Cooper-Bredehoeft injection tests in well USW H-4. From Whitefield et al. (1984)



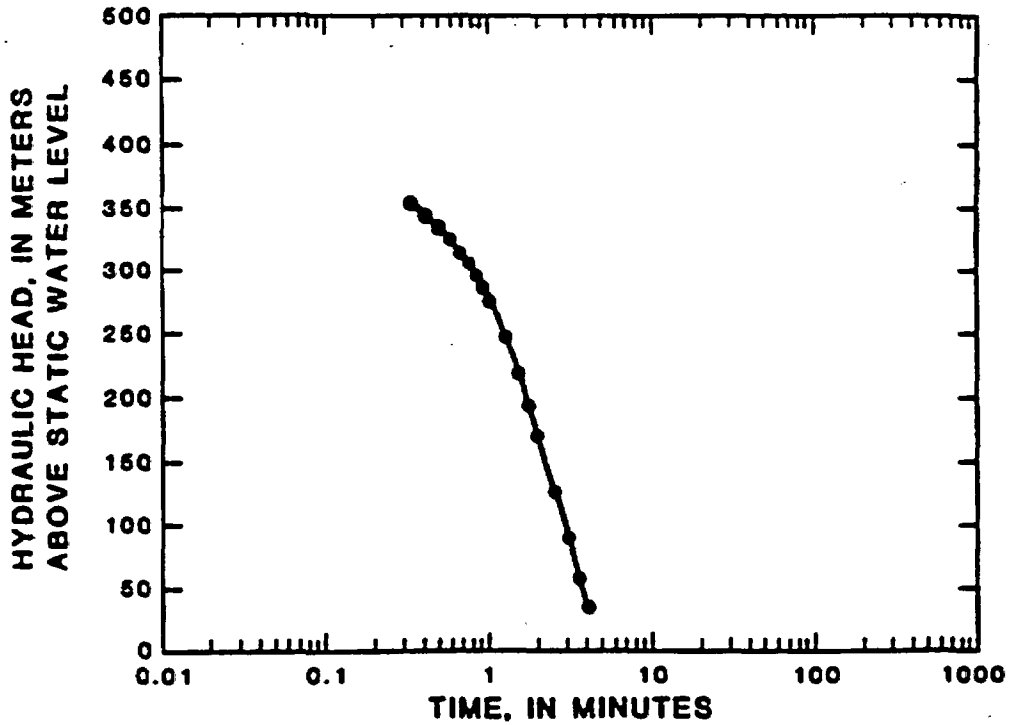
Results of the Cooper-Brederhoft injection tests in well USW H-4. From Whitefield et al. (1984)



Results of the Cooper-Bredehoeft injection tests in well USW H-4. From Whitefield et al. (1984)

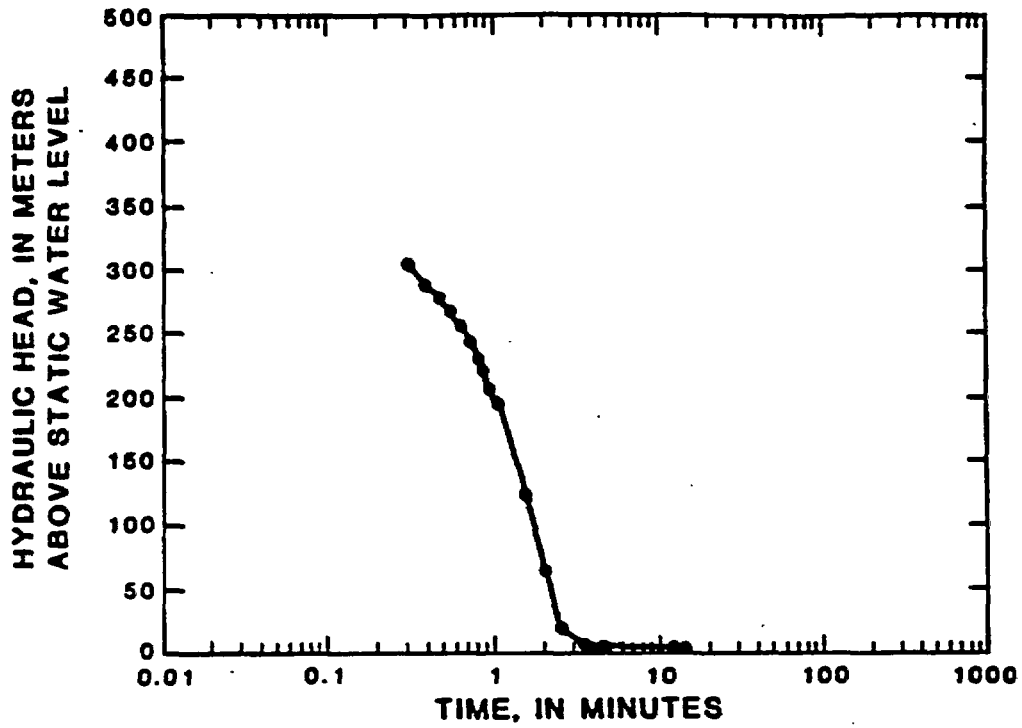


TEST INTERVAL 892m - 910m.

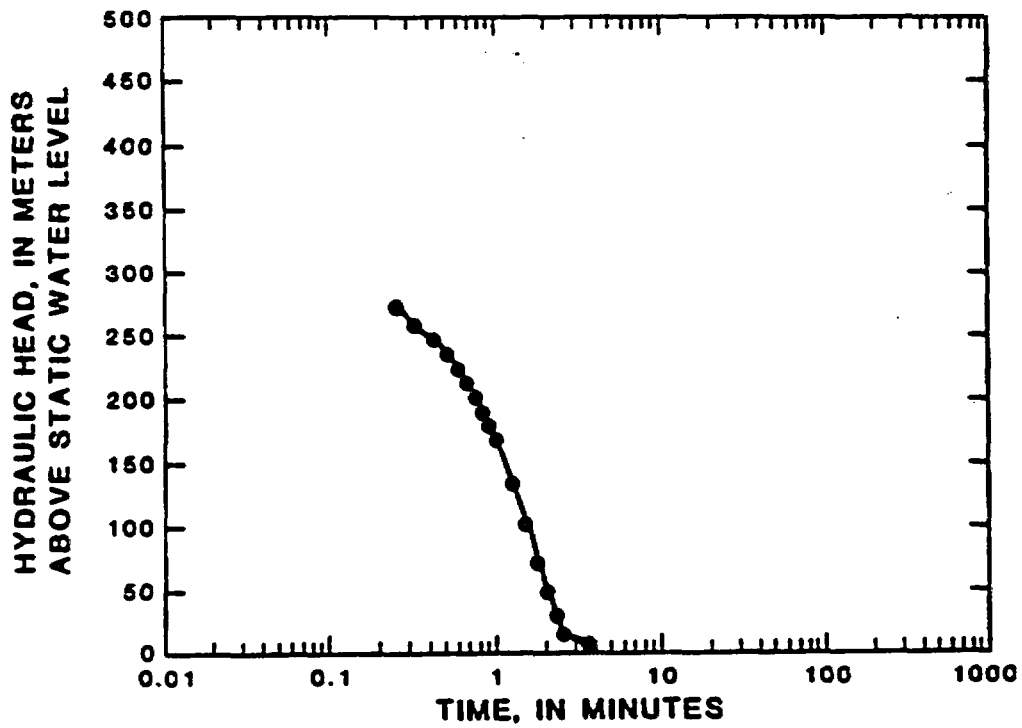


TEST INTERVAL 910m - 926m.

Results of the Cooper-Brederhoeft injection tests in well USW H-4. From Whitefield et al. (1984).

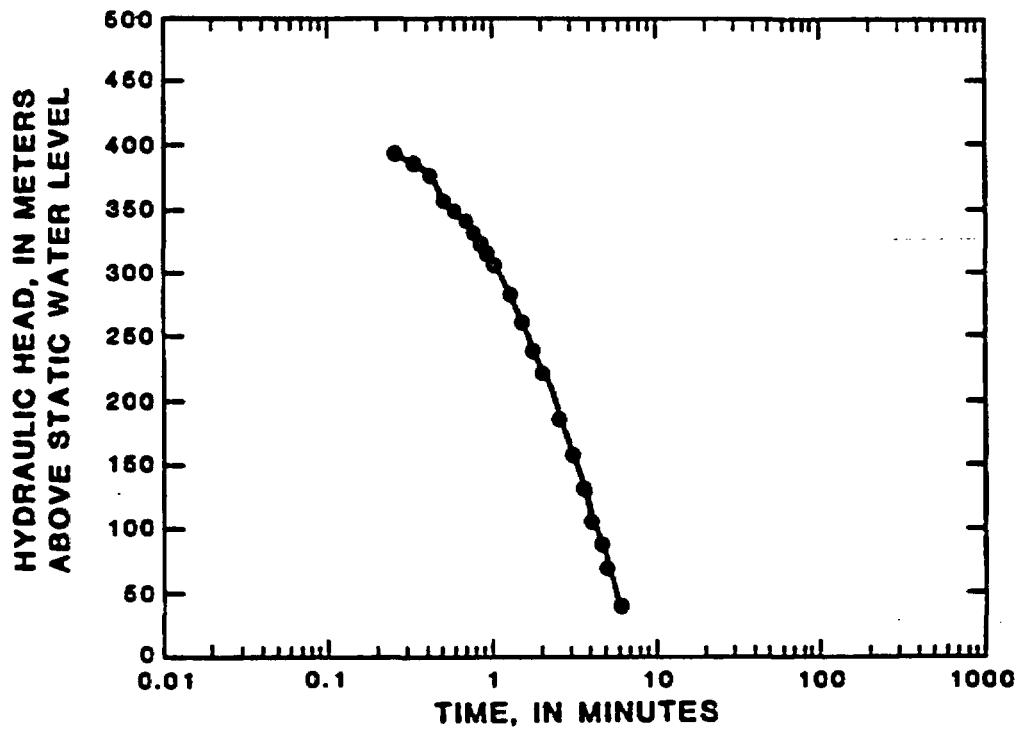


TEST INTERVAL 928m - 1219m.



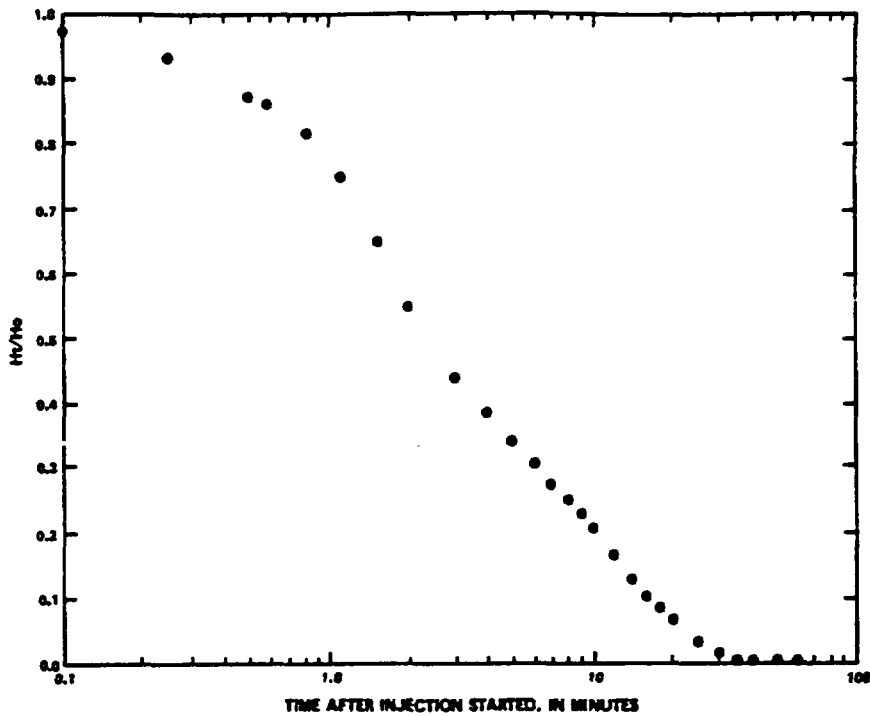
TEST INTERVAL 1173m - 1192m.

Results of the Cooper-Brederhoft injection tests in well USW H-4. From Whitefield et al. (1984).

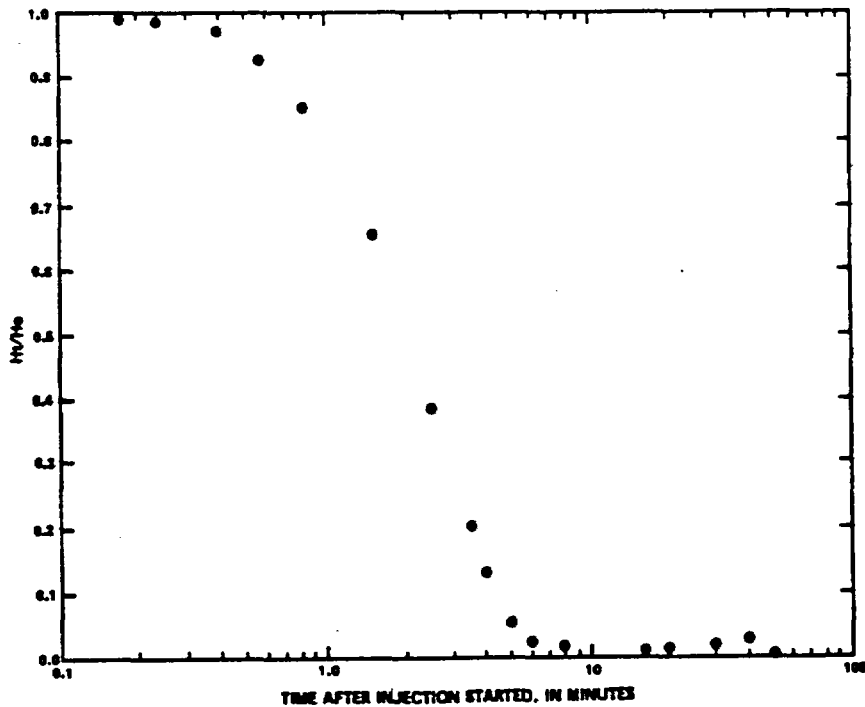


TEST INTERVAL 1195m - 1219m.

Results of the Cooper-Bredehoeft injection tests in well USW H-4. From Whitefield et al. (1984).

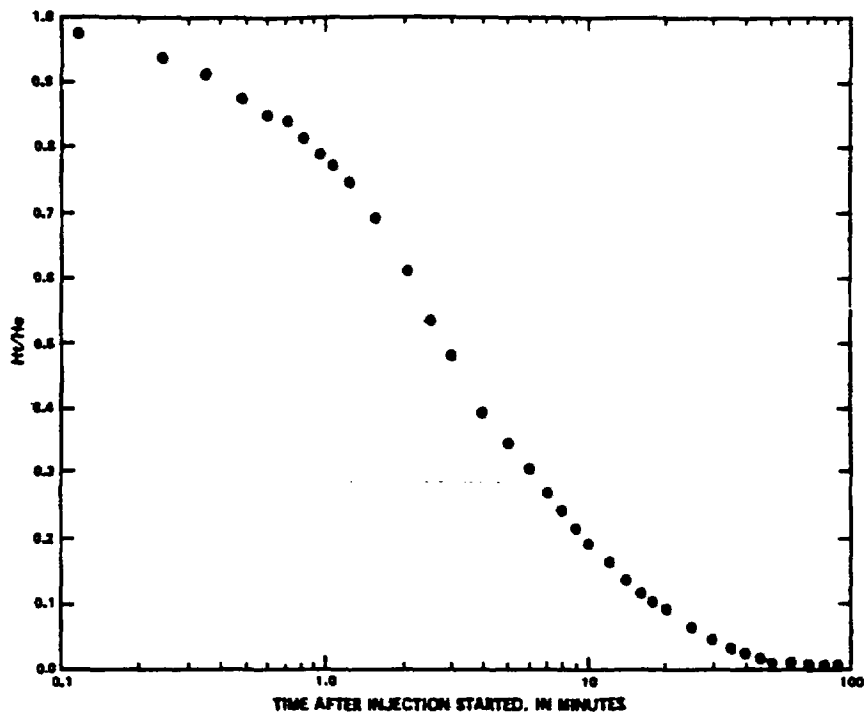


-Packer-injection test for depth interval from 790 to 796 meters.

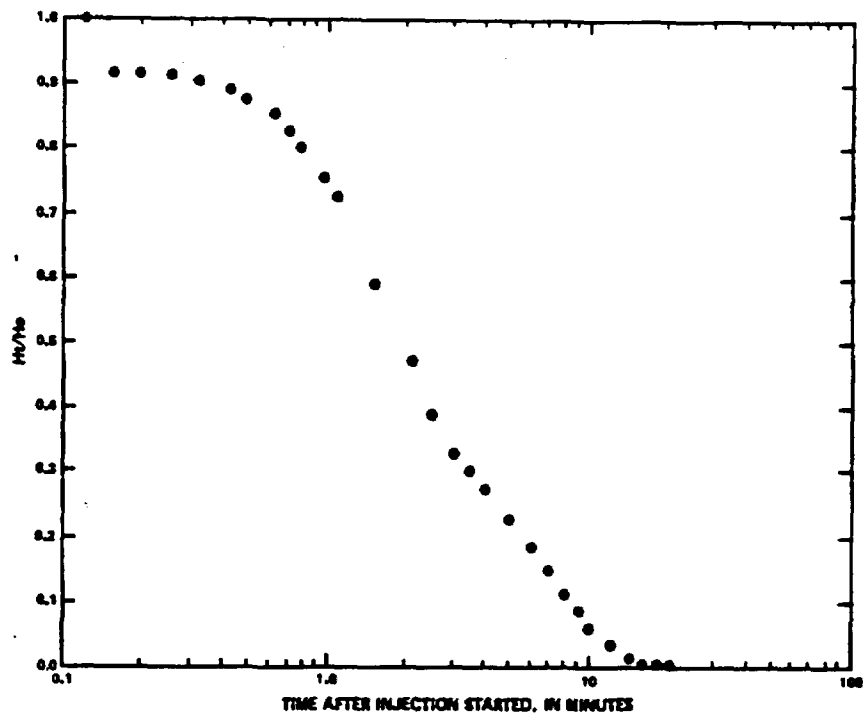


-Packer-injection test for depth interval from 796 to 815 meters.

Results of the Cooper-Bredehoeft injection tests in well USW H-5. From Bentley et al. (1983).

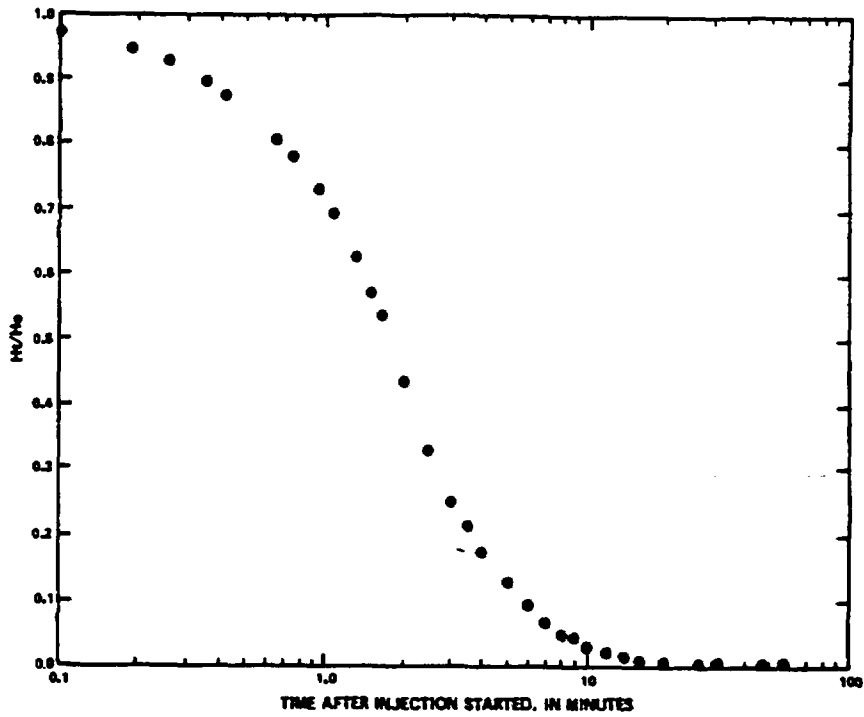


Packer-injection test for depth interval from 834 to 895 meters.

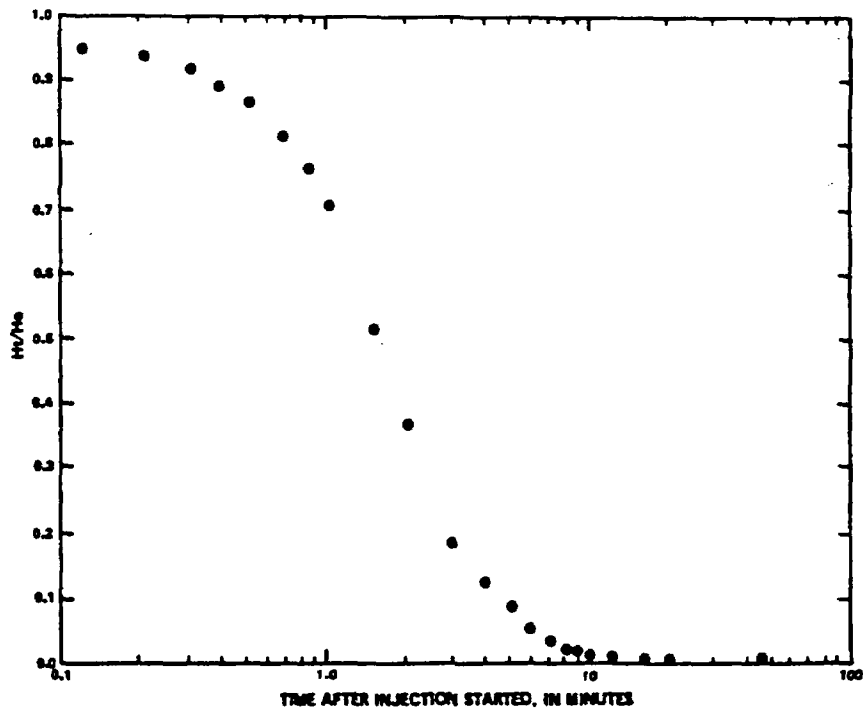


-Packer injection test for depth interval from 815 to 834 meters.

Results of the Cooper-Bredehoeft injection tests in well USW H-5. From Bentley et al. (1983).

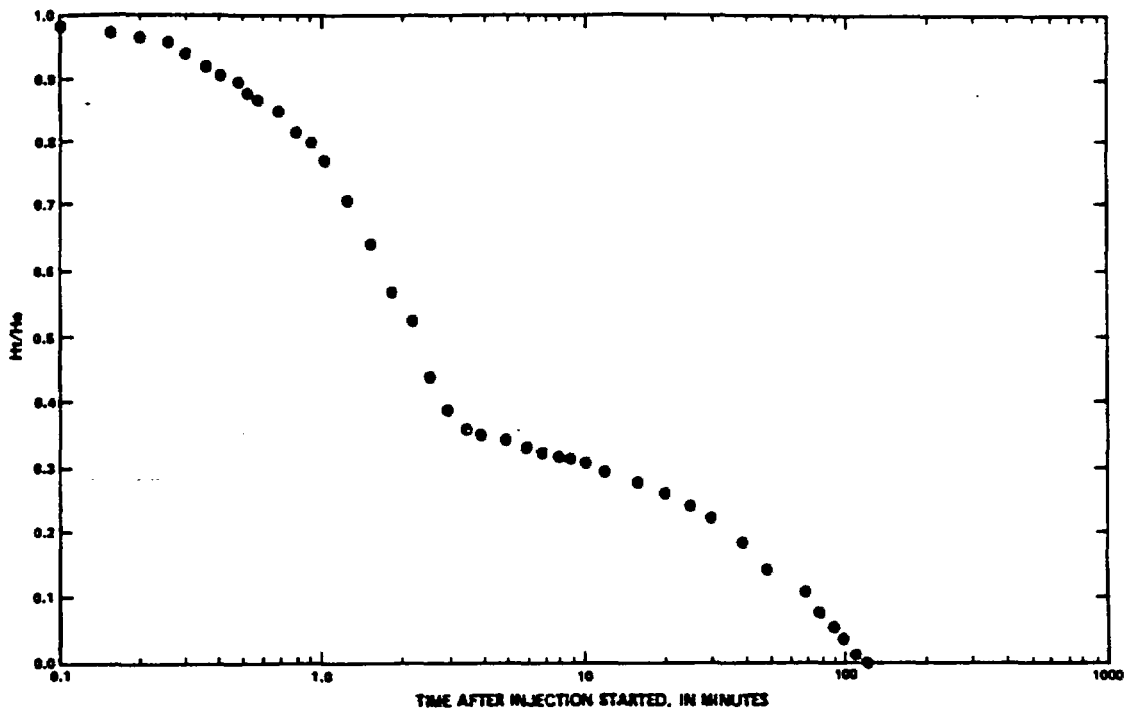


-Packer-injection test for depth interval from 887 to 947 meters.

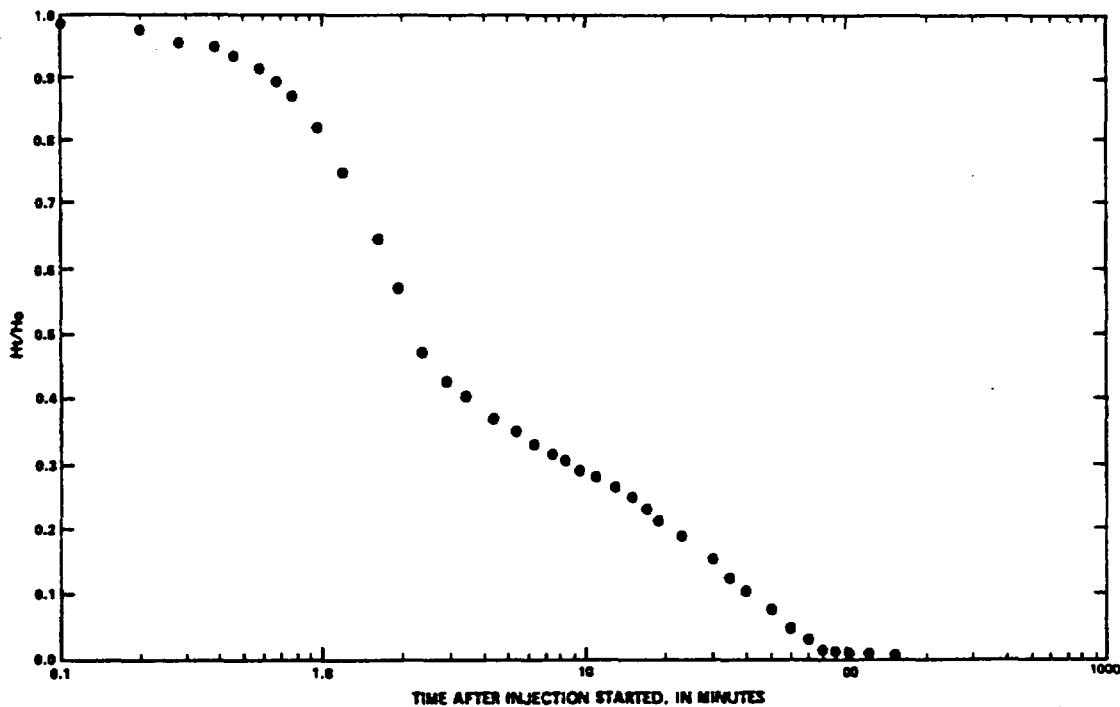


-Packer-injection test for depth interval from 888 to 949 meters.

Results of the Cooper-Bredehoeft injection tests in well USW H-5. From Bentley et al. (1983).

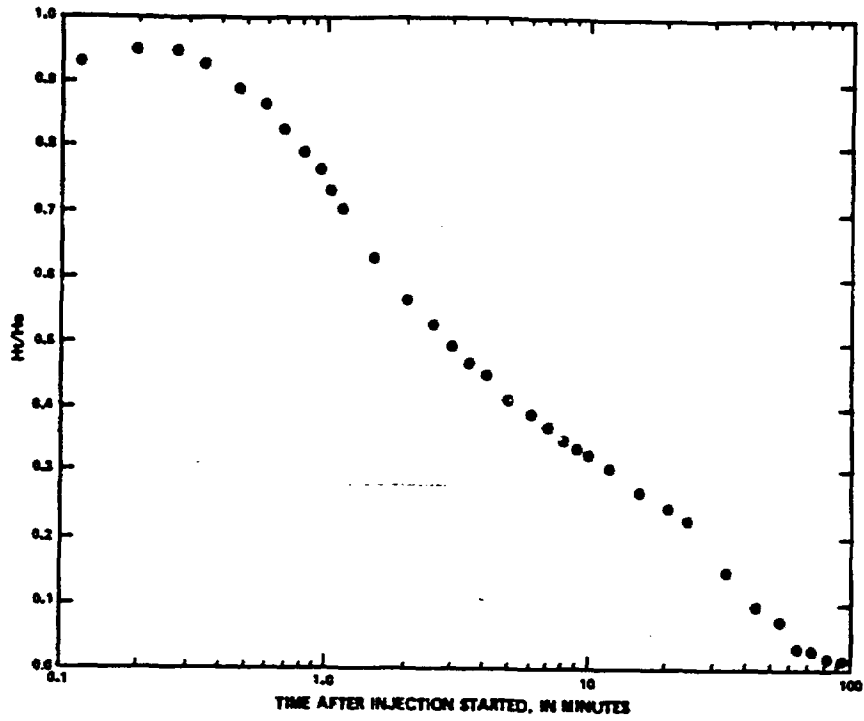


--Packer-injection test for depth interval from 949 to 1,010 meters.

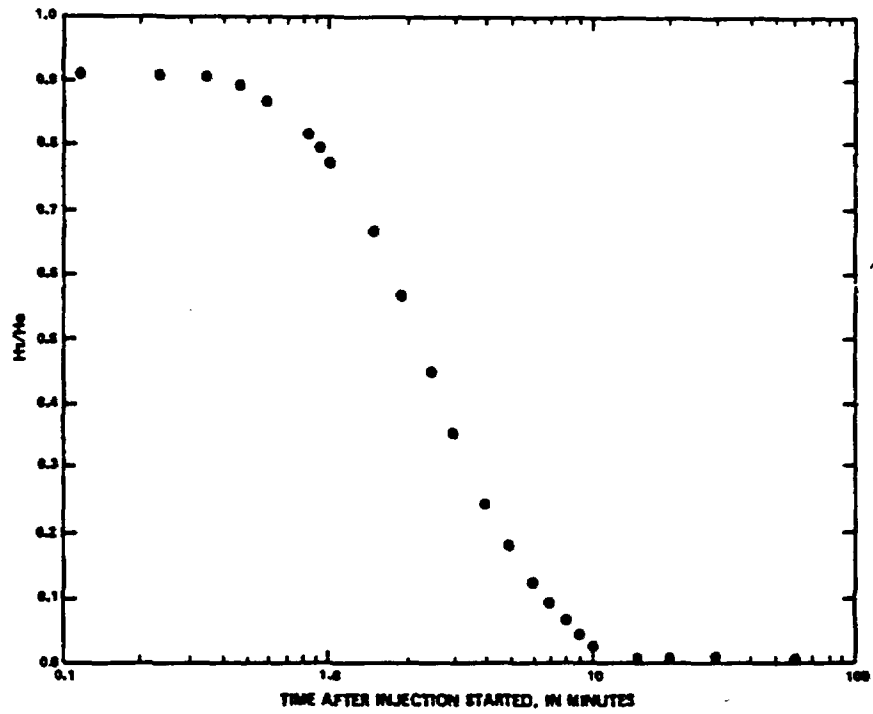


Packer-injection test for depth interval from 1,015 to 1,033 meters (first test).

Results of the Cooper-Bredehoeft injection tests in well USW H-5. From Bentley et al. (1983).

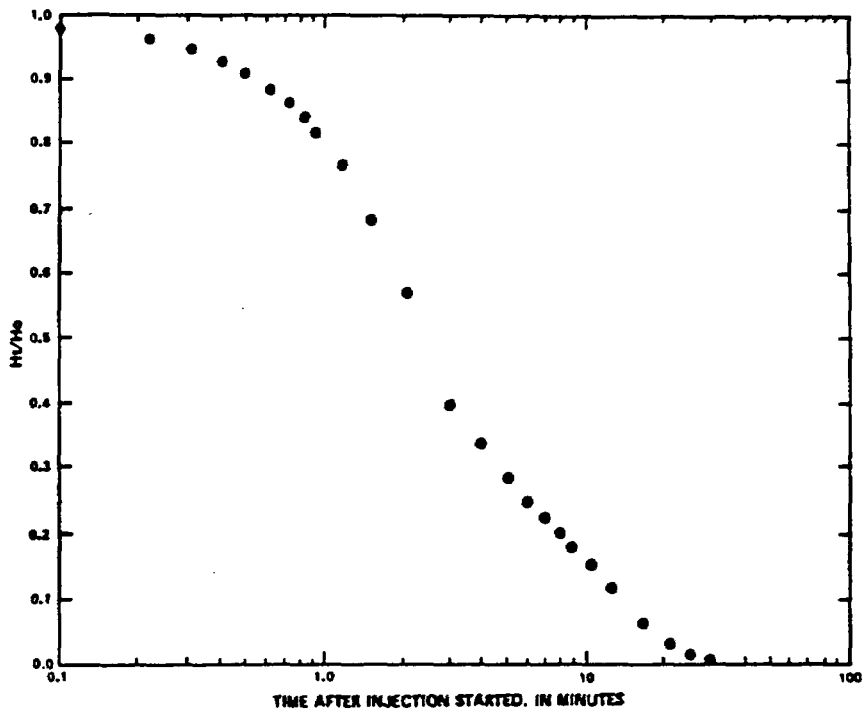


-Packer-injection test for depth interval from 1,015 to 1,033 meters (second test).



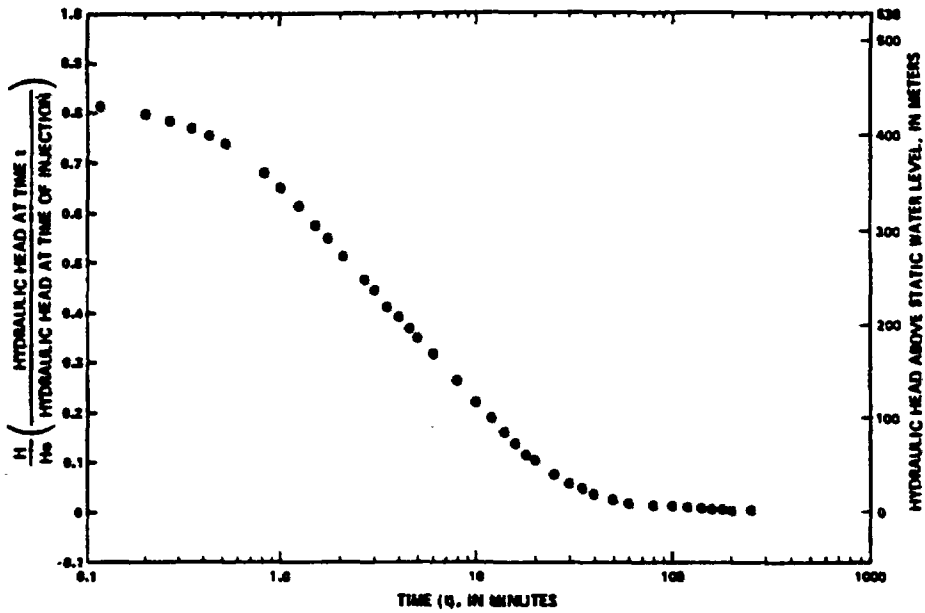
-Packer injection test for depth interval from 1,033 to 1,052 meters.

Results of the Cooper-Bredehoeft injection tests in well USW H-5. From Bentley et al. (1983).

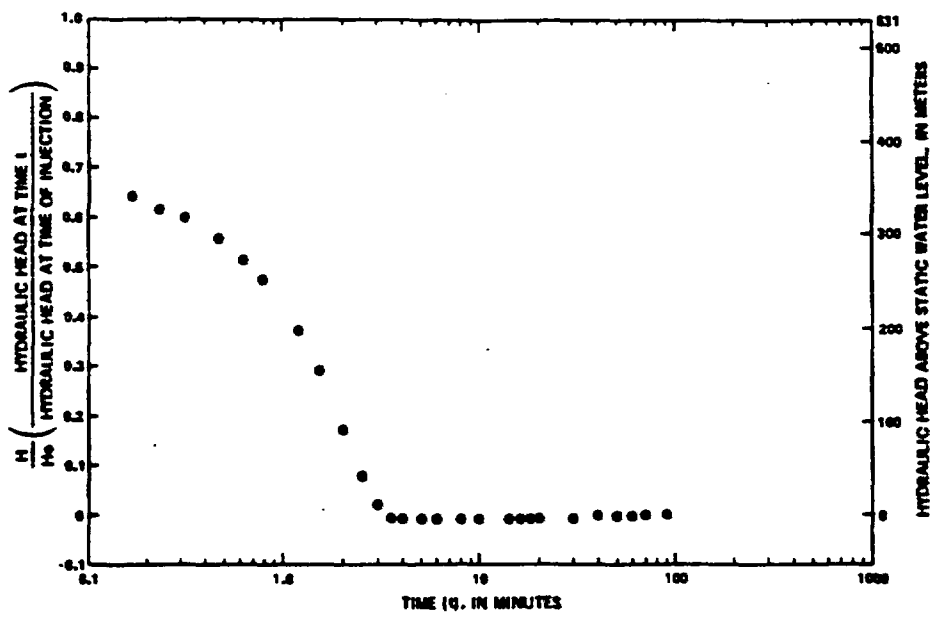


Packer-injection test for depth interval from 1,052 to 1,219 meters.

Results of the Cooper-Bredehoeft injection tests in well USW H-5. From Bentley et al. (1983)

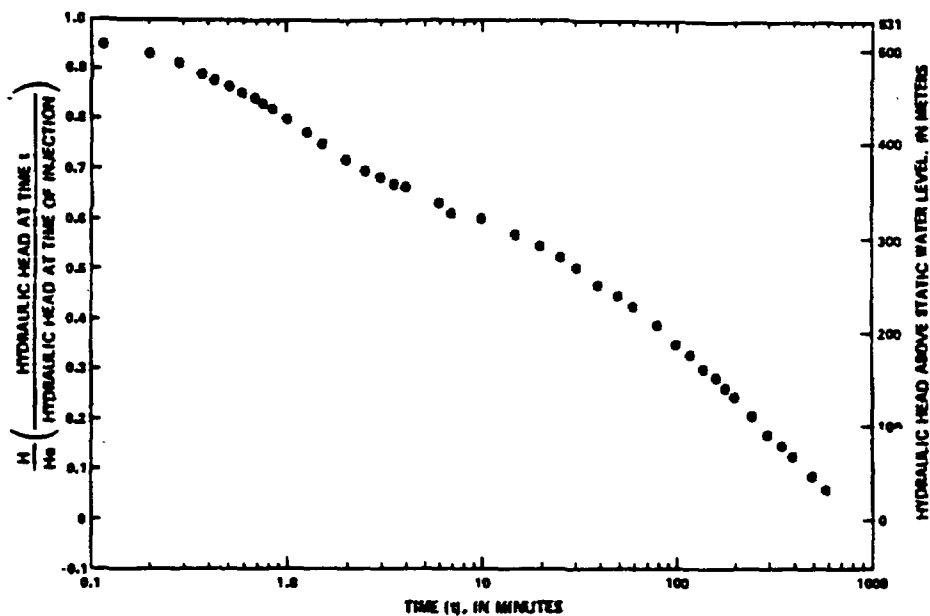


-Packer-injection test 1, depth interval from 581 to 607 meters.

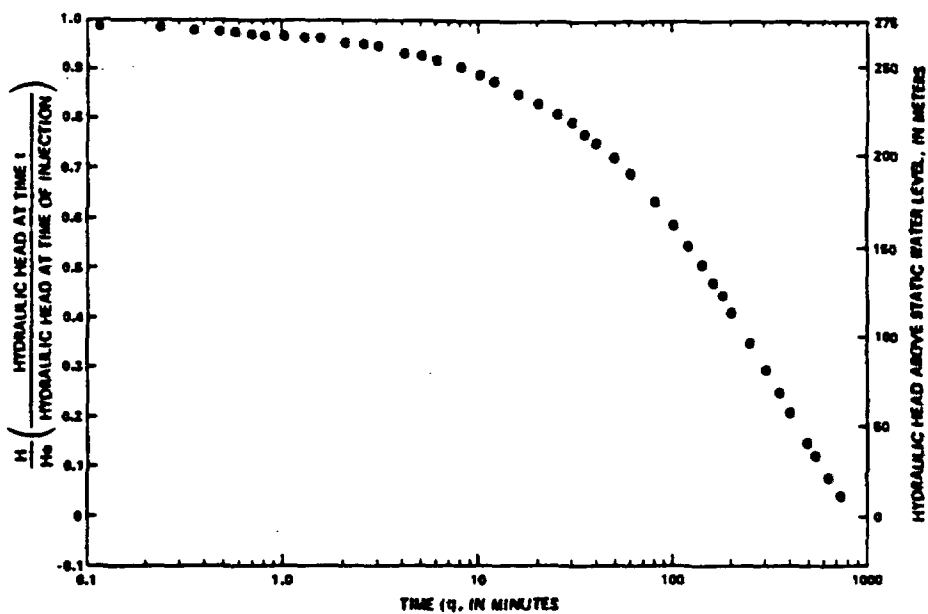


-Packer-injection test 2, depth interval from 606 to 640 meters.

Results of the Cooper-Bredehoeft injection tests in well USW H-6. From Craig et al. (1983).

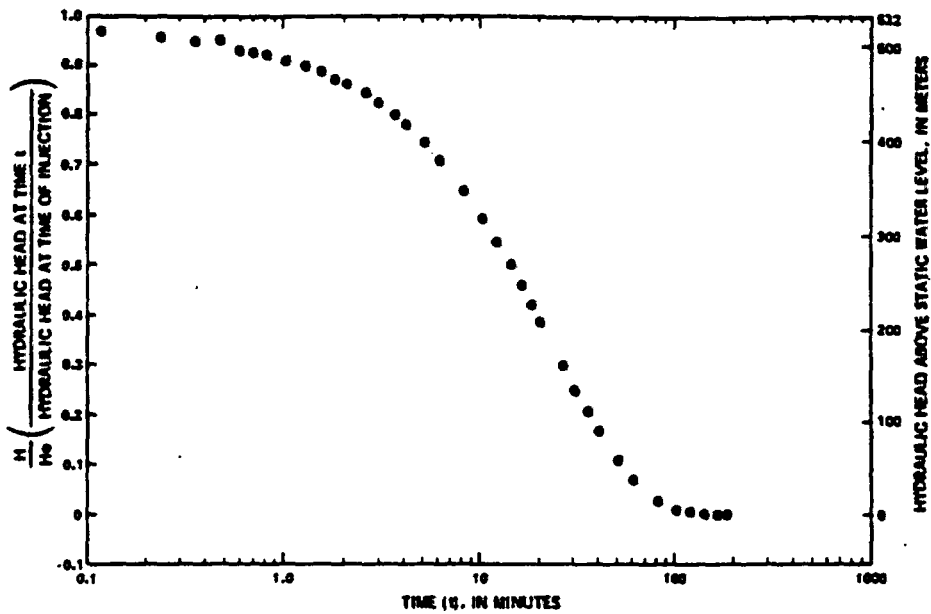


-Packer-injection test 3, depth interval from 649 to 683 meters.

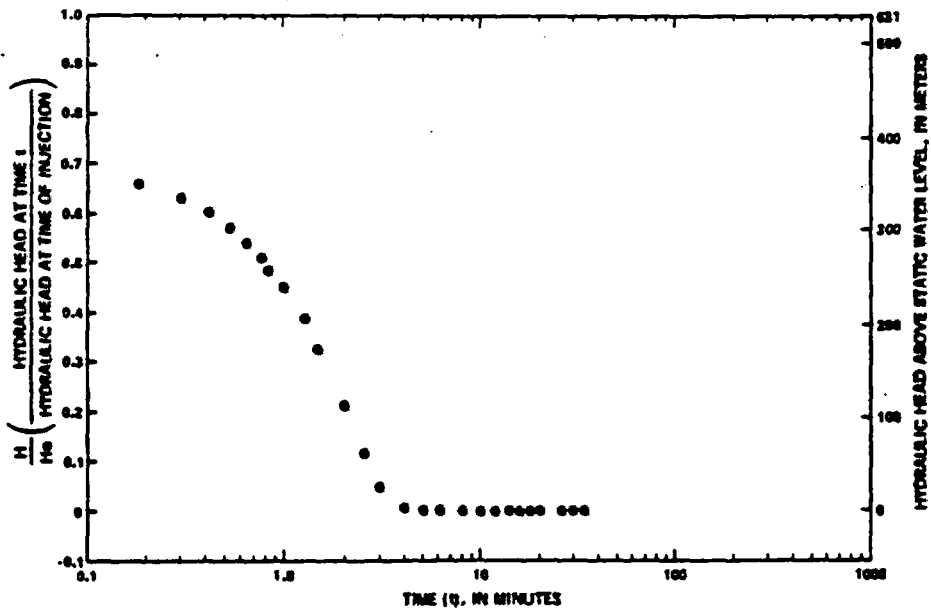


-Packer-injection test 3A, depth interval from 649 to 683 meters.

Results of the Cooper-Bredehoeft injection tests in well USW H-6. From Craig et al. (1983).

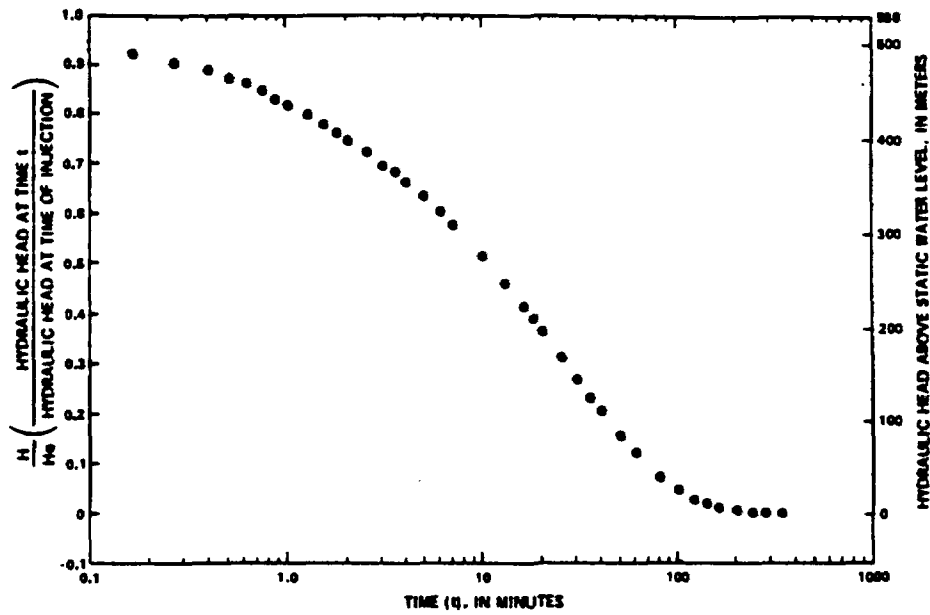


-Packer-injection test 4, depth interval from 686 to 753 meters.

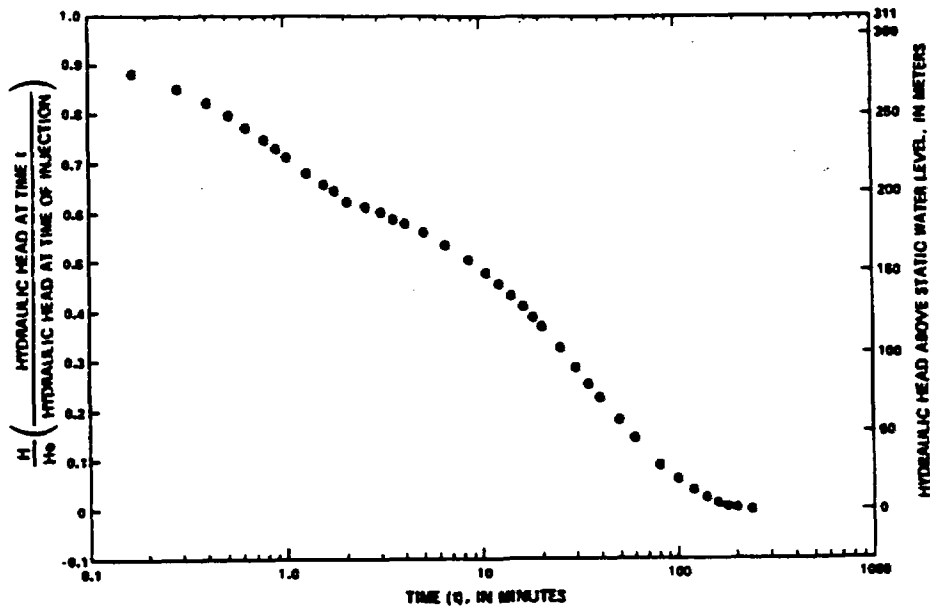


--Packer-injection test 5, depth interval from 753 to 787 meters.

Results of the Cooper-Bredehoeft injection tests in well USW H-6. From Craig et al. (1983).

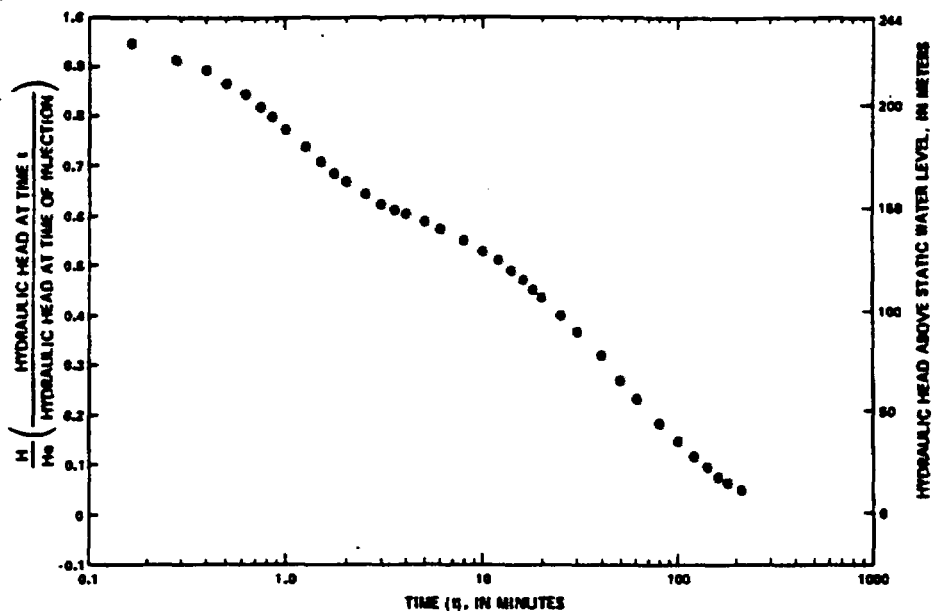


-Packer-injection test 6, depth interval from 804 to 838 meters.

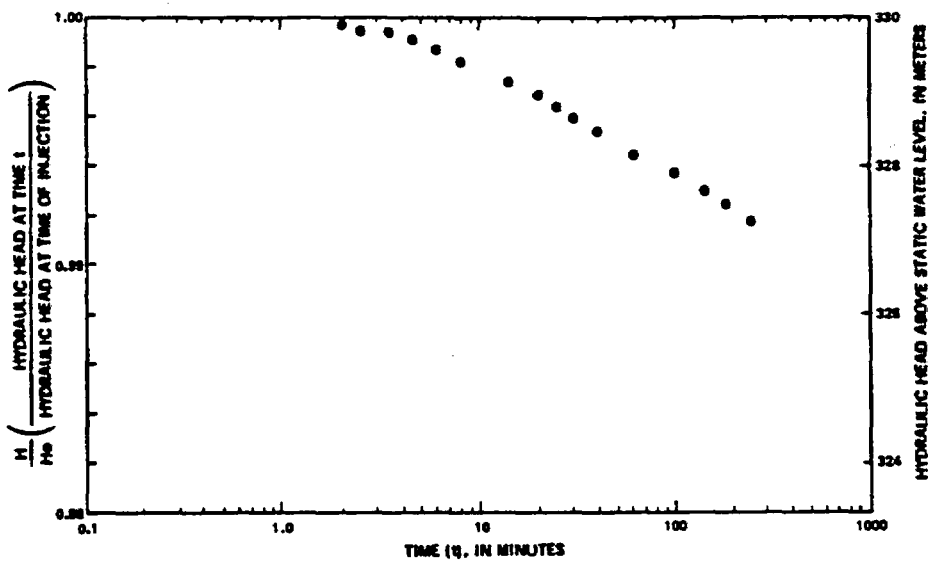


-Packer-injection test 7, depth interval from 835 to 869 meters.

Results of the Cooper-Bredehoeft injection tests in well USW H-6. From Craig et al. (1983)

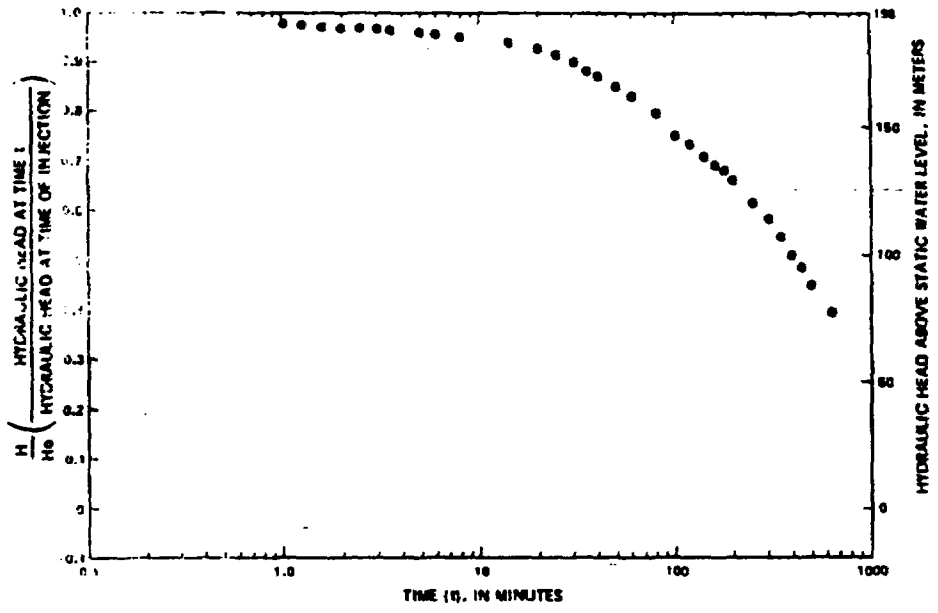


Packer-injection test 8, depth interval from 871 to 1,220 meters.



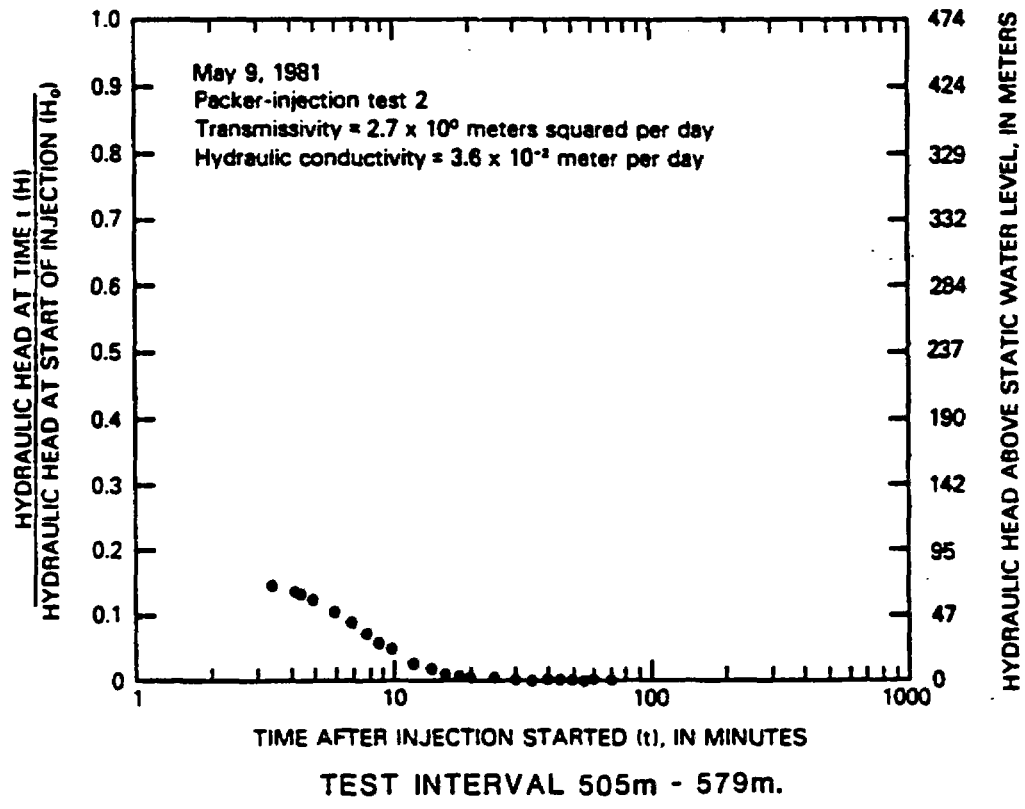
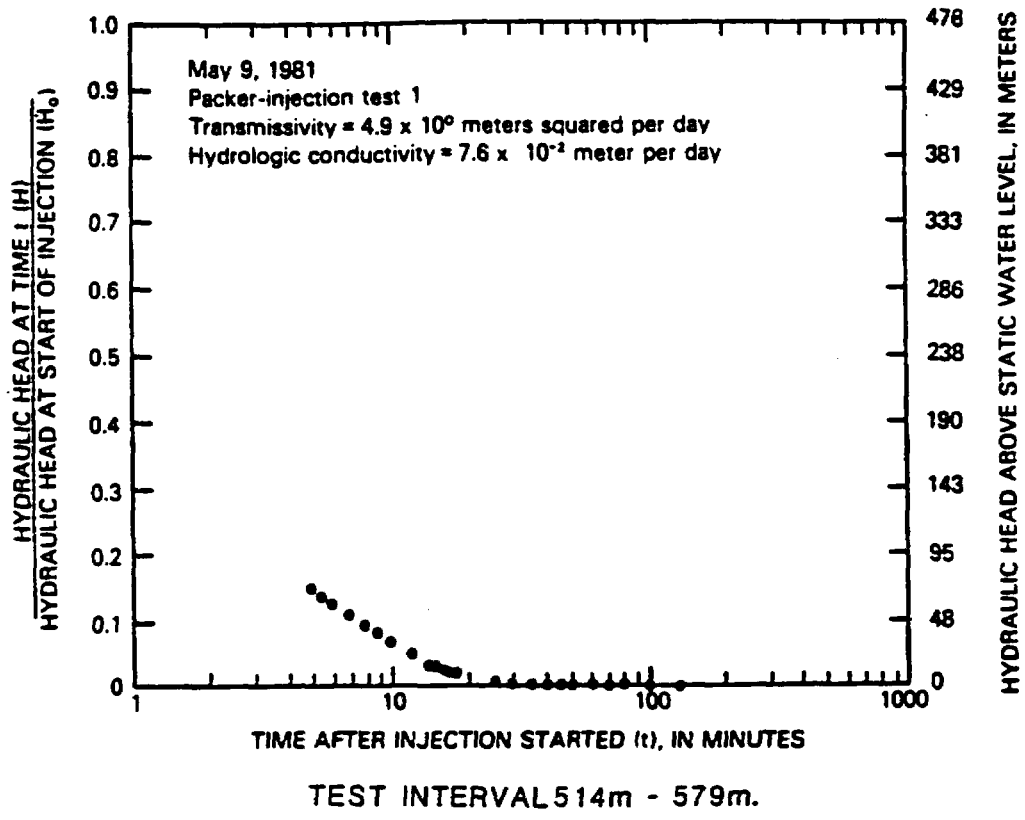
Packer-injection test 9, depth interval from 1,118 to 1,152 meters.

Results of the Cooper-Bredehoeft injection tests in well USW H-6. From Craig et al. (1983).

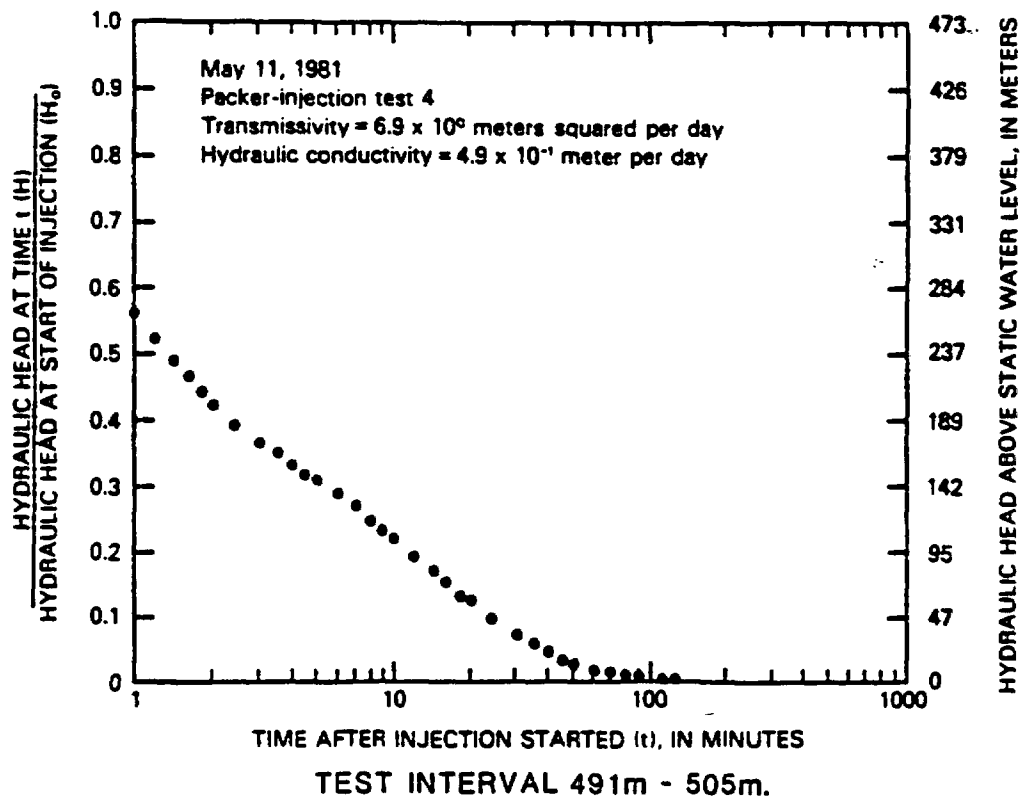
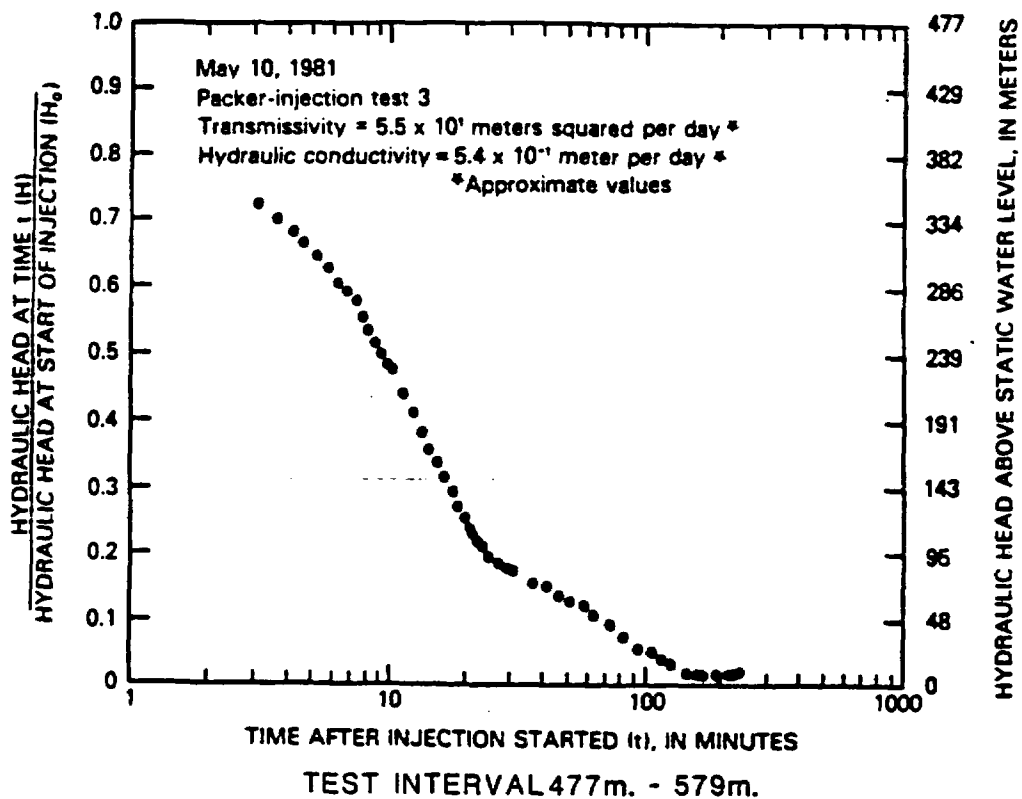


Packer-injection test 10, depth interval from 1,155 to 1,220 meters.

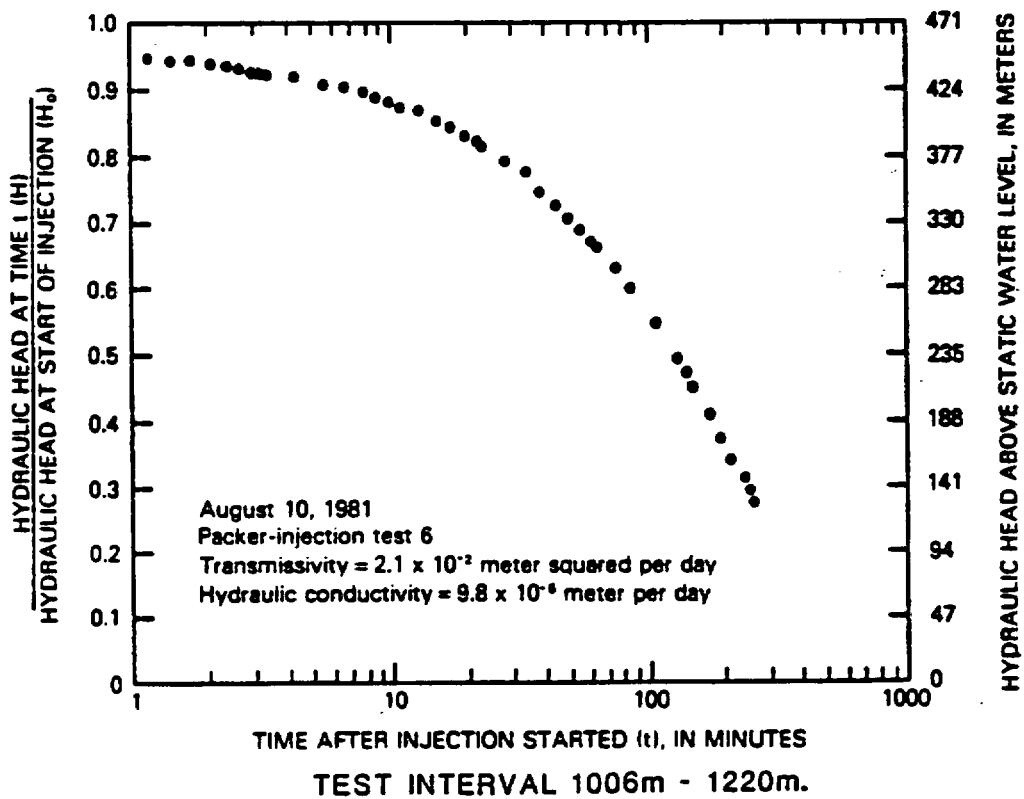
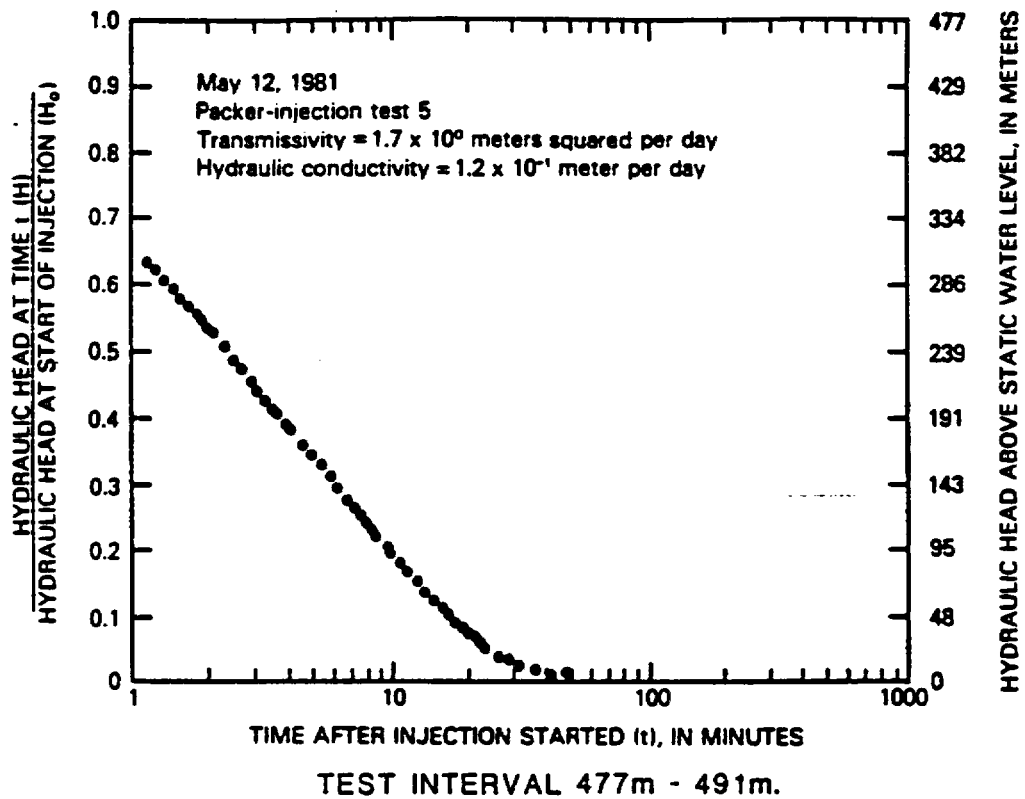
Results of the Cooper-Bredehoeft injection tests in well USW H-6. From Craig et al. (1983).



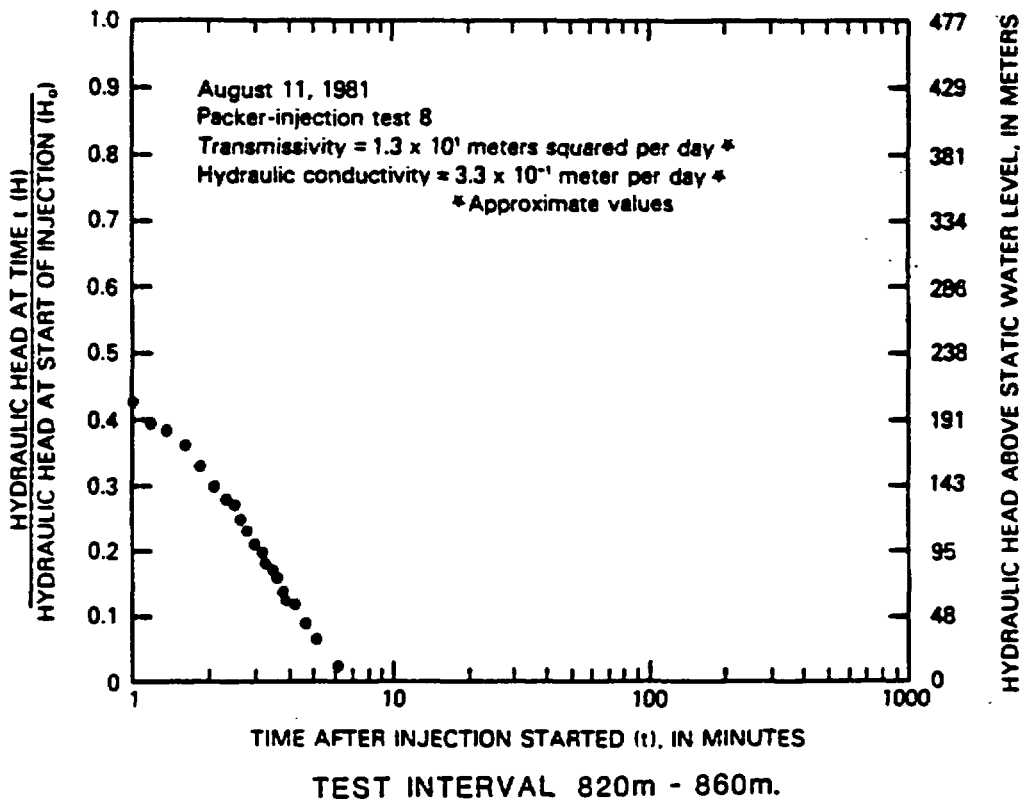
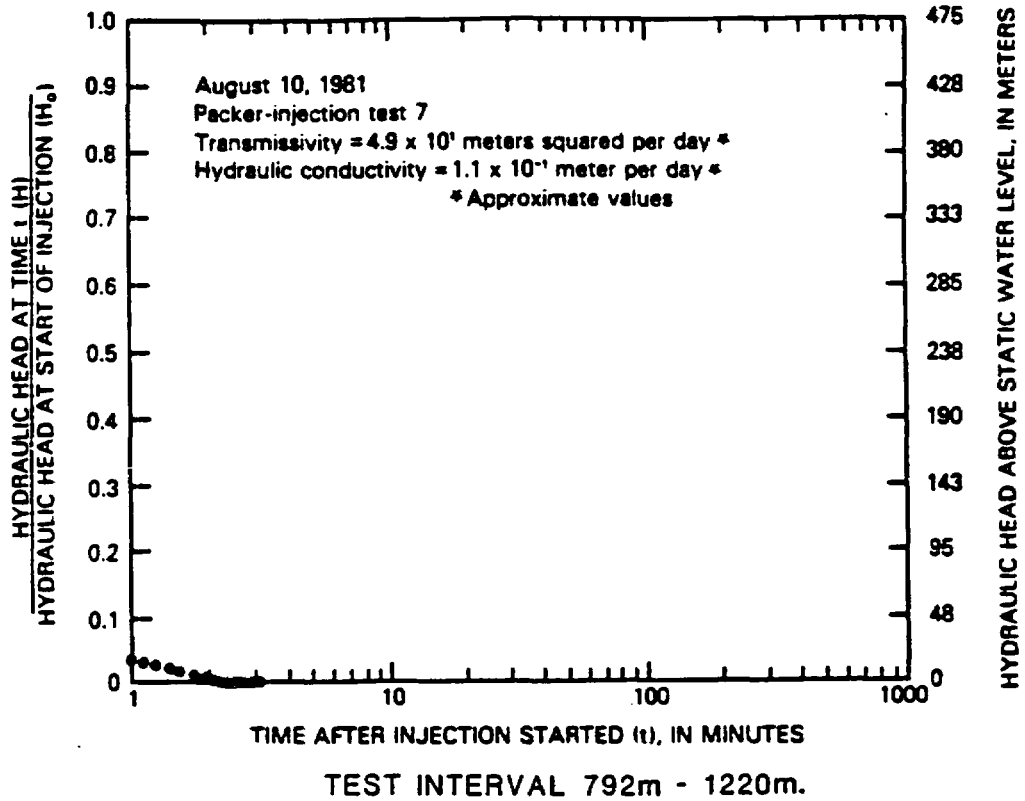
Results of the Cooper-Bredehoeft injection tests in well UE-25b#1. From Lahoud et al. (1984).



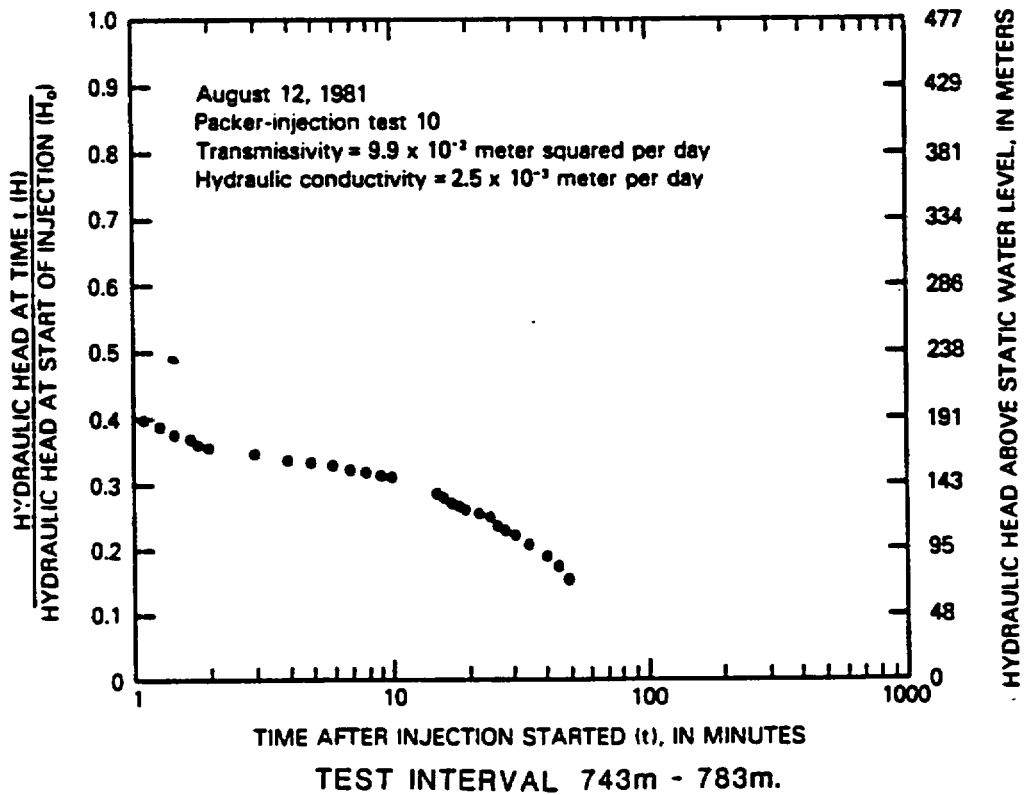
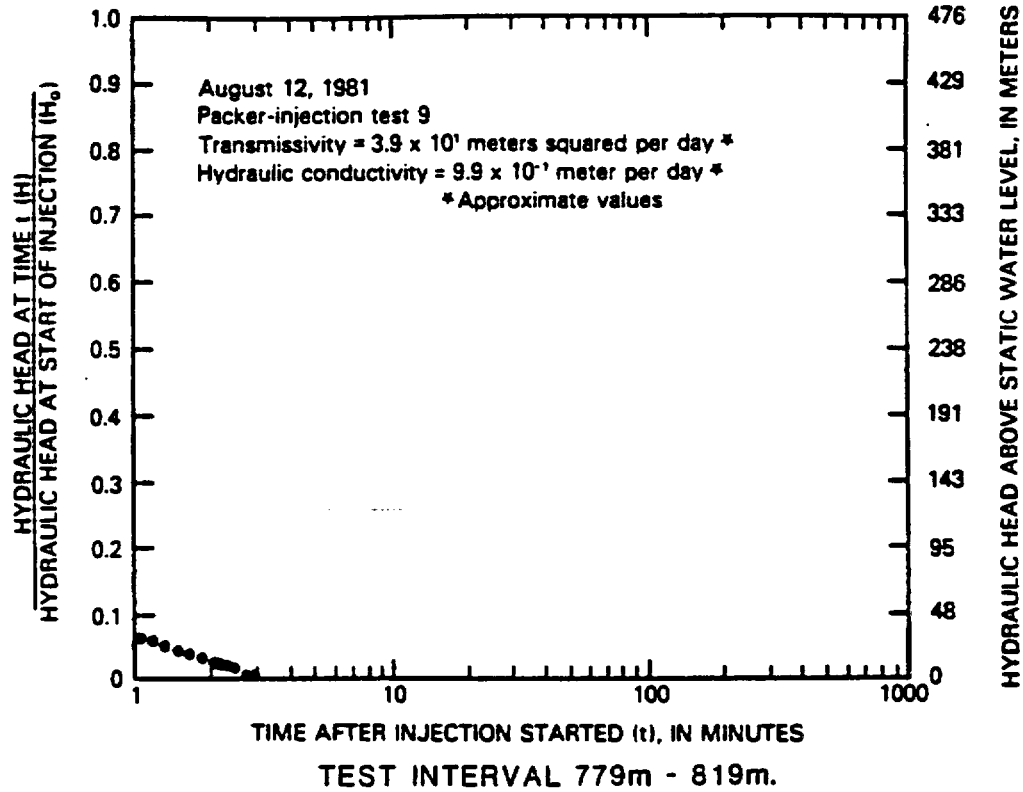
Results of the Cooper-Bredehoeft injection tests in well UE-25b#1. From Lahoud et al. (1984).



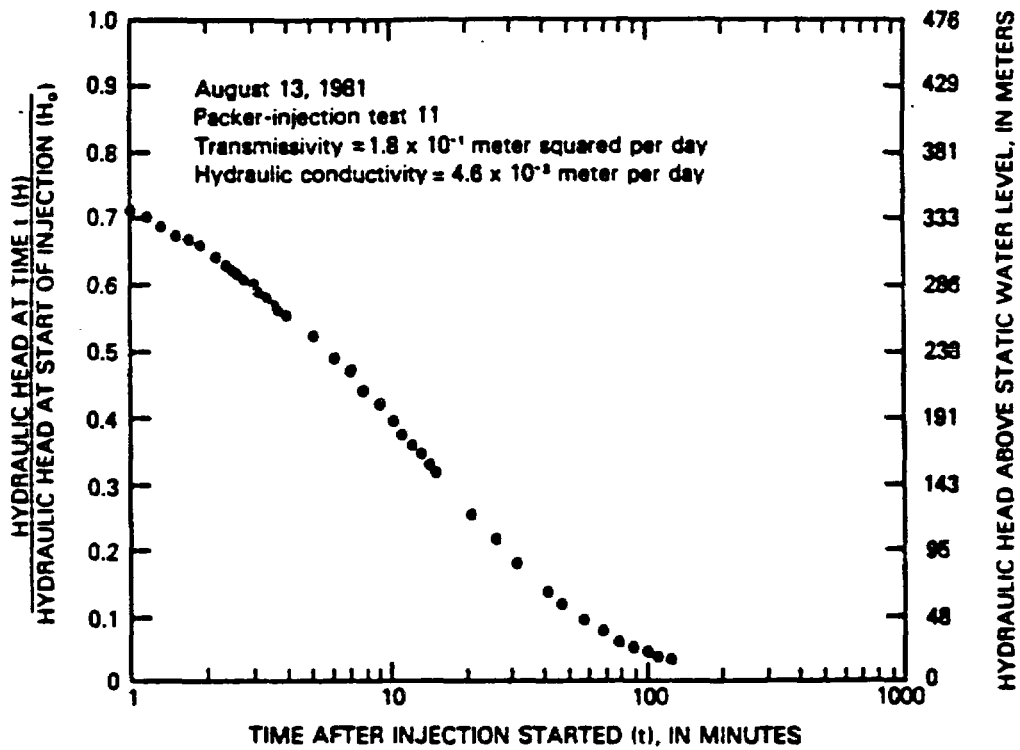
Results of the Cooper-Bredehoeft injection tests in well UE-25b#1. From Lahoud et al. (1984)



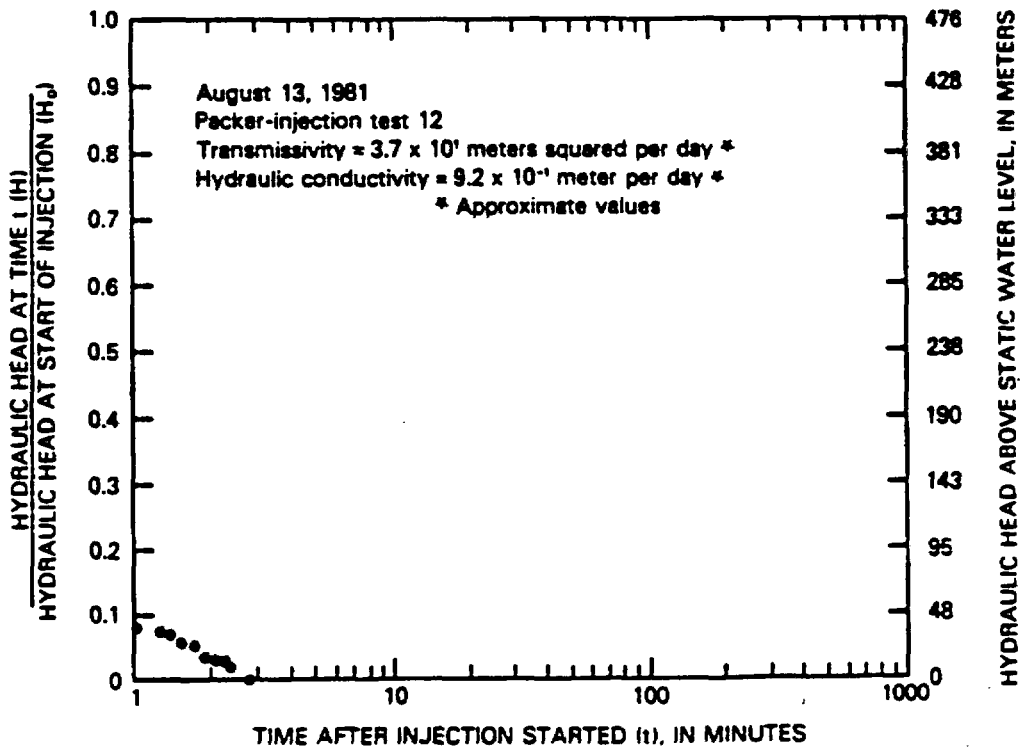
Results of the Cooper-Bredehoeft injection tests in well UE-25b=1. From Lahoud et al. (1984).



Results of the Cooper-Bredehoeft injection tests in well UE-25b#1. From Lahoud et al. (1984).



TEST INTERVAL 703m - 743m.

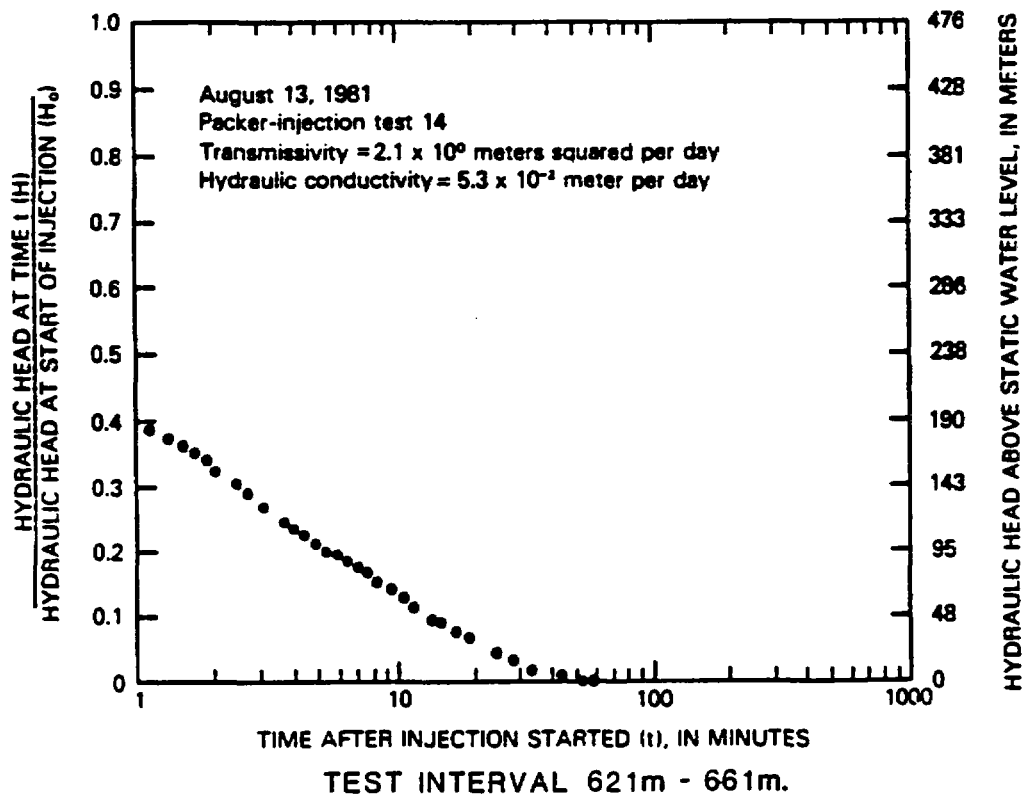
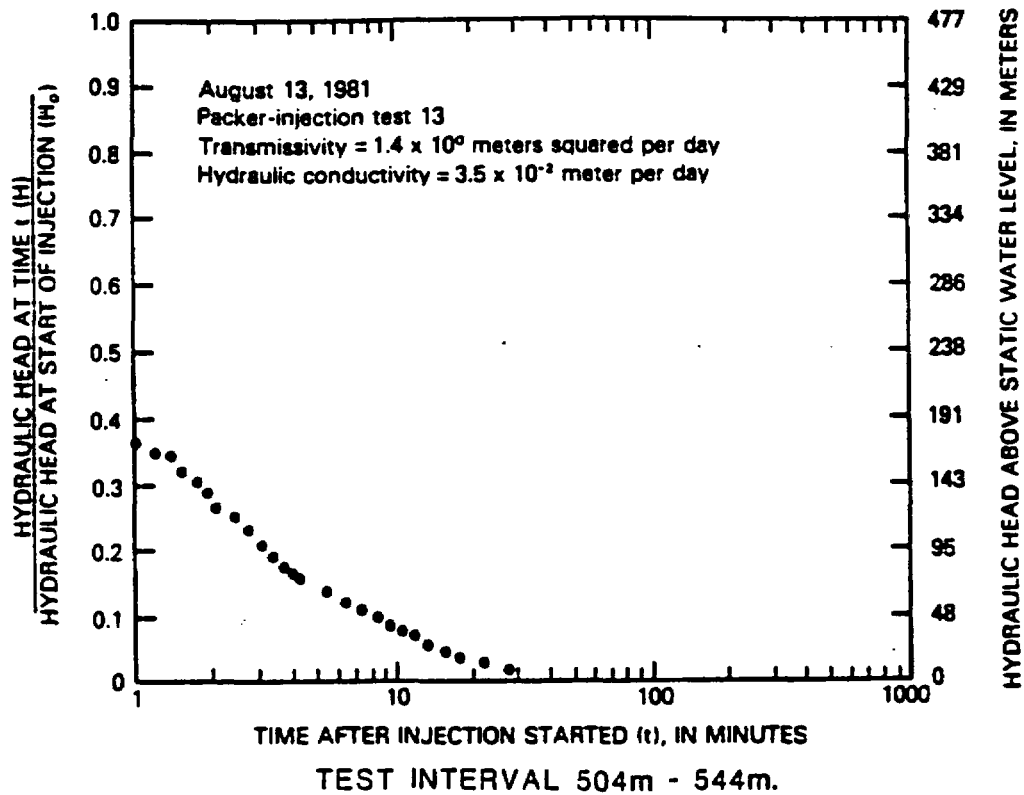


TEST INTERVAL 581m - 621m.

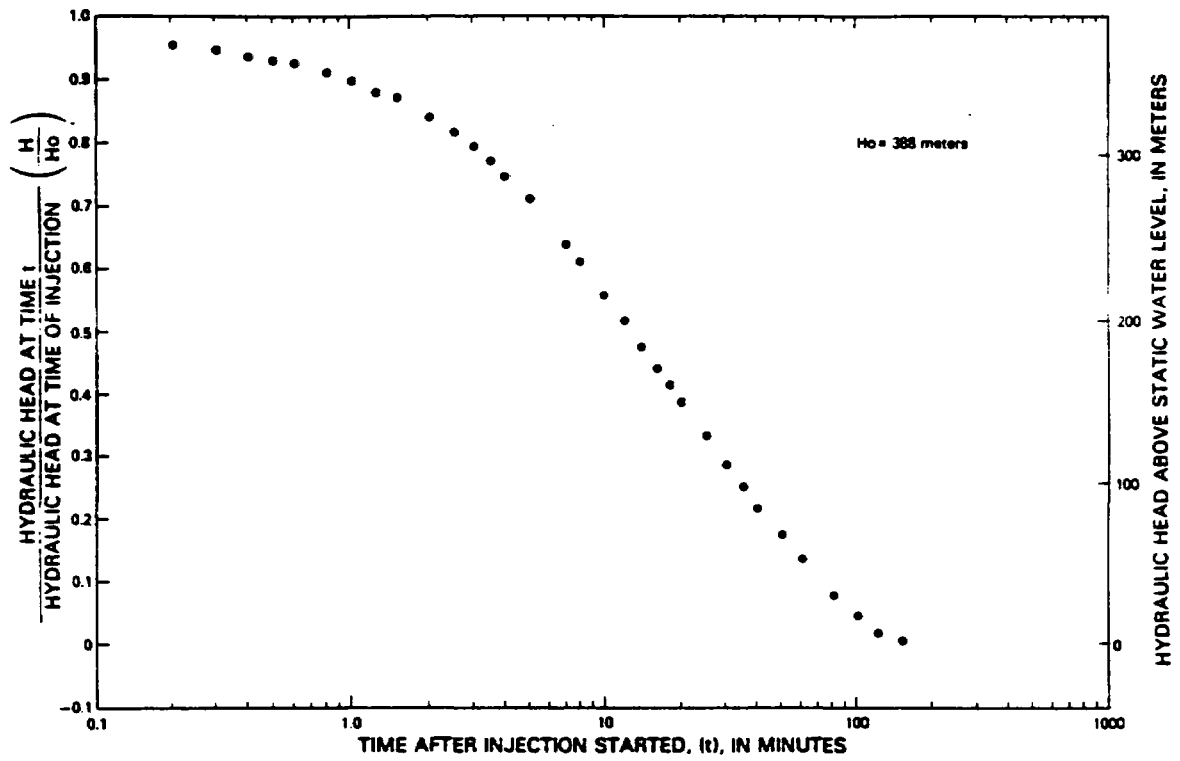
Results of the Cooper-Bredehoeft injection tests in well UE-25b#1. From Lahoud et al. (1984).

BOREHOLE	DEPTH (m)	TEMPERATURE (°C)
UE-25 a#1	34	26
	283	38
	611	46.5
USW G-3	63	22
	131	24
	147	24.5
	318	28.5
	331	31
USW G-2	280	29
	318	29
	346-359	37-34

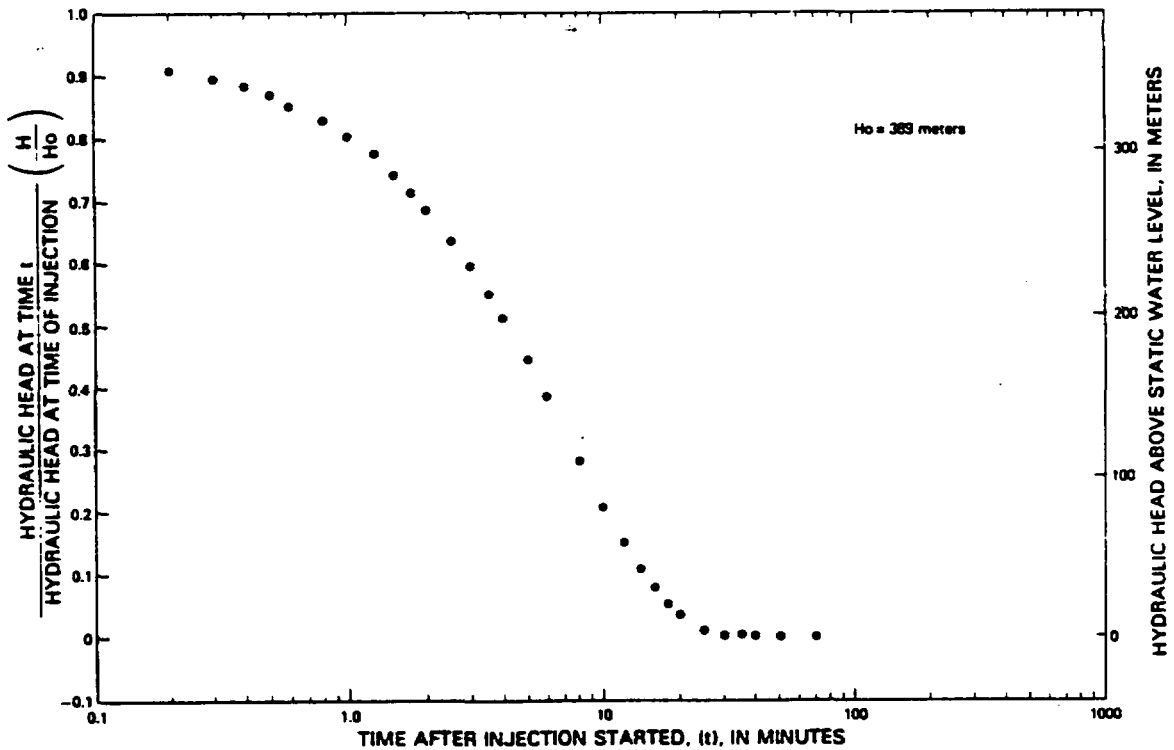
Estimate of paleo-temperatures based on stable isotope content of calcites from Yucca Mountain. Modified from Szabo and Kyser (1981).



Results of the Cooper-Bredehoeft injection tests in well UE-25b#1. From Lahoud et al. (1984)

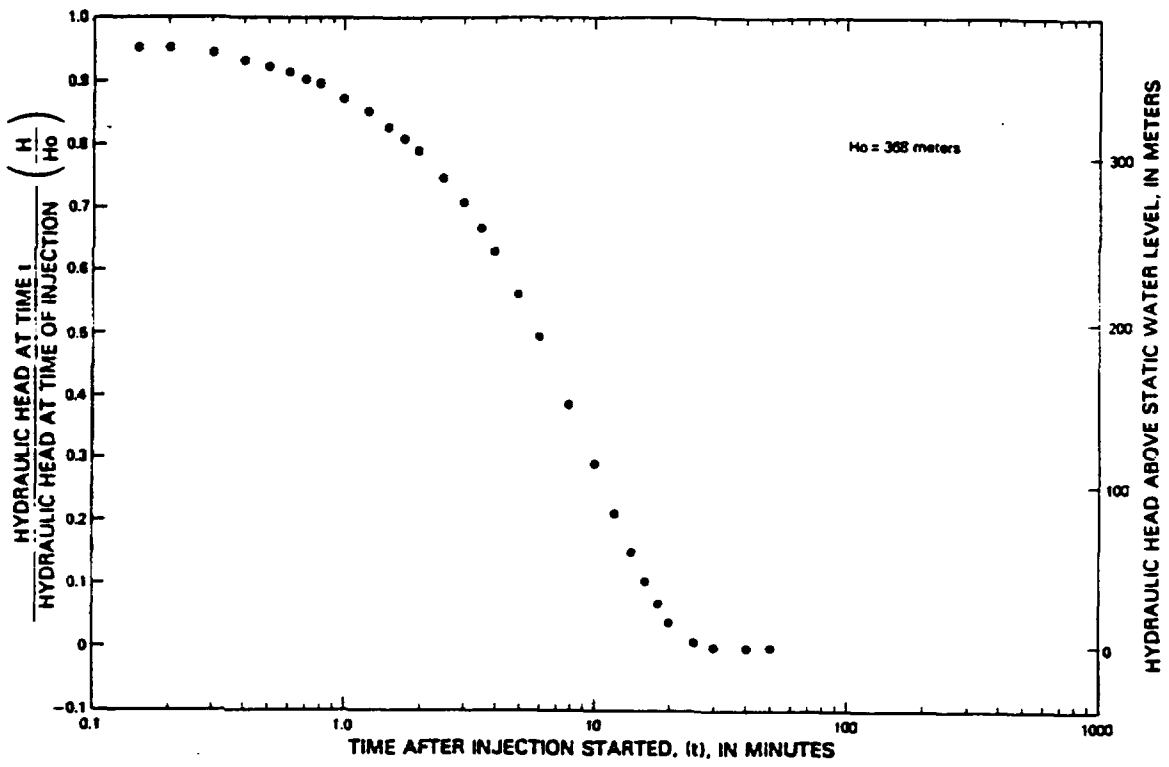


Packer-injection test 2, depth interval from 500 to 550 meters.

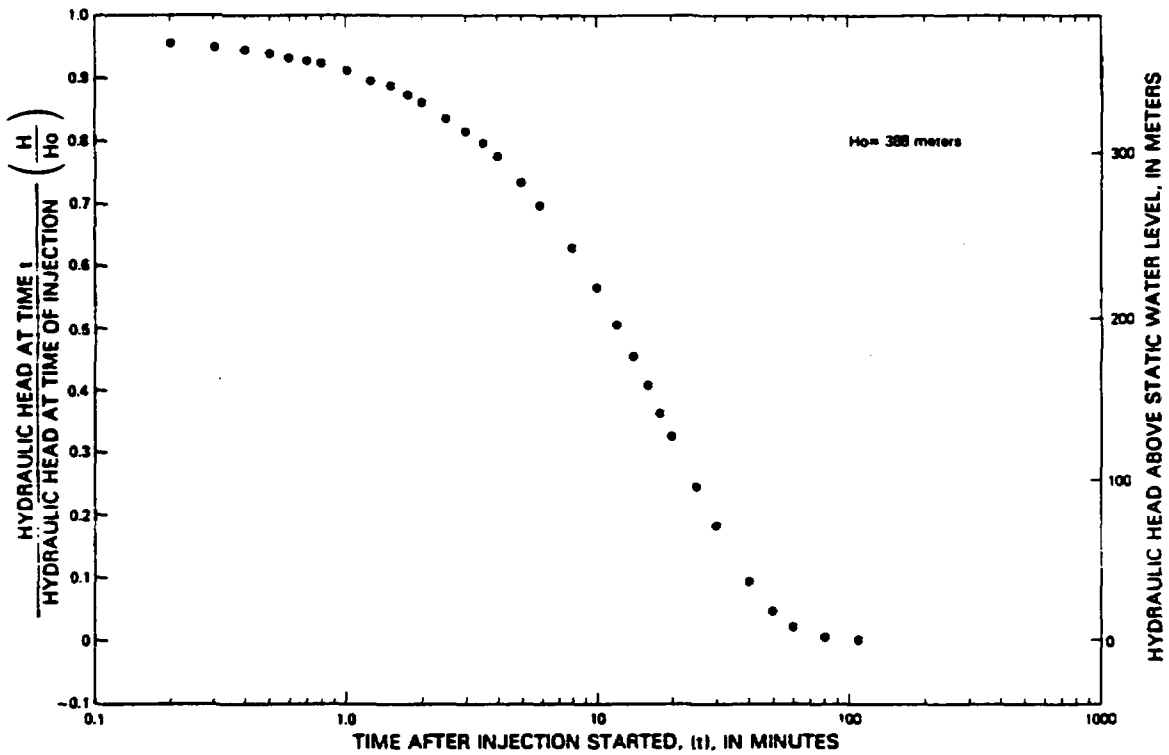


Packer-injection test 3, depth interval from 550 to 600 meters.

Results of the Cooper-Bredehoeft injection tests in well UE-25p#1. From Craig and Johnson (1984).

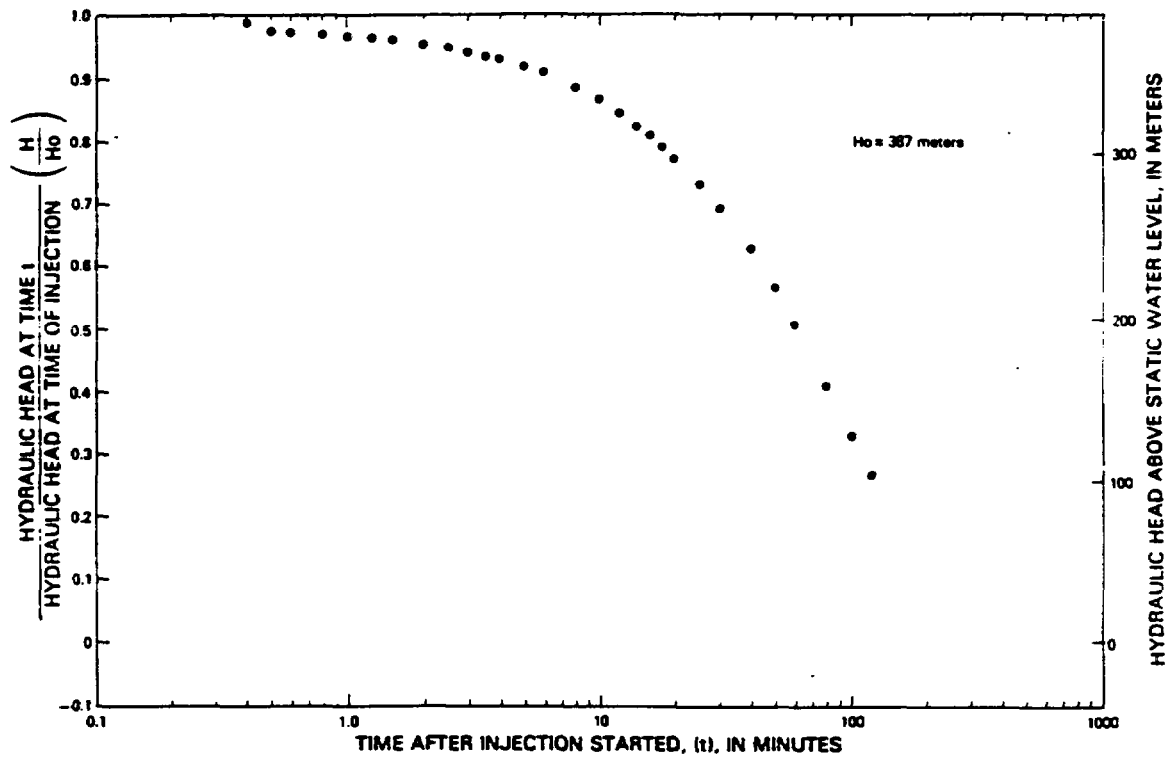


Packer-injection test 4, depth interval from 600 to 650 meters.

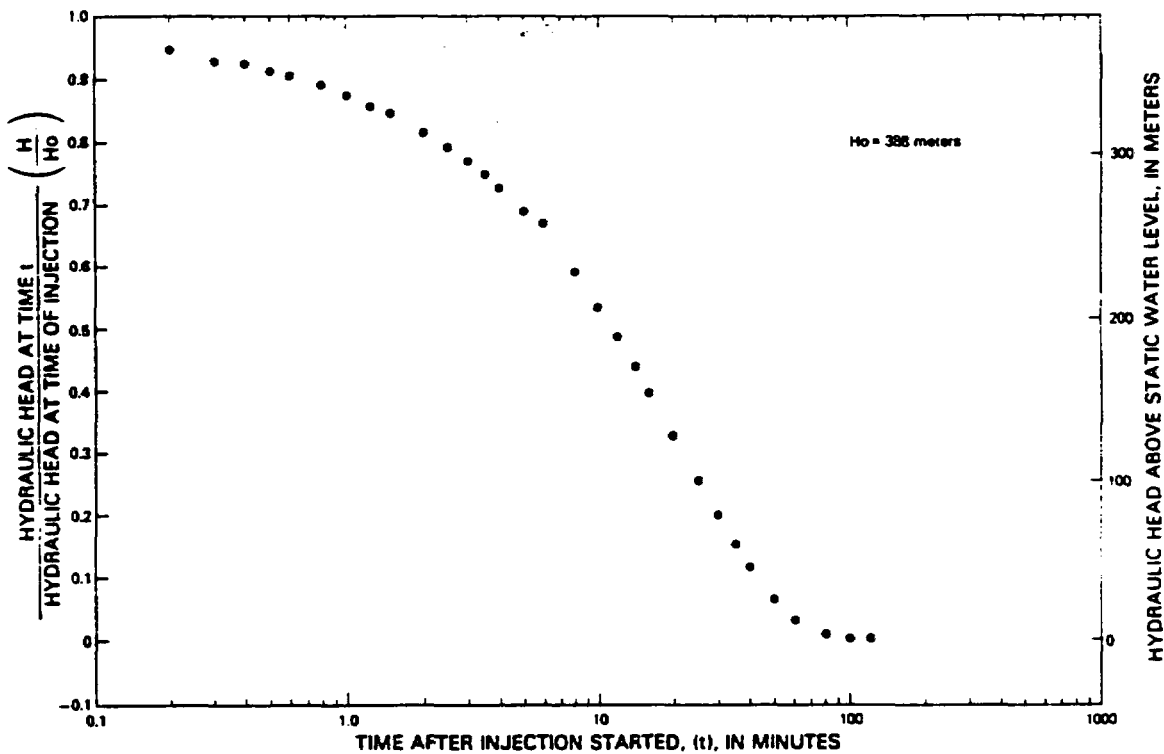


Packer-injection test 5, depth interval from 640 to 690 meters.

Results of the Cooper-Bredehoeft injection tests in well UE-25p#1. From Craig and Johnson (1984).

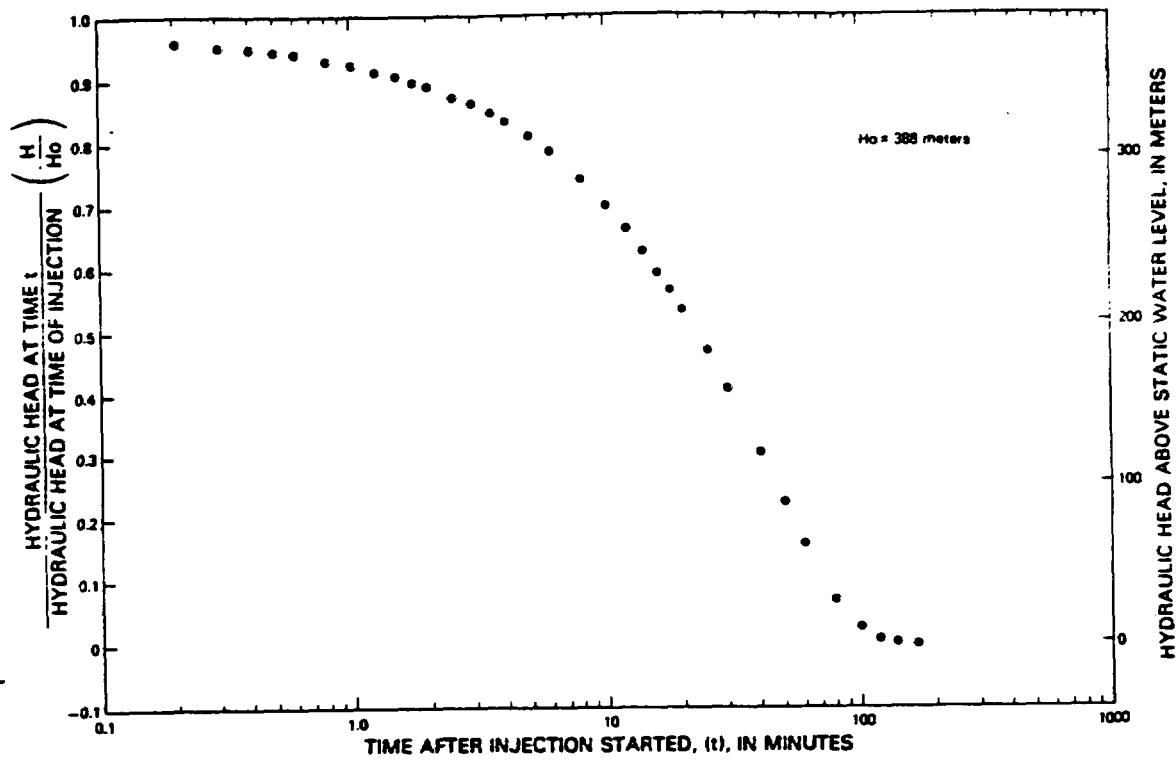


Packer-injection test 6, depth interval from 690 to 740 meters.

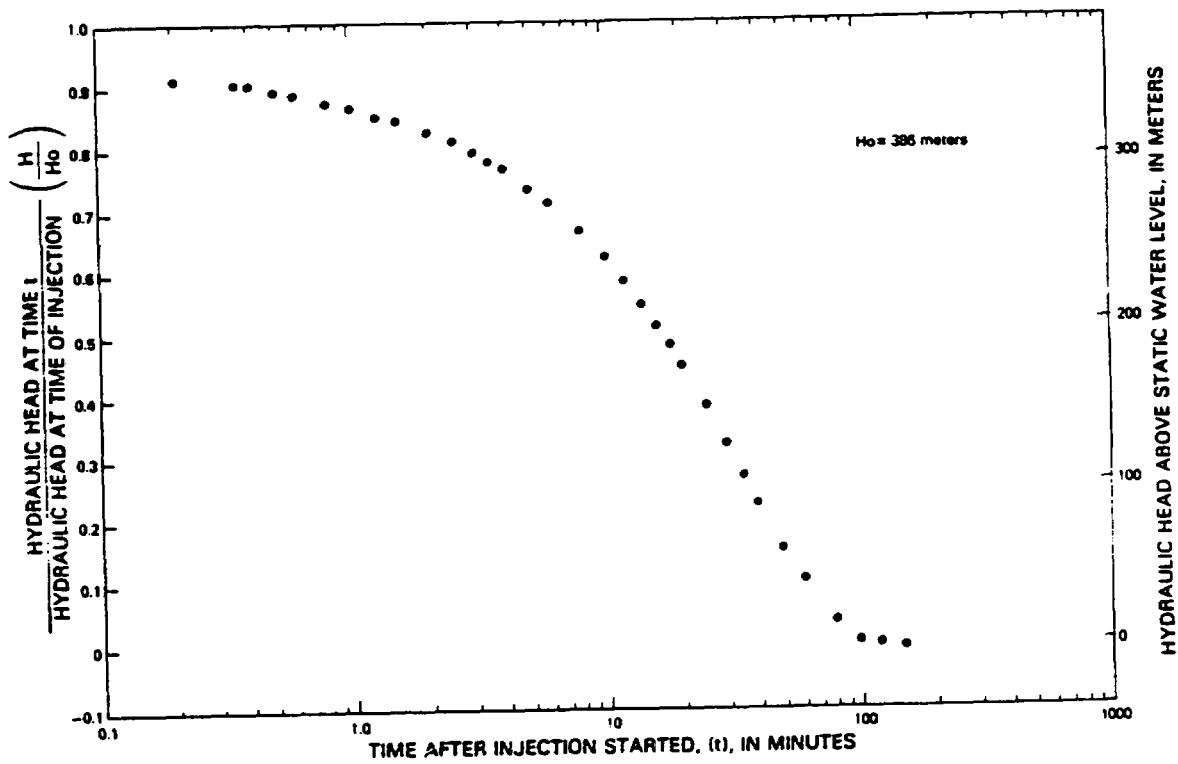


Packer-injection test 7, depth interval from 739 to 789 meters.

Results of the Cooper-Bredehoeft injection tests in well UE-25p#1. From Craig and Johnson (1984).

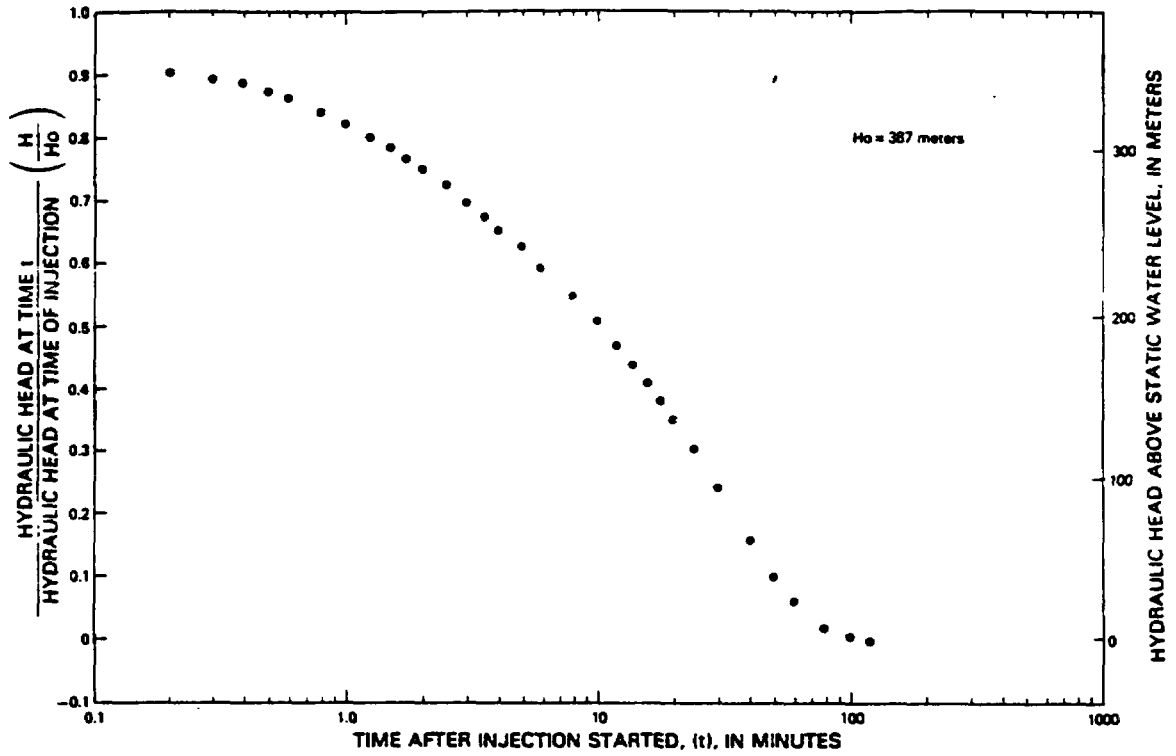


Packer-injection test 8, depth interval from 764 to 834 meters.

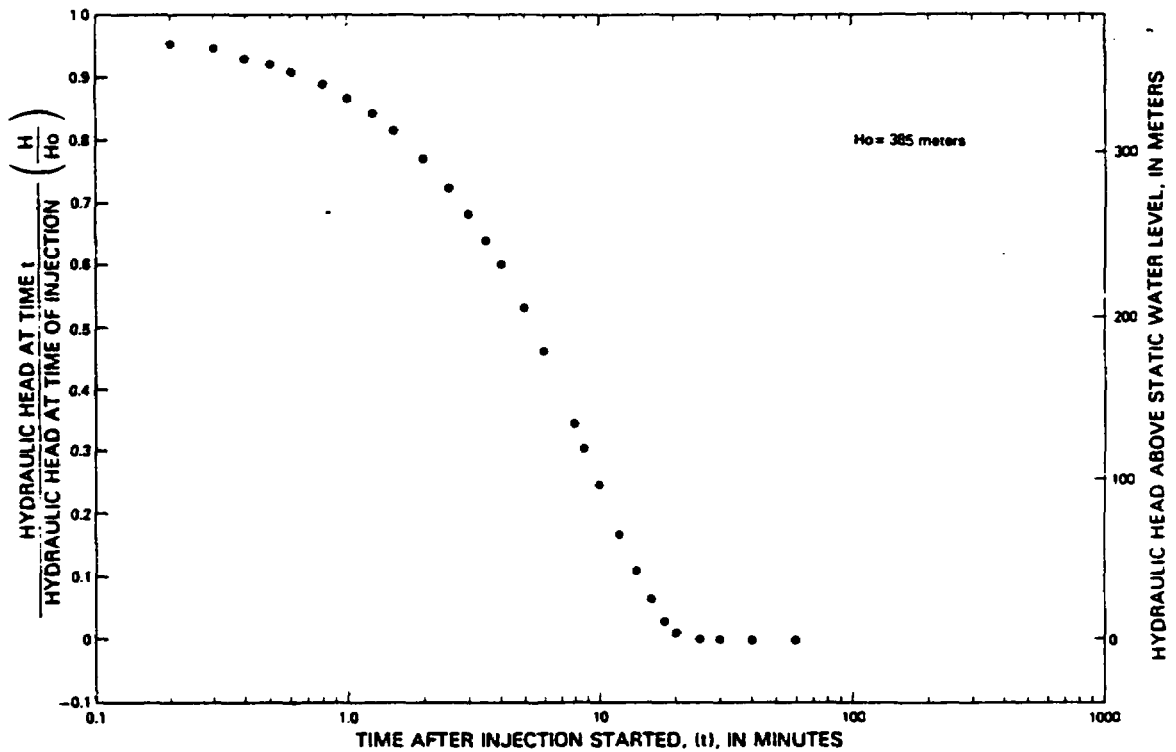


Packer-injection test 9, depth interval from 834 to 904 meters.

Results of the Cooper-Bredehoeft injection tests in well UE-25p#1. From Craig and Johnson (1984).

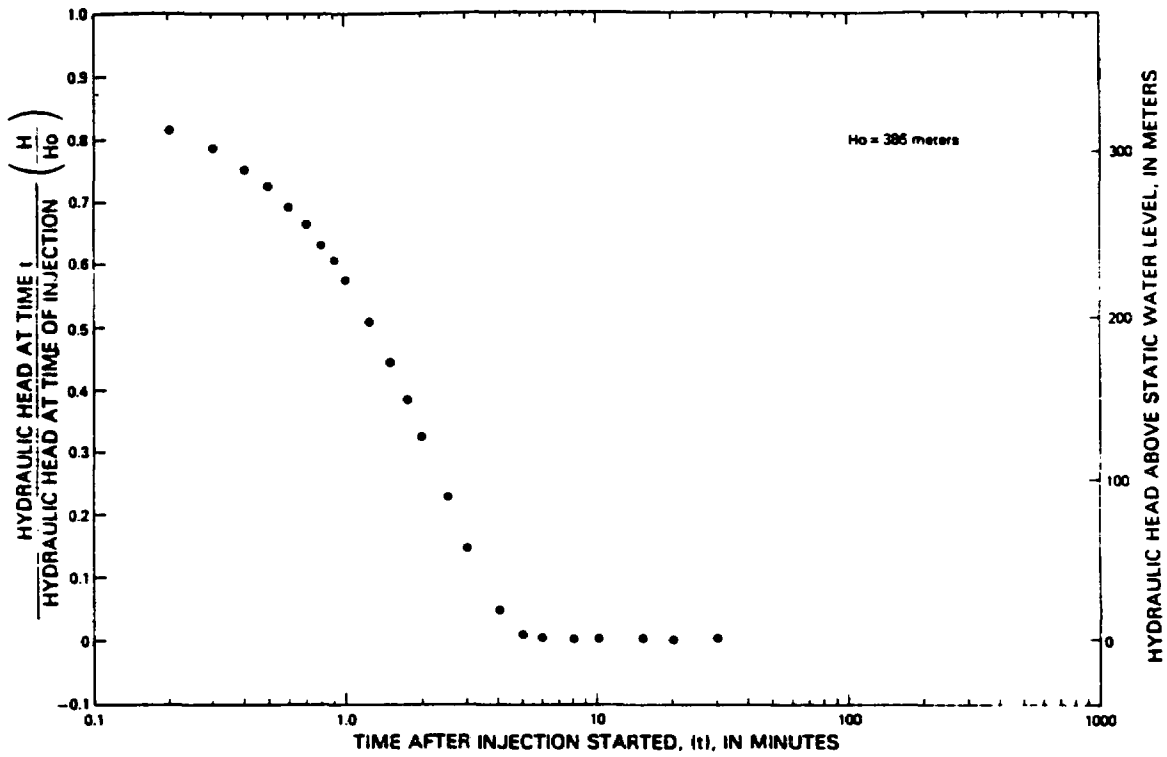


Packer-injection test 10, depth interval from 904 to 974 meters.

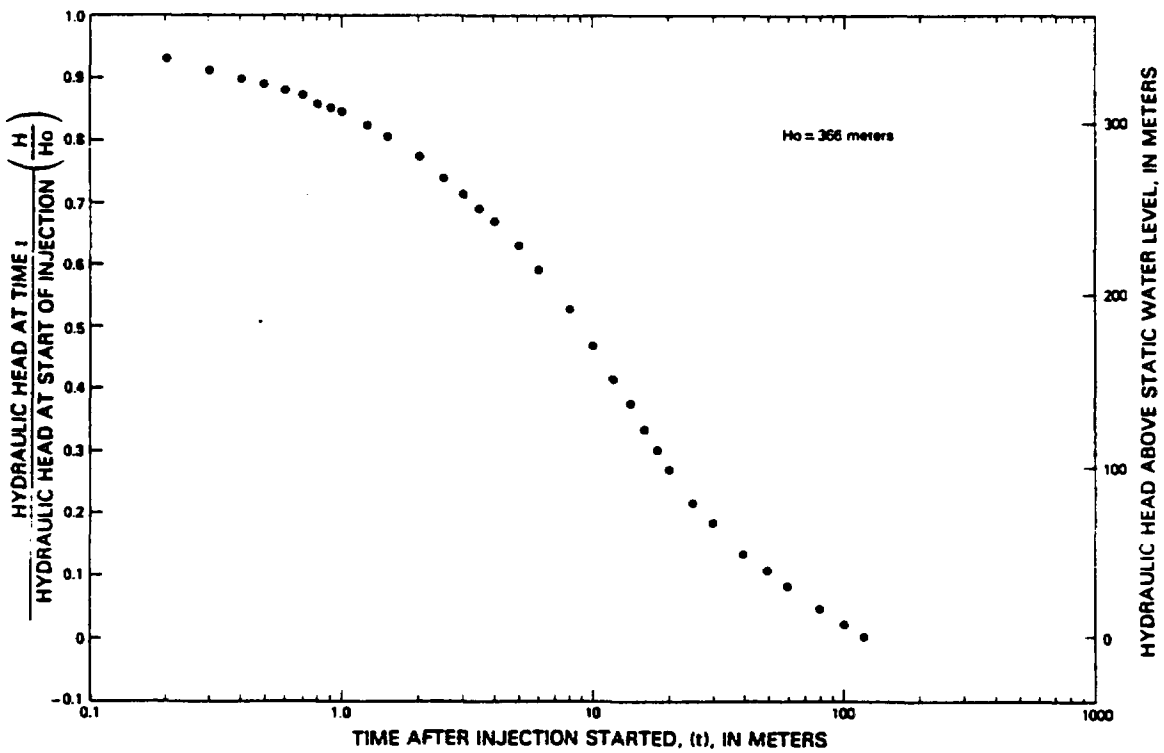


Packer-injection test 11, depth interval from 974 to 1,044 meters.

Results of the Cooper-Bredehoeft injection tests in well UE-25p=1. From Craig and Johnson (1984).

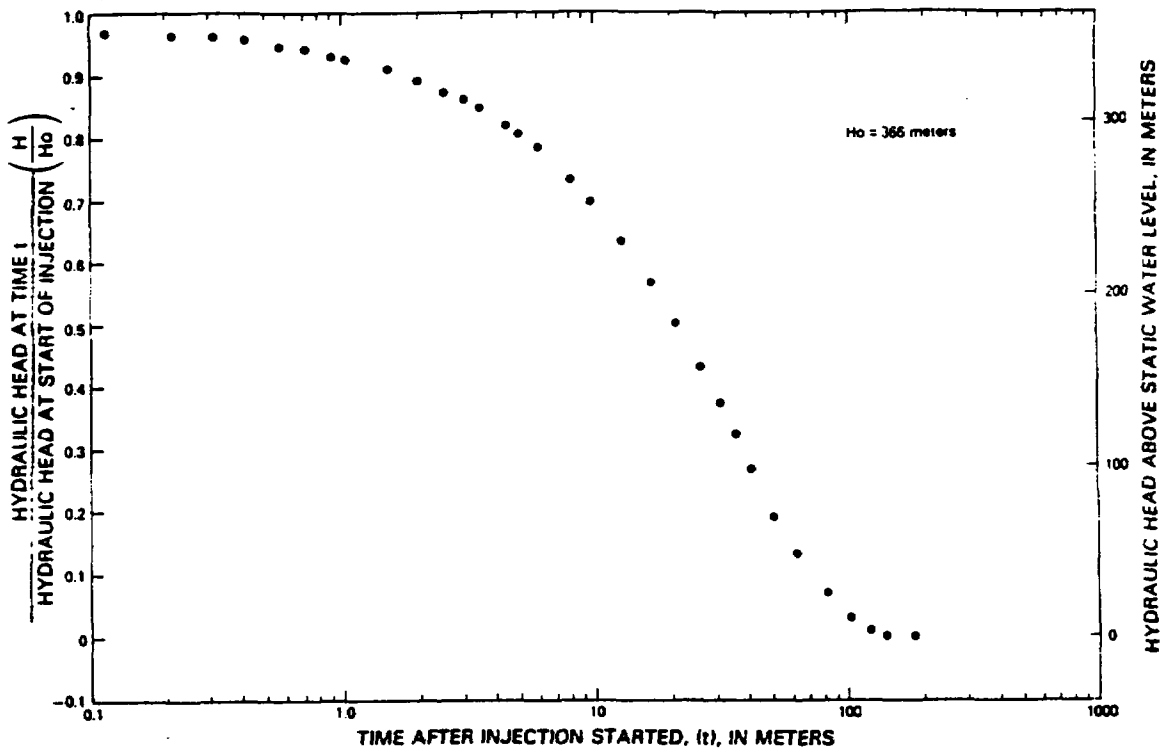


Packer-injection test 12, depth interval from 1,044 to 1,114 meters.

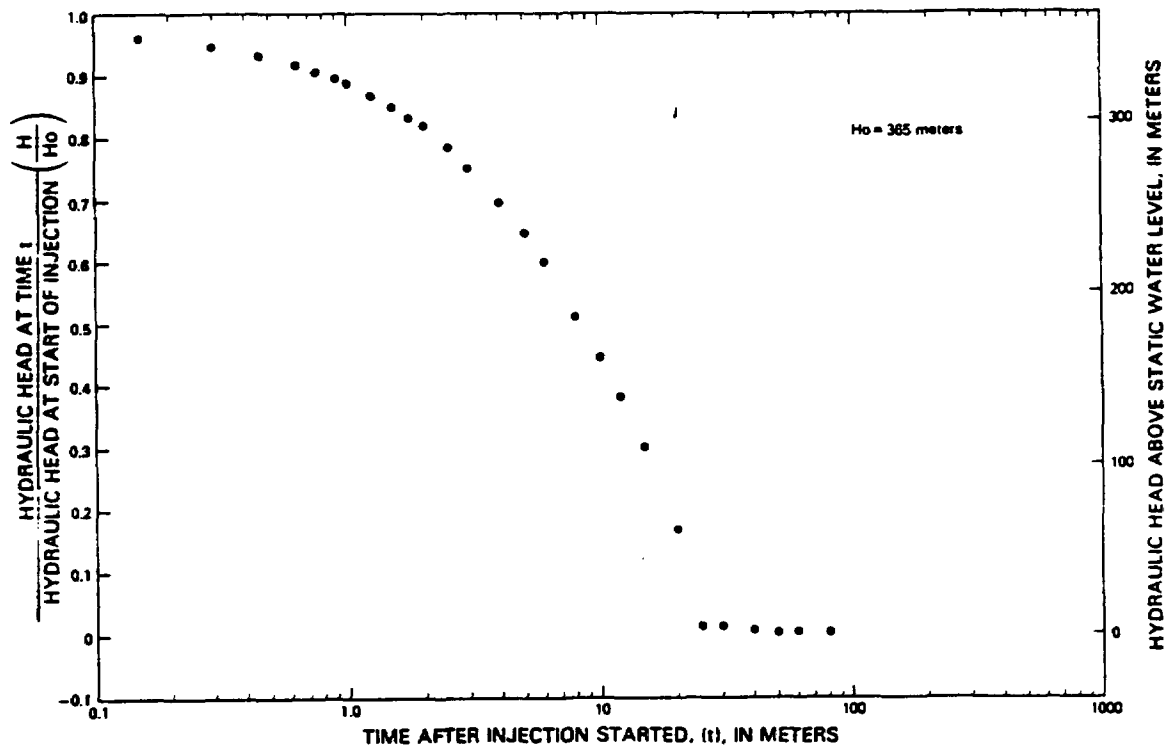


Packer-injection test 13, depth interval from 1,110 to 1,180 meters.

Results of the Cooper-Bredehoeft injection tests in well UE-25p=1. From Craig and Johnson (1984)

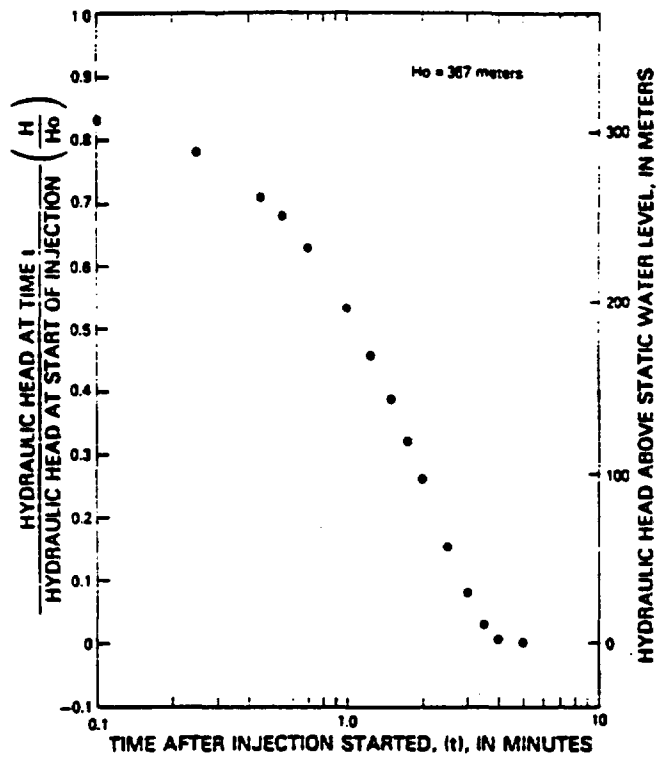


Packer-injection test 15, depth interval from 1,297 to 1,308 meters.

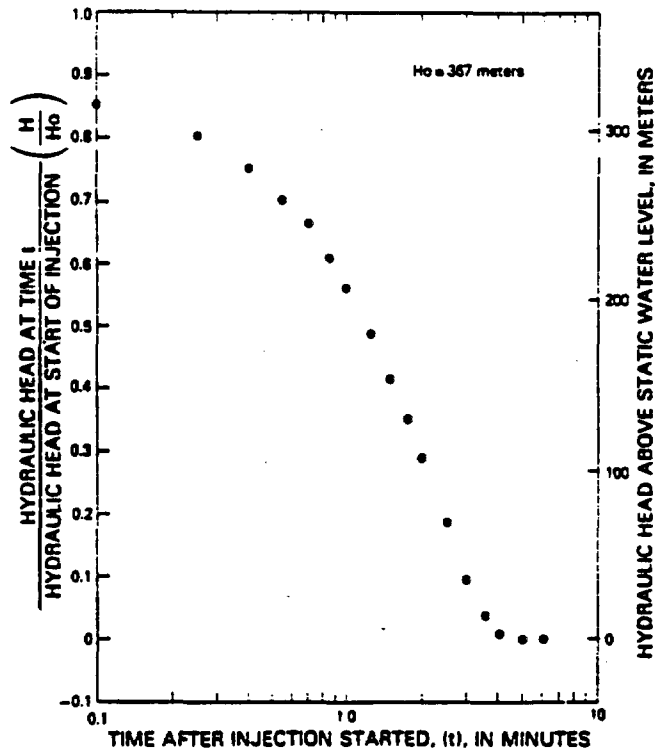


Packer-injection test 16, depth interval from 1,297 to 1,337 meters.

Results of the Cooper-Bredhoeft injection tests in well UE-25p=1. From Craig and Johnson (1984)

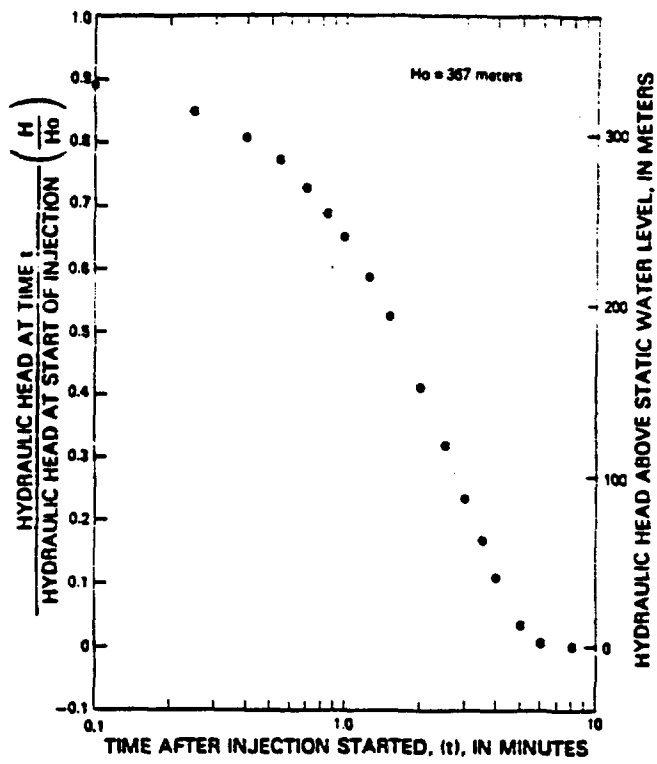


Packer-injection test 17, depth interval from 1,341 to 1,381 meters.

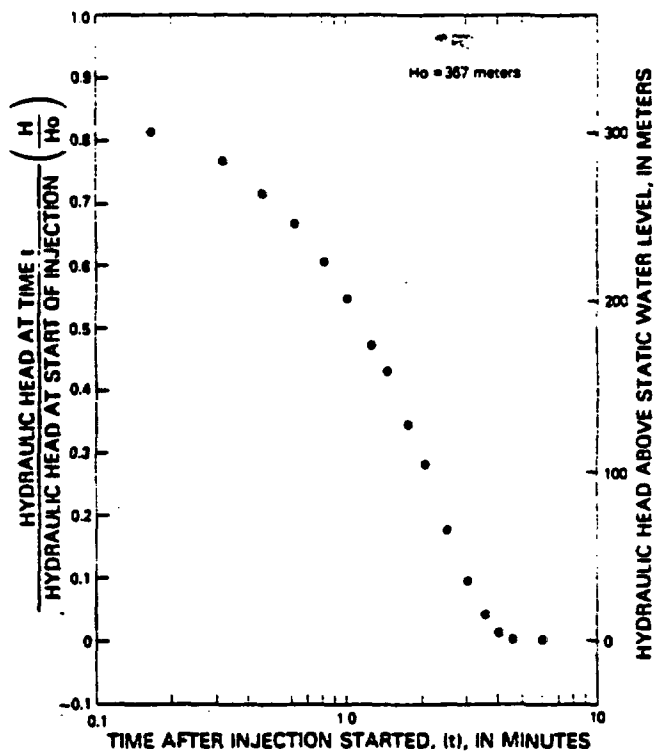


Packer-injection test 18, depth interval from 1,381 to 1,421 meters

Results of the Cooper-Bredehoeft injection tests in well UE-25p#1. From Craig and Johnson (1984).

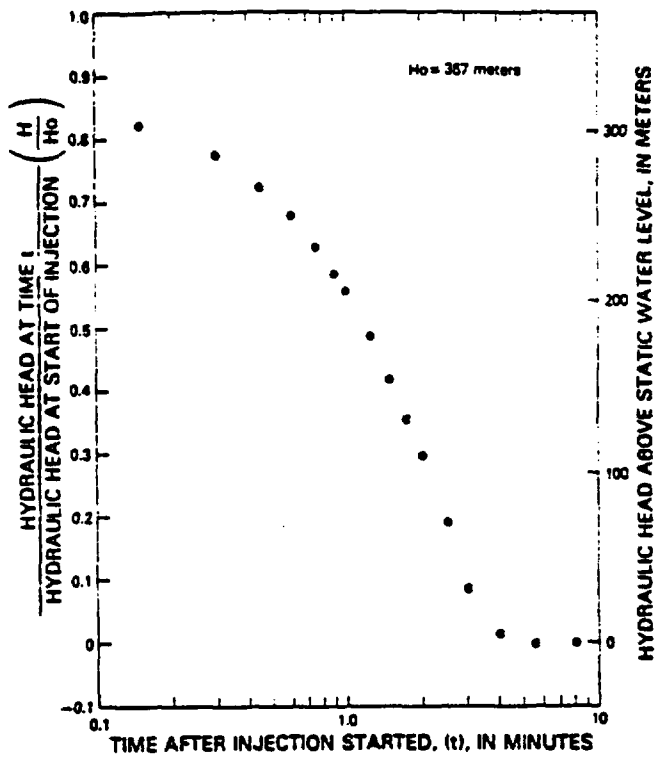


Packer-injection test 19, depth interval from 1,423 to 1,463 meters.

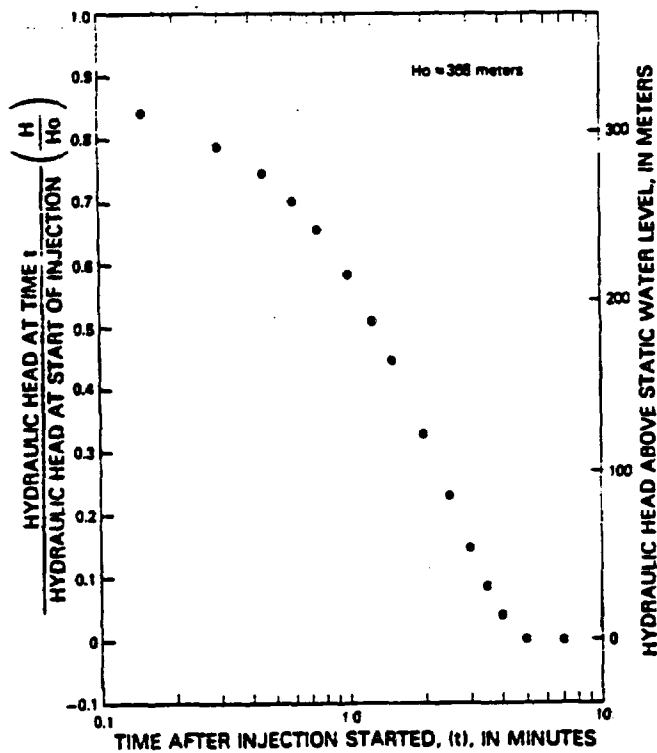


Packer-injection test 20, depth interval from 1,463 to 1,509 meters.

Results of the Cooper-Bredehoeft injection tests in well UE-25p±1. From Craig and Johnson (1984).

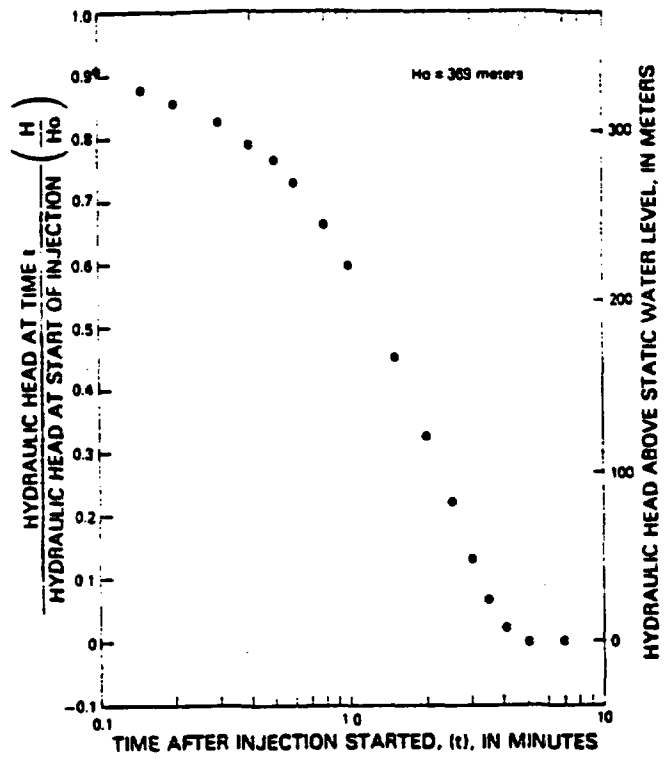


Packer-injection test 21, depth interval from 1,509 to 1,555 meters.

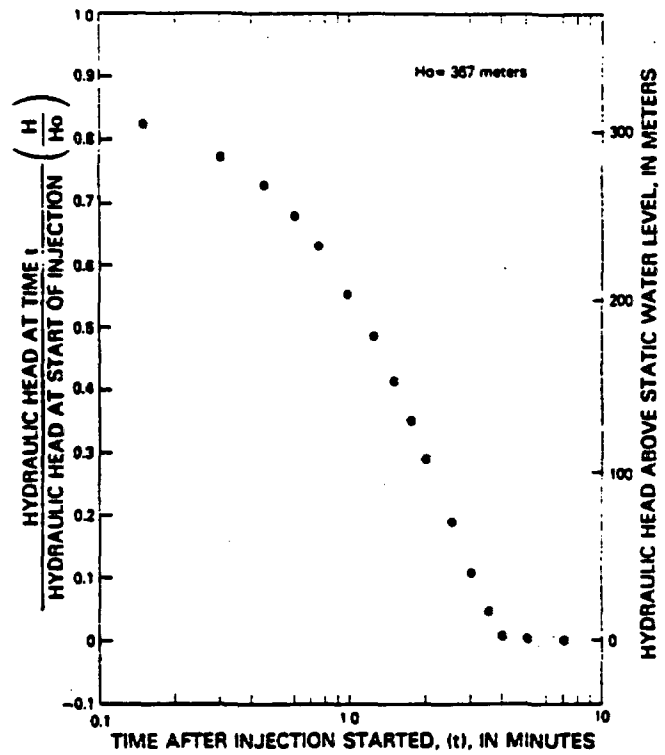


Packer-injection test 22, depth interval from 1,558 to 1,805 meters.

Results of the Cooper-Bredehoeft injection tests in well UE-25p#1. From Craig and Johnson (1984).

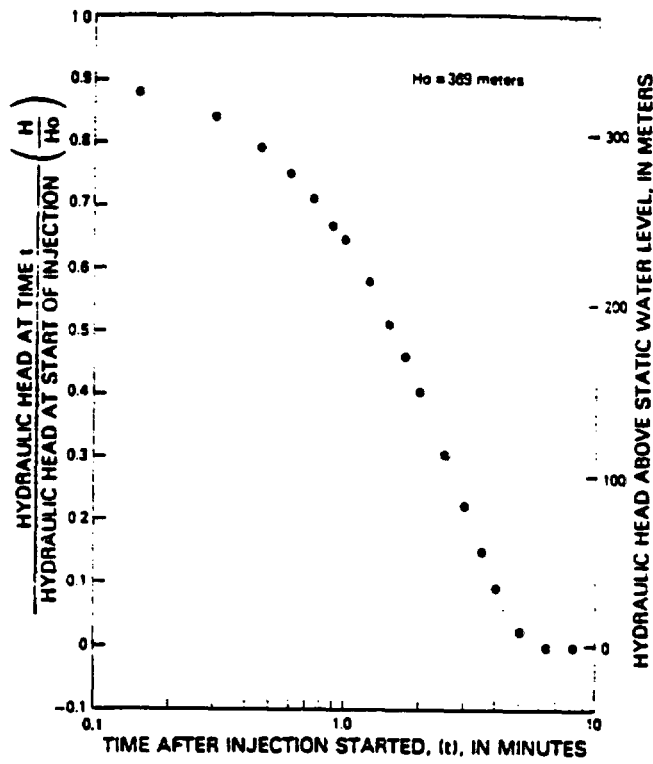


Packer-injection test 24, depth interval from 1,597 to 1,643 meters.

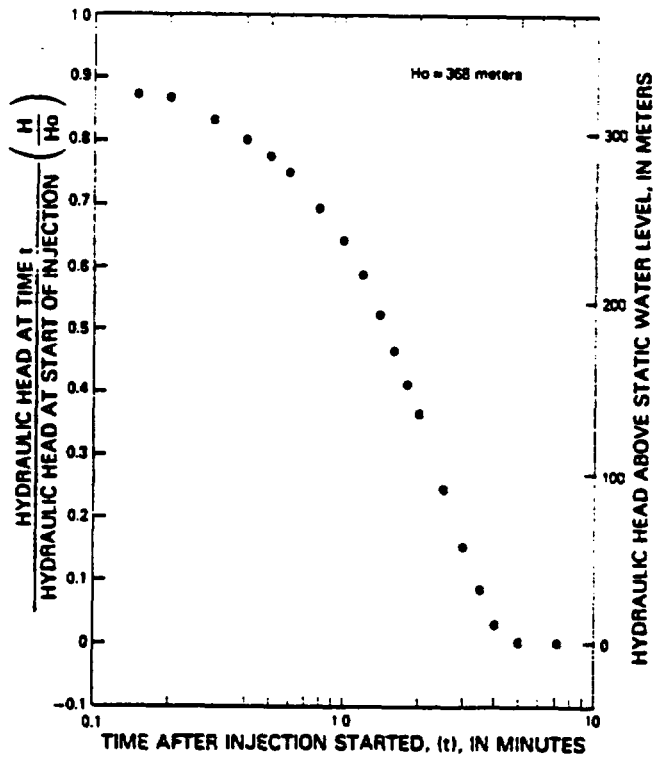


Packer-injection test 23, depth interval from 1,554 to 1,600 meters.

Results of the Cooper-Bredehoeft injection tests in well UE-25p#1. From Craig and Johnson (1984)

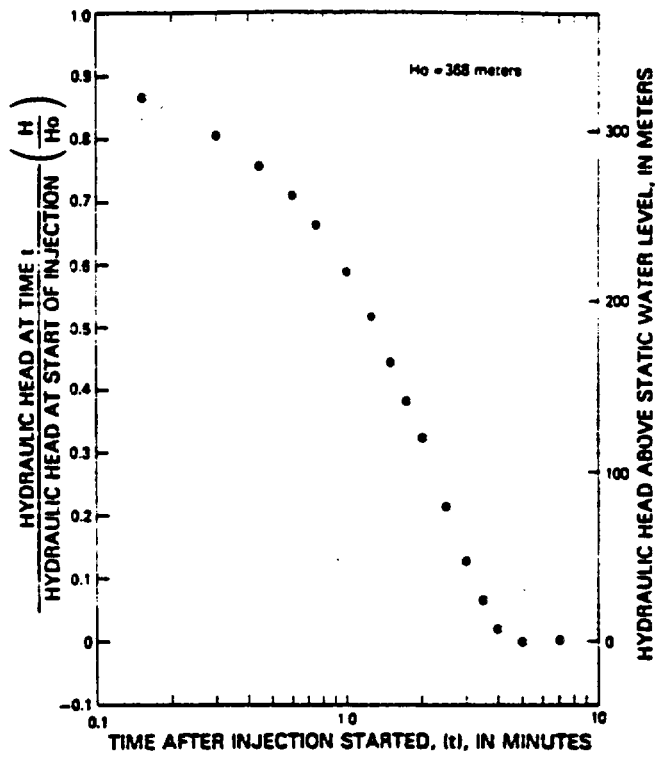


Packer-injection test 25, depth interval from 1,646 to 1,805 meters.

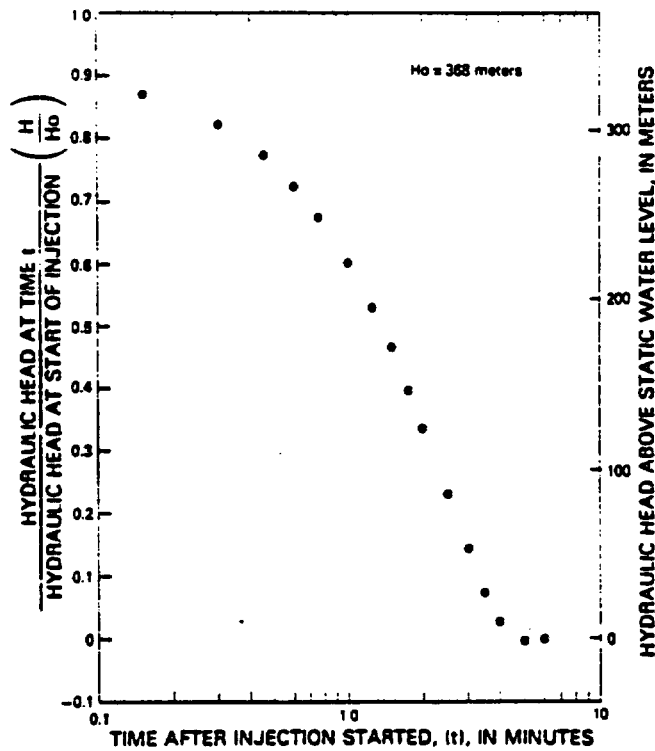


Packer-injection test 26, depth interval from 1,643 to 1,689 meters.

Results of the Cooper-Bredehoeft injection tests in well UE-25p#1. From Craig and Johnson (1984).

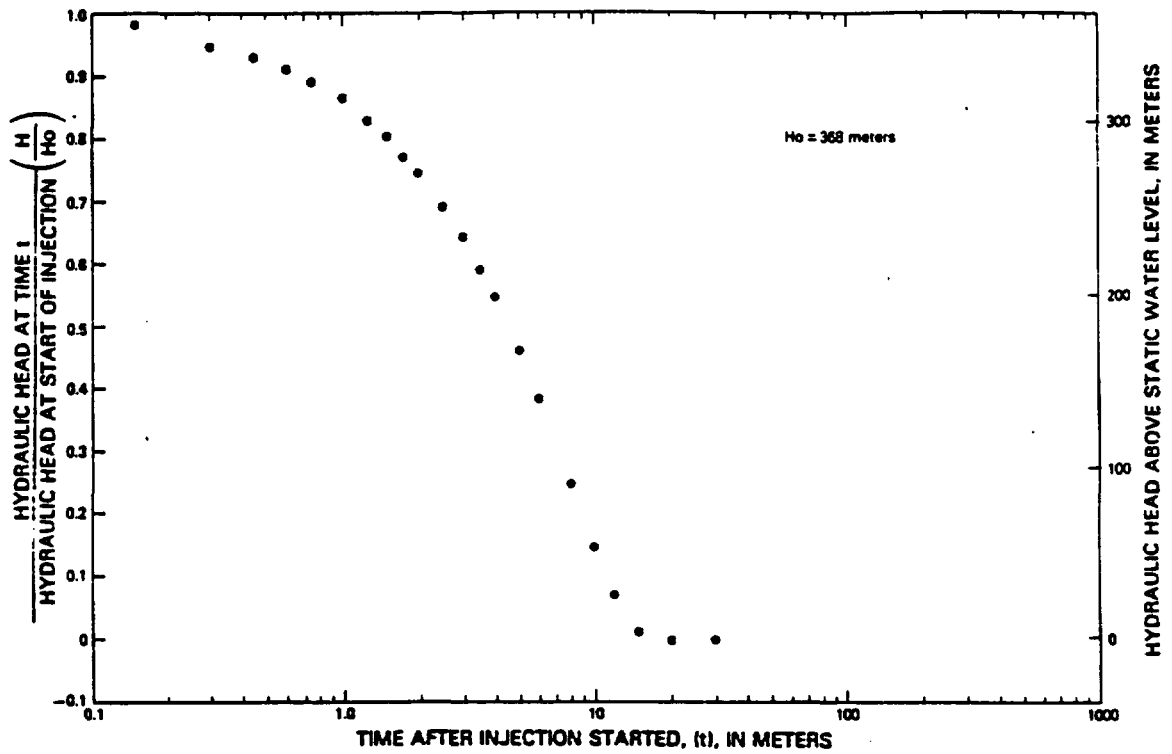


Packer-injection test 27, depth interval from 1,689 to 1,735 meters



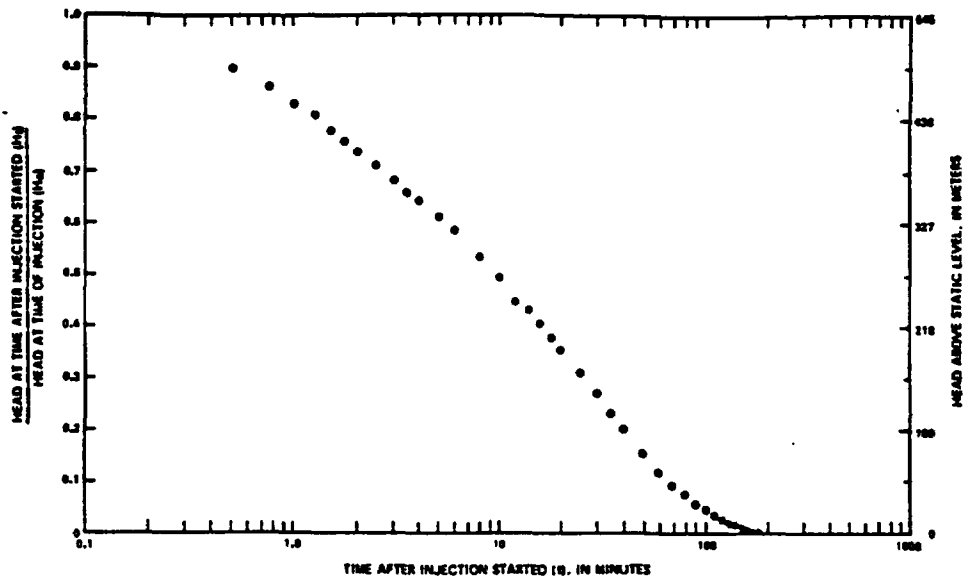
Packer-injection test 28, depth interval from 1,735 to 1,781 meters.

Results of the Cooper-Bredehoeft injection tests in well UE-25p#1. From Craig and Johnson (1984).

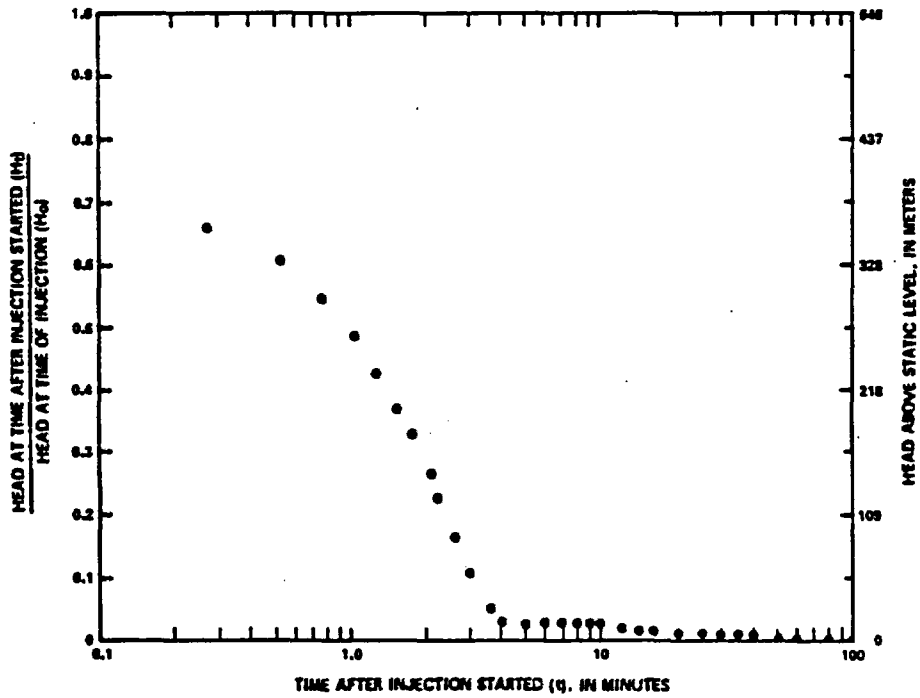


Packer-injection test 29, depth interval from 1,783 to 1,805 meters.

Results of the Cooper-Bredehoeft injection tests in well UE-25p#1. From Craig and Johnson (1984).

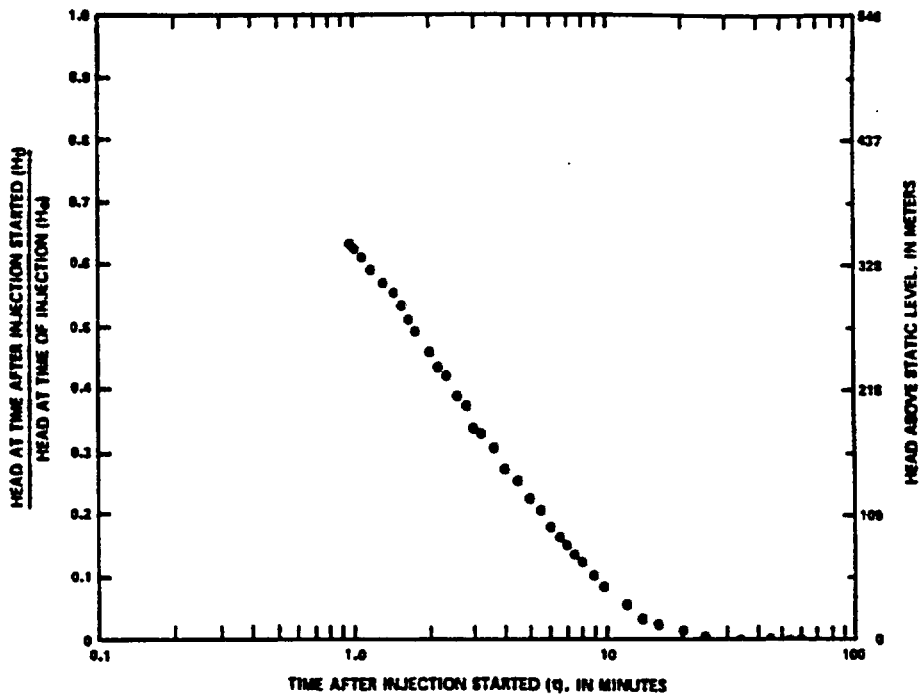


Packer-injection test for depth interval from 698 to 722 meters.

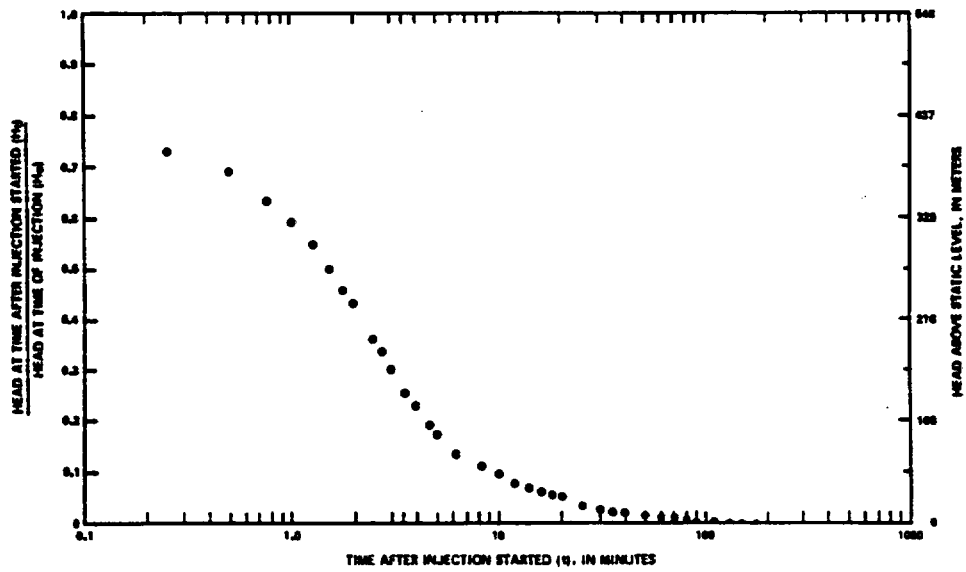


Packer-injection test for depth interval from 702 to 747 meters.

Results of the Cooper-Bredehoeft injection tests in well USW G-4. From Bentley (1984).

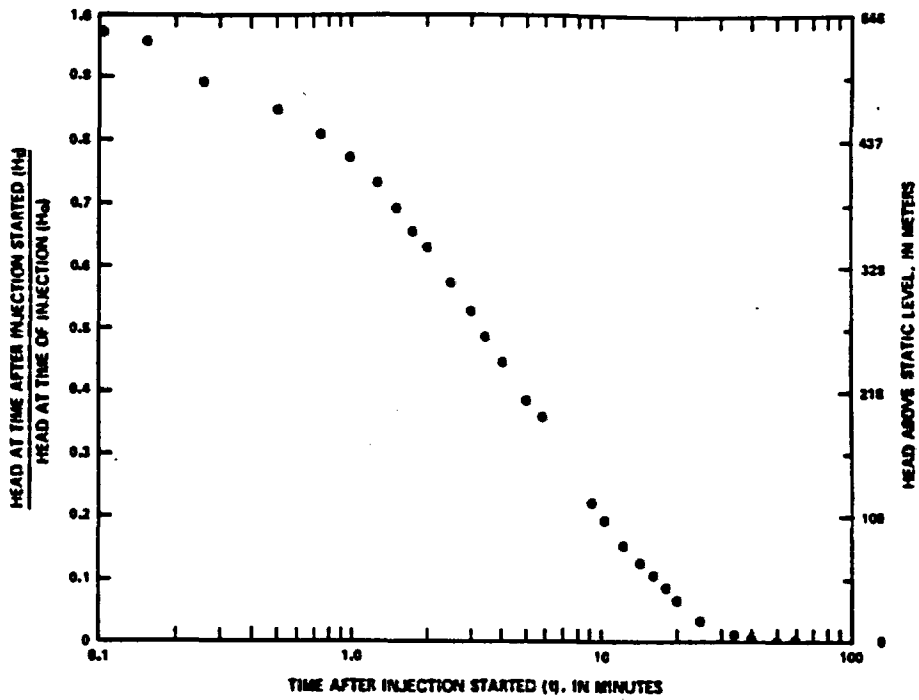


Packer-injection test for depth interval from 615 to 655 meters.

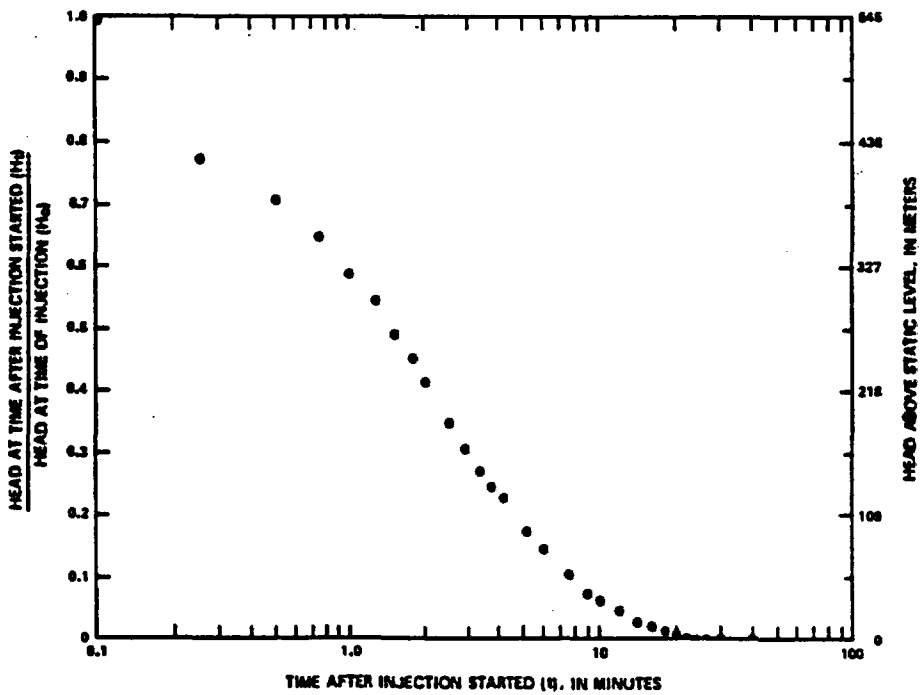


Packer-injection test for depth interval from 655 to 701 meters.

Results of the Cooper-Bredehoeft injection tests in well USW G-4. From Bentley (1984).

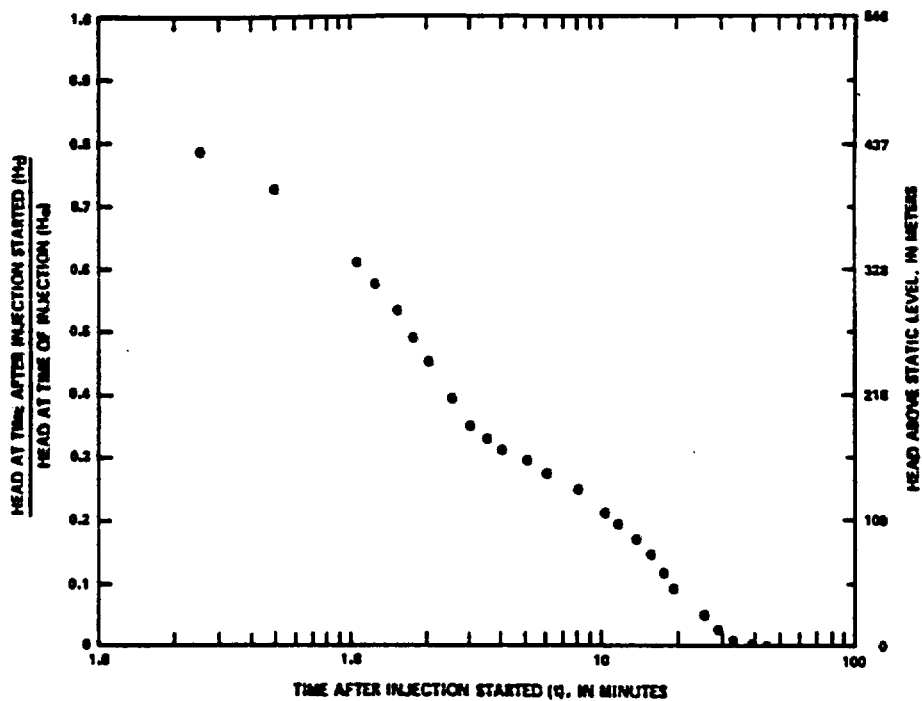


Packer-injection test for depth interval from 722 to 747 meters.

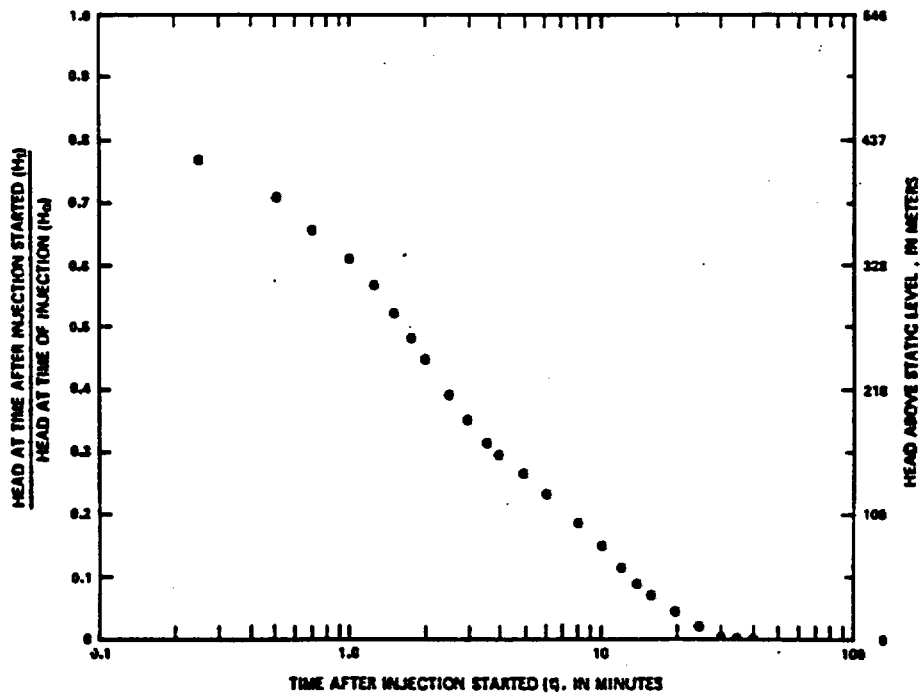


Packer-injection test for depth interval from 747 to 792 meters.

Results of the Cooper-Bredehoeft injection tests in well USW G-4. From Bentley (1984).

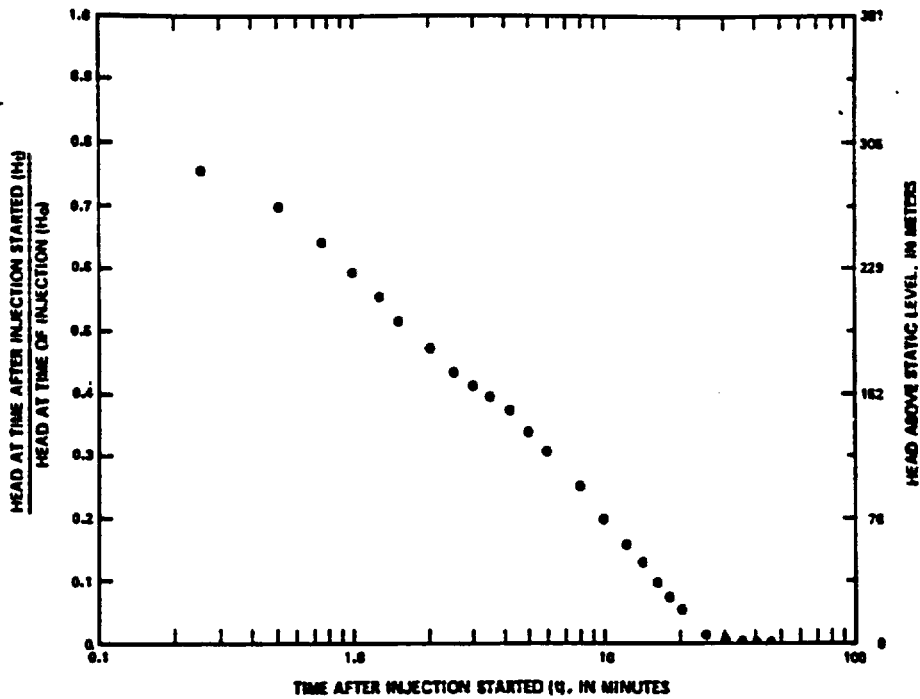


-Packer-injection test for depth interval from 792 to 838 meters.

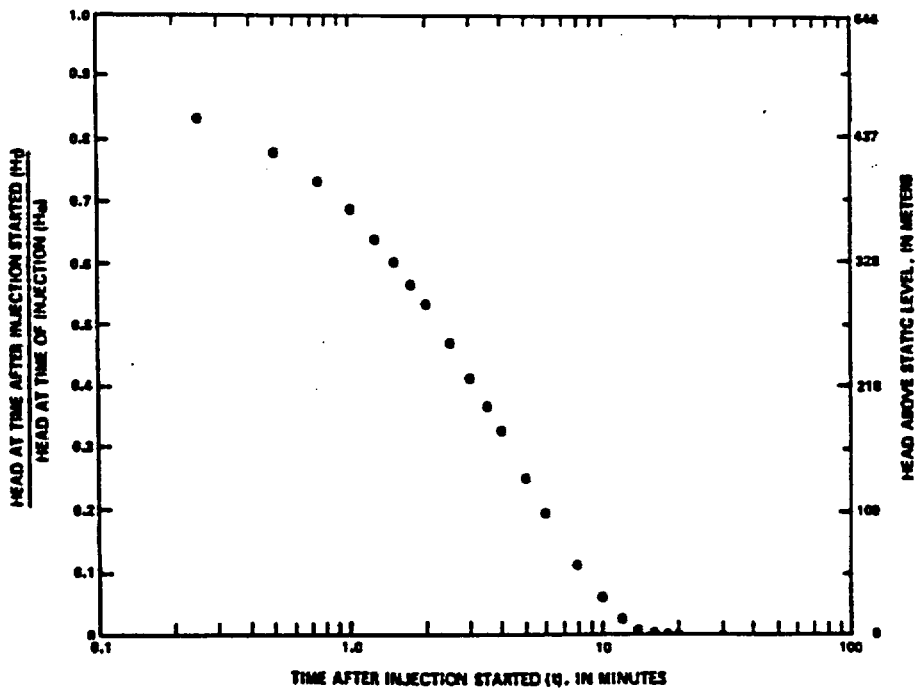


Packer-injection test for depth interval from 802 to 826 meters (first test).

Results of the Cooper-Bredehoeft injection tests in well USW G-4. From Bentley (1984).

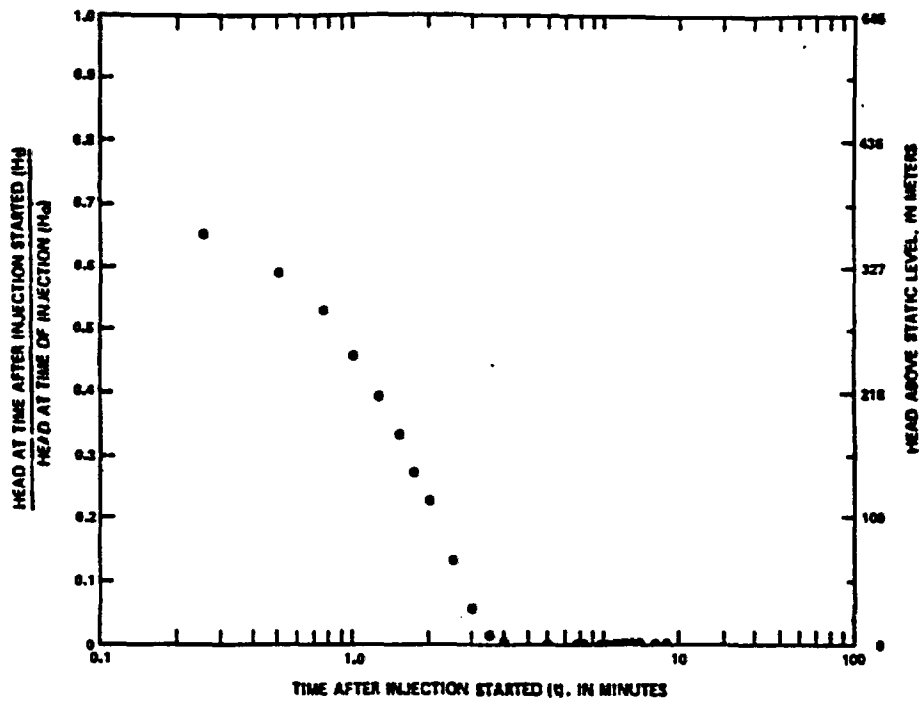


-Packer-injection test for depth interval from 802 to 826 meters (second test).

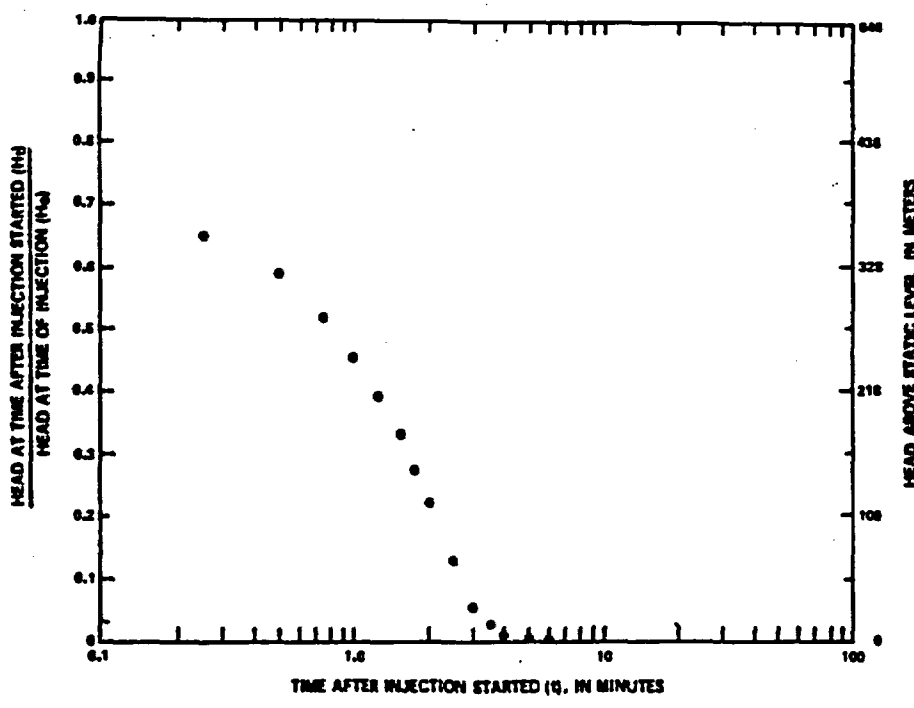


-Packer-injection test for depth interval from 826 to 850 meters.

Results of the Cooper-Bredehoeft injection tests in well USW G-4. From Bentley (1984)

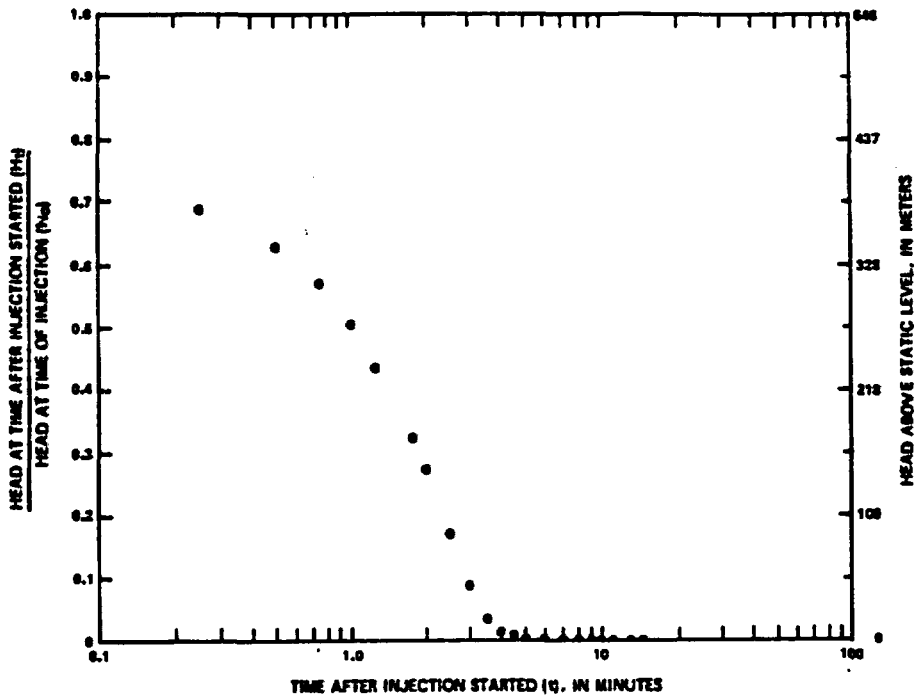


Packer-injection test for depth interval from 850 to 875 meters.



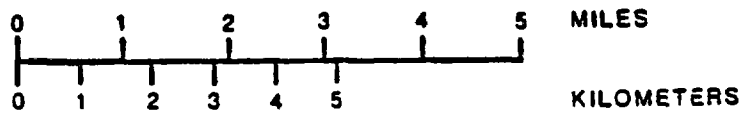
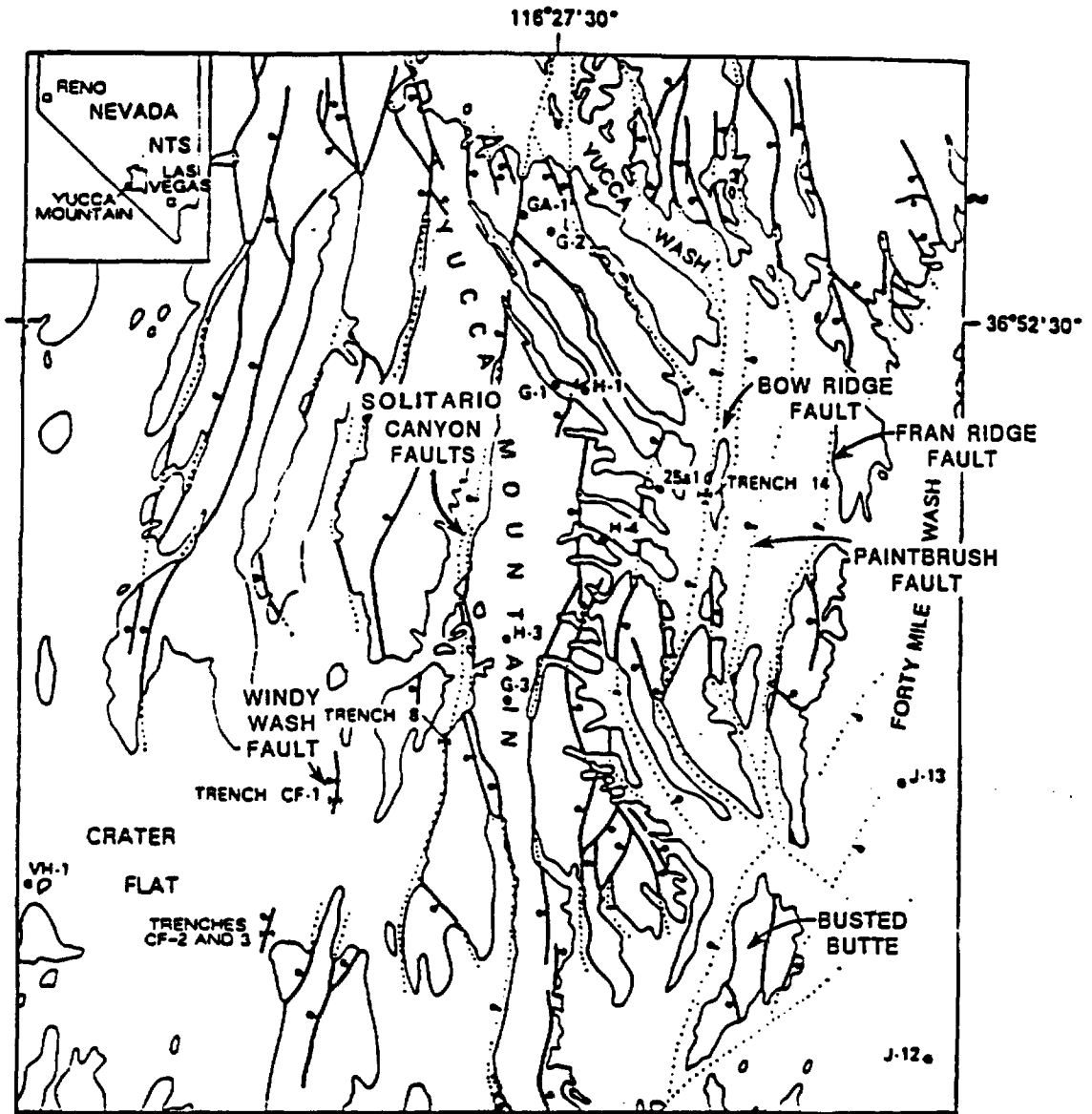
Packer-injection test for depth interval from 875 to 899 meters.

Results of the Cooper-Bredehoeft injection tests in well USW G-4. From Bentley (1984)



-Packer-injection test for depth interval from 899 to 915 meters.

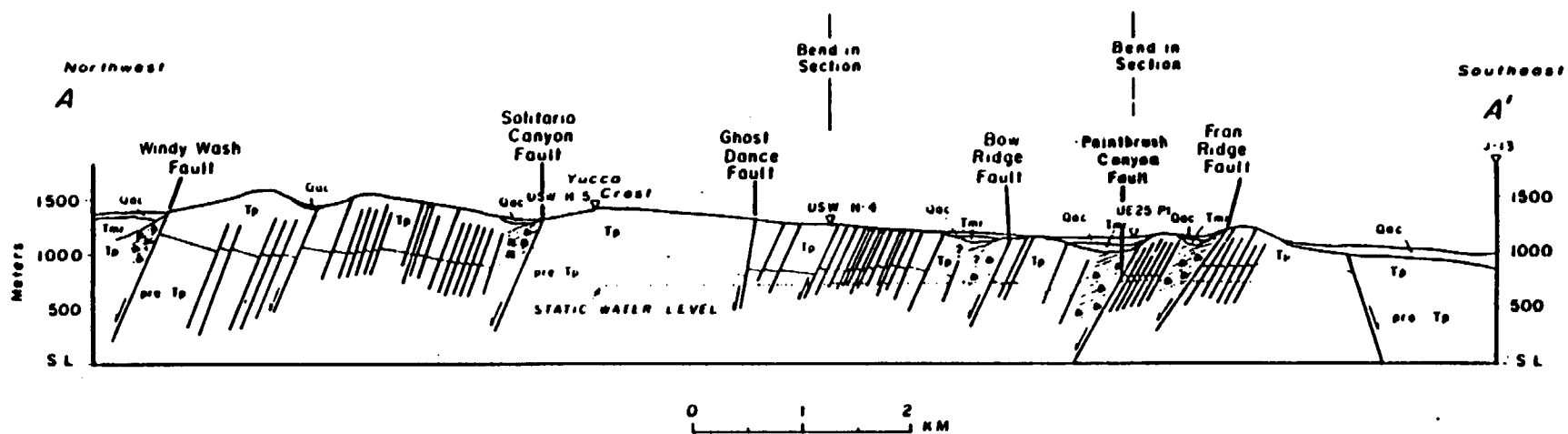
Results of the Cooper-Bredehoeft injection tests in well USW G-4. From Bentley (1984).



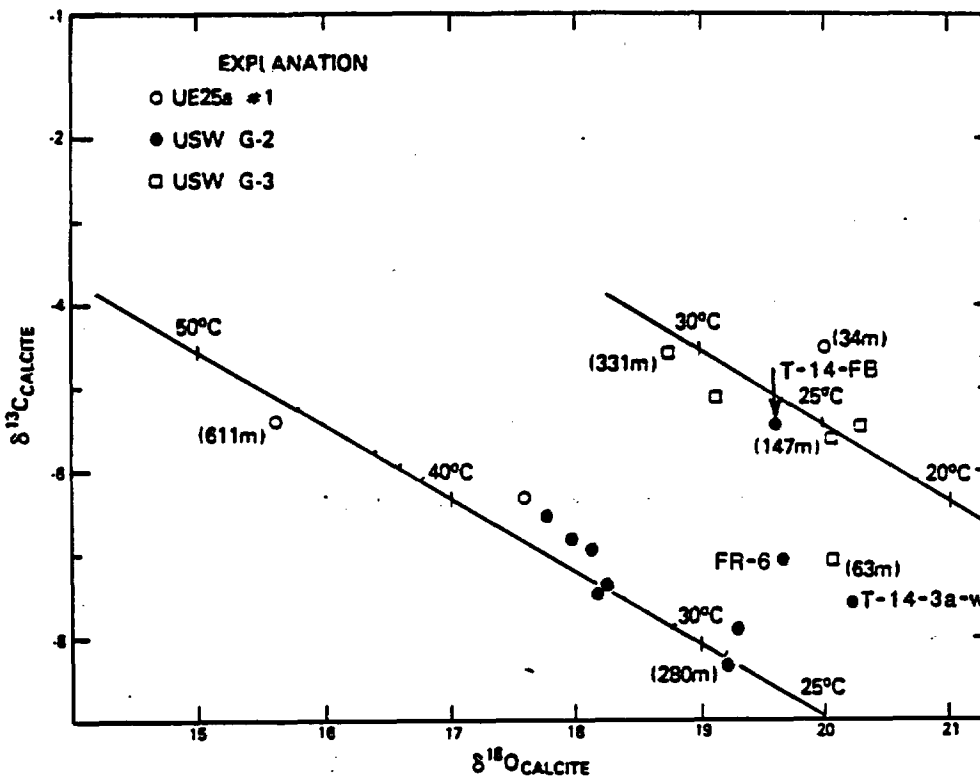
EXPLANATION

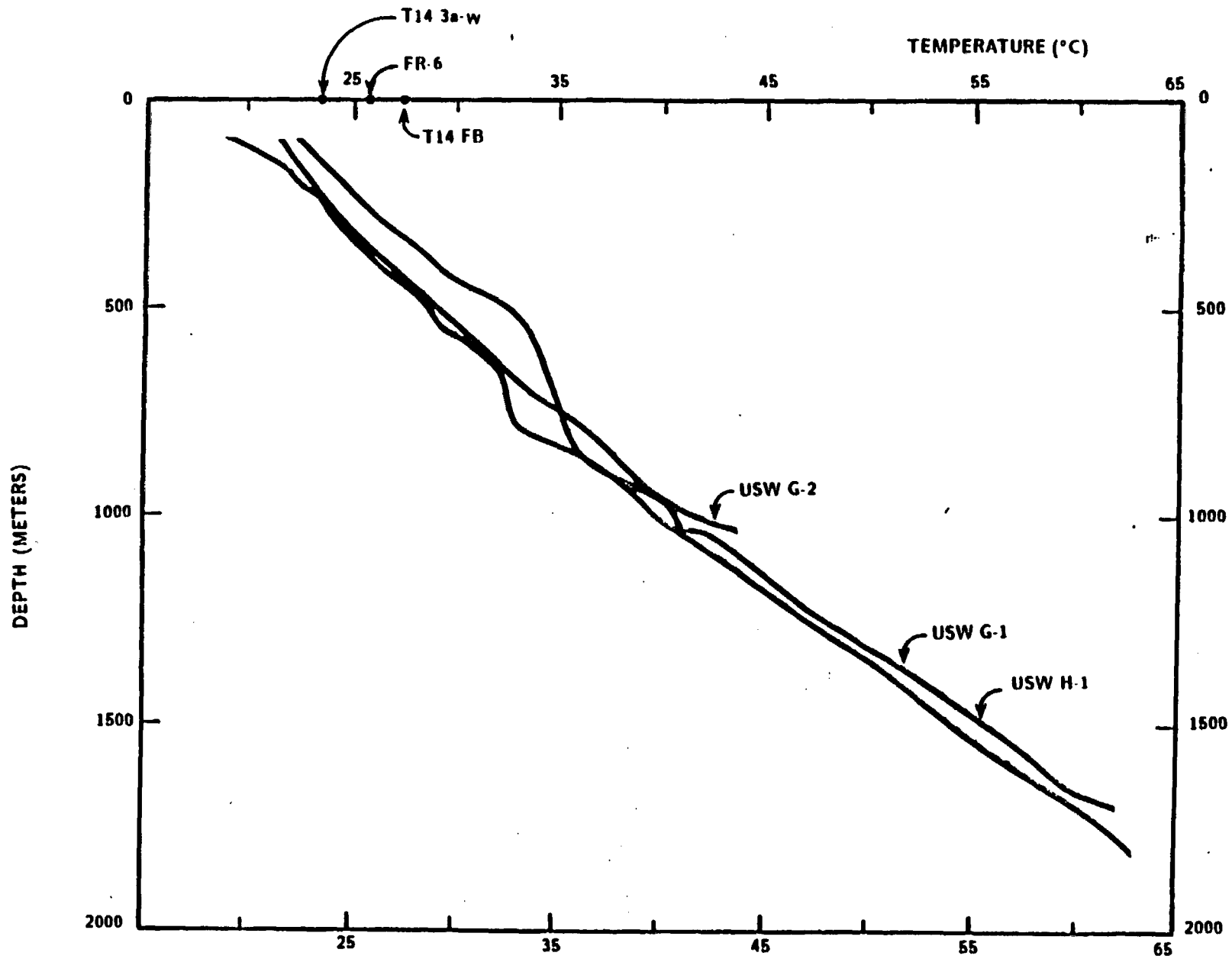
- G-2 DRILL HOLE
- TRENCH
- NORMAL FAULT—BAR AND BALL ON DOWNTHROWN SIDE

Location of faults containing calcite-silica veins of Quaternary age-Yucca Mountain.

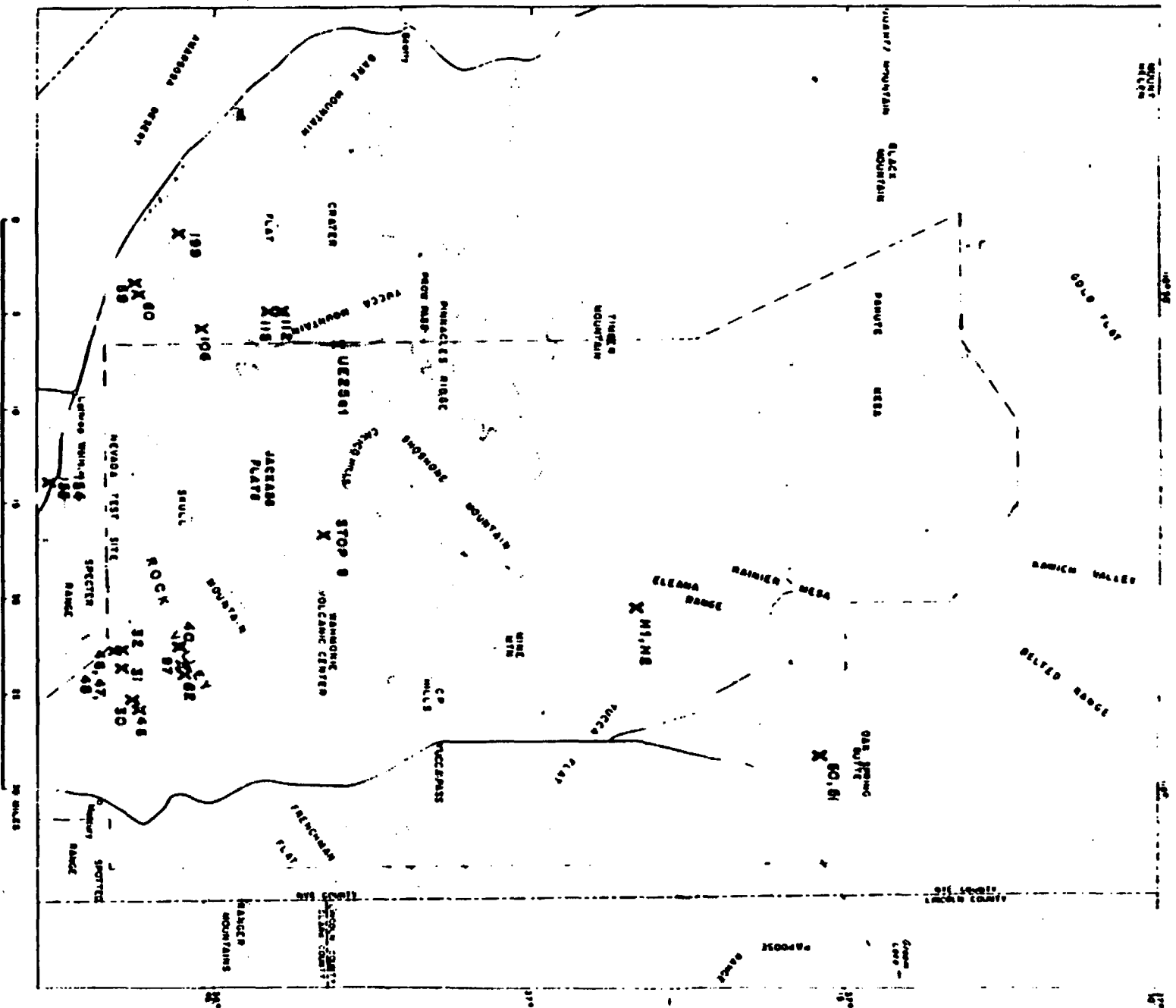


Geologic section across Yucca Mountain showing location and thicknesses of breccias. From Scott and Bonk (1984)





Comparison of temperature of formation of calcite-silica deposits, based on isotopic composition of three samples, with contemporary temperature at Yucca Mountain.



Location of samples analyzed and dated by Szabo et. al., 1981. From Szabo et. al., 1981.

Sample No.	Material	Percent residue	Fraction	Uranium (ppm)	$\frac{^{234}\text{U}}{^{238}\text{U}}$	$\frac{^{230}\text{Th}}{^{232}\text{Th}}$	$\frac{^{230}\text{Th}}{^{234}\text{U}}$	Uranium-series age (years)
MERCURY VALLEY AREA								
30-A <sup>1</sup>	Trav	0	S	0.038 ± 0.001	1.00 ±0.02	43. ±10.	0.844 ±0.042	>700,000
30-B <sup>2</sup>	Trav	0	S	0.066 ± 0.001	0.987 ±0.030	77. ±15.	0.992 ±0.040	>700,000
32	Trav	0	S	0.016 ± 0.002	1.00 ±0.05	4.05 ± 0.41	1.12 ±0.11	>700,000
45-A <sup>3</sup>	Trav	0	S	0.495 ± 0.007	0.981 ±0.015	6.92 ± 0.21	1.00 ±0.03	>700,000
45-C <sup>4</sup>	Trav	5	S	1.10 ± 0.17	0.999 ±0.015	10.2 ± 0.3	1.06 ±0.03	>700,000
			R	0.52 ± 0.05	0.95 ±0.09	5.5 ± 0.6	1.21 ±0.18	-
47-A <sup>5</sup>	Trav	20	S	4.71 ± 0.07	1.12 ±0.02	5.08 ± 0.15	0.846 ±0.025	104,000 ± 8,000
			R	2.84 ± 0.09	0.980 ±0.015	2.20 ± 0.07	1.58 ±0.05	-
47-B <sup>6</sup>	Trav	22	S	3.16 ± 0.05	1.17 ±0.02	5.37 ± 0.16	0.957 ±0.029	97,000 ± 8,000
			R	2.51 ± 0.05	1.00 ±0.05	3.42 ± 0.10	1.42 ±0.07	-
48	Calcr	18	S	3.17 ± 0.05	1.06 ±0.02	7.65 ± 0.23	0.730 ±0.022	100,000 - 150,000
			R	21.1 ± 0.3	1.01 ±0.02	16.7 ± 0.5	1.08 ±0.03	-
46	TTrav	23	S	5.19 ± 0.08	1.04 ±0.02	38.2 ± 1.5	0.999 ±0.030	>70,000
			R	10.6 ± 0.9	1.05 ±0.02	34.0 ± 1.4	1.15 ±0.12	-
31-A <sup>7</sup>	Calcr	70	S	19.7 ± 0.03	1.45 ±0.02	13.1 ± 0.4	0.750 ±0.030	102,000 ± 8,000
			R	5.61 ± 0.08	1.37 ±0.02	4.38 ± 0.13	1.16 ±0.05	-

Analytical data and uranium series ages of carbonates at the Nevada Test Site [Trav. travertine; TTrav. tuffaceous travertine; Calcr. calcrete; SC. soil caliche; S. acid soluble solution; R. acid insoluble residue]. From Szabo et al. (1981)

Sample No.	Material	Percent Residue	Fraction	Uranium (ppm)	$\frac{^{234}\text{U}}{^{238}\text{U}}$	$\frac{^{230}\text{Th}}{^{232}\text{Th}}$	$\frac{^{230}\text{Th}}{^{234}\text{U}}$	Uranium-series age (years)
31-B <sup>7</sup>	Calcr	75	S	2.21 + 0.03	1.10 +0.02	4.66 +0.14	0.751 +0.030	96,000 ± 8,000
			R	1.86 + 0.03	1.07 +0.02	1.45 +0.04	1.79 +0.07	
ROCK VALLEY FAULT AREA								
154	TTrav	55	S	2.23 + 0.03	1.17 +0.02	5.03 +0.13	1.72 +0.09	(8)
			R	0.630 + 0.010	1.03 +0.02	2.48 +0.07	1.98 +0.10	
155	TTrav	80	S	4.96 + 0.07	1.27 +0.02	9.73 +0.29	0.650 +0.033	70,000 - 110,000
			R	18.8 + 0.3	1.31 +0.02	23.4 +0.7	0.790 +0.040	
40	Calcr	45	S	6.90 + 0.10	1.13 +0.02	16.4 +0.7	0.435 +0.013	≈20,000
			R	12.3 + 0.2	1.13 +0.02	11.8 +0.4	0.824 +0.025	
82	SC	62	S	3.79 + 0.06	1.41 +0.02	1.81 +0.07	0.0747 +0.0022	>5,000
			R	3.02 + 0.05	1.24 +0.02	1.10 +0.04	1.06 +0.04	
97	SC	48	S	1.19 + 0.02	1.35 +0.02	1.33 +0.05	0.119 +0.004	>5,000
			R	2.91 + 0.04	1.20 +0.02	1.22 +0.05	1.44 +0.06	
JACKASS FLATS								
Stop-9	SC	90	S	4.75 + 0.06	1.34 +0.02	3.28 +0.10	0.240 +0.010	~24,000
			R	2.79 + 0.04	1.17 +0.02	0.961 +0.029	1.14 +0.05	

Analytical data and uranium series ages of carbonates at the Nevada Test Site [Trav. travertine; TTrav. tuffaceous travertine; Calcr. calcrete; SC. soil caliche; S. acid soluble solution; R. acid insoluble residue]. From Szabo et al., (1981).

Sample No.	Material	Percent Residue	Fraction	Uranium (ppm)	$\frac{^{234}\text{U}}{^{238}\text{U}}$	$\frac{^{230}\text{Th}}{^{232}\text{Th}}$	$\frac{^{230}\text{Th}}{^{234}\text{U}}$	Uranium-series age (years)
LATHROP WELLS AREA								
60-A	Calcr	35	S	5.32 + 0.08	1.23 +0.21	6.98 +0.21	1.05 +0.03	345,000 + 180,000 - 71,000
			R	3.73 + 0.06	1.06 +0.02	1.46 +0.04	1.14 +0.03	
60-B	Calcr	46	S	5.37 + 0.08	1.20 +0.02	5.62 +0.17	1.09 +0.03	345,000 + 180,000 - 70,000
			S	5.03 + 0.10	1.20 +0.02	5.53 +0.17	1.03 +0.05	
			R	6.11 + 0.09	1.10 +0.02	1.62 +0.05	1.04 +0.03	
59	SC	47	S	2.14 + 0.03	1.53 +0.02	1.99 +0.06	0.425 +0.013	25,000 + 10,000
			R	1.94 + 0.03	1.21 +0.02	1.13 +0.03	1.72 +0.05	
YUCCA MOUNTAIN AREA								
113	Calcr	75	S	2.78 + 0.04	1.03 +0.02	0.687 +0.027	0.146 +0.006	>5,000
			R	4.17 + 0.06	0.986 +0.015	0.620 +0.002	0.837 +0.025	
115	Calcr	80	S	10.6 + 0.2	1.46 +0.03	16.7 +1.7	0.422 +0.017	>20,000
			R	9.44 + 0.14	1.51 +0.02	22.4 +0.9	1.19 +0.04	
106	Ttrav	70	S	9.53 + 0.14	1.26 +0.19	4.53 +0.14	0.660 +0.026	78,000 + 5,000
			R	3.66 + 0.05	1.33 +0.02	2.43 +0.07	0.860 +0.034	
CRATER FLAT								
199	TTrav	30	S	1.81 + 0.03	2.16 +0.03	2.57 +0.08	0.290 +0.012	~30,000
			R	1.58 + 0.02	1.17 +0.02	2.81 +0.08	1.47 +0.06	

Analytical data and uranium series ages of carbonates at the Nevada Test Site [Trav. travertine; TTrav. tuffaceous travertine; Calcr. calcrete; SC. soil caliche; S. acid soluble solution; R. acid insoluble residue]. From Szabo et al., (1981).

Sample No.	Material	Percent Residue	Fraction	Uranium (ppm)	$\frac{^{234}\text{U}}{^{238}\text{U}}$	$\frac{^{230}\text{Th}}{^{232}\text{Th}}$	$\frac{^{230}\text{Th}}{^{234}\text{U}}$	Uranium-series age (years)
ELEANA RANGE								
H-1	SC	49	S	6.51 ± 0.10	1.21 ± 0.02	2.95 ± 0.09	0.877 ± 0.026	128,000 ± 20,000
			R	4.09 ± 0.06	1.10 ± 0.02	1.37 ± 0.04	1.18 ± 0.04	
H-2	SC	40	S	16.8 ± 0.3	1.34 ± 0.02	2.90 ± 0.09	0.0806 ± 0.0024	>5,000
			R	11.4 ± 0.2	1.35 ± 0.02	1.82 ± 0.06	0.331 ± 0.010	
BOUNDARY FAULT AREA								
50	SC	40	S	6.21 ± 0.09	1.37 ± 0.02	11.2 ± 0.5	0.242 ± 0.007	≈ 24,000
			R	4.36 ± 0.07	1.34 ± 0.02	4.56 ± 0.14	0.279 ± 0.008	
51	SC	31	S	4.77 ± 0.07	1.37 ± 0.02	1.62 ± 0.05	0.164 ± 0.005	>8,000
			R	3.50 ± 0.50	1.20 ± 0.02	1.07 ± 0.03	0.587 ± 0.018	

<sup>1</sup>The outside, oldest part of travertine vein TSV-30.

<sup>2</sup>The center, youngest part of travertine vein TSV-30.

<sup>3</sup>The outside, oldest part of travertine vein TSV-45.

<sup>4</sup>The center, youngest part of travertine vein TSV-45.

<sup>5</sup>Sample represents 1/3 of full vein width of sample TSV-47.

<sup>6</sup>Sample represents 2/3 of full vein width of sample TSV-47.

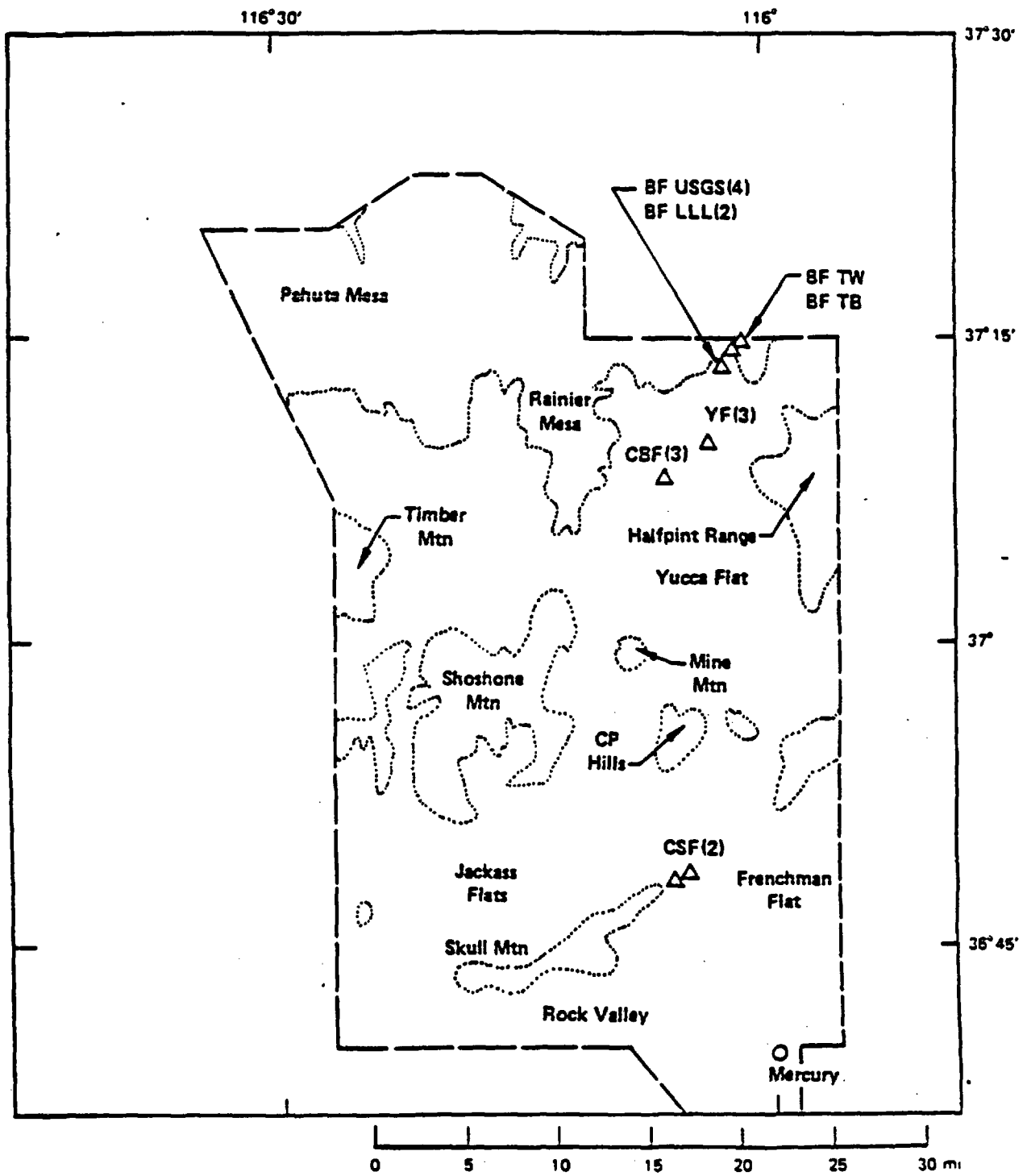
<sup>7</sup>Different aliquots of calcrete cement sample TSV-31.

<sup>8</sup>Age cannot be calculated.

<sup>9</sup>Inner part of dense carbonate rind growing on cobbles.

<sup>10</sup>The softer and porous outer part of the same rind as 9 (above).

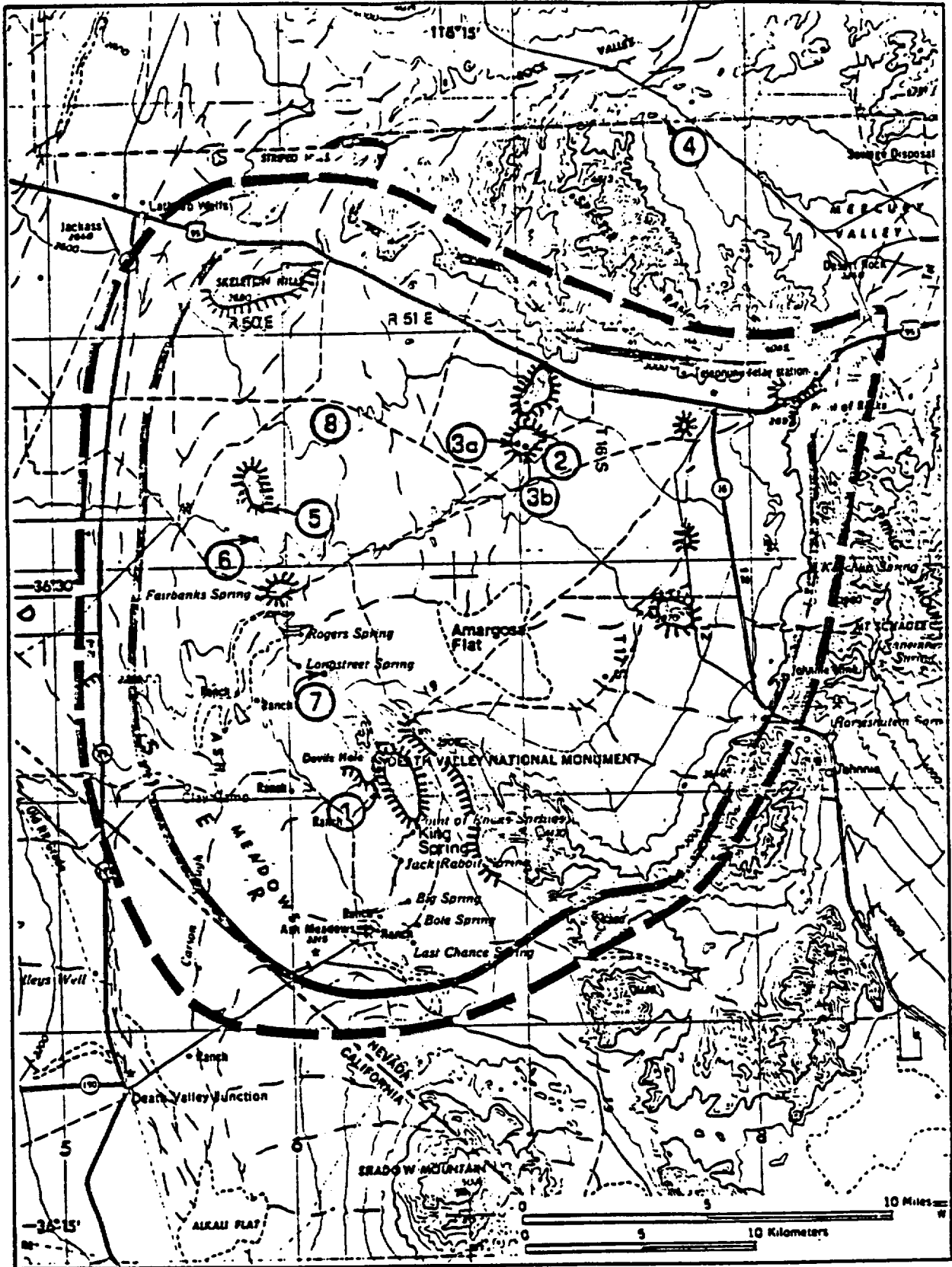
Analytical data and uranium series ages of carbonates at the Nevada Test Site [Trav. travertine; TTrav. tuffaceous travertine; Calcr. calcrete; SC, soil caliche; S, acid soluble solution; R, acid insoluble residue]. From Szabo et al. (1981).



Location map of samples analyzed and dated by Knauss (1981). From Knauss (1981)

Sample No.	Uncorrected ( $\times 10^3$ yr)	Isochron plot ( $\times 10^3$ yr)
CSF 1	34	41
CSF 2	4.8	2
BF USGS5 5a	$\geq 400$	$\geq 400$
BF LLL1 1	$\geq 400$	$\geq 400$

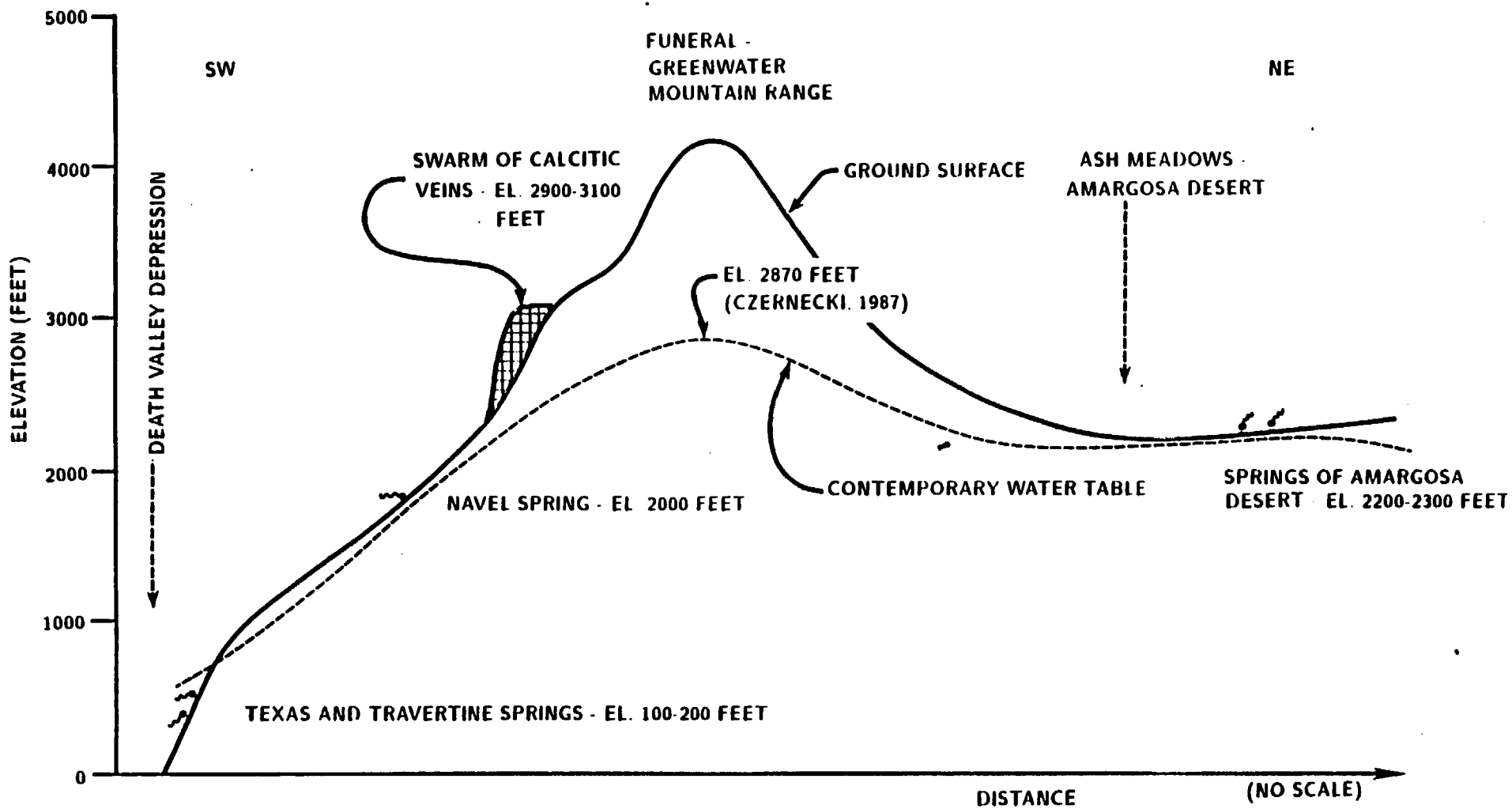
Radiometric ages of samples of travertine and tuffaceous travertine analyzed by Knauss (1981). From Knauss (1981).



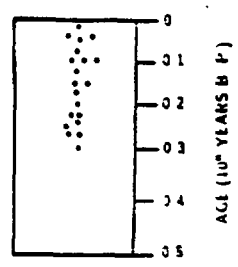
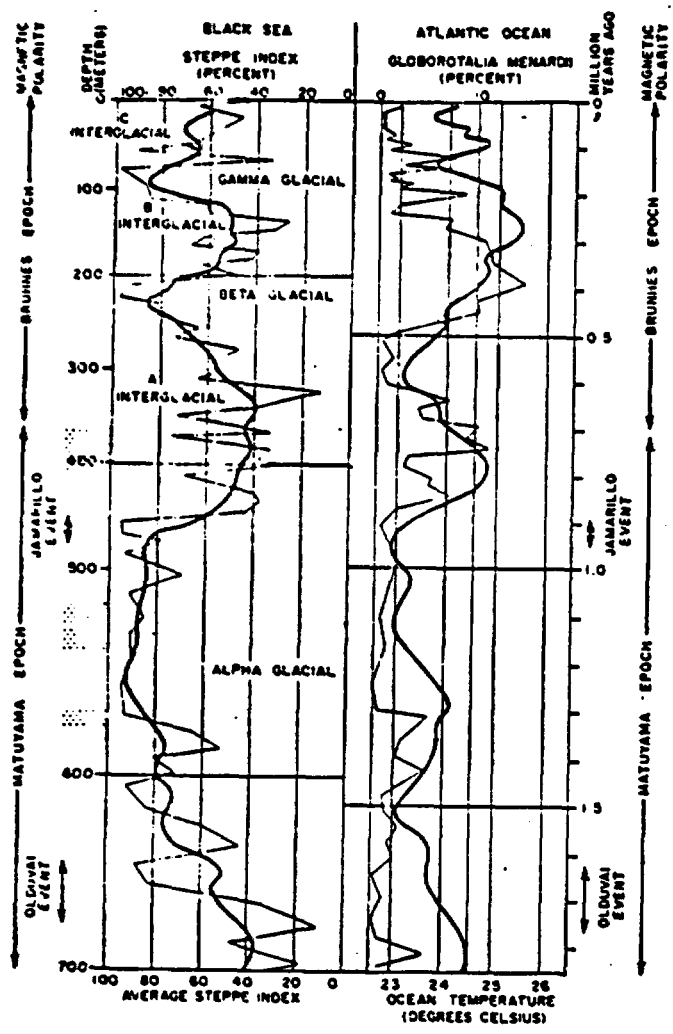
MAP FROM AMS NJ 11-11 1:250,000



Location map-sampling Site 4. From Winograd and Doty (1980).



Idealization of contemporary and paleo-hydrologic situation between Death Valley and Amargosa Desert



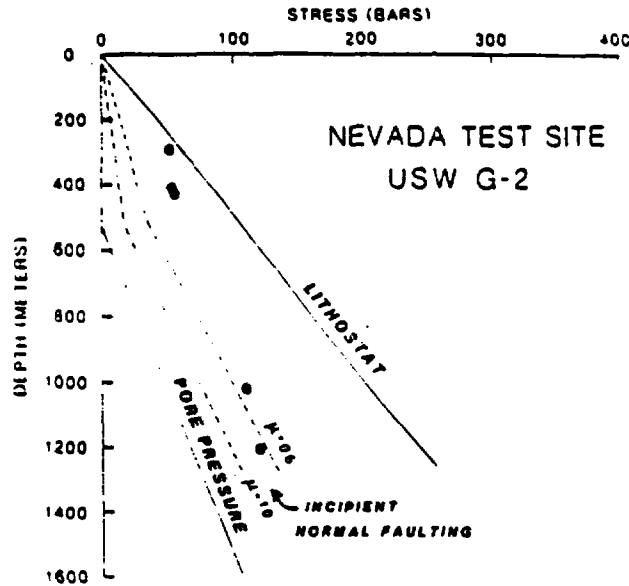
SAMPLES FROM THE NEVADA TEST SITE  
 PLATE 4.6.4-3:  
 PLATE 4.8-6 a. b. c:  
 PLATE 4.8-8: AND  
 WINOGRAD AND DOTY, 1980.

EXPLANATION:  
 ——— INDIVIDUAL MEASUREMENTS  
 ——— SMOOTHED OR AVERAGE CURVE

**NOTE:**

1. A DECREASE IN STEPPE INDEX CORRESPONDS TO A WARMING TEMPERATURE TREND. STEPPE INDEX IS PERCENTAGE OF THE POLLEN FOUND, THAT COMES FROM STEPPE VEGETATION.
2. INDIVIDUAL MEASUREMENTS CURVE FOR ATLANTIC OCEAN ARE CORRELATION OF PERCENT OF *GLOBOROTALIA MENARDII* WITH MEAN OCEAN TEMPERAURE.
3. AVERAGE CURVE FOR ATLANTIC OCEAN BASED ON SEVERAL FOSSIL SPECIES IN ADDITION TO *GLOBOROTALIA MENARDII*.

Comparison of ages of travertines from Nevada Test Site with global temperature fluctuations during Pleistocene  
 Modified from Hsu (1978)

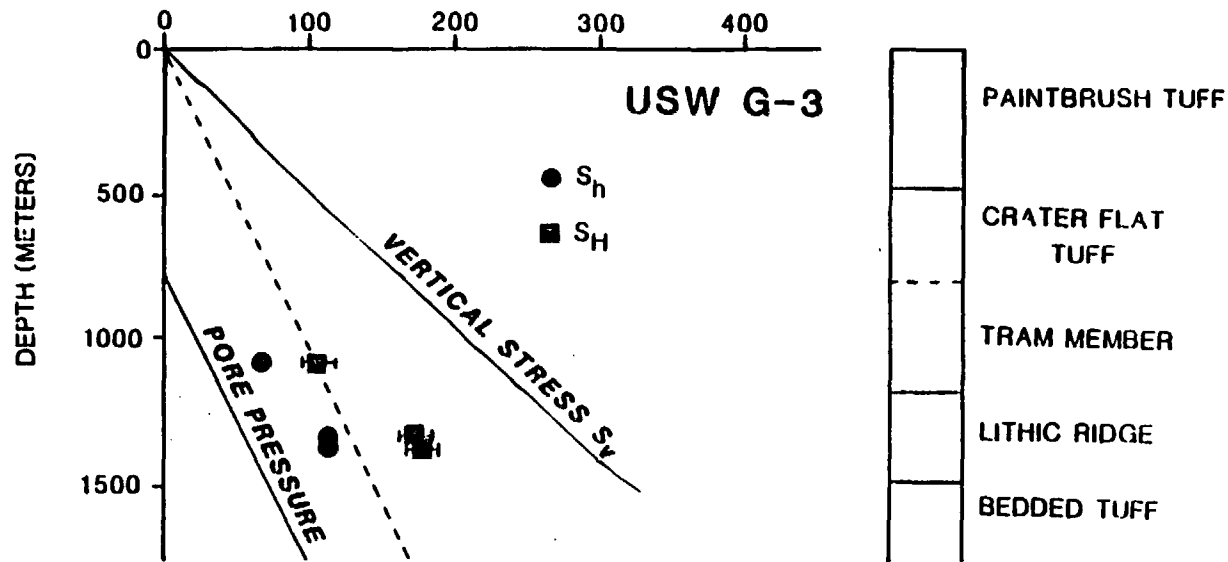


Depth, m	Hydraulic Fracturing Data				Principal Stresses		Comments
	Breakdown Pressure, MPa	Shut-In Pumping Pressure, MPa	Hydrostatic Pressure, MPa	Pore Pressure,*† MPa	Minimum Horizontal Stress, MPa	Vertical Stress MPa*	
<i>USW G-2</i>							
295	5.1	5.1 ± 0.1	2.9	0.0	5.1 ± 0.1	6.1	Reopening preexisting fracture of unknown orientation: shut-in pumping pressure is upper bound on $S_1$ .
418	5.4	5.4 ± 0.1	4.1	0.0	5.4 ± 0.1	8.4	Same as above.
432	5.5	5.5 ± 0.1	4.2	0.0	5.5 ± 0.1	8.7	Same as above.
1026	16.3	11.1 ± 0.2	10.1	4.9	11.1 ± 0.2	20.8	Minimum horizontal stress from stable pumping pressure on multiple cycles.
1209	18.2	12.0 ± 0.2	11.8	6.7	12.0 ± 0.2	25.5	Minimum horizontal stress from flat pumping pressure attained on second cycle. $S_1$ thus may be several bars too high due to pressure gradient in fracture.

\*Calculated for the appropriate density and depth.

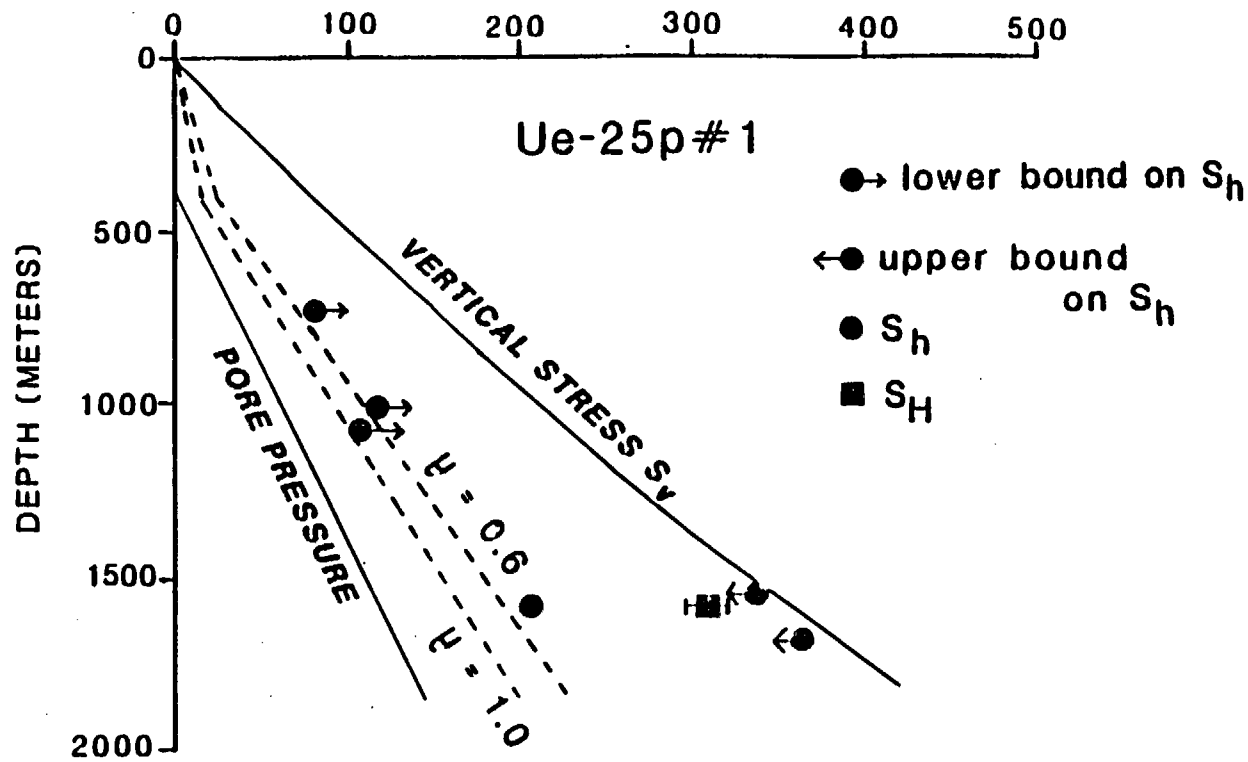
†Based on water table at 576 m depth in USW G-1 and 526 m depth in USW G-2.

Results of in-situ stress determinations in well USW G-2, Yucca Mountain. From Stock et. al., (1985).



Hole	Logged depth (m)	Breakdown pressure <sup>1</sup> (bars)	Shut-in pumping pressure (bars)	Hydrostatic pressure (bars)	Pore <sup>2</sup> pressure (bars)	$S_h$ (bars)	$S_v$ <sup>3</sup> (bars)	$T^4$ (bars)	$S_H$ (bars)	Comments
G-3	1,074	79	68	105	31	68 <sub>-2</sub>	206	13	107 <sub>+10</sub>	
G-3	1,338	173	115	131	56	115 <sub>-2</sub>	258	59	175 <sub>+9</sub>	Interpretation based on first two cycles only.
G-3	1,356	168	114	133	57	114 <sub>-2</sub>	263	64	181 <sub>+8</sub>	

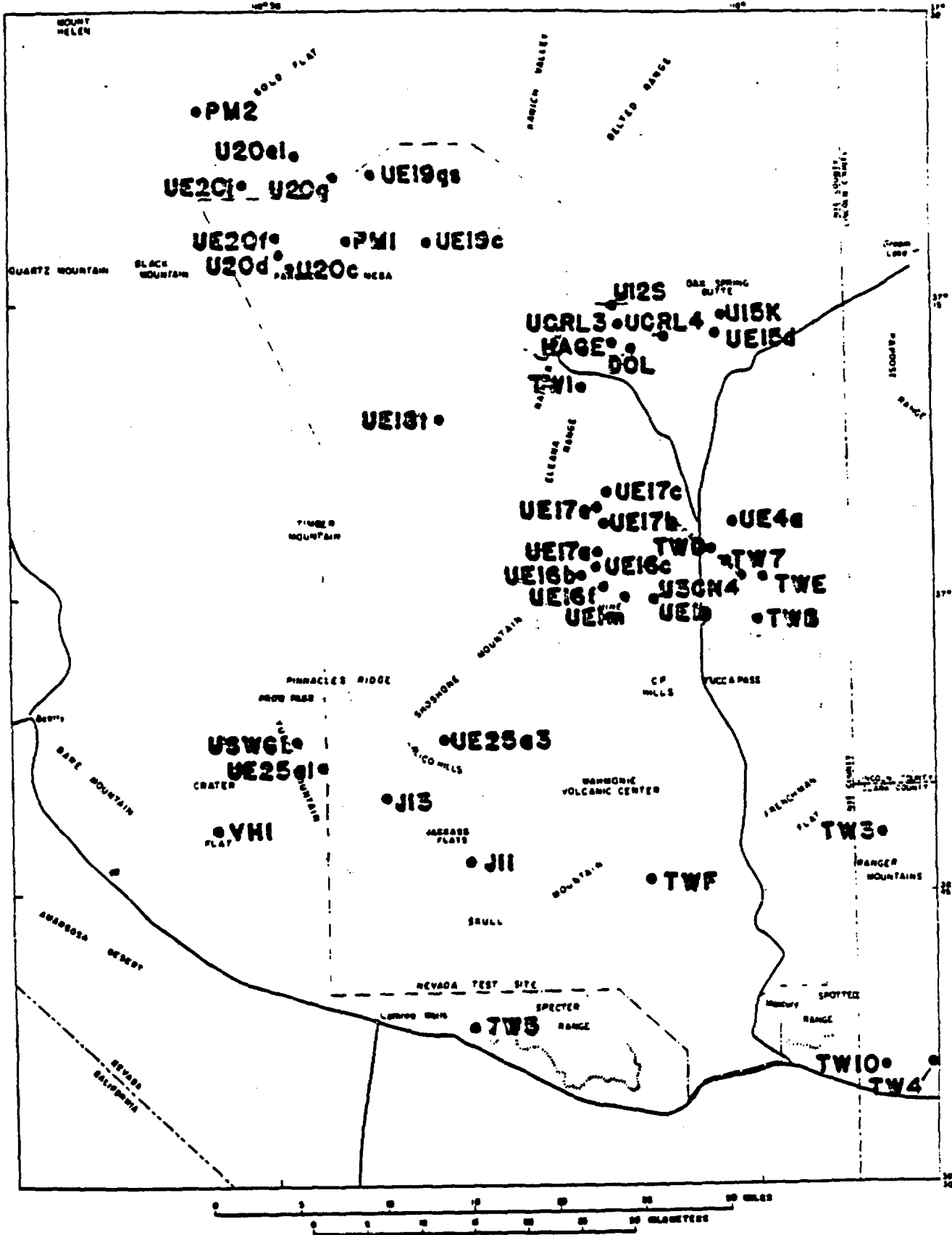
Results of in-situ stress determination in well USW G-3, Yucca Mountain. From Stock et. al., (1986)



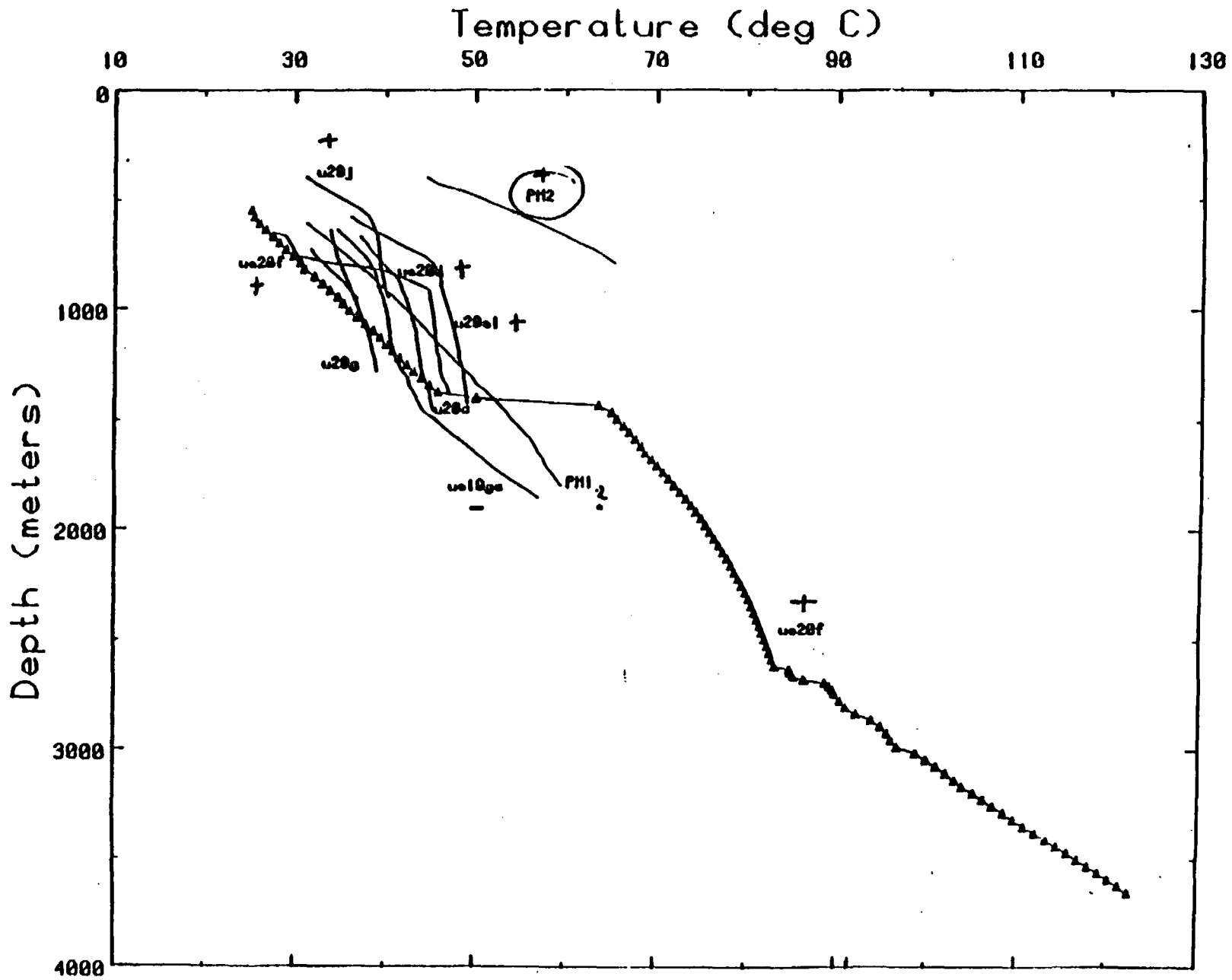
Hole	Logged depth (m)	Breakdown pressure <sup>1</sup> (bars)	Shut-in pumping pressure (bars)	Hydrostatic pressure (bars)	Pore <sup>2</sup> pressure (bars)	$S_h$ (bars)	$S_v$ <sup>3</sup> (bars)	$T^4$ (bars)	$S_H$ (bars)	Comments
P1	1,564	none <sup>1</sup>	337	153	115	337 <sub>+2</sub>	353			Reopening preexisting fracture
P1	1,573	236	207	154	116	207 <sub>+2</sub>	356	41	310 <sub>+11</sub>	
Pa1	1,693	none <sup>1</sup>	366	166	128	365 <sub>+10</sub>	388			Reopening preexisting fracture

1. No clear breakdown pressures seen

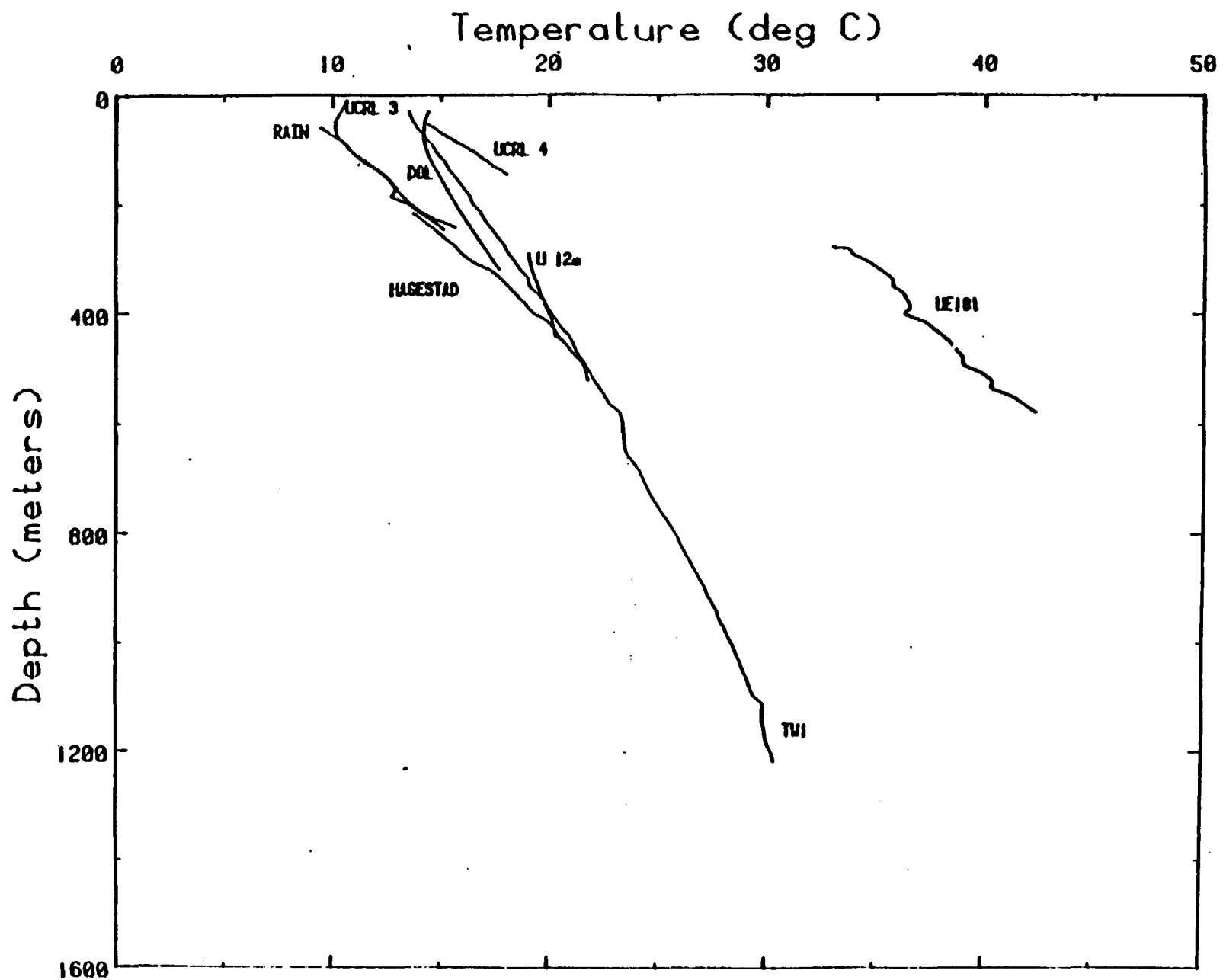
Results of in-situ stress determination in well Ue-25p#1, Yucca Mountain. From Stock et. al. (1986)



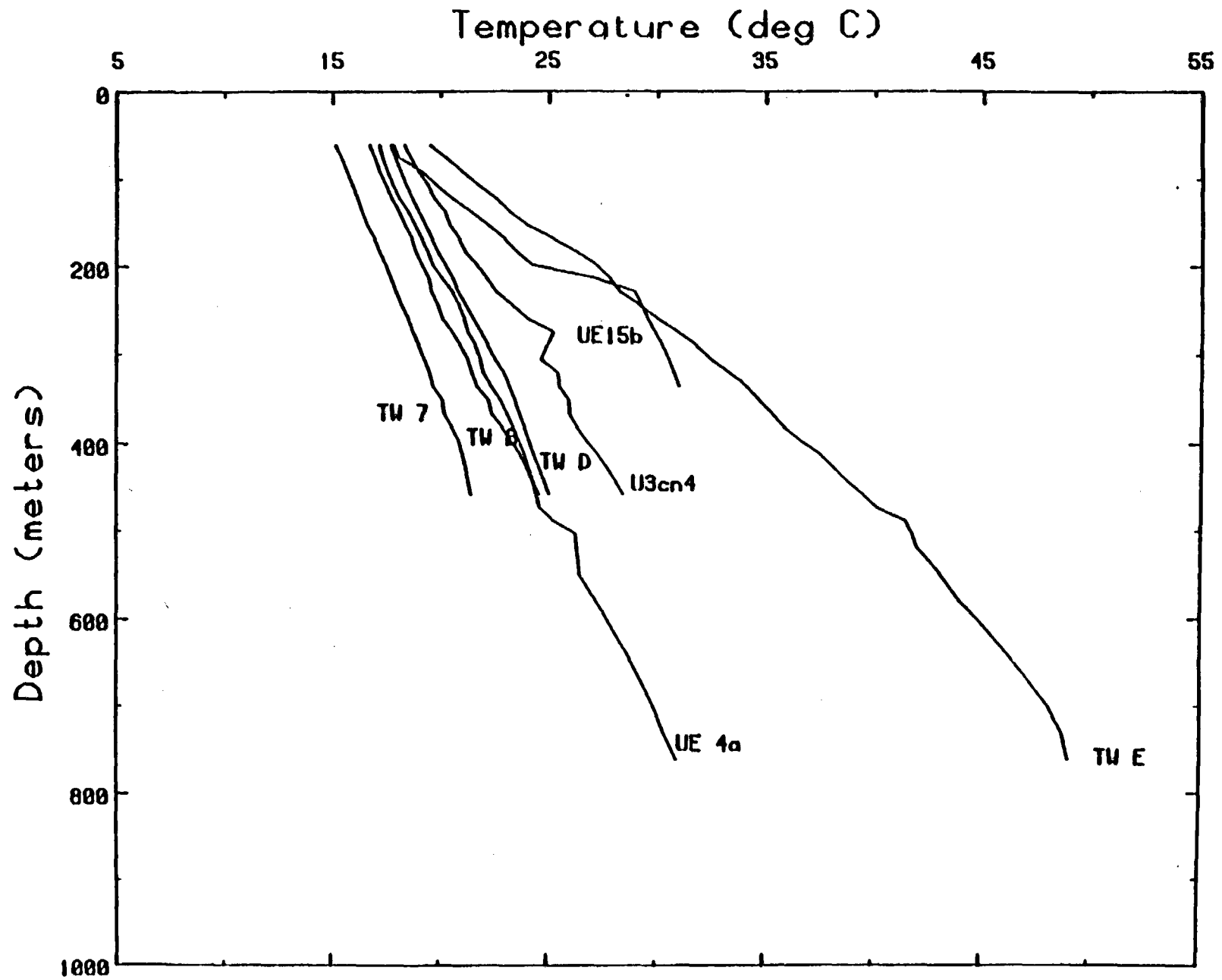
Location of wells where in-situ temperature measurements were performed. From Sass and Lachenbruch (1982).



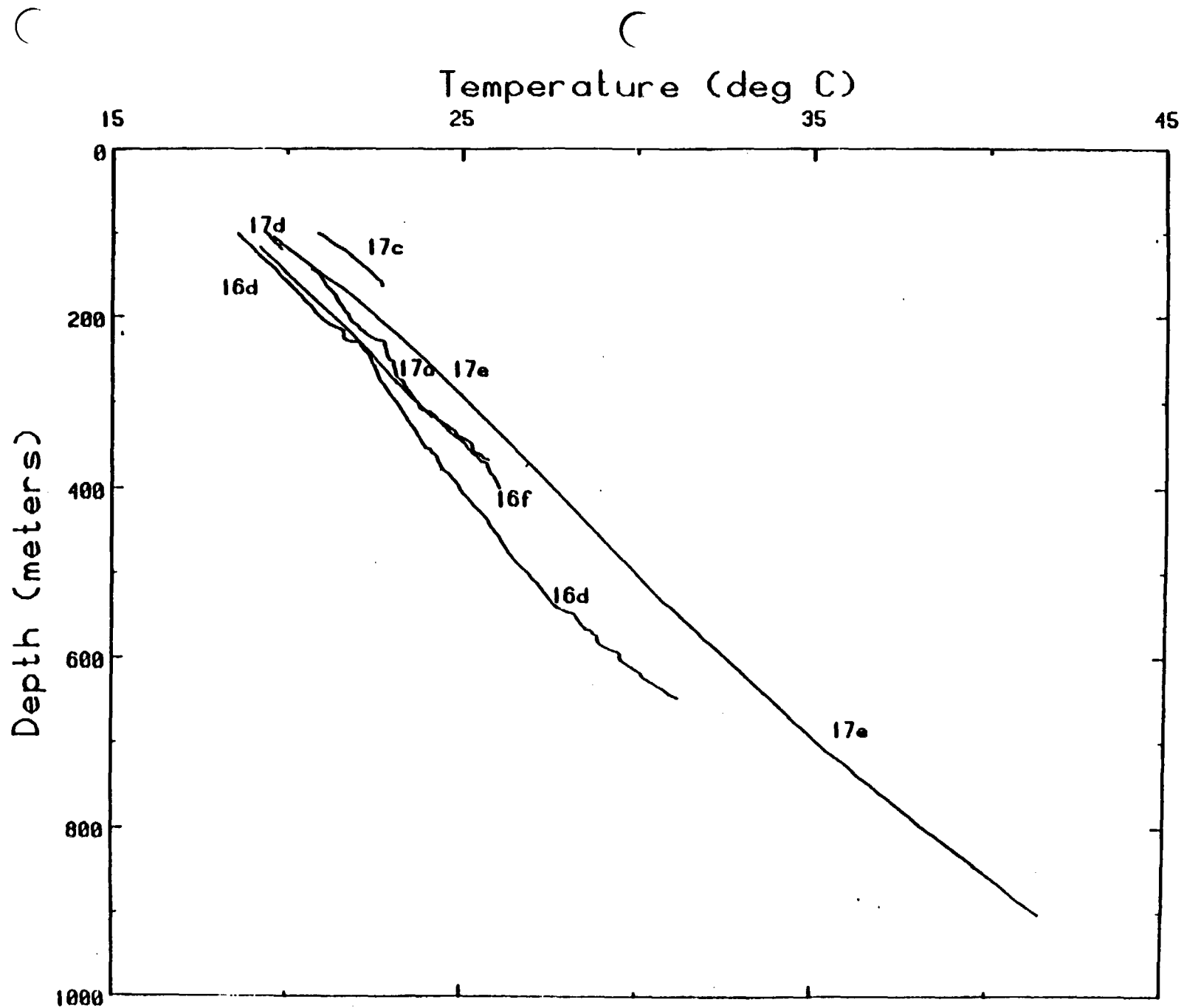
Composite temperature profile, Pahute Mesa From Sass and Lachenbruch (1982)



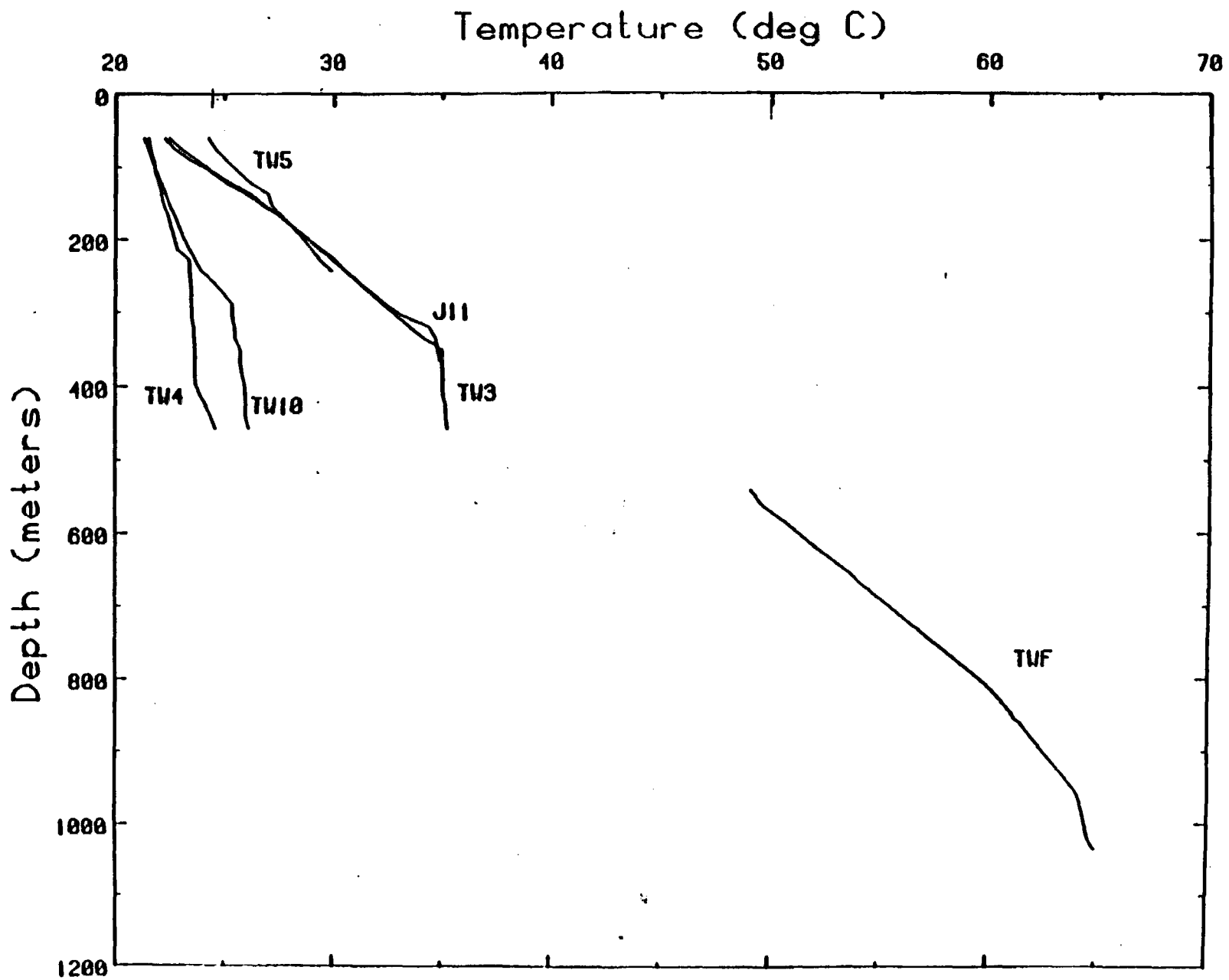
Composite temperature profile for Rainier Mesa and environments. From Sass and Lachenbruch (1982)



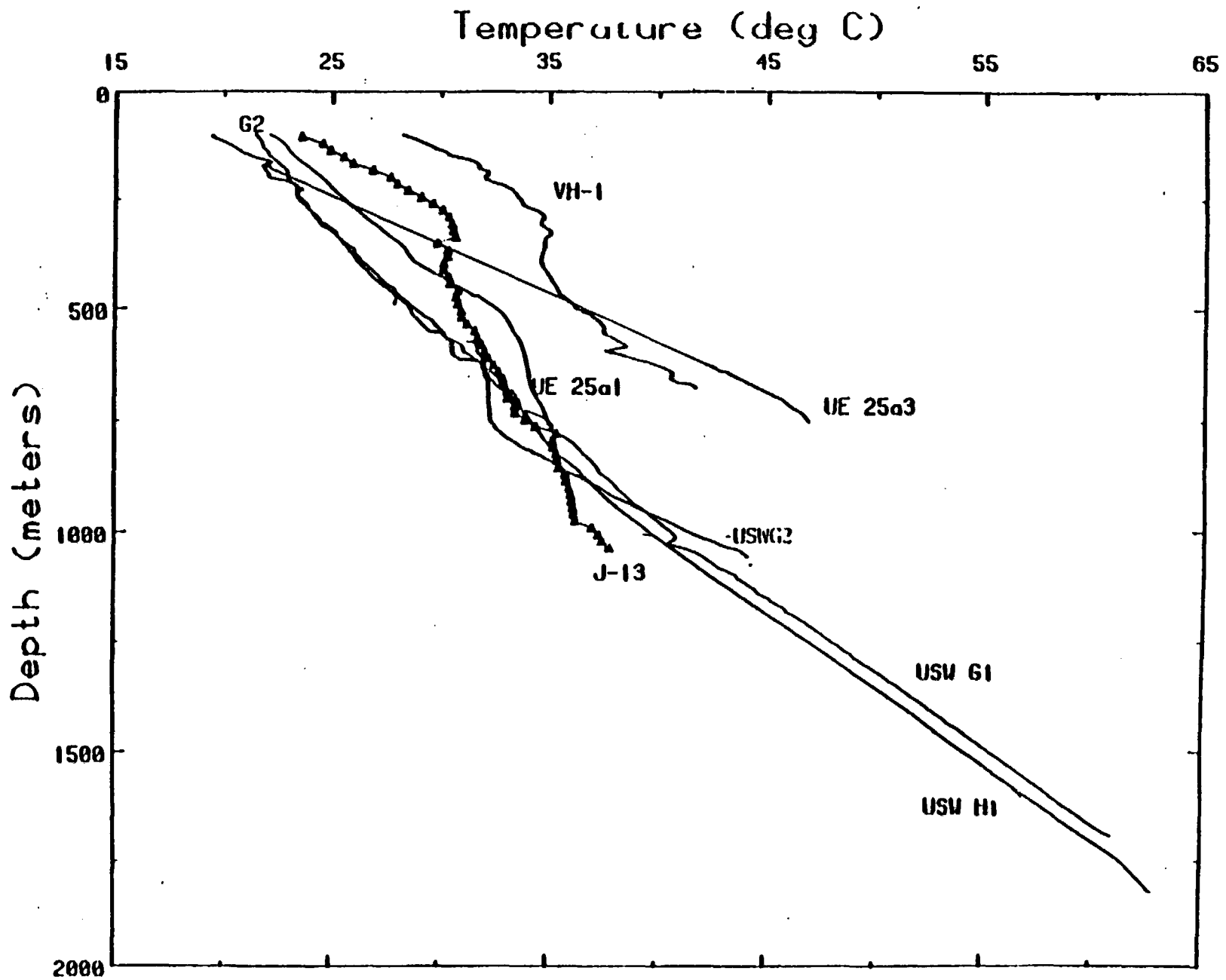
Composite temperature profile for Yucca Flat area From Sass and Lachenbruch (1982)



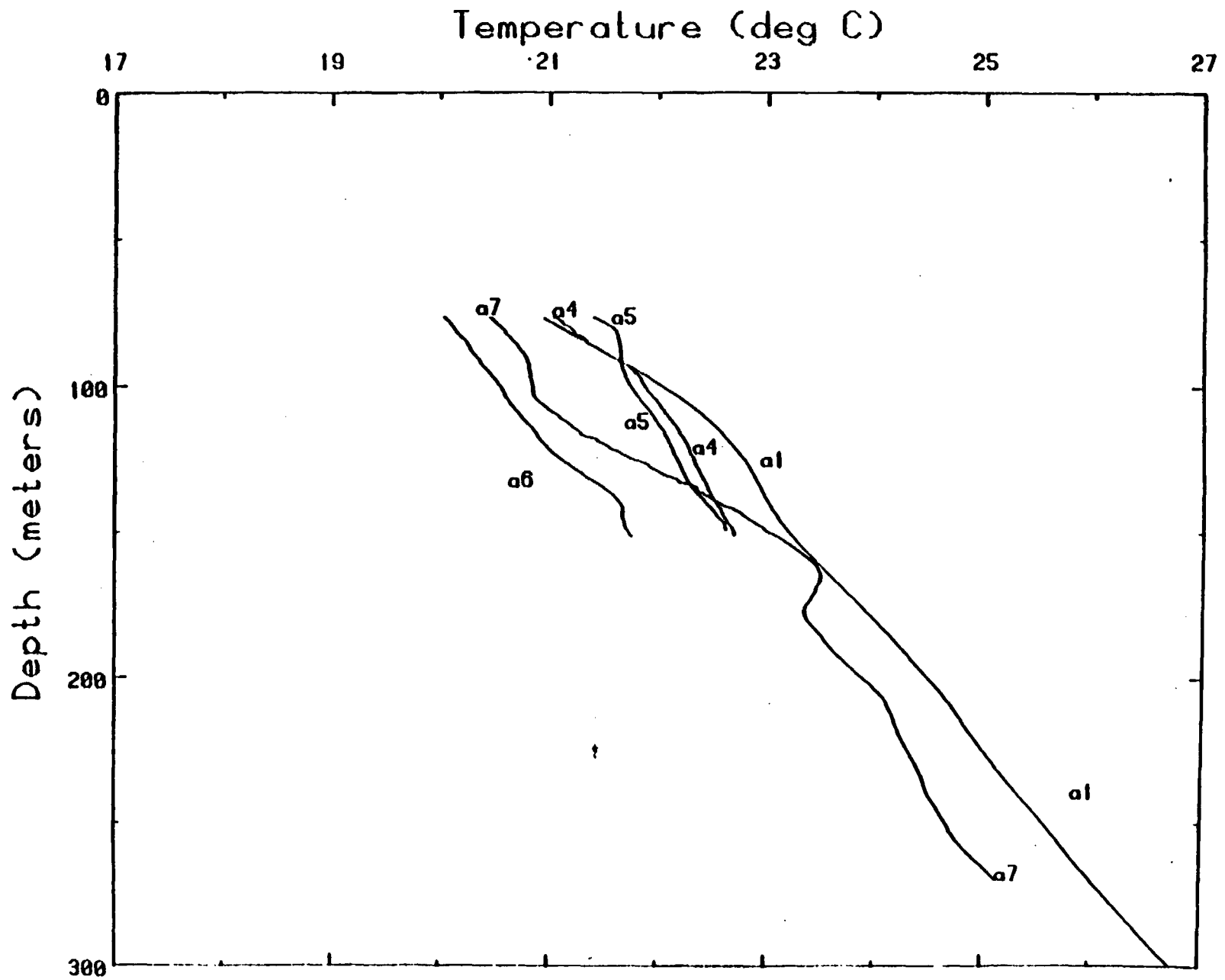
Composite plot of temperatures below 100 m, Syncline Ridge area. From Sass and Lachenbruch (1982).



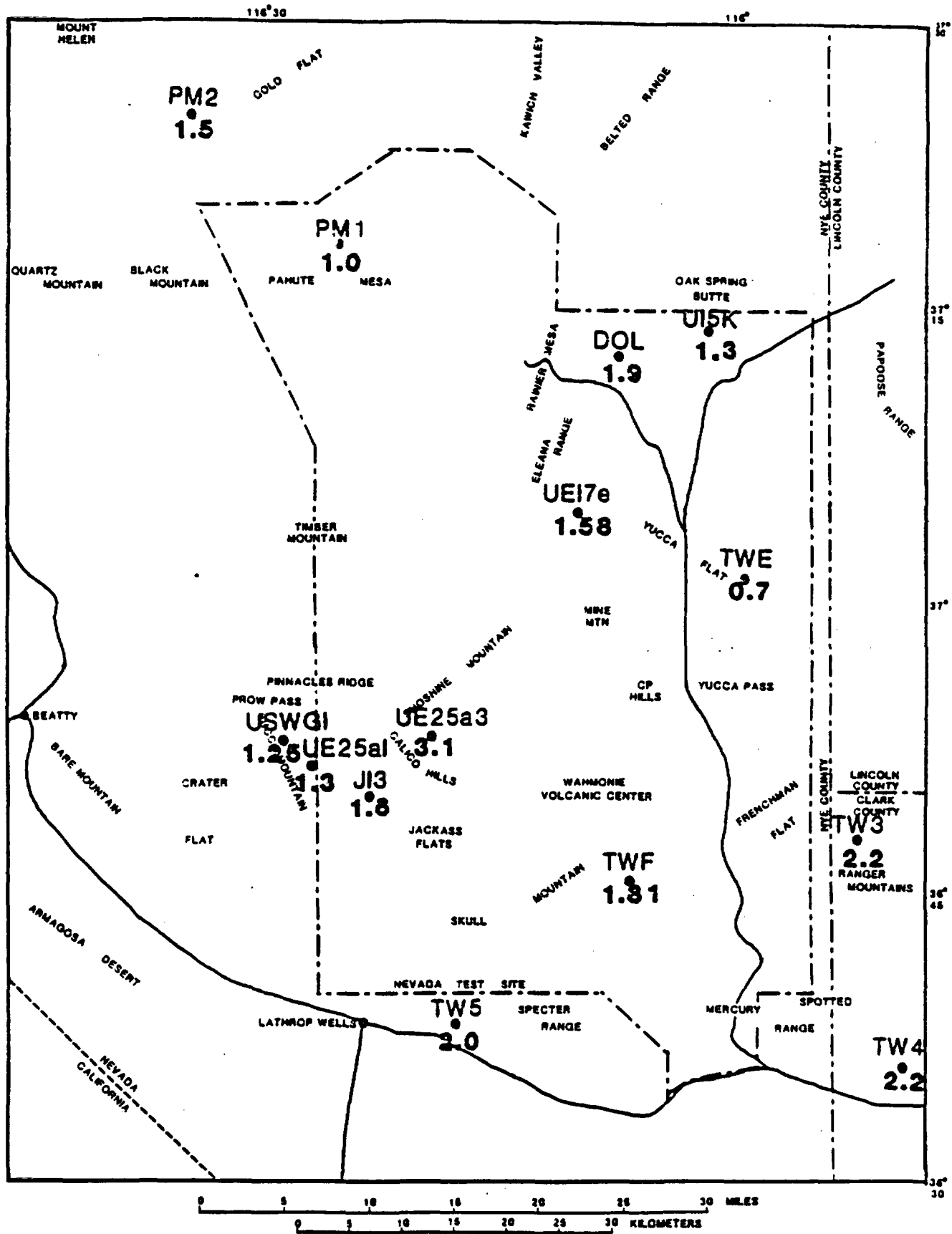
Composite temperature profile for the Southern NTS. From Sass and Lachenbruch (1982)



Temperatures in wells deeper than 600 m, Yucca Mountain. From Sass and Lachenbruch (1982)



Temperatures from UE25a1 and the "conductor holes", Yucca Mountain. From Sass and Lachenbruch (1982)



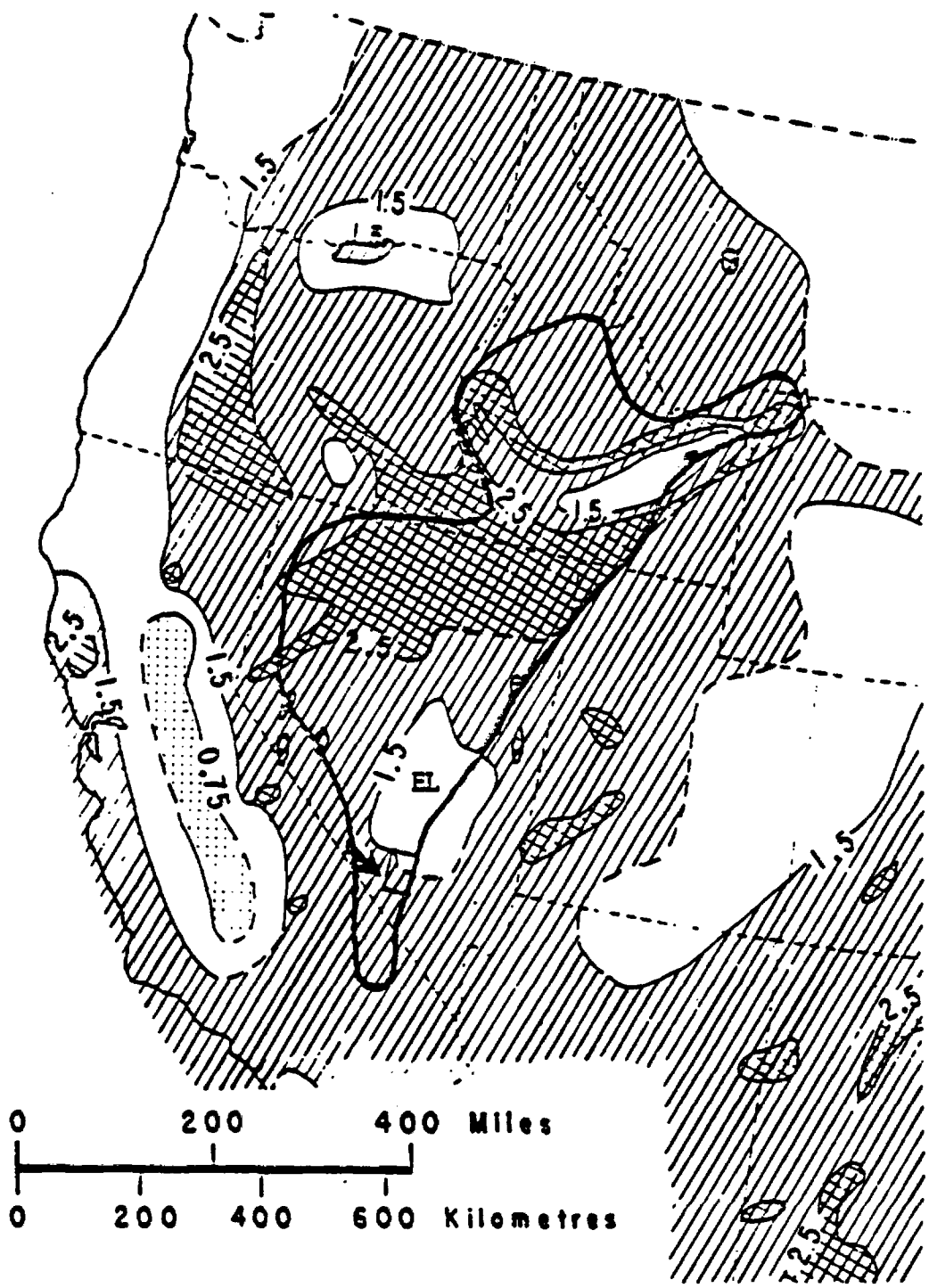
Intensities of heat flow in near ground surface rocks at the Nevada Test Site. From Sass and Lachenbruch (1982)

TABLE 1. Heat-flow determinations in and adjacent to the Nevada Test Site (see Figures 2 and 3 for locations)

Well	Heat flow		Reference
	$\text{mWm}^{-2}$	HFU	
PM2	63	1.5	Sass and others, 1971
PM1	42	1.0	Sass and others, 1971
DOL	80	1.9	Sass and others, 1971
U15K	56	1.3	USGS unpublished
Ue17e	66	1.58	USGS unpublished
TWE	29	0.7	Sass and others, 1971
J-13	67	1.6	Sass and others, 1971
Ue25a1	54	1.3	Sass and others, 1980
Ue25b1	47	1.1	USGS unpublished
Ue25a3	130	3.1	Sass and others, 1980
USWG1*	52	1.25	Table 2, this paper
TWF	76	1.81	Sass and others, 1971
TW3	92	2.2	Sass and others, 1971
TW5	84	2.0	Sass and others, 1971
TW4	91	2.2	Sass and others, 1971

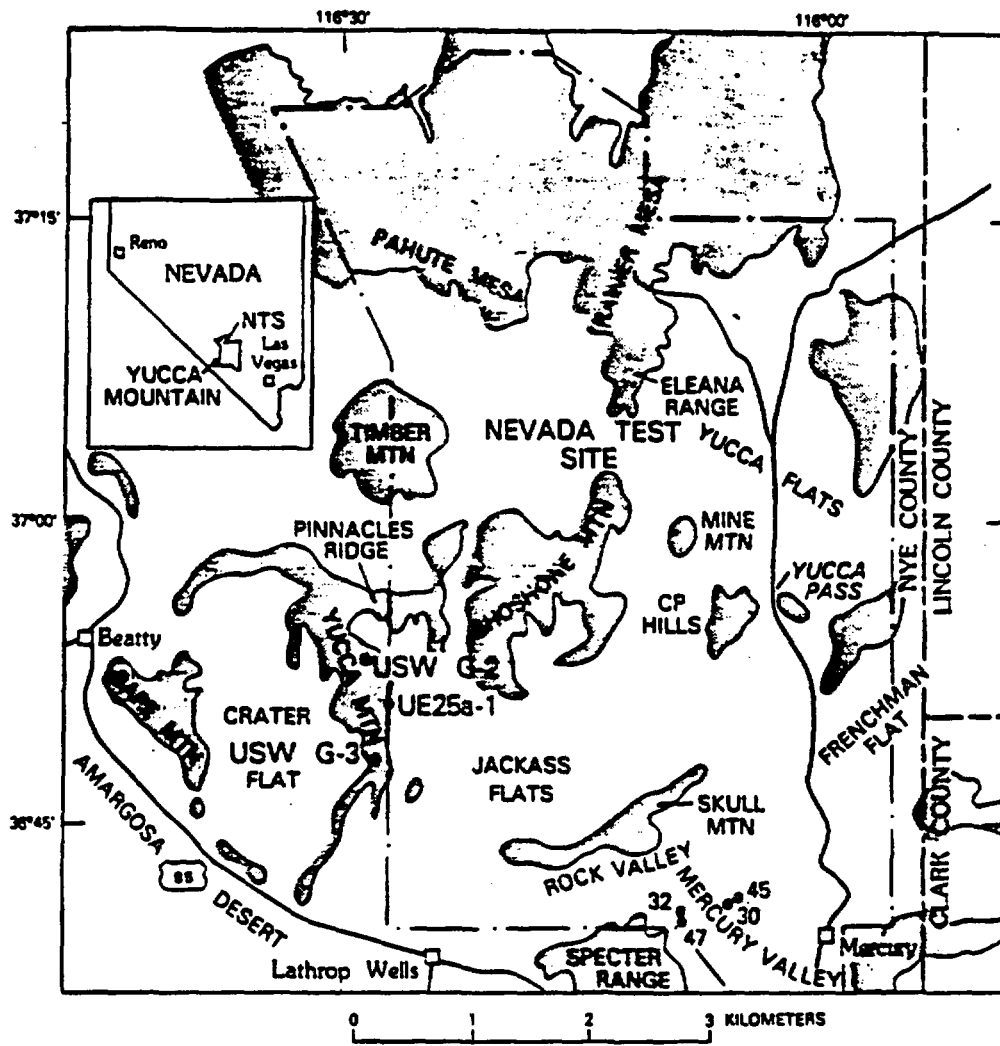
\*Average heat flow in lowermost ~600 m.

Intensities of heat flow at the Nevada Test Site. From Sass and Lachenbruch (1982)



Explanation: (1) Contour lines are heat flow units (HFU); (2) EL is Eureka Low; (3) Arrow indicates outline of the Nevada Test Site; (4) Heavy line is 2.5 HFU contour (Swanberg and Morgan, 1978)

Map of Western United States showing intensities of heat flow. From Sass and Lachenbruch (1982).



Location of boreholes where calcite samples from Yucca Mountain were collected. From Szabo and Kyser (1985)

Sample depth (m)	Material	Uranium (ppm)	$^{235}\text{U}/^{238}\text{U}$	$^{230}\text{Th}/^{232}\text{Th}$ (activity ratio)	$^{230}\text{Th}/^{234}\text{U}$	$\delta^{13}\text{C}$ (‰)	$\delta^{18}\text{O}$ (‰)
34	Calcite	0.767 ±0.015	1.17 ±0.02	2.37 ±0.07	1.02 ±0.04	-4.52	+20.00
283	Calcite	5.03 ±0.10	1.47 ±0.02	22.2 ±0.7	1.04 ±0.04	-6.33	+17.60
611	Calcite	3.43 ±0.07	1.29 ±0.02	72 ±3	1.19 ±0.05	-5.41	+15.60

Sample depth (m)	Fraction	Percent carbonate	Uranium (ppm)	$^{235}\text{U}/^{238}\text{U}$	$^{230}\text{Th}/^{232}\text{Th}$ (activity ratio)	$^{230}\text{Th}/^{234}\text{U}$	$\delta^{13}\text{C}$ (‰)	$\delta^{18}\text{O}$ (‰)
280	Calcite	>99	0.500 ±0.010	1.032 ±0.015	12.0 ± 2.4	1.023 ±0.041	-8.35	+19.21
302	Calcite	n.d.	n.d.	n.d.	n.d.	n.d.	-7.90	+19.31
346.7	Calcite	64	0.405 ±0.008	1.167 ±0.018	4.29 ±0.21	0.915 ±0.037	-7.43	+18.22
346.8	Calcite	n.d.	n.d.	n.d.	n.d.	n.d.	-7.37	+18.30
348.7	Calcite	>99	0.073 ±0.006	1.02 ±0.03	4.6 ±0.5	0.73 ±0.06	-7.47	+18.19
348.8-A	Calcite	97	0.136 ±0.004	0.937 ±0.028	10.7 ±1.6	1.010 ±0.040	-6.93	+18.13
348.8-B	Calcite	63	33.3 ±0.7	1.026 ±0.015	94 ±15	0.093 ±0.037	n.d.	n.d.
359-A	Calcite	61	1.21 ±0.06	1.020 ±0.015	261 ±80	0.795 ±0.032	-6.82	+17.98
359-B	Calcite	75	0.644 ±0.013	0.965 ±0.014	36 ±11	0.811 ±0.032	n.d.	n.d.

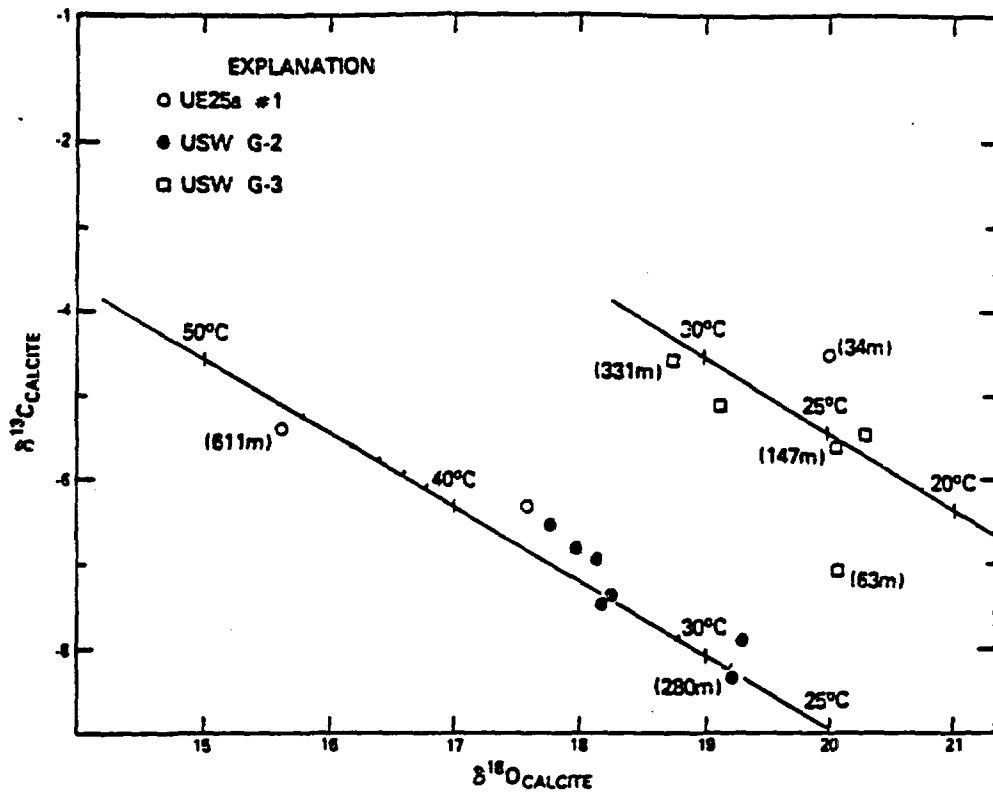
Analytical data from fracture filling calcites from Yucca Mountain. From Szabo and Kyser (1985)

Sample depth (m)	Fraction	Percent carbonate	Uranium (ppm)	$^{235}\text{U}/^{238}\text{U}$	$^{230}\text{Th}/^{232}\text{Th}$ (activity ratio)	$^{230}\text{Th}/^{234}\text{U}$	$\delta^{13}\text{C}$ (‰)	$\delta^{18}\text{O}$ (‰)
361	Calcite	n.d.	n.d.	n.d.	n.d.	n.d.	-6.56	+17.77
63	Calcite	95	0.558 $\pm 0.011$	2.26 $\pm 0.03$	35 $\pm 4$	1.00 $\pm 0.03$	-7.06	+20.23
131	Calcite	52	3.02 $\pm 0.06$	1.43 $\pm 0.02$	84 $\pm 40$	0.216 $\pm 0.009$	-5.11	+20.16
147	Calcite	n.d.	n.d.	n.d.	n.d.	n.d.	-5.58	+20.04
159	Calcite	n.d.	n.d.	n.d.	n.d.	n.d.	-5.44	+20.28
318	Calcite	95	0.0836 $\pm 0.0017$	0.991 $\pm 0.020$	2.58 $\pm 0.13$	1.10 $\pm 0.06$	-5.10	+19.11
331	Calcite	87	0.36 $\pm 0.01$	1.06 $\pm 0.04$	10 $\pm 5$	0.24 $\pm 0.02$	-4.54	+18.73

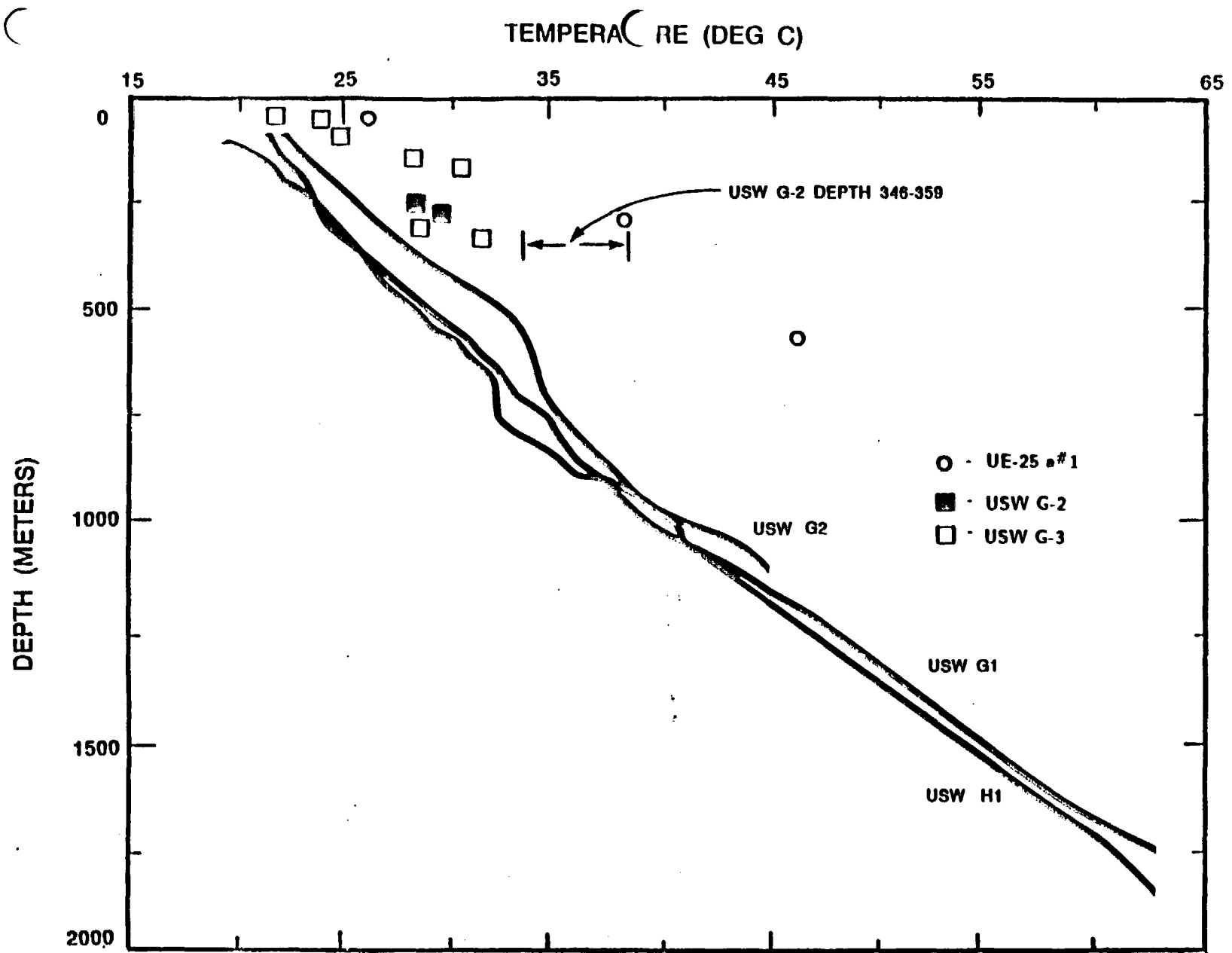
Analytical data from fracture filling calcites from Yucca Mountain (continued). From Szabo and Kyser (1985).

Drill hole	Depth (m)	Uranium (ppm)	Calculated age (x10 <sup>3</sup> years)
Calcite			
UE25a#1	34	0.77	310 <sup>+60</sup> <sub>-50</sub> (a)
GU-3	63	0.56	227±20
GU-3	131	3.0	26±2
USW-G2	280	0.50	>400
UE25a#1	283	5.0	310 <sup>+70</sup> <sub>-55</sub>
GU-3	318	0.084	>400
GU-3	331	0.36	30±4
USW-G-2	346.7	0.40	190±20 (b)
USW-G-2	348.7	0.073	142±30
USW-G-2	348.8-A	0.14	>400
USW-G-2	348.8-B	33	280±70
USW-G-2	359-A	1.2	170±18
USW-G-2	359-B	0.64	185±18
UE25a#1	611	3.4	>400

Calculated uranium series ages of fracture filling calcite from Yucca Mountain. From Szabo and Kyser (1985)

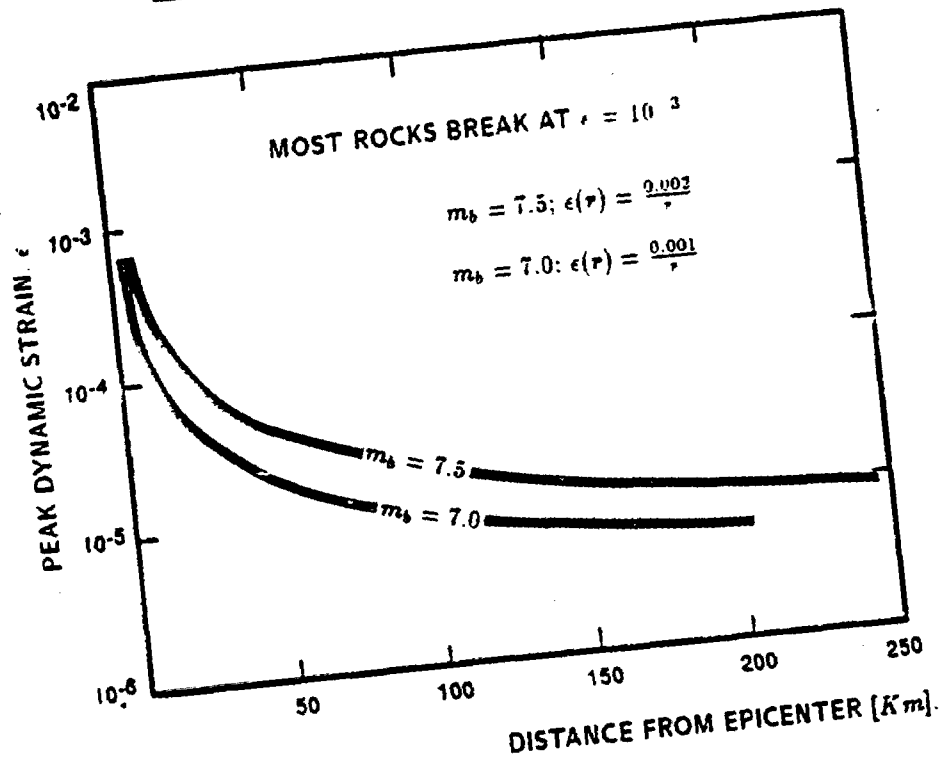


Plot of  $\delta^{18}\text{O}$  versus  $\delta^{13}\text{C}$  values of calcites from Yucca Mountain. From Szabo and Kyser (1985).



Comparison of contemporary and late Quaternary in-situ temperatures at Yucca Mountain

PEAK DYNAMIC STRAIN FROM WOOD (1985)



DURATION OF STRESSING AND WIDTH OF STRESSED INTERVAL

FREQ. SEISMIC WAVE	WIDTH OF STRESSED INTERVAL $\frac{\lambda}{4}$	TIME OF STRESSING
.5 Hz 10 Hz 100 Hz	3.0 Km .15 Km .015 Km	.5 SEC. .025 SEC. .0025 SEC.

PORE PRESSURE INCREASE

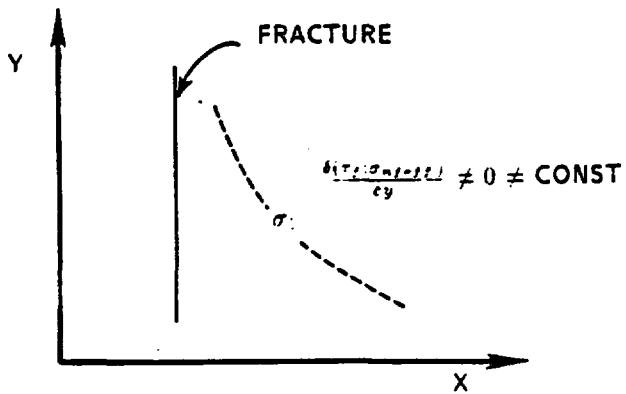
$$\Delta p = \frac{1}{\beta} \cdot \frac{\Delta \sigma}{\nu}$$

ASSUME  $\epsilon = \frac{\Delta \sigma}{\nu} = 10^{-4}$

$$\beta = 4.5 \times 10^{-5} (\text{Mpa})^{-1}$$

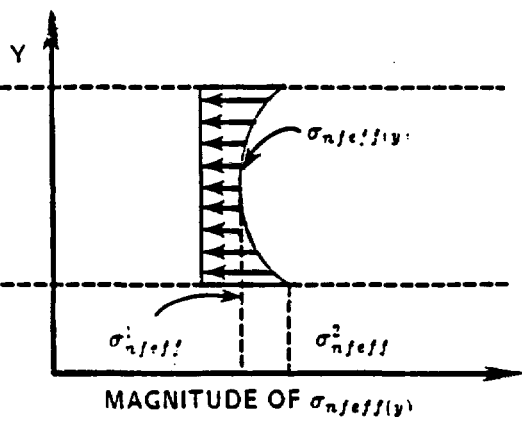
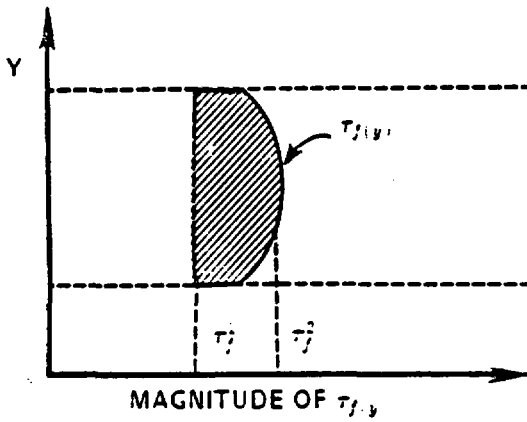
$$\Delta p = 2.3 \text{ Mpa} = 333 \text{ psi}$$

Potential increase of pore pressure caused by the vibratory ground motion.

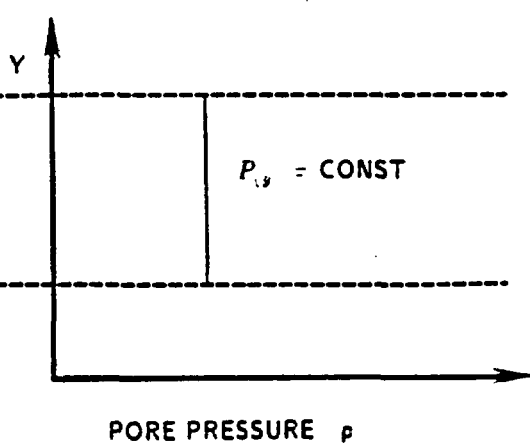
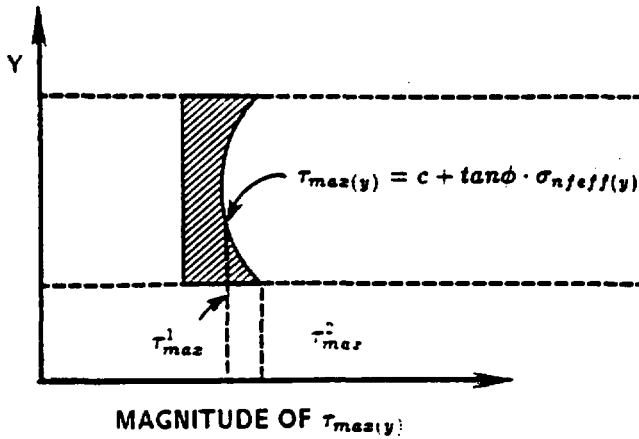


ALONG THE FRACTURE. GRADIENTS OF NORMAL AND SHEAR STRESS EXIST

INITIAL RELATIONSHIP BETWEEN IN-SITU STRESS AND FRACTURE

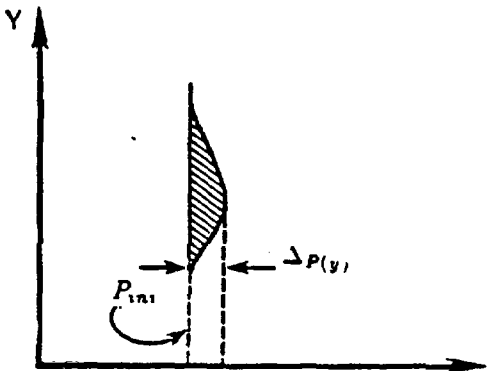


INITIAL DISTRIBUTION OF  $\tau_f(y)$  and  $\sigma_{nfeff}(y)$



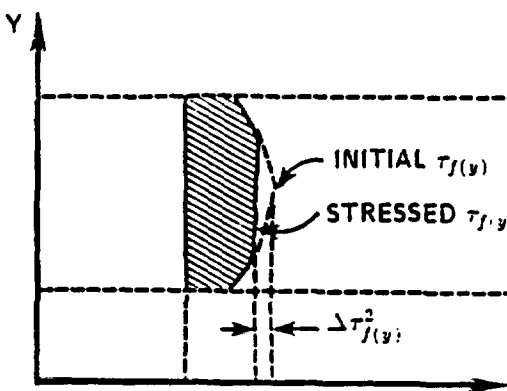
INITIAL DISTRIBUTION OF  $\tau_{max}(y)$  and  $p$

Assumed initial in-situ stress configuration along a fracture.

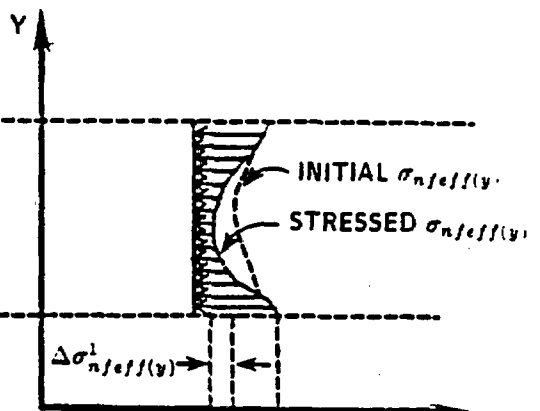


PORE PRESSURE -  $P$

PORE PRESSURE BUILD-UP.

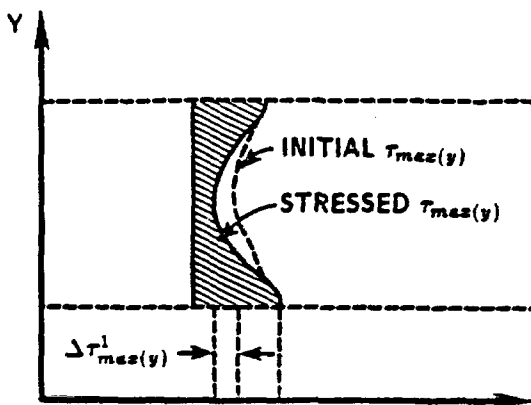


MAGNITUDE OF  $\tau_f(y)$



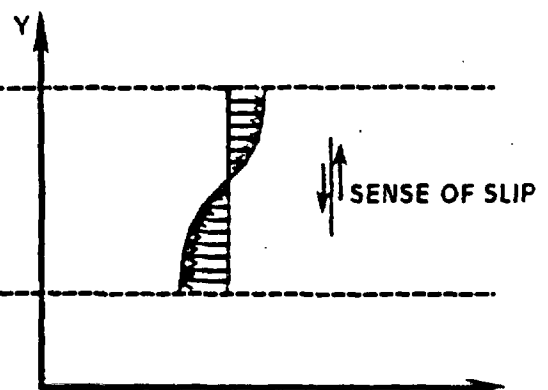
MAGNITUDE OF  $\sigma_{n,eff}(y)$

PERTURBED DISTRIBUTION OF  $\tau_f(y)$  AND  $\sigma_{n,eff}(y)$



MAGNITUDE OF  $\tau_{max}(y)$

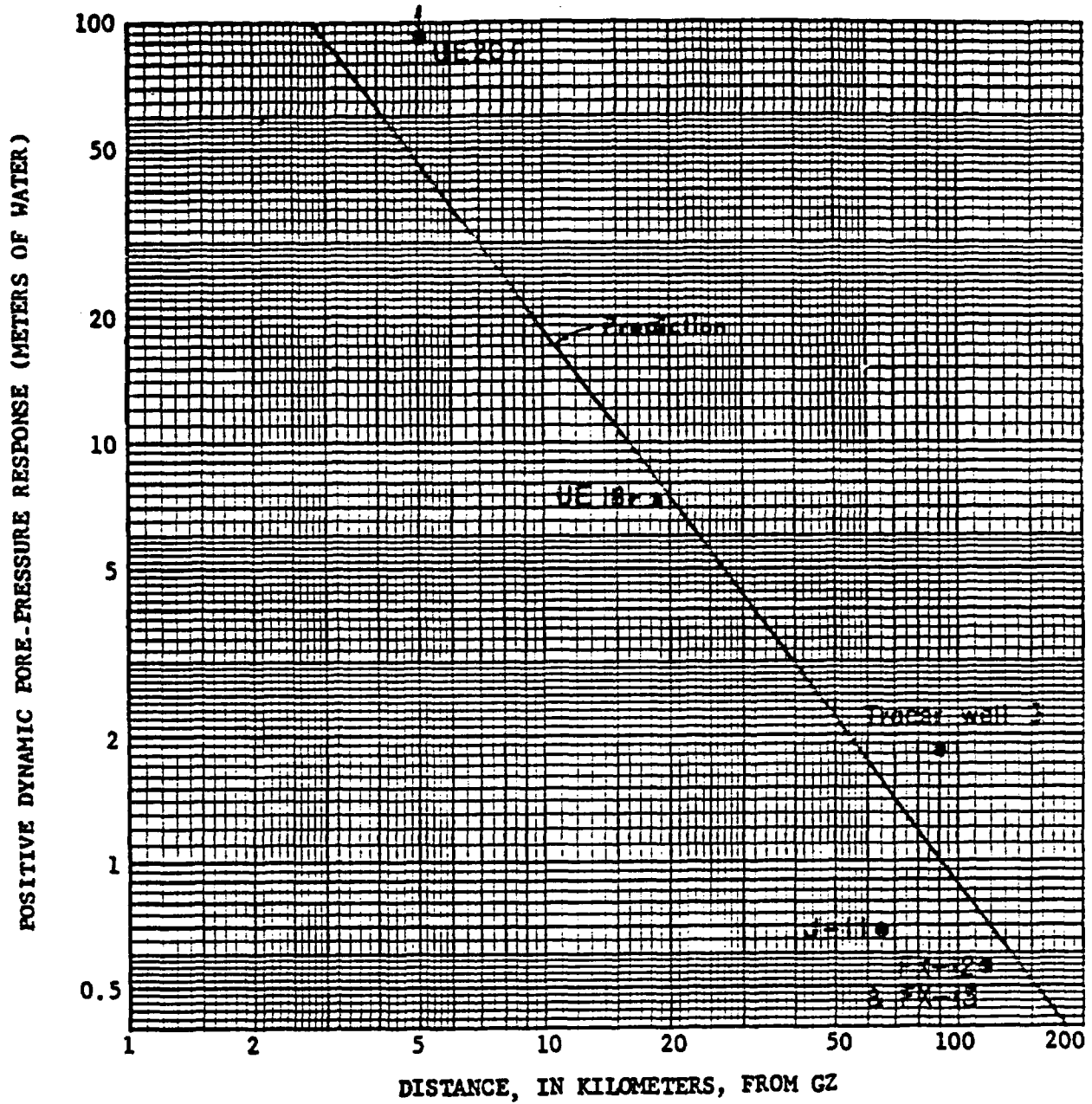
CHANGE IN MAGNITUDE OF  $\tau_{max}(y)$



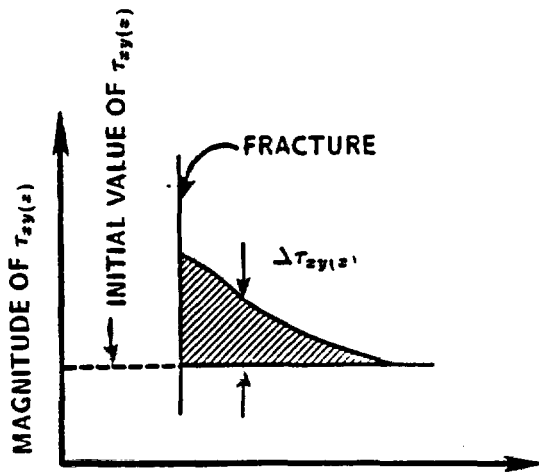
STRESS GRADIENT  $\sigma_n^i(y)$

RESULTING GRADIENT OF NORMAL STRESS

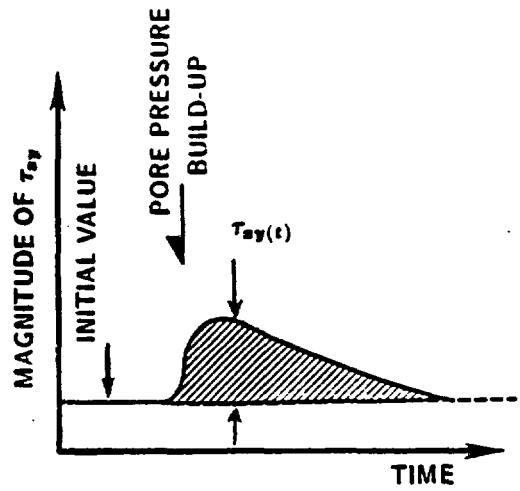
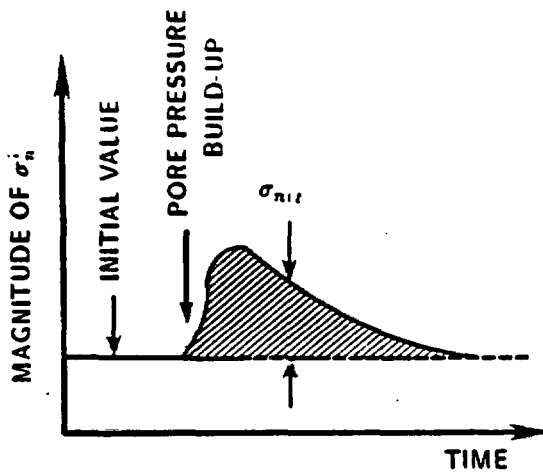
Perturbation of the in-situ stress caused by local build-up of pore pressure -  $\Delta P(y)$ .



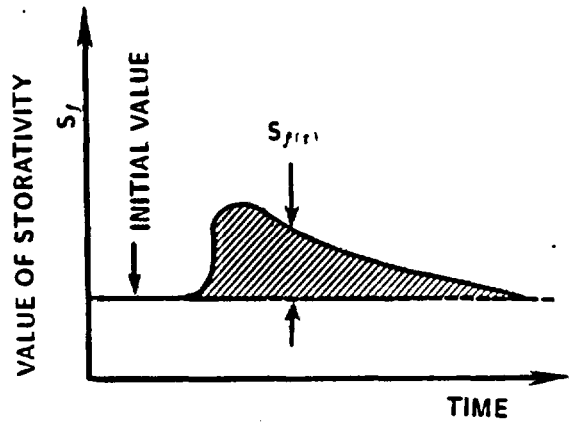
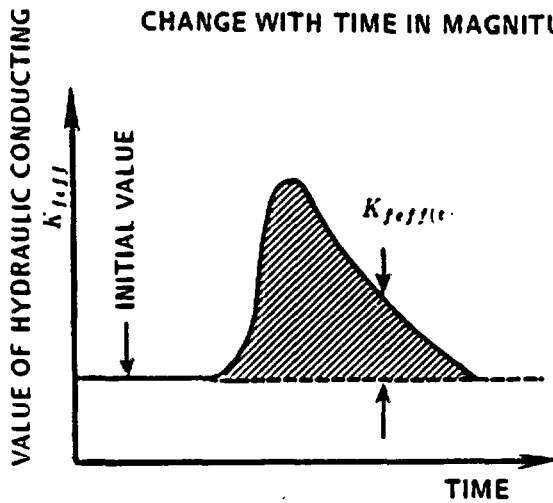
Dynamic fluid overpressure produced by the shock wave of the Handley detonation. From Dudley et. al. (1971)



RESULTING GRADIENT OF SHEAR STRESS



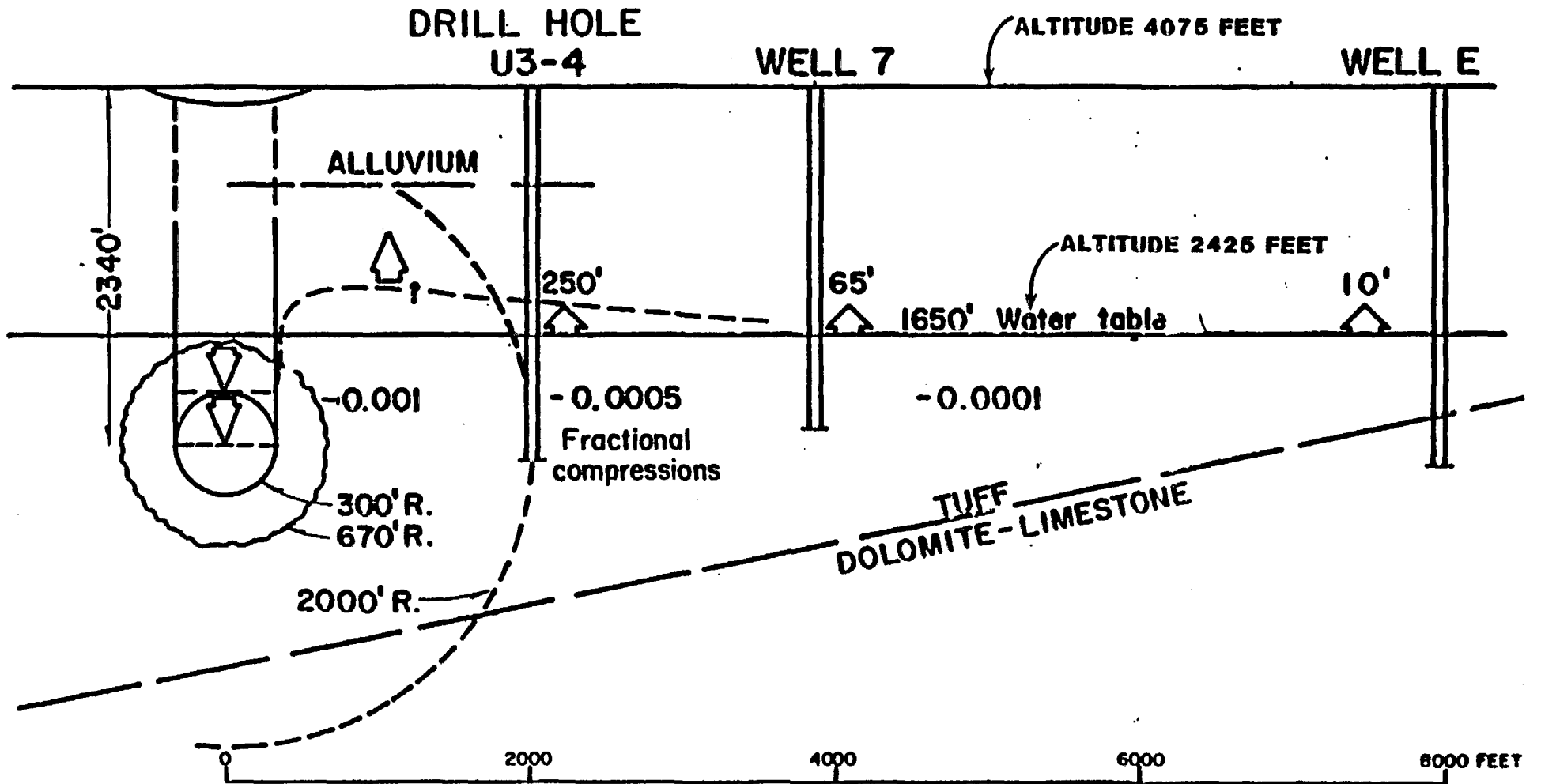
CHANGE WITH TIME IN MAGNITUDE OF  $\sigma_n^1$  AND  $\tau_{xy}$  FOR A GIVEN POINT (x,y).



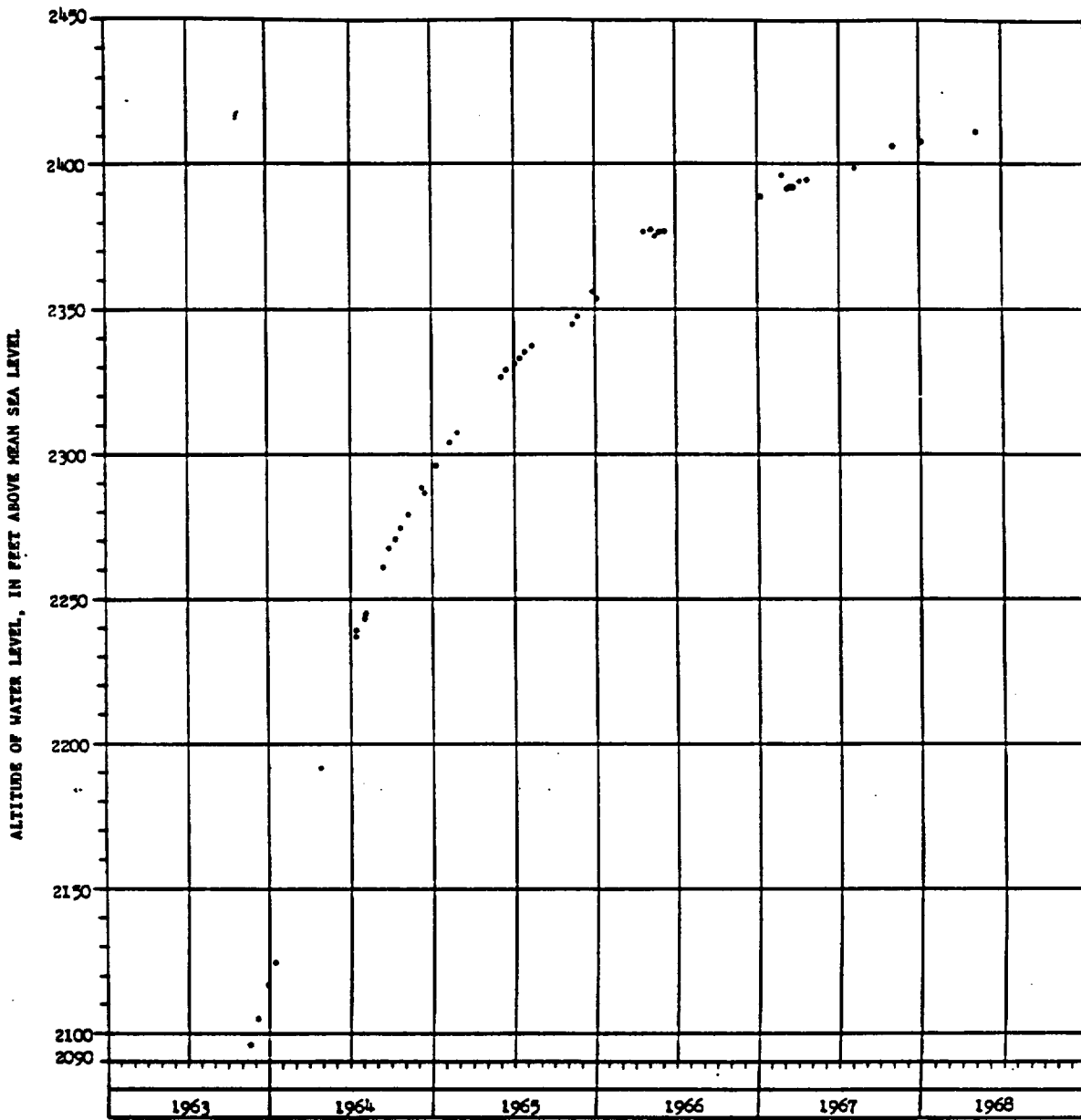
CHANGE WITH TIME IN MAGNITUDE OF FRACTURE  $K_{eff}$  AND  $S_f$

Perturbation of the in-situ stress caused by local build-up of pore pressure and resulting change in hydraulic parameters.

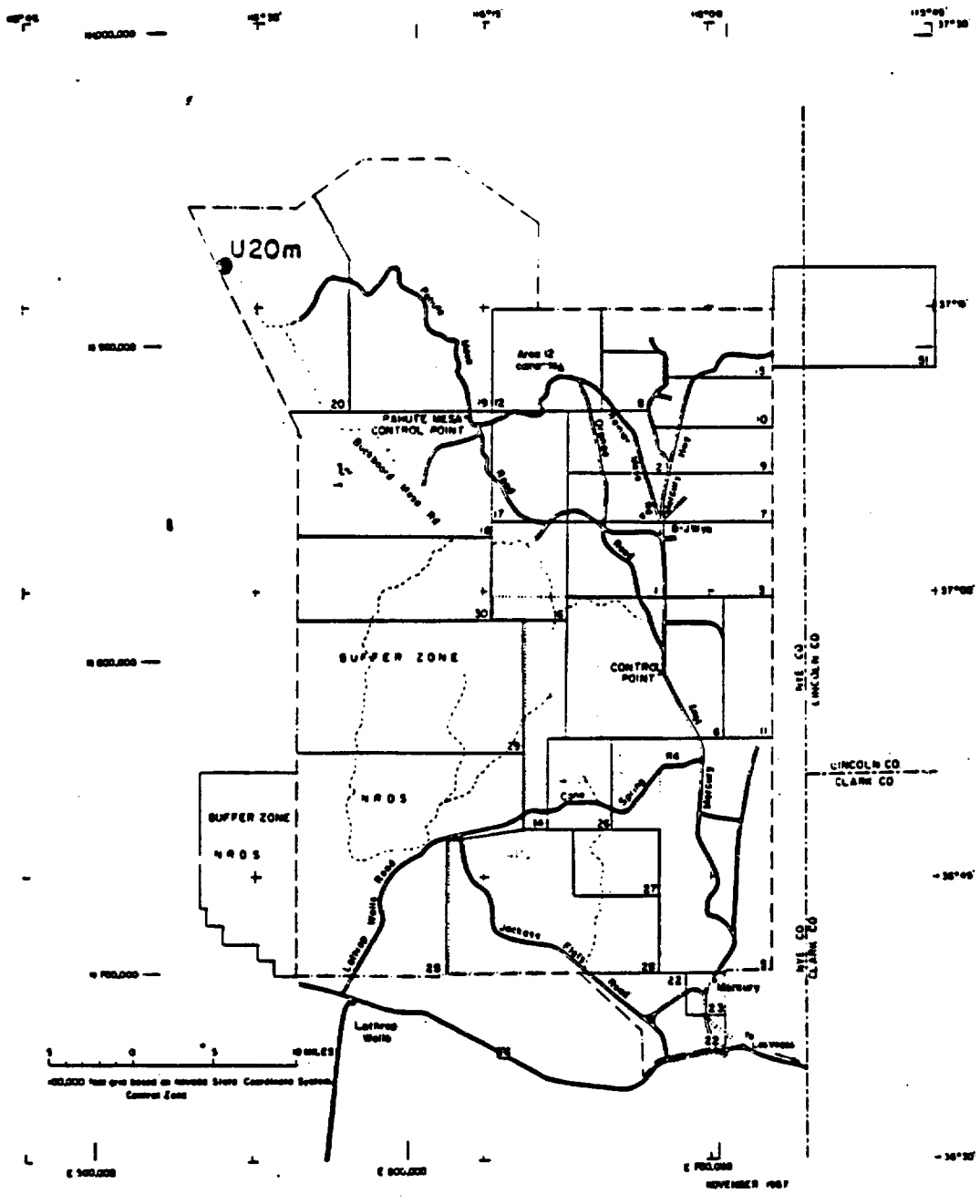




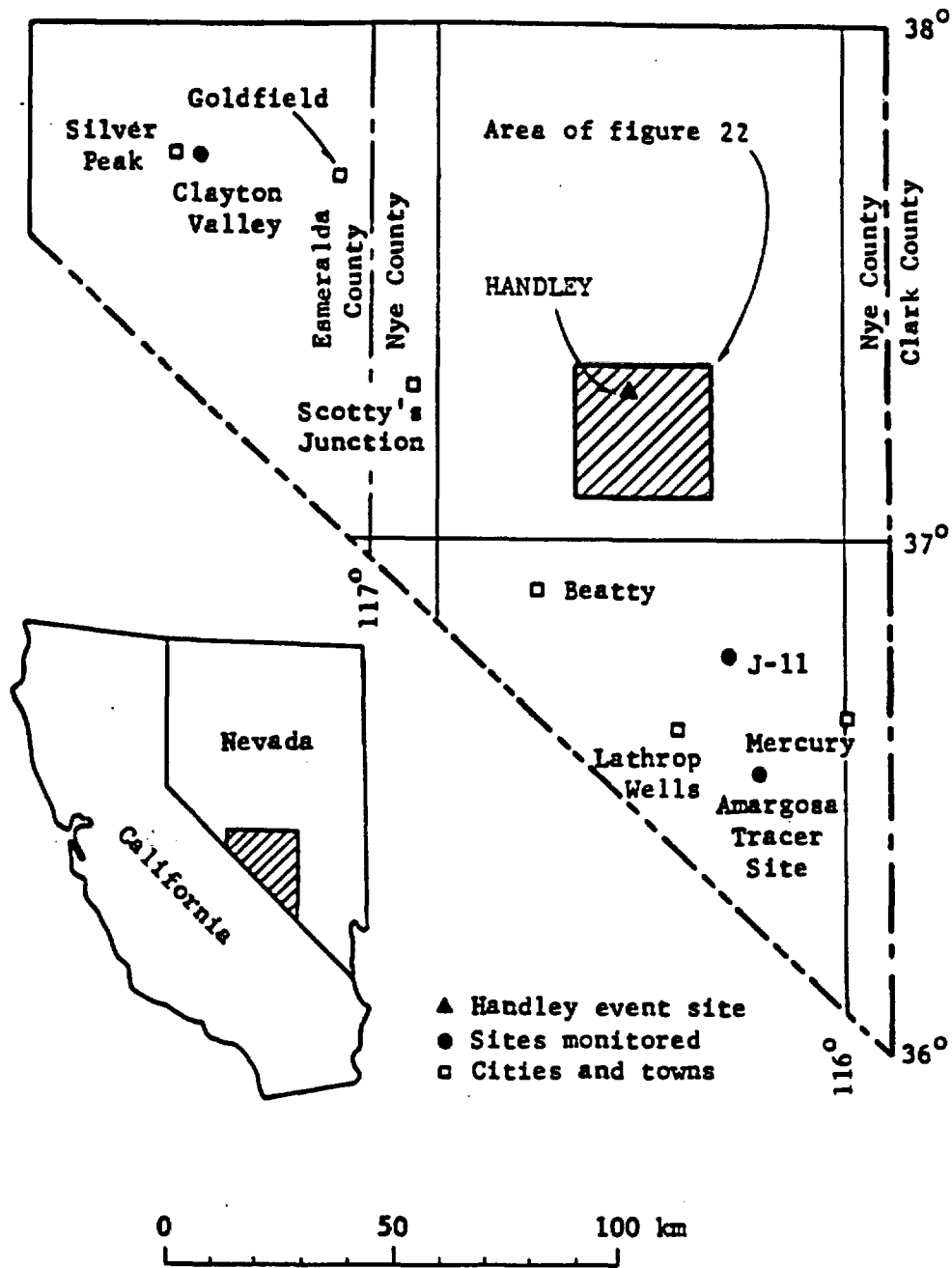
Dynamic fluid overpressure caused by the Bilby shock wave. From Corchary and Dinviddie (1975).



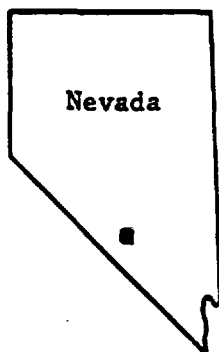
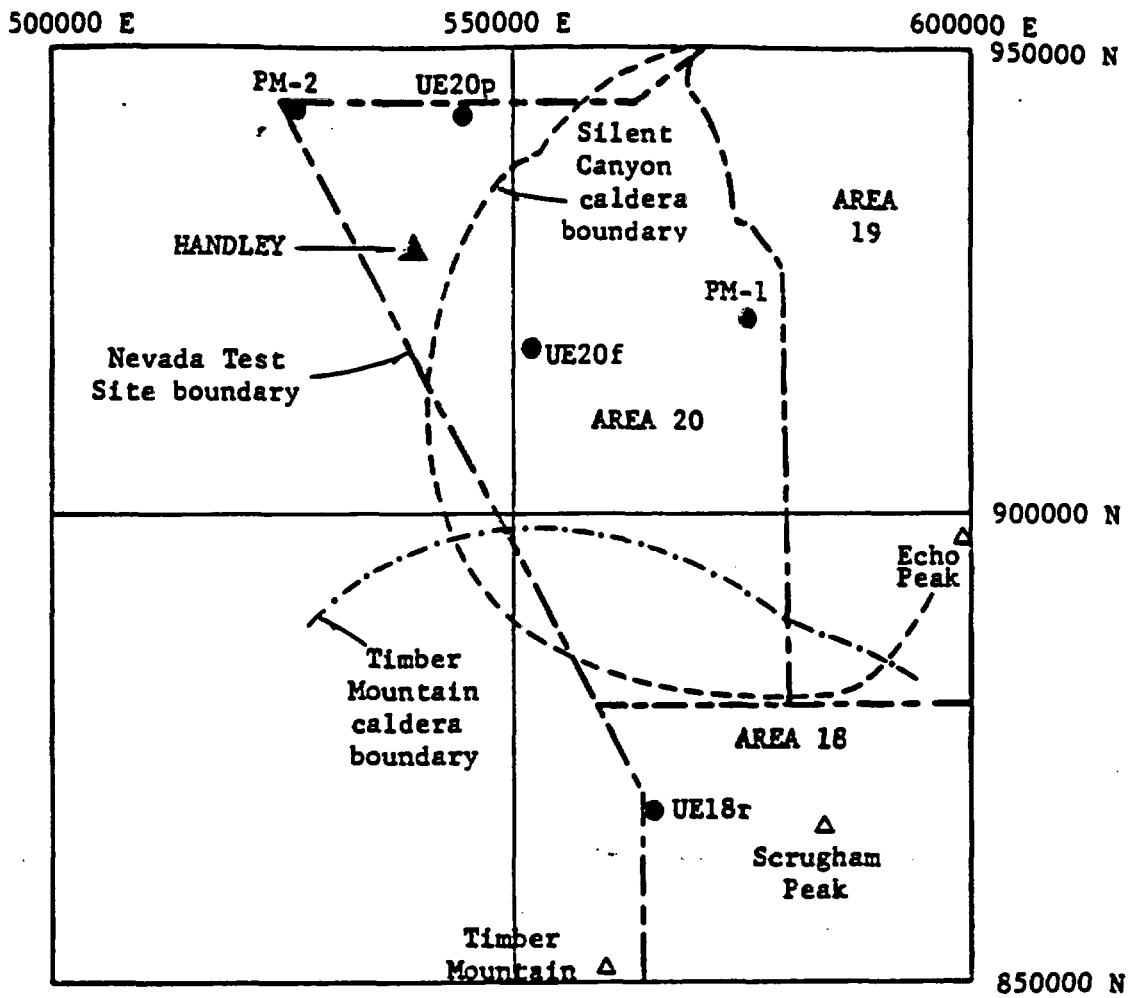
Fluid level rise in U-3cn PS#2. From Garber (1971).



Location of detonation site of the Handley nuclear device. From Morris (1971).

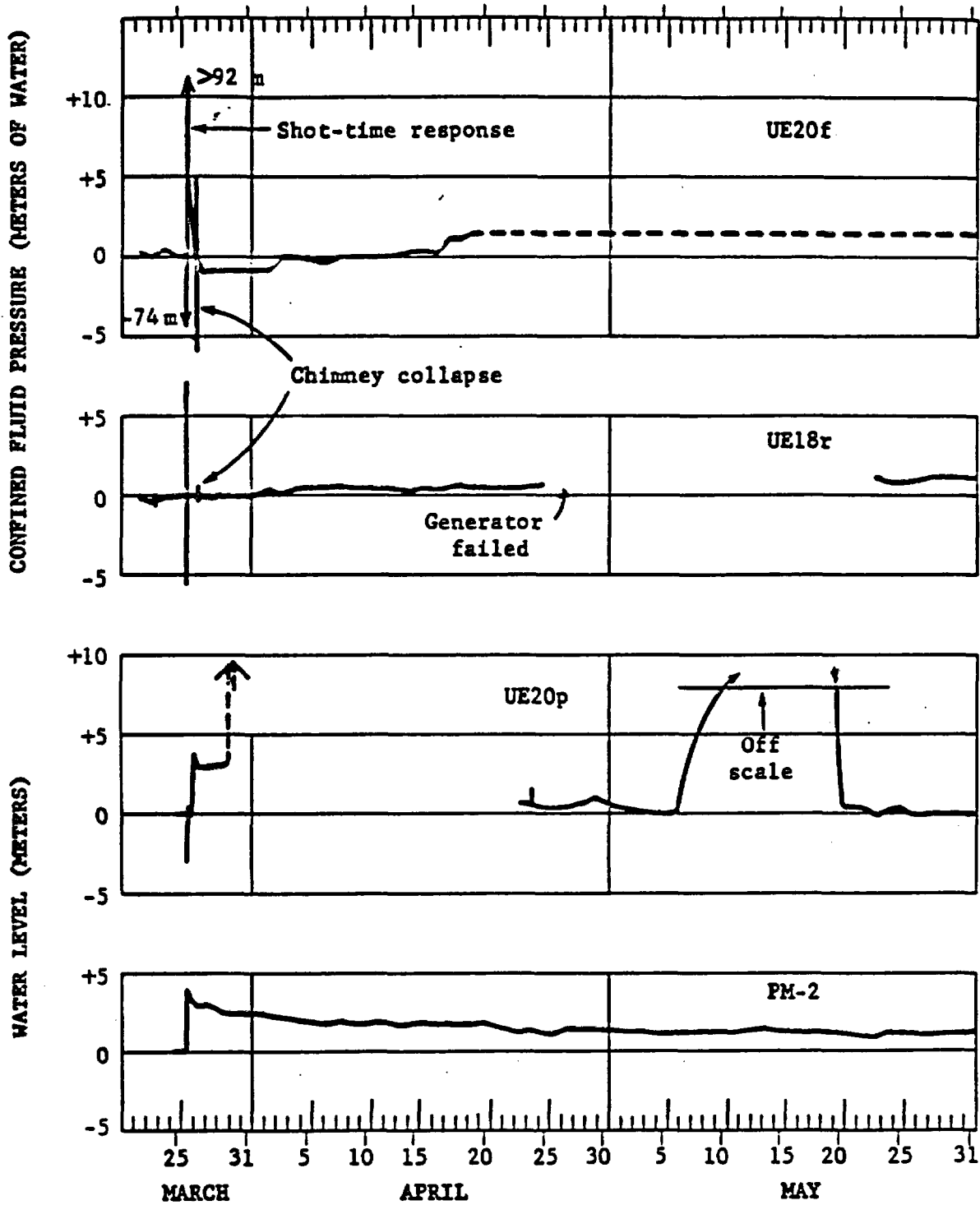


Location of offsite wells monitored during the Handley Event. From Dudley et. al. (1971).



- ▲ Handley event site
- Wells monitored
- △ Mountain peaks

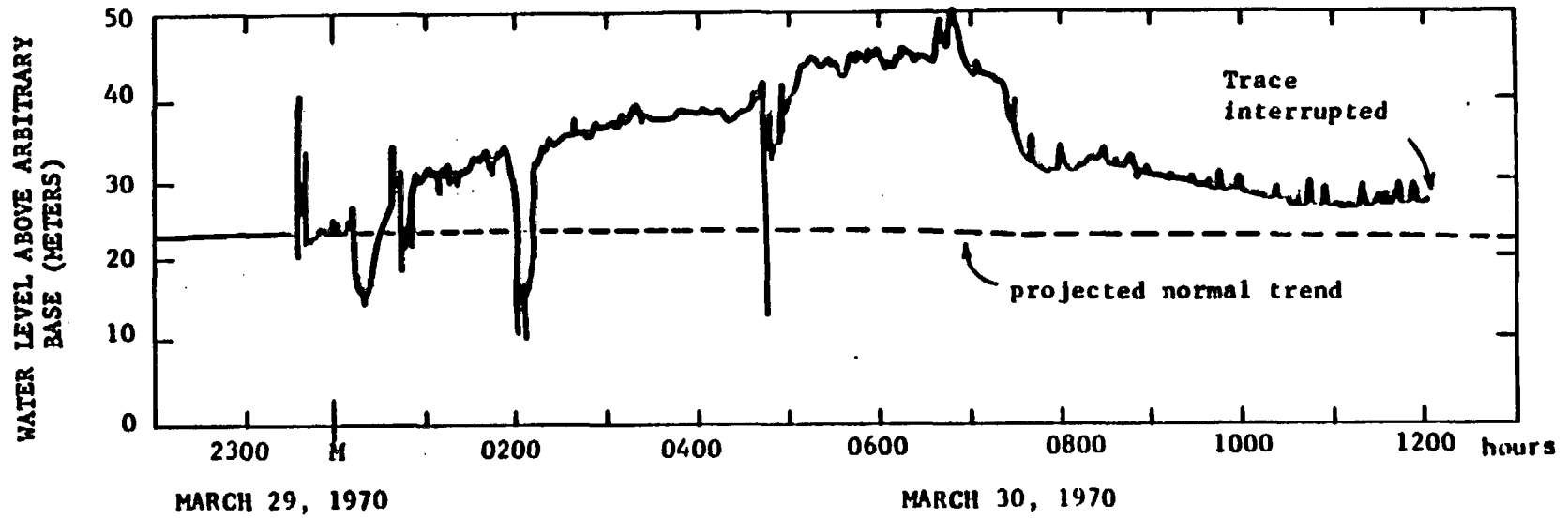
Location of monitoring wells in the Pahute Mesa. Handley detonation. Dudley et. al. (1971)



Hydrologic response in Pahute Mesa to the Handley detonation. From Dudley et. al. (1971)

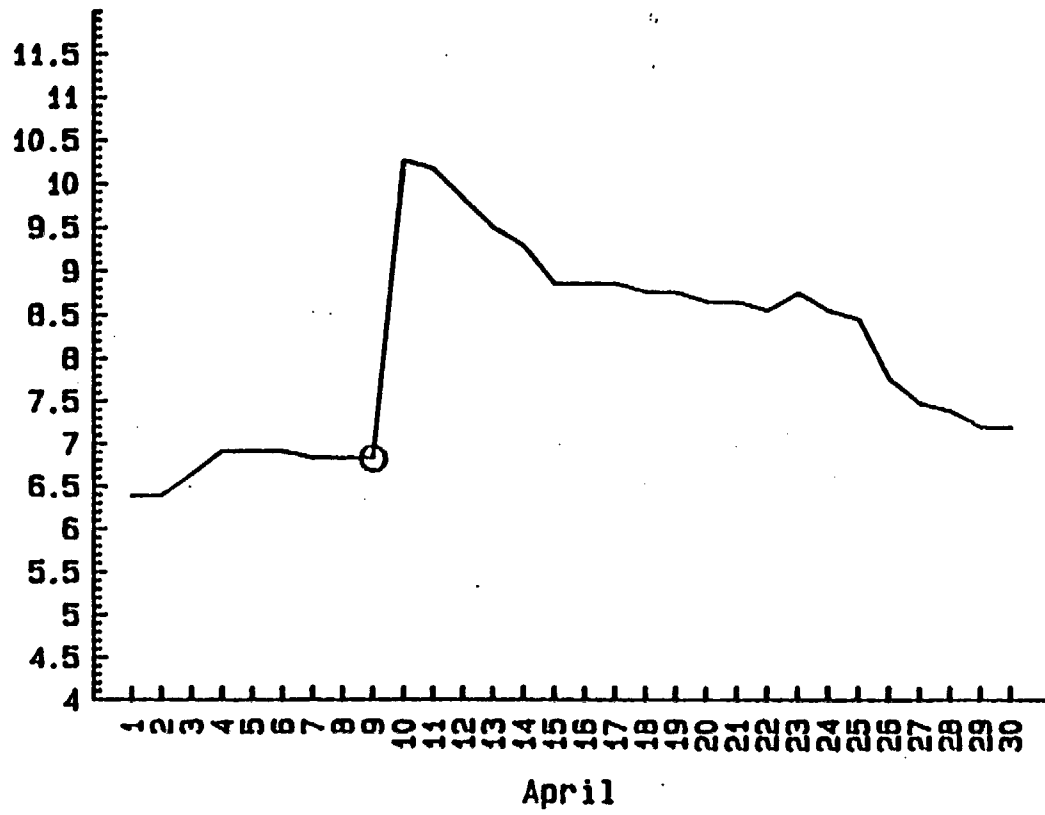
<u>Time postshot (in minutes)</u>	<u>Remarks</u>
3.4	+15.4 m to -28.7 m arrival.
3.4- 5.0	Numerous excursions to $\pm 10$ m.
5.0- 7.4	Smooth decay of primary step.
7.4- 12.2	Continuous activity, including excursion of +24.5 m to -28.7 m at 8.7 min.
12.2- 15.3	Smooth decay of primary step.
15.3- 18.8	Continuous activity with prominent peaks at 15.9, 17.5, and 18.2 min.
18.8- 23.0	Smooth decay of primary step.
23.0	Arrival of +9.8 m to -12.2 m excursions and secondary pressure step of +15.4 m.
23.0- 27.1	Erratic and cyclic decay of secondary pressure step to -9.5 m.
27.1- 30.0	Erratic recovery to +4.5 m.
30.0- 31.0	Decline to primary decay curve.
31.0-214.0	Continuous activity, particularly intense at 74 to 80 min., where excursions of $\pm 7$ m occur, and at 85 to 87 minutes. Ends abruptly at 214 minutes postshot (1434 hrs. PST).

Hydrologic response to the Handley Event in well UE-20f. From Dudley et. al. (1971).



Hydrologic response to the Handley Event in well UE-20p. From Dudley et. al (1971)

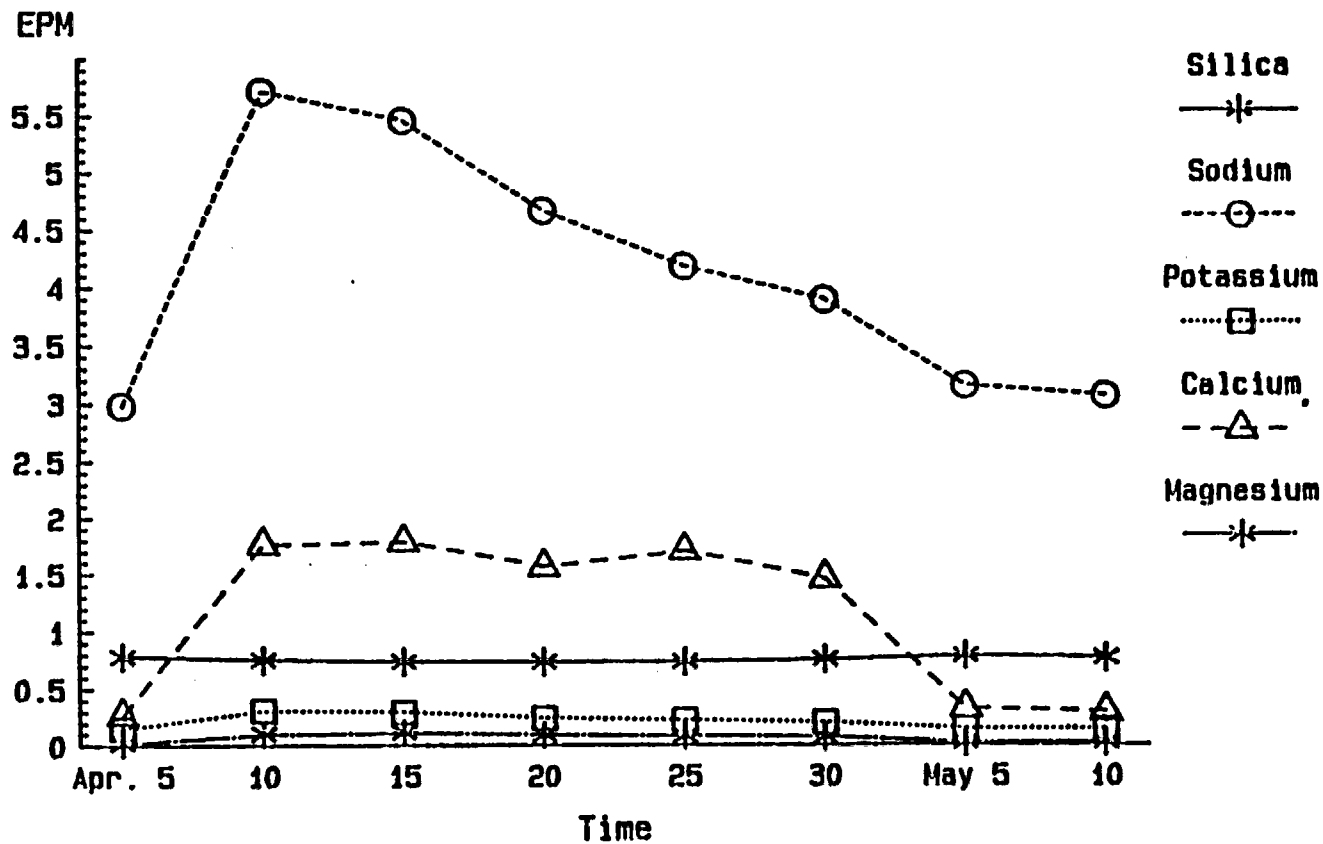
Liters/Minute



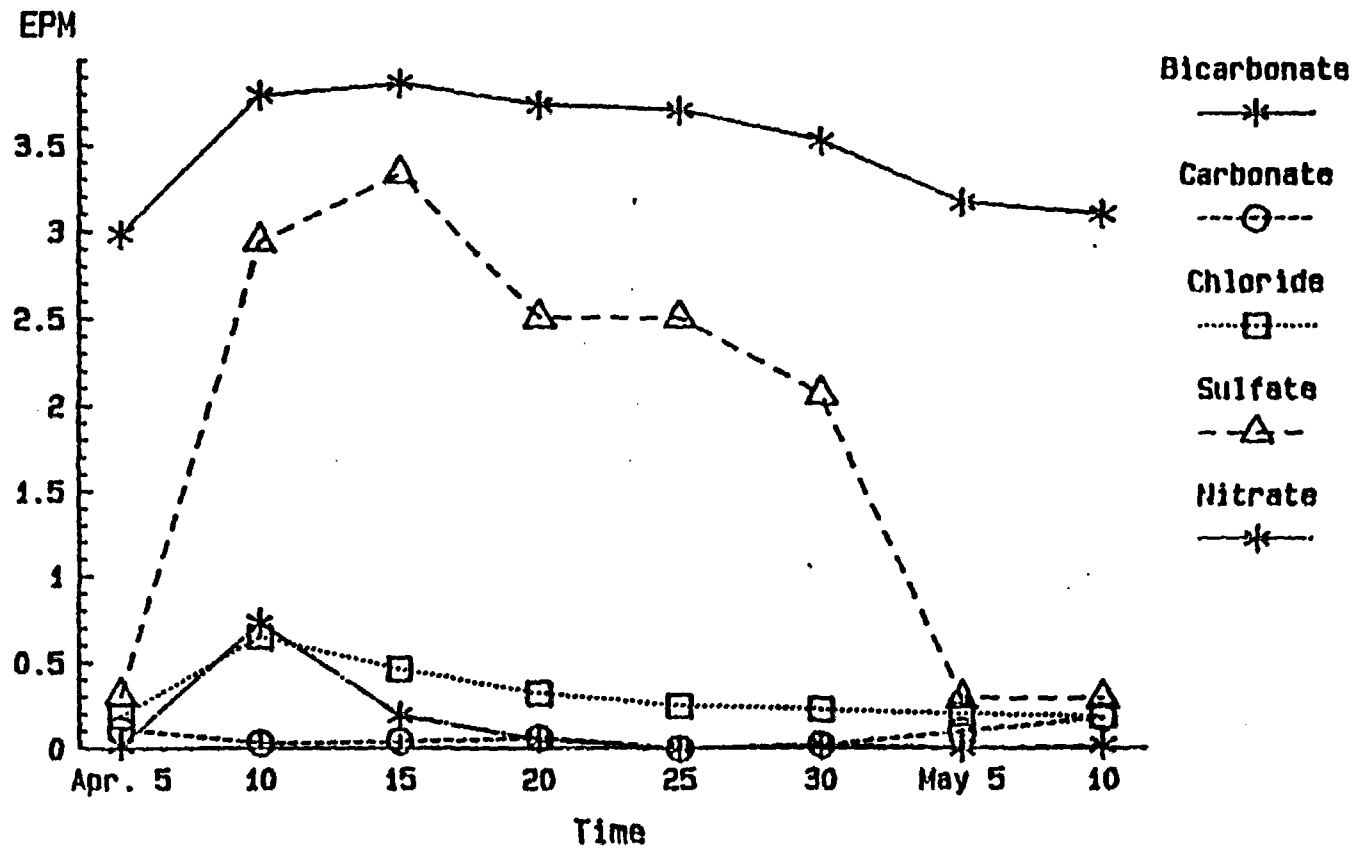
Date of Nuclear Test



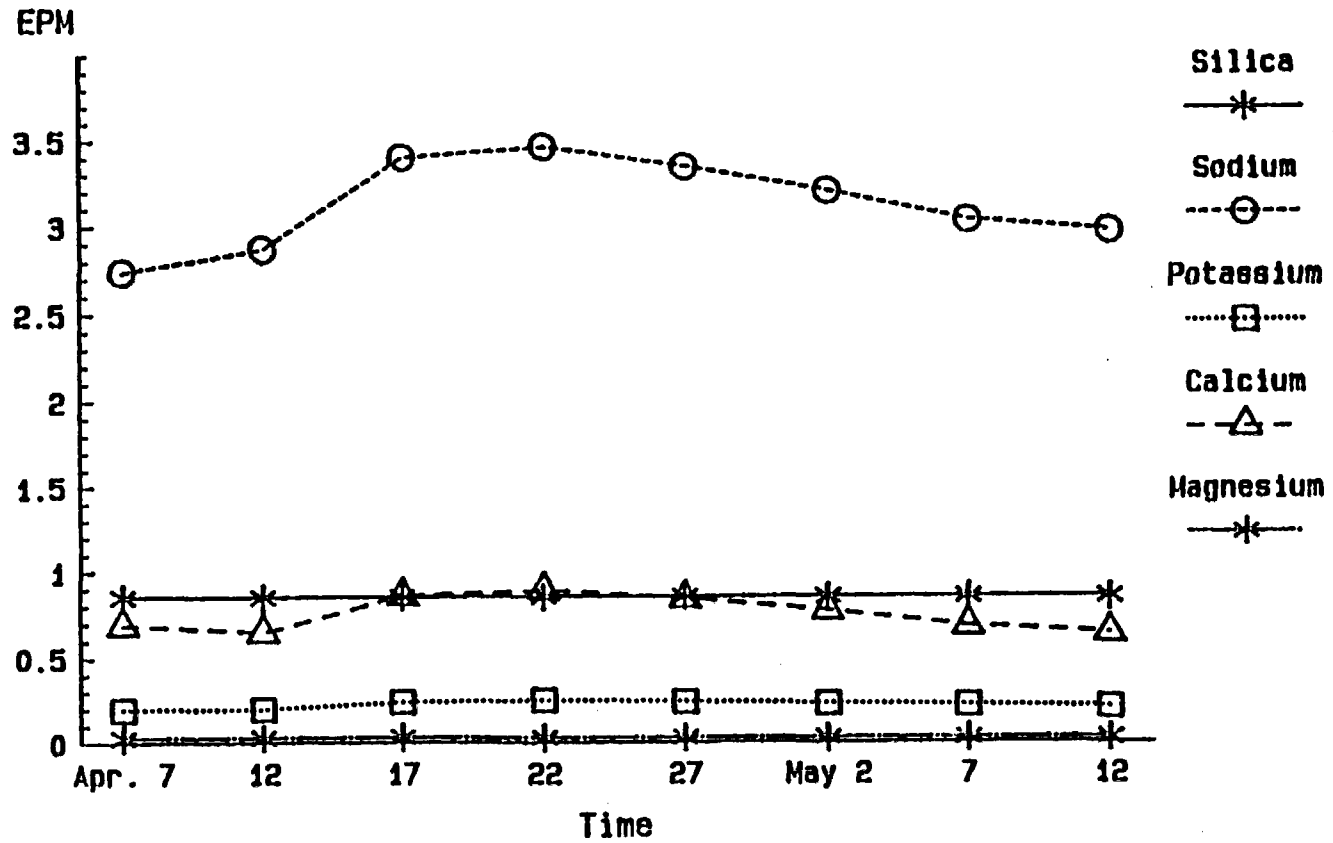
Increased discharge from a seep caused by the April 10, 1986 nuclear detonation. From Russell (1987)



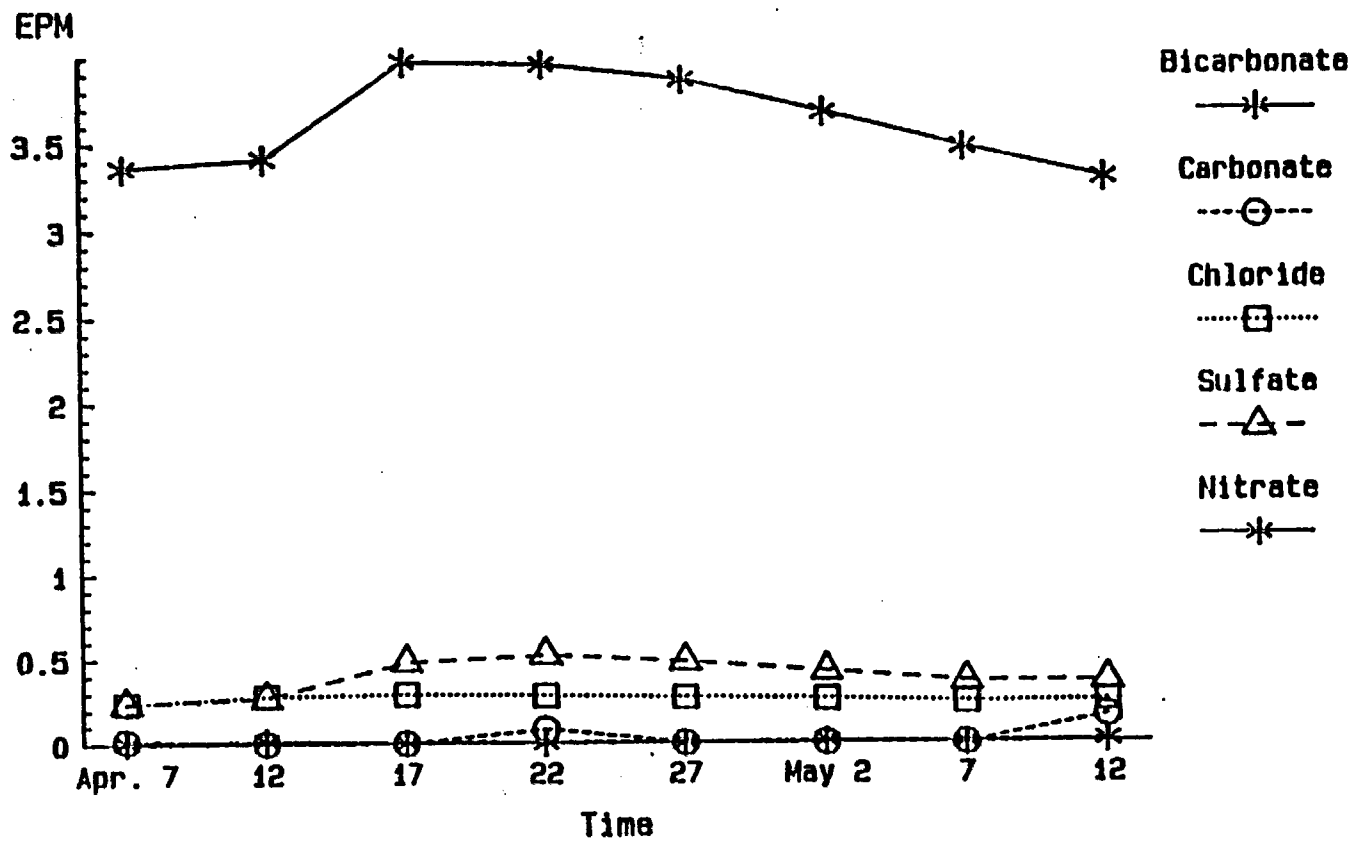
Change in aqueous chemistry caused by the April 6, 1985 detonation. From Russell (1987)



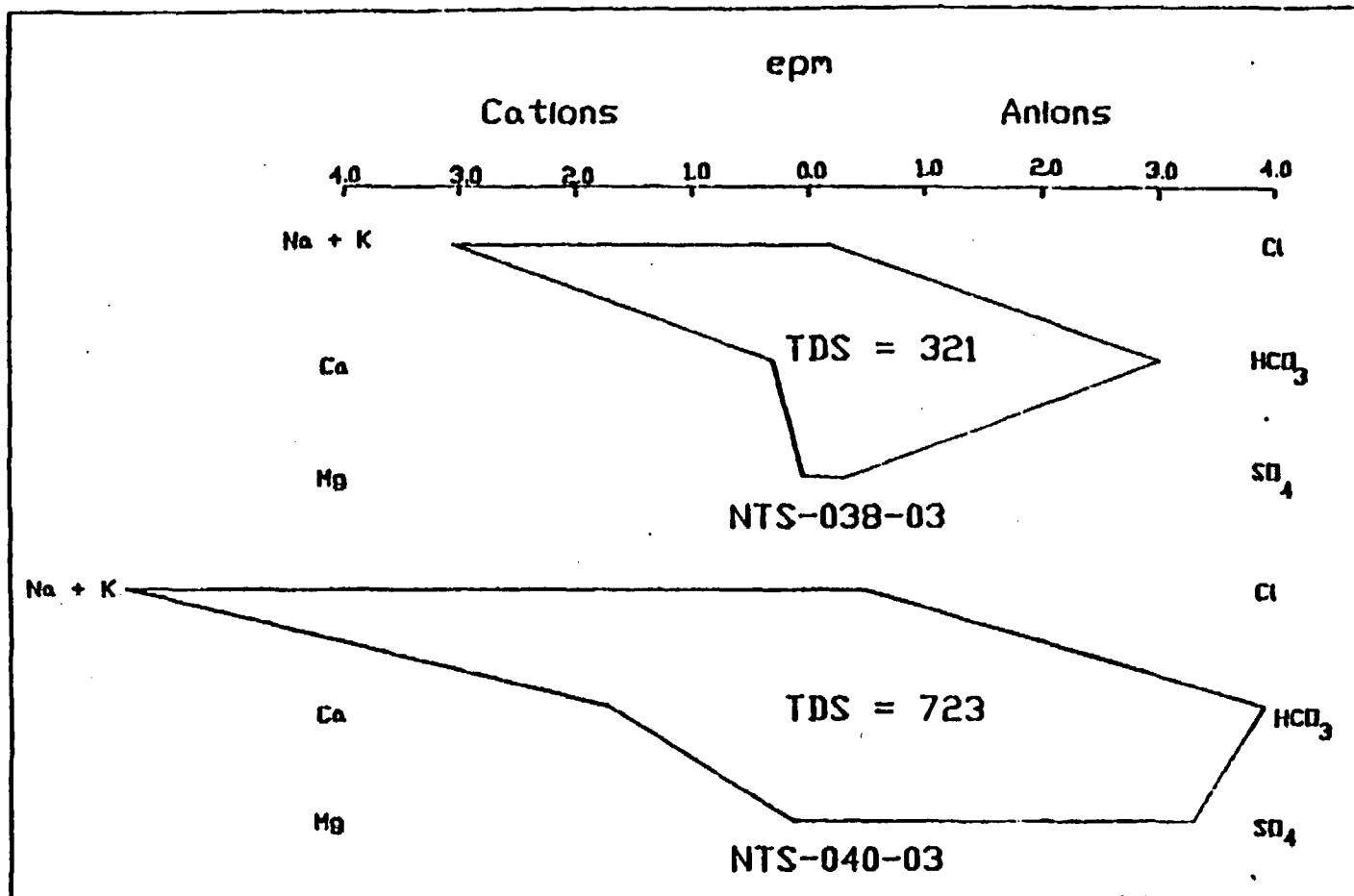
Change in aqueous chemistry caused by the April 6, 1985 detonation From Russell (1987)



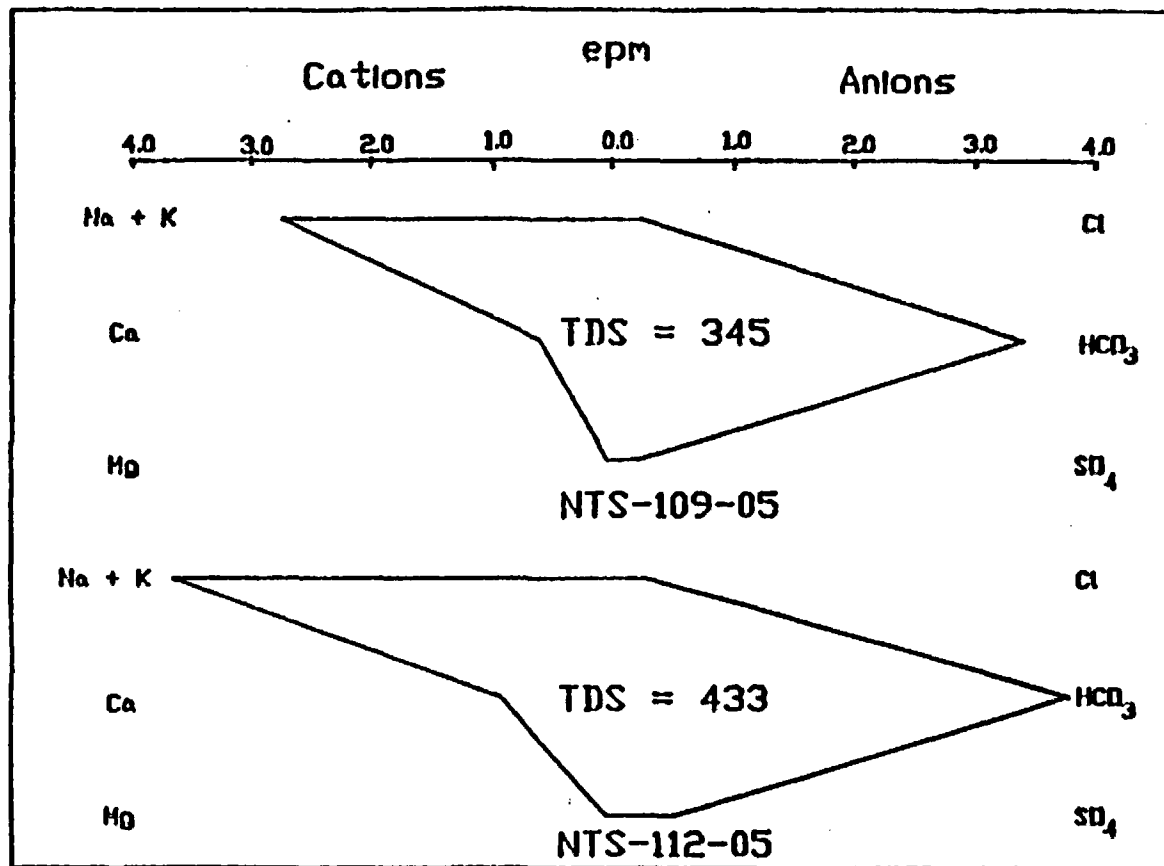
Change in aqueous chemistry caused by the April 10, 1986 nuclear detonation. From Russell (1987)



Change in aqueous chemistry caused by the April 10, 1987 nuclear detonation. From Russell (1987)

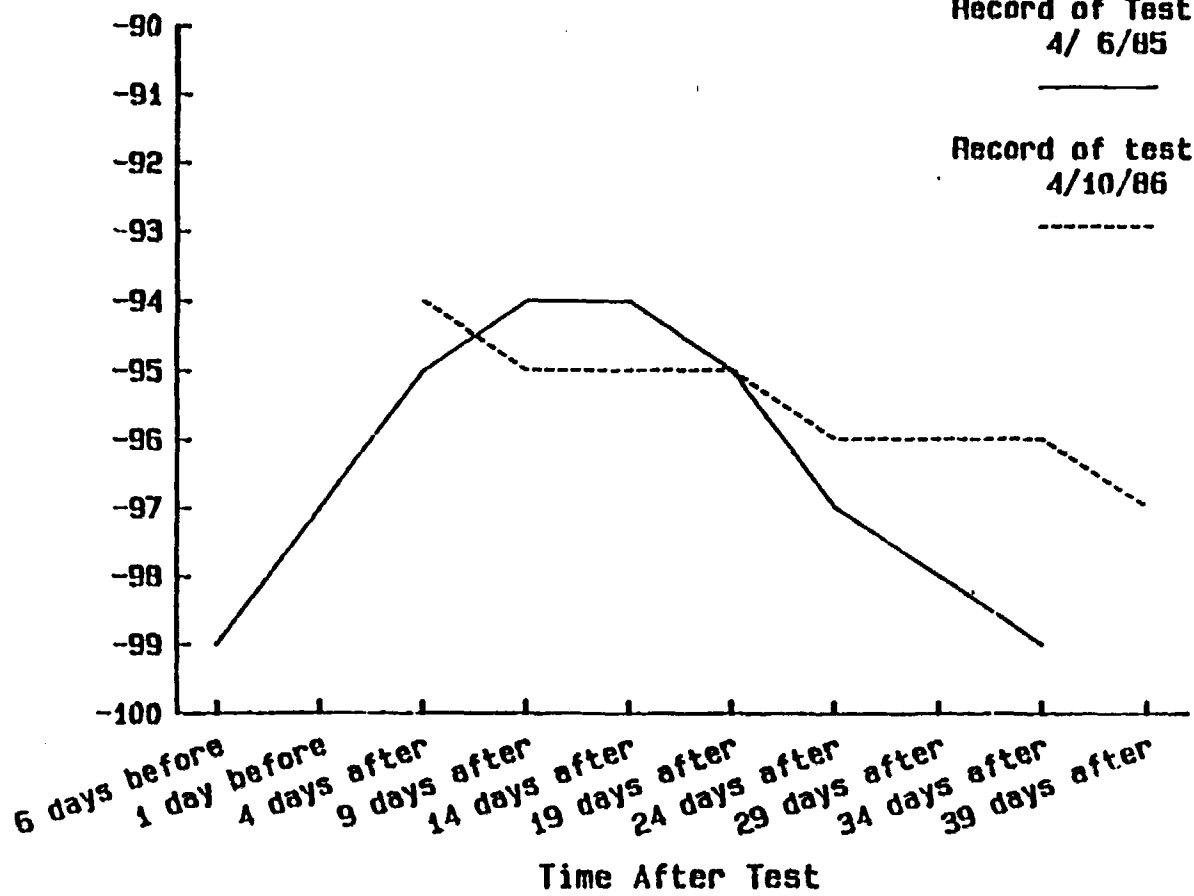


Stiff diagrams of aqueous chemistry before and after the April 6, 1985 nuclear detonation. From Russell (1987).



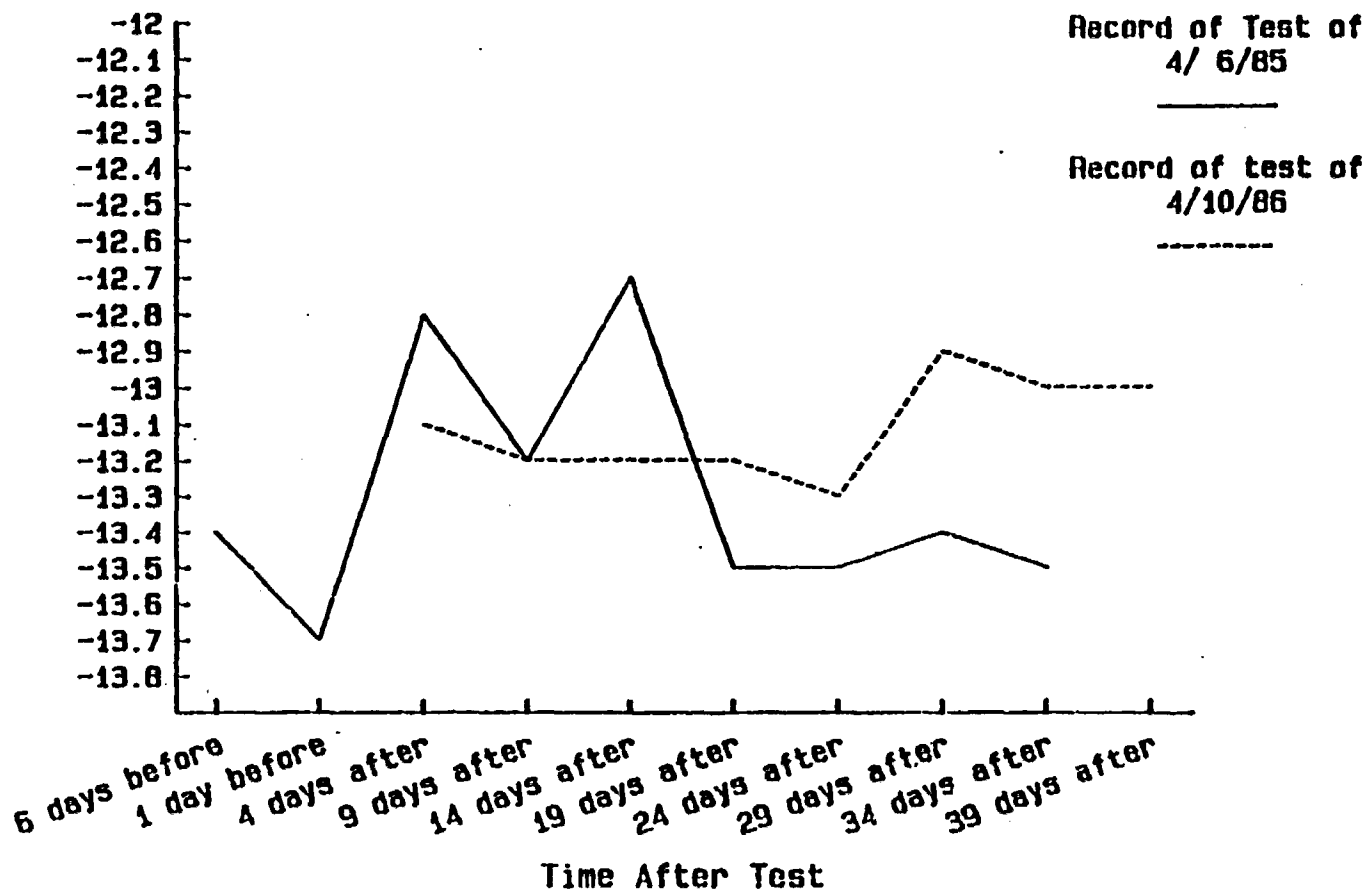
Stiff diagrams of aqueous chemistry before and after the April 10, 1986 nuclear detonation. From Russell (1987)

Del Deuterium

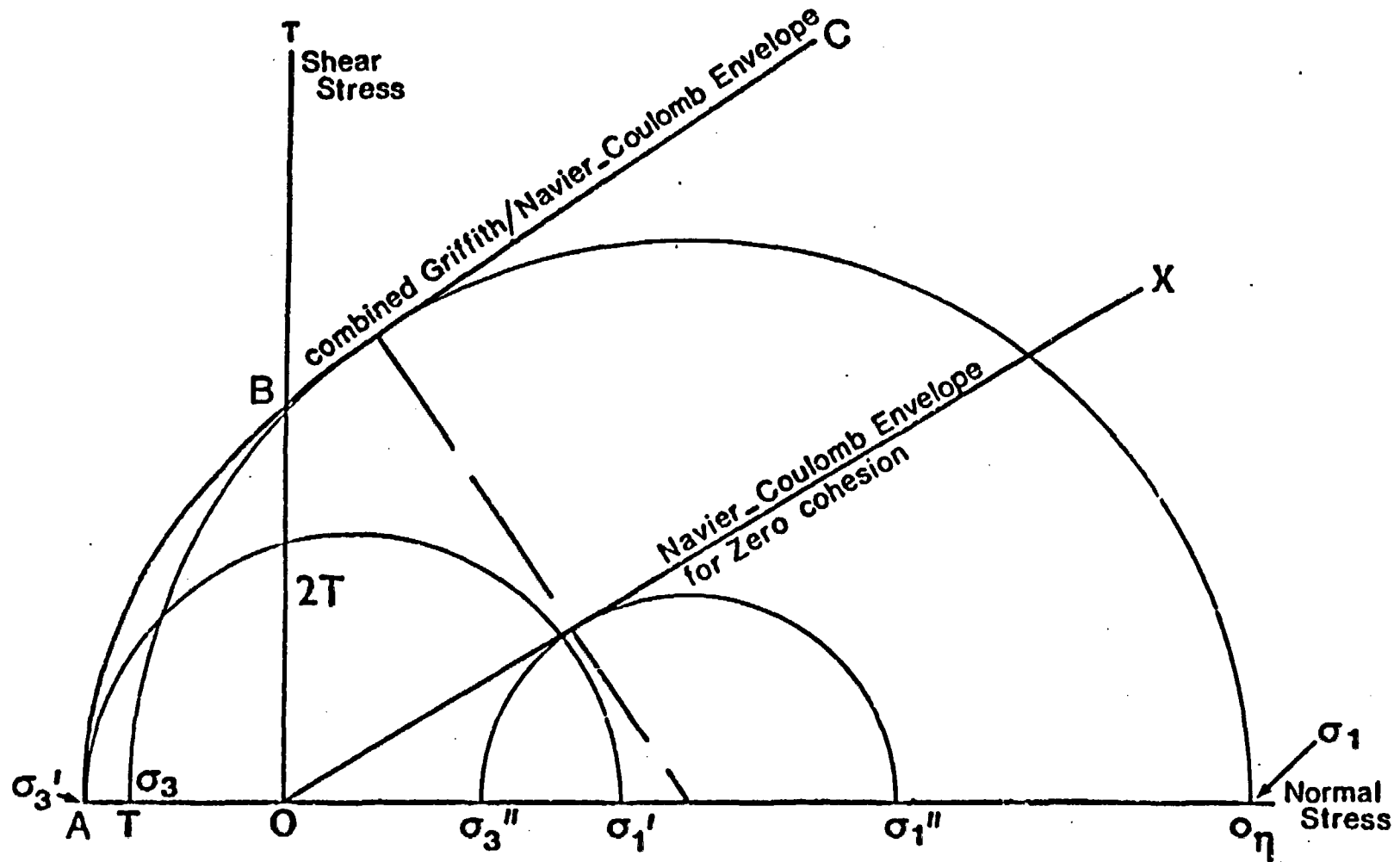


Change in deuterium content caused by two nuclear detonations From Russell (1987)

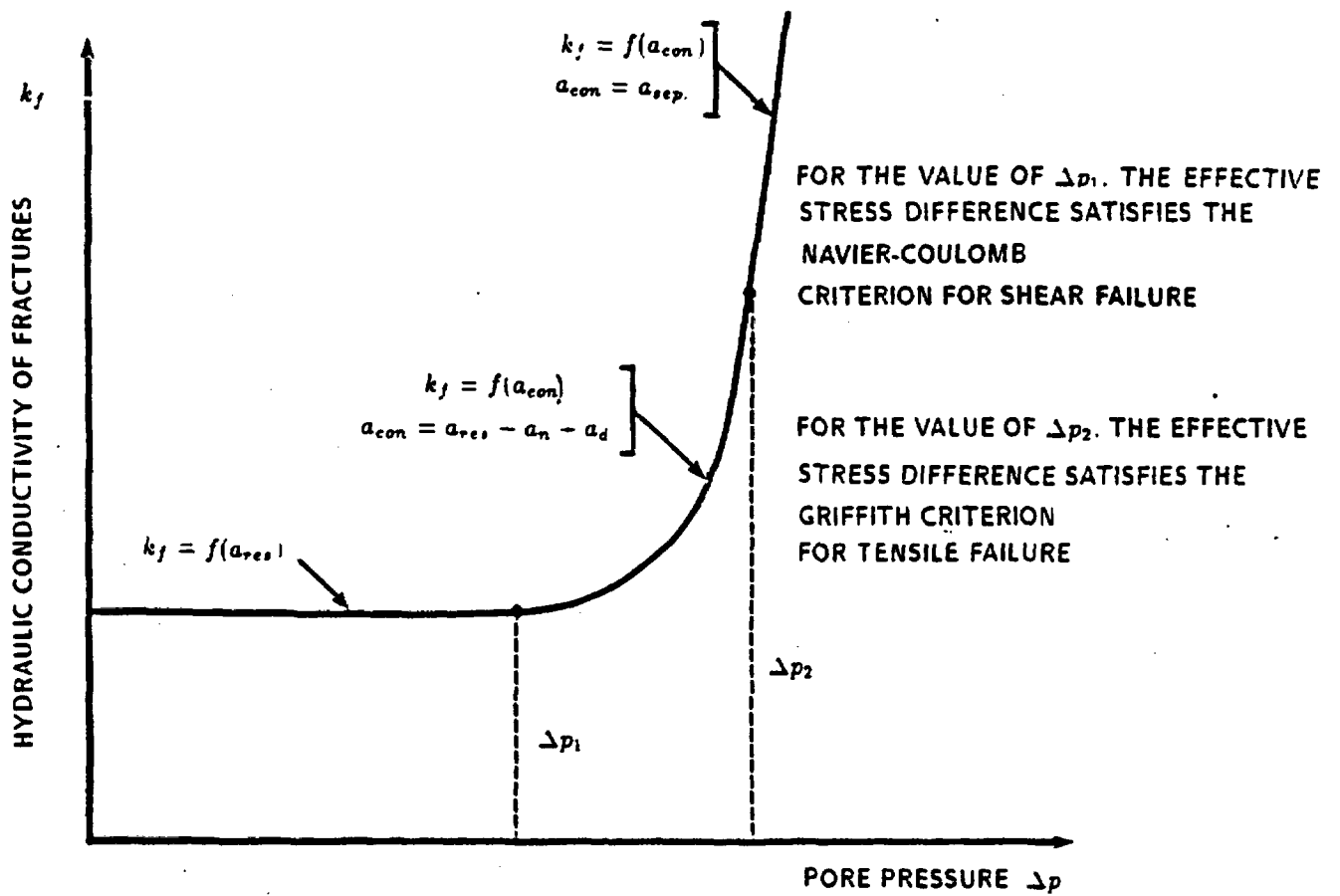
Del Oxygen-18



Change in oxygen-18 content caused by two nuclear detonations From Russell (1987)

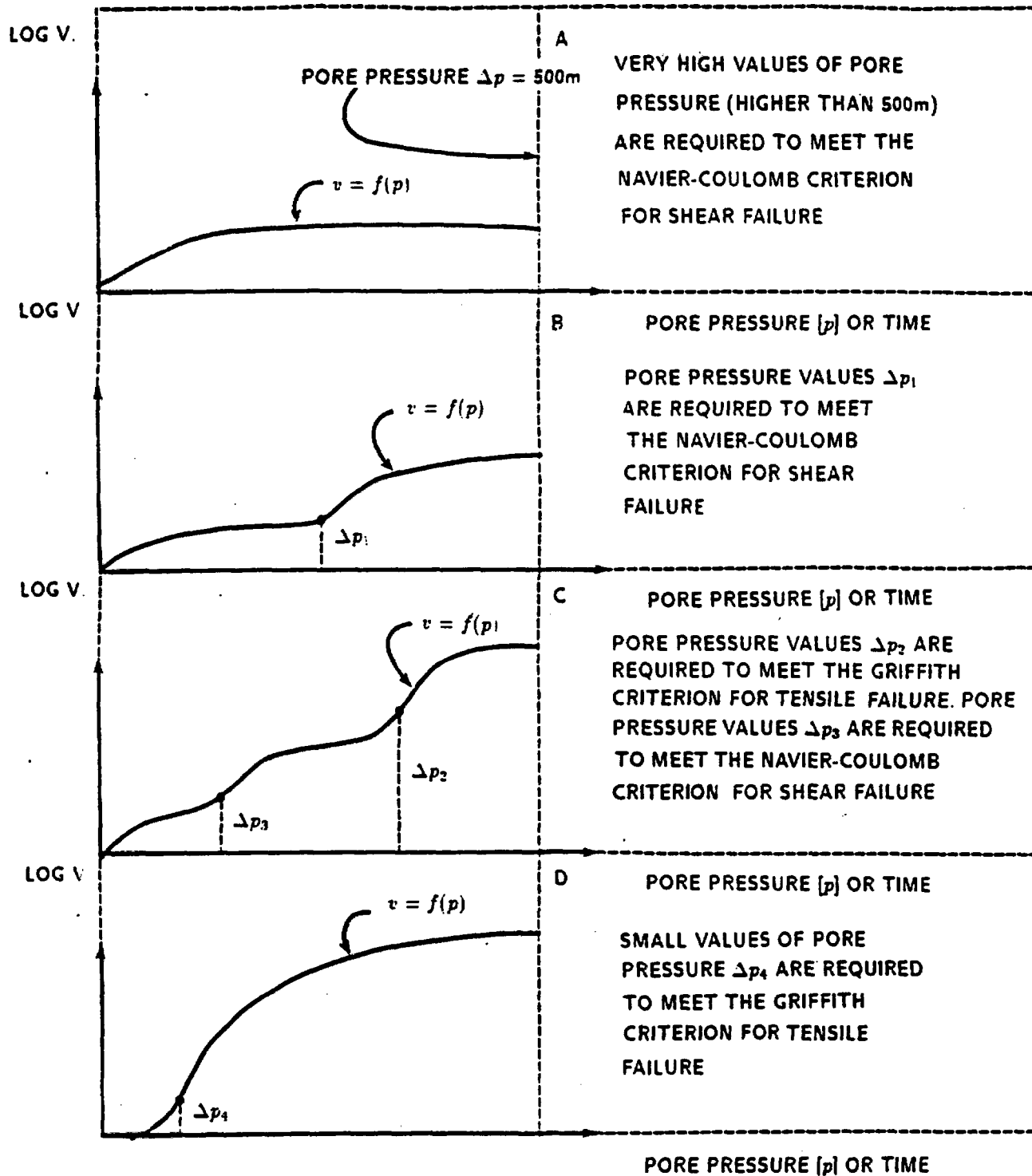


Mohr's representation of stresses in two dimensions and combined Griffith/Navier-Coulomb failure envelope

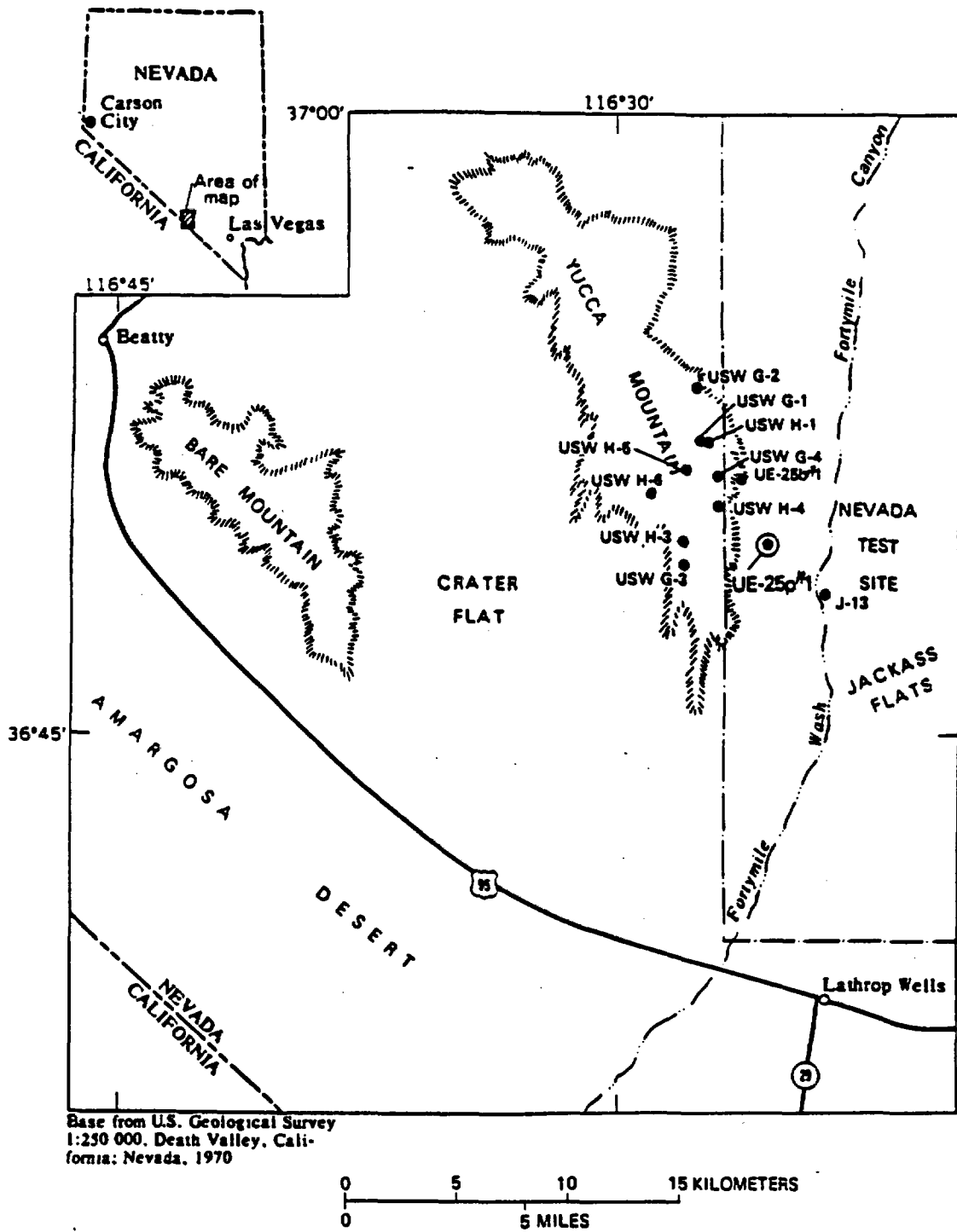


Constitutive relationship between hydraulic conductivity of fractures and pore pressure.

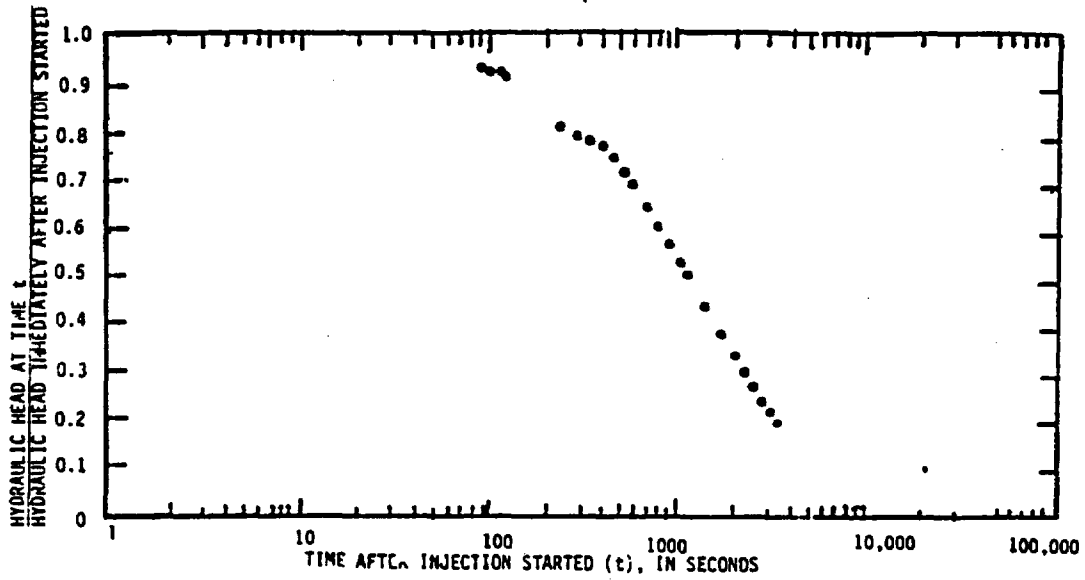
V · VELOCITY OF WATER MOVEMENT IN INJECTION TUBING



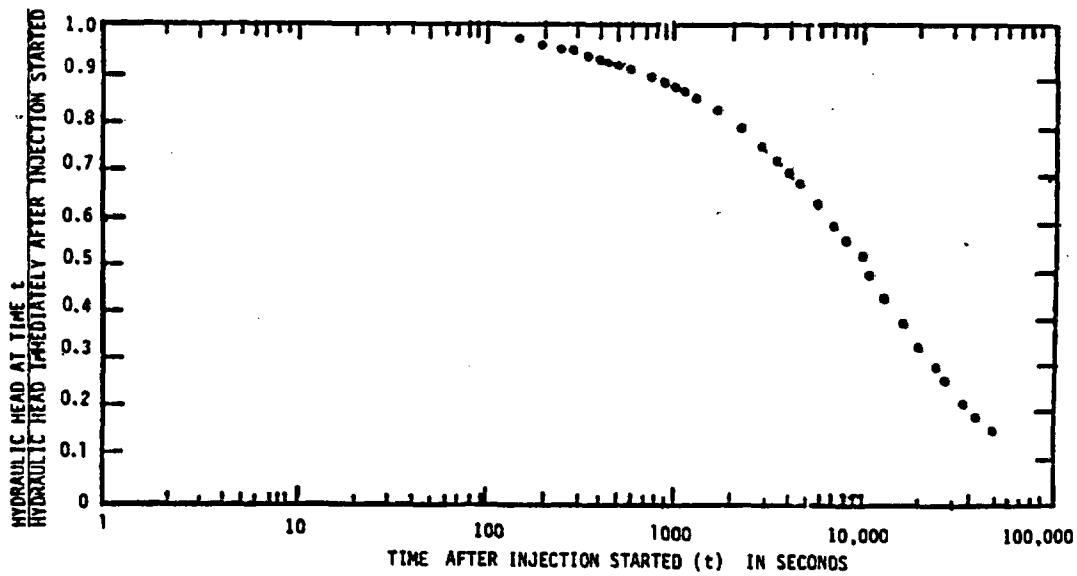
Idealization of relationship between velocity of slug movement and value of pore pressure for different assumed in-situ stress conditions



Location of wells where the Cooper-Brederhoff injection tests were performed. From Craig and Johnson (1984).

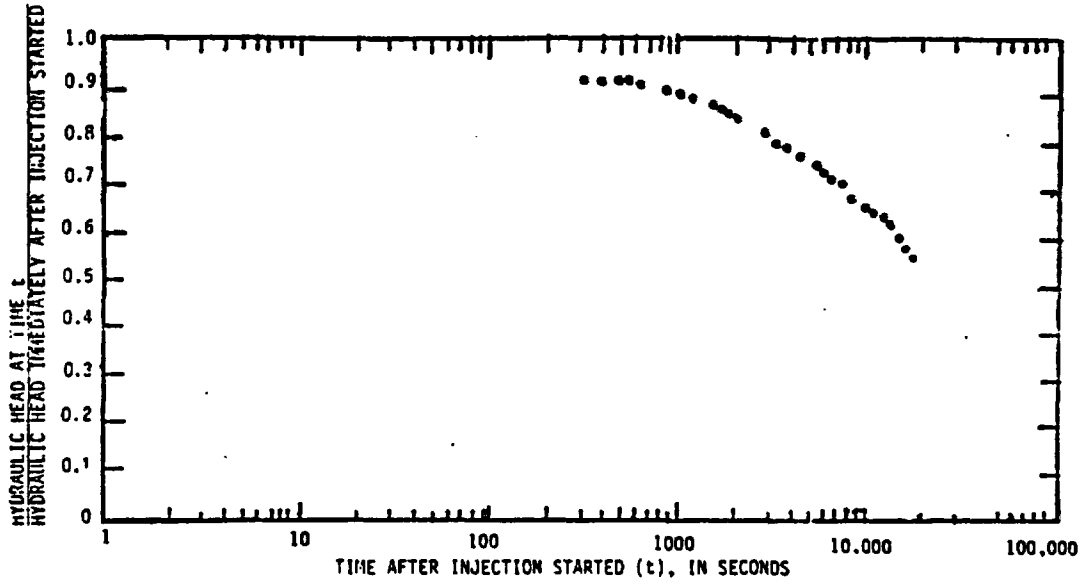


--Injection-test data for depth interval from 687 to 697 meters.

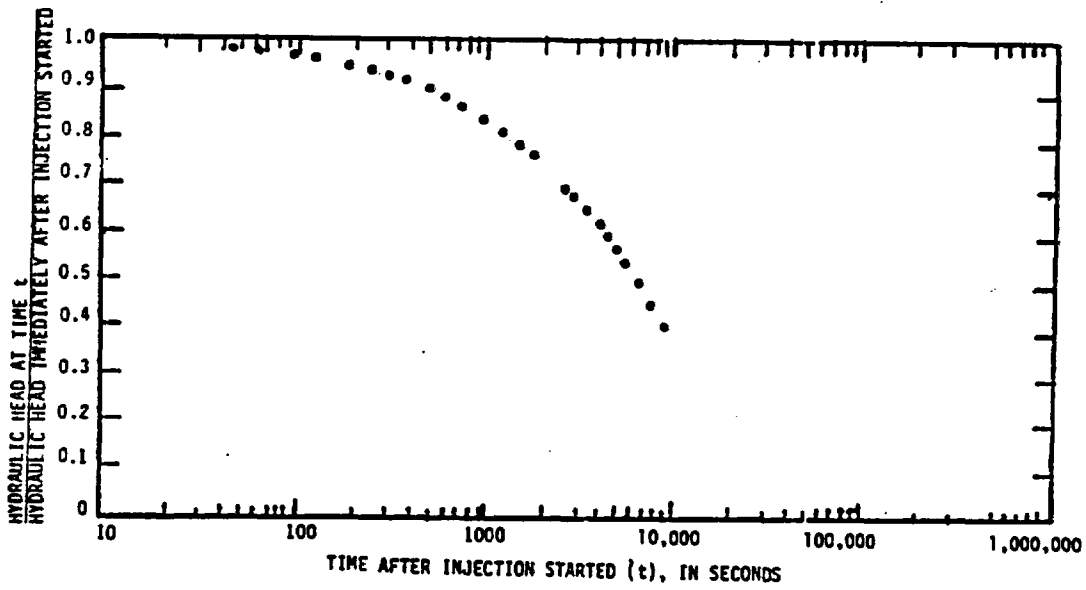


--Injection-test data for depth interval from 811 to 1,829 meters.

Results of the Cooper-Bredehoeft injection tests in well USW H-1. From Rush et al. (1983).

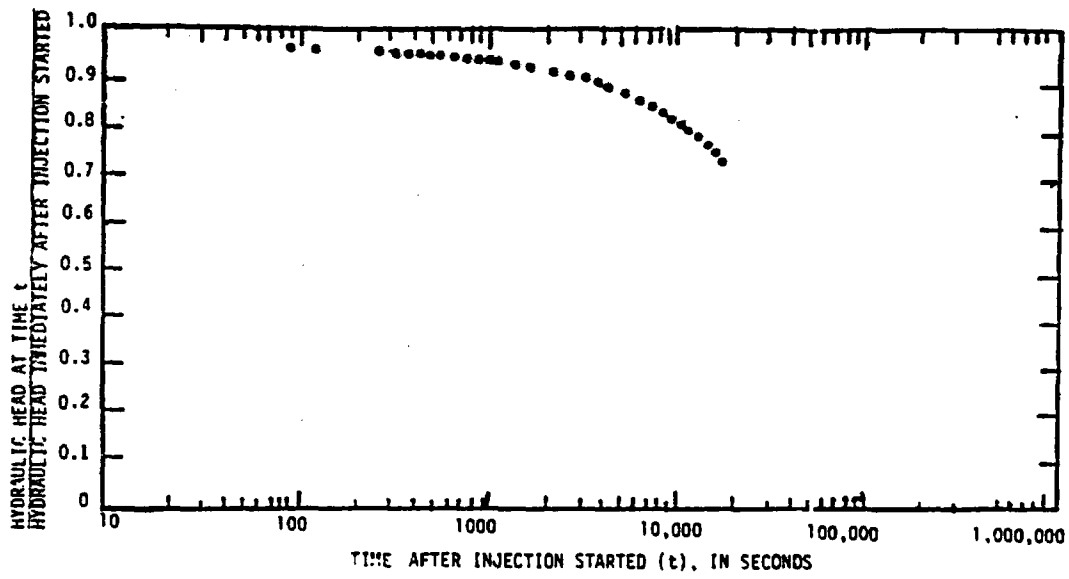


--Injection-test data for depth interval from 926 to 1,829 meters.

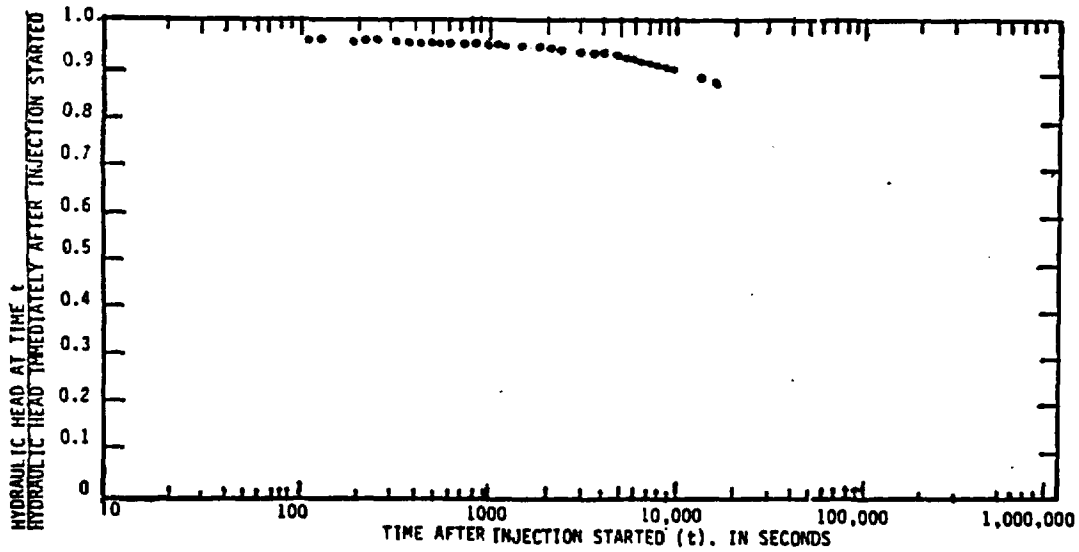


Injection-test data for depth interval from 1,200 to 1,829 meters.

Results of the Cooper-Bredehoeft injection tests in well USW H-1. From Rush et al. (1983).

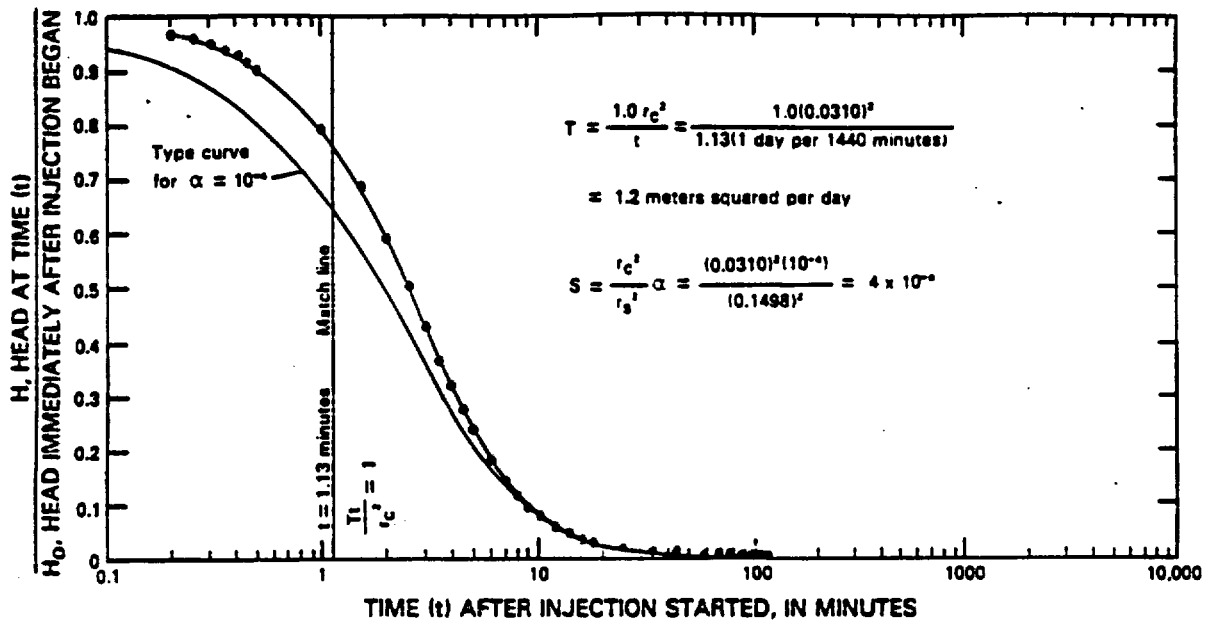


-injection-test data for depth interval from 1,407 to 1,829 meters.

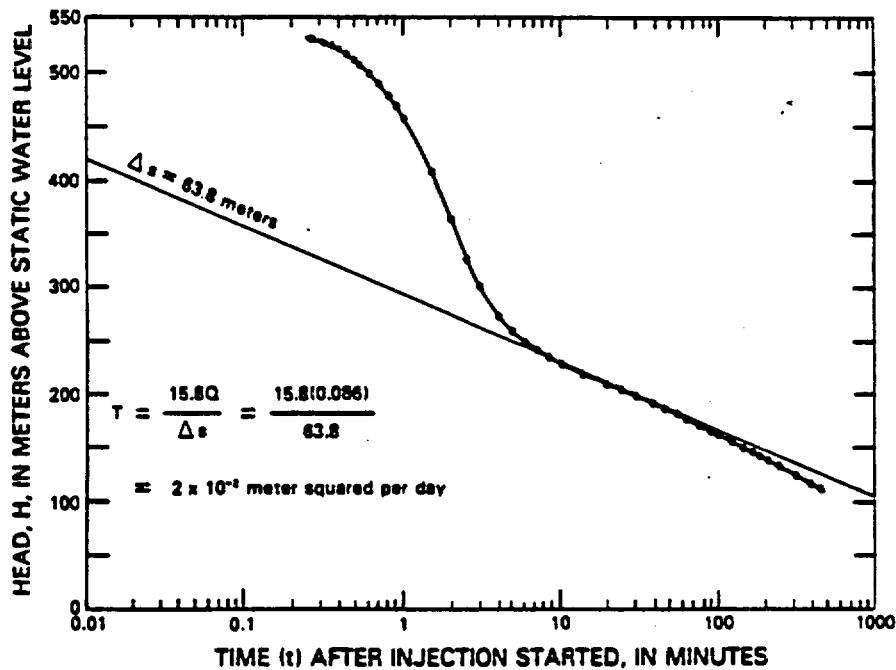


Injection-test data for depth interval from 1,621 to 1,829 meters.

Results of the Cooper-Bredehoeft injection tests in well USW H-1. From Rush et al. (1983).

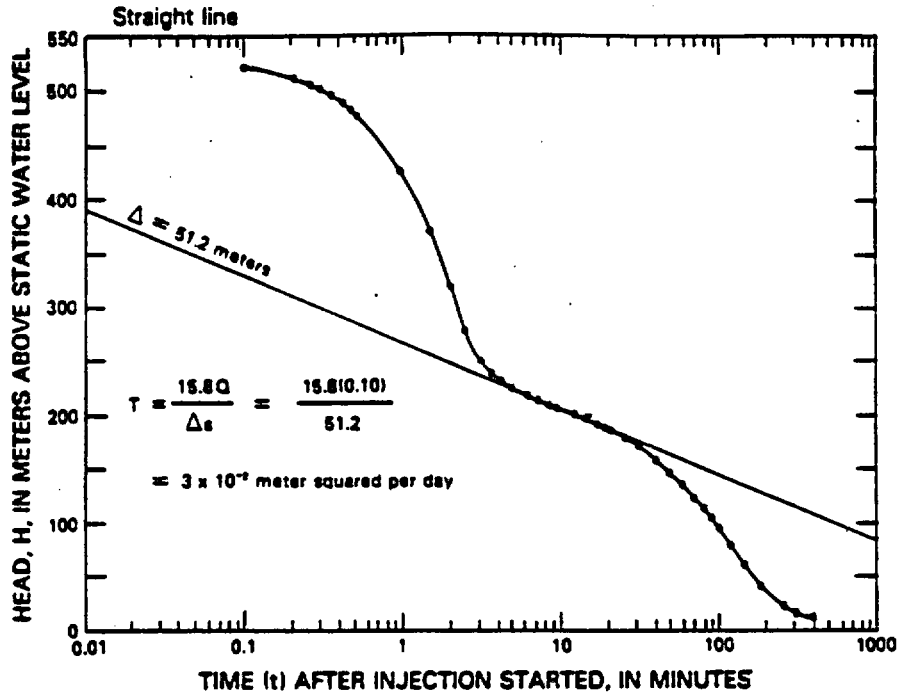


TEST INTERVAL 792m - 850m.

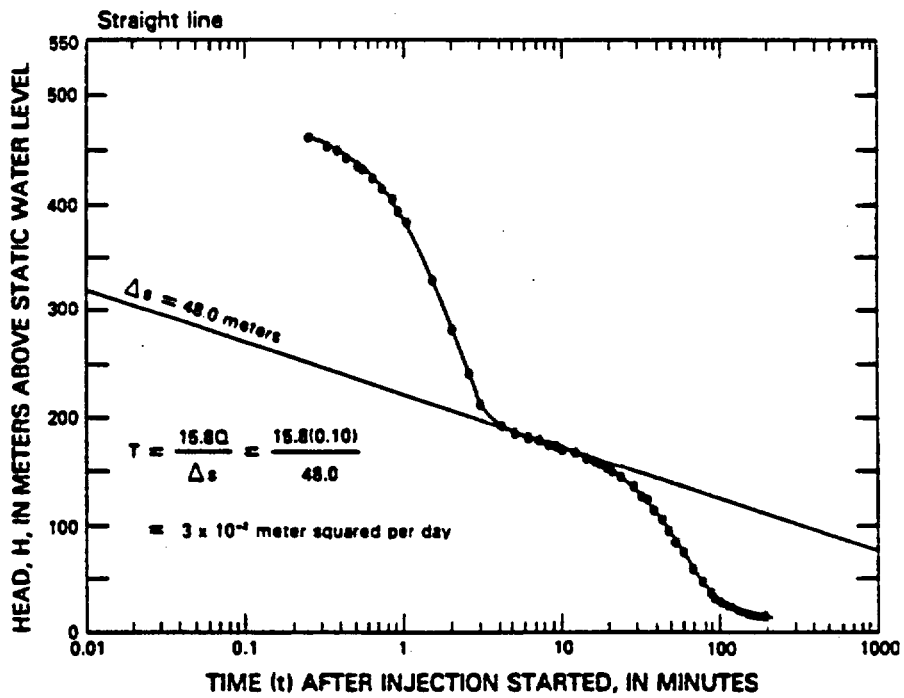


TEST INTERVAL 851m - 917m.

Results of the Cooper-Bredehoeft injection tests in well USW H-3. From Thordarson et al. (1985).

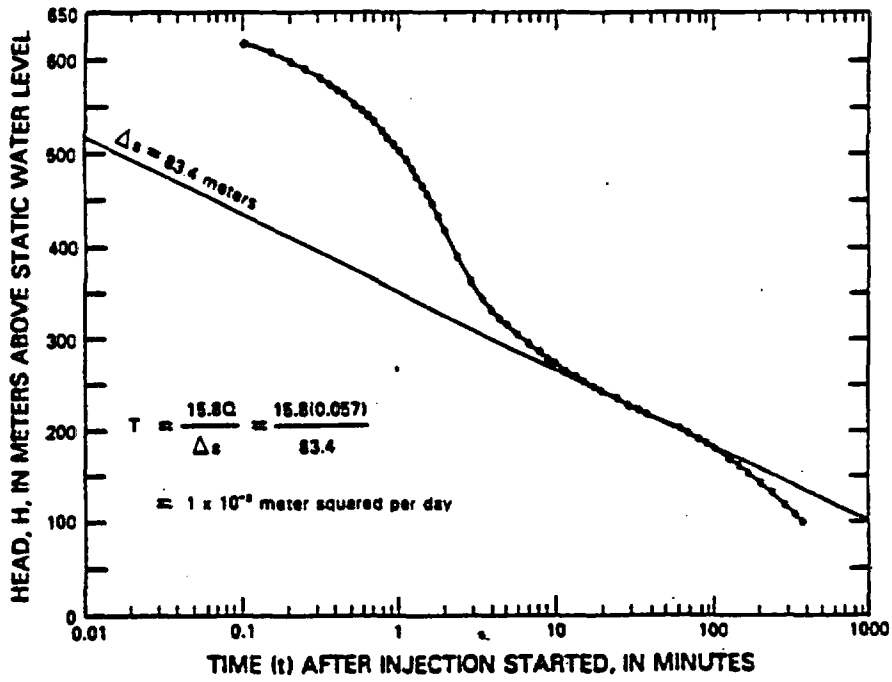
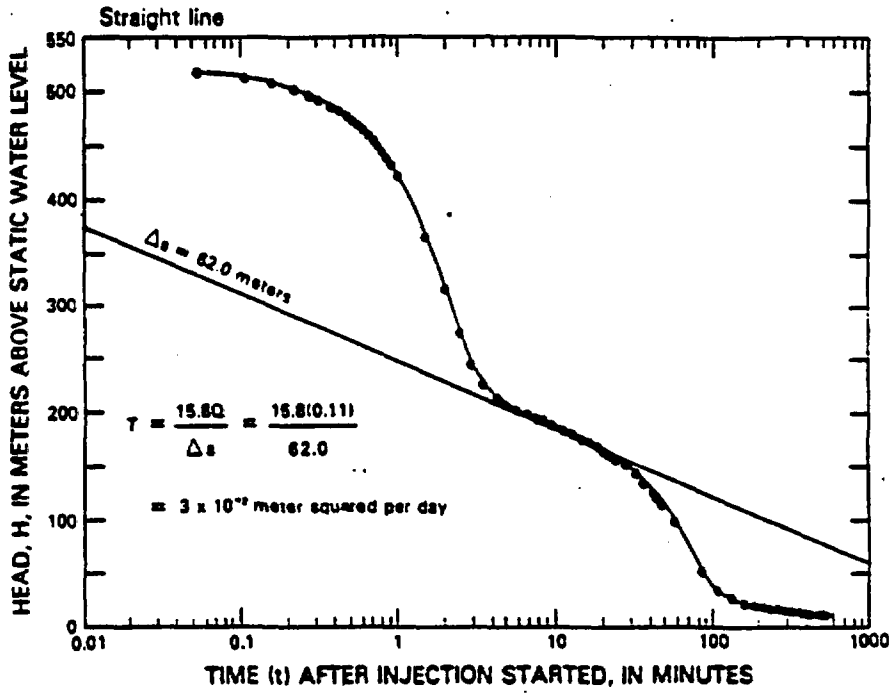


TEST INTERVAL 911m - 972m.



TEST INTERVAL 972m - 1219m.

Results of the Cooper-Bredehoeft injection tests in well USW H-3. From Thordarson et al. (1985).



Results of the Cooper-Bredehoeft injection tests in well USW H-3. From Thordarson et al. (1985).